

THE SEDIMENTARY GEOCHEMISTRY OF THE
MOFFAT SHALES : A CARBONACEOUS SEQUENCE IN
THE SOUTHERN UPLANDS OF SCOTLAND

Stewart W. Watson

A Thesis Submitted for the Degree of PhD
at the
University of St Andrews



1976

Full metadata for this item is available in
St Andrews Research Repository
at:
<http://research-repository.st-andrews.ac.uk/>

Please use this identifier to cite or link to this item:
<http://hdl.handle.net/10023/15471>

This item is protected by original copyright

THE SEDIMENTARY GEOCHEMISTRY OF THE
MOFFAT SHALES : A CARBONACEOUS SEQUENCE
IN THE SOUTHERN UPLANDS OF SCOTLAND

by

STEWART W. WATSON, BSc.

V O L U M E 1 T E X T

Thesis presented for the degree of Doctor of Philosophy of
the University of St. Andrews in the Faculty of Science.

1976.



ProQuest Number: 10170836

All rights reserved

INFORMATION TO ALL USERS

The quality of this reproduction is dependent upon the quality of the copy submitted.

In the unlikely event that the author did not send a complete manuscript and there are missing pages, these will be noted. Also, if material had to be removed, a note will indicate the deletion.



ProQuest 10170836

Published by ProQuest LLC (2017). Copyright of the Dissertation is held by the Author.

All rights reserved.

This work is protected against unauthorized copying under Title 17, United States Code
Microform Edition © ProQuest LLC.

ProQuest LLC.
789 East Eisenhower Parkway
P.O. Box 1346
Ann Arbor, MI 48106 – 1346

Th 8942

We declare that Mr. STEWART WILLIAM WATSON has fulfilled the regulations of study for the Degree of Doctor of Philosophy and is thereby entitled to present this thesis.

J.A. WEIR

(Supervisors)

J.A.W. P/P

P. BOWDEN

DECLARATION

I hereby declare that the following thesis is based on work carried out by me, that the thesis is my own composition, and that no part of it has been presented previously for a higher degree.

The research was carried out in the Department of Geology of the University of St. Andrews, under the direction of Dr. J. A. Weir and Dr. P. Bowden.

S. W. Watson.

ACADEMIC RECORD

I matriculated at the University of St. Andrews in October 1967, and graduated with the degree of Bachelor of Science, Second Class Honours, upper division, in Geology in June 1971.

In October 1971, I matriculated as a research student at the University of St. Andrews.

DEDICATION

For their guidance and encouragement
this work is dedicated to Mum and Dad.

ACKNOWLEDGEMENTS

During my period of research at the Geology Department of St. Andrews University I profited considerably from the excellent facilities provided and am most grateful to Professor E.K. Walton for making them available to me.

Dr. P. Bowden originally suggested this study which was supervised by himself and Dr. J.A.Weir. To them both I am indebted for their guidance and stimulating discussions and in particular I thank Dr. Weir for introducing me to the complexities of the geology of the Southern Uplands. I would also wish to express my gratitude to all the many other members of the department for discussions, advice and tuition in various techniques used in the study. Particular thanks go to Dr. W.E. Stephens for advice and tuition in the use of statistics and the manipulation of the data by computer. Mr. S. Bateman and his technical staff are also thanked for their assistance in analysing the sediments and preparing photographs.

The theme of this thesis has been greatly influenced by one year of attendance at the Organic Geochemistry Unit of the University of Newcastle upon Tyne. Many of the techniques used were taught to me at the Unit and most of the organic analyses were performed on equipment made available through the generosity of Dr. D.G. Murchison. I sincerely thank Dr. Murchison and Dr. A.G. Douglas for tuition in the techniques of the coal-petrographer and organic geochemist and

am indebted to Mr. E. Scott for instruction and assistance in the operation of reflected light microphotometers.

A great deal of the tedious tasks associated with the analytical work and the preparation of this thesis have been made more pleasant by my wife who has helped and encouraged me at every stage. Her assistance has been invaluable.

The receipt of a Natural Environmental Research Council studentship is acknowledged.

CONTENTS

| | Page |
|------------------|--------|
| Declaration | ii |
| Academic record | iii |
| Dedication | iv |
| Acknowledgements | v |
| Contents | viii |
| List of Tables | xvii |
| List of Plates | xxvi |
| Summary | xxviii |

| | Page |
|--|------|
| I. <u>STRATIGRAPHY AND STRUCTURE</u> | 1 |
| 1. INTRODUCTION | 2 |
| 2. STRATIGRAPHY AND SEDIMENTATION | 2 |
| a) Regional | 2 |
| b) Local | 3 |
| 3. STRUCTURE | 5 |
| a) Introduction | 5 |
| b) Ettrick Valley region | 6 |
| c) Dobb's Linn | 6 |
| d) Hartfell | 7 |
| e) Structural synthesis | 8 |
| 4. EVOLUTION OF THE SOUTHERN UPLANDS | 9 |
| a) Introduction | 9 |
| b) Evolution of Zone B | 9 |
| 5. CONCLUSION | 12 |
| | |
| II. <u>MINERALOGY</u> | 14 |
| 1. INTRODUCTION | 15 |
| 2. METHOD | 15 |
| 3. DETAILS OF THE MINERALOGY | 16 |
| a) Component minerals | 16 |
| b) Layered minerals | 17 |
| c) Interpretation | 21 |

| | Page |
|--|------|
| 4. QUANTITATIVE MINERALOGICAL ANALYSIS | 21 |
| a) Introduction | 21 |
| b) Theory of quantitative analysis by X-ray diffraction | 23 |
| c) Method of grinding | 24 |
| d) Preparation of calibration curves | 24 |
| e) Procedure | 25 |
| f) Stratigraphic variation | 26 |
| g) Discussion | 29 |
| 5. CURRENT DIRECTIONS AS DEDUCED FROM GRAPTOLITE STIPE ORIENTATIONS | 33 |
| a) Introduction | 33 |
| b) Method of analysis | 33 |
| c) Interpretation and future work | 34 |
| 6. VARIATION IN MUSCOVITE BASAL-SPACING | 34 |
| a) Introduction | 34 |
| b) Experimental method | 35 |
| c) Results | 36 |
| d) Discussion | 36 |
| III <u>INORGANIC CHEMISTRY</u> | 39 |
| 1. INTRODUCTION AND OBJECTIVES | 40 |
| 2. PREVIOUS RESEARCH | 40 |
| 3. SAMPLE COLLECTION AND ANALYTICAL TECHNIQUES | 41 |
| 4. SUMMARY STATISTICS AND ELEMENT FREQUENCY DISTRIBUTIONS | 43 |

| | Page |
|---|------|
| 5. THE AREAL DISTRIBUTION OF ELEMENT OXIDES AND TRACE ELEMENTS | 44 |
| a) Introduction | 44 |
| b) Application of trend surface analysis | 45 |
| c) The cubic surfaces | 45 |
| d) The iterative surfaces | 47 |
| e) Conclusion | 47 |
| 6. ELEMENT DISTRIBUTIONS THROUGH THE STRATIGRAPHIC SEQUENCE | 48 |
| a) Computation of vertical profile curves | 48 |
| b) Relationship between the vertical profiles | 49 |
| 7. ELEMENT DISTRIBUTIONS AT HARTFELL | 50 |
| a) Profiles computed for the north cliff | 50 |
| b) Restoration profiles | 51 |
| c) Interpretation | 52 |
| 8. BIVARIANT CORRELATION AND ELEMENT ASSOCIATIONS | 54 |
| a) Introduction | 54 |
| b) The correlation matrices | 54 |
| c) Element associations | 55 |
| d) Association of elements with minerals | 58 |
| 9. PRINCIPAL COMPONENTS ANALYSIS | 59 |
| a) Introduction | 59 |
| b) Results of principal components analysis | 61 |

| | Page |
|---|------|
| 10. ELEMENT ASSOCIATIONS AND CONTROLS OF MINERAL FORMATION | 62 |
| a) Free silica | 62 |
| b) Clays | 63 |
| c) Carbonate | 65 |
| d) Metals | 65 |
| e) Sodium and yttrium | 66 |
| 11. THE THREE PRINCIPLE COMPONENTS IN RELATION TO THE CONTROLS OF SEDIMENTATION | 67 |
| 12. TIME DEPENDENCE OF THE PRINCIPAL COMPONENTS | 69 |
| IV <u>ORGANIC CHEMISTRY</u> | 71 |
| 1. INTRODUCTION | 72 |
| 2. AMINO ACIDS | 72 |
| a) Introduction | 72 |
| b) Sample collection and analytical techniques | 74 |
| c) Results | 75 |
| d) Discussion | 75 |
| 3. HYDROCARBONS | 77 |
| a) Introduction | 77 |
| b) Sample collection and preparation | 78 |
| c) Extraction and analytical procedures | 79 |
| d) Results | 80 |
| e) Stratigraphic distribution of organic material | 82 |
| f) The variation in yield of organic compounds with distance from the dyke at Clanyard Bay | 83 |

| | Page |
|---|------|
| g) Composition of the organic extract:- the A/S ratio | 84 |
| h) Chromatographic analysis of the total alkane fraction | 85 |
| i) Calculation of odd-even preference values | 89 |
| j) Conclusions | 95 |
| 4. KEROGEN | 95 |
| a) Introduction | 95 |
| b) Isolation and analytical techniques | 97 |
| c) Chemical analysis | 98 |
| d) X-ray diffraction | 100 |
| e) Infra-red absorption | 103 |
| f) Conclusion | 105 |
| V <u>REFLECTED LIGHT STUDIES ON GRAPTOLITE FRAGMENTS</u> | 107 |
| 1. INTRODUCTION | |
| 2. PRINCIPLES OF REFLECTANCE MEASUREMENT ON COALS | 113 |
| 3. METHOD OF MEASURING GRAPTOLITE REFLECTIVITY VALUES | 114 |
| 4. PRELIMINARY INVESTIGATION OF GRAPTOLITE REFLECTIVITY VALUES | 114 |
| 5. THE POSITION OF THE ISOTROPIC SECTION IN GRAPTOLITES | 115 |
| a) Results | 115 |
| b) Discussion | 117 |
| 6. THE VARIABILITY OF MEAN-REFLECTANCE VALUES | 119 |
| a) Variation within a total sample | 119 |
| b) Variation over a single fragment | 120 |

| | Page |
|---|------|
| c) Computation of trend surfaces for reflectivities generated at random over the surface of a fragment | 122 |
| d) Discussion | 123 |
| 7. THE REFLECTIVITY OF CARBONIZED GRAPTOLITES | 125 |
| a) Introduction | 125 |
| b) Sample collection | 125 |
| c) Petrography of the dyke | 126 |
| d) Macroscopic variation in the samples with distance from the dyke | 126 |
| e) Microscopic changes in the graptolite fragments with distance from the dyke | 127 |
| f) Variation in reflectivity with distance from the dyke | 130 |
| g) Variation in the bireflectance ratio with distance from the dyke | 132 |
| h) Discussion | 133 |
| 8. DISPERSION WITH WAVELENGTH OF THE OPTICAL PROPERTIES OF CARBONIZED GRAPTOLITES | 135 |
| a) Reflectivity | 135 |
| b) Refractive and absorptive indices | 138 |
| c) Discussion | 141 |
| 9. VARIATION IN THE OPTICAL PROPERTIES OF GRAPTOLITES WITH TEMPERATURE | 144 |
| a) Introduction | |
| b) Variation in reflectivity with temperature | 146 |
| c) Variation in refractive index with temperature | 147 |

| | Page |
|---|------|
| d) Variation in absorptive index with temperature | 148 |
| e) Discussion | 148 |
| | |
| VI <u>APPLICATION OF GRAPTOLITE REFLECTIVITY</u> | |
| <u>AS A RANK PARAMETER</u> | 152 |
| 1. INTRODUCTION | 153 |
| 2. AREAS OF STUDY | 153 |
| 3. VARIATION IN GRAPTOLITE REFLECTANCE VALUES ALONG | |
| THE EASTERN MARGIN OF LUCE BAY | 154 |
| a) Sample collection | 154 |
| b) Results | 154 |
| c) Interpretation | 155 |
| 4. VARIATION IN GRAPTOLITE REFLECTANCE VALUES IN | |
| THE VICINITY OF MOFFAT | 157 |
| a) Sample collection and analysis of textures | 157 |
| b) Results | 157 |
| c) Interpretation | 159 |
| 5. THE STRATIGRAPHIC VARIATION IN REFLECTIVITY | 161 |
| a) Introduction | 161 |
| b) Stratigraphic variation at Dobb's Linn | 162 |
| c) Stratigraphic variation at Hartfell | 163 |
| d) Conclusions | 163 |
| 6. THE SPECTRAL VARIATION IN OPTICAL PROPERTIES OF | |
| GRAPTOLITE FRAGMENTS FROM HARTFELL | 164 |
| a) Introduction | 164 |
| b) Reflectivity trends | 165 |

| | Page |
|---|------|
| c) Refractive index trends | 166 |
| d) Absorptive index trends | 166 |
| e) Discussion | 166 |
| 7. VARIATION IN THE REFLECTIVITY OF GRAPTOLITES IN THE VICINITY OF IGNEOUS PLUTONS | 167 |
| a) Introduction | 167 |
| b) Results | 167 |
| c) Computation of temperatures outside a cooling pluton and their relationship with reflectivity | 168 |
| d) Conclusion | 169 |
| VII <u>ELECTRICAL RESISTIVITY</u> | 170 |
| 1. INTRODUCTION | 171 |
| 2. EXPERIMENTAL | 173 |
| 3. THE EFFECT OF PRESSURE ON RESISTIVITY MEASUREMENTS | 174 |
| a) Introduction | 174 |
| b) Experimental details and results | 176 |
| c) Conclusion | 177 |
| 4. VARIATION IN RESISTIVITY FOR SAMPLES FROM CLANYARD BAY | 177 |
| 5. REGIONAL VARIATION IN RESISTIVITY FOR SAMPLES COLLECTED FROM SEDIMENTS EXPOSED ALONG THE EASTERN MARGIN OF LUCE BAY | 179 |
| 6. REGIONAL VARIATION IN RESISTIVITY FOR SAMPLES COLLECTED IN THE VICINITY OF MOFFAT | 180 |

| | Page |
|--|---------|
| 7. THE STRATIGRAPHIC VARIATION IN RESISTIVITY | 181 |
| a) In the Moffat Region | 181 |
| b) At Hartfell | 182 |
| c) Discussion | 183 |
| 8. THE VARIATION IN RESISTIVITY OF TWO COMPONENT MINERAL MIXTURES | 184 |
| a) Introduction | 184 |
| b) Method and results | 184 |
| c) Discussion | 185 |
| VIII <u>FACTORS AFFECTING COALIFICATION AND CARBONIZATION</u> <u>OF THE ORGANIC MATERIAL IN THE MOFFAT SHALES</u> | 187 |
| 1. INTRODUCTION | 188 |
| 2. FACTORS AFFECTING RANK | 190 |
| a) Thermal alteration | 190 |
| b) Pressure effects | 193 |
| c) Radiochemical effects | 194 |
| d) The effect of geological time | 194 |
| 3. CONCLUSION | 195 |
| REFERENCES | 197 |

LIST OF TABLES

- Table 1-1 Stratigraphy of the Moffat Shales.
- Table 1-2 Location of samples at Hartfell.
- Table 2-1 Assignment of mineral reflections to X-ray diffractogram peaks occurring between 2 and 14 Å in sample DCYP-3.
- Table 2-2 Peak positions employed in modal analysis by X-ray diffraction.
- Table 2-3 Summary of mean mineral contents in the Moffat Shales.
- Table 2-4 Summary statistics for the minerals analysed by X-ray diffraction from the Moffat Shales at Dobb's Linn and Hartfell.
- Table 2-5 Regression parameters for the variation of X-ray diffraction peak-intensity ratios for mixtures of quartz with various minerals.
- Table 2-6 Analysis of variance for polynomial curves fitted to the stratigraphic variation of mineral contents and the variation of the muscovite basal spacing.
- Table 3-1 Location, zone and elements analysed for the Moffat Shale samples.
- Table 3-2 Univariant statistics for elements analysed in the total suite of samples collected in the vicinity of Moffat.
- Table 3-3 Comparison of mean element values in Moffat Shales from different localities.
- Table 3-4 Univariant statistics for chemical analyses from samples collected on a grid basis in the vicinity of Moffat.

| | |
|------------|---|
| Table 3-5 | Percentage surface fits for the distribution of elements in the vicinity of Moffat. |
| Table 3-6 | Analysis of variance for polynomial curves fitted to the stratigraphic variation of chemical analyses. |
| Table 3-7 | Analysis of variance for polynomial curves fitted to the stratigraphic variation of chemical analyses from the north cliff at Hartfell. |
| Table 3-8 | Analysis of variance for polynomial curves fitted to the stratigraphic variation of chemical analyses at Hartfell after restoration of the north cliff to the pre-fault sequence. |
| Table 3-9 | Comparison of significance levels for vertical profiles of chemical analyses at Hartfell. |
| Table 3-10 | Kendall rank order and product moment correlation matrices for the Moffat Shales. |
| Table 3-11 | Loadings and eigenvalues for the first three principal components. |
| Table 4-1 | Location of those samples analysed for hydrocarbons. |
| Table 4-2 | Yield of organic materials after soxhlet extraction for samples collected in the vicinity of Moffat. |
| Table 4-3 | Yield of organic materials after soxhlet extraction for samples collected adjacent to the dyke at Clanyard Bay. |
| Table 4-4 | Mean values for the yield of organic fractions at three localities. |

- Table 4-5 Extractability of organic fractions.
- Table 4-6 Analysis of variance for polynomial curves fitted to the stratigraphic variation in organic extracts.
- Table 4-7 Ratio of aromatic to saturated-aliphatic hydrocarbons in the Moffat Shales.
- Table 4-8 Classification of total alkane chromatograms.
- Table 4-9 Odd-even predominance values for samples from Clanyard Bay.
- Table 4-10 Odd-even predominance values in the Moffat Shales.
- Table 4-11 Comparison of mean odd-even predominance values at three localities.
- Table 4-12 Analysis of variance for polynomial curves fitted to the stratigraphic variation in odd-even predominance values.
- Table 4-13 Elemental composition of kerogen isolates.
- Table 4-14 Analysis of variance for polynomial curves fitted to the stratigraphic variation in elemental composition of kerogen.
- Table 4-15 Descriptive parameters characterizing different stages in the graphite-d-graphite series with respect to the [002] peak.
- Table 4-16 X-ray diffraction parameters and degree of disordering of carbonaceous material isolated from the Moffat Shales.

- Table 4-17 Wavenumbers in the infra-red of the quantitatively important minerals in sedimentary rocks.
- Table 5-1 Dispersion with wavelength of minimum and maximum reflectance values in air and in oil of graptolite fragments cut at various angles to the plane of the bedding.
- Table 5-2 Regression line parameters for the variation of minimum and maximum reflectance values in air and in oil with wavelength for a series of measurements made at various angles to the bedding.
- Table 5-3 Variation with wavelength of maximum minus minimum reflectance values in air and in oil of graptolite fragments cut at various angles to the plane of the bedding.
- Table 5-4 Single variable statistics for mean reflectance values measured in oil at 546 nm for sample LBR-29.
- Table 5-5 Observed and random reflectance values in oil at 546 nm for a grid distribution of points across a single graptolite fragment.
- Table 5-6 Computed fit values for surfaces derived by trend surface analysis for the areal variation in reflectance values over a graptolite fragment.
- Table 5-7 Description of samples collected from Clanyard Bay.
- Table 5-8 The variation in reflectance values of graptolite fragments with distance from the centre of a 9.18 metre thick porphyrite dyke.

- Table 5-9a Regression parameters for the variation in mean reflectance of graptolite fragments with distance along the measured section at Clanyard Bay.
- Table 5-9b Observed reflectance values at 546 nm in oil and those obtained from the regression equations in Table 5-9a.
- Table 5-10 Variation of reflectivity in oil at 546 nm with distance for samples collected to the north of the dyke at Clanyard Bay.
- Table 5-11 Variation in optical properties of graptolites with wavelength for selected samples from Clanyard Bay.
- Table 5-12 Statistical regression parameters at various wavelengths for the variation in the logarithm of estimated reflectance values in oil with perpendicular distance from the centre of the dyke.
- Table 5-13 Linear regression parameters for the dispersion with wavelength of reflectivity in oil for samples collected from Clanyard Bay.
- Table 5-14 Statistical regression parameters at various wavelengths for the variation of absorptive index values with perpendicular distance from the centre of the dyke.
- Table 5-15 Calculated maximum temperatures at various points outside the dyke at Clanyard Bay.
- Table 5-16 Regression parameters for the variation of mean reflectance values in oil at 546 nm with maximum temperature for various equivalent temperatures.
- Table 5-17 Variation of refractive index with temperature at selected wavelengths.

- Table 5-18 Regression parameters for the variation in refractive index with temperature at selected wavelengths.
- Table 5-19 Variation in absorptive index with temperature at selected wavelengths.
- Table 5-20 Regression parameters for the variation in absorptive index with temperature at selected wavelengths.
- Table 6-1 Mean reflectance values of samples from the east coast of Luce Bay.
- Table 6-2 Mean reflectance values of samples collected in the vicinity of Moffat.
- Table 6-3 Stratigraphic location of those samples from Hartfell which were used for dispersion analysis.
- Table 6-4 Variation in optical properties of graptolites with wavelength for selected samples from Hartfell.
- Table 6-5 Variation in graptolite reflectance values with distance from granite contacts.
- Table 6-6 Variation in graptolite reflectance values with temperature outside a cooling sphere.
- Table 7-1 Resistivity values of natural minerals.
- Table 7-2 Resistivity values for selected rocks.
- Table 7-3 Variation of resistivity with pressure for samples from Clanyard Bay.
- Table 7-4 Summary of parameters measured for samples collected from the south side of the dyke at Clanyard Bay.

| | |
|-----------|--|
| Table 7-5 | Correlation matrix for samples collected from the south side of the dyke at Clanyard Bay. |
| Table 7-6 | Abstract from correlation matrices to illustrate the variation of resistivity with selected parameters. |
| Table 7-7 | Summary of mean values for selected parameters at Hartfell and Dobb's Linn. |
| Table A-1 | Stratigraphic succession at the north end of Clanyard Bay. |
| Table B-1 | Instrumental conditions for the analysis of major elements by atomic absorption spectroscopy. |
| Table B-2 | Replicate analyses of major elements in standard rock BMS. |
| Table B-3 | Elementary statistics for replicate analyses of major elements in standard rock BMS. |
| Table B-4 | Comments pertaining to the choice of analytical lines in the analysis of trace elements by X-ray fluorescence. |
| Table B-5 | Instrumental conditions for the analysis of trace elements by X-ray fluorescence. |
| Table B-6 | Mineralogy and chemistry of the standard rock BMS. |
| Table B-7 | Replicate estimates of mass absorption coefficients for standard rock BMS. |
| Table B-8 | Elementary statistics for replicate estimates of mass absorption coefficients in standard rock BMS. |

- Table B-9 Replicate analyses of trace elements in standard rock BMS.
- Table B-10 Elementary statistics for replicate analyses of trace elements in standard rock BMS.
- Table B-11 Desalting method scheme.
- Table B-12 Variation in the refractive index of diamond with wavelength.
- Table B-13 Variation in the refractive index of Zeiss immersion oil with wavelength.
- Table B-14 Variation in reflectance values of diamond in oil and in air with wavelength.
- Table C-1 List of computer programs used during the study.
- Table C-2 Glossary of statistical and mathematical terms.
- Table D-1 Regression line parameters for the dispersion of mean reflectance values of graptolite fragments in oil with wavelength for selected samples from Clanyard Bay.
- Table D-2 Regression line parameters for the dispersion of mean reflectance values of graptolite fragments in air with wavelength for selected samples from Clanyard Bay.
- Table D-3 Regression line parameters for the dispersion of mean reflectance values of graptolite fragments in oil with wavelength for selected samples from Hartfell.
- Table D-4 Regression line parameters for the dispersion of mean reflectance values of graptolite fragments in air with wavelength for selected samples from Hartfell.

Tables E1 to E96 Analytical results.

Tables E97 to E99 Standard deviation values for graptolite
reflectivity measurements.

LIST OF PLATES

- Plate 1 Photomicrograph illustrating the mineralogy of the sheared porphyrite dyke at Clanyard Bay.
- Plate 2 Photomicrograph illustrating zoned pyroxenes in the sheared porphyrite dyke at Clanyard Bay.
- Plate 3 Photomicrograph illustrating vesiculation within a graptolite fragment from sample LB-13.
- Plate 4 Photomicrograph illustrating larger scale vesiculation within a graptolite fragment from sample LBR-15.
- Plate 5 Photomicrograph illustrating fractured graptolite fragments within sample LBR-29.
- Plate 6 Photomicrograph illustrating mineral contaminated granular mosaic within graptolite fragments in sample LBR-9.
- Plate 7 Photomicrograph illustrating banding within a graptolite fragment in sample LBR-7.
- Plate 8 Photomicrograph illustrating mineral contaminated granular mosaic within graptolite fragments in sample LBR-3.
- Plate 9 Photomicrograph illustrating vesiculated granular mosaic within graptolite fragments in sample LB-18.
- Plate 10 Photomicrograph illustrating sheared graptolite fragments within sample LBR-8.
- Plate 11 Photomicrograph illustrating strained extinction in a graptolite fragment within sample MG-3.
- Plate 12 Photomicrograph illustrating flow banding in graptolite fragments within sample HCL-30.

Plate 13 Photomicrograph illustrating granular mosaic texture within a graptolite fragment in sample HL-8.

Plate 14 Photomicrograph illustrating granular mosaic within possibly a glyptograptid theca in sample MG-14.

Plate 15 Photomicrograph illustrating mineral interfered granular mosaic in proximal end of graptolite rhabdasome in sample MG-14.

SUMMARY

The Moffat Shales form a 100-metre condensed pelitic succession of middle Ordovician to Silurian age. 210 samples were collected from several inliers and were dated by contained graptolites. Mineralogy indicates low greenschist facies regional metamorphism. Correlation and multivariate statistical techniques assess the interdependence of the range of major and trace elements analysed, and demonstrate progressive change related to an increasing input of clay. Physiography is deduced as the main factor controlling sedimentation with physico-chemical conditions and the decay of organic matter having important influences.

Amino acids were not detected. Minor amounts of alkanes occur, with the highest average yield extracted from sediments at the locality of Hartfell, and lesser amounts from Dobb's Linn and Clanyard Bay. Their abundance and distribution is related to thermal effects of metamorphism and to biodegradation. Metamorphism of kerogen has produced a graphite- d_{1a} structure. Structural ordering is highest in Hartfell kerogens and can be related to the proximity of reverse faults.

Optical properties and textural relationships of carbonized graptolite fragments are related to distance from a porphyrite dyke. Samples show increasing reflectivity, refractive and absorptive indices approaching the intrusion from the south. To the north, three discontinuities in the reflectivity trend are attributed to reactivation

of reverse faults following intrusion. Dispersion of reflectivity with wavelength shows a rise from blue to red corresponding to that of anthracitic vitrinites. The relationship between optical parameters and temperature indicates that carbonization has occurred at lower temperatures than for the coal-carbon transformation. Contrasts are attributed to initial chemistry, and rank, also to the unknown effects of time and tectonically induced pressure and temperature.

Reflectivity of dispersed graptolite fragments is used as a rank index for Moffat Shales cropping out in Luce Bay and near Moffat. At Luce Bay values correspond to those of coals in the low volatile bituminous to anthracitic range with high values occurring near faults. Coalification is related mainly to regional metamorphism; secondary processes, e.g. migration of hot fluids along fractures, may also have operated. At Moffat, comparable rank ranges are distributed along the southeast flank of a Caledonoid trending dome, low values occurring adjacent to the Ettrick Valley Thrust, high at Hartfell. Secondary thermal effects from an unexposed pluton are deduced.

Further evidence of enhanced thermal activity in the Hartfell sediments is presented from a study of the electrical conduction of powdered samples. The low resistance of Hartfell samples is attributed to the graphitic nature of the relatively abundant carbonaceous material.

CHAPTER I

STRATIGRAPHY AND STRUCTURE

1. INTRODUCTION

This study was initiated to investigate the geological setting, mineralogy, chemistry and degree of metamorphism of the 100 metre thick succession of Ordovician and Silurian graptolitic mudstones designated the Moffat "Series" (Lapworth 1878), subsequently amended as the Moffat Shales (Peach and Horne 1899), which designation is currently accepted. The Moffat Shales crop out as a series of strike-orientated, fault-bounded inliers, the occurrence of which defines the Central Belt of the Southern Uplands of Scotland (Peach and Horne 1899). The Northern Belt comprises mostly Ordovician rocks and lies to the north-west of the Central Belt which has mainly Lower Silurian rocks with some Ordovician inliers. The Southern Belt consists mainly of Wenlock rocks (Fig.1).

2. STRATIGRAPHY AND SEDIMENTATION

a) Regional

The Moffat Shale succession of the Southern Uplands of Scotland consists of predominantly black marine shales, cherts and mudstones which are noteworthy for their abundant and varied graptolites by which they are conveniently zoned. Claystones of variable thickness are particularly common in the upper part of the succession.

At no single locality in the Southern Uplands can a complete succession of the Moffat Shales be observed. The following summary presented by Weir (1973), has therefore been drawn up from several sources; Toghill 1968 (Birkhill Shales, Dobb's Linn [NT 198159]); Toghill 1970a (Hartfell Shales, Dobb's Linn); Watson 1971 (Hartfell and Glenkiln Shales, Hartfell [NT 094115]); Peach and Horne 1899 (Glenkiln Shales, Berrybush Burn, Ettrickdale, Selkirkshire, p.119; Lower Hartfell Shales, Dobb's Linn

p.97). Subdividing the Ordovician in accordance with Williams et al., (1972) and using the Silurian zones of Cocks et al., (1971), the composite stratigraphic sequence is given in Table 1-1 and is illustrated in Figs.2,3.

The Moffat Shales are interpreted (Walton 1965, p.205) as having been deposited on an axial rise within the Caledonian Geosyncline. This rise formed the south-eastern limit of a depositional trough, the Southern Uplands Trough, which accumulated a thick spread of flysch during the latter half of the Lower Palaeozoic. This flysch, derived mainly from the Laurentian continent to the north-west and with some contribution from intra-geosynclinal island arcs (Weir in litt.) advanced south-eastwards to progressively encroach and finally obliterate the axial rise during the Llandovery.

Transgression of the graptolite shales by the succeeding flysch facies of the Gala formation is delayed longest at Craigmichan Scaurs about 2 kilometres south-east of Moffatdale (Fyfe and Weir 1976). Here, strata of higher turriculatus age are in the graptolitic facies whereas at Dobb's Linn greywackes come in at a lower level within the same zone (the maximus sub-zone). The south-eastern outcrop of the graptolitic facies is bounded however by the Ettrick Valley fault (Toghill 1970b) suggesting that the axial rise of the Moffat Geosyncline may have been situated further to the south-east.

b) Local

In this study three inliers of Moffat Shales have been extensively sampled. These are situated at Dobb's Linn, Hartfell and Clanyard Bay. The former two localities are situated in the vicinity of Moffat (Dumfries and Galloway Region: Annandale and Eskdale District, Fig.4) while the latter is situated in the Rhinns of Galloway (Dumfries

and Galloway Region: Galloway District, Fig.5).

Summaries of the successions at Dobb's Linn [NT 198159] and Hartfell [NT 094115] are given in Appendix A. No recent account of the geology of Clanyard Bay [NX 101381] exists, and a statement follows, with a stratigraphical summary in Appendix A.

47.98 m of Moffat Shales have been recognized at the north end of Clanyard Bay (Fig.5). Here, the first rock exposure to the north of the pebble filled embayment consists of 13.73 m of very fissile platy grey shales which weather out to give a distinct red colouration. These are succeeded to the north by 0.76 m of non-fossiliferous black shales which give way after an apparent dislocation of small magnitude to 0.71 m of black blocky mudstone.

The succession is then interrupted by a 1.72 m wide gap filled with beach debris before the occurrence of a 0.35 m thick unit of very hard light grey mudstone. There then follow 5.8 m of black blocky mudstones which are intercalated by a few thin claystone bands. 6.5 m of Barren Mudstone lithology succeed.

The sediments are then pierced by a 9.18 m wide porphyrite dyke which is bounded on its northern margin by approximately 9 m of black shales which are fossiliferous in parts. These shales then grade into 7.2 m of black fossiliferous shales containing many nodular claystones. Throughout this and the preceding unit many small-scale dislocations are apparent. These culminate in a strike-orientated fault which occurs towards the top of the unit.

The fault is succeeded by 3.0 m of unfossiliferous blue-black shales and clays which are intruded by a 1.40 m wide dyke. There then follow 2.3 m of grey black sparsely fossiliferous shales and mudstones before the occurrence of another slightly thicker dyke (2.2 m). The

succession is capped by a thick sequence of well jointed greywackes.

Nowhere in the succession are graptolites prolific but the few which have been recovered indicate that the sequence encompasses the vesiculosus to turriculatus Zones. That the sequence commences in the Barren Mudstone facies of the Upper Hartfell Shales is without doubt. The immediately succeeding shales and mudstones may however only be assigned to the Upper Ashgill by lithological comparison with the type section at Dobb's Linn.

Repetition of the Barren Mudstones has been attributed by Peach and Horne (1899) to anticlinal folding. There is however no evidence to suggest a change from the dominant very steep north-westerly dip and reverse faulting probably accounts for the appearance and repetition of the unit.

The lack of strict palaeontological control is unfortunate since the overall aspect of the sequence indicates that it is punctuated by a series of small scale faults. The effect of these will be examined in greater detail in Chapter V.

3. STRUCTURE

a) Introduction

The Moffat Shales outcrop in the Central Belt of Peach and Horne (1899) as inliers within a large area of Llandovery greywackes. These inliers follow the regional Caledonoid trend and two modes of origin have been invoked:- (1) as fold cores (Lapworth 1878); (2) introduced by reverse strike faulting (Harkness 1851; Toghil 1970b; Fyfe and Weir 1976).

b) Ettrick Valley region

Toghill (1970b) has demonstrated that the south-east limit of the Moffat Shale inliers in the Llandoverly greywackes of the Moffat area is a major thrust trending NE-SW. This dislocation, the Ettrick Valley Thrust (Fyfe and Weir 1976), thrusts the tightly folded Moffat terrain over younger greywackes which dip, and young, to the north-west. A zone of imbrication, in which slices of Moffat Shales and Gala greywackes are reduplicated, occupies a zone around one kilometre wide immediately northwest of the fault. This imbrication Toghill (ibid) considers was caused by the shearing out of inverted limbs of isoclinal folds.

Fyfe and Weir (1976) have recently shown that the Ettrick Valley Thrust is traceable to the south-west into Craigmichan Scaurs where it is inclined north-westwards at about 70 degrees (Figs. 7,8). Near the head of the Selcoth Burn shales of the sedgwickii Zone are carried south-eastwards over Gala greywackes whereas at Park's Well [NT 169062], where a lesser thrust splays from the main structure, Glenkiln Shales are in contact with greywackes (Fig.7). Weir (1968) likens the wide zone of imbrication to that associated with major thrusts of the North-west Highlands of Scotland.

c) Dobb's Linn

The Dobb's Linn inlier, 4 kilometres north-west of the Ettrick Valley Thrust (Fig.4) is a complex reverse-faulted anticline showing little sign of imbrication (Peach and Horne 1899). At this locality tight anticlines are cut by a series of early northwestward translating thrusts which are intersected by later normal and also vertical strike faults (Ingham in prep.). This type of structure recalls the diapiric fold of the Broadford Mountains anticline, (Weir 1962), which emplaces

correlatives of the Moffat Shales into the structural context of the overlying flysch. The initiation of similar structures in the Southern Uplands probably predated the propagation of the Ettrick Valley Thrust (Weir 1974).

d) Hartfell

At Hartfell, 9 kilometres from the Ettrick Valley Thrust (Fig.4), it is again an asymmetric anticline that brings the shales to the surface (Watson 1971). The situation is complicated however by the presence of many southeastward translating reverse faults causing imbrication within the Moffat Shales. In the north cliff four major reverse faults are recognised. These are associated with many other smaller faults of the same generation (Fig.9). The most important of the major faults occurs at the base of the cliff and coinciding with the anticlinal axial plane it separates the Lower and Middle Hartfell Shales of the north cliff from the Lower Birkhill Shales of the south cliff.

A series of small scale folds is associated with the faults. These folds are fairly tight and could have originated in one of three ways:- (1) formed before the main anticline; (2) formed as parasitic drag folds on the limbs of the major fold; (3) formed as drag folds as a result of faulting. Detailed study of the sequence of graptolite assemblages within the zones, and of the orientation of the fold axial planes of the minor folds, indicates that they are a result of drag caused by the formation of the main anticlinal structure (Watson 1971).

A total of 63 samples has been collected from the north cliff at Hartfell (Fig.6). The true stratigraphic positions of these before faulting and folding have been reconstructed from the detailed palaeontological and structural information given in Appendix A. The positions

of the samples relative to the major thrust at the base of the cliff and their stratigraphic position after structural restoration is given in Table 1-2.

e) Structural synthesis

The prevalence of imbricate zones associated with thrust faulting in the vicinity of Moffat and the fact that such zones can be traced across the breadth of Scotland has prompted Weir (in litt.) to consider that each of the five main outcrops of Moffat Shales which traverse the Southern Uplands is controlled by a major southeastward translating thrust (Fig.10). These thrust were developed by décollement along the Moffat Shales which always occur in the bases of the thrust slices and are characteristically involved in an overlying schuppen zone. In southeastward succession the thrusts have been named (Weir in litt.) Leadhills, Tweedale, Talnoy, Moffatdale and Ettrick Valley. The Ettrick Valley Thrust which delimits the tectonically and stratigraphically contrasting Central and Southern Belts is the largest of these structures (Toghill 1970b; Fyfe and Weir 1976). Both the Moffatdale (through Dobb's Linn) and the Talnoy (through Hartfell) thrusts are of lesser importance and possibly connect at depth to the Ettrick Valley Thrust (Weir 1974, Fig. 2).

Tectonic transport is southeastward in the Central Belt of the Southern Uplands. Powell (1972) proposes that the Moffat Shales rested initially on a lower turbidite sequence which is perhaps represented at outcrop by the Coldingham Beds of Berwickshire. These beds in turn may have sheared off from crystalline basement at a depth of about twelve kilometres.

The Girvan district of Ayrshire to the north-west of the

Southern Uplands displays by contrast northwestward tectonic transport. In this area low angle thrusts prevail but with no sign of décollement. Here the thrust masses incorporate slices of basement ophiolites of the Ballantrae Igneous Complex (Williams 1959).

The above observations have led Weir (1974) to propose that the structure of the entire Southern Uplands may be interpreted as a double nappe with a form similar to that of the Tay Nappe in the Grampian orogen (Rast 1963).

4. EVOLUTION OF THE SOUTHERN UPLANDS

a) Introduction

The Caledonides of Scotland and Ireland have been divided into two tectonically and metamorphically contrasting zones, respectively the northern metamorphic and the southern non-metamorphic belts (Reid 1961). The northern zone deformed and metamorphised by the Grampian Orogeny which reached an early Ordovician climax (Dewey et al., 1970) is distinguished as the orthotectonic Zone A (Alpinotype tectonics) of the orogen (Dewey 1969).

The southern non-metamorphic Caledonides are subdivided into two; the paratectonic Zone B (Germanotype tectonics) which extends southeastwards to the north-west margin of the Irish Sea Horst and has a late Silurian deformational climax and Zone C, again orthotectonic (Alpinotype tectonics), to the south which has a late Precambrian climax and a complex Lower Palaeozoic history (Dewey 1969).

b) Evolution of Zone B

Dewey (1969, 1971) has interpreted the evolution of the southern part of the Scottish Caledonides from detailed stratigraphical

and structural work of Kennedy (1958), George (1960), Kelling (1961), Williams (1962), Walton (1963) and Ziegler (1970) in terms of plate tectonics. Eocaledonia is diagnosed as part of a North Atlantic (Laurentian) continental plate, and is approximately coextensive with Zone A of the Caledonides under which a 'Proto-Atlantic' plate was being consumed. This occurred during the late Cambrian and early Ordovician along a Benioff zone which outcrops within the Glen App Trench. The Ballantrae Igneous complex is proposed as representing a tectonic mélange developed on top of the Benioff zone. This is considered to extend northwestwards to the Highland Boundary Fault which originated with a northward downthrow prior to the Arenig (George 1960, Dewey 1961, Cobbing 1964).

On Dewey's hypothesis, plate consumption was largely completed by the close of the Arenig, but uplift of Zone A continued through the remainder of the Lower Palaeozoic. A southward-expanding flysch wedge spread across the mélange and thence over the oceanic plate.

Crustal shortening continued due to the squeezing of Zone B between Zone A and the Afro-European Plate which includes the Irish Sea Horst, and southwards, the Midland Platform, together comprising the orthotectonic Zone C. Cockburnland (Walton 1963, Ziegler 1970) and later Solwayland, running between the Southern Uplands and the Lake District (Walton 1963), grew in response to crustal shortening of the flysch sequence. Continued southward spreading of the flysch during Wenlock times united Cockburnland and Solwayland so that by early Ludlow times both were joined as a continuous mass. Between Eocaledonia and the now greatly expanded Cockburnland, the Midland Valley was established as a sedimentary basin receiving high rank metamorphic material from the north and low rank metamorphic material from the south.

Weir (in litt.) criticises the synthesis of Dewey (1971) for not explaining the occurrence of rocks with Precambrian structural imprints, for not defining the spatial distribution of the axial rise of the Protoacadic ocean, for not explaining the occurrence of the Tweedale riebeckite-keratophyres and the Bail Hill andesites and finally for not discussing the apparent absence of pre-flysch basement in the Southern Uplands.

Weir recognises four tectonically contrasting belts within Zone B of the Scottish Caledonides. The first in southward succession from the Highland Boundary Fault includes the Silurian inliers of the Midland Valley which are characterised by low dips. The second comprises the Girvan Thrust Belt (Williams 1959, 1962), which involves the Ballantrae mélange and is typified by northwestward transport. The Southern Uplands Thrust Belt, displaying southeastward transport is the third belt while the fourth, delimited by the Ettrick Valley Thrust, includes the monoclinial folds of the Galloway coast (Craig and Walton 1959, Weir 1968). Northwestward transport again dominates in the southernmost belt.

These four belts are related to the influence of four island arc systems identified as the Connemara Cordillera, the Munster-Galloway arc (Fig.11), Cockburnland and the Tweedale arc. The first two named both had a Dalradian stratigraphy and are considered to have been detached from the south-eastern margin of the Laurentian continent late in the Cambrian. Cockburnland developed in the Arenig as a tectonic mélange associated with the Glen App Benioff Zone and the Tweedale arc contributed andesitic sediments to the Southern Uplands Trough during the Caradoc (Fig. 12).

Evolution of Zone B continued with segmentation controlled by crustal shortening. Initially over-riding was northwestwards forming in southeastward succession the 'rejuvenated' Cockburnland (controlled by the Southern Uplands Fault) and Solwayland as part of the Munster-Galloway arc, the whole defined northwestwards by the Nenagh-Hawick Line. Later development took place under the control of the Moffat décollement forming the succession of lesser wedges expressed in the linear outcrops of Moffat Shales and in the Galloway monoclines (Fig.13).

The formation of the Southern Uplands Tay Nappe type structure (Rast 1963) is interpreted by Weir (in litt.) as having been caused by the movement of Eocaledonia southeastwards in such a way as to drive into the Ballantrae mélange. This would then have rammed into the flysch pile of the Southern Uplands Trough which in turn sheared off along the Moffat décollement to form a Nappe designated by Weir as the Southern Nappe. The Southern Uplands thrust belt probably formed by upward propagation of the décollement in response to continued crustal shortening in an area bounded by the now stable cratonic Zone C. The thrust belt is termed the Moffat Nappe. The Girvan Nappe, to the north-west, was probably formed by extrusion and back thrusting to the north-west of the south-east margin of the original Cockburnland.

The structural evolution of the Southern Uplands is summarised in the form of NNW-SSE trending sections (Fig.14).

5. CONCLUSION

A basic structural and stratigraphical description of the Moffat Shales together with a brief outline of the postulated evolution and development of the Southern Uplands has been presented. Much of the

information presented results from discussions with other members of the group project and is therefore in no way exhaustive but simply serves to introduce the geological background of the sediments and their regional setting before describing their chemical and physical attributes.

(Top of succession)

Upper Birkhill Shales, 26.9 m , Llandovery (Idwian-Fronian).

Compact grey mudstones with black graptolitic mudstones (decreasing upwards both in thickness and in number) and claystones, the thicker containing calcareous nodules. Zones of Mongr. gregarius, M. convolutus (Idwian), M. sedgwickii, M. turriculatus, (Rastrites maximus sub-zone) (Fronian).

Lower Birkhill Shales, 14.6 m , Llandovery (Rhuddanian).

Black graptolitic mudstones, mostly massive and flaggy but shaley in two lowest zones, with abundant thin claystones. Zones of Glypto. persculptus, Akidogr. acuminatus, Cystogr. vesiculosus M. cyphus.

Upper Hartfell Shales, 18.9 m , Caradoc (Onnian)-Ashgill.

(2) Barren grey mudstones, 14.0 m,⁺ massive flaggy mudstones with occasional thin, black graptolitic seams. Dicellogr. complanatus (Pusgillian) and D. anceps (position debatable, Cautleyan-Hirnantian) faunas.

(1) Massively-bedded, blocky-jointed black mudstones, 4.9 m . Zone of Pleurogr. linearis (Caradoc, Onnian — Ashgill, Pusgillian).

Lower Hartfell Shales, 10.1 m , Caradoc (?Soudleyan-Onnian).

Thinly-bedded black shales with pyritised graptolites preserved in half-relief, becoming progressively more massively-bedded higher in the succession. ~~Course~~ ashcs occur at Hartfell (Watson 1971, p10). Zones of Climacogr. wilsoni (?Soudleyan), Dicrano. clingani (?Longvillian-Onnian).

Glenkiln Shales, maximum recorded complete succession 18.9 m ,
Middle Llandeilo-Caradoc (?Harnagian).

(2) Pyritous black shales, grey mudstones and some claystones,
7.2 m . Zones of Nemagr. gracilis (M.Llandeilo-Caradoc, Costonian)
and Climagr. peltifer (?Harnagian).

(1) Ashy sandstones and mudstones, 11.7 m .

(Bottom of succession)

TABLE 1-1 Stratigraphy of the Moffat Shales (after Weir 1973).

+ Barren mudstone thickness may be greater than 20 m.

| Sample | Observed height up cliff (metres) | Distance up succession after structural restoration (metres) | Sample | Observed height up cliff (metres) | Distance up succession after structural restoration (metres) |
|--------|-----------------------------------|--|--------|-----------------------------------|--|
| HG-1 | 35.0 | 0.80 | HCL-25 | 70.0 | 11.10 |
| HG-2 | 98.0 | 2.00 | HCL-26 | 70.5 | 11.60 |
| HG-3 | 15.0 | 2.50 | HCL-27 | 71.0 | 12.10 |
| HW-1 | 99.6 | 6.60 | HCL-28 | 70.8 | 12.12 |
| HW-2 | 23.0 | 5.60 | HCL-29 | 70.0 | 11.45 |
| HW-3 | 38.5 | 4.50 | HCL-30 | 71.0 | 12.50 |
| HW-4 | 24.8 | 7.40 | HCL-31 | 69.0 | 10.40 |
| HW-5 | 100.6 | 7.50 | HCL-32 | 25.4 | 10.15 |
| HCL-1 | 41.4 | 8.80 | HCL-33 | 42.75 | 12.10 |
| HCL-2 | 41.6 | 9.00 | HCL-34 | 27.3 | 10.35 |
| HCL-3 | 70.5 | 11.60 | HL-1 | 47.7 | 14.30 |
| HCL-4 | 27.0 | 9.80 | HL-2 | 49.5 | 14.30 |
| HCL-5 | 45.7 | 12.90 | HL-3 | 71.3 | 13.95 |
| HCL-6 | 68.5 | 9.60 | HL-4 | 5.3 | 17.25 |
| HCL-7 | 41.5 | 8.70 | HL-5 | 1.9 | 14.00 |
| HCL-8 | 42.0 | 9.20 | HL-6 | 5.3 | 17.35 |
| HCL-9 | 42.5 | 9.70 | HL-7 | 3.0 | 15.20 |
| HCL-10 | 43.0 | 10.20 | HL-8 | 2.0 | 14.60 |
| HCL-11 | 43.5 | 10.70 | HL-9 | 0.8 | 13.30 |
| HCL-12 | 44.0 | 11.20 | HL-10 | 15.9 | 13.30 |
| HCL-13 | 44.5 | 11.70 | HL-11 | 18.8 | 13.90 |
| HCL-14 | 45.0 | 12.20 | HL-12 | 55.0 | 17.50 |
| HCL-15 | 45.5 | 12.70 | HL-13 | 74.6 | 15.70 |
| HCL-16 | 66.0 | 8.60 | HL-14 | 78.1 | 14.60 |
| HCL-17 | 66.5 | 9.10 | HL-15 | 81.7 | 15.00 |
| HCL-18 | 67.0 | 9.60 | HL-16 | 88.5 | 15.50 |
| HCL-19 | 67.5 | 8.60 | HL-17 | 16.0 | 13.50 |
| HCL-20 | 68.0 | 9.10 | HIC-1 | 7.0 | 19.90 |
| HCL-21 | 68.5 | 9.60 | HIC-2 | 6.6 | 19.50 |
| HCL-22 | 69.0 | 10.10 | HC-3 | 8.6 | 21.50 |
| HCL-23 | 68.8 | 10.10 | HC-4 | 10.6 | 23.50 |
| HCL-24 | 69.5 | 10.60 | | | |

TABLE 1-2 Location of samples at Hartfell.

C H A P T E R I I

MINERALOGY

1. INTRODUCTION

In any geochemical study it is first necessary to have a prior knowledge of the mineralogy of the rocks being examined so that a realistic interpretation of the element associations may be derived from the analytical results. This chapter is included to provide the necessary mineralogical control for the chapters which follow.

2. METHOD

The identification of the component minerals of the shales, mudstones and cherts comprising the Moffat Shales was made from X-ray diffractograms run on a Philips PW 1012/20 diffractometer, using copper K α radiation generated by a current of 18 mA at 36 kV, an attenuation of 1×10^3 and a time-constant of 8. Each slide was scanned at 1° per minute over a two-theta range of $6-60^\circ$. These conditions gave adequate sensitivity to detect most components but not to differentiate feldspars and phyllosilicates where amounts were low. Such samples were re-run at an attenuation of 4×10^2 , damped by an increased time-constant of 16, and scanned at $\frac{1}{2}^\circ$ per minute. To aid the fast efficient identification of the minerals, the X-ray diffractions were overlaid by a series of computer drawn templates. These were computed and drawn to the same scale as the diffractograms for a series of the more common rock-forming minerals from data given for the d - spacings and relative intensities in the A.S.T.M. Powder Data File (1967). As an example, the template for chalcocite is illustrated in Fig.15.

3. DETAILS OF THE MINERALOGY

a) Component minerals

The sediments are composed mainly of quartz with subsidiary amounts of feldspar (plagioclase), mica (sericite), pyrite, chlorite and occasionally haematite. Strong plagioclase reflections corresponding to d - spacings of 6.37 \AA $[001]$, 4.02 \AA $[20\bar{1}]$, 3.85 \AA $[111]$, 3.66 \AA $[130 : 131]$ and 3.18 \AA $[002 : 040]$ have been recorded. These spacings match closely those quoted for low temperature albite (Brown 1961,p.480).

Out of a total of 130 samples analysed, only 6 gave indications of the presence of a carbonate mineral phase. These are samples ID-3, ID-4, ID-5, ID-6, 2E-6 and 2F-10 all of which were collected from Dobb's Linn. Samples ID-3 to ID-6 are grey mudstones from the D.anceps Zone while 2E-6 is a claystone from the M.convolutus Zone and 2F-10 is a greywacke from the M.sedgwickii Zone (Fig.16).

It was possible by using the quartz reflection at 2.46 \AA $[110]$ as an internal standard to assess accurately the d - spacing for the principal reflection from the carbonate mineral in each of the six samples. The calculated d - spacings approximate to 3.04 \AA (corresponding to the calcite $[104]$ at 29.43°) except only in sample 2F-10 in which a reflection at 29.56° corresponds to the dolomite $[104]$ peak at 2.95 \AA .

The observed reflections were all at slightly higher spacings than those published for the pure minerals, indicating the presence of iron within the carbonate. This was confirmed by staining thin sections of the samples with a 3:2 ratio mixture of alazarin red S and potassium ferricyanide in 1.5 per cent hydrochloric acid. When stained, sample 2F-10 assumed a patchy appearance. Some patches were mauve in colour whereas others were blue, indicating the presence of both ferroan calcite and

ferroan dolomite in the sample. The other five samples assumed a mauve coloration when stained, indicating the presence of ferroan calcite.

b) Layered minerals

Preliminary X-ray examination revealed the presence of a 7 Å layered mineral in most samples. The exact nature of this material was not immediately obvious, and therefore, a series of experiments was undertaken upon a sample displaying strong reflections in the region of 12.5° in order to identify each reflection occurring between 2 and 14 Å. The sample chosen was DCYP-3 which was collected from the M.cyphus Zone at Dobb's Linn.

After eliminating from the diffractogram those reflections attributable to quartz, there remained a series of unidentified peaks with d - spacings of between 2 and 14 Å. These are listed in Table 2-1. Three of the peaks correspond to spacings of 4.01 Å, 3.65 Å and 3.18 Å representing albite $[20\bar{1}]$, $[\bar{1}3\bar{1} : 1\bar{3}0]$ and $[002]$ reflections respectively. Peaks at 3.12 Å and 2.70 Å correspond to pyrite $[111]$ and $[200]$ reflections.

The remaining peaks are illustrated in Fig.17. The relatively strong peaks which occur at 3.52 Å and 7.01 Å and the weaker peaks at 4.70 Å and 13.86 Å are assigned to chlorite $[004]$, $[002]$, $[003]$ and $[001]$ reflections respectively. The dominance of the $[004]$ and $[002]$ reflections diagnosis the ferroan as opposed to the magnesium chlorite (Brindley, 1961 p.262).

The presence of expanding lattice chlorites and montmorillonite minerals may be ruled out, because after treatment with glycerol, the peaks exhibited no apparent change in d-spacing (Fig.17).

It is to be noted that the peaks corresponding to spacings of 3.52 Å and 7.01 Å, coincide with kaolinite reflections. Kaolinite,

however, has a diagnostic though weak reflection corresponding to 2.38 Å. If kaolinite is present only in small amounts the diagnostic reflection could be submerged by the background and its absence is not to be taken that chlorite alone is present (cf. Weir 1974).

Treatment in dilute acid dissolves chlorite whilst leaving kaolinite substantially unaffected to continue production of its strong reflections corresponding to spacings of 3.5 Å and 7.0 Å (Brindley 1961 p.264). Sample DCYP-3 was digested for 15 hours in 10 per cent hydrochloric acid at 80°C, washed until neutral to litmus paper and then dried for 4 hours at 100°. A diffractogram was then run at the more sensitive instrumental setting quoted above.

Acid treatment completely removed the reflections corresponding to 13.86 Å and 4.70 Å and considerably weakened those corresponding to 4.95 Å, 7.01 Å and 3.52 Å (Fig. 17). No change in intensity was observed for the other peaks. The former two are assigned to chlorite [001] and [003] while the latter two are assigned to chlorite [002] and [004]. The calculated d - spacings of 9.86 Å, 4.95 Å, 4.46 Å and 3.75 Å are assigned to sericite [002], [004], [110] and [023] reflections (A.S.T.M. Powder Data File 2-0056). The assignment of each peak in the range from 2 Å to 14 Å is given in Table 2-1.

Thermal treatment is also a valuable auxiliary technique for identifying chlorites positively. Chlorites tend when heated to dehydrate in three stages (Caillière and Hénin 1957). The first stage corresponds to loss of water from the brucite layers with only minor resultant changes in unit cell parameters. There is however, considerable rearrangement in structure. This is manifested by changes in X-ray reflection intensities. The second stage corresponds to loss of water from the talc layer. The third and final stage is recrystallisation to form new products notably

olivine $(\text{MgFe})_2 \text{SiO}_4$. The temperature of the dehydration reactions and the extent to which they are clearly separated depends on the composition, on the crystallinity and on the particle size of the chlorites as well as on the thermal conditions (Brindley 1961).

In general, chlorites which are low in iron and predominantly magnesian in character, dehydrate between 600° and 800°C , whereas the reaction of chlorites which are rich in iron take place at lower temperatures (Brindley and Youell 1953). Chlorites when heated to the dehydration temperature exhibit increased intensity of the $[001]$ reflections and decreased intensity of the $[002]$, $[003]$ and $[004]$ reflections. Iron rich chlorites show slightly greater shrinkage parallel to 'c' than magnesian chlorites (Martin 1955).

As with chlorite, the dehydration of muscovite also depends on the crystallinity of the material. Fine grained muscovite is reported to dehydrate at 750°C whereas coarse grained material dehydrates in the region of 900°C (Bradley and Grim 1961). The results of step-heating and continuous heating of fine grained muscovites indicate that water is released over three temperature intervals. These correspond to the release of superficial adsorbed water, the release of water in cracks and inclusions and the release of the water of constitution, (Zimmerman 1970). The first interval occurs between 100°C and 400°C , the second between 400°C and 700°C and the third in the region of 700°C . Associated with the release of water there is progressive dilation in the basal spacing. This commences at about 300°C (Reif 1966).

Portions of sample DCYP-3 were heated for 60 minutes at temperatures of 450° , 500° , 600° , 800° and 820°C and diffractograms of the roasted powder were run at the more sensitive settings given above. The results of the heating experiments are depicted in Fig.18.

This illustrates that with increasing temperature, up to a maximum of 600°C, there is a progressive increase in the intensity of the chlorite [001] peak relative to the other chlorite reflections. The change in intensity can readily be picked out by comparing the ratio of the intensity of the chlorite [001] reflection to the intensity of the chlorite [002] reflection. This ratio increases from 0.51 for the untreated sample to 0.80 for the sample heated at 450°C and then to 0.86 at 500°C before attaining a maximum value of 1.79 at 600°C.

The peaks which are present at 2.56 Å and 3.52 Å in the diffractograms of the sample heated at 800°C are attributable to sericite [202] and [114] reflections. It is noteworthy that the chlorite basal reflections re-appear in the sample which was heated at 820°C. An explanation is not immediately forthcoming but the re-appearance of the peaks may be related to disequilibrium within the resultant mineral assemblage.

The reflection intensities of sericite exhibit similar changes. At temperatures of 450°C and above, the sericite [110] reflection is the most intense. Increasing temperature decreases the intensity of the sericite [004] and [002] reflections. The peak attributable to a mixture of the sericite [202] and the chlorite [132 : 201] reflections is not evident in the sample heated to 820°C. Associated with the variation in peak intensities the sericite basal spacings increase with increasing temperature. This may be illustrated by examining the sericite [002] reflection which occurs at 9.86 Å in the untreated sample and at 9.90 Å in the sample heated at 600°C.

The above experiments were repeated on samples collected from the P.linearis Zone at Hartfell, the D.clingani Zone at Dobb's Linn, and the A.acuminatus Zone at Dobb's Linn. In each case, results similar to

those outlined have been obtained. It is therefore concluded that both sericite and an iron-rich chlorite, possibly clinochlore, contribute along with quartz, albite and pyrite to the mineralogy of the Moffat Shales.

c) Interpretation

The observed mineral assemblage of quartz-albite-sericite-chlorite is characteristic of the low-temperature zone of the greenschist facies (Winkler 1967). This facies, occurring at the boundary between diagenesis and metamorphism, is related to temperatures of 300°C and is almost independent of pressure. Such a temperature can be attained in burial metamorphism at normal geothermal gradients (30°C/km) at depths of 10 km. It is likely however that since the Moffat Shales have been subjected to large scale orogenesis there has been additional thermal energy produced so that the critical transitional temperature which delineates diagenesis from metamorphism must surely have occurred at much shallower depths.

4. QUANTITATIVE MINERALOGICAL ANALYSIS

a) Introduction

It is essential in any geochemical study of sedimentary rock sequences that a reliable quantitative assessment of mineral composition is available. Estimation of the quantitative mineralogical composition of sediments, particularly those of fine grain size, is extremely difficult. Three main techniques are available:

- (1) Conventional modal analysis using a petrographic microscope and an integrating stage.

(2) Recalculation of chemical analysis into mineralogical composition as suggested by Nicholls (1962) and by Miesch (1962).

(3) Quantitative X-ray diffractometry.

Petrographic modal analysis involves spot counting of mineral grains and has long been applied to igneous rocks with a high degree of success. The technique although of great use in some sedimentary studies, could not be applied in this work due to the very fine nature of the sediments which comprise the Moffat Shales.

The second technique requires a knowledge of the qualitative mineralogy. This may be determined by X-ray diffraction. The technique is only of limited use since it is no longer possible to correlate mineralogy and major element chemistry because the two are not independent variables.

Modal analysis of igneous rocks by X-ray diffraction methods has been described by Bristol (1968) and Otalora and Hess (1969). X-ray diffractometry has been employed in a quantitative investigation of bauxite (Black 1953), in studies of modern sediments (Smaltz and Zen 1959) and in studies of Cretaceous shales (Mitchell 1960). More recently, Kaye et al. (1968) have assessed the relative merits of quantitative X-ray diffraction analysis and optical modal analysis of sedimentary rocks. It was concluded that X-ray diffraction produced the more reliable mineral abundance data.

The purpose of this study was to develop an X-ray diffraction method to assess quantitatively the mineralogical composition of the Moffat Shales.

b) Theory of quantitative analysis by X-ray diffraction

In general terms, the estimation by X-ray diffraction of the relative quantities of mineral phases in rocks is based on the relationship between peak intensities and the absorptive properties of the minerals. This subject is treated in detail by Nuffield (1966).

The intensity of diffraction from a mineral is a function of its concentration in a mixture. Correlation of the peak intensities with mineral concentration depends largely on the accuracy with which peak intensities can be reproduced. The factors controlling this are instrumental and sample preparation techniques. Particular care must be taken to ensure constant particle size because crystallite size greatly influences peak intensity (Weiskirchner 1960).

Theoretically the peak intensity can be expressed by the equation:-

$$I_1 = \frac{K_1 x_1}{\left[p_1 x_1 (u_1^* - u_m^*) + u_m^* \right]}$$

Where I_1 is the peak intensity of component 1, p_1 is the density of the component, x_1 is its weight fraction, and u_1^* its corresponding absorption coefficient. u_m^* is the mass absorption of the matrix and K_1 is a constant which depends upon the nature of component 1 and the geometry of the apparatus. This formula, given by Klug and Alexander (1954), shows that for mineral assemblages with similar absorption coefficients, $u_1^* = u_m^*$, peak heights change linearly with concentration. If, however, u_1^* does not equal u_m^* , the intensity-concentration curve is no longer linear.

c) Method of grinding

Since peak intensity depends on crystallite size (Weiskirchner 1960) it is important to use a grinding technique that will ensure adequate reproducibility of peak intensities in replicate specimens. A standard grinding procedure was accordingly adopted. Samples were crushed in a ball-mill until the powder passed freely through a 200 mesh sieve. The time taken was of the order of 10-15 minutes, and the error involved in reproducing relative peak intensities was in the region of 10 per cent.

d) Preparation of calibration curves

Calibration curves were constructed firstly, by preparing a series of two-component mineral mixtures. These consisted of different proportions of chlorite (var.clinochlore), pyrite, albite, muscovite and graphite in a quartz matrix. Each mineral mixture was homogenised in a ball-blender and then 4 glass slides were prepared for analysis by X-ray diffraction.

In order to have useful calibration charts the minimum detectable limit (MDL) of a mineral should be as low as possible. This limit is defined here as the peak-to-background ratio which satisfactorily establishes the presence of the mineral in a diffraction pattern. The lowest MDL values are obtained by utilising the strongest mineral reflections. This is however not always possible because other rock-forming mineral reflections may interfere with the strongest peak. In this case less intense reflections which are not overlapped must be employed regardless of the resulting reduction in the MDL for the mineral.

Each point plotted on the calibration curves illustrated in Fig. 19 represents the average results for four glass-slide mounts. In each case the abscissa is the weight per cent of the mineral relative to quartz. Having determined the most appropriate peaks to be measured, (Table 2-2), the height of the selected peak is measured above a straight line through the average background in the vicinity of the peak. The ordinate is expressed as $\text{ht.mineral}/(\text{ht.mineral} + \text{ht.quartz}) \times 10^2$ where ht.mineral is the height of the selected peak for the mineral and ht.quartz is the height of the selected quartz peak. Because only peak height ratios are required in this technique, diffractometer parameters may be varied to facilitate measurement of peak heights.

The curves which are drawn through the calibration points plotted in Fig. 19 are a result of 'least-squares' polynomial regression analysis. The equations of the curves, which are all significant at the 99.9 per cent confidence level, are given in Table 2-5.

e) Procedure

For routine rock analysis, a reconnaissance X-ray run to determine the minerals present was made at a speed of 1° two-theta per minute. Having identified the peaks produced and made sure that no other mineral was interfering with the peaks chosen for measurement a slow scan was run at $1/4^\circ$ two-theta per minute over the interval to be measured. The ratio of the height of the mineral peak to the height of the mineral peak plus the height of the quartz peak was calculated, and the amount of mineral present in the sample relative to the amount of quartz derived from the appropriate calibration curve. The assumption was made in this study that the samples are totally composed of quartz,

sericite or illite, chlorite, pyrite and albite and the final modal analysis was expressed as a percentage of the total mineral content.

It was not possible to calculate the amount of graphite within the samples due to the variation in the degree of structural ordering within this mineral.

f) Stratigraphic variation

Modal analysis by X-ray diffraction was conducted on 119 samples collected from the Moffat Shales which outcrop in the vicinity of Moffat. The total sample suite is composed of 43 samples from Dobb's Linn, 60 samples from Hartfell and the remaining 16 from Mountbenger, Carrifran Burn and Glenkiln (Fig.4). Mineral content of the samples is given in Appendix E and mean values for the localities are summarised in Table 2-3. Summary statistics illustrating the variation in mineral contents at Hartfell and Dobb's Linn are presented in Table 2-4.

The mineral distributions over all 14 graptolite zones in the stratigraphic succession are displayed in Figs. 20-23. The divisions of ordinate of each plot have been made proportional to the zone thickness at the type section of Dobb's Linn using the data of Toghill (1968, 1970a). There is an apparent increase up the succession in the amounts of albite, chlorite and sericite and an overall decrease in the amount of quartz. The stratigraphic distribution of pyrite is more complex with a noticeable maximum at the base of the Upper Birkhill Shales.

In order to clarify and to simplify the relationship of the amount of a particular mineral with respect to the position in the stratigraphic succession, polynomial regression curves have been calculated over all zones for each of the five minerals. The method

employed was the progressive fit of higher order polynomials, starting at the first order, until no improvement in the sums of squares resulted between one order and the next. If the F-value for the lower of the two curves was greater than that tabulated for the given degrees of freedom at the 0.99 confidence level, the regression was considered significant and the curves superimposed on the scatter plots. All five minerals yielded significant curves (Table 2-6) and the vertical profiles are considered to represent time dependence of the abundance of those minerals.

The polynomial regression curves which have been computed (Figs 20-23) indicate the following changes with respect to time:-
Albite (Fig.21)

The amount of albite falls from 2.95 per cent in the Glenkiln Shales to 2.56 per cent in the wilsoni Zone. There is then a gradual increase in the amount present until a value of 6.60 per cent is obtained at the top of the persculptus Zone. There is a slight increase in amount from the top of the persculptus Zone to a value of 8.03 per cent in the convolutus Zone. Thereafter, there is a sharp increase so that by the maximus Zone there is a 13.51 per cent albite present.
Chlorite (Fig.21)

There is little change in the amount of chlorite present in the Moffat Shales between Glenkiln Shales and the base of the linearis Zone. The amount then increases from 3.57 per cent in the linearis Zone to 4.45 per cent at the base of the vesiculosus Zone. There follows a period in which the amount of chlorite present does not appreciably change. This period ends mid-way through the convolutus Zone from which time the amount present increases from 4.45 per cent to reach a maximum of 8.11 per cent in the maximus Zone.

Sericite (Fig.22)

The amount of sericite present within the sediments drops from 9.48 per cent in the Glenkiln Shales to 8.61 per cent in the wilsoni Zone. Thereafter there is a pronounced increase, with the amount present equalling 16.12 per cent in the vesiculosus Zone. There is no variation in the amount present between the vesiculosus and convolutus Zones but there is an increase in the amount present between the top of the convolutus Zone and the maximus Zone. A maximum sericite content of 19.05 per cent is computed for the maximus Zone.

Pyrite (Fig.22)

The computed stratigraphic profile for pyrite is the most complex of all examined. The amount of pyrite present increases from 5.69 per cent in the Glenkiln Shales to 7.33 per cent at the top of the wilsoni Zone. The amount present then decreases in the Barren Mudstones where a value of 4.82 per cent is computed. Thereafter, the amount of pyrite present increases rapidly to reach a maximum of 25.12 per cent at the top of the cyphus Zone. There is then a sharp drop into the sedgwickii Zone which only contains 2.67 per cent of pyrite.

Quartz (Fig.23)

The general variation in the amount of quartz present with time is the inverse of that described for the other four minerals. After a brief period between the Glenkiln Shales and the wilsoni Zone in which the amount of quartz rises from 78.1 per cent to 80.7 per cent there is a pronounced decrease in the amount present between the clingani and the gregarius Zones. A minimum quartz content of 53.66 per cent is computed for the gregarius Zone. Thereafter the amount of quartz present increases to reach a computed value of 65.83 per cent in the maximus Zone.

g) Discussion

Weir (1973) has proposed that two major sedimentary cycles may be recognised within the Moffat Shales on the basis of lithological differences. The ideal cycle commences in a strongly reducing euxinic facies characterised by sulphide-rich, fissile black shales with interbedded radiolarites, progressing upwards through platy, sulphide bearing shales and cherts, blocky and massively bedded black and dark grey mudstones to a climax in well oxidised brown mudstones with trilobites. The first cycle spans the Caradoc and Ashgill Series, and the second encompasses most of the Llandovery Series. Weir (ibid) relates the development of the cycles to a progressive increase in current activity.

On the basis of the modal mineral analyses presented in this work it is only the stratigraphic variation of pyrite which may even loosely be termed cyclical. The repetition is of the ~~sample~~ ABABAB type where A is a point of flexure at the low pyrite end in the stratigraphic profile and B is a point of flexure at the high pyrite end in the profile (Fig.24). This type of repetition may be termed rhythmic (Duff et al., 1967).

The observed maxima which occur in the wilsoni and gregarius Zones are interpreted as being related in part to the availability of sulphur and iron within the unconsolidated sediments. The presence of pyrite is indicative of a reducing environment and at least some of the pyrite present within the sediments may be attributed to the fixation of iron with reduced sulphur derived from bacterial activity. Sulphate reduction can be readily effected by a specialist group of bacteria known as the sulphate reducing bacteria. The most important species in the group belong to the genera Desulfovibrio and Desulfotomaculum (Wedepohle 1974). Sulphate-reducing bacteria are all obligate anaerobes

although they may live in a dormant state for long periods in aerobic environments. The result of their metabolism is the release of large quantities of sulphide into the environment. ($S^{2-} \rightleftharpoons HS^- \rightleftharpoons H_2S$). The H_2S produced when in the presence of dissolved iron-hydroxides is transferred into black hydro-troilite ($FeS \cdot nH_2O$) which after a short time stabilises to form pyrite (Love 1964).

Anticipating the chemical results, it is pertinent to note that whereas the stratigraphic profiles of pyrite and of sulphur peak within the C.wilsoni and M.gregarius Zones (Figs 22,57) that of carbon (Fig.57) peaks at slightly higher stratigraphic levels i.e. within the D.clingani and M.convolutus Zones. Furthermore, whereas the profile for carbon displays an overall reduction in carbon through the sequence, that for iron (Fig.49) and to a lesser extent those of sulphur and pyrite indicate increases through the succession. Such observations may imply (assuming reasonable statistical fluctuations in the positions of the peak maxima) that local concentrations of pyrite are related to the quantity of organic matter and to the relative proportions of iron and sulphur in the sediments. The less carbonaceous nature of the sediments towards the top of the succession coupled with the presence of large quantities of pyrite is taken to imply the introduction of epigenetic pyrite into the sediments. Volcanic exhalation could have been the source.

The stratigraphic profiles for the variation of albite, chlorite and sericite are not strictly cyclical but nevertheless indicate a progressive increase in the amount of mineral present with time. Superimposed upon the overall increase, are periods in which the rates of change of mineral content vary. Thus, the variation with time may be expressed in the form of an ABCDE sequence where the

arbitrary parameters A,B,C,D and E are again situated at the points of flexure in the vertical profile curves (Fig.24). The rate of change in the amount of mineral present between A and B is slow, between B and C is fast, between C and D is slow and between D and E is fast. This is again a rhythmic sequence and is interpreted as being related to the overall rate of sedimentation.

The rate of deposition is therefore slow between the Glenkiln Shales and the wilsoni Zone, becomes more rapid and reaches a climax towards the base of the Lower Birkhill Shales where there is mineralogical evidence for the presence of a carbonate phase (Section 3a) and palaeontological evidence for the presence of blind trilobites (Weir 1973). There is then a drop in the rate of sedimentation which remains slow until the Upper Birkhill Shales where it again increases. This time-sequence for the variation in the rate of deposition within the Moffat Shales accords well with that proposed by Weir (1973) who described the occurrence of cyclical climaxes around the Purgillian/Cautleyan boundary and high in the Fronian.

Although the rate of deposition appears to increase with time, and the fissile-shale lithology is replaced by first platy-shale and blocky mudstone phases, grain size does not increase to a degree commensurate with the thickness increase. It has been concluded, (Weir, *ibid*), that neither a marked increase in subsidence rate nor a pronounced change in depth of deposition is likely to have occurred (the dominance of planar bedding within the strata denotes deposition below wave base at all times). Progressive modification of the pattern of oceanic circulation is the most probable cause of this change. Thicker deposition would be expected in areas on which major oceanic currents have effected sedimentation and more typical pelagic deposition

expected in areas devoid of strong currents. Fine grained, fissile shales and radiolarites would form in these latter areas.

These current variations may be considered in a broader context and related to the initiation of a period of uplift which began in Ireland during the Arenig (Dewey 1963, 1971) and spread to the Southern Uplands in the early Caradoc (Weir 1975). The diachronism of this uplift lengthwise to the geosyncline was demonstrated within Connemara by Stanton (1960). There is a corresponding west-east diachronism in the appearance of the Barren Mudstone facies though this does not appear until later. The facies was fully established by about wilsoni times in the Broadford Mountains (Weir 1973) but transgression was delayed longest in the Southern Uplands. Sedimentation within the South Mayo trough was probably completed by the Upper Llandeilo (Williams et al., 1972) and followed by a period of uplift equated with the Taconic phase (Dewey 1963). This uplift coincides broadly with the climax of the first mineralogical rhythm and the first lithological cycle.

The climax of the Silurian part of the rhythmic sequence is less clearly defined due partly to overtaking of the evolution of the mudstone cycle by the transgression of the Gala facies. Regional uplift may however have been an important controlling mechanism in the development of the mineral rhythms. Transgression of the shales by the succeeding flysch facies is again diachronous and is delayed longest in the vicinity of the Ettrick Valley Thrust (Toghill 1970b ; Fyfe and Weir 1976).

5. CURRENT DIRECTIONS AS DEDUCED FROM GRAPTOLITE STIPE ORIENTATIONS

a) Introduction

If the controlling mechanism in the development of the rhythmic sequence is the modification of oceanic circulation caused by emergent landmasses, confirmation should be gained by detailed analysis of current circulation. The only such study to date was conducted by the present author as part of earlier work (Watson 1971). That study was concerned with the orientation of graptolite stipes within the Hartfell Shales. No enlargement on the previous study is presented here, but in the interests of completeness a brief account of the methods employed and of the results found, follows.

b) Method of analysis

Orientated blocks were collected from the wilsoni, clingani and linearis Zones at Hartfell and the direction of the long axes of graptolite stipes, present within the plane of the bedding, was measured. The most abundant graptolite within the wilsoni and clingani Zones is Corynoides calycularis (Nicholson). The stipes are about 1 cm long in contrast to the 5 cm long stipes observed for specimens of Orthograptus truncatus (Lapworth) which are prevalent in the linearis Zone. A histogram illustrating the distribution of stipe orientations is given in Fig. 25.

A statistical test based on chi-square and vector summations was then applied to each distribution to test the hypothesis of random orientation (Rusnack 1957). Values of chi-squared for the three zones were well within the 90 per cent confidence limit and the hypothesis was rejected. The mean direction of current flow was then computed

from the method of Rusnack (ibid). Two assumptions were made. These were that the graptolite stipes were aligned parallel to current flow and that the distal ends of Corynoides, being larger than the proximal, were preferentially aligned up current as in the 'tear-drop' effect (Dapples and Rominger 1945).

It was concluded that the oceanic currents flowed at Hartfell from the north-east to the south-west during deposition of the wilsoni and linearis Zones and from the east-north-east during deposition of the clingani Zone.

c) Interpretation and future work

The current directions found by the above method coincide with the alignment of the axial rise in Caradocian times (Walton 1965). During upper Ordovician times it is believed that the northern margin of the Southern Uplands trough lay in the Girvan area and followed a north-easterly trend. The main provenance lay to the north-west. This explains in part, the slow rate of sedimentation in the lower part of the sequence.

Current directions from only the lower part of the lower rhythmic sequence have been measured. Lack of suitable material precludes extension of the study into the higher Hartfell and Birkhill Shales though intraformational conglomerates (Weir 1973) and other sedimentary structures might yield pertinent data.

6. VARIATION IN MUSCOVITE BASAL-SPACING

a) Introduction

The discovery that paragonite is a common rock-forming mineral in highly aluminous pelitic schists of low to medium grades

of metamorphism prompted investigation into the composition of co-existent muscovite and paragonite (Eugster and Yoder 1955; Rosenfeld et al., 1958). The latter authors observed that the basal spacings show progressive changes according to the grade of metamorphism. For rocks with both micas present, the lowest paragonite spacings (and correspondingly the highest muscovite spacings) occur in rocks which are in the biotite or even the chlorite zone of metamorphism. With prograde metamorphism the spacings for muscovite and paragonite converge as the metamorphism passes through the biotite, the almandine, the staurolite and finally into the kyanite zone.

Arising from the work of Rosenfeld et al., (1958) it has been demonstrated that the spacings of either white mica, in single mica rocks, may be used to monitor the minimum metamorphic grade of these rocks (Zen and Albee 1964). The linear regression curve proposed by Zen and Albee (ibid) for the variation of basal spacings for the binary two-phase system containing muscovite and paragonite predicts basal spacings of 10.03 Å and 9.607 Å for end-member muscovite and paragonite respectively.

The object of this present study was to investigate the variation in basal spacings of muscovite within the Moffat Shales in an attempt to define more accurately the grade of metamorphism to which the sediments have been subjected.

b) Experimental method

There was no indication of the presence of paragonite in preliminary X-ray diffraction scans, therefore only values for the basal spacing of muscovite were measured. Measurements were taken

from diffractograms which were run on a Philips PW 1012/20 diffractometer using copper K α radiation generated by a current of 18 mA at 36 kV, an attenuation of 4×10^2 and a time constant of 16. The slides were scanned at $\frac{1}{2}^\circ$ two-theta per minute over a range of 6° to 40° . The quartz [110] reflection was used as an internal standard.

c) Results

Measurements were taken from the same suite of samples as that analysed for modal mineral composition. Basal spacings for the muscovite reflections are given in Appendix E. The average values at each of the main localities are given in Table 2-3 and summary statistics illustrating the variation about the mean value are presented in Table 2-4.

The vertical profile for the stratigraphic variation of the muscovite basal-spacing was computed in the same way as before. The profile is illustrated in Fig. 56. Analysis of variance for the computed curve, which is significant at the 97.5 per cent confidence level, is presented in Table 2-6. The profile indicates that the spacing decreases from 10.12 Å in Glenkiln Shales to 10.036 Å in the wilsoni Zone. Thereafter, there is a gradual decrease in values until the cyphus Zone for which a spacing of 9.98 is computed. There is then an apparent reversal in the trend and values reach 10.12 Å again in the sedgwickii Zone.

d) Discussion

In soils and unmetamorphosed rocks, paragonite is rare, although muscovite (illite) is nearly ubiquitous. Although there

have been reports of the presence of paragonite in kaolinite soils (Cook and Rich 1962) and in shales (Bannister 1943), the general rule is that the lowest grade rocks which bear paragonite are chloritoid-bearing phyllites of the biotite zone.

Paragonite becomes unstable at a lower temperature than does muscovite under comparable conditions (Eugster and Yoder 1954). The mineral is not observed in zones higher than the kyanite zone and it has been concluded, Zen and Albee (1964), that rocks in the almandine and low kyanite zones of metamorphism are the most likely hosts to paragonite.

If it is assumed that the chemistry of the Moffat Shales is conducive to the formation of paragonite then its absence may be taken to imply that the sediments are either in the chlorite grade or in a zone higher than the kyanite grade of metamorphism. This latter implication can obviously be immediately discounted since the observed mineral assemblage indicates a greenschist facies. Further evidence for the sediments having undergone only mild regional metamorphism is afforded by the mean basal-spacing for muscovite in the total sample suite. The mean value of 10.02 \AA is close to the value of 10.034 \AA which has been assigned to end-member muscovite (Zen and Albee 1964).

The stratigraphic variation about the mean basal-spacing value may be attributed to the variation of Na^+ within the sediments. If the chemical results of the next chapter are anticipated it may be observed that there is a noticeable increase in the sodium content of the Upper Birkhill Shales relative to the Glenkiln Shales (Fig.51). Mean sodium values are also greater at Dobb's Linn than

at Hartfell (Table 3-3). Both observations are consistent with the inverse relationship reported for the variation of muscovite basal-spacing with the amount of sodium in the lattice. (Zen and Albee 1964). It would therefore appear that there is within the Moffat Shales, a limited amount of ionic substitution of sodium for potassium at the muscovite end of the muscovite-paragonite solid solution series.

| I ₁₀₀ | Two-theta degrees | d-spacing Å | Peakshape | Mineral | h k l |
|------------------|----------------------|----------------|--------------|----------|---------------|
| 19 | 6.38 | 13.86 | sharp | chlorite | [001] |
| 44 | 8.97 | 9.86 | fairly sharp | sericite | [002] |
| 37 | 12.62 | 7.01 | fairly sharp | chlorite | [002] |
| 18 | 17.93 | 4.95 | broad | sericite | [004] |
| 16 | 18.88 | 4.70 | broad | chlorite | [003] |
| 8 | 19.23 | 4.62 | sharp | chlorite | [020] |
| 43 | 19.93 | 4.46 | broad | sericite | [110] |
| 29 | 22.18 | 4.01 | sharp | albite | [201] |
| 17 | 23.75 | 3.75 | broad | sericite | [023] |
| 19 | 24.37 | 3.65 | sharp | albite | [131̄ : 130̄] |
| 23 | 25.31 | 3.52 | very broad | chlorite | [004] |
| | | | | sericite | [114] |
| 67 | 28.06 | 3.12 | broad | pyrite | [111] |
| 38 | 28.63 | 3.18 | sharp | albite | [002] |
| 14 | 31.39 | 2.85 | sharp | chlorite | [005] |
| | | | | sericite | [115] |
| 100 | 33.15 | 2.70 | sharp | pyrite | [200] |
| 53 | 35.01 | 2.56 | very broad | chlorite | [132̄ : 201̄] |
| | | | | sericite | [202] |

TABLE 2-1 Assignment of mineral reflections to X-ray diffractogram peaks occurring between 2 Å and 14 Å in sample DCYP-3 (quartz reflections neglected).

| Mineral | Two-theta | d-spacing | hkl |
|-----------|-----------|-----------|---------|
| chlorite | 12.50° | 7.08Å | [002] |
| pyrite | 33.04° | 2.71Å | [200] |
| albite | 28.02° | 3.18Å | [002] |
| muscovite | 45.33° | 2.00Å | [00.10] |
| graphite | 54.79° | 1.68Å | [100] |
| quartz | 36.70° | 2.45Å | [110] |

TABLE 2-2 Peak positions employed in modal analysis by X-ray diffraction.

| | Total | Dobb's Linn | Hartfell | Other localities |
|-----------------------------------|-------|-------------|----------|------------------|
| number of samples | 119 | 43 | 60 | 16 |
| albite % | 4.20 | 6.88 | 2.37 | 3.86 |
| chlorite % | 4.22 | 4.44 | 3.54 | 3.10 |
| sericite % | 12.60 | 15.10 | 9.43 | 8.90 |
| pyrite % | 8.40 | 12.39 | 5.36 | 9.11 |
| quartz % | 72.20 | 61.18 | 79.34 | 75.03 |
| muscovite spacing \AA | 10.02 | 10.01 | 10.04 | 9.98 |

TABLE 2-3

Summary of mean mineral contents in the Moffat Shales. (Calculated values have a relative error of 3% for chlorite and pyrite determinations and 5% for albite, sericite and quartz determinations. Muscovite basal-spacing values are quoted with an absolute error of 0.005 \AA).

DOBB'S LINN

| mineral | minimum | maximum | mean | std. dev. | no. of samples |
|---------------|---------|---------|-------|-----------|----------------|
| d-muscovite Å | 9.83 | 10.19 | 10.01 | 0.08 | 43 |
| albite % | 0.13 | 23.67 | 6.88 | 4.09 | 43 |
| chlorite % | 0.79 | 9.05 | 4.44 | 1.58 | 43 |
| sericite % | 6.27 | 22.91 | 15.10 | 3.85 | 43 |
| pyrite % | 4.05 | 29.89 | 12.39 | 7.58 | 43 |
| quartz % | 44.20 | 85.58 | 61.18 | 9.75 | 43 |

HARTFELL

| mineral | minimum | maximum | mean | std. dev. | no. of samples |
|---------------|---------|---------|-------|-----------|----------------|
| d-muscovite Å | 9.88 | 10.58 | 10.04 | 0.09 | 60 |
| albite % | 0.0 | 8.92 | 2.37 | 1.83 | 60 |
| chlorite % | 1.58 | 5.39 | 3.54 | 0.94 | 60 |
| sericite % | 1.96 | 24.60 | 9.43 | 3.90 | 60 |
| pyrite % | 1.82 | 24.00 | 5.36 | 2.68 | 60 |
| quartz % | 46.18 | 88.25 | 79.34 | 6.69 | 60 |

TABLE 2-4

Summary statistics for the minerals analysed by X-ray diffraction from the Moffat Shales at Dobb's Linn and Hartfell.

| Mineral | Intercept | Regr. coeff-1 | Regr. coeff-2 | Regr. coeff-3 | F-value |
|-----------|----------------|----------------|----------------|---------------|---------|
| chlorite | -0.1024109E 01 | 0.7148733E 00 | -0.2273371E-01 | 0.2598944E-03 | 1303.9 |
| pyrite | 0.4995987E 01 | 0.1430253E 00 | 0.8033186E-02 | - | 350.2 |
| albite | -0.8309479E 01 | 0.9358759E 00 | -0.2489454E-01 | 0.2809551E-01 | 68.9 |
| muscovite | -0.3570747E-01 | 0.1088352E 01 | -0.7771153E-03 | - | 7048.2 |
| graphite | 0.4002960E 01 | -0.3113171E 00 | 0.1162571E-01 | - | 314.0 |

TABLE 2-5

Regression parameters for the variation of X-ray diffraction peak-intensity ratios for mixtures of quartz with various minerals.

| Variable | N | Order of chosen polynomial | DEGREES OF FREEDOM | | F-value |
|-------------|-----|----------------------------------|----------------------|----------------------------------|--------------------|
| | | | Due to regression | Deviation about regression | |
| d-muscovite | 118 | 5 | 5 | 112 | 2.83 |
| albite | 119 | 4 | 4 | 114 | 20.80 ⁺ |
| chlorite | 119 | 4 | 4 | 114 | 13.62 ⁺ |
| sericite | 119 | 4 | 4 | 114 | 15.69 ⁺ |
| pyrite | 119 | 5 | 5 | 113 | 30.73 ⁺ |
| quartz | 119 | 4 | 4 | 114 | 38.17 ⁺ |

TABLE 2-6 Analysis of variance for polynomial curves fitted to the stratigraphic variation of mineral contents and the variation of the muscovite basal spacing.

+ = significant at the 99.9% confidence level.

CHAPTER III

INORGANIC CHEMISTRY

1. INTRODUCTION AND OBJECTIVES

The 100 m thick Moffat Shale sequence (Fig.3) is a group of black marine shales, cherts and mudstones which are noteworthy for their abundant and varied graptolites by which they are conveniently zoned. It was thought that a chemical investigation of this condensed marine succession might be useful in three ways; firstly, to investigate whether studies of element associations might elucidate environments in which these sediments accumulated, and also any gradational or other changes in depositional environment. Secondly, to test whether chemical abundance patterns at the type localities could be used to predict the stratigraphic position of samples in other sequences where the faunal control is poor or even absent. Thirdly, to ascertain whether the black "shales" would provide an adequate source of base metals for the mineralization of the region.

2. PREVIOUS RESEARCH

A considerable body of chemical data has been accumulated on black shales much of which is collected in the bibliography of Tourtelot (1970). Most of these studies are orientated towards minor element abundances and enrichments, and the review of Vine and Tourtelot (1970) is valuable in this respect. A rather different approach was taken by Spencer (1966) in using factor analysis to identify the controls over element distributions in a Silurian graptolite band. Hirst and Kaye (1971) used the same

technique on analyses from an Upper Viséan sequence of argillaceous and arenaceous rocks. They recognised controls in the form of pH, and processes such as rate of deposition and diagenesis in their factors. Cosgrove (1973) also applied factor analysis in a study of red beds in S.W.England and recognised in his factors both mineral controls such as clay, quartz, feldspars and calcite, and chemical controls such as Eh.

Factor analysis has also been used in the study of recent sediments to examine the controls of continental margin sedimentation (Summerhayes 1972). A study of element combinations and ratios was however preferred for an investigation of pelagic sediments (Boström et al., 1972, 1973).

Using some of the techniques just described, the present study sets out to examine element associations and distributions through the Moffat Shale sequence which spans much of the Upper Ordovician and the Lower Silurian.

3. SAMPLE COLLECTION AND ANALYTICAL TECHNIQUES

Samples were collected from most of the main inliers in the vicinity of Moffat (Fig.4) and from the inliers exposed in Wigtownshire (Fig.26). Where the fauna permitted accurate zoning an attempt was made to retrieve a representative sample for analysis. At many horizons no fossils were present or the material had been considerably weathered. This led to selectivity in the sampling procedure which resulted in the preferential sampling of certain horizons, especially the P.linearis and D.clingani Zones. This selectivity is considered an inevitable consequence of the nature of

the problem and the nature of the material but it should not invalidate the final conclusions.

Of the inliers sampled, those at Dobb's Linn, Hartfell, Glenkiln, Carrifran Burn and Mountbenger yielded samples suitable for accurate zonal classification. An attempt was made to locate accurately each sample within its zone by measuring the height from the base of the zone. The graptolite zones are defined according to the terminology of Williams et al., (1972) for the Ordovician and Cocks et al., (1971) for the Silurian.

A total of 159 bulk rock samples were retrieved in the vicinity of Moffat and 27 samples collected from inliers exposed in Wigtownshire. Of the Moffat suite, 29 samples were collected by W.E.Stephens and J.A.Weir, 2 by T.B.Fyfe and the remainder by the present author. All the Wigtownshire samples, designated the LB-series, were collected by the author (Appendix E).

Those samples collected by W.E.Stephens and J.A.Weir were analysed by X-ray fluorescence techniques for both major and trace elements. Major elements were determined at Exeter University using a fusion method based on that of Norrish and Hutton (1969). Minor elements were determined at St. Andrews University on pressed powder discs. Sulphur determinations were made according to the technique of Schapiro (1973).

Major elements were determined on the remaining samples by a rapid, wet chemical technique which employs fusion and acid digestion. Details of the techniques used are given in Appendix B.

Although all the LB-series of samples was analysed for 16 elements, not all the samples collected in the vicinity of Moffat

were similarly treated. Some were analysed for 16 elements plus sulphur, some for 16 elements, some for only Si, Al, Mg and the trace elements, and others for the 7 trace elements only. Details are given in Table 3-1.

4. SUMMARY STATISTICS AND ELEMENT FREQUENCY DISTRIBUTIONS

Analytical results for the complete data set are presented in Appendix E. Table 3-2 is a list of the mean, standard deviation and range of each of the chemical elements. All values for Si, Ti, Al, Fe, Mn, Mg, Ca, Na, K, loss-on-ignition, C and S are quoted in per cent, the remainder are quoted as ppm. Fe is quoted as the Fe³⁺ cation. Mean values for the elements present in the inliers exposed at Hartfell, Dobb's Linn and in Wigtownshire are compared in Table 3-3.

The mean values for the Moffat Shales, collected in the vicinity of Moffat, when plotted (Fig.27) and compared with the 95th percentile ranges and enrichment values which are given by Vine and Tourtelot (1970) for various North American Shales, indicate that they are 'normal' or slightly depleted in most elements relative to the American Shales. This is partly attributable to the sample set being biased towards comparatively fresh mudstones and cherts by the selectivity of the sampling procedure.

Histograms for the element frequency distributions (Figs. 28-29) were prepared using a class interval of one-half of the standard deviation as suggested by Chayes (1954). The frequency distribution of the trace elements in the Moffat Shales seems in

general to be positively skewed which is a common feature of the trace-element distributions in most rocks (Ahrens 1954, 1957).

In many cases in the literature, the assumption of a lognormal distribution is made when a histogram appears to be positively skewed. This assumption was tested by means of the KOLMOGOROV-SMIRNOV test which is concerned with the degree of agreement between the distribution of a set of sample values and some theoretical distribution (Siegel 1956). Both lognormal and normal distributions have been tested for at the 0.95 confidence level. It was found that no element satisfied the probability requirements for rejection of the null hypothesis that the sample set was not drawn from a normal or lognormal distribution. The application of the KOLMOGOROV-SMIRNOV test in this case demonstrates that the assumption of a lognormal distribution when a histogram appears to be positively skewed is not always valid.

In summary, the Moffat Shales suite shows no unusual chemical abundances and as a suite conforms neither to normal nor lognormal distributions. No assumptions regarding the population distribution can therefore be made. This latter fact has a bearing on later applications of multivariate statistical techniques.

5. THE AREAL DISTRIBUTION OF ELEMENT OXIDES AND TRACE ELEMENTS

a) Introduction

Representative samples from each of the major inliers in the vicinity of Moffat have been grouped together to form the Moffat Grid series of samples (Fig.4). For the purposes of this

study, where more than one sample has been analysed at a given locality, the results have been combined and a mean value for each element computed for that locality. The discussion of the areal variation for most of the elements is based on the results at 32 regional points but that for the trace elements Rb, Sr, Y and Zr, and also C is based on only 30 and 27 points respectively. A summary of the univariate statistics for the elemental composition of the grid samples is given in Table 3-4.

b) Application of trend surface analysis

Many authors have pointed to the dangers of plotting areally distributed data using contours determined by human judgement, e.g. Whitten (1963). In this study an objective contouring method is used, which is a modification of the general trend surface analytical technique. This involves the iterative modification of a polynomial surface and is known as iterative trend surface analysis (Cole 1969). The merits of this technique will be discussed in more detail in Appendix C.

Linear, quadratic and cubic surfaces have been calculated for each element. In every case it was found that the cubic surface explained more 'sums of squares'. This was taken to indicate that the cubic surfaces approximated the data distribution most closely. Iterative surfaces have also been computed. These are a result of 10 iterations over the chosen cubic surface.

c) The cubic surfaces

The percentage fits of the cubic surfaces for each of the

elements are given in Table 3-5. The surface computed for Cu accounts for 78 per cent of the variance whereas those quoted for Si, Fe and Y account for more than 40 per cent and those computed for Mn, Na, Zn, Sr and Zr account for more than 30 per cent. The cubic surfaces which have been computed for the remaining elements only account for less than 30 per cent of the variance and are therefore not considered to be significant.

The boundary between significance and non-significance has been arbitrarily fixed at the 30 per cent degree-of-fit level. This was necessary because the measure of reliability of the fitted surface is based on a sums of squares test. This test does not define confidence limits. It has been demonstrated that if for a 100 points, a sums of squares test produces values that fall below 6.0, 12.0 and 16.2 per cent for the linear, quadratic and cubic surfaces respectively, the distribution of data points is not significantly different from random at the 0.05 level (Howarth 1967). Critical sums of squares values have not as yet been proposed for surfaces defined on less than 100 points but intuition suggests that they must be higher than those quoted for 100 points.

The cubic surfaces for each of the elements are illustrated in Figs 30-47. It is interesting that all eight significant surfaces are centred around the Hartfell and Carrifran Burn exposures. All surfaces, except for those for Si and Na which take the form of elongate domes, conform to a general pattern of elongate basins. The basins computed for Cu and Mn are aligned in a north-west to south-east direction and as such they are orientated across the regional strike. Those basins computed for the variation of Fe, Zr, Zn and

Y are orientated parallel to the Caledonian strike. The structural dome for Si follows the same NW-SE trend as displayed by both Cu and Mn. The Na surface is unique in that it is orientated east to west.

d) The iterative surfaces

The cubic surfaces are highly smoothed expressions of the main geographic trend in the data. The iterative surface for an element begins with the chosen cubic surface and progressively modifies it until after a specified number of iterations, ten in this work, it has improved the fit of the data but has lost much of the original form (Table 3-5). It is therefore not possible to generalise as much for the iterative map patterns as it was for the cubic surfaces.

It was noted above that the peak of the dome or the lowest part of the basin was located in the same general area over most of the cubic surfaces. This is to some extent still true for the iterative surfaces, Figs. 30 to 47, but the accurate position of the 'lows' and 'highs' is more difficult to define because of small-scale fluctuations in the computed trends.

e) Conclusion

The irregular nature of the geographic orientations of the trend surfaces is taken to imply that the distribution of the elements is not governed by areal processes. In this study no attempt has been made, nor would it have been possible, to sample a common graptolite zone within each inlier. Although the maximum

vertical thickness of sediments between samples is less than 100 m there is a large time difference. This is attributable to an exceptionally slow overall rate of deposition. The points of inflection in the surfaces coincide with those localities which are predominantly composed of Ordovician sediments. Perhaps therefore, the trend-surface maps are depicting stratigraphic time variations in the chemical abundances.

6. ELEMENT DISTRIBUTIONS THROUGH THE STRATIGRAPHIC SEQUENCE

a) Computation of vertical profile curves

The element distributions over all 14 graptolite zones in the sequence are depicted for those samples which have been accurately zoned on the basis of their graptolite assemblage (Figs 48-57). The divisions of ordinate of each plot have again been made proportional to the zone thicknesses at Dobb's Linn (Toghill 1968, 1970a). It may be observed that though some elements such as Na and Pb show apparent dependence on position in the succession, others such as Zr and Si, increase or decrease in amount upwards through the succession.

The time-stratigraphic relationships of the elements have been simplified by the computation of polynomial regression curves for each element over all zones. The technique used was that described above (Chapter II 4f). 13 of the 18 elements analysed have yielded curves which are significant at the 0.99 confidence level (Table 3-6). The significant curves are superimposed upon the scatter plots of the data and are considered to represent time-dependence of the abundance of the elements (Figs 48-57).

b) Relationship between the vertical profiles

Inspection of the 13 significant profiles reveals that there is an inverse relationship between Si and all the other elements except C. It appears from the profiles that both Si and C progressively decrease up the succession while Al, Fe, K, Mn, Mg, Ti, S, Cu, Zn, Al and Zr all show an overall increase in the same direction. This may be attributable to the inverse relationship between free silica and the other rock-forming minerals.

The other striking relationship which may be observed on comparison of the vertical profiles is the similarity in form of the curves generated for Ti, K, Rb, Al and Zr. The grouping of these five elements together by the similarity of their profiles is not without reason as will be shown below (Section 8b).

Although detailed discussion of the origin and meaning of this group of elements is held over (Section 10b), the similarity of the K and Rb profiles may be noted, notwithstanding that the profile for Rb is based on 133 analyses, whereas that for K is based on only 77 analyses. These elements are known to be correlated in a wide variety of geological environments. Furthermore, the profile for K is almost identical to that computed when only 33 analyses were available (Stephens et al., 1975). These observations lend confidence to the method of polynomial fitting and suggest that the significant profiles represent fundamental patterns in the sequence which can easily be defined by just a few samples.

7. ELEMENT DISTRIBUTIONS AT HARTFELL

a) Profiles computed for the north cliff

Polynomial regression curves have been computed to illustrate the variation in element concentrations in the 100 m thick sequence of mudstones, shales and cherts which is exposed in the north cliff at Hartfell. The analysis of variance for the computed curves is given in Table 3-7. Out of a total of 17 elements considered, only Cu, Mn, Mg and Sr yield profiles which are significant at the 99 per cent confidence level. The profiles for Al, K and Pb are significant at the 95 per cent level.

All those profiles which are significant at the 95 per cent level have been superimposed upon the scatter plots (Figs 59a - 76a). The curves for K and Pb are similar in that both display trends which increase for the first 15 m from the base of the cliff and then decrease for the next 10 m. Values then increase once more and both elements have their greatest concentrations in the P.linearis Zone, 87 m from the base of the cliff.

The profiles for Al and Cu are essentially the same as for K and Pb for the first 85 m up the cliff. Thereafter, values increase more rapidly. This observation is also true for the trends computed for Mn and Mg. These, although not varying much for the first 85 m, begin to change rapidly around the 85 m mark. The profile for Sr also exhibits inflexions at around 15 m and 85 m up the cliff.

b) Restoration profiles

The true stratigraphic position of the samples before faulting and folding have been calculated (Chapter I, 3d) and the results are given in Table 1-2. Polynomial regression curves were then computed to illustrate the variation of element concentration through the structurally restored succession. The analysis of variance for the restored curves is given in Table 3-8.

Out of a total of 17 elements considered, only Al, Cu and C yield restoration profiles which are significant at the 99 per cent confidence level. The profiles for Fe and Na are significant at the 95 per cent level. The six profiles which are significant at the 95 per cent level have been superimposed upon scatter plots of the data (Figs 61b, 62b, 65b, 68b, 69b, 76b). These profiles exhibit the same trends, although with greater detail, as the lower parts of the profiles which have been computed for the total suite of the samples (cf. Figs 49, 51, 52, 53 and 57).

The significance levels of the vertical profiles for the sequence as exposed, and for the sequence of samples after structural restoration are compared in Table 3-9. It is found that the profiles for Mn, Mg, Sr, K and Pb are more significant when computed in the in-situ position, whereas structural restoration improves the fit of the profiles computed for Al, Fe, Na and C. Although both profiles for Ca lie outside the chosen confidence limits it is noteworthy that the F-value is greater for the in-situ profile. This may mean that the in-situ profile of Ca is more significant than the restoration profile. These results imply that the profiles for Al, Fe, Na and C represent time

stratigraphic variations whereas the profiles for Mn, Mg, Ca, Sr, K and Pb represent variations attributable to effects associated with faulting.

c) Interpretation

The element assemblage involved with the effects associated with faulting indicates that a carbonate phase may have been introduced into the sediments at Hartfell. This phase was not detected in the mineralogical examination of the samples but as the mean values of Ca, Mn and Mg at this locality are only 0.02, 0.01 and 0.48 per cent respectively, only small quantities of a carbonate mineral could possibly be present. Two possibilities can be considered for the introduction of a carbonate into the sediments: firstly, metasomatism related to an igneous source, and secondly, diagenesis related to carbonate-bearing groundwaters. In the first connexion, Weir (1974) has related the presence of carbonate minerals in the Silurian rocks of Gatehouse to granitic emanations. In the Gatehouse area there is ample evidence for surface and sub-surface igneous activity. However, there is little evidence for such activity in the vicinity of Hartfell. The nearest proven igneous body lies below the surface at Leadhills about 25 km to the north-west of Hartfell. A recent geophysical survey has outlined the presence of a strong magnetic anomaly in the vicinity of Moffat (Powell, pers comm.). This anomaly follows the Caledonoid trend and may indicate the presence of a concealed igneous body. Carbonate metasomatism may therefore be related to this body.

In support of the second consideration, carbonate

replacement is a widespread feature of the Lower Palaeozoic greywackes (Weir 1974). Such replacement has been observed in inliers in S.W.Ireland which are well removed from any exposed centre of igneous activity (Weir 1962). In these instances the outcrops occur in Carboniferous Limestone terrain and it is likely that the sediments have been exposed for a considerable period of time to the circulation of carbonate-rich groundwaters. Calcite is observed to replace quartz at outcrop in sandstones exposed to semi-desert conditions (Dapples 1967). As the Hartfell Shale sequence is predominantly quartz rich it is possible that calcite replacement could be related to circulating carbonate-saturated groundwater following the Carboniferous episode of limestone deposition. However, in contrast to Ireland, carbonate rocks are not prevalent components of the Scottish Carboniferous. Moreover, deposition of Carboniferous rocks in the Southern Uplands was almost certainly confined largely to the basins in which they now occur.

On balance therefore, it would appear that the small amount of carbonate introduced into the sequence at Hartfell is metasomatic in origin.

Other than the visual similarity between the profiles for K and Pb, there is no evidence to support an inter-relationship between these two elements. Indeed, as will be shown later, K is considered to be associated with the clay factor and Pb with the metal factor. Lead is known to be a common substitute for potassium, especially in igneous rocks (Fairbridge 1972). This substitution is most frequently observed in potassium feldspars and micas both of which have, on average, 25-30 ppm Pb.

8. BIVARIANT CORRELATION AND ELEMENT ASSOCIATIONS

a) Introduction

Bivariant statistics describe the relationships between pairs of variables. A variable in this case is either the amount of a major or minor element in a sample. In most cases the most useful device for the presentation of the data is a scatter diagram. Usually, the data can be quantified in terms of regression and correlation coefficients.

The coefficient of correlation between two variables that is conventionally used in scientific studies is the product moment correlation coefficient. There are however a number of objections to using this coefficient. These are discussed in Appendix C. In this work the Kendall rank order correlation coefficient is also used because it is less sensitive to the constraints that apply to the former.

b) The correlation matrices

The correlation coefficients for both methods of calculation are presented in Table 3-10. This is a matrix for all combinations of variables. The matrix is based on the maximum possible number of comparisons within the data set eg. the coefficient for Si with Al is based on 107 points and that for Si with C on 60 points. It should be noted that the values of the coefficients may be affected by the phenomenon of closure which arises when data are referred to a constant total such as 100 in the case of percentage major element analyses. The correlation

coefficient calculated from such data may be quite anomalous, with the effect being most marked between the most abundant variables (Chayes 1971). Caution must accordingly be exercised in the interpretation of such matrices.

It is pertinent to observe here that when the two coefficients of correlation are compared, the sign is the same for each but in most cases the degree of estimated correlation of the rank order correlation coefficient is lower than that of the product moment coefficient. There are exceptions however, eg. the correlation coefficient calculated between K and Al is 0.48 when calculated by the product moment method and 0.60 when calculated by the Kendall rank order method.

Sulphur has not been included in the correlation matrix because only 27 analyses are available. It however correlates well with Fe. Correlation analysis provides a product moment correlation coefficient of 0.81 and a Kendall rank order correlation coefficient of 0.50.

c) Element associations

Most of the comparisons yield positive correlations except Si, which has negative correlation coefficients with all other elements except C. The strongest correlations generally appear to be associated with the major elements; this may be partly due to the closure phenomenon. If an arbitrary figure of 0.50 is chosen for the Kendall rank order correlation coefficient, it is found that the linear regression for all element pairs exceeding this value is significant at the 99 per cent confidence level. Scatter plots

and regression lines for those element pairs which have a correlation coefficient equal to or greater than 0.50 are presented in Figs. 77-85.

There are 31 strongly correlated pairs of elements out of a possible 136 pairs. Although Sr is not well correlated with Mn, Mg and Ca when the total sample suite is considered, it is found that when only those samples from Dobb's Linn are considered, these elements correlate well. Correlation analysis for the Dobb's Linn sub-set of samples yields Kendall rank order correlation coefficients of 0.55, 0.53 and 0.59 for the variation of Sr with Mn, Mg and Ca respectively. When these correlations and that of Fe with S are included, there is a grand total of 35 correlatable pairs of elements within the data set (Fig. 86a).

It is possible to assign most of the better correlated element pairs to one of four groups (Fig. 86b). The first group consists of all ten possible combinations of the elements Al, K, Ti, Rb and Zr. Attention has already been drawn above (Section 6b) to the similarity of the vertical profiles of the elements in this group. The second group consists of all six possible combinations of the elements Ca, Mg, Mn and Sr. This group of elements is most significant at Dobb's Linn. The third group of elements may be divided into two parts. The first part consists of all six possible combinations of the elements Fe, Al, Mg and Zn whereas the second part consists of two of the three possible combinations between the elements Fe, S and Cu. The fourth group is composed of negative correlations between Si and the elements Ti, Al, Fe, Mg, Zn, Rb, Sr and Mn. The other two correlations not assigned

to any of the four groups are Zn with Mn and Zr with Mg.

The first three groups, with their high positive internal correlations, are clearly very significant and are considered below in greater detail. The fourth group with its negative correlations based on Si, may be attributed to a greater or lesser extent, to closure. Where elements are presented in a given mineral species in approximately constant proportions, high positive correlations may reflect the variation in abundance of that mineral in a range of rocks.

The regressions for all 10 combinations of the Al - K - Ti - Rb - Sr group pass close to the origin and suggests that the majority, but not all, of these elements are found in one mineral species. X-ray diffraction studies have confirmed the presence of a mica conforming to the 2M type of the illite group. If the element associations are indicating this mineral species, then the mica must contain trace quantities of Rb and Sr.

The approximate proportions of each element within the mineral species have been calculated from the slope of the regression lines. A composition of Al 75.6%, K 19.1%, Ti 5.0%, Rb 0.1% and Zr 0.2% resulted. These proportions are not dissimilar to those of the type Fithian illite which contains 71.5% Al, 26.2% K and 3.7% Ti (Weaver and Pollard 1973). This lends support to the diagnosis of illite.

In the sedimentary environment the elements Ca, Mg, Sr and Mn are commonly associated as components of carbonate minerals. X-ray diffraction studies have shown that only a few samples have a high carbonate content. The element associations also indicate

that Mn correlates to a limited extent with Fe (Fig. 83). The regression slopes for the correlation of these five elements indicate the presence within the Moffat Shales of a carbonate with 63.1% Ca, 7.2% Mn, 25.7% Mg, 1.4% Fe and 0.1% Sr.

Element proportions calculated from the regression slopes for the third group of elements are not as meaningful as those computed for the first two groups. This is partly due to the link through Al with the group one elements, partly to the common link through Fe with the group two elements and partly to the common link with Fe within the group (Fig. 86a).

The regression slopes of the Fe - S - Cu sub-group indicate the presence of a pyritic mineral with 42.3% Fe, 57.2% S and 0.4% Cu. Similarly an iron-rich chlorite, related to clinocllore, of composition Fe 36.3 : Mg 14.7 : Al 49.0 : Zn 0.05, is indicated by the regression slopes of the Fe - Mg - Al - Zn sub-group.

d) Association of elements with minerals

The variation of element concentration has been correlated with mineral content as calculated from X-ray modal analysis. Product moment and Kendall rank order correlation coefficients are given in Table 3-10. The correlation matrix indicates 13 mineral-element pairs with a Kendall rank order coefficient greater than 0.50. Not included in the matrix is the variation of sulphur with pyrite. This combination gives a product moment correlation coefficient of 0.81 and a Kendall rank order correlation coefficient of 0.50.

The more significant element-mineral correlations are

illustrated in Fig. 86c and scatter plots with superimposed regression lines are given in Figs. 87-89. It is observed that Si exhibits negative correlations with albite and sericite but is positively correlated with the amount of quartz in the sediments. Al, Fe and Mg yield negative correlations with quartz, and Ti, Al and Mg are positively correlated with the amount of sericite. Albite, although not recognised as a distinct mineral species when considering element associations, is found to correlate with both Al and Mg. Pyrite, iron and sulphur intercorrelate lending confidence to the observed vertical mineral distribution (cf Figs. 22,49,57). Correlations within the mineral group itself indicate that as the amounts of sericite and albite increase within the sediments there is a decrease in the amount of quartz present.

In certain horizons within the sequence, notably within the M.cyphus Zone, pyrite is visible in hand specimen. This observation plus the good statistical correlations between Fe, S and modal pyrite indicate that Fe is principally bound up in the sulphide phase. Cu, Pb and Zn can be present in pyrite in the form of admixtures of other minerals such as chalcopyrite, galena and sphalerite (Fleischer 1955) or as small amounts in solid solution with pyrite (Deer et al., 1962).

9. PRINCIPAL COMPONENTS ANALYSIS

a) Introduction

Principal components analysis and factor analysis have recently been used to examine the relationships between elements

in sediments and in sedimentary rocks. The techniques have been used by Spencer (1966) on a Silurian claystone, Hirst and Kaye (1971) on a suite of argillaceous and arenaceous rocks, Cosgrove (1973) on red beds and by Summerhayes (1972) on recent continental margin sediments. The factor, or principal component vectors indicate associations of elements and interpretation of the vectors can lead to the recognition of the relationships between mineral phases. In some cases the vector may be a simple reflection of a fundamental chemical or physical control such as pH or supply of terrigenous debris.

Principal components analysis is a useful means by which the complex relationships between variables in a data set can be reduced to simple components. This statistical approach accounts for the variation in a data set in terms of vectors. It also defines the amount of variation in the data set for which a component accounts.

Two methods exist for the calculation of the eigen-vectors or principal components. The first begins with the covariance matrix and produces vectors which are related to the original magnitudes of the variables, ie. in this study S_i would be the major contributor to the vectors. The second method begins with the correlation matrix and produces vectors which are composed of variables which have equal weighting regardless of their magnitude ie. in this study S_i , and T_i would be given equal importance. The second method was favoured in this work in order to eliminate undue bias towards S_i .

Factor analysis is a mathematical extension of principal

components analysis but unlike the latter it requires a prior knowledge of the number of factors to be extracted. It also suffers from the constraint that the original input variables must have normal distributions. As has been already demonstrated, the normality assumption is not valid and no prior knowledge of the number of factors exists. For these reasons, principal components analysis rather than factor analysis has been applied in this study. Further description of the techniques is given in Appendix C.

b) Results of principal components analysis

The input correlation matrix was based on the results of only 33 samples. All elements except C were analysed. The samples were collected by Stephens, Weir and Watson as part of the Southern Uplands Research Project and include 16 from Dobb's Linn, 8 from Hartfell, 5 from Glenkiln, 3 from Mountbenger and one from Carrifran. The correlation matrix differs only slightly from that described in the previous section where a larger number of samples was examined. Three eigen vectors have eigen values greater than 1.0 (that being equivalent to a single original variable) and these together account for 80 per cent of the variance in the data set. The construction of each principal component is given in Table 3-11 and represented diagrammatically in Fig.90.

The first principal component is dominated by the positive loading of Si and the negative loadings of the Al - K - Ti - Rb - Zr (clay) group and the Ca - Mg - Mn - Sr (carbonate) group. Si is present in these sediments both as uncombined silicon in quartz and as combined silicon in silicates, principally aluminosilicates.

Thus the first principal component can be interpreted as reflecting the antipathetic relationships between quartz on the one hand and clay and carbonate on the other.

The second principal component is also bipolar with a marked positive contribution from the carbonate group of elements. Negative contributions are provided by the clay group of elements along with the metals Pb, Fe and Cu. This component appears to reflect associated clays and metals in an inverse relationship with carbonates.

The main positive contribution to the third principal component is provided by Cu, Pb, Fe and Na. The negative contribution comes mainly from the clay elements and Sr. This vector is interpreted as the formation of metals at the expense of clay and quartz.

10. ELEMENT ASSOCIATIONS AND CONTROLS OF MINERAL FORMATION

a) Free silica

The amount of silica in the Moffat Shales varies widely from over 95 per cent in the cherts to much lower values in the shales. The origin of the free silica presents a problem. Certain cherts from the Ordovician are known to be radiolarian (Peach and Horne 1899) and in these cases much of the silica may be biogenic. In contrast, the true shales contain much less silica and a large proportion of the free silica may be quartz of detrital origin. Some silicification may however have occurred during diagenesis (Weir 1974). The origin of the silica could not be deduced,

because of extensive recrystallisation, by use of either the petrographic or the scanning electron microscope. It seems that the silica has several sources but it is not possible to quantify their varying contributions to each lithology.

b) Clays

Chemical evidence indicates that illite and chlorite are the dominant clay minerals in the suite. Such an indication does not conflict with the X-ray diffraction findings. Pre-Upper Palaeozoic shales are known to consist largely of illite and chlorite while younger rocks have a more varied mineralogy (Weaver 1967). It therefore seems likely that the original clay minerals have been modified to the phyllosomorph stage by the processes of diagenesis. Similar processes have been demonstrated in overlying turbidites of the region (Weir 1974).

If it is assumed that strongly correlated elements are to be found largely in the same mineral species then Ti, Rb and Zr (grouped with Al and K) are likewise located in illite. Ti is usually quoted in the group of octahedrally co-ordinated elements eg. Deer et al. (1962). Boström (1970) claims that when Al and Ti are correlated the ratio of Al to Ti indicates the material source. A high value (near 20) is supposed to suggest a terrigenous source, while weathering products of average oceanic rock should have low Al/Ti ratios of about 5. The regression of Al against Ti for the total suite of Moffat-Shale samples gives a slope of 15.2. This then suggests a dominantly terrigenous source with little contribution from weathered ocean-floor basalt. If however the

total sample suite is divided into three parts and the Al/Ti ratios calculated separately for those samples from Dobb's Linn, those from Hartfell and those from all other localities, values of 17.6, 3.0 and 20.2 are respectively obtained. As the sequence in the north cliff at Hartfell is exclusively composed of Ordovician sediments and that at Dobb's Linn is predominantly Silurian in age, it might be implied that there was a change in the type of source material with time.

TiO₂ occurs as anatase and rutile in pelagic clays (Goldberg and Arrhenius 1958) and also can be concentrated in dinoflagellates (Collier 1953). The strong correlation of Ti with Al and K however, favours its presence in illite rather than denoting significant concentrations of alternative sources.

There is also good correlation of Rb with K and thus Rb is probably substituting for K at the interlayer sites in illite. It is known that carbonate rocks containing authigenic illite yield high K/Rb ratios of around 500 whereas rocks containing detrital illite of continental origin have a lower ratio of about 240 (Schroll 1968). The samples from Dobb's Linn give a K/Rb ratio of 250 and therefore, if the above relationships are extendable to shales, it is likely the clays in the sediments at Dobb's Linn have largely originated as continental detritus. The K/Rb ratio of the Hartfell samples can not be considered as the regression of K with Rb for samples from this locality is not within the chosen significance level.

The other trace element which is statistically associated with illite is Zr. This element is known to substitute for Al in

the octahedral sites of clays (Chave and Mackenzie 1961). Although the presence of zircon is not indicated this mineral may well be present within the sediments.

c) Carbonate

The presence of a carbonate of composition Ca 63.1%, Mn 7.2%, Mg 26.7%, Fe 1.4% and Sr 0.1% has been postulated on the basis of regression line slopes. It is noteworthy that a ferroan carbonate phase was detected in the X-ray diffractograms of a few samples (Chapter II). The significance of a substantial amount of manganese in a high magnesium calcite is not clear though admittedly only five samples from three horizons are significantly enriched in carbonate (Fig. 51). The amount of carbonate in these samples accounts for less than 30 per cent of the total, the remainder consisting largely of clay minerals.

The original textures having been destroyed, the origin of the carbonate in the Moffat Shales remains problematical. The carbonates at Dobb's Linn, unlike the trace amounts at Hartfell, may be of primary origin for recently a blind trilobite fauna has been collected from certain horizons in the Barren Mudstone facies (J. G. Ingham pers.comm.). Dolomitization and iron replacement likely took place during diagenesis.

d) Metals

The metals Fe, Cu, Pb and Zn are grouped together by principal components analysis and from the slopes of the regression lines the relative proportions of each in a single mineral phase

would be of the order of Fe 99.7%, Cu 0.1%, Pb 0.1% and Zn 0.1%. Apart from the ferroan carbonate, X-ray diffraction also indicates the presence of pyrite and a chlorite.

The main sources of Fe in the pelagic environment are Fe-rich minerals, in the absorbed coating of ferric oxides on detrital clay minerals and from solution of Fe during submarine volcanic exhalation (Berner 1971, Boström 1970). The range of Fe in the Moffat Shales is wide (19%) and it is possible that a proportion of this was contributed by submarine volcanism. Whatever the source, fixation of Fe as a sulphide has been a major process during the formation of these shales. Much of the pyrite formation may have been effected by the bacterial decay of organic matter but migration of Fe and S during diagenesis must be invoked to explain localised concentrations (Berner 1969).

e) Sodium and Yttrium

These are the only two elements which are not easily assigned to any of the groups so far recognised. Na is undoubtedly present in feldspar and may be substituting for K in clays but it is not found to correlate with either Al, K or the modal amount of albite. This may be a reflection of the poor analytical precision for this element. There are no statistical indications as to the location of Y in this suite of samples.

11. THE THREE PRINCIPAL COMPONENTS IN RELATION TO THE
CONTROLS OF SEDIMENTATION.

In view of the extensive recrystallisation and obliteration of original textures, interpretation of the principal components in relation to sedimentation will be somewhat speculative. The three principal components are orthogonal vectors. Such a three dimensional system can be projected on to a plane (Cole and Adamson 1969). Using this method, which has been applied to geological problems by Stephens (in litt.), the positions of the elements in relation to the principal components are located by means of spheres whose sizes are inversely related to the distance from the viewer (Fig.91).

The first principal component reflects the bipolar relationship between quartz and all other minerals, and with clay in particular. This is interpreted as the diluting effect of quartz on all other minerals. If, as it is believed, much of the free silica contribution comes from the silicious skeletons of micro-organisms, then the first principal component depends on the abundance of these micro-organisms or alternatively on the lack of detrital clay. The depositional relationship between organic silica and detrital clay probably depends to a great extent on physiographic location in the pelagic environment, with increasing depth and distance from the source being the main suppressing controls over clay and carbonate deposition.

The second principal component probably represents that part of the first vector in which the proportion of clay is high

and probably reflects the conditions under which carbonate is stable in such an environment. This principal component is thus interpreted as the chemical controls of carbonate formation.

Finally, the third principal component with its high positive loadings for the metals against the negative loadings for the main rock forming minerals of quartz, clays and carbonates can be related to the conditions of pyrite fixation and to the total amount of degradable organic matter. Some horizons in the Moffat Shales yield abundant graptolites which may have provided ample material for bacterial decomposition leading to the reduction of sulphate and the formation of H_2S . It is noteworthy in this respect, although it is the exception rather than the rule, that the graptolites themselves are pyritised.

In summary the three principal component system is dominated by the first component with an eigen value of 45 per cent. This vector has been interpreted as the physiographic control over sedimentation. The second process within the system reflects the formation of a carbonate phase. This has an eigen value of 20 per cent. The third process recognised, with an eigen value of 14.6 per cent, is interpreted as the early diagenetic formation of pyrite controlled by the amount of organic decay. The relationships of the elements to these three postulated controls of sedimentation are shown in Fig.91.

12. TIME DEPENDENCE OF THE PRINCIPAL COMPONENTS

A principal component consists of a vector of weightings for each variable. A principal component score (which may be treated in the same way as any other variable) can be computed by summing the products of the weightings and the values for a given sample over all variables (elements). Plots of the variations of the principal component scores with stratigraphic zone are presented in Fig. 92.

The first principal component is the only one to yield a curve which is significant at the 99% confidence level. Predictably the profile of this component is very similar to those of Si and modal quartz (cf. Figs 48,23).

In accordance with the interpretation of the first principal component, it is proposed on the basis of chemical analysis that quartz decreases upwards in the succession relative to clay minerals, and that cherty mudstone gives way to less silicious mudstone. The change is fairly rapid near the Ordovician/Silurian boundary and then conditions appear to stabilise higher in the Llandovery. This probably reflects a change in the physiographic environment. The second and third principal components show high score values where they are rich in carbonates and metal elements respectively but neither shows a distinct variation with time.

The twofold cyclicity diagnosed from lithologies (Weir 1973) is not substantiated by the geochemical trends presented in this work. The cycle starts with fissile black shales and passes

through a succession of transitional lithologies to culminate in barren grey mudstones. A comparison of bulk chemical composition with rock type, fissility and colour of these samples shows a lack of any systematic relationship. It is thus concluded that although the lithological characteristics are influenced by primary sedimentation they are more a function of diagenesis, compaction and burial metamorphism.

| ZONE | INLIER | NUMBER OF SAMPLES | ELEMENTS ANALYSED |
|--------------------|-------------|----------------------|----------------------|
| <u>maximus</u> | Dobb's Linn | 2 | 17 |
| | Dobb's Linn | 1 | 16 |
| <u>sedgewickii</u> | Dobb's Linn | 2 | 17 |
| | Dobb's Linn | 1 | 16 |
| <u>convolutus</u> | Dobb's Linn | 2 | 17 |
| | Dobb's Linn | 2 | 16 |
| | Mountbenger | 1 | 17 |
| <u>gregarius</u> | Dobb's Linn | 1 | 16 |
| <u>cyphus</u> | Dobb's Linn | 2 | 17 |
| | Dobb's Linn | 1 | 16 |
| | Dobb's Linn | 11 | 10 |
| | Dobb's Linn | 2 | 7 |
| <u>vesiculosus</u> | Dobb's Linn | 2 | 16 |
| <u>acuminatus</u> | Dobb's Linn | 1 | 17 |
| | Dobb's Linn | 2 | 16 |
| <u>persculptus</u> | Dobb's Linn | 1 | 17 |
| | Dobb's Linn | 3 | 16 |
| <u>anceps</u> | Dobb's Linn | 5 | 17 |
| | Dobb's Linn | 3 | 16 |
| | Dobb's Linn | 1 | 7 |
| <u>complanatus</u> | Dobb's Linn | 2 | 16 |
| | Dobb's Linn | 1 | 7 |
| | Hartfell | 4 | 10 |

TABLE 3-1 Location, zone and elements analysed for the Moffat Shale samples.

/continued

| ZONE | INLIER | NUMBER OF SAMPLES | ELEMENTS ANALYSED |
|-----------------|-------------|----------------------|----------------------|
| <u>linearis</u> | Dobb's Linn | 4 | 16 |
| | Hartfell | 2 | 17 |
| | Hartfell | 8 | 16 |
| | Hartfell | 8 | 10 |
| | Mountbenger | 2 | 17 |
| | Carrifran | 1 | 17 |
| <u>clingani</u> | Hartfell | 2 | 17 |
| | Hartfell | 5 | 16 |
| | Hartfell | 29 | 10 |
| | Dobb's Linn | 1 | 16 |
| <u>wilsoni</u> | Hartfell | 1 | 17 |
| | Hartfell | 5 | 16 |
| | Glenkiln | 2 | 17 |
| | Glenkiln | 2 | 16 |
| Glenkiln | Dobb's Linn | 1 | 17 |
| | Hartfell | 3 | 16 |
| | Glenkiln | 2 | 17 |

Key to ELEMENTS ANALYSED.

- 17 Si, Ti, Al, Fe, Mn, Mg, Ca, Na, K, Cu, Pb, Zn, Rb, Sr, Y, Zr, S.
16 Si, Ti, Al, Fe, Mn, Mg, Ca, Na, K, Cu, Pb, Zn, Rb, Sr, Y, Zr.
10 Si, Al, Mg, Cu, Pb, Zn, Rb, Sr, Y, Zr.
7 Cu, Pb, Zn, Rb, Sr, Y, Zr.

TABLE 3-1 continued.

| Element | Mean | Std.Dev. | Minimum | Maximum | No.of samples |
|--------------------------------|-------|----------|---------|---------|---------------|
| SiO ₂ | 72.78 | 13.21 | 46.40 | 95.08 | 159 |
| TiO ₂ | 0.60 | 0.21 | 0.12 | 1.08 | 107 |
| Al ₂ O ₃ | 10.13 | 4.82 | 2.68 | 23.67 | 159 |
| Fe ₂ O ₃ | 5.23 | 4.33 | 0.13 | 19.39 | 107 |
| MnO | 0.10 | 0.20 | 0.0 | 1.22 | 107 |
| MgO | 1.68 | 1.68 | 0.22 | 7.63 | 158 |
| CaO | 0.65 | 2.10 | 0.0 | 11.86 | 107 |
| Na ₂ O | 1.09 | 1.08 | 0.0 | 6.89 | 107 |
| K ₂ O | 2.40 | 1.30 | 0.59 | 10.29 | 107 |
| LOI | 7.28 | 2.90 | 1.40 | 16.12 | 77 |
| S | 1.41 | 2.33 | 0.0 | 10.59 | 27 |
| Cu | 73 | 43 | 0 | 223 | 163 |
| Pb | 54 | 51 | 12 | 440 | 163 |
| Zn | 36 | 41 | 0 | 174 | 163 |
| Rb | 93 | 38 | 25 | 199 | 161 |
| Sr | 61 | 56 | 9 | 474 | 161 |
| Y | 29 | 19 | 0 | 139 | 161 |
| Zr | 139 | 85 | 34 | 652 | 161 |
| C | 1.89 | 1.16 | 0.05 | 5.43 | 129 |

TABLE 3-2

Univariate statistics for elements analysed in the total suite of samples collected in the vicinity of Moffat. Values for Cu, Pb, Zn, Rb, Sr, Y and Zr in ppm, others in per cent.

| Element | Hartfell | Dobb's Linn | Luce Bay |
|--------------------------------|----------|-------------|----------|
| SiO ₂ | 83.12 | 61.33 | 69.99 |
| TiO ₂ | 0.54 | 0.74 | 0.61 |
| Al ₂ O ₃ | 6.73 | 13.82 | 12.50 |
| Fe ₂ O ₃ | 1.20 | 6.86 | 5.28 |
| MnO | 0.01 | 0.20 | 0.07 |
| MgO | 0.48 | 2.99 | 1.94 |
| CaO | 0.02 | 1.55 | 0.02 |
| Na ₂ O | 0.38 | 1.53 | 0.29 |
| K ₂ O | 2.28 | 3.00 | 4.27 |
| LOI | 5.80 | 8.60 | 4.66 |
| Cu | 45 | 90 | 98 |
| Pb | 31 | 60 | 36 |
| Zn | 4 | 64 | 60 |
| Rb | 69 | 119 | 113 |
| Sr | 73 | 60 | 58 |
| Y | 22 | 34 | 33 |
| Zr | 86 | 220 | 144 |
| C | 2.33 | 1.66 | 0.82 |

TABLE 3-3 Comparison of mean element values in Moffat Shales from different localities. Values for Cu, Pb, Zn, Rb, Sr, Y and Zr in ppm, others in per cent.

| Element | Mean | Std.Dev. | Minimum | Maximum | No.of Samples |
|--------------------------------|-------|----------|---------|---------|---------------|
| SiO ₂ | 66.86 | 11.35 | 51.89 | 95.08 | 32 |
| TiO ₂ | 0.57 | 0.22 | 0.12 | 0.90 | 32 |
| Al ₂ O ₃ | 12.38 | 5.40 | 2.68 | 20.60 | 32 |
| Fe ₂ O ₃ | 6.59 | 3.52 | 0.13 | 13.73 | 32 |
| MnO | 0.07 | 0.08 | 0.01 | 0.39 | 32 |
| MgO | 2.38 | 1.80 | 0.22 | 6.55 | 32 |
| CaO | 0.30 | 1.01 | 0.0 | 5.68 | 32 |
| Na ₂ O | 0.59 | 0.44 | 0.0 | 1.88 | 32 |
| K ₂ O | 2.22 | 0.90 | 0.59 | 4.09 | 32 |
| LOI | 6.99 | 2.83 | 1.40 | 16.12 | 31 |
| Cu | 100 | 40 | 26 | 223 | 32 |
| Pb | 67 | 49 | 20 | 197 | 32 |
| Zn | 58 | 41 | 0 | 145 | 32 |
| Rb | 109 | 42 | 27 | 175 | 30 |
| Sr | 44 | 24 | 9 | 116 | 30 |
| Y | 32 | 11 | 10 | 62 | 30 |
| Zr | 133 | 56 | 34 | 228 | 30 |
| C | 1.06 | 0.81 | 0.05 | 3.71 | 27 |

TABLE 3-4 Univariate statistics for chemical analyses from samples collected on a grid basis in the vicinity of Moffat. Values for Cu, Pb, Zn, Rb, Sr, Y and Zr in ppm, others in per cent.

| Element | Linear surface | Quadratic surface | Cubic surface | Iterative fit for 10 iterations on the cubic surface |
|--------------------------------|----------------|-------------------|---------------|--|
| SiO ₂ | 3.10 | 23.78 | 40.28 | 96.41 |
| TiO ₂ | 0.50 | 13.55 | 19.02 | 96.30 |
| Al ₂ O ₃ | 1.92 | 14.54 | 23.02 | 94.20 |
| Fe ₂ O ₃ | 0.24 | 16.35 | 46.54 | 98.68 |
| MnO | 0.54 | 22.45 | 35.06 | 98.79 |
| MgO | 1.35 | 3.04 | 11.73 | 97.65 |
| CaO | 1.23 | 12.06 | 18.36 | 98.56 |
| Na ₂ O | 11.70 | 21.68 | 39.31 | 98.75 |
| K ₂ O | 0.94 | 13.34 | 22.40 | 99.06 |
| LOI | 10.28 | 26.58 | 49.28 | 99.11 |
| Cu | 0.59 | 33.97 | 78.17 | 99.54 |
| Pb | 1.47 | 3.80 | 23.10 | 97.91 |
| Zn | 1.36 | 8.20 | 39.42 | 98.46 |
| Rb | 0.39 | 22.25 | 28.20 | 94.83 |
| Sr | 6.05 | 24.67 | 34.05 | 98.84 |
| Y | 3.81 | 32.58 | 43.38 | 100.0 |
| Zr | 0.76 | 26.09 | 30.63 | 97.79 |
| C | 11.85 | 17.31 | 28.38 | 99.20 |

TABLE 3-5 Percentage surface fits for the distribution of elements in the vicinity of Moffat.

| Variable | N | Order of chosen polynomial | DEGREES OF FREEDOM | | F-value |
|--------------------------------|-----|----------------------------------|----------------------|----------------------------------|--------------------|
| | | | Due to regression | Deviation about regression | |
| SiO ₂ | 129 | 3 | 3 | 125 | 79.24 ⁺ |
| TiO ₂ | 77 | 5 | 5 | 71 | 7.49 ⁺ |
| Al ₂ O ₃ | 129 | 4 | 4 | 124 | 54.00 ⁺ |
| Fe ₂ O ₃ | 77 | 4 | 4 | 72 | 27.24 ⁺ |
| MnO | 77 | 4 | 4 | 72 | 4.06 ⁺ |
| MgO | 128 | 4 | 4 | 123 | 38.98 ⁺ |
| CaO | 77 | 6 | 6 | 70 | 2.33 |
| Na ₂ O | 77 | 4 | 4 | 72 | 3.19 |
| K ₂ O | 77 | 4 | 4 | 72 | 4.42 ⁺ |
| LOI | 48 | 5 | 5 | 42 | 3.25 |
| S | 27 | 4 | 4 | 22 | 4.93 ⁺ |
| Cu | 133 | 5 | 5 | 127 | 14.31 ⁺ |
| Pb | 133 | 5 | 5 | 127 | 2.74 |
| Zn | 133 | 4 | 4 | 128 | 32.97 ⁺ |
| Rb | 133 | 4 | 4 | 128 | 17.50 ⁺ |
| Sr | 133 | 5 | 5 | 127 | 1.94 |
| Y | 133 | 5 | 5 | 127 | 1.90 |
| Zr | 133 | 6 | 6 | 126 | 22.88 ⁺ |
| C | 104 | 4 | 4 | 99 | 6.39 ⁺ |

TABLE 3-6 Analysis of variance for polynomial curves fitted to the stratigraphic variation of chemical analyses.

+ = significant at the 99% confidence level.

| Variable | N | Order of chosen polynomial | DEGREES OF FREEDOM | | F-value |
|--------------------------------|----|----------------------------------|----------------------|----------------------------------|--------------------|
| | | | Due to regression | Deviation about regression | |
| SiO ₂ | 62 | 5 | 5 | 56 | 1.33 |
| TiO ₂ | 21 | 4 | 4 | 16 | 0.63 |
| Al ₂ O ₃ | 62 | 5 | 5 | 56 | 3.32 ⁺ |
| Fe ₂ O ₃ | 21 | 5 | 5 | 15 | 1.26 |
| MnO | 21 | 4 | 4 | 16 | 5.00 ⁺ |
| MgO | 61 | 4 | 4 | 56 | 4.32 ⁺ |
| CaO | 21 | 8 | 8 | 12 | 1.31 |
| Na ₂ O | 21 | 4 | 4 | 16 | 2.10 |
| K ₂ O | 21 | 5 | 5 | 15 | 3.35 ⁺ |
| LOI | 21 | 3 | 3 | 17 | 0.04 |
| Cu | 62 | 3 | 3 | 58 | 21.07 ⁺ |
| Pb | 62 | 4 | 4 | 57 | 3.54 ⁺ |
| Zn | 62 | 4 | 4 | 57 | 1.42 |
| Rb | 62 | 4 | 4 | 57 | 2.11 |
| Sr | 62 | 5 | 5 | 56 | 4.57 ⁺ |
| Y | 62 | 4 | 4 | 57 | 0.90 |
| Zr | 62 | 4 | 4 | 57 | 1.58 |
| C | 62 | 5 | 5 | 56 | 1.49 |

TABLE 5-7 Analysis of variance for polynomial curves fitted to the stratigraphic variation of chemical analyses from the north cliff at Hartfell.

+ = significant at the 95% confidence level.

| Variable | N | Order of chosen polynomial | DEGREES OF FREEDOM | | F-value |
|--------------------------------|----|----------------------------------|----------------------|----------------------------------|-------------------|
| | | | Due to regression | Deviation about regression | |
| SiO ₂ | 62 | 6 | 6 | 55 | 1.05 |
| TiO ₂ | 21 | 5 | 5 | 15 | 1.86 |
| Al ₂ O ₃ | 62 | 6 | 6 | 55 | 4.28 ⁺ |
| Fe ₂ O ₃ | 21 | 6 | 6 | 14 | 2.95 ⁺ |
| MnO | 21 | 4 | 4 | 16 | 2.67 |
| MgO | 61 | 5 | 5 | 55 | 1.27 |
| CaO | 21 | 4 | 4 | 16 | 0.58 |
| Na ₂ O | 21 | 3 | 3 | 17 | 3.71 ⁺ |
| K ₂ O | 21 | 5 | 5 | 15 | 1.48 |
| LOI | 21 | 4 | 4 | 16 | 4.32 ⁺ |
| Cu | 62 | 6 | 6 | 55 | 4.59 ⁺ |
| Pb | 62 | 6 | 6 | 55 | 1.38 |
| Zn | 62 | 5 | 5 | 56 | 0.30 |
| Rb | 62 | 10 | 10 | 51 | 0.45 |
| Sr | 62 | 3 | 3 | 58 | 0.68 |
| Y | 62 | 6 | 6 | 55 | 0.45 |
| Zr | 62 | 5 | 5 | 56 | 0.13 |
| C | 62 | 5 | 5 | 56 | 5.18 ⁺ |

TABLE 3-8 Analysis of variance for polynomial curves fitted to the stratigraphic variation of chemical analyses at Hartfell after restoration of the north cliff to the pre-fault sequence.

+ = significant at the 95% confidence level.

LEVEL OF SIGNIFICANCE

| Variable | Original profile | Restoration profile |
|--------------------------------|------------------|---------------------|
| SiO ₂ | 10.0 | 10.0 |
| TiO ₂ | 10.0 | 10.0 |
| Al ₂ O ₃ | 5.0 | 1.0 |
| Fe ₂ O ₃ | 10.0 | 5.0 |
| MnO | 1.0 | 10.0 |
| MgO | 1.0 | 10.0 |
| CaO | 10.0 | 10.0 |
| Na ₂ O | 10.0 | 5.0 |
| K ₂ O | 5.0 | 10.0 |
| LOI | 10.0 | 2.5 |
| Cu | 0.1 | 0.1 |
| Pb | 2.5 | 10.0 |
| Zn | 10.0 | 10.0 |
| Rb | 10.0 | 10.0 |
| Sr | 1.0 | 10.0 |
| Y | 10.0 | 10.0 |
| Zr | 10.0 | 10.0 |
| C | 10.0 | 0.1 |

TABLE 3-9

Comparison of significance levels for vertical profiles of chemical analyses at Hartfell.

Principal components

| Variable | 1st | 2nd | 3rd |
|--------------|--------|--------|--------|
| Si | 0.359 | 0.009 | -0.112 |
| Ti | -0.318 | -0.194 | -0.184 |
| Al | -0.327 | -0.177 | -0.118 |
| Fe | -0.213 | -0.207 | 0.411 |
| Mn | -0.230 | 0.427 | -0.028 |
| Mg | -0.287 | 0.184 | -0.040 |
| Ca | -0.215 | 0.434 | -0.050 |
| Na | -0.075 | 0.143 | 0.413 |
| K | -0.279 | -0.281 | -0.247 |
| Cu | -0.171 | -0.115 | 0.450 |
| Pb | -0.050 | -0.211 | 0.458 |
| Zn | -0.303 | 0.037 | 0.176 |
| Rb | -0.253 | -0.312 | -0.269 |
| Sr | -0.185 | 0.423 | -0.028 |
| Y | -0.107 | 0.218 | 0.030 |
| Zr | -0.346 | -0.040 | -0.135 |
| Eigenvalue | 7.273 | 3.207 | 2.334 |
| Eigenvalue % | 45.5 | 20.0 | 14.6 |

TABLE 3-11

loadings and eigenvalues for the first three principal components.

C H A P T E R I V

ORGANIC CHEMISTRY

1. INTRODUCTION

This part of the study is an enlargement upon an earlier work (Watson 1971) which investigated the presence of amino acids and the maturity of the kerogen isolate in Ordovician shales from the north cliff at Hartfell. It was found that although the sediments yielded relatively large amounts of amino acids, the isolated kerogen was graphitic in nature. The present study was initiated firstly to investigate the anomalous association of amino acids with chemically mature organic material, and secondly to attempt to determine from the distribution and yield of hydrocarbons the palaeo-chemical history of the sediments.

2. AMINO ACIDS

a) Introduction

Amino acids are the principal components of proteins which, while accounting for most of the nitrogen compounds present in living systems, also make up over 50 per cent of the bulk dry weight of many organisms (Florkin 1949). Of the twenty or so amino acids which combine to form proteins, all except glycine exhibit optical activity. This property has been utilised in geochemical studies as an aid in determining the origin of the acids (Kvenvolden 1973, Dungworth 1976) and also as a means of dating recent sediments (Bada et al., 1970).

Most of the amino acids which enter geological systems originate from organisms in the biosphere. Those acids which survive the transition from the biosphere to the lithosphere become incorporated in modern sedimentary deposits where they undergo a number

of diagenetic changes. Proteins begin to hydrolyze and the process of racemization is initiated. Some new amino acids are formed and the concentration of all amino acids is reduced with time and temperature through degradation. The occurrence of amino acids in fossils, soils and sediments has been reviewed by Hare (1969). They have been reported present in many diverse sample groups eg. shells, (Abelson 1954); graptolites, (Foucart et al., 1965); fossil bones, (Bada et al., 1973); carbonaceous chondrites, (Cronin and Moore 1971); recent sediments (Emery 1964; Clarke 1967) and Precambrian sediments (Abelson et al., 1969; Vologdin et al., 1971).

The discovery of amino acids in meteorites and Precambrian sediments has prompted many workers to suggest an origin of terrestrial biological contamination. Such a deduction is based on the observation that the detected kinds and the distribution patterns of the isolated amino acids are very similar to those attributable to human finger prints and other laboratory contaminants (Hayes 1967). Contamination was also detected in the amino acids extracted from the Fig Tree chert (Kvenvolden et al., 1969). The presence of predominantly L - configured amino acids in three carbonaceous chondrites indicates a comparable origin (Oró et al., 1971).

Not all meteoritic amino acids are necessarily attributable to contamination; enantiomeric amino-acid distributions have been diagnosed from the Murchison and the Murray meteorites (Kvenvolden et al., 1970, 1971; Lawless et al., 1971). Along with the racemic mixture of protein amino acids there was found a series of non-protein amino acids. The latter have subsequently been synthesized in the laboratory by electric discharge techniques and it is now believed

that amino acids are formed in meteorites by abiotic chemical processes (Ring et al., 1972; Wolman et al., 1972).

A survey of contamination arising from the gas liquid chromatographic method of analysis for amino acids has been conducted (Rash et al., 1972). It was found that common laboratory agents such as water, butanol and hydrochloric acid and sources such as dust, latex gloves, cellulosic tissues, finger prints, skin fragments, hair, dandruff and saliva were all possible sources of amino acid contamination in the laboratory.

Such an impressive list of contaminants, many of which contribute the same amino acids as those found in the Hartfell Shales, casts doubt upon the original nature of these compounds in the Lower Palaeozoic of the South of Scotland (Watson 1971). Therefore, the occurrence and original nature of the amino acids in the Moffat Shales was reappraised.

b) Sample collection and analytical techniques

Six samples, each of approximately 500 g, were collected specifically from the Moffat Shales for amino acid analysis. Two samples were collected from the topmost linearis exposure at Hartfell (Fig.6), two from the middle exposure of the D.clingani Zone at Hartfell and two from P.linearis Zone at Dobb's Linn.

The samples were broken into small chips and ultrasonically extracted with 0.25 M hydrochloric acid for four periods, each of 15 minutes. The chips were then filtered and washed thoroughly with distilled and deionised water before crushing. After crushing, 200 g portions of the samples were hydrolyzed for 22 hours with 400 ml 6M hydrochloric acid (constant boiling). After evaporation

to dryness each of the samples yielded large quantities of inorganic salts. The quantities ranged from 3.6 g for one of the clingani Zone samples to 6.4 g for one of the Dobb's Linn linearis Zone samples. The extracts were then desalted by the method of Pollock and Miyamoto (1971) and then converted to the N - heptafluorobutyl n - propyl derivative using the method of Moss et al., (1971). The derivative was then chromatographed on a 10' x 1/16" glass column containing 3% OV - 1 on Varaport-30. A more detailed account of the desalting technique, the preparation of the derivative and the analytical method is given in Appendix B.

c) Results

Even after repeating the final stages of the desalting method, there remained associated with the hydrolyzate trace quantities (10 mg) of inorganic salts. The presence of salt within the extracts inhibited the ninhydrin reaction and consequently only one sample from Dobb's Linn gave a positive test (Appendix B). None of the six samples when chromatographed, yielded peaks at the position of any of the twenty common protein amino acids. The sample from Dobb's Linn that gave a positive ninhydrin test did, however, yield one strong peak on the chromatogram. This lay between the positions of glutamic acid and lysine and it may be that this peak is attributable to a non-protein amino acid. A more accurate determination of the compound could not be made because the limited amount of extract available was exhausted after one reconnaissance and one coinjection chromatographic analysis.

d) Discussion

Three causes may contribute to the absence of protein amino

acids in the Moffat Shales. Firstly, loss may have occurred through mishandling of the extract during the isolation procedure. (Conversely there was ample opportunity for the introduction of contamination). Secondly, there may not have been any input of amino acids into the sequence from the biosphere. Thirdly, amino acids may have been lost in diagenesis and metamorphism. It is not likely that the technique is at fault, the same method of extraction, isolation and purification having been employed successfully by the present author in the investigation of the amino acid composition of a Tertiary fossil wood from the island of Rhum (Allan et al., 1975).

The postulation of a limited supply of amino acids to the sediments is likewise considered invalid. Indeed, the opposite may have been the case due to the breakdown of large amounts of proteinaceous material derived from graptolite cortical periderms which are believed to have been composed of collagen-like fibrils (Towe and Urbanek 1972).

Diagenetic and metamorphic processes are the most likely cause of the depleted amino acid distribution. The sequence being in the greenschist facies of regional metamorphism, must have been subject to PT conditions of between 4 and 8 kb and 200-300°C (Landis and Coombs 1967). Laboratory studies indicate that for 1000 moles of amino acid present in aqueous solution only trace quantities remain after a period of 500,000 years at 100°C (Vallentyne 1964). There are many arguments for not equating these results directly with sedimentary processes, but nevertheless these laboratory experiments indicate that it is unlikely that much, if any, of the original proteinaceous material would be recognised in a 400 MY old sequence within the greenschist facies.

In conclusion, it is suggested that the amino acids previously reported from the Hartfell Shales were the result of contamination (Watson 1971). The findings of this work are in keeping with laboratory predicted models for the stability of amino acids in the sedimentary environment.

3. HYDROCARBONS

a) Introduction

Hydrocarbons are among the most ubiquitous organic compounds known. They are extensively found in nature as components or products of living organisms (eg. Eglinton and Hamilton 1963; Douglas and Eglinton 1966; Oró et al., 1967). They are widely distributed as components in recent sediments (eg. Stephens et al., 1956; Kvenvolden 1963), in ancient sedimentary rocks (eg. Hunt 1961; Bray and Evans 1965; Tissot et al., 1971), in Precambrian rocks (eg. Oró and Skenes 1965; Johns et al., 1966), in meteorites (eg. Noonan and Oró 1967; Hayes 1967; Oró et al., 1971), and in natural graphite (eg. Lam and Peterson 1968; Gelpi et al., 1969).

The existence of hydrocarbons in such diverse geochemical environments is related to shared-electron (covalent) bonding between carbon and hydrogen atoms and between carbon and carbon atoms. This latter bonding gives rise to chains of carbon atoms which commonly range in length from two to forty atoms. Since any carbon atom may combine with more than two other carbon atoms the carbon chains can not only be straight (normal) but also branched. A special style of branching leads to the formation of cyclic structures comprising rings of five or six carbon atoms.

Hydrocarbons, (except olefins and highly undersaturated compounds which are susceptible to attack at the position of the double bond), are chemically unreactive relative to most organic compounds. In general, only severe oxidation, thermal destruction or bacterial activity is effective in modifying or destroying this group of compounds.

Hydrocarbons are therefore more likely to be present within the Moffat Shales than any other class of organic compounds. This section summarises a preliminary study on the occurrence of hydrocarbons in the sequence.

b) Sample collection and preparation

A total of 43 samples, each of approximately 500 g, was collected from the Moffat Shales for hydrocarbon analysis. Of this, 21 samples were collected from the north cliff at Hartfell, 11 from Dobb's Linn, 3 from Glenkiln and 1 from Mountbenger (Fig.4). In addition, 7 samples were collected from the north side of the porphyrite dyke exposed at the north end of Clanyard Bay [NX 101381]. Details of sample locations are presented in Table 4-1.

To minimize contamination each sample was retrieved from the deepest accessible part of the exposure. Each was then wrapped in aluminium foil for transport to the laboratory.

Before crushing and extraction, the samples were broken into small chips, the surface weathering removed and then ultrasonically washed with dichloromethane (redistilled) for four periods each of five minutes. After each wash, the chips were filtered and dried at room temperature. They were then crushed in a 'Tema' mill which had previously been well washed with solvent. During

crushing and in all subsequent steps, care was taken not to handle the material.

c) Extraction and analytical procedures

After washing and crushing, 300 g samples were soxhlet extracted with 600 ml of a 50:50 v/v dichloromethane-methanol mixture for 200 hours. The solvent in the syphon-arm always assumed a slight yellow coloration shortly after commencement of extraction but other than this, the extracts were completely colourless. Evaporation of the solvent in a rotary evaporator left substantial quantities of free sulphur associated with the organic extract. The sulphur was removed by reaction with freshly precipitated copper in a 10 x 1 cm glass column.

The total extract was then chromatographed over 15 g of activated silica gel (60-120 mesh) using a sequential elution system of petroleum ether (25 ml : boiling range 40-60°C), benzene (30 ml) and methanol (35 ml). The base of the glass column was packed with 1 cm of freshly precipitated copper to remove any remaining traces of sulphur. Column chromatography separated the extract into aliphatic hydrocarbons, aromatic compounds and resins and asphaltenes. A total alkane fraction was separated using preparative argentatious thin layer chromatography (5% AgNO₃, 0.50 mm Keiselgel G plate activated at 120°C for one hour) with petroleum ether as developer. This was conducted as a routine procedure to perform two functions viz; to separate saturated hydrocarbons from non-saturated hydrocarbons and to remove any impurities from the alkane fraction. It is noteworthy that alkenes were not detected in any of the 43 samples investigated.

The total alkane fraction was then analysed by low-resolution gas-liquid chromatography using either OV - 1 or OV - 101 as the liquid phase. Carbon numbers were identified by coinjection with standard n - alkanes. Further details of the analytical methods employed are given in Appendix B.

d) Results

The yields of organic materials recovered after soxhlet extraction are given for those samples collected in the vicinity of Moffat in Table 4-2 and for the Clanyard Bay samples in Table 4-3. Large quantities of sulphur were associated with the organic extracts. Sulphur values are grouped about a mean of 278.9 mg / 100 g of sediment extracted, and range from less than 3 mg / 100 g in a sample from the wilsoni Zone at Hartfell, to nearly 1500 mg / 100 g in the sample from the convolutus Zone at Mountbenger. Mean values when calculated independently for Dobb's Linn (248.5 mg / 100 g) and Hartfell (149.4 mg / 100 g) indicate that the sediments at the former locality are more sulphurous. This is consistent with the observed chemical (S and Fe) and mineralogical (pyrite) variation through the succession. The extracts from the sediments collected adjacent to the dyke at Clanyard Bay are the least sulphurous of all, yielding on average 113.8 mg of sulphur per 100 g of sediment.

Of the three localities investigated the highest average yield of total alkanes was obtained from the Hartfell samples (0.87 mg/100 g). Smaller quantities were extracted from the sediments at Dobb's Linn (0.51 mg / 100 g) and the sediments at Clanyard Bay (0.49 mg / 100 g).

Aromatic compounds (benzene fraction) are only slightly

more abundant in the samples from Clanyard Bay (0.53 mg / 100 g) than those collected from Hartfell (0.46 mg / 100 g). Only 0.34 mg / 100 g of aromatic compounds were extracted, on average, from the sequence at Dobb's Linn. The highly polar organic material which constitutes the methanol eluates varies at Dobb's Linn from 0.2 mg / 100 g to 278.6 mg / 100 g. The mean abundance of the polar material at Dobb's Linn is 38.97 mg / 100 g whereas it is only 14.63 mg / 100 g and 4.57 mg / 100 g at Clanyard Bay and Hartfell respectively. Mean abundances of the organic fractions at each of the three localities are given in Table 4-4.

Extractabilities of the organic fractions are expressed relative to the amount of carbon within the samples (Table 4-5). Data are not available for the Clanyard Bay samples. Mean extractabilities of the aliphatic hydrocarbons, aromatic compounds and polar material for the Hartfell samples are 0.05, 0.03 and 0.34% respectively whereas the same parameters attain values of 0.03, 0.02 and 2.21% in the samples from Dobb's Linn. Even although carbon has been taken into account, the relative differences between the extractabilities at Dobb's Linn and Hartfell are similar to the differences noted for the organic fraction yields at the two localities.

The extractability of the aliphatic hydrocarbon fraction is plotted against the combined extractabilities of the aromatic and polar fractions in Fig.93. There is no apparent simple relationship between the two parameters but it may be pertinent to observe that the majority of the samples (27) group in a cluster centred towards the origin while, if an arbitrary dividing line is constructed to pass through the aliphatic hydrocarbon axis at about 0.09 and through

the other axis at about 0.5, nine samples lie outside the cluster zone. Of these nine samples eight were collected from Hartfell and one from Dobb's Linn. An inverse relationship between the aliphatic hydrocarbon extractability and the combined extractabilities of the aromatic and polar fractions may be inferred for these few samples but as yet there is insufficient data to justify such a claim.

e) Stratigraphic distribution of organic material

The distribution of organic material over all 14 zones in the stratigraphic sequence is depicted in Fig.94. As before, the divisions of ordinate of each plot have been made proportional to the zone thicknesses at the type succession of Dobb's Linn using the data of Toghil (1968, 1970a). Trends have again been simplified by the computation of a polynomial regression curve for each parameter over all zones.

Only the regression curve for the extractability of the total alkanes is not significant at the 0.95 confidence level. Of the four remaining parameters, the curves for the variation of the total hydrocarbon extract, the total hydrocarbon extractability and the extractability of the polar material are significant at the 97.5 per cent level and the curve computed for the variation in extractability of aromatic compounds is significant at the 95 per cent level (Table 4-6).

It is noteworthy that the vertical profiles for the total hydrocarbon extract, the total hydrocarbon extractability and the extractability of the polar material are all similar in form to that calculated for the variation of sulphur in the sequence (Fig.57). This, in part, substantiates the earlier suggestion that pyrite formation

may have been effected by the bacterial decay of organic matter.

f) The variation in yield of organic compounds with distance from the dyke at Clanyard Bay.

The yields of alkanes, aromatic compounds and polar material for the samples collected to the north of the 9.18 m wide porphyrite dyke at Clanyard Bay are given in Table 4-3. Their trends with distance from the dyke contact are illustrated in Fig.95. The trends for the distribution of the alkane and polar material fractions are similar over the total distance examined whereas, for the first three metres from the contact, the amount of aromatic compounds appears to vary inversely with the amount of material in the other fractions. Between six and fifteen metres from the contact the amount present in all three fractions decreases with distance. The maximum yield of organic material was obtained from the sample collected 6.4 m from the dyke contact i.e. at a distance equal to just over half the thickness of the dyke.

Holmes (1971) has studied the variation in yields of organic fractions in a series of Lower Carboniferous sediments adjacent to a 10 m thick quartz-dolerite dyke of Upper Carboniferous age. Yields of alkanes of at least five times greater than that found in the sediments at Clanyard Bay were obtained by Holmes. The maximum yield of alkanes was found at about 7 m from the dyke i.e. at a distance equal to about three-quarters the thickness of the dyke. Two causes may have influenced the poor yield of alkanes at Clanyard Bay relative to the sediments studied by Holmes (1971). Firstly, the original organic input was less at Clanyard Bay. Secondly, greater thermal or biological destruction may have occurred.

The variety of depositional environments indicated suggests a correspondingly variable contribution of organic compounds to the sediments. There is, however, no reason to propose a lesser input of organic material into the notably stagnant environment represented by the Clanyard Bay sequence. Evolution of the latter was probably influenced initially by penecontemporaneous biodegradation and subsequently by greenschist-facies metamorphism (in contrast to the aforementioned Carboniferous sediments, which have undergone only compaction and minor diagenesis).

g) Composition of the organic extract:- the A/S ratio.

The ratio of the amount of aromatic hydrocarbons (A) to the saturated aliphatic hydrocarbons (S), expressed as the A/S ratio of the sediments, has been shown to decrease with an increase in the degree of diagenesis (Baker and Claypool 1970; Connan 1972; Le Tran et al., 1974). Similar changes have also been demonstrated by thermal experiments in the laboratory (Bajor et al., 1969). It is found that immature sediments which have been buried by less than 2000 m of sediment yield A/S values of about 5.0 whereas mature sediments at depths greater than 5000 m under the influence of normal geothermal gradients ($3^{\circ}\text{C}/100\text{ m}$) yield A/S values of less than 0.5 (Le Tran et al., 1974).

A/S values are presented for the total sample suite in Table 4-7. Mean values of the A/S ratio for the samples from Hartfell, Dobb's Linn and Clanyard Bay are 0.9, 1.05 and 1.91 respectively. When taken at face value these results imply that the sediments at Hartfell are more mature than those at Dobb's Linn which in turn are more mature than those at Clanyard Bay. This implication may, however,

be without foundation since some abnormally high values (>1.5) have been included in the calculation. The phenomenon of abnormally high A/S values has been ascribed to bacterial alteration which preferentially removes the saturated aliphatic hydrocarbons, and first of all the saturated straight chain alkanes below nC25* (William and Winters 1969; Bailey and Krause 1970; Bailey et al., 1973).

h) Chromatographic analysis of the total alkane fraction.

Gas-liquid chromatographic analysis has been performed on the total alkane fraction of the extracts. Chromatograms are illustrated in Figs 96-109. Visual inspection of the chromatograms indicates that they may be grouped on the basis of the distribution of compounds into five different types. Type I distributions are characterized by a lack of peaks at the positions of the normal hydrocarbons, and the chromatograms exhibit pronounced unresolved envelopes centred in the vicinity of nC20. The chromatograms of type II are skewed towards the low molecular weight end and are enriched in normal hydrocarbons in the region of nC21. Type III chromatograms also exhibit unresolved envelopes centred about nC20 and are thus similar to those of type I. They are characterized, however, by the presence of larger quantities of normal hydrocarbons. The hydrocarbon distributions of the type IV chromatograms are again skewed but in this case towards the high molecular weight end. Type IV distributions are characterized by peak maxima in the nC27 to nC29 range. Type V distributions are bimodal and are dominated by large quantities of n-alkanes in the nC19 to nC21 range and in the nC27 to nC29 range.

* nC25 : indicates a normal alkane with 25 carbon atoms in a chain.

The chromatograms of the total alkanes extracted from the Moffat Shales have been classified in accordance with the above scheme (Table 4-8). It is not possible to classify the hydrocarbon distributions of samples HCL-2, CLAN-1 and DCV-2. The chromatograms of the former two samples (Figs.103 and 107) are however, similar, in that both exhibit prominent single peaks protruding from an unresolved envelope. Coinjection of isoprenoids reveals that pristane and phytane are present in samples CLAN-1 and HCL-2 respectively. The chromatogram for sample DCV-2 (Fig.98) exhibits a series of total alkanes which are skewed towards low molecular weights but differ from the type II distribution by the relative dominance of peaks which coinject with nC19 and nC21.

Those samples which have already been shown to have high A/S values also have either type III, IV or V total alkane distributions. The common link between those three distribution types is that each exhibits enrichment in high molecular weight n-alkanes at the expense of low molecular weight material. Such distributions are similar to those of oils which have been biodegraded (Bailey et al., 1973). Bailey (ibid) also finds that branched isoprenoid compounds resist bacterial attack to a greater extent than normal hydrocarbons. Hence, if only a limited amount of bacterial degradation is postulated for samples HCL-2 and CLAN-1, the relative abundance of the isoprenoids phytane and pristane may possibly be explained.

Alkanes, cycloalkanes and aromatics are all metabolized by bacteria. The order of attack upon saturated hydrocarbons, is light and then heavy normal alkanes followed by isoprenoids (Williams and Winters 1969; Bailey et al., 1973). After a period of time,

which depends on the type of culture, only complex, branched and cyclic components remain and the resulting chromatogram takes the form of an unresolved envelope. Type I total alkane distributions may therefore have originated as a result of intense prolonged bacterial activity. However, none of the Moffat Shale extracts assigned to this type exhibit abnormally high A/S values (Table 4-8). Bacterial degradation may therefore not be the controlling mechanism in the formation of type I distributions.

A clue to the origin of the hydrocarbons with type I distributions is afforded by the location of samples CLAN-2 and CLAN-3. The saturated hydrocarbons from both of these samples have been assigned to type I distributions and the extracts do not exhibit abnormally high A/S values (Table 4-8). That these samples have been subjected to thermal activity is without doubt since both were collected from within 1.5 metres of the contact of the 9.18 metre thick dyke at Clanyard Bay. Comparable hydrocarbon distributions have been observed in terrestrial graphites (Gelpi et al., 1969) and have also been produced by artificially heating vitrinite (Allan 1975). It is therefore suggested that type I hydrocarbon distributions have been derived as a result of thermal activity.

Hydrocarbon distributions resembling those of type II have been described for a high rank (89.5% d.a.f.C) Permian coal, and for a Lower Permian bituminous shale (Brooks and Smith 1967; Connan and Orgeval 1973). The observed distributions have been explained in two completely different ways. Brooks and Smith believe it is a result of increasing metamorphism on a hydrocarbon distribution which was originally rich in C₂₉ and C₃₁ alkanes. Connan and Orgeval

conclude that the distribution indicates large quantities of either algae or plankton.

As will be shown later (Chapter VI), the Moffat Shales are of high rank and it therefore does not seem likely that the hydrocarbons could have survived in their original form even although large quantities of algae and plankton might well have been incorporated into the sediments. Metamorphic alteration of the organic material seems a more likely explanation for the observed distribution. It is therefore considered that type II total alkane distributions are a result of metamorphic degradation of high molecular weight organic material. This degradation, in the case of the Moffat Shales, causes enrichment in the region of nC₂₁.

Thermal degradation may also explain the observed distribution of total alkanes in sample DCV-2 (Fig.98). At this stage however, it is still uncertain how thermal degradation of high molecular weight compounds can result in the preferential enrichment of only two alkanes.

So far, only the mode which occurs at the high molecular weight end of the type V distribution has been discussed. The low molecular weight mode may be the result of thermal degradation of high molecular weight compounds and if so the type V distributions are intermediate between types IV and II.

In summary, saturated total alkane distributions of types III, IV and V are interpreted as having been influenced by bacterial activity. Later thermal effects may be represented in type V distributions. Distribution types I and II represent the results of more pronounced thermal activity.

i) Calculation of odd-even preference values

There is a noticeable predominance of odd over even chain lengths in most biologically produced n-alkanes. This observation has been quantified by calculating a single value, termed the carbon preference index (CPI), to express the ratio of odd-carbon-numbered to even-carbon-numbered n-alkanes in any given sample (Bray and Evans 1961; Cooper and Bray 1963). Recent sediments generally have high CPI values while mature sediments, because of the effects of temperature and time, tend to exhibit CPI values in the region of 1.0.

The main disadvantage of CPI values is that, by definition, they must be calculated from the weight percentages of a sequence of eleven consecutive n-alkanes. This results in the loss of detail over limited carbon-number ranges. For example, in some Persian Gulf sediments there is a change from even to odd-number predominance with increasing carbon-number (Welte and Ebhardt 1968). Such an observation cannot be accurately quantified unless running CPI ratios are calculated. These, however, are not reliable since they are susceptible to changing trends in the weight percentage of alkanes with chain length.

A formula has been proposed for the calculation of odd-to-even ratios which is less sensitive to general trends in relative abundances and which is a more sensitive measure of the local odd-even ratio (Scalan and Smith 1970). This ratio has been named the odd-even predominance (OEP) value. This incorporates only five weight percentages, rather than eleven, and the three homologues in the centre of the range are weighted more heavily in the calculation.

The odd-even predominance function is calculated from the following equation:-

$$\text{OEP}(C_{i+2}) = \left[\frac{C_i + 6C_{i+2} + C_{i+4}}{4C_i + 4C_{i+3}} \right] (-1)^{i+1}$$

Where C_i is the relative weight per cent of a n-alkane containing i carbons per molecule.

Inspection of the gas-liquid chromatograms of the total alkanes from the Moffat Shales (Figs.96-109) reveals that most samples show a predominance of odd-number n-alkanes, especially in the high molecular weight region, but that some samples eg. DAC-1 and DVE-2 (Fig.97) exhibit a predominance of even-number alkanes. Visual comparison of the odd-even ratio from one part of a chromatogram to another is difficult especially as in the case of sample HL-9 (Fig.100) where there is a large disparity in the average weight percentages between different parts of the chromatograph. In order to compensate for such variations, running OEP values have been computed for each sample.

OEP values have been computed for the peaks occurring at the positions of n-alkanes in the total alkane chromatograms, rather than for the distribution of isolated n-alkanes. This course was necessary because repeated coinjection of standards with the hydrocarbon extract exhausted most of the available material. Attempts were made to sieve the extracts, which remained after coinjection, with a 5 Å molecular sieve but they were not successful. Peak intensities were measured relative to the baseline which in the case

of type I and type III distributions took the form of a normal curve. By following such a procedure it is realised that great care must be taken when interpreting the derived values since it is possible that the true n-alkane distribution is masked by the high proportion of branched and cyclic material.

OEP values from C18 to C29 are presented for the Clanyard Bay samples in Table 4-9. When plotted versus carbon chain length, (Fig.110), there is an apparent trend, especially at C18, in OEP values for all samples except CLAN-1, with distance from the dyke contact. Values at C18 range from 0.19 (evens dominant) at 0.53 m from the dyke contact to 1.39 (odds dominant) at 15.15 m from the contact. This trend is less marked at higher carbon chain lengths. The implication is that perhaps OEP values may be useful in elucidating the thermal history of mature organic extracts. Further work is obviously required before a relationship between OEP values and the degree of metamorphism of organic material can be substantiated and perhaps quantified.

OEP values are presented in Table 4-10 for those samples collected in the vicinity of Moffat. Values range from 0.43 at nC22 in sample DSE-1 to 8.39 at nC19 in sample DCV-2. Mean OEP values for various carbon chain lengths are given for each of the three main localities studied (Table 4-11). From these, average values of OEP C18 - C19 have been computed for Hartfell, Dobb's Linn and Clanyard Bay. The derived values of 1.06, 1.31 and 1.10 indicate that, on average, the total alkane extracts at each of the localities are only slightly enriched in odd-numbered n-alkanes relative to even-numbered n-alkanes. Such an observation confirms that the organic material

in the sediments at each of the three localities is chemically mature.

The stratigraphic variation in OEP values has been studied in the usual manner by computing polynomial regression curves over all 14 graptolite zones in the sequence. Analyses of variance are given for the computed curves in Table 4-12. It may be observed that of the 12 curves generated, only five are significant at the 0.95 confidence level. The significant curves are the vertical profiles for the stratigraphic variation in OEP at nC18, nC19, nC20 nC28 and nC29.

Even although only five curves are statistically significant, all twelve are presented because there is a remarkable similarity in the shape of the vertical profiles through the carbon number range (Figs.111-112). Points to observe are the occurrence of pronounced OEP maxima for lower carbon number curves in the region of the convolutus and gregarius Zones and also the variation in slope of the regression curves in the Hartfell Shales. This latter point is best amplified by comparing the profiles of the OEP values generated between chain lengths of 18 and 21 carbon atoms. OEP values at nC18 and nC19 are computed to decrease between the wilsoni and anceps Zones whereas at nC20 there is little change and at nC21, values first increase to a maximum in the linearis Zone and then decrease towards the anceps Zone.

The biomodal nature of the computed curves for OEP at nC19 and nC21 (Fig.111) is very much reminiscent of the computed profiles for the stratigraphic variation in the amount of pyrite, sulphur and total organic extract eluted from a silica gel column (Figs.22, 57, 94). In each case vertical profiles exhibiting two .

maxima were computed; one in the Lower Hartfell Shales and the other, more pronounced, in the Upper Birkhill Shales. Perhaps there is a sedimentary association between these variables.

The common link may be bacterial activity. Such activity may have reached a climax contemporaneously with the extreme development of the euxinic facies i.e. during the Idwian and Onnian. During these periods, bacteria, especially of the sulphate-reducing type, may have metabolized large quantities of n-alkanes and sulphur and so produced quantities of sulphide ions which on reaction with iron and water formed pyrite. After death of the bacteria it is possible that abnormally large quantities of organic material, derived from the decomposing cell walls of the organisms, entered the sediments.

The cell walls of many micro-organisms contain appreciable quantities of even carbon number dominated fatty acids (Sokatch 1969; Eisima and Jurg 1969). Such compounds when heated produce quantities of n-alkanes with one less carbon number than the starting material. The mechanism of the reaction is one of simple decarboxylation to form an intermediate radical which hydrogenates to form the n-alkane (Cooper and Bray 1963). This type of reaction may explain the presence of unusually high amounts of nC19 and nC21 alkanes in sample DCV-2. This implies that C20 and C22 acids were the source of the alkanes in this sample. These particular acids however, have not as yet been reported as constituents of bacterial cell walls (Sokatch 1969).

The occurrence of even-dominated (OEP < 1.0) n-alkane distributions in the Moffat Shales is unusual. Smooth n-alkane distributions (OEP \approx 1) are typical of marine organic facies whereas a relative predominance of high molecular weight n-alkanes with possibly an odd carbon preference (OEP > 1.0) in the C20 to C30 range may be

evidence for a non-marine origin of some sediments (Kvenvolden 1966) and crude oils (Reed 1969). Recently, predominances of n-alkanes with even numbered carbon chains have been reported in a Spanish petroleum (Albaiges and Torradas 1974), in native bitumens (Grantham and Douglas 1973), in the pyrolysis of kerogen (Dungworth 1972), from pyrolyzed alginites and resinites (Allan 1975) and from algal rich Mississippian carbonates (Dembicki et al., 1976).

It has been proposed that even number predominances may have been caused by either reductive processes acting upon the fatty acids and alcohols (Welte and Ebhart 1968; Albaiges and Torradas 1974) or by the condensation of two fragments originating from the decarboxylation of fatty acids (Robinson 1966). Simple thermal degradation of n-alkanes may also cause an enrichment in even-numbered n-alkanes.

Any one of the above processes may have been responsible for the enrichment in even number n-alkanes in some of the Moffat Shale samples. Thermal degradation of fatty acids is preferred as the mechanism by the present author because it is a kinetically favourable simple reaction capable of taking place in a number of diverse environments. This reaction produces free radicals as intermediates. Free radicals are extremely reactive and it is possible that if formed in a sedimentary environment they would combine to form larger molecules. In this way an even-numbered fatty acid could decarboxylate to form an odd-numbered radical which could either combine with another odd-numbered radical to form an even-numbered alkane or with an even-numbered radical to form an odd-numbered alkane. As even-numbered fatty acids are more common in nature (Eisima and Jury 1969) the statistical chance that even-

numbered compounds result from the condensation of two radicals is greater than from the formation of odd-numbered compounds.

As previously stated, it is also possible that the free radicals, produced after the decarboxylation of fatty acids, combine with hydrogen to form alkanes with one less carbon atom than the original acid. Thermodynamically there is little to choose between which of the two reactions occur as the bond energies for C-C and C-H bonds are similar (80 and 98 K cal's respectively, Glasstone and Lewis 1966). The size of the radicals may however in some instances hinder the condensation reaction and thus favour the formation of alkanes of lower molecular weight.

j) Conclusions

It is considered that biodegradation has initially influenced the yield and distribution of organic material in the Moffat Shales. Bacterial death assemblages may have contributed large quantities of fatty acids to the sediments. Metamorphic processes have subsequently modified these fatty acids to give a variety of hydrocarbon distributions, notably those with a dominance of even-numbered alkanes. Bacterial activity reached a climax during the Onnian and Idwian, and is reflected in the deposition of large quantities of pyrite. This is ascribed to the bacterial reduction of sulphate ions to sulphide, releasing them to combine with iron.

4. KEROGEN

a) Introduction

Organic matter dispersed in sediments consists of complex biotic remains which can either be highly concentrated as in a coal

bed or dispersed as kerogen in a mineral matrix. For this study, kerogen is defined according to Laplante (1974) as the bitumen-free biotic remains disseminated in a rock. Kerogen appears to be formed by condensation or polymerization of microbially altered products originating from carbohydrates, proteins, lipids and perhaps other organic material (Mc Iver 1967).

The natural sequence of transformation of organic substances has been formulated in a series of laws (Andreev 1962). These laws which are based on chemical thermodynamic principles, describe how organic matter in living organisms is transformed as a result of oxidation and coalification. In the living organism, organic substances are at relatively high energy levels and are therefore very unstable. After death of the organisms, the high energy levels can no longer be sustained and the original organic substances decompose into compounds of greater thermodynamic stability.

The processes of oxidation, coalification and carbonization continue after death the transformation of the organic remains into more stable substances. If there is an excess of oxygen, the organic remains are quickly oxidized to the thermodynamically stable end-products of carbon dioxide and water. If however the system is deficient in oxygen, coalification and/or carbonization occurs. Both processes result in a continual carbon enrichment of the organic residue accompanied by the evolution of volatile substances which are relatively enriched in hydrogen and oxygen. The stable end-products are graphite for the solid phase, and methane, carbon dioxide and water for the volatile phase.

The most relevant studies of the transformation of sedimentary organic matter are those related to coalification and the coal series (Himus 1951;

van Krevelen 1961). Coal-forming organic debris, after deposition, passes consecutively through peat-lignite-bituminous and anthracite coal stages. These changes are marked by an ever-increasing percentage of carbon and correspondingly decreasing percentages of oxygen, and in the final stages, decreasing hydrogen. The ultimate coalification product is 100 per cent carbon or graphite.

Kerogen isolated from sedimentary rocks is affected by coalification in a similar way to that of coal forming detritus (Long et al., 1968; Tissot et al., 1974). As depth of burial and temperature increase, a series of stages can be recognised from changes in the kerogen H/C and O/C ratios. The first stage corresponds to the release of hetero-atoms, such as oxygen, in the form of water, and carbon dioxide. Increasing temperature then liberates hydrocarbons from the kerogen, and in the final stage the breaking of C-C bonds becomes important. The relative importance of each of the three evolutionary steps is governed, especially at low temperatures, by the composition of the original kerogen.

In the preceding section it was concluded that metamorphism has affected the amount and distributions of hydrocarbons in the Moffat Shales. The effects of metamorphism upon the kerogen are investigated in this section by means of chemical analysis and infra-red and X-ray spectroscopy.

b) Isolation and analytical techniques

Kerogenous extracts were isolated from the bitumen-free inorganic matrix by digesting the sediments with mixtures of hydrofluoric and hydrochloric acids following the procedure of Saxby (1970) (see Appendix B). The purity of the kerogenous extract

was assessed by measuring the ash content after ignition and also by X-ray diffraction. All samples contained between 30 and 60 wt. per cent ash (Table 4-13) indicating that perhaps the method of isolation was not the most satisfactory. X-ray analysis indicated that although there had been effective removal of clay minerals, feldspars and quartz, there remained within the extracts significant amounts of pyrite and insoluble fluorides. These fluorides, formed as artefacts of the separation process, are very complex and contain the ammonium ion within their lattices. The most common contaminants were ammonium fluoranate (ASTM 16-647) and a complex fluoride of the formula $MgF_2 (NH_4)FA1F_3$ (ASTM 3-99).

The kerogenous isolates were analysed for carbon, hydrogen and nitrogen using a Perkin Elmer automatic micro-analyser. X-ray diffractograms of the isolates were run on a Philips PW 1012/20 diffractometer using copper $K\alpha$ radiation generated by a current of 18 mA at 36 kV, with an attenuation of 2×10^2 and a time constant of 16. Each slide was scanned at $1/4^\circ/\text{min}$ over a two-theta range of 24 to 27 degrees. Infra-red spectra were run on KBr discs which were prepared by homogenizing 0.1 mg kerogen with 350 mg KBr. The instrument used was an Infracan mk II H900.

c) Chemical analysis

The results of chemical elemental analysis and the H/C ratios for the Moffat Shale kerogenous isolates are given in Table 4-13. The values, when plotted on an ash-free basis in the form of a triangular diagram (Fig.113), indicate that the organic isolates lie within the zone of coaly-type kerogens (Forsman and Hunt 1958). A coalification trend is also apparent with the extracts

from Hartfell being of highest rank and those from Clanyard Bay being the most immature.

It is considered significant that although most samples (considered as ash free) have around 2.5% nitrogen, some are relatively enriched in this element. Certain samples, notably HL-14, DCV-2 and CLAN-1 have been shown above to exhibit high A/S values. These were attributed to bacterial activity. Nitrogen enrichment may be a result of degradation of protein-rich bacterial cells and if so this may contribute further evidence that biodegradation has altered the organic matter of the Moffat Shales.

The variation in elemental chemistry of the kerogen with distance from the 9.18 m thick porphyrite dyke at Clanyard Bay is illustrated in Fig.95. The amounts of hydrogen and carbon both increase with distance from the dyke to reach maximum values at about 3 metres from the contact. Thereafter, there is little change in hydrogen values but the amount of carbon in the isolates decreases steadily with distance. The variation in the H/C ratio with distance from the dyke is almost the inverse of that of carbon.

The variation in elemental distribution of the kerogens over all 14 zones in the stratigraphic sequence is illustrated in Fig.114. The computed polynomial regression curves for the stratigraphic variation of carbon, hydrogen and the H/C ratio are significant at the 97.5 per cent confidence level whereas the profile for the variation of nitrogen is not even significant at the 0.90 level. Analysis of variance is given for the curves in Table 4-14.

The vertical profiles indicate that the kerogen becomes more carbonaceous as the sequence is ascended from the Glenkiln Shales to the top of the Lower Hartfell Shales. From this point

upwards there is then a steady decrease in the amount of carbon present within the isolates. Hydrogen values do not exhibit any change in the upper part of the succession but show the reverse of the carbon trend in the lower part. It is pertinent once again to observe that the lower part of the succession is dominated by samples from Hartfell and therefore the computed variation may not be related to stratigraphic differences but may have resulted in response to regional effects. If this is so, then it may be concluded that the sedimentary organic matter at Hartfell is, on average, more carbonaceous than that at Dobb's Linn and thus that the former locality has been subjected to more severe metamorphic effects than the latter.

d) X-ray diffraction

X-ray diffractograms have been run for the kerogen isolates over a two-theta range of 25.5 to 27.5° (Fig.115). In most cases there is a reflection present that corresponds to a d-spacing of 3.35 Å. This is attributable to the graphite $\boxed{002}$ peak (ASTM 13-148). The shape, intensity and two-theta position of the peaks vary quite considerably through the stratigraphic sequence, justifying an attempt to establish a classification of the carbonaceous material based on that of Landis (1971). In this classification, all sub-graphitic carbon can be designated graphite-d and increased disorder within the material can be expressed in terms of subscript values (d_1, d_2, d_3).

The term graphite is used here to describe only that material whose pattern is essentially identical to fully ordered

graphite (Smith 1969). All other material is graphite-d. It has been proposed that four fairly distinctive stages in the graphitization series can be recognized (Landis 1971). The characteristics of these are summarized in Table 4-15. Fully ordered graphite is characterized by a diffractometer trace with an intense, sharp and symmetrical $[002]$ reflection at $3.35 - 3.36\text{\AA}$ as well as other considerably weaker reflections, (eg. $[100]$, $[101]$, $[104]$), at higher angles. Graphite-d₁ is characterized by a relatively intense $[002]$ peak at $3.35 - 3.36\text{\AA}$ which is noticeably broader and markedly skewed towards lower angles. Reflections other than $[002]$ are absent. Material classified as graphite-d_{1A} produces very similar diffractograms to those classified as graphite-d. The main difference is that the former material gives a less skewed $[002]$ reflection of slightly higher d-spacing (ca. 3.4\AA).

In less well ordered samples (d₂), the single peak is broader and has a conspicuously larger spacing (ca. 3.5\AA) than fully ordered graphite or graphite-d₁. Diffractograms of graphite-d₃ material range from featureless charts to those containing broad low intensity peaks with a mean spacing of $3.50 - 3.75\text{\AA}$. Material showing such a diffractogram is best considered amorphous (French 1964).

The degree of disordering of the carbonaceous material within the Moffat Shales has been estimated. Using basal spacing as the classification criterion all samples, with the exception of sample DL-4, contain graphite-d₁ (Table 4-16). Most samples appear more disordered, however, when the height to width-at-half-peak-height of the $[002]$ reflection is used. This discrepancy may reflect differences in experimental conditions between those used in this study and those of Landis (1971).

The data presented in Table 4-16 and the shape and position of the peaks illustrated in Fig.115 indicate that the carbonaceous material of the Moffat Shales can be classified, on average, as graphite- d_{1A} . Furthermore it appears that the organic material in the Hartfell samples is more ordered than that isolated from the Dobb's Linn samples.

There is an apparent progressive increase in spacing of the $\boxed{002}$ reflection with distance up the north cliff at Hartfell (Table 4-16). When examined more closely, this trend appears to be punctuated by the occurrence of thrusts. Thus it is implied that graphitization of the kerogen occurred contemporaneously with or before, thrusting. This will be investigated in greater detail in the next chapter.

Advances in metamorphic geology, experimental petrology and isotope studies have permitted increased understanding of the p-t fields occupied by the various metamorphic facies (eg. Fyfe and Turner 1966; Hietanen 1967). Data presented by Quin and Glass (1958), French (1964) and Landis (1971) indicate that fully ordered graphite first appears in uppermost greenschist facies to lower amphibolite facies rocks whereas graphite- $d_{1,2}$ is more often associated with the pumpellyite-actinolite and greenschist facies (Fig.116). Average p-t conditions for the formation of graphite- $d_{1,2}$ are therefore in the region of 5 kb and 350°C.

It is concluded that the degree of crystallinity of the carbonaceous material isolated from the Moffat Shales indicates that the sediments have been subjected to p-t conditions comparable to those of the greenschist facies. This finding is consistent with the observed mineralogy (Chapter II). The X-ray studies also indicate

that the organic material at Hartfell is of higher metamorphic grade than that at Dobb's Linn.

e) Infra-red absorption

It is only comparatively recently that infra-red spectra of difficult carbonaceous materials such as graphite and carbon black have been obtained (Friedel and Carlson 1972). Experimental results indicate that spectral resolution improves with extensive grinding and that it is often necessary to grind such materials for periods of up to 96 hours before good infra-red spectra can be obtained.

In a preliminary investigation to study the effect of grinding time upon the infra-red spectrum of a Moffat Shale kerogenous isolate, portions of the insoluble organic material from sample HW-4, collected from the north cliff at Hartfell (Fig.6), were crushed first by hand and then for fixed time intervals in a small reciprocating ball-mill for periods ranging from 5 minutes to 36 hours. Care was taken not to overfill the mill as large amounts of powder were found to cushion the blow of the grinding balls. The infra-red spectra are illustrated in Fig.117 for the sample after crushing for periods of 1, 5 and 10 minutes, and 2, 12 and 36 hours.

Absorption bands are present in all the displayed spectra (Fig.117) in the vicinity of 1640, 1590 and 1400 cm^{-1} . In addition, there is a band present after crushing for periods of up to 10 minutes at 1740 cm^{-1} . Periods of crushing of greater than 10 minutes did not cause an improvement in the resolution or intensity of the bands and therefore this time was chosen as a standard in this study.

Infra-red absorption spectra were run between 3500 and 750 cm^{-1} on the complete set of powdered kerogen isolates. In each

case there was no indication of the presence of any absorption bands above 2000 cm^{-1} or below 1000 cm^{-1} . Representative spectra of the samples between these latter limits are illustrated in Fig.118. Examination of the spectra reveals a series of absorption bands superimposed upon a strong background absorption.

The presence of aliphatic (CH_3) groups is evident, especially in samples collected from the lower parts of the section at Dobb's Linn. (eg. sample DL-4 exhibits weak absorptions at 1470 and 1336 cm^{-1}). These, although present in other samples are always much weaker. The observed band in the region of 1300 cm^{-1} may be attributed to aromatic ethers or phenols (Friedel 1966) but this assignment cannot be confirmed due to the lack of complementary absorptions. The strong absorption band at 1635 cm^{-1} that occurs in most spectra is likely attributable to false bands caused by the mixing and grinding together of KBr and water-containing substances such as inorganic hydrates which are present in the kerogens as a result of the isolation procedure (Friedel 1966).

The bands at 1400 , 1120 and 1080 cm^{-1} are also probably related to artefacts of the isolation procedure. The former is assigned to the bending mode of the ammonium fluoride molecule (Plumb and Hornig 1955) but the latter two, although likely to be of inorganic origin, cannot be easily identified. The bands at 1120 and 1080 cm^{-1} cannot be assigned to any of the rock-forming minerals present in the original sediment (compare Table 4-17). It is possible therefore that they are attributable to absorptions arising from complex inorganic fluorides produced during isolation of the kerogen.

There is a relatively intense absorption band present in the spectra of all Hartfell samples at 1589 cm^{-1} . This is not

evident in any of the spectra of the Dobb's Linn samples. Such an absorption and a complementary, though much weaker, band at 1359 cm^{-1} is attributable to vibrations within a graphite structure (Friedel and Carlson 1972). The presence of this band in the spectra and the lack of absorption due to the organic functional groups which are normally present in low to medium rank kerogens indicate that the kerogenous isolates from Hartfell have been strongly carbonized (Grasselly et al., 1972).

It may be argued that the lack of organic absorption bands in the spectra is due in some way to the drastic chemical treatment which is involved in the isolation procedure. This possibility was checked by using the same technique to isolate kerogen from five Lower Carboniferous Shales collected from the east coast of Fife. The recorded infra-red spectra yield absorption bands which are attributable to C-H, O-H, C=O and CH_2 CH_3 groups. It is therefore concluded that chemical degradation of the organic material during the isolation procedure is not responsible for the scarcity of absorption bands in the spectra of the Moffat Shale kerogenous isolates.

The absence of graphite-type absorption bands in the isolates of Dobb's Linn samples lends support to the statement made above (Section 4d) that the organic material at this locality is of lower metamorphic grade than that at Hartfell.

f) Conclusion

The use of chemical, X-ray and infra-red techniques has illustrated that the Moffat Shale kerogen, or perhaps more correctly because of the limited success of the isolation technique, the

kerogenous isolate, is sub-graphitic. The degree of graphitization is more enhanced in the Hartfell than in the Dobb's Linn samples. Graphitization of the organic matter at Hartfell may have occurred contemporaneously with, or before, the onset of strike reverse faulting.

| Zone | Inlier | Number of samples |
|--------------------|--------------|-------------------|
| <u>maximus</u> | Dobb's Linn | 1 |
| <u>sedgwickii</u> | Dobb's Linn | 1 |
| <u>convolutus</u> | Dobb's Linn | 1 |
| | Mountbenger | 1 |
| <u>gregarius</u> | Dobb's Linn | 1 |
| | Clanyard Bay | 2 |
| <u>cyphus</u> | Dobb's Linn | 1 |
| | Clanyard Bay | 2 |
| <u>vesiculosus</u> | Dobb's Linn | 1 |
| | Clanyard Bay | 3 |
| <u>acuminatus</u> | Dobb's Linn | 1 |
| <u>persculptus</u> | Dobb's Linn | 1 |
| <u>complanatus</u> | Dobb's Linn | 1 |
| | Hartfell | 1 |
| <u>linearis</u> | Dobb's Linn | 1 |
| | Hartfell | 6 |
| <u>clingani</u> | Dobb's Linn | 1 |
| | Hartfell | 6 |
| | Glenkiln | 1 |
| <u>wilsoni</u> | Hartfell | 5 |
| | Glenkiln | 2 |
| Glenkiln | Hartfell | 3 |

TABLE 4-1 Location of those samples analysed for hydrocarbons.

| Sample | Total extract | Sulphur | Total organic extract | Total alkanes | Benzene fraction | Methanol fraction |
|--------|---------------|---------|-----------------------|---------------|------------------|-------------------|
| HL-9 | 306.2 | 284.5 | 21.8 | 0.5 | 0.7 | 12.7 |
| HL-7 | 346.0 | 327.6 | 18.4 | 1.2 | 0.4 | 3.9 |
| HLC-1 | 99.2 | 96.7 | 2.5 | 0.1 | 0.2 | 3.4 |
| HLC-1 | 68.6 | 43.6 | 25.0 | 0.5 | 0.3 | 2.3 |
| HL-11 | 184.0 | 170.0 | 13.8 | 0.2 | 0.4 | 6.5 |
| HW-2 | 72.2 | 58.5 | 13.8 | 1.3 | 0.3 | 5.3 |
| HW-4 | 33.4 | 23.1 | 10.2 | 0.4 | 0.3 | 5.8 |
| HCL-4 | 307.7 | 302.2 | 5.5 | 0.3 | 0.2 | 3.4 |
| HG-1 | 45.3 | 41.5 | 3.8 | 0.3 | 0.3 | 3.3 |
| HW-3 | 283.9 | 281.2 | 2.7 | 0.3 | 0.2 | 1.1 |
| HCL-1 | 183.2 | 170.6 | 12.6 | 1.4 | 0.8 | 6.5 |
| HCL-2 | 81.3 | 76.8 | 4.4 | 1.1 | 0.3 | 1.8 |
| HCL-5 | 148.1 | 132.0 | 16.1 | 1.5 | 2.5 | 2.5 |
| HCL-6 | 321.1 | 288.7 | 32.5 | 0.6 | 0.2 | 4.4 |
| HCL-3 | 20.6 | 19.0 | 1.7 | 0.4 | 0.1 | 0.1 |
| HL-3 | 45.7 | 20.5 | 23.7 | 1.2 | 0.5 | 2.8 |
| HL-14 | 321.0 | 313.0 | 8.1 | 0.1 | 0.4 | 7.3 |
| HL-15 | 243.3 | 226.8 | 16.5 | 4.1 | 1.2 | 7.0 |
| HG-2 | 25.6 | 16.9 | 8.6 | 0.2 | 0.2 | 4.5 |
| HW-1 | 8.9 | 2.5 | 6.4 | 0.4 | 0.0 | 0.8 |
| HW-5 | 83.3 | 70.9 | 12.4 | 1.2 | 0.2 | 10.6 |
| | | | | | | |
| DCL-1 | 118.8 | 113.7 | 5.3 | 1.2 | 0.0 | 0.8 |
| DL-4 | 203.7 | 155.9 | 47.6 | 1.5 | 0.7 | 3.0 |
| DC-1 | 12.2 | 7.6 | 1.5 | 0.3 | 0.0 | 0.4 |
| DPE-2 | 1390.2 | 1101.6 | 288.6 | 1.2 | 0.6 | 14.3 |
| DAC-1 | 1028.8 | 238.4 | 790.4 | 0.2 | 0.0 | 0.2 |
| DVE-2 | 152.4 | 150.3 | 1.9 | 0.3 | 0.1 | 0.3 |
| DCYP-1 | 63.4 | 59.0 | 4.4 | 0.3 | 1.3 | 2.8 |
| DGR-1 | 520.4 | 62.1 | 458.4 | 0.3 | 0.4 | 278.6 |
| DCV-2 | 607.8 | 183.7 | 424.1 | 0.3 | 0.6 | 126.0 |
| DSE-1 | 1592.4 | 638.3 | 954.1 | 0.2 | 0.0 | 0.2 |
| DMAX-1 | 46.5 | 22.6 | 23.8 | 0.4 | 0.0 | 1.0 |
| | | | | | | |
| GL-W1 | 872.3 | 860.7 | 11.6 | 0.3 | 0.1 | 7.9 |
| GL-W2 | 878.5 | 877.5 | 1.0 | 0.0 | 0.0 | 0.8 |
| GL-CL1 | 1104.3 | 1103.0 | 0.9 | 0.2 | 0.0 | 0.7 |
| MB4X | 1513.5 | 1498.1 | 13.7 | 1.0 | 1.4 | 2.2 |

TABLE 4-2

Yield of organic materials after soxhlet extraction for samples collected in the vicinity of Moffat, (all values expressed as mg/100g sediment).

| Sample | Perpend. distance from dyke contact m. | Total extract | Sulphur | Total organic extract | Total alkanes | Benzene fraction | Methanol fraction |
|--------|--|------------------|---------|-----------------------------|------------------|---------------------|----------------------|
| CLAN 1 | 0.13 | 113.5 | 108.4 | 5.2 | 0.3 | 1.0 | 2.7 |
| CLAN 2 | 0.53 | 37.9 | 23.2 | 14.7 | 0.7 | 0.4 | 10.0 |
| CLAN 3 | 1.49 | 239.8 | 231.6 | 8.9 | 0.5 | 0.4 | 4.1 |
| CLAN 4 | 3.20 | 164.4 | 146.9 | 17.5 | 0.2 | 1.5 | 6.2 |
| CLAN 5 | 6.40 | 337.8 | 250.3 | 87.6 | 1.0 | 0.3 | 64.4 |
| CLAN 6 | 10.70 | 49.3 | 26.2 | 23.1 | 0.5 | 0.1 | 10.8 |
| CLAN 7 | 15.15 | 30.7 | 10.1 | 20.7 | 0.2 | 0.0 | 4.2 |

TABLE 4-3 Yield of organic materials after soxhlet extraction for samples collected adjacent to the dyke at Clanyard Bay, (distance in metres, extracts expressed as mg/100g sediment).

| | Hartfell | Dobb's Linn | Clanyard Bay |
|-------------------|----------|-------------|--------------|
| Sulphur | 149.4 | 248.5 | 113.8 |
| Total alkanes | 0.87 | 0.51 | 0.49 |
| Benzene fraction | 0.46 | 0.34 | 0.53 |
| Methanol fraction | 4.57 | 38.87 | 14.63 |

TABLE 4-4 Mean values for the yield of organic fractions at three localities, (values expressed as mg/100g sediment extracted).

| Sample | EXTRACTABILITY | | | | | |
|--------|----------------|----------|--------------------|---------------|----------------|-----------------|
| | Total extract | Carbon % | Total ⁺ | Total alkanes | Benzene eluate | Methanol eluate |
| HL-9 | 13.9 | 1.97 | 0.71 | 0.03 | 0.04 | 0.65 |
| HL-7 | 5.5 | 1.08 | 0.51 | 0.11 | 0.04 | 0.36 |
| HC-1 | 3.7 | 0.88 | 0.42 | 0.01 | 0.02 | 0.39 |
| HRC-1 | 3.1 | 0.49 | 0.63 | 0.10 | 0.06 | 0.47 |
| HL-11 | 7.1 | 3.40 | 0.21 | 0.01 | 0.01 | 0.19 |
| HW-2 | 6.9 | 4.98 | 0.14 | 0.03 | 0.01 | 0.11 |
| HW-4 | 6.5 | 2.40 | 0.27 | 0.02 | 0.01 | 0.24 |
| HCL-4 | 3.9 | 3.66 | 0.11 | 0.01 | 0.01 | 0.09 |
| HG-1 | 3.9 | 0.35 | 1.11 | 0.09 | 0.09 | 0.94 |
| HW-3 | 1.6 | 1.93 | 0.08 | 0.02 | 0.01 | 0.06 |
| HCL-1 | 8.7 | 1.68 | 0.52 | 0.08 | 0.05 | 0.39 |
| HCL-2 | 3.2 | 3.78 | 0.08 | 0.03 | 0.01 | 0.05 |
| HCL-5 | 6.4 | 3.40 | 0.19 | 0.05 | 0.07 | 0.07 |
| HCL-6 | 5.2 | 1.85 | 0.28 | 0.03 | 0.01 | 0.24 |
| HCL-3 | 0.6 | 4.01 | 0.02 | 0.01 | 0.00 | 0.01 |
| HL-3 | 4.5 | 4.73 | 0.10 | 0.03 | 0.01 | 0.06 |
| HL-14 | 7.8 | 4.06 | 0.19 | 0.00 | 0.01 | 0.18 |
| HL-15 | 12.3 | 3.28 | 0.38 | 0.13 | 0.04 | 0.21 |
| HG-2 | 4.9 | 0.33 | 1.48 | 0.06 | 0.06 | 1.36 |
| HW-1 | 1.2 | 1.29 | 0.09 | 0.03 | 0.00 | 0.06 |
| HW-5 | 12.0 | 1.17 | 1.03 | 0.10 | 0.02 | 0.91 |
| | | | | | | |
| DCL-1 | 2.0 | 1.81 | 0.11 | 0.07 | 0.00 | 0.04 |
| DL-4 | 5.2 | 3.29 | 0.16 | 0.05 | 0.02 | 0.09 |
| DC-1 | 0.8 | 0.65 | 0.12 | 0.05 | 0.00 | 0.07 |
| DPE-2 | 16.1 | 1.51 | 1.07 | 0.08 | 0.04 | 0.95 |
| DAC-1 | 0.4 | 0.72 | 0.06 | 0.03 | 0.00 | 0.03 |
| DVE-2 | 0.8 | 1.48 | 0.05 | 0.02 | 0.01 | 0.02 |
| DCYP-1 | 4.4 | 1.28 | 0.34 | 0.02 | 0.10 | 0.22 |
| DGR-1 | 279.3 | 1.99 | 14.04 | 0.02 | 0.02 | 14.00 |
| DCV-2 | 126.9 | 1.46 | 8.69 | 0.02 | 0.04 | 8.63 |
| DSE-1 | 0.4 | 1.76 | 0.02 | 0.01 | 0.00 | 0.01 |
| DMAX-1 | 1.4 | 0.59 | 0.24 | 0.07 | 0.00 | 0.17 |
| | | | | | | |
| GL-W1 | 8.3 | 5.01 | 0.28 | 0.01 | 0.00 | 0.26 |
| GL-W2 | 0.9 | 2.61 | 0.03 | 0.00 | 0.00 | 0.03 |
| GL-CL1 | 0.9 | 2.39 | 0.04 | 0.01 | 0.00 | 0.03 |
| MB4X | 4.6 | 1.69 | 0.27 | 0.06 | 0.08 | 0.13 |

TABLE 4-5 Extractability of organic fractions. Total extract expressed in mg/100g rock, extractabilities expressed in g/g C per cent.

+ only includes that material eluted from a silica gel column.

| EXTRACTABILITY | Variable | N | Order of chosen polynomial | DEGREES OF FREEDOM | | F-value |
|----------------|-----------------|----|----------------------------------|----------------------|----------------------------------|-------------------|
| | | | | Due to regression | Deviation about regression | |
| | Total | 36 | 7 | 7 | 28 | 3.12 ⁺ |
| | Alkanes | 36 | 6 | 6 | 29 | 1.07 |
| | Benzene eluate | 36 | 6 | 6 | 29 | 2.51 ⁺ |
| | Methanol eluate | 36 | 5 | 5 | 30 | 3.85 ⁺ |
| | Total extract | 36 | 5 | 5 | 30 | 3.40 ⁺ |

TABLE 4-6 Analysis of variance for polynomial curves fitted to the stratigraphic variation in organic extracts.

+ = significant at the 95% confidence level.

| Sample | A/S | Sample | A/S |
|--------|------------------|--------|------------------|
| HL-9 | 1.4 | DCL-1 | 0.0 |
| HL-7 | 0.3 | DL-4 | 0.5 |
| HC-1 | 2.0 ⁺ | DC-1 | 0.0 |
| HRC-1 | 0.6 | DPE-2 | 0.5 |
| HL-11 | 2.0 ⁺ | DAC-1 | 0.0 |
| HW-2 | 0.2 | DVE-2 | 0.3 |
| HW-4 | 0.8 | DCYP-1 | 4.3 ⁺ |
| HCL-4 | 0.7 | DGR-1 | 1.3 |
| HG-1 | 1.0 | DCV-2 | 2.0 ⁺ |
| HW-3 | 0.7 | DSE-1 | 0.0 |
| HCL-1 | 0.6 | DMAX-1 | 0.0 |
| HCL-2 | 0.3 | CLAN 1 | 3.3 ⁺ |
| HCL-5 | 1.7 ⁺ | CLAN 2 | 0.6 |
| HCL-6 | 0.4 | CLAN 3 | 0.8 |
| HCL-3 | 0.3 | CLAN 4 | 7.5 ⁺ |
| HL-3 | 0.4 | CLAN 5 | 0.3 |
| HL-14 | 4.0 ⁺ | CLAN 6 | 0.2 |
| HL-15 | 0.3 | CLAN 7 | 0.7 |
| HG-2 | 1.0 | GL W1 | 0.3 |
| HW-1 | 0.0 | GL W2 | 0.0 |
| HW-5 | 0.2 | GL CL1 | 0.0 |
| | | MB4X | 1.4 |

TABLE 4-7 Ratio of aromatic to saturated-aliphatic hydrocarbons in the Moffat Shales, (⁺values considered to be abnormally high).

| Sample | DISTRIBUTION TYPE | | | | | A/S |
|--------|-------------------|----|----------------|----|---|------------------|
| | I | II | III | IV | V | |
| HL-9 | | X | | | | 1.4 |
| HL-7 | | | | | X | 0.3 |
| HC-1 | | | | | X | 2.0 ⁺ |
| HRC-1 | | | | | X | 0.6 |
| HL-11 | | | | X | | 2.0 ⁺ |
| HW-2 | X | | | | | 0.2 |
| HW-4 | | | | X | | 0.8 |
| HCL-4 | | | X | | | 0.7 |
| HG-1 | | | | | X | 1.0 |
| HW-3 | | | | X | | 0.7 |
| HCL-1 | X | | | | | 0.6 |
| HCL-2 | | | NOT CLASSIFIED | | | 0.3 |
| HCL-5 | | | | X | | 1.7 ⁺ |
| HCL-6 | | X | | | | 0.4 |
| HCL-3 | X | | | | | 0.3 |
| HL-3 | X | | | | | 0.4 ⁺ |
| HL-14 | | | | X | | 4.0 ⁺ |
| HL-15 | | | | X | | 0.3 |
| HG-2 | | | | X | | 1.0 |
| HW-1 | X | | | | | 0.0 |
| HW-5 | | | X | | | 0.2 |
| DCL-1 | X | | | | | 0.0 |
| DL-4 | X | | | | | 0.5 |
| DC-1 | X | | | | | 0.0 |
| DPE-2 | X | | | | | 0.5 |
| DAC-1 | | | | | X | 0.0 |
| DVE-2 | | | | | X | 0.3 |
| DCYP-1 | | | X | | | 4.3 ⁺ |
| DGR-1 | | | X | | | 1.3 |
| DCV-2 | | | NOT CLASSIFIED | | | 2.0 ⁺ |
| DSE-1 | | | | X | | 0.0 |
| DMAX-1 | | | X | | | 0.0 |
| CLAN 1 | | | NOT CLASSIFIED | | | 3.3 ⁺ |
| CLAN 2 | X | | | | | 0.6 |
| CLAN 3 | X | | | | | 0.8 ⁺ |
| CLAN 4 | | | | X | | 7.5 ⁺ |
| CLAN 5 | | | | X | | 0.3 |
| CLAN 6 | | | | X | | 0.2 |
| CLAN 7 | | | | X | | 0.7 |

TABLE 4-8 Classification of total alkane chromatograms.

(⁺ indicates abnormally high values).

CARBON NUMBER

| Sample | C18 | C19 | C20 | C21 | C22 | C23 | C24 | C25 | C26 | C27 | C28 | C29 |
|--------|------|------|------|------|------|------|------|------|------|------|------|------|
| CLAN 1 | 1.35 | 1.14 | 1.12 | 1.13 | 1.05 | 1.00 | 1.03 | 1.10 | 1.15 | 1.20 | 1.23 | 1.34 |
| CLAN 2 | 0.19 | 0.34 | 0.40 | 0.44 | 0.96 | 1.45 | 1.45 | 1.24 | 1.12 | 1.10 | 1.33 | 1.37 |
| CLAN 3 | 0.66 | 0.72 | 0.54 | 0.38 | 0.71 | 1.20 | 1.33 | 1.22 | 1.18 | 1.16 | 1.19 | 1.30 |
| CLAN 4 | 0.98 | 1.05 | 1.05 | 1.00 | 1.00 | 1.03 | 1.08 | 1.15 | 1.23 | 1.35 | 1.61 | 1.95 |
| CLAN 5 | 1.10 | 1.03 | 1.03 | 1.07 | 1.06 | 1.02 | 1.03 | 1.05 | 1.08 | 1.13 | 1.23 | 1.41 |
| CLAN 6 | 1.22 | 1.05 | 1.06 | 1.13 | 1.09 | 1.00 | 1.02 | 1.08 | 1.12 | 1.21 | 1.33 | 1.55 |
| CLAN 7 | 1.39 | 1.14 | 1.09 | 1.15 | 1.12 | 1.09 | 1.07 | 1.03 | 1.03 | 1.05 | 1.07 | 1.16 |

TABLE 4-9 Odd-even predominance values for samples from
Clanyard Bay.

| Sample | CARBON NUMBER | | | | | | | | | | | |
|--------|---------------|------|------|------|------|------|------|------|------|------|------|------|
| | C18 | C19 | C20 | C21 | C22 | C23 | C24 | C25 | C26 | C27 | C28 | C29 |
| HL-9 | 1.27 | 0.91 | 0.92 | 1.10 | 1.13 | 1.02 | 0.99 | 1.02 | 1.09 | 1.20 | 1.32 | 1.47 |
| HL-7 | 1.09 | 1.10 | 1.00 | 0.97 | 1.04 | 1.05 | 1.07 | 1.12 | 1.17 | 1.22 | 1.28 | 1.33 |
| HC-1 | 1.21 | 0.85 | 0.85 | 1.03 | 1.08 | 0.95 | 0.95 | 1.01 | 1.06 | 1.17 | 1.35 | 1.58 |
| HRC-1 | 1.28 | 0.95 | 0.92 | 1.06 | 1.11 | 1.01 | 1.01 | 1.03 | 1.05 | 1.11 | 1.21 | 1.32 |
| HL-11 | 0.99 | 0.94 | 1.13 | 1.12 | 1.03 | 0.98 | 0.98 | 1.00 | 1.06 | 1.15 | 1.26 | 1.41 |
| HW-2 | 1.00 | 0.81 | 0.77 | 0.68 | 0.48 | 0.39 | 0.58 | 0.79 | 0.83 | 0.90 | 1.04 | 1.25 |
| HW-4 | 0.93 | 0.81 | 0.89 | 1.02 | 1.01 | 0.95 | 0.94 | 0.97 | 1.03 | 1.07 | 1.12 | 1.18 |
| HCL-4 | 1.04 | 0.87 | 0.97 | 1.09 | 1.08 | 1.04 | 1.07 | 1.12 | 1.15 | 1.18 | 1.19 | 1.18 |
| HG-1 | 1.48 | 1.02 | 0.96 | 1.05 | 1.05 | 1.01 | 1.05 | 1.08 | 1.11 | 1.18 | 1.29 | 1.45 |
| HW-3 | 1.29 | 1.03 | 1.05 | 1.10 | 1.11 | 1.10 | 1.14 | 1.22 | 1.29 | 1.34 | 1.39 | 1.47 |
| HCL-1 | 0.92 | 0.71 | 0.66 | 0.63 | 0.58 | 0.67 | 0.88 | 0.94 | 0.99 | 1.10 | 1.16 | 1.19 |
| HCL-2 | 2.11 | 1.53 | 1.16 | 1.11 | 1.16 | 0.89 | 0.68 | 0.69 | 0.71 | 0.68 | 0.89 | 1.62 |
| HCL-5 | 1.07 | 1.03 | 0.98 | 1.01 | 1.09 | 1.12 | 1.13 | 1.16 | 1.20 | 1.27 | 1.33 | 1.38 |
| HCL-6 | 1.00 | 0.86 | 0.84 | 0.98 | 1.08 | 0.99 | 0.97 | 1.03 | 1.04 | 1.07 | 1.13 | 1.19 |
| HCL-3 | 1.24 | 1.03 | 0.85 | 0.68 | 0.60 | 0.67 | 0.85 | 0.93 | 0.93 | 0.96 | 1.02 | 1.15 |
| HL-3 | 0.95 | 0.90 | 0.87 | 0.74 | 0.78 | 1.02 | 1.29 | 1.37 | 1.25 | 1.11 | 1.05 | 1.09 |
| HL-14 | 1.42 | 1.09 | 1.12 | 1.05 | 0.98 | 0.99 | 1.01 | 1.03 | 1.05 | 1.09 | 1.17 | 1.31 |
| HL-15 | 1.00 | 0.88 | 0.87 | 0.90 | 0.91 | 0.88 | 0.91 | 0.94 | 0.94 | 0.97 | 1.07 | 1.21 |
| HG-2 | 1.61 | 1.28 | 1.26 | 1.20 | 1.11 | 1.12 | 1.24 | 1.35 | 1.39 | 1.47 | 1.71 | 2.07 |
| HW-1 | 1.01 | 0.89 | 0.90 | 0.93 | 0.97 | 0.94 | 0.93 | 1.00 | 1.04 | 1.03 | 1.08 | 1.44 |
| HW-5 | 1.11 | 0.95 | 0.97 | 1.01 | 1.03 | 1.03 | 1.07 | 1.09 | 1.12 | 1.19 | 1.23 | 1.24 |
| DCL-1 | 0.90 | 0.76 | 0.58 | 0.38 | 0.31 | 0.45 | 0.88 | 1.05 | 1.00 | 1.02 | 1.09 | 1.17 |
| DL-4 | 0.97 | 1.44 | 2.56 | 3.72 | 3.41 | 1.88 | 1.12 | 1.00 | 1.00 | 0.90 | 0.92 | 1.06 |
| DC-1 | 1.02 | 0.88 | 0.87 | 0.85 | 0.80 | 0.80 | 0.87 | 0.89 | 0.88 | 0.96 | 1.06 | 1.39 |
| DPE-2 | 0.87 | 0.75 | 0.67 | 0.53 | 0.44 | 0.46 | 0.66 | 0.78 | 0.85 | 0.95 | 1.03 | 1.15 |
| DAC-1 | 0.69 | 0.57 | 0.54 | 0.51 | 0.52 | 0.60 | 0.75 | 0.85 | 0.87 | 0.86 | 0.89 | 0.98 |
| DVE-2 | 0.74 | 0.57 | 0.56 | 0.59 | 0.66 | 0.72 | 0.79 | 0.83 | 0.82 | 0.81 | 0.84 | 0.91 |
| DCYP-1 | 1.00 | 0.96 | 1.01 | 1.02 | 0.93 | 0.89 | 1.08 | 1.23 | 1.13 | 0.99 | 1.00 | 1.18 |
| DGR-1 | 5.06 | 4.53 | 3.68 | 2.96 | 1.93 | 1.07 | 0.96 | 1.04 | 1.01 | 0.99 | 1.01 | 1.10 |
| DCV-2 | 5.94 | 8.39 | 6.25 | 2.55 | 1.14 | 0.94 | 0.97 | 1.15 | 1.27 | 1.23 | 1.03 | 0.92 |
| DSE-1 | 0.70 | 0.81 | 0.88 | 0.65 | 0.43 | 0.44 | 0.81 | 1.05 | 1.04 | 1.02 | 1.04 | 1.11 |
| DMAX-1 | 0.61 | 0.52 | 0.57 | 0.67 | 0.75 | 0.81 | 0.88 | 0.92 | 0.92 | 0.95 | 1.04 | 1.18 |

TABLE 4-10 Odd-even predominance values in the Moffat Shales.

/continued

| Sample | CARBON NUMBER | | | | | | | | | | | |
|--------|---------------|------|------|------|------|------|------|------|------|------|------|------|
| | C18 | C19 | C20 | C21 | C22 | C23 | C24 | C25 | C26 | C27 | C28 | C29 |
| GL-W1 | 0.80 | 0.95 | 1.00 | 1.12 | 1.24 | 1.12 | 1.06 | 1.11 | 1.14 | 1.12 | 1.08 | 1.04 |
| GL-W2 | 1.56 | 1.72 | 1.58 | 1.39 | 1.22 | 1.15 | 1.14 | 1.06 | 1.02 | 1.03 | 1.00 | 0.96 |
| GL-CL1 | 0.86 | 1.12 | 1.29 | 1.39 | 1.38 | 1.31 | 1.24 | 1.13 | 1.07 | 1.08 | 1.09 | 1.11 |
| MB4X | 1.13 | 1.00 | 0.87 | 0.78 | 0.84 | 0.92 | 0.98 | 0.98 | 0.97 | 0.99 | 1.05 | 1.24 |

TABLE 4-10 (Continued) Odd-even predominance values in the
Moffat Shales.

| Variable | Hartfell | Dobb's Linn | Clanyard Bay |
|---------------------|----------|-------------|--------------|
| OEP C18 | 1.19 | 2.08 | 0.98 |
| OEP C19 | 0.97 | 1.83 | 0.92 |
| OEP C20 | 0.95 | 1.65 | 0.90 |
| OEP C21 | 0.97 | 1.31 | 0.90 |
| OEP C22 | 0.97 | 1.03 | 1.00 |
| OEP C23 | 0.94 | 0.82 | 1.12 |
| OEP C24 | 0.99 | 0.90 | 1.14 |
| OEP C25 | 1.04 | 0.98 | 1.12 |
| OEP C26 | 1.07 | 0.98 | 1.17 |
| OEP C27 | 1.11 | 0.97 | 1.17 |
| OEP C28 | 1.20 | 1.00 | 1.28 |
| OEP C29 | 1.36 | 1.10 | 1.44 |
| No. of observations | 21 | 11 | 7 |

TABLE 4-11 Comparison of mean odd-even predominance values at three localities.

| Variable | N | Order of chosen polynomial | DEGREES OF FREEDOM | | F-value |
|----------|----|----------------------------------|----------------------|----------------------------------|-------------------|
| | | | Due to regression | Deviation about regression | |
| OEP C18 | 36 | 5 | 5 | 30 | 3.97 ⁺ |
| OEP C19 | 36 | 5 | 5 | 30 | 4.09 ⁺ |
| OEP C20 | 36 | 7 | 7 | 28 | 2.77 ⁺ |
| OEP C21 | 36 | 6 | 6 | 29 | 0.83 |
| OEP C22 | 36 | 6 | 6 | 29 | 0.32 |
| OEP C23 | 36 | 8 | 8 | 27 | 0.78 |
| OEP C24 | 36 | 6 | 6 | 29 | 0.03 |
| OEP C25 | 36 | 6 | 6 | 29 | 0.83 |
| OEP C26 | 36 | 6 | 6 | 29 | 1.26 |
| OEP C27 | 36 | 6 | 6 | 29 | 2.09 |
| OEP C28 | 36 | 7 | 7 | 28 | 3.50 ⁺ |
| OEP C29 | 36 | 7 | 7 | 28 | 2.52 ⁺ |

TABLE 4-12 Analysis of variance for polynomial curves fitted to the stratigraphic variation in odd-even predominance values.

+ = significant at the 95% confidence level.

| Sample | Purity % | C % | H % | N % | H/C |
|--------|-------------|--------|--------|--------|------|
| HL-9 | 51.8 | 6.78 | 1.72 | 0.15 | 0.25 |
| HL-7 | 62.4 | 22.99 | 1.29 | 0.30 | 0.06 |
| HL-4 | 72.6 | 18.92 | 1.73 | 1.17 | 0.09 |
| HL-10 | 66.9 | 27.17 | 1.61 | 0.27 | 0.06 |
| HRC-1 | 52.4 | 2.01 | 2.15 | 0.18 | 1.07 |
| HL-11 | 64.7 | 21.66 | 1.30 | 0.16 | 0.06 |
| HG-1 | 51.1 | 1.19 | 1.82 | 0.26 | 1.53 |
| HW-3 | 69.1 | 1.96 | 1.97 | 0.25 | 1.01 |
| HCL-1 | 77.1 | 17.88 | 1.31 | 0.40 | 0.07 |
| HL-12 | 64.9 | 27.85 | 1.47 | 0.40 | 0.05 |
| HCL-6 | 56.5 | 12.47 | 1.55 | 0.30 | 0.12 |
| HL-13 | 63.1 | 27.65 | 1.58 | 0.38 | 0.06 |
| HL-14 | 69.6 | 31.45 | 1.35 | 1.96 | 0.04 |
| HL-15 | 63.0 | 30.25 | 1.11 | 0.36 | 0.04 |
| HW-5 | 57.4 | 2.03 | 1.51 | 0.01 | 0.74 |
| DCL-1 | 59.1 | 20.36 | 1.35 | 0.39 | 0.07 |
| DL-4 | 59.3 | 14.09 | 1.10 | 0.11 | 0.08 |
| DA-1 | 44.7 | 6.25 | 1.29 | 0.22 | 0.21 |
| DPE-2 | 61.4 | 5.44 | 1.52 | 0.31 | 0.28 |
| DAC-1 | 41.6 | 5.10 | 1.32 | 0.15 | 0.26 |
| DVE-2 | 50.9 | 3.66 | 1.34 | 0.00 | 0.37 |
| DGR-1 | 47.5 | 3.55 | 1.17 | 0.08 | 0.33 |
| DCV-2 | 59.1 | 3.71 | 1.38 | 0.41 | 0.37 |
| DSE-1 | 47.7 | 3.31 | 1.24 | 0.00 | 0.37 |
| DMAX-1 | 59.3 | 1.06 | 1.45 | 0.39 | 1.37 |
| MB4X | 51.9 | 6.16 | 1.60 | 0.14 | 0.26 |
| CLAN 1 | 44.9 | 1.83 | 1.15 | 0.11 | 0.63 |
| CLAN 2 | 39.7 | 3.01 | 1.20 | 0.10 | 0.40 |
| CLAN 3 | 42.2 | 3.21 | 1.36 | 0.12 | 0.42 |
| CLAN 4 | 45.9 | 4.49 | 1.65 | 0.19 | 0.37 |
| CLAN 5 | 44.8 | 4.24 | 1.47 | 0.15 | 0.35 |
| CLAN 6 | 47.2 | 2.72 | 1.62 | 0.13 | 0.60 |
| CLAN 7 | 38.5 | 1.99 | 1.42 | 0.15 | 0.71 |

TABLE 4-13

Elemental composition of kerogen isolates.

(Values are uncorrected for ash and moisture contents.
Relative errors in the determinations are within 5%).

| Variable | N | Order of chosen polynomial | <u>DEGREES OF FREEDOM</u> | | F-value |
|-------------|----|----------------------------------|---------------------------|----------------------------------|--------------------|
| | | | Due to regression | Deviation about regression | |
| Kerogen C | 26 | 4 | 4 | 21 | 7.61 ⁺ |
| Kerogen H | 26 | 5 | 5 | 20 | 3.82 ⁺ |
| Kerogen N | 26 | 3 | 3 | 22 | 0.99 |
| Kerogen H/C | 26 | 6 | 6 | 19 | 35.16 ⁺ |

TABLE 4-14 Analysis of variance for polynomial curves fitted to the stratigraphic variation in elemental composition of kerogen.

+ = significant at the 97.5% confidence level.

| | Height/width at $\frac{1}{2}$ height | $d_{002}^{\text{\AA}}$ (at I_{maximum}) |
|-----------------------------|---|--|
| graphite (fully ordered) | 30 | 3.35-3.36 |
| graphite-d ₁ | 3-15 | 3.35-3.36 |
| graphite-d _{1a} | 1-3 | 3.37-3.44 |
| graphite-d ₂ | 0.5-1 | 3.45-3.55 |
| graphite-d ₃ | 0.5 | 3.50-3.75 |

TABLE 4-15 Descriptive parameters characterizing different stages in the graphite-d-graphite series with respect to the $[002]$ peak.
(after Landis 1971).

| Sample | d_{002}° (at I_{maximum}) | Height/width at $\frac{1}{2}$ height | Degree of disorder | |
|--------|---|---|---------------------------|------------------------------|
| | | | based on basal spacing | based on ht./ width ratio |
| HL-9 | 3.35 | 0.90 | d_1 | d_2 |
| HL-8 | 3.34 | 3.79 | d_1 | d_1 |
| HL-7 | 3.34 | 1.50 | d_1 | d_{1a} |
| HL-4 | 3.35 | 1.44 | d_1 | d_{1a} |
| HL-6 | 3.36 | 2.83 | d_1 | d_{1a} |
| HC-1 | 3.35 | 2.36 | d_1 | d_{1a} |
| HL-10 | 3.37 | 0.76 | d_{1a} | d_2 |
| HL-11 | 3.36 | 4.00 | d_1 | d_1 |
| HRC-1 | 3.35 | 2.26 | d_1 | d_{1a} |
| HW-2 | 3.36 | 0.75 | d_1 | d_2 |
| HW-4 | 3.35 | 2.38 | d_1 | d_{1a} |
| HCL-4 | 3.35 | 1.60 | d_1 | d_{1a} |
| HG-1 | 3.34 | 2.43 | d_1 | d_{1a} |
| HW-3 | 3.36 | 2.25 | d_1 | d_{1a} |
| HCL-1 | 3.37 | 1.68 | d_{1a} | d_{1a} |
| HL-2 | 3.38 | 0.64 | d_{1a} | d_2 |
| HL-12 | 3.35 | 1.42 | d_1 | d_{1a} |
| HCL-6 | 3.36 | 2.79 | d_1 | d_{1a} |
| HL-13 | 3.41 | 2.20 | d_{1a} | d_{1a} |
| HL-14 | 3.40 | 2.60 | d_{1a} | d_{1a} |
| HL-15 | 3.37 | 0.76 | d_{1a} | d_2 |
| HL-16 | 3.37 | 0.72 | d_{1a} | d_2 |
| HG-2 | 3.31 | 2.42 | - | d_{1a} |
| HW-5 | 3.36 | 1.13 | d_1 | d_{1a} |
| DCL-1 | 3.35 | 1.76 | d_1 | d_{1a} |
| DL-4 | nd | nd | d_3 | d_3 |
| DA-1 | 3.35 | nd | d_1 | d_3 |
| DPI-2 | 3.37 | 0.81 | d_{1a} | d_2 |
| DAC-1 | 3.36 | 0.80 | d_1 | d_2 |
| DVE-1 | 3.35 | 0.73 | d_1 | d_2 |
| DGR-1 | 3.36 | 1.25 | d_1 | d_{1a} |
| DCV-2 | 3.40 | 0.80 | d_{1a} | d_2 |
| DSE-1 | 3.40 | 0.71 | d_{1a} | d_2 |
| DMAX-1 | 3.40 | 5.75 | d_{1a} | d_1 |

TABLE 4-16

X-ray diffraction parameters and degree of disordering of carbonaceous material isolated from the Moffat Shales.

| | | | | | | | |
|-----------------|----------------|-------------------------|--------|-----------------------|------------------------|--------------|--------------|
| Quartz | 1961w | 1613w | 1163sd | 1087s | 909sd | 800m 781m | 694m |
| Opal | 3333w 1859w | 1639w | 1220sd | 1087s | 952sd | 794m | |
| Chlorite | 3571 3125w | 1667w 1639w 1325w | | 1075sd 1026sd | 990s 952sd 870m | | 694m |
| Illite | 3597 3125w | 1667w 1639w 1325m | 1156sd | 1091sd 1026s | 909w | | |
| Kaolinite | 3636sh 3401 | 1667w 1639w 1325w | 1112 | 1100s 1030 1010 | 935sd 909s | 800m | 752m 690m |
| Montmorillonite | 3571 3125w | 1626w 1325m | | 1095sd 1025s | 909w 877sd 840sd | | |
| Calcite | 2488w 1792w | 1429sb | | | 877ssh 848w | | 709ssh |
| Magnesite | 2488w 1812w | 1449sb | | | 885ssh 848wsh | | 746ssh |
| Dolomite | 2500w 1812w | 1441sb | | | 877ssh 855w | | 725ssh |
| Aragonite | 2488w 1792w | 1456mb | | | 855ssh | | 709ssh |

TABLE 4-17

Wavenumbers in the infra-red absorption bands of the quantitatively important minerals in sedimentary rocks. (Adapted after Chester and Green 1968).

s = strong; m = medium; w = weak; sh = sharp;
b = broad; sd = shoulder.

C H A P T E R V

REFLECTED LIGHT STUDIES ON GRAPTOLITE FRAGMENTS

1. INTRODUCTION

The yield and distribution of soluble hydrocarbons and the sub-graphitic nature of the Moffat Shale organic isolates indicate that the sedimentary organic material in the sequence has been subjected to coalification and/or carbonization processes. The nature of the energy source responsible for the observed effects and the regional and stratigraphic variation of its strength is investigated in this chapter. The method employed incorporates the principal technique of the ore-microscopist and coal-petrographer, namely the measurement of reflectivity values of microscopic-sized particles. The particles used in this case to assess the rank of the sediments are the fossilised graptolite fragments which are common in most parts of the succession.

Throughout this chapter the optical properties of naturally carbonized graptolites will be compared and contrasted to those of coals of varying rank. At all times however, it must not be forgotten that coal and fossil graptolites have different chemical ancestries. Coal is an accumulation of carbonaceous material derived from the breakdown of vegetation with cellulosic, lignitic and proteinaceous affinities (Flaig 1968), whereas graptolites are of animal origin (Moore 1955; Bulman 1970) and are derived from proteinaceous material which is similar in structure and chemistry to types of collagen (Foucart et al., 1965; Towe and Urbanek 1972).

The physical, chemical and optical properties of coals which have been carbonized by the thermal effects of igneous intrusions have received widespread attention for many years. It has been reported that a low volatile coal (19 per cent volatile matter) was

unaffected by a 1200 feet thick dyke at a distance from it equal to the thickness of the intrusion (Heslop 1899). Later, it was found that the zone of alteration for coals cut by dykes in the Transvaal was related to the dyke thickness (Whitehead 1904). Contemporaneously, it was concluded that the form of alteration was also influenced by the nature of the dyke (Russel 1904).

Similar conclusions were reached from studies on heat-altered British coals (Hinxman et al., 1920; Macgregor and Anderson 1923). Consideration was then given to describing the various stages through which coal passed when subjected to rapid thermal metamorphism (Marshall 1936). Marshall not only described the changes in the original coal constituents as the dyke was approached, but also brought attention to the fact that with increasing temperature all but the inert materials disappear. He also observed the formation of a 'groundmass' which was composed of a granular aggregate of bodies intimately intergrown to form a dense mosaic. The description of mosaic textures and their relationship with coal rank and to discrete petrographic components was discussed later by Stach (1952).

Attention was drawn between 1950 and 1960 to the heat transfer properties and the carbonization characteristics of the coal components. Initially, it was concluded that the near horizontal attitude of coke prisms lying adjacent to dyke walls resulted from the poor thermal conductivity of coal in comparison to that of the enclosing sedimentary rocks (Marshall 1936). Later however, he implied the existence of two heat-flow regimes within the coal; one in the unaltered coal and the other in the zone of altered coal (Marshall 1945). Subsequently it was found by experiment that the

highest thermal gradient was found not in the unaltered coal as suggested by Marshall but in a very narrow zone, termed the plastic zone, which formed a boundary between the altered and unaltered coal (Brown 1956).

The carbonization behaviour of the individual petrological coal components has been related to rank (Abramski and Mackowsky 1952; Taylor 1957). It was found that the rate of heating of the coal specimens influenced the size of the coke mosaic units with higher heating rates being equated with larger areas of anisotropic coke having similar optical extinction. Taylor (ibid) concluded that the coal constituents could be divided into four groups whose boundaries were determined by the degree of anisotropy and mosaic-unit size in the resultant coke. Vitrinite was related to the predominant mosaic-like material in the coke and semi-fusinite to non-mosaic components showing slight shrinkage and general morphological affinities with unaltered semi-fusinite. Exinite was mostly expelled during carbonization but the fate of this component was found to be determined by maceral association and carbonization conditions (Alpern 1956; Taylor 1957). Exinite when slowly heated ($2^{\circ}\text{C}/\text{minute}$ to 500°C) was found not to fuse (Ergun et al., 1959).

In the past ten years or so the investigations of heat-affected coals have tended to centre on their optical and crystallographic properties, with special interest being taken in studies directed towards the investigation of the fine structure in the crystallites of the mosaic. Techniques such as mass-spectroscopy, NMR study, optical and electron microscopy and X-ray diffraction have been directed towards this end (Marsh et al., 1971).

Many petrographers have studied reflectance profiles of coals in contact with igneous intrusions (eg. Chandra 1963; Chatterjee et al., 1964; Pareek 1964; Kisch 1966a, 1966b; Schapiro and Grey 1966). In general, increasing reflectivity is found in the coal as the dyke is approached.

In the broader context, regional metamorphic effects have received detailed consideration by Teichmüller (1966); Mackowsky (1968); Paproth and Wolf (1973). They jointly conclude that time, pressure and temperature play important roles in determining the rank and reflectivity values reached by coals during metamorphism. Temperature is believed to be the most important factor influencing the reflectivity of coals (Teichmüller 1949; Dulhunty 1954; Huck and Karweil 1955) while pressure can influence, in an unpredictable manner, the maximum reflectivity or the degree of anisotropy (Chandra 1965; Mackowsky 1961).

In the last decade the study of the change in coal rank by coal petrographers has firmly established the notion of the metamorphic nature of progressive coalification. Attempts have been made to correlate the changes in the rank of coals with the changes in the mineralogy of associated sedimentary and volcanic rocks (eg. Kisch 1966, 1968, 1969, 1974; Kisch and Taylor 1966).

Data collected from coals and coaly matter associated with various burial and regional metamorphic facies show that the 'anchimetamorphic' zone (Kubler 1968) and the 'stage of early metagenesis' (Kossovskaya and Shulov 1970) are normally associated with coals of anthracite rank but locally also with semi-anthracites (Kisch 1974). It is also considered that the prehnite-pumpellyite-

metagreywacke facies and the glaucophane-lawsonite-schist facies are associated with a similar range of anthracite coal ranks, although the beginning of the prehnite-pumpellyite-metagreywacke facies is associated with lower rank coals (low-volatile bituminous) than is the beginning of 'anchimetamorphism'.

The transition of 'anchimetamorphism' or 'very low stage' metamorphism (Winkler 1970) to the epizonal greenschist facies appears to be associated with coals close to the anthracite to meta-anthracite boundary and generally with low-grade meta-anthracites (Kisch 1974).

The variation of vitrinite reflectance values has also been related to the lithology of the enclosing sediments and in particular to that of the roof strata (Jones et al., 1971). It is believed that there are two coalification tracks for vitrinite reflectivities; one for seams overlain by shales, the other for seams with sandstone roofs.

It is now possible with careful preparation to isolate and measure the reflectivities of tiny carbonaceous particles in shales and limestones and thereby determine the rank of the organic material in the sediments. This rank is of interest to oil and gas exploration companies who have related the metamorphic regime in the reservoir basin to the genesis of hydrocarbon deposits (Hacquebard and Donaldson 1970; Shibaoka et al., 1973; Eames 1974).

Now that equipment is available for measuring the reflectivity of very small coal particles it seems logical that a study be made of other types of dispersed carbonaceous fragments in rocks. Land plant fragments are customarily used in rank studies,

but are largely absent from the Lower Palaeozoic. Graptolites are, however, most commonly preserved as carbonaceous films, thus lending themselves to study by this technique, and extending rank studies to the Lower Palaeozoic, as well as to the marine sedimentary environment.

2. PRINCIPLES OF REFLECTANCE MEASUREMENT ON COALS

Measurement of the reflectivity of coals shows that with increasing rank there is a progressive increase in both maximum reflectivity and bireflectance. Maximum reflectivity is always quoted in percentage terms and has a real unitary basis whereas bireflectance, being derived from the difference between maximum and minimum reflectivity has only a numerical value.

Almost all reflectivity measurements on coal are made on the vitrinite component which mostly behaves as if it was a crystallographic uniaxial negative mineral. In some instances however, vitrinites affected by high geothermal gradients behave as if they were biaxial minerals (Cook et al., 1972a). The crystallographic configuration of the vitrinite determines the form of the reflectivity measurement. For example if an uniaxial negative coal is rotated on a microscope stage and the reflectivity measured, a series of maximum and minimum signal peaks are produced. This series, because of the symmetry of the system, is made up of two maximum and two minimum peaks each separated by 90 degrees. The maximum reflectivity remains constant and is unaffected by the orientation of the coal sample, while the minimum value varies in relation to the orientation of the crystallographic section. Coal sections cut perpendicular to the bedding exhibit the true minimum reflectance value and hence the greatest bireflectance.

In sections parallel to the bedding the maximum and minimum values converge and consequently this section is isotropic.

The maximum reflectivity value of a coal is therefore always taken as the diagnostic value. When it is required to measure the minimum value or to assess the bireflectance it is necessary to prepare perpendicular sections.

3. METHOD OF MEASURING GRAPTOLITE REFLECTIVITY VALUES

Small fragments of shale and mudstone were mounted in resin and the surface polished with alumina powders. Reflectance measurements were then made on the graptolite fragments with micro-reflectivity equipment which comprised a Leitz MPV microscope photometer connected to a Philips PM 8220 pen recorder. Absolute reflectivity values were obtained by comparing the signals from the graptolite fragments with that of a polished diamond standard mounted in 'Bakelite' in the form of a wedge. Further details of the method and of the equipment used are given in Appendix B.

4. PRELIMINARY INVESTIGATION OF GRAPTOLITE REFLECTIVITY VALUES

The level of reflectivity attained by graptolite fragments in the Lower Palaeozoic of the South of Scotland was assessed initially by measuring a fossiliferous mudstone containing abundant examples of Orthograptus truncatus (Lapworth). The sample was collected from the linearis Zone exposed in the Main Cliff at Dobb's Linn. The block was cut, mounted and polished in the usual manner and reflectivity measurements taken under oil at 546 nm over the surface of a single graptolite lying in the plane of the bedding.

The resulting chart recording (Fig.119) indicates that with each rotation through 360° there are alternating peaks and troughs every 90° . These are of varying intensity and can be related to minimum and maximum reflectance values. By taking only the largest peak of each rotation a mean reflectance value (R_o mean-max) of 6.57 ± 0.6 per cent is computed. Such a value implies, if direct comparison can be made with the behaviour of vitrinite, that the organic material in the sample is of anthracite rank with a dry-ash-free carbon content of about 96 per cent (McCartney and Teichmüller 1972).

Vitrinites however, are normally considered to be crystallographically uniaxial negative with the isotropic section in the plane of the bedding. This specimen is clearly not displaying an isotropic section in the bedding-plane nor are the maximum reflectance values constant with varying minimum values. The question is therefore raised as to whether or not these graptolite remains can be treated as an uniaxial negative material.

5. THE POSITION OF THE ISOTROPIC SECTION IN GRAPTOLITES

a) Results

A detailed investigation of the variation of the reflectivity of graptolites cut at various angles to the plane of the bedding was performed on a block of black mudstone collected from an exposure of the clingani Zone at Hartfell in an attempt to determine the position of any isotropic sections and determine the crystallographic indicatrix to which the graptolites of the Moffat Shales approximate.

Reflectivity measurements were made in air and in oil at various wavelengths over a specimen of Climacograptus scalaris (Hisinger), which exhibited a good polish with negligible relief effects, firstly, in the plane of the bedding and then after repeated cutting and repolishing, at angles of 57° , 74° and 90° to the plane of the bedding (Fig.120). Maximum and minimum reflectivities in oil and in air at each of the four positions are given in Table 5-1.

Inspection of the reflectivity data indicates that there is a linear relationship with wavelength (Fig.121). This relationship has been quantified by means of linear regression analysis which indicates that the reflectance values for each of the four sections are linearly related to wavelength at the 99.9 per cent confidence level. Random fluctuations in the results have been eliminated by calculating estimated reflectivity values from the regression parameters which are given in Table 5-2. Estimated bireflectance values were then found from the difference between estimated maximum and estimated minimum reflectivities (Table 5-3).

In no instance do the bireflectance values indicate an isotropic section. The nearest they approach a zero bireflectance is in the section parallel to the bedding measured at 410 nm where even then there is a noticeable difference between maximum and minimum values of 0.3. Bireflectance is at a maximum of 1.6 in the 57° section measured in air at 710 nm. Values then decrease in the 74° section and finally drop to an intermediate value of 0.5 in oil and 0.75 in air at 410 nm in the section cut perpendicular to the bedding plane.

The variation in bireflectance with the angle of section is obviously a function of the trends in maximum and minimum reflectance values (Fig.122). For a fixed wavelength the maximum

reflectivity decreases slowly while the minimum drops more markedly between the parallel and the 57° section. At angles of between 57° and 74° both minimum and maximum reflectivities increase at similar rates while between 74° and the perpendicular section both minimum and maximum values decrease in the sections measured in oil but there is a slight tendency for minimum reflectivities measured in air to increase.

b) Discussion

The bireflecting property of coals and cokes is often likened to the birefringence of many rock-forming mineral crystals and the concept of a birefringence indicatrix has been translated to a bireflectance indicatrix. Such an indicatrix represents by means of three orthogonal axes the relative reflectivities of the organic material measured in differing directions usually with respect to the bedding plane. The lengths of the axes are proportional to the reflectivities in these directions.

Normal coals usually have a uniaxial negative bireflecting indicatrix with the axes in the horizontal (bedding) plane equal in length and longer than the single vertical axis (Fig.123). A positive uniaxial figure is the reverse of this configuration ie. the single vertical axis is longer than the horizontal axes. The biaxial configuration is rather more complex with all three axes of unequal length (Fig.123).

In the uniaxial configuration there is only one possible circular section ie. a section containing the two equal axes which is therefore isotropic since it does not exhibit bireflectance. This

section lies in the horizontal plane. With a biaxial indicatrix there are two possible circular sections, both of which are equally inclined to the horizontal. In common with terminology related to birefringence indicatrices, the term optic axis is retained to indicate that axis which lies in a direction perpendicular to the circular section. A uniaxial indicatrix has thus one and a biaxial indicatrix two optic axes.

The results presented for the variation of graptolite reflectance values with the angle of section are inconclusive. The variation in both maximum and minimum values from one part of the sample to another renders the possibility of a uniaxial configuration unlikely. Until the positions of the isotropic sections are located, it must however remain a tentative suggestion that the graptolites of the Moffat Shales are behaving as a biaxial material.

The anisotropy displayed by the graptolite fragment in the plane of the bedding may be due to a number of causes which may have acted singly or jointly to produce the observed effects. Firstly, as graptolites tend to be long and slender it may be that they are displaying a form of zoological anisotropy in the same way as some of the form anisotropy of vitrinite is mimetic after that of the parent-plant material (Saleh 1968).

Another cause might be that the growth of structural elements in the graptolites was governed by the pressure field acting upon them. In coals, the lamellae appear to grow so that the plane of the lamellae is orientated perpendicular to the direction of maximum stress (Cook et al., 1972a). In a triaxial stress regime it is considered that the lamellae would tend to be elliptical rather than

circular discs, with the long axes of the disc parallel with the minimum stress direction. Such a structure should have biaxial optical properties and with a small degree of ellipticity it would be optically negative. Pressure may well have influenced the anisotropy of the graptolite fragment because it and the enclosing sediment have without doubt suffered the full effects of the Caledonian orogenic movements.

Thermal alteration might also give a biaxial character to the graptolite fragment. This type of effect has been described for a British Devonian meta-anthracite coal (Cook et al., 1972b). It is of relevance to observe that both this meta-anthracite and the graptolite fragment show a pronounced increase in reflectance values from the blue to the red in the visible spectrum whereas coals of lesser rank show decreasing values from the blue to the red (Cook et al., 1972b).

6. THE VARIABILITY OF MEAN-REFLECTANCE VALUES

a) Variation within a total sample

So far in this study the reflectance values of the graptolites have been examined using the method of rotation to find the position of the maximum reflectivity. This technique however is not satisfactory when dealing with extremely small carbonaceous fragments because due to the inherent physical instability of the microreflectivity equipment it is not possible to rotate exactly about a fixed point. cursory examination of the resin blocks prepared from the Hartfell Shale samples revealed that many contained organic fragments which were too small for rotation analysis.

A series of experiments was therefore conducted with a view to ascertaining the variability of mean reflectance values in a sample. In this work mean reflectance values are defined as the average reflectivity at a particular wavelength in a plane perpendicular to the bedding and as such do not have the same connotation of the 'mean' value of coal petrographers which is a function of the reflectivity of particles measured in unpolarised light.

A total of 53 reflectivity measurements was made at random in oil at 546 nm over the surface of the organic material in sample LBR-9. This sample was collected 5.7 metres from the 9.18 metre thick porphyrite dyke exposed in Clanyard Bay. The computed single variable statistics for the reflectivity of the total sample are given in Table 5-4. In statistical terms, the null hypothesis that the distribution of values illustrated in Fig.124a is normal, can be rejected with a probability of 0.98 of being incorrect.

b) Variation over a single fragment

The variation in mean reflectance values over a single carbonaceous fragment measuring 50 x 35 microns was investigated. A total of 135 measurements were made in oil at 546 nm over most of the surface of the particle at the intersections of a rectangular grid using a 1 micron measuring aperture. The single variable statistics for the data tabulated in Table 5-5 are given in Table 5-4 and the results are graphed in Fig.124b.

The areal variation of the mean reflectance values was further investigated by means of a contouring technique which utilises trend-surface analysis. The technique and computer program used was

that of Cole (1969). Further details of the method are given in Appendix C.

In normal usage, this computer program provides only iterative-surface, global-fit surface, and difference maps for the 'best-fit' polynomial surface defined in terms of the sums of squares explained. In this study however, first, second and third order polynomial surfaces have been forced upon the data in order to derive the maximum possible information. The degree of fit of the various surfaces is given in Table 5-6 and the computed maps illustrated in Figs.125-133.

Each of the iterative maps (Figs.125, 128, 131) produced after 10 iterations over the linear, quadratic and cubic surfaces indicate a general rise in reflectivity from the lower left to the upper right corner of the fragment. There are several localised areas with either elevated or depressed reflectivities superimposed upon the general trend. These localized 'anomalous' areas are mapped in detail in the difference maps (Figs.127, 130, 133) which although of similar form for each of the three surfaces show differences in the distribution of the 'anomalous' areas. Such areas are more widely distributed in the difference maps of the higher order surfaces.

The global-fit surface maps which are essentially trend maps with local peculiarities in the data filtered out become, by definition, more complex with higher orders of surface (Figs. 126, 129, 132). Examination of the maps for all three orders of surface reveals that in each case there is an overall increase in reflectance values over the fragment from the lower left to the upper right. Fit-values for the quadratic and cubic global-fit surfaces (Table 5-6) indicate that more significant maps are obtained when some of the

elevated reflectivities of the upper left corner are contoured more accurately.

c) Computation of trend surfaces for reflectivities generated at random over the surface of a fragment

The technique used in the program of Cole (1969) to estimate the degree of fit (ie. a sums of squares method) although informative, is not decisive when assessing the significance of a chosen surface. However it has been found that if a sums of squares test for greater than 100 data points produces values that are greater than 6.0, 12.0 and 16.2 per cent for the linear, quadratic and cubic surfaces respectively then the distribution of data is significantly different from random at the 0.05 level (Howarth 1967).

Although the diagnostic values proposed by Howarth (1967) are exceeded in this work, the significance of the computed surfaces was investigated further by computing the trend surface maps for randomly generated reflectivity data distributed over the area of the graptolite fragment examined above. Reflectivity values produced at random using an IBM 44 MFT package (CLNORM) to give a normal distribution with the properties of that illustrated in Fig.124b were positioned at the intersections of the rectangular grid constructed over the surface of the particle. The derived random reflectance values are given in Table 5-5.

The linear, quadratic and cubic iterative, global-fit and difference maps resulting from trend surface analysis over the distribution of random reflectance values are illustrated in Figs. 134-142. The sums of squares fit values are given for each surface in Table 5-6.

Several observations result from comparison of the maps produced for the random data with those produced for the measured data viz:- the iterative and global-surface fits are poorer for the random data; sums of squares fit values for the quadratic and cubic surfaces generated for the random data lie within the proposed limits set by Howarth (1967) for random data, while that of the linear surface lies just above the critical value; the iterative surface fits of the random data decrease with increasing order of surface whereas those of the observed data increase; the iterative and difference maps are more complex for the random data and finally the global-fit maps for the random data indicate shallower structures dipping in a perpendicular direction to those of the observed data.

d) Discussion

The results presented indicate that the maps derived for the variation in reflectance values over the surface of the graptolite fragment are statistically significant and that the variation in values has a real cause. The interpretation of the variation in values depends upon which order of surface is statistically most significant. This was found to be the cubic surface by the sums of squares method but this need not have been so if for example a more complex analysis of variance test of significance had been used.

Considering firstly the planar global-fit trend. The variation in reflectance values might be explained if the sample was tilted during measurement. It has been found that when using the Berek-prism illuminator the reflectivity increased to a value greater than the normal maximum as the angle of tilt was increased from the horizontal to about 3° (Melvin 1973). Thereafter values dropped with

increasing amount of tilt. This effect in itself does not explain the computed trend in values but if the sample was tilted and the microscope focus was not adequately adjusted to compensate for the changing focal distance, the reflectivity values would vary in accordance with the trend observed by Jones (1961). In this latter work it was noted that departure from focus in a direction which diminished the stage-objective distance apparently decreased the reflectivity of the specimen, whereas values increased with larger distances (Fig.143).

The effects of tilt can always be recognised on reflectivity chart records produced by rotation analysis. Several rotation measurements were made over the surface of the fragment and the resulting trace did not display the consistently asymmetrical peak maxima lying in the same direction which are typical of tilted samples but instead the maximum peak heights were observed to vary in an irregular manner. Such a variation may indicate relief effects produced as a result of polishing.

The more complex quadratic and cubic trends may indicate some form of folded layered structure within the fragment similar to the primary structures of graptolites (Urbanek and Towe 1974 Plate 23). It is also possible that the variation in reflectivity values is attributable to heat flow structures as a result of thermal metamorphism of the carbonaceous material (Aganoglu 1972).

7. THE REFLECTIVITY OF CARBONIZED GRAPTOLITES

a) Introduction

During the preliminary work on the reflectivity of graptolites it was thought possible that the carbonaceous fragments examined were displaying the effects of heat. It was therefore decided to investigate the reflected light properties of naturally carbonized graptolites.

The locality chosen for such a study was the northern part of Clanyard Bay situated on the west coast of the Rhinns of Galloway [NX 101381] (Fig.5). Here, there is exposed a series of graptolitic shales and mudstones of Upper Hartfell to Upper Birkhill age. These are cut by a number of porphyrite dykes, the largest of which is 9.18 metres thick. The detailed geology of this locality is described above (Chapter I, section 2b).

b) Sample collection

Two suites of samples were collected at Clanyard Bay. The first suite, designated the LB-series, was collected along a parallel trend to that of the sinistral wrench fault (ie. 330°) and includes samples from both sides of the dyke (Fig.144). Samples LB-12 to LB-18 are from the south side and samples LB-20 to LB-24 are from the north side of the dyke. The second suite of samples designated the LBR-series, was collected at an oblique angle to the northern contact of the dyke so that samples could be collected from either side of the fault. Samples LBR-1 to LBR-19 are from the east side of the fault and samples LBR-20 to LBR-24 are from the west side of the fault. The position of the samples with respect to the dyke and details of the sample lithologies are given in Table 5-7.

c) Petrography of the dyke

The 9.18 m thick dyke at the north end of Clanyard Bay is similar in composition and texture to the majority of those from the Caledonian dyke swarm in South Galloway which have been described as sheared porphyrites (Blyth 1949). The dyke displays typical directional textures, due to shearing, which are discernible under the microscope by the alignment of mafic constituents.

In hand specimen the rock is pale grey in colour and even textured. Under the microscope it is observed to have a porphyritic texture consisting of phenocrysts of plagioclase, pyroxene and quartz set in a fine grained groundmass of feldspar, chlorite, muscovite and quartz. Some of the larger crystals of chlorite pseudomorph biotite. Accessory minerals include sphene, pyrite and magnetite. The most abundant phenocrysts are of well zoned sericitised plagioclase feldspar. Quartz phenocrysts are rare but when observed they display undulatory extinction. Representative fields of view are illustrated in Plates 1 and 2.

d) Macroscopic variation in the samples with distance from the dyke

Approaching the 9.18 metre thick dyke from the south, the sediments do not appear to have been heat affected to any great extent. Indeed, the pyrite mineralization associated with some of the samples is similar to that found at Hartfell and Dobb's Linn, the type localities for the Hartfell and Birkhill Shales. Lithological description of the samples is given in Table 5-7.

On the north side of the dyke, the sediments are more obviously heat affected. This may partly be because whereas grey

mudstones predominate on the south side, black shales and mudstones are more common on the north side. Immediately adjacent to the northern contact of the dyke there is a 0.76 metre wide wave-eroded depression containing crumbly, badly sheared pyritised shales which as well as being slickensided appear to have flowed. As a result of the nature of the sediments, great difficulty was experienced in collecting samples of suitable size for reflectivity measurement from this zone. At one stage a portable drilling machine was employed but attempts were unsuccessful due to the friable state of the sediments. There are no obvious signs in any of the hand-specimens that samples collected further than one metre from the dyke have been heat affected.

e) Microscopic changes in the graptolite fragments with distance from the dyke

The field orientated samples were cut perpendicular to the bedding plane, set in resin and polished according to the standard procedure for microscopic examination under reflected light. The polished surfaces were studied with a Zeiss 'Standard Universal' microscope using both strain-free planachromatic air and oil immersion 'Eiplan Pol' objectives and 'Antiflex' oil-immersion objectives. Magnifications employed ranged from x 150 to x 400.

In polarised light with air objectives the polished surfaces of the organic material show no structures but do exhibit small cracks and scratches which were produced during preparation. Individual fragments are highly reflecting. When immersed in oil and examined under partly crossed polars various types of structure

are visible in the samples. The occurrence of each type may be related to the distance the sample is from the dyke contact.

Structures, which are similar to those found in carbonized coal macerals, are first observed in the graptolite fragments at a perpendicular distance of 15.4 metres from the dyke contact. The organic material in sample LB-13 although very sparse and finely comminuted displays a noticeable vesiculation. (Plate 3). This vesiculation pervades the surface of the fragments in such a way that quantitative measurement of reflectivity is rendered very difficult. Moving nearer the dyke, the amount of vesiculation decreases until in sample LB-14 (11.1 metres from the contact) only a few vesicles pock the surface of the organic material. In sample LB-15 (7.6 metres from the dyke) the few remaining vesicles are much enlarged (Plate 4). Vesiculation is almost absent in sample LBR-29 (5.3 metres from the dyke). In this sample a brittle texture is manifested by a series of fractures cutting through and splitting the organic material (Plate 5). Larger scale vesiculation is evident once more in sample LBR-15 (2.30 metres from the dyke).

A new texture appears 1.10 m from the dyke in sample LBR-9 and consists of distinct anisotropic granular aggregates forming a mosaic which is pocked by vesicles. Mineral interference is not uncommon (Plate 6). This granularity is not evident in sample LBR-7 (0.9 metres from the dyke) but instead a texture consisting of a number of concentric, alternating dark and light bands is observed under partially crossed polars (Plate 7). The appearance of this flow texture close up to the dyke is discussed below (p.129).

Granularity is again evident in sample LBR-3 (0.76 metres from the dyke, Plate 8). As the dyke is approached, the granules

increase in size until at 0.69 metres from the contact the organic material in sample LB-18 displays a pronounced granularity superimposed upon which there is a series of large scale vesicles. These are now more variable both in shape and size and are often infilled with mineral matter (Plate 9).

The sequence of textural changes in the graptolite fragments is closely analogous to that described for thermally altered vitrinites (Aganoglu 1972). The main contrast lies in the position of the flow stage. The graptolite fragments exhibit flow-type textures closer to the dyke than the first indication of shearing and the development of granularity. In the progressive thermal alteration of vitrinites, flow is known to occur between shearing which occurs before the development of granularity (Aganoglu 1972).

The observed flow-type texture may not be the result of thermally induced processes but instead, could be a manifestation of the original layered structure of the graptolite periderm (Urbanek and Towe 1974). If carbonization is responsible then it is likely that some form of physical break occurs between samples LBR-9 (granular texture) and LBR-7 (flow texture). Field evidence for such a break is lacking but examination of sample LBR-8 which was collected between sample LBR-7 and sample LBR-9 reveals that it is a badly cleaved flaky black shale similar to those found adjacent to the thrusts at Hartfell. The organic material in this sample is also sheared (Plate 10).

The indications therefore are that there is a fault in close proximity to sample LBR-8. The observed sequence of textures would be explained if this fault was of the reverse type. Such

faulting has already been described at Clanyard Bay (Chapter I section 2b) and is not uncommon in the Lower Palaeozoic of the Southern Uplands (Mitchell 1974; McKerrow and Mitchell 1975).

f) Variation in reflectivity with distance from the dyke

Mean-maximum reflectivities of the LB-series of samples collected from the south side of the dyke were assessed at 546 nm in oil using a rotation technique. As many of the graptolite fragments were extremely small the method employed was to centre each particle on the microscope stage and measure the reflectance. The stage was then rotated through 15° and the reflectance of the particle measured after re-centring. This procedure was repeated until values were obtained for one complete revolution. Twenty particles in each sample were measured in this way and the mean-maximum reflectivity was obtained by averaging the twenty strongest signals. An estimate of the minimum reflectivity was obtained by averaging the twenty least intense signals (Table 5-8).

The variation of mean-maximum reflectivity with distance along the measured section at Clanyard Bay is illustrated in Fig.145. It is apparent that values increase towards the dyke but it is difficult to fit an accurate curve to the few data points. When the best-fit second order polynomial curve is computed it is found to be significant only at the 95 per cent confidence level (F-value = 3.59). Although the best-fit third order polynomial gives a F-value of 5.54 it is significant only at the 90 per cent level.

Incremental rotation of a sample to derive the mean-maximum reflectivity is a very laborious procedure which without doubt

gives rise to many errors. It was therefore decided to measure the mean reflectance values of the samples and compare the results with those found above. Mean reflectance values measured perpendicular to the bedding were calculated from the results of 20 or so measurements over the surface of each sample. A representative chart-recording is illustrated in Fig.146 and the results are given in Table 5-8. Comparing the results of the two methods it is found that there is a high linear correlation between mean-maximum reflectivity and mean reflectivity (correlation coefficient 0.90). The linear regression line drawn through the data points (Fig.147) is significant at the 99.9 per cent confidence level and is computed to have an intercept of 1.223 and a slope of 1.574. It is appreciated that the true maximum reflectivity is not recorded when assessing mean values but nevertheless it is considered that more accurate and meaningful trends can be constructed for this parameter.

Fig.148 is the plot of mean reflectivity of graptolite fragments in oil at 546 nm versus distance along the section at Clanyard Bay. The data for the samples collected from the south side of the dyke fit a second order polynomial regression curve at the 95 per cent confidence level. A curve with similar confidence limits is obtained for the data from the north side of the dyke when the reflectance value of sample LB-20, collected adjacent to the dyke, is omitted from the calculation. The anomalously low reflectivity of the organic material in this sample is a common phenomenon that has been attributed to adsorption effects by mineral material (Melvin 1967; Aganoglu 1972). Regression parameters and values of reflectance estimated from the curves are given in Table 5-9.

The reflectivity of the organic material in the LBR-series of samples was measured in an attempt to elaborate upon the trend displayed by the LB-series on the north side of the dyke. The values obtained are reported in Table 5-10 and their relationship with the perpendicular distance to the middle of the dyke is illustrated in Fig.149.

The data may conveniently be subdivided into three sub-groups viz:- values for samples LBR-1 to LBR-12, samples LBR-13 to LBR-18 and samples LBR-20 to LBR-25 (sample LBR-19 was not measured). The data of the first sub-group which encompasses the first 1.5 metres from the dyke contact displays no obvious trend with distance from the dyke. The second group of reflectance values, encompassing the next 1.5 metres of strata, is linearly correlated with distance. Regression analysis reveals a line with an intercept of 27.5 and a slope of -3.3 which is significant at the 99.9 per cent confidence level. The third group of reflectance values, extending from 8.0 to 12.0 metres from the contact, is also linearly correlated with distance. This line however, with an intercept of 9.73 and a slope of 0.38 is only significant at the 97.5 per cent confidence level.

g) Variation in the bireflectance ratio with distance from the dyke

It is possible, knowing maximum and minimum reflectance values, to derive an estimate of the degree of molecular ordering in the graptolite carbonaceous fragments by calculating the parameter described as the bireflectance ratio. This is defined in the following way:-

$$\text{Bireflectance ratio} = \frac{\text{Ro(max)} - \text{Ro(min)}}{\text{Ro(max)}}$$

Where $R_o(\max)$ is the maximum reflectivity in oil at a fixed wavelength and $R_o(\min)$ is the minimum reflectivity in oil at the same wavelength.

Bireflectance ratios were calculated for samples LB-12 to LB-18 collected from the south side of the dyke (Table 5-8). Values range from 0.26 at 12.21 metres from the dyke centre to 0.75 at 6.58 metres from the dyke centre (Fig.150). Because of the large spread in the data it was not possible to compute any realistic trends for the variation in the bireflectance ratio with distance from the dyke but the following general observations may be made. It appears that on approaching the dyke the bireflectance ratio first increases then falls to a minimum value at approximately 9 metres from the dyke contact. The value then increases to a maximum of 0.75 within 2 metres from the contact before plunging steeply to a value of 0.33 near the contact.

h) Discussion

On the south side of the dyke, the variation in graptolite reflectance values with distance from the dyke is qualitatively similar to the changes observed in vitrinites which have been carbonized by the thermal effects of intrusive bodies. Quantitatively however, the values recorded for the graptolites are much greater than for vitrinites. For example, the mean-maximum reflectivity of vitrinite adjacent to a 100 mm thick tholeiite dyke at Collywell Bay in Northumberland increases from 1.0 per cent at 50 mm from the contact to a maximum of 5.0 per cent at the contact (Aganoglu 1972). The enhanced values at Clanyard Bay may possibly be related to the higher

metamorphic grade of the sediments at this locality.

Likewise, the variation in the bireflectance ratio with distance from the dyke is comparable in trend, although not in absolute values, to the variation observed in carbonized vitrinites (Aganoglu 1973). The bireflectance ratio of the vitrinite at Collywell Bay ranges from zero, indicating complete disorder, at a distance equal to the thickness of the dyke to a maximum of 0.21, indicating relatively good ordering of the carbonaceous material 20 mm from the dyke. It is noteworthy that maximum disorder occurs in both the vitrinite and graptolite fragments at a distance equal to the thickness of the intrusion.

The maximum degree of ordering in both types of particle occurs a short distance away from the dyke contact. This is so in the graptolites because the bireflectance ratio of the sample immediately adjacent to the dyke is depressed because of an unusually high minimum reflectance value (Table 5-8). This may be attributed to absorption effects on the organic material by mineral matter produced from percolating hot solutions. These effects can be particularly strong in the vicinity of fault planes (Cooper et al., 1974).

On the north side of the dyke there are three obvious discontinuities in the graptolite reflectivity trend with distance. These breaks occur between samples LBR-7 and LBR-8 (5.5 metres from the centre of the dyke), between samples LBR-12 and LBR-13 (6.2 metres from the centre of the dyke) and between samples LBR-18 and LBR-20 (about 10 metres from the centre of the dyke). From observations on the textures developed in the carbonaceous material it was concluded

in section 7c of this chapter that the discontinuity in the vicinity of sample LBR-8 was probably due to a reverse fault. This hypothesis is further substantiated by the break in the trend of reflectivity at this point. It therefore seems not unreasonable to postulate that the other two breaks in the reflectivity trend also indicate the position of reverse faults. If this is so then it is implied that reverse faulting at Clanyard Bay post-dates the intrusion of the dyke. This is consistent with the proposal that the Caledonian porphyrite dykes of this region were intruded along fault planes which were later reactivated (Blyth 1949).

8. DISPERSION WITH WAVELENGTH OF THE OPTICAL PROPERTIES OF CARBONIZED GRAPTOLITES

a) Reflectivity

The spectral variation in the reflectivity of carbonized graptolites was assessed both in air and in oil for samples LB-12 - 18 and samples LBR-3, LBR-7, LBR-8, LBR-9 and LBR-13. Ten reflectance measurements were made in each of the two media at 410, 442, 502, 546, 590, 651 and 710 nm over a surface of each sample cut perpendicular to the bedding. Average values at each of the seven wavelengths are given for the samples in Table 5-11.

Spectral trends for the variation in reflectivity have been computed by fitting least-squares polynomial regression curves to the data. Regression line parameters are given for the curves in Appendix D and the values estimated from the curves for the reflectivities in oil and in air ($Rest^1$ and $Rest^2$) are tabulated in Table 5-11.

As a result of correlation analysis it is found that there is an excellent linear correlation at each wavelength between the logarithm of the estimated reflectance in oil and the perpendicular distance of the sample from the centre of the dyke. The correlation coefficients derived from product moment correlation analysis exceed 0.90 in every case and the resulting regression lines are all within the 99 per cent confidence level. The regression parameters for the lines which are illustrated in Fig.151 are presented in Table 5-12.

The equation of the line for the variation in reflectance with distance at 546 nm has been used to calculate, using the mean reflectance values of the LBR-series of samples, the approximate position of these samples relative to the dyke before thrust-faulting. These estimated distances are given in Table 5-9.

Inspection of Fig.151 drawn to illustrate the variation in reflectivity at several wavelengths with distance from the dyke, reveals that there is a larger variation in values at the blue end of the visible spectrum. From this, it might be implied that the most suitable wavelength for the study of reflectance values of carbonized graptolites is to be found in the vicinity of 400 nm. Any sensitivity gained by measuring in this region would, however, be undoubtedly lost due to the inherent inefficiency of the apparatus at low wavelengths (for further details see Appendix B).

Observations pertaining to the spectral variation of the reflectivities in oil and in air for the graptolite fragments in the samples collected from the south of the dyke at Clanyard Bay are described in Appendix D.

The computed trends for the variation with wavelength of

the reflectivity of the samples from the north side of the dyke are similar to those described for the majority of the samples from the south side of the dyke with the reflectance values of all five samples increasing from the blue to the red (Figs 156-158). Unlike the samples from the south of the dyke, the reflectance values at a fixed wavelength of the samples to the north do not increase with distance from the dyke but appear to vary in an irregular manner.

The variation in reflectivity with wavelength for the twelve samples has been further simplified by computing linear regression curves for the data. This simpler statistical technique has been employed in preference to the more complex polynomial regression analysis in order to amplify general trends in the data. These trends are illustrated by the lines depicted in Fig.159 while the regression parameters of the lines are given in Table 5-13.

The trends illustrated in Fig.159 for the LB-series of samples indicate that as the dyke is approached there is a gradual increase in the rate of change of reflectivity with wavelength and that most samples display a direct relationship with wavelength. The reflectivity of samples close to the dyke appears to vary inversely with wavelength.

If this relationship holds for the LBR-series, then the position and slope of the curves pertaining to this series indicates that the samples may be arranged with respect to distance from the dyke at the time of intrusion. In this way it is assessed that sample LBR-8 was closer to the dyke than sample LBR-7 which was closer than samples LBR-3 and LBR-9. Such a sequence is consistent with that which may be deduced from reflectivity values alone. Further evidence

for tectonic activity after intrusion of the dyke is therefore afforded by studying the dispersion with wavelength of the reflectivity of graptolite fragments.

b) Refractive and absorptive indices

Since the variation of reflectivity with distance from the dyke showed certain significant features it was decided also to examine the trends of the fundamental parameters which combine together to produce the reflectivity value, namely the refractive and absorptive indices. The reflectivity R_o , of a specimen having a refractive index n , and an absorptive index k , when measured in a medium of refractive index n_o , is given by;

$$R_o = \frac{(n - n_o)^2 + n^2 k^2}{(n + n_o)^2 + n^2 k^2}$$

Clearly, by measuring the reflectivity of a sample in two media of differing refractive index, both n and k can be calculated.

If one of the media is air, ie. $n_o = 1$ then the reflectivity in air R_a , is given by;

$$R_a = \frac{(n - 1)^2 + n^2 k^2}{(n + 1)^2 + n^2 k^2}$$

Then by solving the two equations for n and k the following is obtained;

$$n = \frac{(n_o^2 - 1) / 2}{\frac{n_o (1 + R_o)}{(1 - R_o)} - \frac{n_a (1 + R_a)}{(1 - R_a)}}$$

$$\text{and } k^2 = \frac{R_a (n + 1)^2 - (n - 1)^2}{n^2 (1 - R_a)}$$

Values of refractive and absorptive indices have been calculated for those samples collected from Clanyard Bay which have been subjected to dispersion analysis (Table 5-11). These values have been calculated from the estimated reflectance values derived from the dispersion curves depicted in Figs. 152-157. This procedure has been adopted in preference to calculating the indices from 'raw' reflectance data in order to minimize random fluctuations in the reflectance values and thus improve the precision of the absorptive and refractive indices.

Refractive index values of the LB-series of samples at 546 nm correlate with distance from the dyke in a similar fashion to mean maximum reflectance values. When subjected to polynomial regression analysis, a third order curve significant at the 95 per cent confidence level is computed. The curve drawn through the data points in Fig.145 has the following regression parameters;

| | |
|-------------------------|---------------|
| Intercept | 0.1464420E 01 |
| Regression coefficients | |
| 1. | 0.1878120E 00 |
| 2. | 0.2410650E-01 |
| 3. | 0.8167794E-03 |

The trends of refractive index with distance illustrated in Fig.160 indicate that on approaching the dyke there is, after an initial rise in values, a sharp fall to a minimum at approximately five metres from the dyke. Moving nearer the dyke, the values steadily increase to a maximum at the contact. The observed minimum is not confined to measurements of refractive index made at 546 nm. Indeed, it is equally obvious at 442, 502, 590 and 651 nm. Furthermore, the trends of refractive index with wavelength of a single sample indicate

that values decrease from the red to the blue in the visible spectrum.

Spectral trends for the variation in refractive index of the graptolite fragments in the samples from Clanyard Bay are described in Appendix D and are illustrated in Figs.161-166.

The variation in absorptive index with wavelength for the samples is illustrated in Figs.161-166. Of the optical parameters in the Fresnel-Beer equation (Stach et al., 1975, p.263), the absorptive index generally has the lowest accuracy and often, especially when dealing with low rank material, negative values of k^2 are found. This problem has not been encountered in this work due to the high rank of the material studied.

It is found that absorptive index values at 546 nm for the LB-series of samples have a linear correlation with distance from the dyke. When subjected to statistical analysis a line, significant at the 99 per cent confidence level, may be drawn through the data points. This line illustrated in Fig.145c, has a computed slope of 0.015 and an intercept of 0.169.

The variation in absorptive index with distance is more enhanced at the blue end of the visible spectrum. Values at the seven wavelengths used in this work are given in Table 5-11. There is at all wavelengths a linear increase in absorptive index with increasing proximity to the dyke. Correlation coefficients of the lines which are illustrated in Fig.167 vary from -0.88 at 710 nm to -0.96 at 410 nm (Table 5-14). A more detailed description of the spectral trend in absorptive index of the samples is given in Appendix D.

c) Discussion

Dispersion data for the optical properties of carbonized graptolites have not been previously reported. Dispersion trends have however been published for naturally occurring vitrinites of varying rank and for artificially carbonized macerals (Gilbert, 1960; Ergen and McCartney, 1960; Gilbert, 1962; Marshall and Murchison 1971). In studies of both naturally and laboratory carbonized vitrinites it is found that reflectivity shows a rise towards the blue in lower-rank bituminous coals whereas the trend is reversed in anthracites. High rank bituminous vitrinites lying between the two extremes show only a slight increase towards the blue.

The dispersion trends for the graptolitic material collected furthest away from the dyke would by comparison with the vitrinite trends seem to indicate a material similar in composition to a semi-anthracite (ie. with a d.a.f carbon content of between 86 and 92 per cent. Approaching the dyke, the rise in values towards the red is enhanced thus indicating progressive carbonization of the organic material.

The reversal in the dispersion trends for the reflectivity of the two samples immediately adjacent to the dyke on the south side remains unexplained. It is certainly unusual for high rank organic material to show an increase in reflectivity towards the blue but that the material in sample LB-18 is organic is without question. There is some doubt however as to the affinities of the finely comminuted material within sample LB-17A (J.Melvin pers.comm.).

Except for these two samples, the dispersion trends for the graptolitic material are similar to those derived from coals.

Furthermore, by comparison with the spectral properties of coals it would appear that the starting material at the time of intrusion was similar to a low-volatile bituminous coal containing 88 per cent d.a.f. carbon (Marshall and Murchison, 1971). If this was so then the original sclero-proteinaceous material of the graptolite periderm must have been transformed into a substance with a high lipid content before intrusion of the dyke (Towe and Urbanek, 1972).

Further evidence that the material before intrusion of the dyke was similar to a low-volatile bituminous coal is given by observing that the graptolite material displays plastic properties and optical mosaic textures. Such observations imply that the material at the time of intrusion was already similar to coals of coking-range rank (85-92 per cent d.a.f. carbon). It is true that the carbonization conditions of the material within the shales are hardly comparable with those of commercially produced cokes, firstly in terms of length of time during which heating took place and secondly, in terms of the considerable hydrostatic pressure due to the depth of overlying strata. Doubtless, these factors will have had some effect and they thus increase the area of uncertainty regarding the initial rank of the graptolitic material. For example, it is known that natural coals of 80.5 and 79.0 per cent carbon are able to develop mosaic textures in the vicinity of igneous dykes whereas the same coals do not form mosaics when carbonized in the laboratory (Melvin, 1967; Aganoglu, 1972).

Clearly, while the behaviour of the graptolite reflectivities at different wavelengths is relatively straightforward, that of the refractive index follows a more complex pattern. As previously noted, some of the variation in refractive index trends may

be accounted for in terms of analytical errors since the error in refractive index determinations includes that of the two reflectivity determinations.

Dispersion curves for the spectral variation in refractive index of the highest rank vitrinites show an increase in refractive index from the blue to the red in a similar manner to that described for the graptolites (Gilbert, 1962; McCartney et al., 1965). These high rank vitrinites also display an increase in the general level of refractive index throughout the visible spectrum when compared with vitrinites of lower rank.

The increase in the refractive index of naturally occurring coals correlates well with the increase in layer diameters, the improvement of stacking order and the increase in the amount of carbon present, all of which were observed by Hirsch (1954). It would therefore seem feasible to postulate that some form of structural ordering is being manifested by the increase of refractive index values of the graptolite fragments close to the dyke. Confirmation of this will not be easy since most carbonized graptolites are preserved as thin organic films on rock surfaces thus rendering their uncontaminated isolation very difficult.

It has been demonstrated that with increasing rank there is a marked increase in the diameters of the aromatic lamellae that form the crystallites of anthracitic vitrinites when compared with vitrinites of lower rank (Hirsch, 1954). The rise in optical absorption in the high rank vitrinites is attributable to electronic absorption within the lamellae which are rapidly increasing in size at this level of coalification. If the rise in the absorptive indices of the heat

affected graptolites is attributable to the same cause then it is suggested that the maximum layer diameter is attained for the aromatic lamellae some distance away from the dyke contact. This distance cannot be accurately defined from a study of spectral trends.

9. VARIATION IN THE OPTICAL PROPERTIES OF GRAPTOLITES
WITH TEMPERATURE

a) Introduction

Now that the variation in the various parameters which are interrelated with reflectivity has been described in relation to the distance from the dyke, it remains to relate the optical properties of graptolites to temperature. This is not an easy task since before any estimate of palaeotemperature can be given there are many factors which must be considered. In general terms the information that is required is a knowledge of the amount of heat and the temperature at which it is available but several other factors have an influence on any estimate of temperature. Some of the more important of these factors include:-

- 1) Size (thickness) of the intrusion.
- 2) Time during which the intrusion was active.
- 3) Initial temperature of the intrusion.
- 4) Degree of superheat of the magma.
- 5) Latent heat of crystallisation of the magma.
- 6) Temperature range of crystallisation.
- 7) Amount of heat transferred by convecting gases and liquids.
- 8) Initial temperature of the country rock.
- 9) Thermal conductivity of the country rocks.

Some of the above factors are more important than others. For example it has been demonstrated that the liberation of latent heat has a very important effect on contact temperature whereas the solidification range of the magma has in comparison very little effect (Jaeger 1959). The effect of the latent heat of crystallisation is of lesser importance when dissolved water is present (Kesler and Heath 1968).

It is possible to arrive at a formula for the temperature at a point some distance away from an intrusion if the problem is simplified by making certain assumptions. These are, that the magma is intruded at a fixed temperature, that the effect of transport of heat by volatiles is small and that the physical properties of thermal conductivity, specific heat and density of the country rocks and of the magma are invariant. Jaeger (1964 p.454) has derived, using these assumptions, the following formula for the maximum temperature at a point outside a cooling sheet;

$$T_m = 0.484 T_o^*/E \text{ - - - - - Equation A}$$

where T_m is the maximum temperature at a point outside a cooling sheet

T_o^* is the equivalent initial temperature of the magma

$$T_o^* = T_o + L/C \text{ - - - - - Equation B}$$

T_o is the initial temperature of the magma

L is the latent heat of the magma

C is the specific heat of the country rock

E is the dimensionless quantity = x/d

x is the distance from the centre of an intrusive sheet

and d is the half thickness of an intrusive sheet

Equation (A) can therefore be simplified to give

$$T_m = 0.484 T_o^* \frac{d}{x} \text{ - - - - - Equation C.}$$

Before values of T_m can be calculated it is first necessary to estimate the equivalent initial temperature of the magma (T_o^*). This estimate may be derived by inserting realistic values for the latent heat of the magma and the specific heat of the country rock into Equation B. Assuming that a lower temperature of 900°C may reasonably be postulated for the magma temperature of the porphyrite dyke at Clanyard Bay, that the latent heat of solidification is of the order of 80 to 100 cal/g and that the specific heat of the country rocks varies within the limits 0.20 to 0.30 (Larsen 1945 and Birch et al., 1942) it is likely that the equivalent initial temperature of the magma lies between 1166 and 1400°C .

Substituting the lower value of 1166°C for T_o^* into Equation C it is possible to calculate the maximum temperature at any point outside the cooling sheet relative to the initial temperature of the country rock which is taken to be zero (Table 5-15).

b) Variation in reflectivity with temperature

There is good correlation between the calculated maximum temperatures (T_m) of the samples and the mean reflectance values in oil at 546 nm. These two parameters when subjected to product moment correlation analysis yield a correlation coefficient of 0.88 and it is possible to draw a line significant at the 99.9 per cent confidence level through the data points. This line with a slope of 68.3 and an intercept of 66.3 is labelled $T_o^* = 1166^{\circ}\text{C}$ in Fig. 168.

The plot of reflectivity versus temperature when $T_o^* = 1166^{\circ}\text{C}$ (Fig. 168) indicates that although there is a large spread in the data points all of these, except one, are enclosed in an envelope

bounded by the best-fit lines for the lowest and highest estimated values for the equivalent temperature ie. 900° and 1400°C . The former temperature could only have resulted if latent heat effects had been negligible while the latter could have resulted if a latent heat of 100 cal/g and a conductivity of 0.20 described the situation. The regression line parameters for the variation of mean reflectance values in oil at 546 nm with maximum temperature for various equivalent temperatures are given in Table 5-16.

c) Variation in refractive index with temperature

Refractive index values at 410, 546 and 710 nm of the 12 samples analysed from Clanyard Bay are summarised in Table 5-17. These values have been correlated with temperature at various distances from the dyke exposed in the Bay. Polynomial least-squares analysis indicates that a second order polynomial regression curve may be drawn with 99 per cent confidence through the data points (Fig.169). Regression parameters for the lines are given in Table 5-18.

All three curves illustrated in Fig.169 indicate a trend in refractive index values that falls between 120 and 250°C . Values then increase to a maximum at 490°C . The decrease in values between 120 and 250°C is most prominent at 546 nm and least prominent at 710 nm. Likewise, the rate of change in refractive index with temperature between 250 and 490°C is greatest at 546 nm. Clearly, 546 nm is the most suitable wavelength for the study of refractive index trends of heat affected graptolites.

It is possible by comparing the refractive index/temperature trends with the changes in textures which are displayed

by the organic matter, to arrive at approximate temperatures at which structural reorganisation takes place in the solid (Fig.170). Temperatures of 200^o, 280^o and 380^o may be assigned by comparison of similar effects in coal to the onset of plasticity, the onset of resolidification and the onset of molecular reorganisation respectively.

d) Variation in absorptive index with temperature

Absorptive indices at 410, 546 and 710 nm are compared with temperature in Table 5-19. 'Best-fit' polynomial regression lines have been derived for the variation of absorptive index with temperature (Fig.171). Regression parameters for these three curves which are all significant at the 99 per cent confidence level are given in Table 5-20. All three curves indicate a rise in the index with temperature up to 360^oC. Thereafter, although values measured at 410 nm continue to rise those measured at 546 and 710 nm level off and then plunge steeply. This reversal of the general trend at temperatures greater than 360^oC is most marked at 710 nm.

e) Discussion

In the normal coalification series an overburden of 2 km together with a normal geothermal gradient is sufficient to produce a vitrinite reflectance value of 1.5 per cent in oil at 546 nm (M. and R. Teichmüller 1968). This reflectivity corresponds to that of a coking coal which is the type of organic material which is suggested as a starting substance at the time of intrusion of the dyke.

The basic mechanisms of the coal-carbon transformation, although rank dependent do not differ much from one coal to another

except in the case of anthracites (Berkowitz 1967). Carbonization is regarded as taking place in three phases, the first at temperatures below 350-400°C and not involving much more than 'molecular stripping' with decarboxylation, elimination of OCH_3 groups, some loss of carbon-bound CH_3 groups and partial dehydroxylation. Some depolymerisation and some condensation may also take place in phase 1. Phase 2 takes place between temperatures of 400° and 650°C and it is during this phase that a coal passes through its decomposition temperature and suffers extensive devolatilization. It is in this region that tars are formed from the aliphatic and alicyclic structures which link the polycondensed components of the coal 'molecule'. These volatiles arise from the degradation of aliphatic structures, from dealkylation of portions of free radicals and from aromatic carbon. There is considerable change in structure and ordering of the coal 'molecule' towards the end of phase 2 but this is not accompanied by any growth of the small aromatic units present. There is however, rapid growth and increased ordering of the aromatic units in phase 3 which takes place between temperatures of 650° and 1000°C. These changes take place by removal of hydrogen which is concentrated round the margins of the polycondensed aromatic structures.

The foregoing generalized description of the carbonization process has to be modified in detail in relation to the starting rank of the coal. In the case of anthracites, for example, it would not be expected that phases 1 and 2 would be much in evidence, if at all, and that the main changes would be those observed in phase 3.

In the present study it appears that phase 1 processes have taken place at temperatures of between 210° and 230°C. Phase 2

processes appear to have taken place in the region of 280°C whereas the re-ordering and rapid growth of the organic 'molecule' associated with phase 3 took place at temperatures in excess of 380°C.

Clearly, the temperatures estimated for the transformation stages of the graptolite fragments are less than those described by Berkowitz (1967). It is possible that the observed textural changes in the graptolites have been promoted at lower temperatures due to the as yet unknown effects of slow rates of heating and the immense time and pressure involved in natural processes.

The most striking difference between the optical behaviour of heat affected graptolites and vitrinites lies in the behaviour of the refractive index above the temperature of molecular reorganisation (T_m). Results for carbonized vitrinites show that immediately after molecular reorganization of the solid there is a sharp drop in refractive index values whereas the absorptive index values continue to rise (Marshall and Murchison 1971; Goodarzi and Murchison 1972). The variation in refractive index has been related to changes taking place in the height of the crystallites and in the packing of the lamellae within the individual crystallites. Although the graptolite fragments exhibit a slight drop in refractive index immediately after the proposed onset of molecular reorganisation the general trend is one of increasing refractive index with temperature. An explanation for the difference in behaviour of the two materials may be in the fact that comparisons are being drawn between natural and artificial processes. For example, it may be that in the artificial carbonization experiments the rate of heating is so fast in comparison to the natural process that the ordering of the

crystallites is inhibited at high temperatures. Another explanation for the observed difference in the refractive index with temperature may be related to the original chemistry of the organic material. This is however not considered to be of any great importance because if locust wings, which are predominantly scleroproteinaceous, are carbonized in the laboratory it is found that the refractive index decreases at temperatures in excess of 600⁰C (Khavari pers.comm.).

The assumptions that have been made in order to determine the temperature at any distance from the dyke may be much too simple. For example, it is possible that the calculated value of the equivalent temperature does not fully describe the heat input at the time of intrusion. Furthermore, maximum temperatures have not been calculated for the now observed distance the samples are from the dyke but for distances reconstructed to compensate for the effects of later thrusting (section 8a). It must be stressed that, in view of the number of variables involved, the quantitative results must be regarded as tentative, and that more emphasis should be laid on relating the optical properties of graptolites with temperature in qualitative terms only.

OIL

| nm. | 0° | | 57° | | 74° | | 90° | |
|-----|------|------|------|------|------|------|------|------|
| | min. | max. | min. | max. | min. | max. | min. | max. |
| 410 | 4.09 | 4.42 | 3.60 | 4.26 | 4.87 | 5.47 | 4.59 | 5.08 |
| 442 | 4.07 | 4.58 | 3.63 | 4.29 | 4.78 | 5.38 | 4.50 | 5.00 |
| 502 | 4.18 | 4.49 | 3.84 | 4.53 | 4.88 | 5.48 | 4.82 | 5.31 |
| 546 | 4.40 | 4.70 | 4.01 | 4.73 | 5.06 | 5.80 | 4.95 | 5.46 |
| 590 | 4.56 | 4.89 | 4.12 | 4.98 | 5.39 | 6.09 | 5.25 | 5.76 |
| 651 | 4.88 | 5.21 | 4.32 | 5.26 | 5.69 | 6.26 | 4.48 | 6.05 |
| 710 | 5.00 | 5.42 | 4.65 | 5.54 | 5.94 | 6.74 | 5.84 | 6.40 |

AIR

| nm. | 0° | | 57° | | 74° | | 90° | |
|-----|-------|-------|-------|-------|-------|-------|-------|-------|
| | min. | max. | min. | max. | min. | max. | min. | max. |
| 410 | 12.16 | 12.50 | 11.18 | 12.16 | 12.73 | 13.67 | 13.05 | 13.78 |
| 442 | 12.24 | 12.58 | 11.23 | 12.26 | 12.71 | 13.61 | 12.68 | 13.39 |
| 502 | 12.85 | 13.20 | 11.85 | 14.04 | 13.42 | 14.40 | 13.39 | 14.35 |
| 546 | 13.20 | 13.61 | 12.04 | 13.49 | 13.93 | 14.95 | 14.08 | 14.86 |
| 590 | 13.70 | 14.08 | 12.40 | 14.04 | 14.38 | 15.40 | 14.55 | 15.35 |
| 651 | 14.20 | 14.66 | 13.05 | 14.56 | 14.99 | 16.08 | 15.10 | 15.81 |
| 710 | 14.59 | 15.18 | 13.55 | 14.95 | 15.26 | 16.42 | 15.48 | 16.43 |

TABLE 5-1 Dispersion with wavelength of minimum and maximum reflectance values in air and in oil of graptolite fragments cut at various angles to the plane of the bedding.

OIL

| Angle of cut | Intercept | Slope | F-value |
|---------------------|---------------|---------------|---------|
| 0 ^o min | 0.2590950E 01 | 0.3386997E-02 | 118.19 |
| 0 ^o max | 0.2787115E 01 | 0.3635461E-02 | 97.39 |
| 57 ^o min | 0.2127858E 01 | 0.3447147E-02 | 295.57 |
| 57 ^o max | 0.2349669E 01 | 0.4451390E-02 | 484.01 |
| 74 ^o min | 0.3037172E 01 | 0.3985912E-02 | 58.12 |
| 74 ^o max | 0.3445012E 01 | 0.4441671E-02 | 62.71 |
| 90 ^o min | 0.2635177E 01 | 0.4410211E-02 | 155.36 |
| 90 ^o max | 0.3007339E 01 | 0.4676342E-02 | 164.83 |

AIR

| | | | |
|---------------------|---------------|---------------|---------|
| 0 ^o min | 0.8554184E 01 | 0.8584961E-02 | 759.33 |
| 0 ^o max | 0.8554275E 01 | 0.9330049E-02 | 1083.84 |
| 57 ^o min | 0.7730429E 01 | 0.8098401E-02 | 404.85 |
| 57 ^o max | 0.8041576E 01 | 0.9921823E-02 | 467.95 |
| 74 ^o min | 0.8785672E 01 | 0.9327512E-02 | 290.04 |
| 74 ^o max | 0.9370858E 01 | 0.1011008E-01 | 304.80 |
| 90 ^o min | 0.8820651E 01 | 0.9500232E-02 | 105.36 |
| 90 ^o max | 0.9418488E 01 | 0.9878095E-02 | 129.20 |

TABLE 5-2

Regression line parameters for the variation of minimum and maximum reflectance values in air and in oil with wavelength for a series of measurements made at various angles to the bedding.

OIL

| nm. | 0° | 57° | 74° | 90° |
|-----|-------------|-------------|-------------|-------------|
| | max. - min. | max. - min. | max. - min. | max. - min. |
| 410 | 0.33(0.30) | 0.66(0.64) | 0.60(0.60) | 0.49(0.49) |
| 442 | 0.31(0.30) | 0.66(0.67) | 0.60(0.61) | 0.50(0.49) |
| 502 | 0.31(0.32) | 0.69(0.72) | 0.60(0.64) | 0.49(0.51) |
| 546 | 0.30(0.33) | 0.72(0.77) | 0.74(0.66) | 0.51(0.52) |
| 590 | 0.33(0.34) | 0.86(0.82) | 0.70(0.68) | 0.51(0.53) |
| 651 | 0.33(0.35) | 0.94(0.88) | 0.57(0.71) | 0.57(0.54) |
| 710 | 0.42(0.37) | 0.89(0.93) | 0.80(0.73) | 0.56(0.56) |

AIR

| nm. | 0° | 57° | 74° | 90° |
|-----|-------------|-------------|-------------|-------------|
| | max. - min. | max. - min. | max. - min. | max. - min. |
| 410 | 0.34(0.31) | 0.98(1.06) | 0.94(0.91) | 0.73(0.75) |
| 442 | 0.34(0.33) | 1.03(1.12) | 0.90(0.93) | 0.71(0.77) |
| 502 | 0.35(0.38) | 1.19(1.22) | 0.98(0.98) | 0.96(0.79) |
| 546 | 0.41(0.41) | 1.45(1.31) | 1.02(1.01) | 0.78(0.80) |
| 590 | 0.38(0.44) | 1.64(1.39) | 1.02(1.05) | 0.80(0.82) |
| 651 | 0.46(0.49) | 1.51(1.50) | 1.09(1.09) | 0.71(0.84) |
| 710 | 0.59(0.53) | 1.40(1.61) | 1.16(1.14) | 0.95(0.86) |

TABLE 5-3

Variation with wavelength of maximum minus minimum reflectance values in air and in oil of graptolite fragments cut at various angles to the plane of the bedding. Values in parenthesis are the differences obtained in maximum and minimum reflectance values derived from the statistical regression line.

| | Total sample | Single fragment |
|--------------------|--------------|-----------------|
| Mean | 4.00 | 4.12 |
| Mode | 4.18 | 4.17 |
| Standard Deviation | 0.39 | 0.19 |
| Variance | 0.15 | 0.04 |
| Minimum | 3.20 | 3.66 |
| Maximum | 4.89 | 4.59 |

TABLE 5-4 Single variable statistics for mean reflectance values measured in oil at 546 nm. for sample LBR-29.

| X | Y | Ro observed per cent | Ro random per cent | X | Y | Ro observed per cent | Ro random per cent |
|-----|-----|----------------------------|--------------------------|-----|-----|----------------------------|--------------------------|
| 040 | 050 | 4.12 | 3.66 | 110 | 060 | 4.48 | 4.09 |
| 040 | 080 | 3.98 | 4.13 | 110 | 070 | 4.31 | 4.20 |
| 040 | 100 | 3.92 | 4.38 | 110 | 080 | 4.31 | 4.06 |
| 040 | 110 | 3.81 | 4.34 | 110 | 090 | 4.06 | 3.93 |
| 040 | 120 | 4.24 | 4.20 | 110 | 100 | 4.16 | 4.38 |
| 040 | 130 | 4.25 | 4.37 | 110 | 110 | 4.16 | 4.14 |
| 040 | 140 | 4.25 | 4.13 | 110 | 120 | 4.26 | 4.17 |
| | | | | 110 | 130 | 4.15 | 4.27 |
| 060 | 050 | 3.88 | 4.07 | 110 | 140 | 4.11 | 4.03 |
| 060 | 060 | 4.18 | 4.27 | 110 | 150 | 4.04 | 4.12 |
| 060 | 070 | 4.20 | 4.05 | | | | |
| 060 | 080 | 4.20 | 3.99 | 130 | 050 | 4.03 | 4.10 |
| 060 | 090 | 4.18 | 4.12 | 130 | 060 | 3.75 | 4.22 |
| 060 | 100 | 4.14 | 3.75 | 130 | 070 | 3.86 | 4.29 |
| 060 | 110 | 4.09 | 3.92 | 130 | 080 | 3.99 | 4.25 |
| 060 | 120 | 4.20 | 4.18 | 130 | 090 | 3.97 | 4.17 |
| 060 | 130 | 4.24 | 4.43 | 130 | 100 | 3.93 | 4.23 |
| 060 | 140 | 4.27 | 4.18 | 130 | 110 | 4.21 | 3.85 |
| 060 | 150 | 4.26 | 4.35 | 130 | 120 | 4.18 | 4.29 |
| | | | | 130 | 130 | 4.27 | 4.13 |
| 070 | 050 | 3.92 | 4.00 | 130 | 140 | 4.26 | 4.04 |
| 070 | 060 | 4.02 | 4.47 | 130 | 150 | 4.30 | 4.25 |
| 070 | 070 | 4.09 | 4.19 | | | | |
| 070 | 080 | 4.08 | 4.09 | 150 | 050 | 3.95 | 3.97 |
| 070 | 090 | 4.21 | 4.15 | 150 | 060 | 3.98 | 4.24 |
| 070 | 100 | 4.16 | 4.21 | 150 | 070 | 3.82 | 4.20 |
| 070 | 110 | 4.16 | 4.28 | 150 | 080 | 3.91 | 4.09 |
| 070 | 120 | 4.20 | 3.96 | 150 | 090 | 4.04 | 3.83 |
| 070 | 130 | 4.21 | 4.38 | 150 | 100 | 4.09 | 4.20 |
| 070 | 140 | 4.25 | 3.98 | 150 | 110 | 4.17 | 4.23 |
| 070 | 150 | 4.25 | 4.28 | 150 | 120 | 4.33 | 4.18 |
| | | | | 150 | 130 | 4.32 | 4.03 |
| 080 | 050 | 4.03 | 4.44 | 150 | 140 | 4.40 | 4.19 |
| 080 | 060 | 4.03 | 4.05 | 150 | 150 | 4.38 | 4.10 |
| 080 | 070 | 4.14 | 4.09 | | | | |
| 080 | 080 | 4.04 | 4.06 | 170 | 050 | 3.91 | 4.08 |
| 080 | 090 | 4.20 | 4.06 | 170 | 060 | 3.93 | 4.03 |
| 080 | 100 | 4.14 | 4.04 | 170 | 070 | 3.95 | 4.02 |
| 080 | 110 | 4.17 | 3.99 | 170 | 080 | 4.12 | 4.10 |
| 080 | 120 | 4.21 | 4.32 | 170 | 090 | 4.04 | 4.18 |
| 080 | 130 | 4.21 | 4.03 | 170 | 100 | 4.14 | 4.29 |
| 080 | 140 | 4.10 | 4.01 | 170 | 110 | 4.32 | 4.32 |
| 080 | 150 | 4.09 | 4.46 | 170 | 120 | 4.31 | 4.33 |
| | | | | 170 | 130 | 4.08 | 4.00 |
| 090 | 050 | 4.21 | 4.17 | 170 | 140 | 4.14 | 4.01 |
| 090 | 060 | 4.08 | 3.83 | 170 | 150 | 4.36 | 4.00 |
| 090 | 070 | 4.01 | 4.09 | | | | |
| 090 | 080 | 4.14 | 4.20 | 190 | 050 | 3.92 | 4.17 |
| 090 | 090 | 4.14 | 4.08 | 190 | 060 | 3.93 | 4.19 |
| 090 | 100 | 4.18 | 4.11 | 190 | 070 | 4.10 | 3.93 |
| 090 | 110 | 4.27 | 4.20 | 190 | 080 | 4.12 | 3.77 |
| 090 | 120 | 4.17 | 4.07 | 190 | 090 | 4.13 | 3.97 |
| 090 | 130 | 4.13 | 4.13 | 190 | 100 | 4.21 | 4.03 |
| 090 | 140 | 4.09 | 4.61 | 190 | 110 | 4.32 | 4.22 |
| 090 | 150 | 3.66 | 4.42 | 190 | 120 | 4.37 | 4.19 |

TABLE 5-5

/ Continued

TABLE 5-5 Continued.

| X | Y | Ro observed per cent | Ro random per cent |
|-----|-----|----------------------------|--------------------------|
| 190 | 130 | 4.37 | 4.07 |
| 190 | 140 | 4.41 | 4.30 |
| 190 | 150 | 4.44 | 4.18 |
| 210 | 050 | 3.89 | 4.54 |
| 210 | 060 | 3.86 | 3.93 |
| 210 | 070 | 4.14 | 4.03 |
| 210 | 080 | 4.36 | 4.10 |
| 210 | 090 | 4.31 | 4.30 |
| 210 | 100 | 4.27 | 4.15 |
| 210 | 110 | 4.33 | 4.10 |
| 210 | 120 | 4.46 | 4.06 |
| 210 | 130 | 4.55 | 4.06 |
| 210 | 140 | 4.59 | 3.96 |
| 210 | 150 | 4.35 | 4.01 |
| 230 | 050 | 4.04 | 4.04 |
| 230 | 060 | 4.03 | 4.20 |
| 230 | 070 | 3.99 | 4.14 |
| 230 | 080 | 4.02 | 3.96 |
| 230 | 090 | 4.19 | 4.17 |
| 230 | 100 | 4.30 | 4.11 |
| 230 | 110 | 3.92 | 4.04 |
| 230 | 120 | 4.08 | 4.23 |
| 230 | 130 | 4.00 | 4.06 |
| 230 | 140 | 4.19 | 3.94 |
| 140 | 040 | 4.06 | 3.94 |
| 180 | 040 | 3.80 | 4.17 |
| 180 | 030 | 3.89 | 4.11 |
| 180 | 020 | 3.81 | 4.19 |
| 180 | 010 | 3.94 | 3.98 |
| 200 | 040 | 3.88 | 4.20 |
| 200 | 030 | 4.04 | 4.04 |
| 240 | 040 | 4.14 | 3.80 |
| 040 | 150 | 4.05 | 4.41 |

TABLE 5-5 Observed and random reflectance values in oil at 546 nm for a grid distribution of points across a single graptolite fragment.

| Surface generated | Fit values for the Measured Fragment | Fit values for the data generated at random |
|-----------------------------|---|---|
| | % | % |
| Iterative Plane Surface | 98.75 | 96.40 |
| Iterative Quadratic Surface | 98.87 | 96.32 |
| Iterative Cubic Surface | 99.41 | 96.02 |
| Global Plane Surface | 31.95 | 7.28 |
| Global Quadratic Surface | 37.81 | 11.95 |
| Global Cubic Surface | 39.66 | 14.26 |

TABLE 5-6 Computed fit values for surfaces derived by trend surface analysis for the areal variation in reflectance values over a graptolite fragment.

| | | |
|--------|----------------------|---|
| LB-12 | 21.74 m ⁺ | Badly cleaved grey mudstone weathered red |
| LB-13 | 20.00 m | Badly cleaved grey mudstone |
| LB-14 | 15.68 m | Hard dark-grey mudstone with some pyrite present |
| LB-15 | 12.21 m | Black blocky mudstone with pyrite and elemental sulphur present |
| LB-16 | 10.05 m | Dark grey shale with quartz veining |
| LB-17 | 6.58 m | Blue-grey platy shale |
| LB-18 | 5.28 m | Very hard steel-grey shale |
| LB-19 | 0.00 m | Course grained porphyrite dyke |
| LB-20 | 4.68 m | Baked, bleached shale with quartz veining |
| LB-21 | 5.46 m | Blocky black sulphurous mudstone |
| LB-22 | 8.05 m | Blocky black mudstone with shale intercalations |
| LB-23 | 10.22 m | Pyritised graptolitic shale |
| LB-24 | 12.38 m | Slickensided black shale |
| LBR-1 | 5.30 m | Friable black shale which appears to have flowed |
| LBR-2 | 5.33 m | Black shale with abundant quartz veins |
| LBR-3 | 5.35 m | Very soft crumbly pyritised dark grey shale |
| LBR-4 | 5.38 m | Pyritised blocky black mudstone |
| LBR-5 | 5.41 m | Pyritised blocky black mudstone |
| LBR-6 | 5.43 m | Soft black crumbly shale |
| LBR-7 | 5.49 m | Graptolitic black shale |
| LBR-8 | 5.56 m | Very flaky, badly cleaved black shale |
| LBR-9 | 5.69 m | Blocky black graptolitic mudstone |
| LBR-10 | 5.78 m | Black graptolitic mudstone |
| LBR-11 | 5.94 m | Crumbly black badly cleaved shale |
| LBR-12 | 6.04 m | Black, blocky mudstone |
| LBR-13 | 6.31 m | Badly cleaved black shale |
| LBR-14 | 6.57 m | Black, blocky mudstone |
| LBR-15 | 6.89 m | Cherty black mudstone |
| LBR-16 | 7.14 m | Platy black shale |
| LBR-17 | 7.47 m | Badly cleaved shale associated with grey claystones |
| LBR-18 | 7.66 m | Fissile black shale |
| LBR-20 | 12.53 m | Badly cleaved black mudstone |
| LBR-21 | 13.12 m | Black blocky mudstone |
| LBR-22 | 13.54 m | Badly cleaved iron stained black shales |
| LBR-23 | 13.91 m | Black blocky pyritised mudstone |
| LBR-24 | 14.44 m | Fine grained greywacke |

+ = Distance from centre of dyke (metres)

TABLE 5-7 Description of samples collected from Clanyard Bay.

| Sample | dm | Ro (mean) | Ro (mean-max) | Ro (min) | Bireflectance |
|--------|--------|-----------|---------------|----------|---------------|
| | metres | % | % | % | ratio |
| LB-12 | 21.74 | 3.29 | 3.29 | 2.29 | 0.30 |
| LB-13 | 20.00 | 3.38 | 4.79 | 1.94 | 0.60 |
| LB-14 | 15.68 | 3.89 | 4.96 | 2.94 | 0.41 |
| LB-15 | 12.21 | 3.98 | 5.55 | 4.12 | 0.26 |
| LB-16 | 10.05 | 4.15 | 4.88 | 3.09 | 0.37 |
| LB-17 | 6.58 | 4.60 | 5.74 | 1.42 | 0.75 |
| LB-18 | 5.28 | 7.60 | 10.80 | 7.27 | 0.33 |

TABLE 5-8 The variation in reflectance values of graptolite fragments with distance from the centre of a 9.18 metre thick porphyrite dyke. (dm is the perpendicular distance to the dyke centre).

| | | |
|-------------------------|-------------------|----------------|
| Samples | LB-12 to 18 | LB-21 to 24 |
| Intercept | 0.3732288E 01 | 0.5698351E 02 |
| Regression coefficients | | |
| | 1. -0.1445017E 00 | -0.2571462E 01 |
| | 2. 0.1353786E-01 | 0.3061407E-01 |
| F-value | 7.00 | 297.71 |

TABLE 5-9a Regression parameters for the variation in mean-reflectance of graptolite fragments with distance along the measured section at Clanyard Bay.

| Sample | Distance along section (m) | Ro (observed) % | Ro (regressed) % |
|--------|----------------------------|-----------------|------------------|
| LB-12 | 1.4 | 3.29 | 3.56 |
| LB-13 | 3.4 | 3.38 | 3.40 |
| LB-14 | 8.4 | 3.89 | 3.47 |
| LB-15 | 12.4 | 3.98 | 4.02 |
| LB-16 | 14.9 | 4.15 | 4.59 |
| LB-17 | 18.9 | 4.60 | 5.84 |
| LB-18 | 20.4 | 7.60 | 6.44 |
| LB-21 | 32.8 | 5.59 | 5.58 |
| LB-22 | 35.8 | 4.11 | 4.16 |
| LB-23 | 38.3 | 3.46 | 3.40 |
| LB-24 | 40.8 | 3.01 | 3.03 |

TABLE 5-9b Observed reflectance values at 546 nm in oil and those obtained from the regression equations in Table 5-9a.

| Sample | Ro (mean) % | log.Ro (mean) | Obs.distance from dyke centre (metres) | Est.distance from dyke centre before faulting (metres) |
|--------|----------------|---------------|---|--|
| LBR-1 | 3.31 | 0.5198 | 5.30 | 14.9 |
| LBR-2 | 4.26 | 0.6294 | 5.33 | 12.1 |
| LBR-3 | 3.88 | 0.5888 | 5.35 | 13.2 |
| LBR-4 | 4.45 | 0.6484 | 5.38 | 11.8 |
| LBR-5 | 4.64 | 0.6665 | 5.41 | 11.5 |
| LBR-6 | 2.68 | 0.4281 | 5.43 | 17.0 |
| LBR-7 | 4.68 | 0.6702 | 5.49 | 11.3 |
| LBR-8 | 6.86 | 0.8363 | 5.56 | 7.2 |
| LBR-9 | 3.52 | 0.5465 | 5.69 | 14.3 |
| LBR-10 | 4.45 | 0.6484 | 5.78 | 11.8 |
| LBR-11 | 4.62 | 0.6646 | 5.94 | 11.4 |
| LBR-12 | 3.90 | 0.5911 | 6.04 | 13.3 |
| LBR-13 | 6.50 | 0.8129 | 6.31 | 8.0 |
| LBR-14 | 6.03 | 0.7803 | 6.57 | 9.1 |
| LBR-15 | 4.55 | 0.6580 | 6.89 | 11.8 |
| LBR-16 | 4.57 | 0.6599 | 7.14 | 11.8 |
| LBR-17 | 2.87 | 0.4579 | 7.47 | 16.2 |
| LBR-18 | 2.00 | 0.3010 | 7.66 | 20.0 |
| LBR-20 | 5.28 | 0.7226 | 12.53 | 10.0 |
| LBR-21 | 4.55 | 0.6580 | 13.12 | 11.6 |
| LBR-22 | 4.99 | 0.6981 | 13.54 | 10.8 |
| LBR-23 | 4.23 | 0.6263 | 13.91 | 12.6 |
| LBR-24 | 4.00 | 0.6021 | 14.44 | 13.1 |
| LBR-25 | 3.84 | 0.5843 | 16.19 | 13.6 |

TABLE 5-10 Variation of reflectivity in oil at 546 nm with distance for samples collected to the north of the dyke at Clanyard Bay.

| Sample | W | Ro | Rest ¹ | Ra | Rest ² | n | k |
|--------------|-----|------|-------------------|-------|-------------------|------|------|
| LB-12 | 410 | 1.79 | 1.90 | 8.86 | 8.79 | 1.69 | 0.25 |
| | 442 | 2.02 | 1.91 | 8.66 | 8.73 | 1.69 | 0.25 |
| | 502 | 1.83 | 1.92 | 8.86 | 8.70 | 1.68 | 0.25 |
| | 546 | 2.04 | 1.93 | 8.21 | 8.75 | 1.69 | 0.24 |
| | 590 | 2.01 | 1.94 | 9.26 | 8.87 | 1.70 | 0.24 |
| | 651 | 1.86 | 1.95 | 9.21 | 9.13 | 1.73 | 0.23 |
| | 710 | 1.95 | 1.96 | 9.39 | 9.49 | 1.78 | 0.21 |
| LB-13 | 410 | 1.61 | 1.87 | 6.21 | 5.78 | 1.44 | 0.28 |
| | 442 | 2.19 | 1.79 | 6.93 | 7.80 | 1.61 | 0.26 |
| | 502 | 1.72 | 1.73 | 10.12 | 9.70 | 1.83 | 0.17 |
| | 546 | 1.54 | 1.78 | 10.38 | 10.01 | 1.86 | 0.16 |
| | 590 | 1.94 | 1.89 | 9.57 | 9.83 | 1.82 | 0.19 |
| | 651 | 2.25 | 2.17 | 9.25 | 9.47 | 1.74 | 0.24 |
| | 710 | 2.54 | 2.56 | 9.98 | 9.85 | 1.73 | 0.27 |
| LB-14 (1) | 410 | 2.52 | 2.72 | 9.66 | 10.31 | 1.74 | 0.29 |
| | 442 | 2.85 | 2.49 | 10.56 | 10.24 | 1.77 | 0.26 |
| | 502 | 2.03 | 2.12 | 10.82 | 10.10 | 1.81 | 0.21 |
| | 546 | 1.75 | 1.90 | 9.68 | 9.99 | 1.84 | 0.18 |
| | 590 | 1.72 | 1.72 | 10.03 | 9.89 | 1.86 | 0.15 |
| | 651 | 1.67 | 1.53 | 9.65 | 9.75 | 1.88 | 0.11 |
| | 710 | 1.36 | 1.42 | 9.49 | 9.61 | 1.88 | 0.08 |
| LB-14 (2) | 410 | 3.89 | 3.96 | 11.50 | 11.50 | 1.69 | 0.37 |
| | 442 | 4.07 | 3.97 | 11.57 | 11.57 | 1.70 | 0.37 |
| | 502 | 4.15 | 4.10 | 11.92 | 11.89 | 1.72 | 0.37 |
| | 546 | 4.13 | 4.28 | 12.18 | 12.24 | 1.74 | 0.37 |
| | 590 | 4.52 | 4.49 | 12.71 | 12.67 | 1.77 | 0.38 |
| | 651 | 4.86 | 4.80 | 13.29 | 13.30 | 1.80 | 0.38 |
| | 710 | 4.98 | 5.01 | 13.87 | 13.87 | 1.85 | 0.37 |

TABLE 5-11 Variation in optical properties of graptolites with wavelength, for selected samples from Clanyard Bay.

/continued

TABLE 5-11 continued.

| Sample | W | Ro | Rest ¹ | Ra | Rest ² | n | k |
|--------|-----|-------|-------------------|-------|-------------------|------|------|
| LB-15 | 410 | 4.05 | 4.05 | 10.62 | 10.33 | 1.56 | 0.41 |
| | 442 | 4.22 | 4.20 | 10.63 | 11.13 | 1.62 | 0.40 |
| | 502 | 4.42 | 4.48 | 12.20 | 12.19 | 1.70 | 0.39 |
| | 546 | 4.67 | 4.67 | 13.03 | 12.68 | 1.74 | 0.39 |
| | 590 | 4.94 | 4.84 | 13.10 | 13.04 | 1.76 | 0.40 |
| | 651 | 4.94 | 5.02 | 13.85 | 13.46 | 1.78 | 0.39 |
| | 710 | 5.13 | 5.11 | 14.14 | 13.10 | 1.73 | 0.41 |
| LB-16 | 410 | 4.55 | 4.51 | 10.38 | 10.46 | 1.52 | 0.44 |
| | 442 | 4.52 | 4.61 | 11.03 | 10.90 | 1.55 | 0.44 |
| | 502 | 4.94 | 4.84 | 11.63 | 11.68 | 1.60 | 0.44 |
| | 546 | 4.96 | 5.02 | 12.29 | 12.23 | 1.63 | 0.44 |
| | 590 | 5.21 | 5.20 | 12.56 | 12.74 | 1.67 | 0.44 |
| | 651 | 5.42 | 5.42 | 13.56 | 13.41 | 1.71 | 0.43 |
| | 710 | 5.55 | 5.55 | 13.92 | 13.97 | 1.77 | 0.42 |
| LB-17A | 410 | 5.87 | 6.10 | 14.28 | 14.49 | 1.72 | 0.47 |
| | 442 | 6.65 | 6.06 | 15.82 | 14.50 | 1.73 | 0.46 |
| | 502 | 5.51 | 5.98 | 14.27 | 14.52 | 1.75 | 0.45 |
| | 546 | 5.63 | 5.92 | 12.96 | 14.54 | 1.77 | 0.44 |
| | 590 | 6.43 | 5.86 | 14.75 | 14.56 | 1.79 | 0.43 |
| | 651 | 5.57 | 5.78 | 14.50 | 14.58 | 1.81 | 0.42 |
| | 710 | 5.75 | 5.71 | 15.20 | 14.60 | 1.83 | 0.41 |
| LB-18 | 410 | 12.37 | 13.82 | 23.63 | 26.31 | 2.18 | 0.60 |
| | 442 | 14.75 | 13.02 | 28.08 | 25.52 | 2.23 | 0.56 |
| | 502 | 12.78 | 11.61 | 26.63 | 24.04 | 2.29 | 0.48 |
| | 546 | 9.25 | 10.66 | 21.70 | 22.94 | 2.30 | 0.45 |
| | 590 | 9.29 | 9.79 | 20.29 | 21.85 | 2.28 | 0.42 |
| | 651 | 9.05 | 8.69 | 19.88 | 20.34 | 2.23 | 0.39 |
| | 710 | 7.87 | 7.76 | 19.68 | 18.88 | 2.15 | 0.38 |

/ continued

TABLE 5-11 continued.

| Sample | W | Ro | Rest ¹ | Ra | Rest ² | n | k |
|--------|-----|------|-------------------|-------|-------------------|------|------|
| LBR-3 | 410 | 3.77 | 3.72 | 8.85 | 9.00 | 1.49 | 0.40 |
| | 442 | 3.78 | 3.86 | 10.65 | 10.40 | 1.60 | 0.39 |
| | 502 | 4.18 | 4.13 | 11.79 | 11.83 | 1.71 | 0.37 |
| | 546 | 4.35 | 4.33 | 12.09 | 12.22 | 1.73 | 0.38 |
| | 590 | 4.36 | 4.53 | 12.43 | 12.37 | 1.72 | 0.39 |
| | 651 | 5.01 | 4.80 | 12.72 | 12.70 | 1.72 | 0.40 |
| | 710 | 4.99 | 5.07 | 13.76 | 13.77 | 1.82 | 0.38 |
| LBR-7 | 410 | 4.39 | 4.31 | 12.15 | 11.85 | 1.68 | 0.40 |
| | 442 | 4.45 | 4.56 | 12.15 | 12.76 | 1.75 | 0.39 |
| | 502 | 4.96 | 5.06 | 14.15 | 13.86 | 1.82 | 0.39 |
| | 546 | 5.51 | 5.44 | 14.64 | 14.30 | 1.82 | 0.40 |
| | 590 | 6.07 | 5.83 | 14.20 | 14.57 | 1.79 | 0.43 |
| | 651 | 6.09 | 6.36 | 14.86 | 14.86 | 1.75 | 0.47 |
| | 710 | 6.93 | 6.85 | 15.38 | 15.34 | 1.73 | 0.49 |
| LBR-8 | 410 | 5.45 | 5.45 | 13.75 | 13.16 | 1.66 | 0.45 |
| | 442 | 5.94 | 5.99 | 13.09 | 13.91 | 1.67 | 0.47 |
| | 502 | 6.71 | 6.66 | 15.04 | 15.17 | 1.73 | 0.49 |
| | 546 | 7.23 | 6.98 | 15.79 | 15.96 | 1.78 | 0.48 |
| | 590 | 6.80 | 7.25 | 18.09 | 16.66 | 1.84 | 0.47 |
| | 651 | 7.93 | 7.67 | 16.22 | 17.46 | 1.89 | 0.47 |
| | 710 | 8.27 | 8.33 | 18.38 | 18.04 | 1.86 | 0.51 |
| LBR-9 | 410 | 3.04 | 3.10 | 8.79 | 9.00 | 1.56 | 0.35 |
| | 442 | 3.37 | 3.28 | 10.47 | 10.02 | 1.63 | 0.35 |
| | 502 | 3.71 | 3.61 | 10.60 | 11.10 | 1.71 | 0.35 |
| | 546 | 3.62 | 3.86 | 11.85 | 11.45 | 1.71 | 0.36 |
| | 590 | 4.21 | 4.10 | 11.44 | 11.63 | 1.70 | 0.37 |
| | 651 | 4.46 | 4.44 | 12.01 | 11.96 | 1.69 | 0.39 |
| | 710 | 4.75 | 4.77 | 12.08 | 12.81 | 1.74 | 0.39 |

/ continued

TABLE 5-11 continued.

| Sample | W | Ro | Rest ¹ | Ra | Rest ² | n | k |
|--------|-----|------|-------------------|-------|-------------------|------|------|
| LBR-13 | 410 | 4.05 | 3.91 | 10.23 | 9.97 | 1.55 | 0.40 |
| | 442 | 3.57 | 3.88 | 9.84 | 10.29 | 1.58 | 0.39 |
| | 502 | 4.44 | 4.13 | 11.26 | 11.09 | 1.63 | 0.39 |
| | 546 | 4.32 | 4.47 | 11.61 | 11.78 | 1.66 | 0.40 |
| | 590 | 4.84 | 4.86 | 13.01 | 12.48 | 1.69 | 0.42 |
| | 651 | 5.36 | 5.34 | 12.88 | 13.38 | 1.72 | 0.43 |
| | 710 | 5.55 | 5.55 | 14.18 | 14.03 | 1.78 | 0.42 |

W = wavelength. (nm)

Ro = mean reflectance value in oil. (%)

Rest¹ = estimated value for mean reflectance in oil
calculated from regression line. (%)

Ra = mean reflectance value in air. (%)

Rest² = estimated value for mean reflectance in air
calculated from regression line. (%)

n = refractive index.

k = absorptive index.

| Wavelength | Slope | Intercept | PMCC | Level of significance of computed curve |
|------------|--------|-----------|-------|--|
| 410 nm | -0.045 | 1.19 | -0.94 | 1.0% |
| 442 nm | -0.045 | 1.99 | -0.95 | 0.1% |
| 502 nm | -0.044 | 1.17 | -0.96 | 0.1% |
| 546 nm | -0.042 | 1.15 | -0.97 | 0.1% |
| 590 nm | -0.040 | 1.13 | -0.98 | 0.1% |
| 651 nm | -0.037 | 1.09 | -0.98 | 0.1% |
| 710 nm | -0.033 | 1.05 | -0.98 | 0.1% |

PMCC is the product moment correlation coefficient.

TABLE 5-12 Statistical regression parameters at various wavelengths for the variation in the logarithm of estimated reflectance values in oil with perpendicular distance from the centre of the dyke.

| Sample | Slope | Intercept | F-value | Ro (mean) | dm |
|--------|---------|-----------|---------|-----------|------|
| LB-18 | -0.0203 | 21.93 | 16.2 | 7.60 | 5.3 |
| LB-17A | -0.0013 | 6.64 | 0.6 | 4.60 | 6.6 |
| LBR-8 | 0.0089 | 1.99 | 61.6 | 6.86 | 5.6 |
| LBR-7 | 0.0085 | 0.79 | 150.9 | 4.68 | 5.5 |
| LB-16 | 0.0036 | 3.03 | 156.1 | 4.15 | 10.1 |
| LB-15 | 0.0037 | 2.62 | 102.1 | 3.98 | 12.2 |
| LBR-3 | 0.0045 | 1.87 | 80.8 | 3.88 | 5.4 |
| LB-14 | 0.0037 | 2.32 | 63.3 | 3.89 | 15.7 |
| LBR-9 | 0.0055 | 0.84 | 120.6 | 3.52 | 5.7 |
| LB-13 | 0.0019 | 0.94 | 1.9 | 3.38 | 20.0 |
| LB-12 | 0.0019 | 1.82 | 0.2 | 3.29 | 21.7 |
| LBR-13 | 0.0061 | 1.22 | 40.0 | 6.50 | 6.3 |

TABLE 5-15 Linear regression parameters for the dispersion with wavelength of reflectivity in oil for samples collected from Clanyard Bay. dm is the distance in metres the sample is from the centre of the dyke.

| Wavelength | Slope | Intercept | PMCC | Level of significance of computed curve |
|------------|--------|-----------|-------|--|
| 410 nm | -0.018 | 0.64 | -0.96 | 0.1% |
| 442 nm | -0.018 | 0.61 | -0.94 | 0.1% |
| 502 nm | -0.017 | 0.58 | -0.90 | 1.0% |
| 546 nm | -0.017 | 0.55 | -0.91 | 1.0% |
| 590 nm | -0.015 | 0.54 | -0.92 | 1.0% |
| 651 nm | -0.013 | 0.50 | -0.91 | 1.0% |
| 710 nm | -0.012 | 0.49 | -0.88 | 2.5% |

PMCC is the product moment correlation coefficient.

TABLE 5-14 Statistical regression parameters at various wavelengths for the variation of absorptive index values with perpendicular distance from the centre of the dyke.

| Sample | x | Tm | Ro (mean) |
|--------|-------|--------------------|-----------|
| LB-18 | 5.3 m | 489 ^o C | 7.60 |
| LB-17A | 6.6 | 392 | 4.60 |
| LBR-8 | 7.2 | 360 | 6.86 |
| LBR-13 | 8.0 | 324 | 6.50 |
| LB-16 | 10.1 | 256 | 4.15 |
| LBR-7 | 11.3 | 229 | 4.68 |
| LB-15 | 12.2 | 212 | 3.98 |
| LBR-3 | 13.2 | 196 | 3.88 |
| LBR-9 | 14.3 | 181 | 3.52 |
| LB-14 | 15.7 | 165 | 3.89 |
| LB-13 | 20.0 | 130 | 3.38 |
| LB-12 | 21.7 | 119 | 3.29 |

$$T_o = 900^{\circ}\text{C}$$

$$L = 80\text{cal/g}$$

$$c = 0.30$$

$$T_o^* = 1166^{\circ}\text{C}$$

$$d = 4.59 \text{ m}$$

$$Z = 0.484T_o^*d = 2590$$

TABLE 5-15 Calculated maximum temperatures at various points
outside the dyke at Clanyard Bay.

| To* | Intercept | Slope | F-value |
|------|-----------|-------|---------|
| 900 | -50.6 | 52.6 | 33.2 |
| 1013 | -57.2 | 59.3 | 33.4 |
| 1166 | -66.3 | 68.3 | 33.5 |
| 1284 | -72.5 | 75.4 | 33.3 |
| 1400 | -79.1 | 82.0 | 33.3 |

TABLE 5-16 Regression parameters for the variation of mean reflectance values in oil at 546 nm with maximum temperature for various equivalent temperatures.

| Sample | Tm ^o C | n(410 nm) | n(546 nm) | n(710 nm) |
|--------|-------------------|-----------|-----------|-----------|
| LB-12 | 119 | 1.69 | 1.69 | 1.78 |
| LB-13 | 130 | 1.44 | 1.86 | 1.73 |
| LB-14 | 165 | 1.72 | 1.79 | 1.87 |
| LBR-9 | 181 | 1.56 | 1.71 | 1.74 |
| LBR-3 | 196 | 1.49 | 1.73 | 1.82 |
| LB-15 | 212 | 1.56 | 1.74 | 1.73 |
| LBR-7 | 229 | 1.68 | 1.63 | 1.73 |
| LB-16 | 256 | 1.52 | 1.63 | 1.77 |
| LBR-13 | 324 | 1.55 | 1.66 | 1.78 |
| LBR-8 | 360 | 1.66 | 1.78 | 1.86 |
| LB-17A | 392 | 1.72 | 1.77 | 1.83 |
| LB-18 | 489 | 2.18 | 2.30 | 2.15 |

TABLE 5-17 Variation of refractive index with temperature at selected wavelengths.

| Wavelength | 410 nm | 546 nm | 710 nm |
|--------------------|----------------|----------------|----------------|
| Intercept | 0.2012677E 01 | 0.2335172E 01 | 0.2013103E 01 |
| Regression | | | |
| coefficients | | | |
| 1 | -0.4142165E-02 | -0.5462755E-02 | -0.2366840E-02 |
| 2 | 0.8979503E-05 | 0.1081352E-04 | 0.5277212E-05 |
| F-value | 15.64 | 27.73 | 20.69 |
| Significance level | 1.0% | 0.1% | 0.1% |

TABLE 5-18 Regression parameters for the variation in refractive index with temperature at selected wavelengths.

| Sample | Tm ^o C | k(410 nm) | k(546 nm) | k(710 nm) |
|--------|-------------------|-----------|-----------|-----------|
| LB-12 | 119 | 0.25 | 0.24 | 0.21 |
| LB-13 | 130 | 0.28 | 0.16 | 0.27 |
| LB-14 | 165 | 0.33 | 0.27 | 0.23 |
| LBR-9 | 181 | 0.35 | 0.36 | 0.39 |
| LBR-5 | 196 | 0.40 | 0.38 | 0.38 |
| LB-15 | 212 | 0.41 | 0.39 | 0.41 |
| LBR-7 | 229 | 0.40 | 0.40 | 0.49 |
| LB-16 | 256 | 0.44 | 0.44 | 0.42 |
| LBR-13 | 324 | 0.40 | 0.40 | 0.42 |
| LBR-8 | 360 | 0.45 | 0.48 | 0.51 |
| LB-17A | 392 | 0.47 | 0.44 | 0.41 |
| LB-18 | 489 | 0.60 | 0.45 | 0.38 |

TABLE 5-19 Variation in absorptive index with temperature at selected wavelengths.

| Wavelength | 410 nm | 546 nm | 710 nm |
|--------------------|----------------|----------------|----------------|
| Intercept | 0.1794449E 00 | -0.7773113E-01 | -0.1115862E 00 |
| Regression | | | |
| coefficients | | | |
| 1 | 0.9811600E-03 | 0.2905287E-02 | 0.3454370E-02 |
| 2 | -0.4010082E-06 | -0.3834837E-05 | -0.5096158E-05 |
| F-value | 26.42 | 23.12 | 13.37 |
| Significance level | 0.1% | 0.1% | 1.0% |

TABLE 5-20 Regression parameters for the variation in absorptive index with temperature at selected wavelengths.

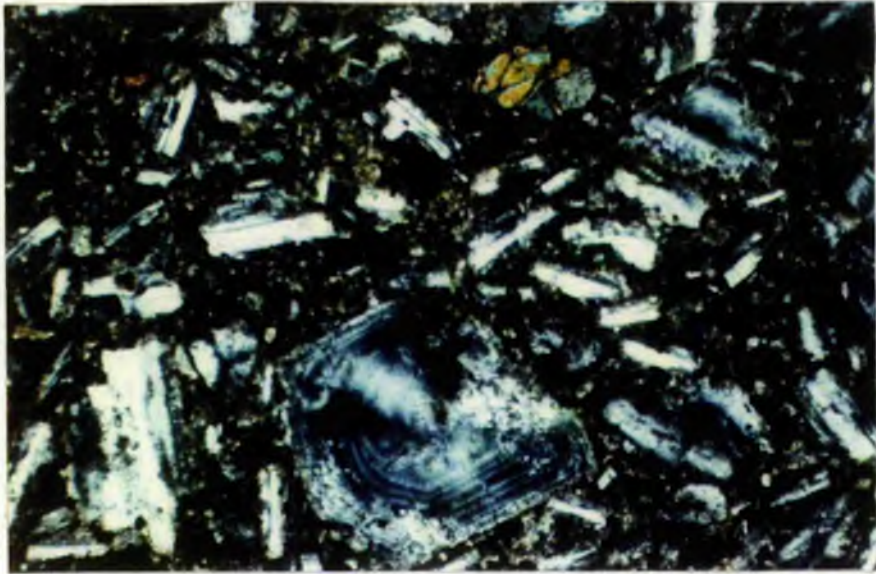


Plate 1. Photomicrograph illustrating the mineralogy of the sheared porphyrite dyke at Clanyard Bay. Magnification X300, transmitted light, crossed polars.

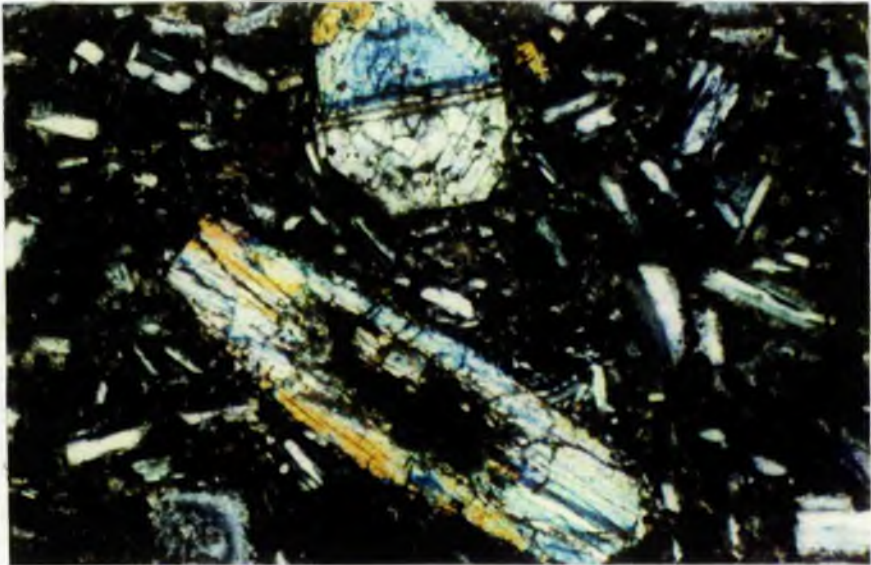


Plate 2. Photomicrograph illustrating zoned pyroxenes in the sheared porphyrite dyke at Clanyard Bay. Magnification X300, transmitted light, crossed polars.

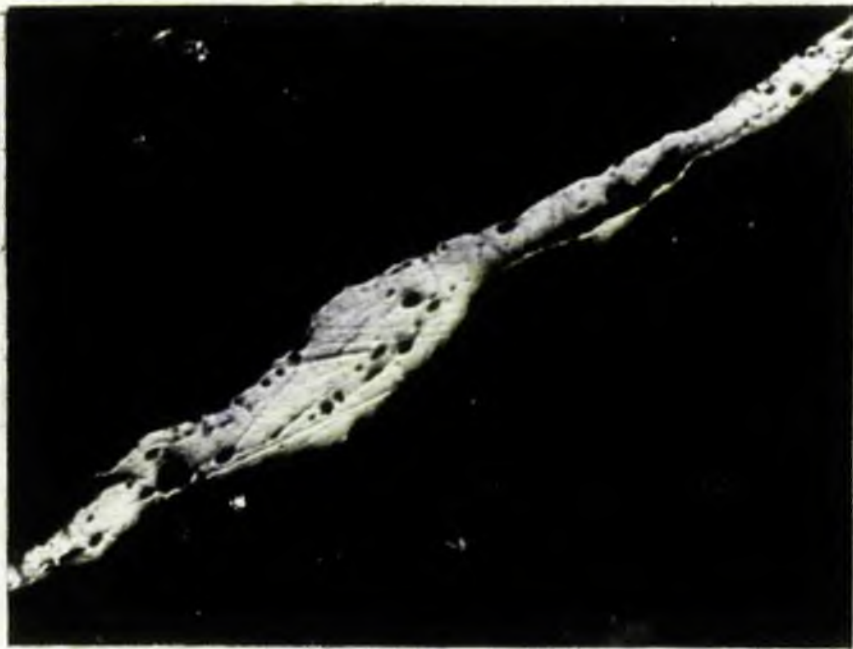


Plate 3. Photomicrograph illustrating vesiculation within a graptolite fragment from sample LB-13. Magnification X600, reflected light, oil immersion.

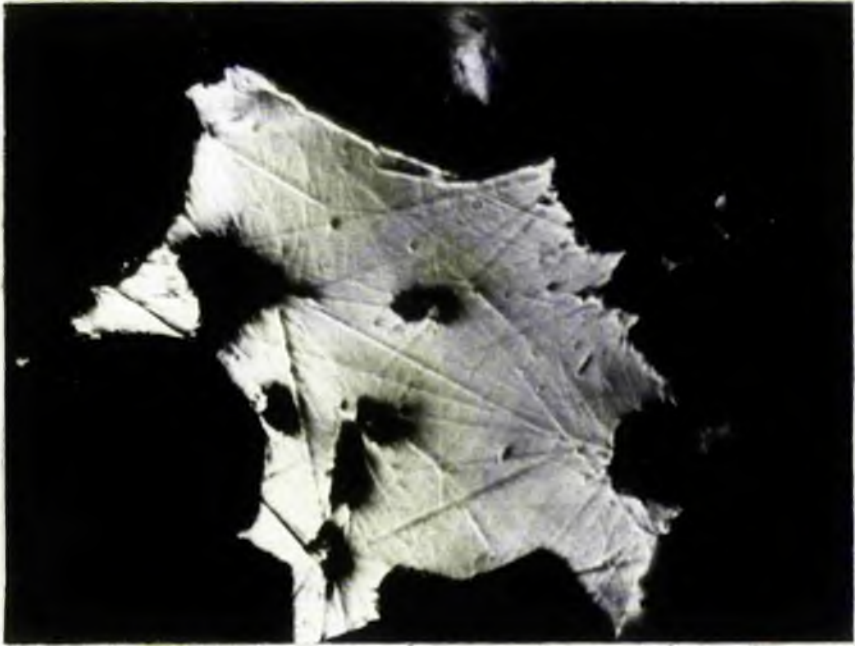


Plate 4. Photomicrograph illustrating larger scale vesiculation within a graptolite fragment from sample LBR-15. Magnification X600, reflected light, oil immersion.

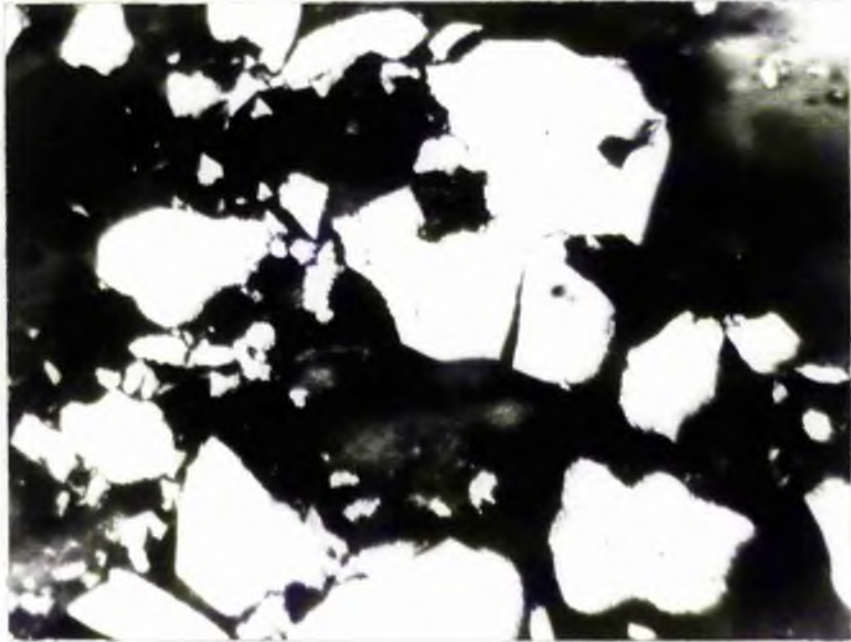


Plate 5. Photomicrograph illustrating fractured graptolite fragments within sample LBR-29.
Magnification X600, reflected light, oil immersion.

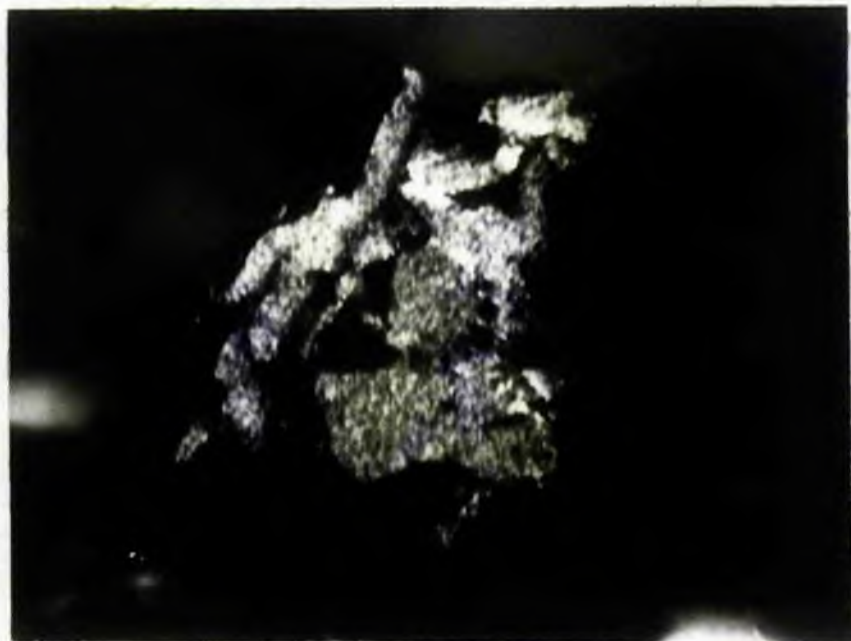


Plate 6. Photomicrograph illustrating mineral contaminated granular mosaic within graptolite fragments in sample LBR-9. Magnification X600, reflected light, partially crossed polars, oil immersion.



Plate 7. Photomicrograph illustrating banding within a graptolite fragment in sample LBR-7. Magnification X600, reflected light, partially crossed polars, oil immersion.

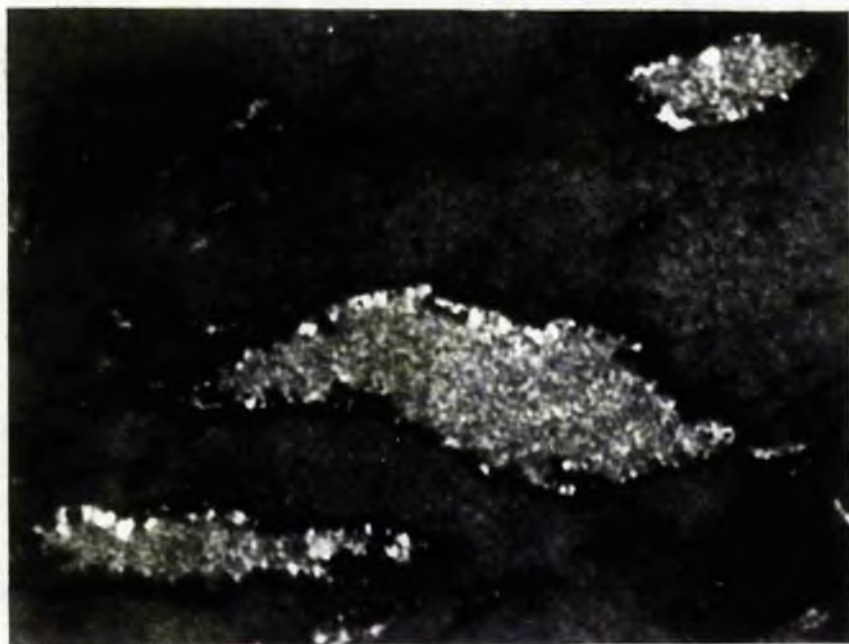


Plate 8. Photomicrograph illustrating mineral contaminated granular mosaic within graptolite fragments in sample LBR-3. Magnification X600, reflected light, partially crossed polars, oil immersion.

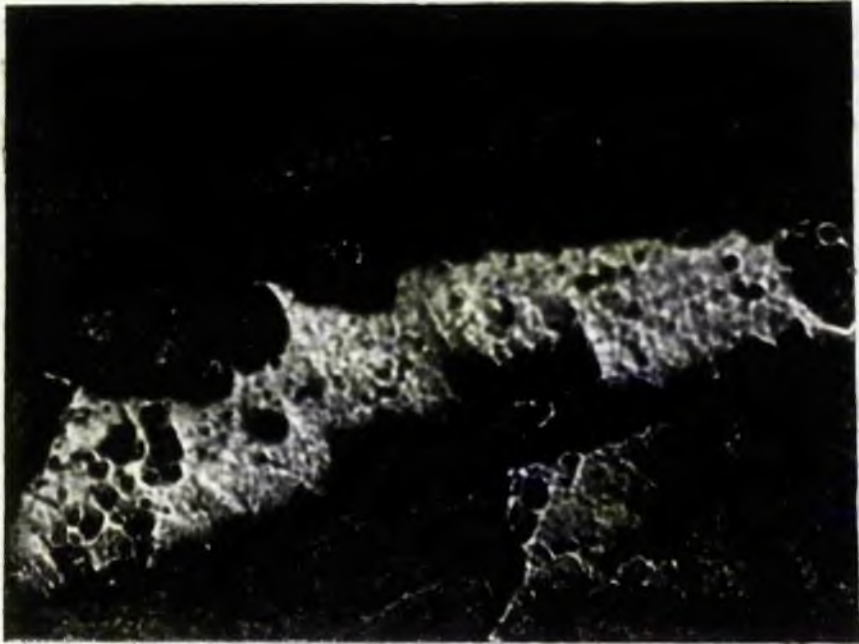


Plate 9. Photomicrograph illustrating vesiculated granular mosaic within graptolite fragments in sample LB-18. Magnification X600, reflected light, partially crossed polars, oil immersion.

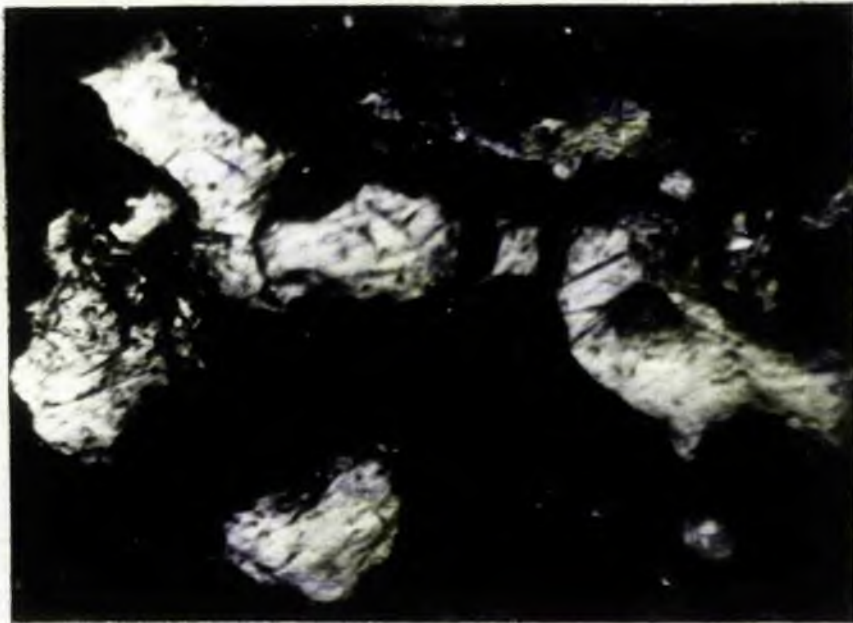


Plate 10. Photomicrograph illustrating sheared graptolite fragments within sample LBR-8. Magnification X600, reflected light, partially crossed polars, oil immersion.

CHAPTER VI

APPLICATION OF GRAPTOLITE REFLECTIVITY
AS A RANK PARAMETER

1. INTRODUCTION

Now that the behaviour of the various optical parameters of carbonized graptolite remains has been discussed it is clear that the reflectivity values give an indication of the rank of the organic material within the sediment. The concept of rank when applied to coals indicates the overall maturity or grade of a given coal but does not give any indication of the geological processes which may have caused the effect. There are various methods of measuring the rank of coals. These include chemical analysis (ultimate analysis) of the important constituent elements; carbon, hydrogen, oxygen, nitrogen and sulphur, measurement of calorific value, determination of coking properties, proximate analysis which determines directly inherent moisture, volatiles, ash and fixed carbon, and reflectance of vitrinite.

All of the above methods may be used to draw rank-maps for a series of coal-bearing strata. If however, the organic matter is finely disseminated throughout a sediment a measure of rank is most easily obtained from reflectivity measurements because all other methods require preliminary time consuming separation of the organic material from the inorganic matrix.

2. AREAS OF STUDY

Two areas have been selected for the study of graptolite reflectance values in a regional context. These include an area of approximately 15x5 km on the eastern margin of Luce Bay just north of Port William (Figs.5 and 26) and an area of approximately 40x16 km

in the vicinity of Moffat (Fig.4). Both areas are geologically similar in that each contains outcrops of Hartfell and Birkhill Shales which have been inlayed into Gala Greywackes as a result of Caledonian thrusting (Mitchell 1974; McKerrow and Mitchell 1975; Weir in litt.). The shale inliers of the Moffat region are bounded to the south-east by the Ettrick Valley Thrust (Toghill 1970b) which is postulated to continue along the Caledonide strike to the east coast of Luce Bay where it bounds the major shale outcrop of the area (Weir in litt.). The thrust then continues in a south-westerly direction into Luce Bay where it is offset by a dextral wrench fault, the Loch Ryan fault, before re-appearing in the Rhinns of Galloway where it delimits the shale outcrop at Clanyard Bay (Fig.10).

3. VARIATION IN GRAPTOLITE REFLECTANCE VALUES ALONG THE EASTERN MARGIN OF LUCE BAY

a) Sample collection

Samples LB-1 - LB-11 and also sample LB-26 were collected from the shale inliers north of Port William on the eastern margin of Luce Bay (Figs.5 and 26). Detailed description and the location of each of these samples is given in Appendix E. The samples were prepared, mounted and polished according to the standard procedure, and mean reflectance values were measured in oil at 546 nm.

b) Results

Reflectivity values derived as a result of about twenty measurements over the surface of each block are tabulated together with the relative grid parameters of the samples in Table 6-1. The

values were subjected to trend surface analysis according to the method of Cole (1969). The computed planar, quadratic and cubic surfaces yield fit values of 17.1, 26.7 and 68.0 per cent respectively. Comparison of these values indicates that the 'best-fit' surface is the cubic surface (Fig.172).

Two separate trends in reflectivity may be observed when the computed 'best-fit' surface is viewed along sections drawn perpendicular to the regional strike. A section through the central area of the southerly inlier indicates a progressive rise in reflectivity towards the main shale outcrop. After attaining a maximum value along the northerly margin of the main outcrop, reflectance values are computed to decrease until a minimum value is attained along the southern margin of the most northerly shale outcrop. In contrast, a section through the western extremity of the inliers, perpendicular to the strike, indicates a northerly decrease in values up to the southern contact of the major inlier. Values thereafter increase to a maximum in the vicinity of the southern limit of the northerly inlier.

c) Interpretation

The majority of the samples examined have reflectivities ranging from 1.31 to 3.26 per cent. By analogy with the response of vitrinite to rank increases, it appears that the graptolite material is similar to a coal series which ranges from low volatile coal to anthracite with the mean composition lying near to a coal equivalent with 92 per cent d.a.f. carbon i.e. at the junction between semi-anthracite and anthracite. Three samples exhibit reflectivity values

in excess of 4.0 per cent. These, by comparison with coal, indicate that the graptolite organic material is of higher rank and similar to coals close to the anthracite to meta-anthracite boundary (McCartney and Teichmüller 1972).

The variation in rank of the organic matter within the sediments exposed along the eastern margin of Luce Bay can be equated to metamorphic stages. Since the determining factor controlling the progressive increase in crystallinity in illite is temperature with little effect from pressure (Kubler 1968) and the main control of the progressive geochemical coalification of organic matter is also temperature with only minor effects from static pressure (Teichmüller and Teichmüller 1966) it is possible to relate the crystallinity of illite to the rank of associated coals and coaly matter in sedimentary rocks. As a result of detailed investigation of the relationship between the crystallinity of illite and the rank of the associated organic matter it has been observed that the stage of "early metagenesis" (Kossovskaya and Shutov 1961, 1970) is associated with coals of anthracite and low grade meta-anthracite rank with local occurrences of semi-anthracites (Kisch 1974). The transition from the stage of "early metagenesis" or "very low stage metamorphism" (Winkler 1970) to the epizonal greenschist facies is associated with coals which are close to the anthracite to meta-anthracite boundary and generally with low grade meta-anthracites. Analysis of rank therefore indicates that the sediments are most probably in the lowest grade of regional metamorphism.

An attempt has been made to minimise local variations in the reflectivity data by the use of trend surface analysis. This

technique however suffers from severe limitations when, as in this case, few data points are considered. The derived trends although informative are only of limited value in interpreting the regional variation in rank. At this stage however, it appears that there may be some relationship between the area of elevated rank and the occurrence of faults (Gordon 1962) but further investigation is required.

4. VARIATION IN GRAPTOLITE REFLECTANCE VALUES IN THE VICINITY OF MOFFAT

a) Sample collection and analysis of textures

The MG-series of samples, collected on a grid basis in the vicinity of Moffat, was again prepared and mounted for microscopic examination in incident light according to the standard technique. Detailed descriptions of the samples are given in Appendix E and the locality of each is illustrated in Fig.4.

Examination of the textures developed in the organic matter reveals that some of the samples have suffered carbonization. For example, strained extinction is evident in the organic material collected from Range Cleuch (sample MG-3, Plate 11) and flow texture is visible in sample HCL-30 collected from Hartfell (Plate 12). Granular mosaic texture is visible in samples from Hartfell (eg. sample HCL-8, Plate 13) and also in sample MG-14 which was collected from Crosscleuch (Plates 14, 15).

b) Results

Mean reflectance values at 546 nm in oil are tabulated

for the samples in Table 6-2. Values quoted for Dobb's Linn (DL) and Hartfell (HL) are averages of the results found for 31 and 53 samples respectively. These averages are quoted at this stage in order to avoid 'over-weighting' of the sample distribution in the following regional assessment.

A grand total of 114 samples collected in the vicinity of Moffat have been subjected to reflectivity analysis. Univariant statistical analysis reveals a population ranging from 0.75 to 6.67 per cent with a mean of 3.67 per cent and a standard deviation of 1.22 per cent.

Trend surface analysis has been conducted on the reflectance values of the MG-series of samples. Values for samples MG-5, MG-5A, MG-6 and MG-7 have been omitted from the study since all four samples were taken from shales which outcrop in stratigraphic continuity with greywackes which are exposed to the south-east of the Ettrick Valley Thrust. This major tectonic feature is taken as the southern boundary of the Moffat Shales (Toghill 1970b; Weir in litt.) and it is therefore not realistic to include data from both sides of the discontinuity in the same statistical analysis.

Trend surface analysis produced linear, quadratic and cubic surfaces with percentage fits of 36.9, 53.3 and 64.5 respectively. The plot of the cubic surface (Fig.173) indicates that the reflectance values are distributed along the south-eastern flank of a north-east to south-west trending dome. Computed values across this dome range from 1.75 per cent along the outcrop of the Ettrick Valley Thrust to 6.75 per cent to the north-west of Hartfell.

c) Interpretation

The computed regional variation in reflectivity for the Moffat region differs markedly from that observed at Luce Bay. In the Moffat region the results indicate that the rank of the organic material increases away from the boundary thrust whereas along the margin of Luce Bay the results seemed to indicate an increase in rank towards faults. Furthermore, in the Moffat region the organic material has attained a higher rank, comparable in places to that of meta-anthracites.

Many workers have noted a progressive rise in rank, particularly in coals, towards zones of intense tectonic deformation. A progressive decrease in volatiles from bituminous coals to anthracites has been demonstrated towards the highly folded and thrust Allegheny Front in the Pennsylvanian of the Appalachian coal belt (White 1913). Similarly it has been shown that a decrease in volatiles occurs above and below the Sutan Thrust in the Ruhr coal field (Teichmüller and Teichmüller 1958). In the South Wales coal field it has been suggested that the volatile content of the coal is determined by the proximity to a major low-angle thrust (Trotter 1948).

More recent data however, have demonstrated that pressure plays only a minor role in the geochemical coalification of organic matter (Teichmüller and Teichmüller 1966). An increase in rank towards a fault plane is therefore not directly related to the origin of the fault but is more probably related to secondary processes such as the preferential percolation of hot fluids along the zone of weakness. That such hydrothermal fluids flowed along fault planes in the Moffat area is perhaps evidenced by the occurrence of old copper

mine workings along the outcrop of the Talnothy Thrust (Weir in litt.) in the Auchencat Burn which drains Hartfell Scaur.

The source of the fluids remains problematical. However, it is perhaps pertinent to observe that the distribution of reflectivity contours within the shales in the vicinity of Moffat is comparable to the distribution of isovols in Carboniferous coals which have been affected by the Weardale granite under the Alston Block in Durham (Trotter 1954). Approaching the Alston Block, Trotter observed a decrease in volatile content of the coals (ie. an increase in rank). The variation in volatile content was found to relate, not only to zones of hydrothermal mineralization, but also to the gravity contours.

Although comparison cannot be made in this study between reflectance and zones of mineralization there is close similarity in the south-west part of the study area between the Bouguer gravity anomaly map and the reflectivity map (compare Figs 173 and 174).

It may therefore be implied that the distribution of rank in the vicinity of Hartfell is either a direct or an indirect result of plutonic activity. In the former case the distribution of rank would be controlled by heat flow from a buried igneous body as indicated by the gravity anomaly map while in the latter case it would be controlled by the passage of hot percolating fluids resulting from igneous activity.

The thermal effects of the postulated igneous body are not manifested along the strike of the Ettrick Valley Thrust and it is possible to trace the 1.75 per cent reflectivity contour along the fault in a north-easterly direction as far as Berrybush Burn (sample MG-16, Figs.4 and 173). At this locality the 1.75 per cent contour

is deflected away from the thrust towards the north-west and after circumventing a computed 'low' of very little significance since it is not based on any data points the contour cuts the inlier at Ettrickbridgend (sample MG-27).

The geological implications of the observed contour pattern are noteworthy since if the Ettrick Valley Thrust bounds the southern limit of the black shale inliers in this area then it must curve away from the Caledonide strike towards the south-east in order to accommodate the inlier exposed around Ettrickbridgend. The reflectivity data however appear to suggest that the Ettrick Valley Thrust has been physically displaced. Such a displacement could take the form of a wrench fault orientated in a north-west to south-east direction. This trend coincides with that described by Weir (1968) for primary dextral wrenches in the Gatehouse area. If a lateral movement of about 6 km is postulated along the wrench it is possible to reconstruct the position of the inliers in the north-eastern part of the study area so that before faulting the exposure of black shale at Ettrickbridgend was along strike from the Ettrick Valley inliers. Assuming continuity of the fault, the inliers at Mountbenger and in the Eldinhope Burn (sample MG-15) can similarly be reconstructed to be along strike from the shales which are exposed in the Carrifran Burn and in the Meggat Valley.

5. THE STRATIGRAPHIC VARIATION IN REFLECTIVITY

a) Introduction

Examination of the regional trend in reflectivity for the Moffat region has indicated that the organic material within the

sediments exhibits increased temperature effects away from the Ettrick Valley Thrust and towards an area which lies slightly north-west of Hartfell. It is now proposed to investigate the stratigraphic variation in reflectivity at two localities. The two localities which immediately lend themselves to such an investigation are Dobb's Linn and Hartfell, primarily because at each there is part of the local type succession (Toghill 1968, 1970a; Watson 1971).

b) Stratigraphic variation at Dobb's Linn

A mean reflectance value of 3.27 per cent has been calculated from 31 samples measured up the stratigraphic succession of shales and mudstones which is exposed in Dobb's Linn. The distribution of the reflectance values over all 14 graptolite zones in the sequence is displayed in Fig.175 where the divisions of the ordinate have been made proportional to the zone thicknesses as proposed by Toghill (1968, 1970a).

In order to clarify and to simplify the stratigraphic relationship of reflectivity, a polynomial regression curve has been calculated. The method employed was to fit progressively higher order polynomials to the data, starting at the first order and continuing until there was no improvement in terms of sums of squares between one order and the next.

A fourth order polynomial curve with an F-value of 4.69 was computed for the variation of reflectivity with stratigraphic thickness at Dobb's Linn. The curve which is significant at the 99 per cent confidence level is superimposed upon the scatter plot of the data (Fig.175). The computed trend indicates a 2.6 per cent

increase in reflectivity between the Glenkiln and the maximus Zone. This increase equals a 0.031 per cent variation in reflectivity per metre of strata.

c) Stratigraphic variation at Hartfell

Mean reflectance values of 53 samples from the north cliff at Hartfell yield an average value of 4.45 per cent. The distribution of values are displayed in Fig.176a. The superimposed third order polynomial regression curve, which is significant at the 99 per cent confidence level, indicates a decrease in values up the cliff with an average rate of decrease of 0.025 per cent reflectivity per metre of sediment.

The time relationship between strike-faulting and the thermal imprinting of the sediments was investigated firstly by restoring the sedimentary succession to its pre-fault position in the manner described in Chapter I, p. 7 . Reflectance values were then correlated with distance up the true stratigraphical succession. A fourth order polynomial curve, significant only at the 90 per cent level and indicating a general rise in reflectivity through the succession, was found to fit the data. This curve is not considered to be within the significance level of the statistical test (Fig.176b).

d) Conclusions

Since the strata at Dobb's Linn and particularly those in the upper part of the succession are effectively vertical, the computed profile showing a general increase in reflectivity up the succession is taken to indicate that the centre of heat which caused

the variation in rank was situated to the north-west of this locality. Comparison of the levels of significance of the two profiles generated for the variation in rank at Hartfell indicates that thermal imprinting of the sediments took place after the onset of f_1 folding and associated strike faulting.

6. THE SPECTRAL VARIATION IN OPTICAL PROPERTIES OF GRAPTOLITE FRAGMENTS FROM HARTFELL

a) Introduction

A detailed description of the spectral variation in the optical properties of carbonized organic material from Clanyard Bay was given in Chapter V. It is now proposed to describe the dispersion trends for reflectivity, refractive and absorptive indices for a series of samples collected from the north cliff at Hartfell. The selected samples are listed in Table 6-3.

Ten reflectance measurements were made over the samples in air and in oil at each of the seven wavelengths. The values at each wavelength were averaged (Table 6-4) and 'best-fit' polynomial regression curves were then computed to illustrate the spectral variation of reflectivity in each of the two media (Figs.177-179). Regression parameters for the curves are given in Appendix D. Estimated reflectance values in air and in oil were then derived at each of the seven wavelengths from the regression equations. Values of refractive and absorptive index were then calculated from the estimated reflectance values (Table 6-4) and plotted versus wavelength (Figs.180-182).

b) Reflectivity trends

All samples, except sample HL-15, display reflectivity trends which increase towards the red in the visible spectrum. Sample HL-15 although displaying a slight rise between 410 and 442 nm exhibits a marked decrease in values between 502 and 710 nm (Fig.177). A similar decrease in reflectance values with increasing wavelength was observed in two samples collected from Clanyard Bay. These samples were collected from immediately adjacent the dyke.

It might therefore be expected that by analogy with the results at Clanyard Bay, sample HL-15 has suffered extreme heat effects. This is not however consistent with the fact that this sample was collected nearer the top of the cliff and hence further away from the postulated plutonic body than any other sample studied (Table 6-3).

The cause of this anomalous behaviour may be related to the fact that sample HL-15 was collected from a blocky mudstone band immediately adjacent to a strike-reverse fault plane (Fig.6). Two possible explanations may therefore be suggested;

either, thermal effects due to the postulated plutonic body have been superimposed upon earlier local effects related to fault initiation,
or, after, or simultaneously with, the imposition of thermal effects due to the plutonic body there was localized hydrothermal activity which preferentially affected material in the vicinity of fault planes.

There is ample evidence to support the presence of hydrothermal activity in the vicinity of the fault planes. Copper has

been worked from small mines associated with the main thrust at Hartfell, and along strike at Talnotry there is extensive evidence of hydrothermal activity (D.R.Cook pers.comm).

c) Refractive index trends

Again, all samples except sample HL-15, display similar trends of increasing refractive index towards the red. Sample HL-15 like sample LB-18 from Clanyard Bay, exhibits a trend in values which firstly rises from a low value at 410 nm to a maximum at 502 nm before falling to a low at 651 nm. Between 651 and 710 nm the trends of the two samples diverge from one another. This may not however be very significant since the overall response of the reflectivity apparatus is very poor at this wavelength.

d) Absorptive index trends

There is little variation in absorptive index with wavelength. Values range from about 0.35 to 0.50 with the majority of dispersion trends exhibiting an increase towards the blue.

e) Discussion

Not only the trends, but also the magnitude of the optical parameters of the organic material in the sediments at Hartfell are similar to those described for the carbonized material from Clanyard Bay. It may therefore be stated that the organic material within the sediments at Hartfell has been thermally affected. The exact nature of the heat source still remains uncertain but as the thermal effects are evident over a vertical distance of 80 metres it

seems unlikely that any small igneous body such as a thin sill or dyke could have caused the increase in rank.

7. VARIATION IN THE REFLECTIVITY OF GRAPTOLITES IN THE VICINITY OF IGNEOUS PLUTONS

a) Introduction

If carbonization of the organic material in the sediments in the vicinity of Moffat has been caused by thermal effects from a deep-seated igneous pluton it is clear that the reflectivity-temperature calibration derived in Chapter V for the Clanyard Bay suite of samples is rendered invalid. It was therefore decided to examine graptolite reflectivities in a contact metamorphic aureole to assess the changes with distance from the pluton, and attempt to calibrate a more realistic geothermometer for the Moffat region.

It was not necessary to collect further samples for this study as several suitable specimens were already housed in the Department of Geology at St. Andrews University. These were collected from black shale sequences along the western margins of the Loch Doon and Flect granites by S. Klimčik and D.R. Cook who mapped the respective areas as part of their undergraduate and PhD dissertations. Sample localities are summarised in Table 6-5.

b) Results

The samples were prepared, mounted and polished for reflectivity determination according to the usual standard process. Mean reflectance values in oil at 546 nm were calculated for each

sample from about 20 individual determinations (Table 6-5).

Even although measurements were made on samples collected from the vicinity of two different plutons and no account was taken of differences in contact characteristics it is found that there is a good linear correlation (PMCC - 0.88) between reflectivity and the distance a sample was from the contact of the intrusion. Regression analysis yields a line, significant at the 99.9 per cent level, of slope -4.66 and intercept 12.46 (Fig.183).

It may therefore be concluded that for distances of between one and two kilometres from the contact of large plutons the reflectivity of graptolite fragments is inversely proportional to distance. This relationship may not hold within areas of higher heat flow.

c) Computation of temperatures outside a cooling pluton and their relationship with reflectivity

The thermal model used in this part of the study was that of Jaeger (1964) who has presented equations which simulate the cooling of a sphere. In the model it is assumed that a constant initial temperature existed over the sphere and that the temperature outside the sphere was zero. Temperature T, at radius x, at time t, is given by

$$T = T_0 \psi (\epsilon \tau)$$

where

$$\psi (\epsilon \tau) = \frac{1}{2} \left[\frac{\operatorname{erf} \epsilon + 1}{2\tau^{1/2}} - \frac{\operatorname{erf} \epsilon - 1}{2\tau^{1/2}} - \frac{2\tau^{1/2}}{\epsilon \pi^{1/2}} \left(e^{-(\epsilon-1)^2/4\tau} - e^{-(\epsilon+1)^2/4\tau} \right) \right]$$

where

$$\epsilon = \frac{x}{d}$$

where

$$\tau = \frac{kt}{d^2}$$

and where T = temperature

To = initial temperature of magma

erf = tabulated error function

k = diffusivity of country rock

t = time after intrusion

d = radius of the sphere

x = distance from outside the sphere

A computer program, written by Stephens (1972), was used to assess the temperature outside a sphere. Time was increased by orders of magnitude in each successive run and within each run the distance from the contact was increased by 25 metres. The estimates used in applying the model are:-

To = 700°C

d = 8 km

k = 0.00721

The maximum temperatures which were calculated using the above estimates at the measured distances that the samples in the LD and DRC series are from the pluton contacts have been abstracted from the results (Table 6-6). These temperatures have been correlated with reflectance values derived from the linear regression line for the variation of reflectivity with distance (Fig.184).

d) Conclusion

If the described thermal model is applicable in the Moffat region then the spread in reflectivities indicates that the temperature never exceeded 180°C at Dobb's Linn and 195°C at Hartfell. Such temperatures are realistic and are in keeping with the observed mineralogy of the sediments (Chapter II).

| Sample | Grid/parameters | | Ro (mean) |
|--------|-----------------|-----|-----------|
| | X | Y | |
| LB-1 | 094 | 056 | 1.31 |
| LB-2 | 095 | 051 | 3.03 |
| LB-3 | 131 | 066 | 2.10 |
| LB-4 | 156 | 074 | 4.40 |
| LB-5 | 186 | 108 | 3.26 |
| LB-5A | 203 | 108 | 3.26 |
| LB-6 | 204 | 103 | n.d. |
| LB-7 | 158 | 041 | 4.12 |
| LB-8 | 053 | 108 | 1.83 |
| LB-9 | 072 | 098 | 4.54 |
| LB-10 | 067 | 102 | 2.54 |
| LB-11 | 084 | 102 | 1.89 |
| LB-26 | 172 | 078 | 3.17 |

n.d. = reflectance value not obtained due to lack of organic particles.

TABLE 6-1 Mean reflectance values of samples from the east coast of Luce Bay.

| Sample | Grid/parameters | | Ro (mean) |
|--------|-----------------|-----|-----------|
| | X | Y | |
| MG-1 | 229 | 070 | 2.10 |
| MG-2 | 262 | 088 | 1.89 |
| MG-3 | 267 | 090 | 2.88 |
| MG-4 | 298 | 077 | 2.81 |
| MG-5 | 286 | 067 | 2.04 |
| MG-5A | 269 | 065 | 3.99 |
| MG-6 | 269 | 065 | n.d. |
| MG-7 | 269 | 065 | 2.56 |
| MG-8 | 306 | 079 | 2.27 |
| MG-9 | 319 | 099 | 2.56 |
| MG-10 | 333 | 087 | 2.32 |
| MG-11 | 299 | 185 | 6.50 |
| MG-12 | 299 | 185 | 2.27 |
| MG-13 | 373 | 123 | 2.16 |
| MG-14 | 431 | 138 | 1.68 |
| MG-15 | 537 | 114 | 1.44 |
| MG-16 | 448 | 100 | 1.54 |
| MG-17 | 422 | 217 | 4.36 |
| MG-18 | 089 | 242 | 6.67 |
| MG-19 | 065 | 226 | 3.14 |
| MG-20 | 041 | 147 | 1.78 |
| MG-21 | 176 | 086 | n.d. |
| MG-22 | 190 | 079 | 0.75 |
| MG-23 | 131 | 068 | 2.50 |
| MG-24 | 107 | 132 | n.d. |
| MG-25 | 377 | 092 | 2.37 |
| MG-26 | 121 | 165 | 5.63 |
| MG-27 | 641 | 028 | 3.42 |
| C1 | 247 | 165 | 3.24 |
| MB | 573 | 124 | 2.20 |
| DL | 328 | 144 | 3.27 |
| HF | 173 | 208 | 4.45 |

n.d. = reflectance value not obtained due to lack of suitable organic particles.

MB Average of three samples collected from Mountbenger.

DL Average of 31 samples collected from Dobb's Linn.

HF Average of 53 samples collected from Hartfell.

TABLE 6-2 Mean reflectance values of samples collected in the vicinity of Moffat.

| Sample | Ro (mean) | Distance up cliff (metres) | Distance up unfaulted stratigraphic succession (metres) |
|--------|-----------|----------------------------|---|
| HL-15 | 4.76 | 81.7 | 15.0 |
| HL-14 | 4.64 | 78.1 | 14.6 |
| HL-13 | 4.59 | 74.6 | 15.7 |
| HCL-26 | 4.60 | 70.5 | 11.6 |
| HCL-29 | 4.41 | 70.0 | 11.5 |
| HCL-31 | 4.72 | 69.0 | 10.4 |
| HCL-16 | 4.51 | 66.0 | 8.6 |
| HL-4 | 5.70 | 5.3 | 17.3 |

TABLE 6-3 Stratigraphic location of those samples from Hartfell which were used for dispersion analysis.

| Sample | W | Ro | Rest ¹ | Ra | Rest ² | n | k |
|---------|-----|------|-------------------|-------|-------------------|------|------|
| HCL-16 | 410 | 3.46 | 3.49 | 9.36 | 9.40 | 1.55 | 0.38 |
| | 442 | 4.05 | 3.97 | 10.21 | 10.14 | 1.56 | 0.40 |
| | 502 | 4.51 | 4.61 | 11.28 | 11.35 | 1.60 | 0.43 |
| | 546 | 4.98 | 4.92 | 12.17 | 12.08 | 1.63 | 0.43 |
| | 590 | 5.13 | 5.13 | 12.55 | 12.65 | 1.67 | 0.43 |
| | 651 | 5.38 | 5.39 | 13.27 | 13.21 | 1.69 | 0.44 |
| | 710 | 5.71 | 5.71 | 13.43 | 13.45 | 1.68 | 0.46 |
| HCL-26 | 410 | 3.85 | 3.80 | 10.51 | 10.51 | 1.61 | 0.38 |
| | 442 | 3.75 | 3.83 | 11.15 | 11.13 | 1.67 | 0.37 |
| | 502 | 4.03 | 4.02 | 12.13 | 12.25 | 1.78 | 0.35 |
| | 546 | 4.28 | 4.24 | 13.09 | 12.98 | 1.84 | 0.34 |
| | 590 | 4.49 | 4.48 | 13.61 | 13.60 | 1.89 | 0.33 |
| | 651 | 4.77 | 4.82 | 14.14 | 14.20 | 1.93 | 0.33 |
| | 710 | 5.08 | 5.06 | 14.43 | 14.41 | 1.92 | 0.35 |
| HCL-26A | 410 | 5.52 | 5.60 | 10.56 | 10.44 | 1.40 | 0.50 |
| | 442 | 5.76 | 5.66 | 11.00 | 11.25 | 1.46 | 0.50 |
| | 502 | 5.98 | 5.89 | 12.91 | 12.68 | 1.56 | 0.49 |
| | 546 | 6.01 | 6.13 | 13.41 | 13.59 | 1.62 | 0.49 |
| | 590 | 6.29 | 6.41 | 14.49 | 14.34 | 1.67 | 0.49 |
| | 651 | 6.94 | 6.77 | 14.95 | 15.06 | 1.71 | 0.49 |
| | 710 | 6.92 | 6.98 | 15.36 | 15.33 | 1.71 | 0.50 |
| HCL-29 | 410 | 3.66 | 3.86 | 10.12 | 12.43 | 1.81 | 0.33 |
| | 442 | 4.63 | 4.06 | 15.55 | 12.71 | 1.82 | 0.34 |
| | 502 | 3.78 | 4.50 | 13.11 | 13.26 | 1.83 | 0.36 |
| | 546 | 4.82 | 4.87 | 13.57 | 13.65 | 1.83 | 0.38 |
| | 590 | 6.03 | 5.28 | 14.12 | 14.05 | 1.82 | 0.40 |
| | 651 | 5.49 | 5.93 | 14.03 | 14.60 | 1.78 | 0.44 |
| | 710 | 6.71 | 6.63 | 15.32 | 15.13 | 1.74 | 0.48 |

TABLE 6-4 Variation in optical properties of graptolites with wavelength for selected samples from Hartfell.

/continued

| Sample | W | Ro | Rest ¹ | Ra | Rest ² | n | k |
|--------|-----|------|-------------------|-------|-------------------|------|------|
| HCL-31 | 410 | 4.23 | 4.23 | 9.36 | 9.30 | 1.46 | 0.43 |
| | 442 | 4.42 | 4.42 | 9.59 | 9.69 | 1.47 | 0.44 |
| | 502 | 4.72 | 4.72 | 10.48 | 10.47 | 1.50 | 0.45 |
| | 546 | 4.91 | 4.90 | 11.14 | 11.05 | 1.53 | 0.45 |
| | 590 | 5.05 | 5.07 | 11.54 | 11.59 | 1.56 | 0.45 |
| | 651 | 5.35 | 5.33 | 12.23 | 12.25 | 1.60 | 0.46 |
| | 710 | 5.65 | 5.65 | 12.74 | 12.73 | 1.61 | 0.47 |
| HL-4 | 410 | 5.60 | 5.61 | 13.25 | 13.27 | 1.65 | 0.46 |
| | 442 | 5.38 | 5.38 | 13.51 | 13.49 | 1.71 | 0.44 |
| | 502 | 5.39 | 5.35 | 13.96 | 13.91 | 1.78 | 0.41 |
| | 546 | 5.49 | 5.55 | 14.16 | 14.26 | 1.80 | 0.42 |
| | 590 | 5.88 | 5.86 | 14.70 | 14.66 | 1.80 | 0.43 |
| | 651 | 6.31 | 6.30 | 15.36 | 15.34 | 1.82 | 0.44 |
| | 710 | 6.05 | 6.50 | 16.16 | 16.17 | 1.92 | 0.42 |
| HL-13 | 410 | 4.72 | 4.73 | 12.45 | 12.30 | 1.67 | 0.42 |
| | 442 | 5.06 | 5.04 | 12.41 | 12.70 | 1.67 | 0.43 |
| | 502 | 5.35 | 5.39 | 13.55 | 13.45 | 1.71 | 0.43 |
| | 546 | 5.52 | 5.53 | 14.17 | 14.01 | 1.77 | 0.43 |
| | 590 | 5.69 | 5.63 | 14.47 | 14.60 | 1.83 | 0.41 |
| | 651 | 5.81 | 5.85 | 15.51 | 15.52 | 1.94 | 0.38 |
| | 710 | 6.34 | 6.33 | 16.62 | 16.60 | 2.03 | 0.37 |
| HL-14 | 410 | 4.40 | 4.33 | 10.86 | 10.65 | 1.56 | 0.42 |
| | 442 | 4.32 | 4.43 | 10.52 | 10.90 | 1.57 | 0.42 |
| | 502 | 4.66 | 4.67 | 11.39 | 11.38 | 1.59 | 0.43 |
| | 546 | 4.98 | 4.87 | 12.19 | 11.72 | 1.60 | 0.44 |
| | 590 | 5.04 | 5.06 | 11.73 | 12.06 | 1.61 | 0.44 |
| | 651 | 5.26 | 5.31 | 12.50 | 12.51 | 1.63 | 0.45 |
| | 710 | 5.54 | 5.52 | 12.96 | 12.93 | 1.65 | 0.46 |

TABLE 6-4 Continued.

/continued

| Sample | W | Ro | Rest ¹ | Ra | Rest ² | n | k |
|--------|-----|------|-------------------|-------|-------------------|------|------|
| III-15 | 410 | 7.53 | 7.59 | 18.73 | 19.04 | 2.15 | 0.39 |
| | 442 | 8.13 | 8.04 | 20.44 | 20.00 | 2.27 | 0.36 |
| | 502 | 8.25 | 8.22 | 20.41 | 20.27 | 2.31 | 0.34 |
| | 546 | 7.90 | 7.95 | 19.41 | 19.69 | 2.26 | 0.35 |
| | 590 | 7.40 | 7.50 | 18.59 | 18.87 | 2.20 | 0.36 |
| | 651 | 6.97 | 6.84 | 18.51 | 18.09 | 2.20 | 0.32 |
| | 710 | 6.47 | 6.51 | 18.46 | 18.59 | 2.40 | 0.16 |

W = wavelength. (nm)

Ro = mean reflectance in oil. (%)

Rest¹ = estimated value for mean reflectance in oil
calculated from regression line. (%)

Ra = mean reflectance in air. (%)

Rest² = estimated value for mean reflectance in air
calculated from regression line. (%)

n = refractive index.

k = absorptive index.

TABLE 6-4 Continued.

| Sample | Distance from contact | Ro (mean) | Grid ref. |
|---------|-----------------------|-----------|---|
| LD-3 | 1000 m | 7.05 | ² ₄₁₆ ⁵ ₈₀₄ |
| DRC-455 | 1200 m | 6.18 | ² ₄₆₅ ⁵ ₆₉₅ |
| DRC-462 | 1600 m | 7.23 | ² ₄₆₅ ⁵ ₆₈₅ |
| LD-2 | 1600 m | 5.55 | ² ₄₁₂ ⁵ ₈₁₈ |
| DRC-457 | 1750 m | 4.51 | ² ₄₆₀ ⁵ ₆₉₀ |
| LD-1 | 2000 m | 3.16 | ² ₄₀₈ ⁵ ₈₁₁ |
| DRC-459 | 2100 m | 1.93 | ² ₄₆₀ ⁵ ₆₈₅ |
| LD-4 | 2100 m | 1.90 | ² ₄₀₈ ⁵ ₈₀₁ |

TABLE 6-5 Variation in graptolite reflectance values with distance from granite contacts.

| Distance | T _m ^o C | Ro (mean) |
|----------|-------------------------------|-----------|
| 1000 m | 250 | 7.80 |
| 1200 m | 230 | 6.87 |
| 1600 m | 185 | 5.00 |
| 1750 m | 168 | 4.31 |
| 2000 m | 140 | 3.15 |
| 2100 m | 128 | 2.68 |

TABLE 6-6 Variation in graptolite reflectance values with temperature outside a cooling sphere.

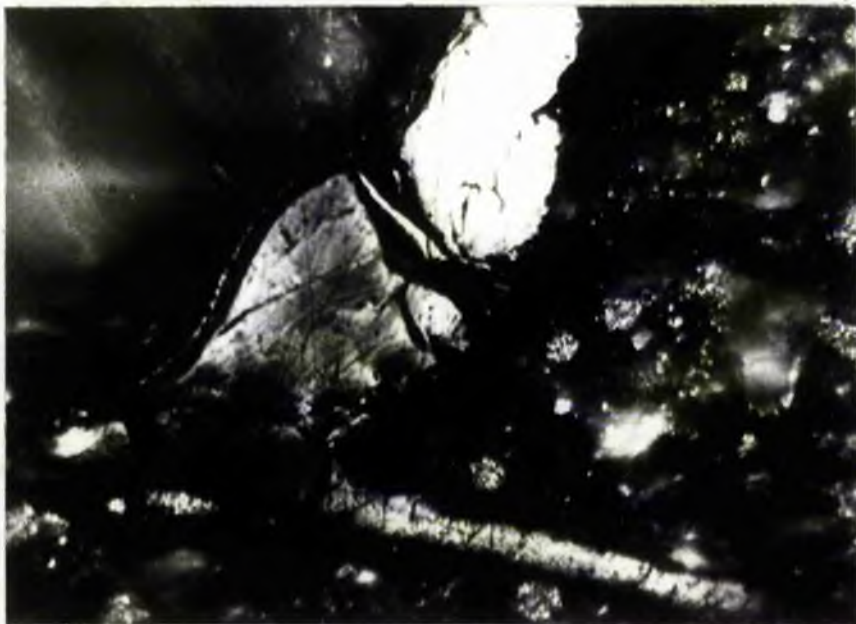


Plate 11. Photomicrograph illustrating strained extinction in a graptolite fragment within sample MG-3. Magnification X600, reflected light, partially crossed polars, oil immersion.

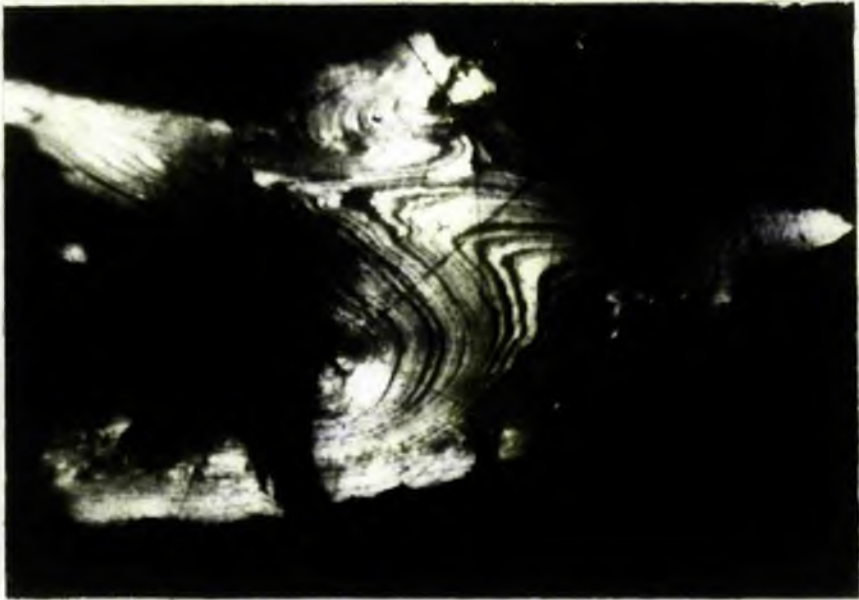


Plate 12. Photomicrograph illustrating flow banding in graptolite fragments within sample HCL-30. Magnification X600, reflected light, partially crossed polars, oil immersion.

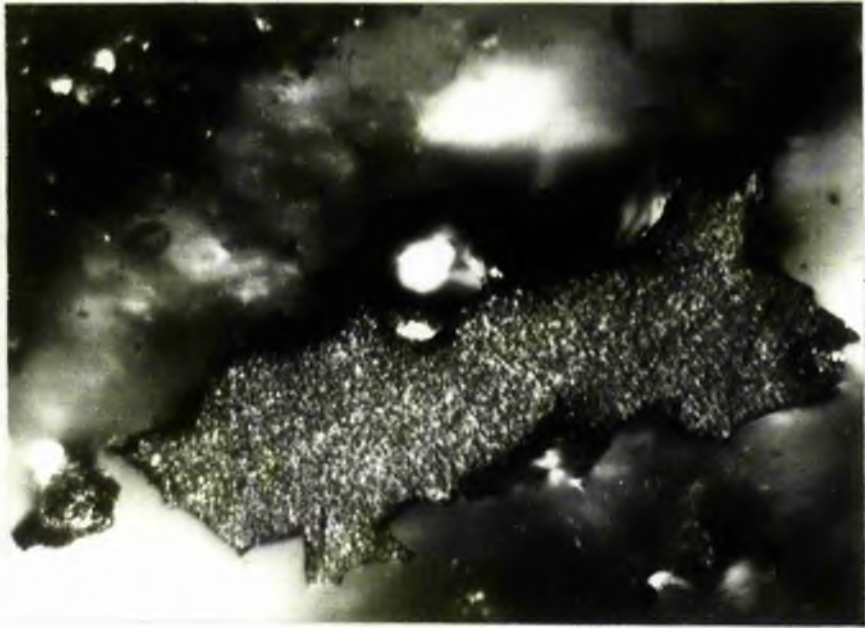


Plate 13. Photomicrograph illustrating granular mosaic texture within a graptolite fragment in sample HL-8. Magnification X600, reflected light, partially crossed polars, oil immersion.

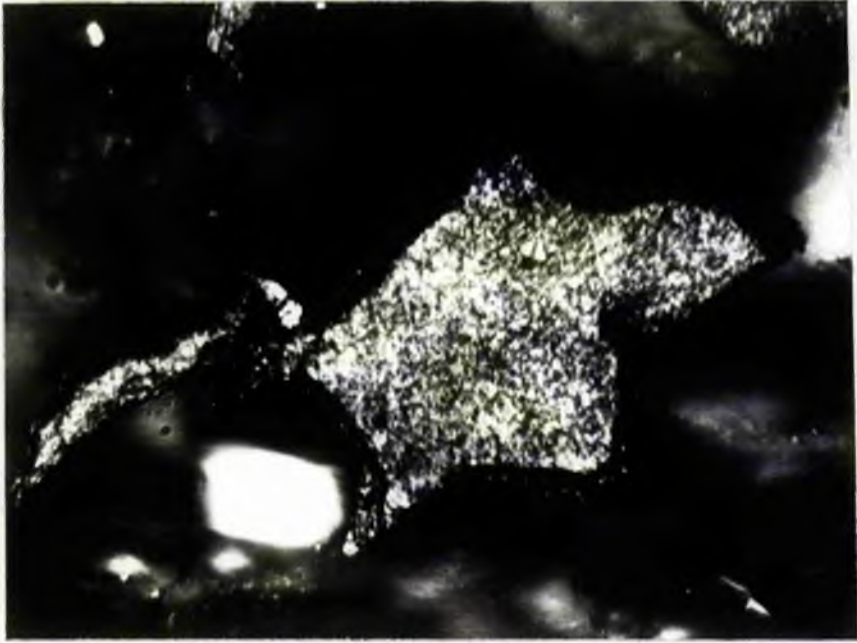


Plate 14. Photomicrograph illustrating granular mosaic within possibly a glyptograptid theca in sample MG-14. Magnification X600, reflected light, partially crossed polars, oil immersion.



Plate 15. Photomicrograph illustrating mineral interfered granular mosaic in proximal end of graptolite rhabdasome in sample MG-14. Magnification X600, reflected light, partially crossed polars, oil immersion.

CHAPTER VII

ELECTRICAL RESISTIVITY

1. INTRODUCTION

The determination of electrical resistivity of rocks in-situ is a technique most often used in geological exploration to determine indirectly the lithology of rock sequences at depth and also parameters such as water and oil saturation levels in porous rocks. In this chapter it is intended to examine the variation in resistivity of crushed samples from the Moffat Shales and to attempt to relate the values to the mineralogy and rank of the sediments.

It is first necessary to outline a few basic points concerning the electrical resistivity of rocks and minerals. All rocks conduct electricity but the degree to which any given rock conducts is a function of the resistivity of each of the component minerals and of the fluid filling any pore space. The great variability of mineral abundances and resistivities imposes a wide range of values upon the electrical resistivity of rocks.

Minerals, as with all solid materials, may be divided into three groups on the basis of the magnitude and mechanism of electrical conduction. Thus a mineral may be classified as a conductor, a semi-conductor or a dielectric. In general, native elements such as gold, copper, tin and platinum are conductors, whereas most sulphide minerals, arsenides, graphite and a few oxides such as cassiterite and cuprite are semi-conductors. The dominant rock-forming minerals - quartz, mica, feldspar and calcite - have very high resistivities, and are dielectrics. Reported resistivity values for selected minerals from each of the three classes are given in Table 7-1.

Most minerals, because of their crystallinity, exhibit

anisotropy thus causing variations in electrical conductance along the different crystallographic axes. This property is particularly pronounced in minerals of the semi-conductor class and has been studied in detail for graphite and molybdenite. Resistivities parallel to the graphite basal cleavage are of the order of 10^{-4} ohm cm^{-1} whereas values perpendicular to the cleavage are about 1.0 ohm cm^{-1} (Krishnan and Ganguli 1939). Values of resistivity measured along the two principal directions for molybdenite have been reported to vary by as much as three orders of magnitude (Dutta 1947).

Resistivities of rocks depend largely on which type of mineral is dominant. Rocks may be divided into two general groups on the basis of resistivity. The first group consists of rocks which contain large amounts of low resistivity ore minerals. These rocks exhibit resistivities which are characteristic of semi-conductors. The second group consists of rocks which are composed of minerals with high resistivities and as such comprises most sedimentary rocks. Examples of both groups are given in Table 7-2.

A detailed study of the variation in resistivity within coals of differing rank has been conducted in order to establish relationships between electrical properties of coal and parameters such as rank and grade. Resistivity values of coals range widely and can extend from the semi-conductor to the insulating regions. Values have been quoted as ranging from 10^9 to 10^{10} ohm cm^{-1} for brown coals to 10^2 ohm cm^{-1} for anthracites (Agroskin and Petrenko 1950).

More recently, the reflectivity, resistivity and hydrogen content of a series of heat affected coals have been correlated with temperature (Johnson et al., 1963). In this work it is found that

all three parameters can be independently used to determine the degree of alteration of the coal.

In Chapter VI of this work it was concluded that the rank of the Moffat Shales, as deduced from graptolite reflectivities, was elevated in part of the region about Moffat. A series of experiments was therefore initiated to examine the variation in resistivity of several Moffat Shale samples in an attempt to ascertain the presence of areas with low resistivity and to attempt to correlate rank with resistivity.

2. EXPERIMENTAL

A direct current method was used to determine the resistivity of the samples. Approximately 1 g of minus 200-mesh rock powder which had been dried for 24 hours at 50^oC was loaded through a funnel into a specially fabricated P.T.F.E. tube with an internal bore-diameter of 10 mm. The lower end of this tube was fitted with a silver-plated brass plug which formed one electrode. A second brass plunger, again silver-plated, formed the upper electrode. The whole assembly was placed in a metallurgical hydraulic press on a thick (5 mm) insulating sheet of P.T.F.E. and was clamped between the asbestos-covered jaws of the press. This was then loaded to pressure and the resistance across the rock powder calculated indirectly by first measuring the voltage across a standardized 100 ohm resistance by means of a Universal Precision Potentiometer (Pye 7565). The current flowing through the circuit was calculated and the voltage across the sample in the press was measured on a Fenlow 701 variable scale digital voltmeter. The resistance across the length of the

rock powder was then calculated using Ohm's Law. A block diagram of the circuit used and a section of the sample holder is given in Fig.185.

3. THE EFFECT OF PRESSURE ON RESISTIVITY MEASUREMENTS

a) Introduction

It is known that the resistivity of rocks decreases with depth and that the rate of change is greatest at depths of between 400 and 500 km (Jain 1964). Various parameters contribute to the observed change. Among these are the effects of pressure, temperature and cementation, all of which have been studied in detail in an attempt to understand the controlling influences that govern the response of electric logs.

The first resistivity-pressure studies demonstrated that for 20 sodium chloride saturated sandstone samples resistivity increased with pressure (Fatt 1957). These results were later amplified to include limestones (Wyable 1958; Glanville 1959).

These earlier works did not consider the effects of cementation upon the resistivity of the rocks. Later work indicated that the largest changes in resistivity with pressure occur in samples with significant amounts of clay cement (Marmorshtein 1962). In addition it was demonstrated that for some samples, particularly those with clay cements, the presence of cement decreases the resistivity whereas those with clay-carbonate cements show an increase in resistivity when pressure is applied.

A decrease in resistivity with increasing pressure was

also noted during a series of experiments in which the pressure ranged from 10 to 600 kg/cm² (Parkhomenko et al., 1960). It was noted that although the decrease was not always of the same magnitude, most of the variation was found at pressures below 300 kg/cm² and that it could be related to the degree of water saturation of the rock. Thus, the rate of change of resistivity of a rock with pressure is influenced by the water content.

The effects of pressure up to 10 kb on the electrical resistivity of 30 crystalline rocks have been studied (Brace and Orange 1968). It was found for rocks of low porosity that grain-size, mineralogy and degree of alteration have almost no effect and at high pressures porosity is the sole property that determines the resistivity of water-saturated rocks composed of non-conducting minerals. At low pressures a partially saturated rock becomes less resistive whereas a saturated rock becomes more resistive as pressure is increased. For rocks composed of conductive minerals pressure first causes a sharp decrease in resistivity and then has almost no effect.

Although temperature does not have a significant effect upon the shape of a resistivity-pressure curve there is a pronounced decrease in resistivity with increasing temperature (Parkhomenko 1967). In the case of an artificially heated basalt it was observed that over the temperature range of 19 to 215^oC pressure changed resistivity by 40 per cent. The effect was not so evident at higher temperatures but nevertheless it is apparent that the effect of temperature upon resistivity is more marked than that of pressure.

In summary, the resistivity of a rock when subjected to pressure is controlled by a number of factors. These include porosity,

water content, mineral content, composition of the cement and temperature. In this present study the effects due to porosity, water content and temperature have been neutralized by crushing the samples to a standard size (-200 mesh) and drying them at 50^oC for 24 hours before measurement at room temperature (23^oC). During crushing, the cement is broken down and therefore only affects the resistivity as part of the overall variation attributable to changes in mineral composition.

The prime aim in investigating the variation of resistivity with pressure was to establish a suitable pressure at which to measure the resistivity of a number of samples at a level of accuracy which would be unaffected by slight changes in pressure.

b) Experimental details and results

Samples LB-12, LB-13, LB-14, LB-15, LB-16 and LB-18, collected from the south side of the dyke at Clanyard Bay (Fig.144) were crushed to -200 mesh and dried for 24 hours at 50^oC. Resistivities were then calculated from measurements taken between 300 psi and 2000 psi at 100 psi intervals and also at 2500 and 3000 psi.

The results indicate that there is a decrease in resistivity with increasing pressure (Figs 186-187). The rate of change in resistivity with pressure is at a maximum for most samples between 300 and 1000 psi and thereafter it decreases slowly so that for pressures greater than 1000 psi there is a linear correlation between resistivity and pressure. Between samples however, there is little difference between the ratio of the resistivity at 300 psi to

that at 3000 psi (Table 7-3). The ratios vary from 0.41 for sample LB-14 to 0.65 for sample LB-16. Absolute values of resistivity range from 2.65×10^7 ohm cm^{-1} at 300 psi for sample LB-18 to 3.5×10^6 ohm cm^{-1} at 3000 psi for sample LB-15.

c) Conclusion

The influence of pressure upon resistivity is less marked at pressures in excess of 1000 psi. Therefore, in order to obtain the most reproducible results, resistivity measurements should be measured at the highest possible pressures. However, it was discovered during the experiments that due to faults in the oil seals of the press, pressures of greater than 1000 psi could not be maintained constant over the time necessary to make a measurement. Although attempts were made to cure the faults the remedies were not entirely satisfactory and a compromise had to be reached in the choice of a suitable pressure for the routine measurement of resistivity. It was necessary to minimize variations caused by reaction of the sample to pressure and yet not exceed the critical value for the efficiency of the press. The value chosen was 1000 psi, this being the lower limit at which the effects of pressure upon the sample began to diminish and the upper limit for the stability of the press.

4. VARIATION IN RESISTIVITY FOR SAMPLES FROM CLANYARD BAY

Resistivity values at 1000 psi have been abstracted from the data given in the preceding section for the LB-series of samples. Values are tabulated in Table 7-4 and are plotted with respect to

distance from the dyke centre in Fig.188.

Inspection of the scatter diagram (Fig.188) reveals that the distribution of points is similar to that described in Chapter V for the variation in the bireflectance ratio of the organic material with distance from the dyke (Fig.150). Both the resistivity and the bireflectance ratio, on approaching the dyke, first increase and then drop to a minimum before increasing to a maximum a little way from the dyke contact. Immediately adjacent to the dyke both parameters fall to an intermediate value.

The visual correlation between the two parameters prompted the application of product moment correlation analysis which revealed a correlation coefficient of 0.75. Thus, there is a good statistical correlation between resistivity of the powdered rock and the bireflectance ratio of the organic material. The positive nature of this correlation is however, not that expected if both parameters are directly related to the rank of the organic material, for if the bireflectance ratio gives an indication of the degree of stacking and ordering of the aromatic lamellae within the organic material it is expected that high values of bireflectance will be associated with low resistivity values.

Obviously it is not realistic to view the variation of resistivity solely in terms of ordering of the aromatic lamellae because measurements were taken from powdered rock samples containing a variety of inorganic minerals. These minerals undoubtedly have some effect upon the resistivity and with this in mind the mineralogy of the samples was assessed quantitatively using the X-ray diffraction method in Chapter II. The amount of albite, chlorite, sericite,

pyrite and quartz present in each of the samples is given in Table 7-4. Correlation analysis indicates that resistivity is not correlatable with any of the mineral constituents (Table 7-5).

Assuming that some other parameter is more closely related to resistivity than any of the mineral contents it might be expected that this is inter-related with both resistivity and bireflectance. Since both parameters intercorrelate, it was felt that perhaps the common link lay through the amount of carbon present within the sediments. This possibility was checked and confirmed by analysing the sediments for carbon and then subjecting the results to correlation analysis (Tables 7-4 and 7-5). A correlation coefficient of -0.81 was obtained indicating that the sediments containing larger amounts of carbon are better conductors of electricity.

5. REGIONAL VARIATION IN RESISTIVITY FOR SAMPLES COLLECTED FROM SEDIMENTS EXPOSED ALONG THE EASTERN MARGIN OF LUCE BAY

Details of the resistivity values obtained at a pressure of 1000 psi for the samples collected from the black shale inliers exposed along the eastern margin of Luce Bay are given in Appendix E. Values range from 1.2×10^7 to 4.8×10^7 ohm cm^{-1} and group about a mean of 3.0×10^7 ohm cm^{-1} . This variation is not considered to be significant for the few samples analysed from the relatively large area (Fig.26) and therefore the data were not subjected to computer mapping techniques.

It may be observed from the data that the mean resistivity of the Luce Bay samples is greater than the mean value of 1.7×10^7

ohm cm⁻¹ calculated for the Clanyard Bay samples. This difference occurs despite the fact that the average carbon content of the Luce Bay samples is 1.02 per cent and that of the Clanyard Bay samples is only 0.39 per cent. In this case, correlation of resistivity with the carbon content of the samples yields a low correlation coefficient of -0.07 indicating little or no correlation between the two parameters.

Thus, although the amount of carbon present within the Moffat Shales can affect the resistivity value it does not always hold that resistivity decreases with increasing amounts of carbon. The physical state of the carbon may be an important factor but as previously stated the resistivity is observed to increase with increasing ordering within the carbonaceous material. Such an observation can not at this stage be explained. It is likely however that the amount of carbon, the physical state of the carbon and the mineralogy of the sediments all inter-relate to produce fluctuations in the resistivity. The net effect will obviously depend on the relative contribution from each variable.

6. REGIONAL VARIATION IN RESISTIVITY FOR SAMPLES COLLECTED IN THE VICINITY OF MOFFAT

The resistivity of a grand total of 130 samples collected within the vicinity of Moffat has been measured at a pressure of 1000 psi. Values for individual samples which were collected from the localities displayed in Fig.4 are given in Appendix E. The total sample suite is composed of 63 samples from Hartfell, 34 samples from

Dobb's Linn and the remainder from various exposures of black shales and mudstones.

The distribution of results for the total sample suite is illustrated in Fig.189. Values, when arranged on a logarithmic scale, range from 2.76 to 7.91 about a mean value of 6.27. This mean value is heavily influenced by the large number of samples from Hartfell and Dobb's Linn. When treated separately, these two localities yield individual averages of 4.89 and 7.64 respectively.

Trend surface analysis, according to the method of Cole (1969) was performed on the resistivity data. The derived cubic global fit surface map (Fig.190) with a sums of squares fit value of 45.6 per cent follows the shape of a basin which is centred to the south of Hartfell and is aligned in a east-north-east to west-south-west direction. The position of the computed trough in resistivity in the vicinity of Hartfell is comparable to that of the dome computed for the variation in reflectivity (Fig.173). There is however no statistical correlation between these two parameters nor has any correlation been found to exist between the resistivity of the samples collected from the Moffat region and any other parameter measured during this study.

7. THE STRATIGRAPHIC VARIATION IN RESISTIVITY

a) In the Moffat region

The resistivity values of those samples collected from the Moffat region which have been accurately zoned on the basis of their graptolite assemblage are plotted in Fig.191 as a function of

height up the stratigraphic succession as proposed by Toghil (1968, 1970a). A fourth order polynomial regression curve, significant at the 99 per cent level, has been superimposed upon the scatter plot in order to indicate the statistical vertical variation within the sequence. The computed curve indicates a general increase in resistivity up the succession.

The degree of linear correlation between the resistivity and all other parameters measured for the sample set was estimated by calculating the product moment correlation coefficient for all possible combinations of parameters. Four separate correlation matrices were computed; one each for correlations within the total sample set, for correlations within samples collected in the Moffat region, for correlations within samples from Dobb's Linn and for correlations within samples from Hartfell. Correlation coefficients within the total sample set only exceeded 0.50 in four cases. These were for the variation of resistivity with the iron, carbon and copper contents of the sediments and for the variation of resistivity with the mean reflectance in oil of the graptolite fragments (Table 7-6).

Inspection of Table 7-6 reveals that although carbon, copper, iron and reflectivity correlate with resistivity in the total sample suite and in those samples collected from Hartfell, only carbon correlates with resistivity in the Dobb's Linn samples and no correlation exists between resistivity and any of the measured parameters in the Moffat Grid series of samples.

b) At Hartfell

The resistivity values of samples collected from Hartfell

range from 5.4×10^2 to 6.7×10^7 ohm cm^{-1} and are grouped about a mean value of 7.8×10^4 ohm cm^{-1} . The distribution of values with respect to height up the north cliff is illustrated in Fig.192a. The superimposed fourth order polynomial regression curve which is computed to be significant at the 97.5 per cent confidence level indicates that the samples become more conductive from the top of the cliff towards the prominent exposure of Glenkiln Shales and then become more resistive towards the base of the cliff.

The vertical profile for the resistivity of the samples when the succession is restored to its pre-fault state is indicated in Fig.192b. In this case the computed curve is significant at the 99.9 per cent level and the trend indicates that between the Glenkiln Shales and the linearis Zone the sediments become more conductive and then on transition to the barren grey mudstone of the complanatus Zone there is a marked increase in resistivity.

c) Discussion

The sub-set of samples collected from Hartfell is responsible for the apparent vertical change in resistivity through the succession of shales and mudstones which is exposed in the vicinity of Moffat. The degree of electrical conduction through the sediments appears to be controlled by the amount of carbon, iron and copper present. Resistivity, being indirectly proportional to the mean reflectance value of the organic material in sediments from Hartfell, may indicate changes in rank, but evidence of such a relationship cannot be given until it is demonstrated that the resistivity is more dependant upon the amount and nature of the carbonaceous material than

upon any other contributing factor.

On the contrary, comparison of the level of significance for the faulted and structurally restored profiles derived for the variation in resistivity at Hartfell, reveals that a curve significant at a higher level may be generated for the original sequence of sediments. From this it is inferred that the resistivity is controlled by the amounts of iron, copper and carbon that were present shortly after deposition of the sediments and before the onset of faulting.

8. THE VARIATION IN RESISTIVITY OF TWO COMPONENT MINERAL MIXTURES

a) Introduction

The three elements which have been demonstrated to correlate with resistivity are iron, copper and carbon. Most of the iron and the copper is present within the sediments in the form of pyrite while some iron is in chlorite (Chapter III). At Hartfell, carbon is present in a structurally immature graphitic phase. Since most sulphide minerals and also graphite may be classed as semi-conductors (Table 7-1) a series of experiments was initiated to investigate by means of artificial mixtures of minerals the relationship between resistivity and mineral content. Mixtures of quartz with varying amounts of chlorite, pyrite, graphite and muscovite were prepared and the resistivity measured.

b) Method and results

Samples of chlorite (var. clinocllore), pyrite, graphite, muscovite and quartz were crushed in a ball-mill to -200 mesh.

Various mixtures were then prepared for each mineral with quartz as the matrix so that a series of samples containing between 1 and 100 per cent mineral was obtained. These samples were then dried at 50°C for 24 hours and the resistivity of each was measured in the previously described manner.

The variation in resistivity with the amount of each mineral in a two component mixture with quartz is illustrated in Fig.193. The greatest changes in resistivity occur in samples containing quartz/pyrite and quartz/graphite mixtures. In the mixtures containing graphite the resistivity drops from 10^7 ohm cm^{-1} for a mixture containing 1 per cent graphite to less than 1 ohm cm^{-1} for a mixture containing 20 per cent graphite. The resistivity continues to decrease with increasing amounts of graphite until finally a value of 10^{-2} ohm cm^{-1} is obtained for a sample consisting solely of graphite. For mixtures of pyrite and quartz the results indicate that for the first 20 per cent pyrite the resistivity increases from 10^6 to 10^7 ohm cm^{-1} . Thereafter the resistivity decreases with increasing amounts of pyrite to reach a minimum value of 5 ohm cm^{-1} in a sample containing 100 per cent pyrite. Muscovite and chlorite both show decreases in resistivity with increasing amounts of mineral present but the rate of change is much less than for pyrite or graphite. Values range from 10^7 to 10^6 ohm cm^{-1} in mixtures of muscovite and quartz and remain in the region of 10^7 ohm cm^{-1} in chlorite/quartz mixtures.

c) Discussion

Relating the amount of carbon, pyrite, chlorite and

sericite found in the sediments at Hartfell and Dobb's Linn (Table 7-7) to the resistivity trends described above it is found that the low resistivity values at Hartfell can only be explained in terms of the amount of carbon present. The high conducting nature of the sediments at this locality is interpreted as being influenced by the graphitic nature of the relatively more abundant carbonaceous material (compare Figs. 76b and 192b). Carbonization and graphitization of the organic material has been attributed to thermal effects from regional metamorphism and a deep seated igneous body which is centred at depth in the vicinity of Hartfell. The thermal effects of this body can be detected on a regional scale from reflectivity measurements on graptolite fragments. Resistivity values however do not indicate any regional effects possibly due to the low carbon contents of many of the rocks studied.

In conclusion, if resistivity measurements are to be used as a useful tool as a means of locating regional thermal anomalies in the Southern Uplands, it is essential that measurements are taken from samples of similar mineralogy and with reasonable carbon contents. Even when these parameters are accurately known and their relationship with resistivity understood in greater detail, it will only be at localities such as Hartfell which have been subjected to substantial geothermal gradients that the method applied in this work will be of use.

| | Mineral | Resistivity (ohm-cm ⁻¹) |
|------------------------|----------------------------|---|
| CONDUCTIVE MINERALS | Gold | 0.22 |
| | Copper | 0.17 |
| | Tin | 1.31 |
| | Platinum | 1.10 |
| SEMI- CONDUCTORS | Pyrite | $2.3 \times 10^{-2} - 1.5 \times 10^2$ |
| | Galena | 3.7×10^{-2} |
| | Chalcopyrite | $1.0 \times 10^{-2} - 7.0 \times 10^{-2}$ |
| | Ilmenite | 2.2×10^2 |
| | Magnetite | $3.6 \times 10^{-2} - 5.0 \times 10^5$ |
| | Graphite | $0.1 - 10^3$ |
| DIELECTRICS | Diamond | 5×10^{14} |
| | Quartz \perp to axis | 2×10^{16} |
| | Quartz \parallel to axis | 10^{14} |
| | Muscovite | $10^{14} - 10^{16}$ |
| | Sulphur | 10^{17} |
| | Phlogopite | $10^{13} - 10^{14}$ |

TABLE 7-1 Resistivity values of natural materials,
(after Parkhomenko, 1967).

| Rock Type | Resistivity (ohm-cm ⁻¹) | |
|-----------------------|-------------------------------------|----------------------|
| | wet | dry |
| Bornite ore | - | 0.3 |
| Galena ore | - | 7.0 |
| Graphitic slate | - | 13.3 |
| Limestone | 4.2x10 ⁷ | 1.2x10 ⁹ |
| Sandstone | 1.4x10 ⁷ | 6.4x10 ¹⁰ |
| Quartzitic slate | 6.4x10 ⁶ | 1.6x10 ⁷ |
| Shaly slate | 4.0x10 ⁵ | 6.0x10 ⁸ |
| Quartz-sericite slate | 5.0x10 ⁶ | 3.6x10 ⁹ |
| Quartz-chlorite slate | 5.0x10 ⁵ | 2.0x10 ⁸ |
| Quartzite | 4.7x10 ⁸ | - |

TABLE 7-2 Resistivity values for selected rocks,
(after Parkhomenko, 1967).

| Sample | ratio | $\frac{\text{resistivity at 300psi}}{\text{resistivity at 3000psi}}$ |
|--------|-------|--|
| LB-12 | | 0.44 |
| LB-13 | | 0.47 |
| LB-14 | | 0.41 |
| LB-15 | | 0.44 |
| LB-16 | | 0.65 |
| LB-17 | | 0.43 |
| LB-18 | | 0.47 |

TABLE 7-3 Variation of resistivity with pressure for samples from Clanyard Bay.

| Sample | Alb | Chl | Ser | Pyr | Qtz | Res | B.R. | C |
|--------|------|-------|-------|-------|-------|-----|------|------|
| LB-12 | 3.89 | 9.31 | 19.51 | 14.64 | 52.65 | 147 | 0.30 | 0.11 |
| LB-13 | 3.90 | 7.81 | 22.69 | 11.64 | 53.97 | 205 | 0.60 | 0.21 |
| LB-14 | 0.0 | 15.44 | 15.77 | 7.70 | 61.09 | 91 | 0.41 | 0.71 |
| LB-15 | 4.06 | 4.04 | 12.30 | 5.29 | 74.30 | 51 | 0.26 | 0.87 |
| LB-16 | 1.96 | 3.41 | 7.35 | 9.23 | 78.05 | 214 | 0.37 | 0.36 |
| LB-17 | 6.07 | 21.67 | 12.55 | 5.15 | 54.56 | 280 | 0.75 | 0.16 |
| LB-18 | 8.49 | 19.43 | 11.66 | 4.43 | 55.99 | 183 | 0.33 | 0.29 |

Alb : Albite %

Chl : Chlorite %

Ser : Sericite %

Pyr : Pyrite %

Qtz : Quartz %

Res : Resistivity $\times 10^{-5}$ ohm cm^{-1}

B.R. : Bireflectance ratio

C : Carbon %

TABLE 7-4 Summary of parameters measured for samples collected from the south side of the dyke at Clanyard Bay.

| | Alb | Chl | Ser | Pyr | Qtz | Res | B.R. | C |
|---------------|-------|-------|-------|-------|-------|-------|-------|-------|
| Albite | 1.00 | 0.48 | -0.10 | -0.40 | -0.40 | 0.40 | 0.14 | -0.43 |
| Chlorite | 0.48 | 1.00 | -0.02 | -0.46 | -0.65 | 0.40 | 0.48 | -0.31 |
| Sericite | -0.10 | -0.02 | 1.00 | 0.64 | -0.69 | -0.10 | 0.21 | -0.29 |
| Pyrite | -0.40 | -0.46 | 0.64 | 1.00 | -0.26 | 0.01 | -0.10 | -0.44 |
| Quartz | -0.40 | -0.65 | -0.69 | -0.26 | 1.00 | -0.34 | -0.46 | 0.63 |
| Resistivity | 0.40 | 0.40 | -0.10 | 0.01 | -0.34 | 1.00 | 0.75 | -0.81 |
| Bireflectance | 0.14 | 0.48 | 0.21 | -0.10 | -0.45 | 0.75 | 1.00 | -0.46 |
| Carbon | -0.43 | -0.31 | -0.29 | -0.44 | 0.63 | -0.81 | -0.46 | 1.00 |

Alb : Albite

Chl : Chlorite

Ser : Sericite

Pyr : Pyrite

Qtz : Quartz

Res : Resistivity

B.R. : Bireflectance ratio

C : Carbon

TABLE 7-5 Correlation matrix for samples collected from the south side of the dyke at Clanyard Bay.

| | Total | MG | DL | HF |
|----------------|-------|-------|-------|-------|
| C/resistivity | -0.60 | -0.23 | -0.54 | -0.78 |
| Ro/resistivity | -0.57 | 0.16 | 0.22 | -0.45 |
| Cu/resistivity | 0.54 | 0.11 | 0.16 | 0.66 |
| Fe/resistivity | 0.53 | 0.14 | -0.07 | 0.54 |

Total = total sample set

MG = sub-set of samples collected on a grid basis
in the Moffat region

DL = sub-set of samples collected from Dobb's Linn

HF = sub-set of samples collected from Hartfell

TABLE 7-6 Abstract from correlation matrices to illustrate
the variation of resistivity with selected parameters.

| | Hartfell | Dobb's Linn |
|-------------|---------------------------------------|---------------------------------------|
| Carbon | 2.33% | 1.66% |
| Pyrite | 5.36% | 12.40% |
| Chlorite | 3.54% | 4.44% |
| Sericite | 9.43% | 15.10% |
| Resistivity | $7.8 \times 10^4 \text{ ohm-cm}^{-1}$ | $4.4 \times 10^7 \text{ ohm-cm}^{-1}$ |

TABLE 7-7 Summary of mean values for selected parameters
at Hartfell and Dobb's Linn.

C H A P T E R V I I I

FACTORS AFFECTING COALIFICATION AND CARBONIZATION
OF THE ORGANIC MATERIAL IN THE MOFFAT SHALES

1. INTRODUCTION

Coalification and carbonization have acted jointly or singly upon the organic material in the Hartfell Shales to produce the range of properties described in the previous chapters. It is found from considerations of a) graptolite reflectance values, b) resistivity measurements on rock powders and c) infra-red and X-ray data from kerogen isolates, that the effects of these processes are firstly, more pronounced at Hartfell than at Dobb's Linn and secondly, that the organic matter at both of these localities is of higher rank than that in most of the sediments sampled from the inliers along the east coast of Luce Bay.

The discussion which follows deals in some detail with the physical processes that affect the coalification and carbonization of organic material. Coalification and carbonization, considered synonymous by some authors (eg. McIntyre 1972), relate to two contrasting processes, both of which involve the cleavage of molecular bonds in a carbonaceous substance to produce carbon dioxide and carbon monoxide, and to leave a residue of higher carbon content than the starting material (Breger 1963a). Both processes lead by separate routes and mechanisms to the (ultimately) formation of graphite. The end product of carbonization may be coke especially if the starting material is a coal containing between 85 and 92 per cent carbon (van Krevelen and Schuyer 1967).

Under conditions of atmospheric pressure, coals outside this limited carbon range do not normally form cokes, but since the coking process is pressure dependent (Francis 1954), it is possible

that even lignites can be coked if high pressures are available (Gray and Boucot 1975).

Coalification occurs during low-grade regional metamorphism and is a long term process (measured in millions of years) involving various sources of energy. These include various different heat sources such as the geothermal gradient which can be related to sedimentary and tectonic overburden, igneous activity, and tectonic pressure. Coalification may also be related to differential pressure (shear) in which heat may, or may not be, a contributing factor (Gray and Boucot 1975).

Carbonization is the result of rapid purely thermal destruction or decomposition of organic material, and may take place during a short time interval measured in hours (Gray and Boucot 1975). High temperatures assist the process, but the rate of temperature increase is critical. Laboratory experiments reveal that microfossils undergo carbonization at temperatures as low as 200°C providing this temperature is attained quickly (Combaz 1971; Gutjahr 1966). Natural cokes (carbonized coals) are normally only found in close proximity to intrusive or extrusive igneous bodies (Chandra 1963).

Coalification and carbonization are accordingly analogous to regional and contact metamorphism respectively (Gray and Boucot 1975). Thus, in the same way as for regional and contact metamorphism, a continuum exists between coalification and carbonization. It is therefore possible that in some cases the thermal effects on particulate organic matter such as dispersed graptolite fragments will be gradational between the extreme processes

of carbonization and coalification. This would occur, for instance, where a buried igneous intrusion sufficiently disturbed the geothermal gradient to alter coal rank or in circumstances similar to those at Clanyard Bay where changes in the reflectance of the graptolite fragments grade from the zone of contact metamorphism (carbonization) into the area of regional metamorphism (coalification).

2. FACTORS AFFECTING RANK

a) Thermal alteration

Particulate organic matter in sediments can be chemically and physically altered by a variety of thermal energy sources. Included in this group are the effects of geothermal heat, tectonically generated heat, heat from igneous sources and superheated fluids.

In regions of thick overburden, the effects of temperature in advancing coalification are directly related to the geothermal gradient (Kuyf et al., 1955; Gutjahr 1966). Organic fragments within sediments of the same age can have different rank depending on the geological evolution of an area. For example, a rise in maximum reflectivity values of particulate plant material in Dinantian sediments of the Rheinisches Schiefergebirge from the north-west to the south-east indicates that the sedimentary sequence was at some time thicker in the south-west of the area (Wolf 1972).

The reflectivity gradient through the Dinantian sequence in the Rheinisches Schiefergebirge can be compared with the graptolite reflectivity gradient through the sequence at Dobb's Linn. In the

former, values range from 0.39% R.max/10 m of sediment to 0.88% R.max/10 m. The lower value is close to that found for the variation in Ro(mean) at Dobb's Linn (0.31% Ro(mean)/10 m) and it may be possible, therefore, that the observed rank gradient in the Moffat Shales is a function of overburden thickness. If this is so, then the areal variation in rank in the vicinity of Moffat indicates that the thickest accumulation of sediments occurred near Hartfell and that thinning took place to the south-east towards the Ettrick Valley Thrust. This would support the location of the axial rise of the Moffat geosyncline to be close to, or beyond, the outcrop of the thrust (Toghill 1970b; Fyfe and Weir 1976).

Tectonically generated heat is claimed to be responsible in some cases for the coalification of organic particles (White 1913; Staplin 1969; Wilson 1971). Processes of folding and faulting within the Moffat Shales undoubtedly generated frictional heat but these may have proceeded at such a slow rate that the temperature of the rocks was not raised sufficiently to effect coalification. Nevertheless, it is probable that in areas subjected to severe faulting (eg. Hartfell) the shear component of the tectonic movements has had a positive effect on the maturation of the organic material (Bridgman 1946).

Natural carbonization of organic material is most commonly effected by thermal energy associated with igneous bodies (eg. Chandra 1963; Chatterjee et al., 1964; Kisch 1966). Carbonization, unlike coalification, is manifested by the presence of vesicular and granular mosaic textures and is mostly confined to narrow zones adjacent to igneous bodies. Although the direct effects

of carbonization are never observed on a regional scale (Gray and Boucot 1975), it is possible that diffused heat from the igneous body may enhance the coalification of organic particles some distance from the contact (Bostick 1971). Thus, it can be explained why the effects of carbonization are evident close to the dyke at Clanyard Bay but not at a distance of 1 km from the Loch Doon and Fleet granites where the reflection level of the graptolites is similar.

A few samples from Hartfell which were collected from the vicinity of fault planes exhibit evidence of plasticity in the organic material. From this it may be concluded that locally the process of carbonization has been superimposed upon coalification. This may have been achieved by the percolation of superheated fluids, derived either from plutonic activity or faulting, through fissures and fractures and along fault planes. This process could also have been responsible for the increase in rank of the organic material close to faults in sediments exposed along the east coast of Luce Bay.

The thermal conductivity of the enclosing matrix will influence the temperature and hence the rank of particulate organic material (M. and R. Teichmüller 1968; Jones et al., 1971). Thus, if a graptolite-bearing rock sequence has been affected by a continuous heat flux since lithification, those strata with low thermal conductivities will have been subjected to higher temperatures for a longer time than those units characterized by high thermal conductivities. The differing thermal conductivities of coal (low), clay minerals (low-moderate), calcite (moderate) and quartz (relatively high) suggest, for example, that under a continuous thermal flux the graptolite fragments in sediments relatively rich in clay, such as

those of the upper part of the succession at Dobb's Linn, will have been subjected to higher thermal energy than those in the more quartzose sediments at the base of the succession. Comparison of the stratigraphic profiles for reflectivity, quartz and sericite (Figs. 191, 23, 22) reveal no significant relationship between the parameters, and therefore it is concluded that although the thermal conductivity of the enclosing sediments may have influenced the ultimate rank of the graptolite fragments, the effect is of only minor importance.

b) Pressure effects

Pressure in the geological environment can be divided into hydrostatic pressure and shear. Hydrostatic pressure refers to the application of the same pressure from all directions whereas shear refers to the application of different pressures from more than one direction. 'Overburden pressure' and 'tectonic pressure' include both hydrostatic pressure and shear components that are difficult to separate.

Hydrostatic pressure alone has minimal effect on the rank of organic material (Breger 1963a). In some cases high pressure of this kind actually retards rather than accelerates the process of coalification (Gutjahr 1966; McIntyre 1972).

The shear potential of a rock is a function of lithology, eg. beds rich in coal should flow most readily, those rich in clay minerals considerably less than coals and those rich in quartz least of all. It may be predicted, therefore, that graptolite fragments embedded in the more quartzose rocks would suffer greater shear than those having matrices dominated by clay. Hence, for the same lithology,

the effect of shear upon the rank of organic material is opposite and in part compensates for the effect of conductivity.

c) Radiochemical effects

Various combinations of radiogenic isotope-bearing minerals occur in sedimentary rocks. If radioactive minerals such as zircon, sphene, apatite, thucholite or potash feldspar are present in abundance in a carbonaceous sequence they cause a change in reflectivity of the organic material which parallels that of coalification and carbonization (Stach 1968). The process of radiochemical decomposition involves however, the loss of both carbon and hydrogen in contrast to the processes of coalification and carbonization which result in an increase in carbon and a loss of hydrogen (Breger and Deul 1959; Breger 1963b).

The overall radioactivity in the Moffat Shales is not volumetrically high but radiochemical decomposition may indeed have affected the graptolite fragments. The not dissimilar stratigraphic profiles for potassium oxide, zirconium and reflectivity may be positive evidence for a large scale stratigraphic effect (Figs 52, 56, 191).

d) The effect of geological time

In a discussion concerning the inducement of rank upon organic matter, the stability of chemical bonds with time must be considered. Both geological and experimental evidence indicates that chemical bonds in organic compounds are exceptionally stable, and provided temperature does not rise above 50°C they can survive intact

for periods greater than 200 million years (M. and R. Teichmüller 1966).

Experimental heating of organic microfossils to 270°C for one day produces a darkening in colour which is related to the chemical degradation of the organic constituents (Gutjahr 1966; Combaz 1971; McIntyre 1972). If however the temperature is not allowed to exceed 200°C, little visible change is observed even when long periods of heating are employed. The inducement of rank is therefore believed by some to be independent of time and closely related to the maximum temperature attained.

A recent study of reflectivity profiles in boreholes suggested that time, as well as temperature, has a profound influence on the ultimate rank of dispersed organic material (Karpov et al., 1976). One of the four models presented in this study predicts that if a temperature of 240°C is maintained for about a million years then original fragments of brown coal rank would be coalified to semi-anthracitic rank. If, however, the same temperature was only effective for 100,000 years, then the ultimate rank would approximate to that of a medium volatile bituminous coal.

3. CONCLUSION

The suite of samples studied indicates that nowhere in the Southern Uplands of Scotland is the rank of graptolites less than that of a low volatile bituminous coal (83% d.a.f. carbon). Both coalification and carbonization processes have acted singly or jointly to produce the observed physical and chemical features. Coalification has been induced over the region by thermal effects resulting from

geothermal and tectonic agencies. Carbonization is only evident in the samples collected adjacent to the dyke at Clanyard Bay and also in the few samples collected in the vicinity of fault planes at Hartfell. The former occurrence is obviously related to a natural coking process brought about by rapid heating in the immediate vicinity of the dyke. The latter, however, may either be related to frictional heat generated by fault movement or to channeled supplies of superheated fluids produced from tectonic processes or from an igneous body at depth. Similar processes have caused the enhanced coalification of the graptolites in the vicinity of faults within the sediments exposed along the eastern margin of Luce Bay.

REFERENCES

- Abelson, P.H., 1954. Amino acids in fossils. *Science*, 119: 576-578.
- Abelson, P.H. and Hare P.E., 1969. Recent amino acids in the Gunflint chert. *Carnegie Inst. Wash., Yearb.*, 67: 208-210.
- Abramski, C. and Mackowsky, M. Th., 1952. Methoden und Ergebnisse der Angewandten Koxmikroskopie. In: H. Freund (Editor), *Handbuch der Mikroskopie in der Technik*, Vol.2, Umschau-Verlag, Frankfurt, pp. 311-410.
- Aganoglu, K., 1972. A comparison of the thermal metamorphism of coal seams in north east England by Carboniferous and Tertiary igneous dykes. M.Sc. Thesis, University of Newcastle upon Tyne.
- Agroskin, A.A. and Petrenko, I.G., 1950. Electrical conductivity of slate and coal on heating, *Akad. Nauk. SSSR, Izv., Ser. Geol.*, 1: 19-34.
- Ahrens, L.H., 1954a. The lognormal distribution of the elements, I. *Geochim. Cosmochim. Acta*, 5: 49-73.
- Ahrens, L.H., 1954b. The lognormal distribution of the elements, II. *Geochim. Cosmochim. Acta*, 6: 121-131.
- Ahrens, L.H., 1957. The lognormal distribution of the elements, III. *Geochim. Cosmochim. Acta*, 11: 205-211.
- Albaiges, J. and Torrados, J.M., 1974. Significance of the even-carbon n-paraffin distribution of Spanish crude oil. *Nature*, 250: 567-568.
- Allan, J., 1975. Natural and artificial diagenesis of coal macerals. Ph.D. Thesis, University of Newcastle upon Tyne.
- Allan, J., Murchison, D.G., Scott, E. and Watson, S.W., 1975. Organic geochemistry of thermally metamorphosed fossil wood. *Fuel*, 54: 283-287.

- Alpern, B., 1956. Die anisotropie der kokse als kriterium für ihre beurteilung und klassifizierung. *Brennstoff. Chemie*, 13/14 : 194-198.
- Andreev, P.F., 1962. Geochemical transformation of petroleum in the lithosphere. *Geochemistry*, 10: 1005-1014.
- Bada, J.L., Luyendyk, B.P. and Maynard, J.B., 1970. Marine sediments: dating by the racemization of amino acids. *Science*, 170: 730-732.
- Bada, J.L. and Protsch, R., 1973. Racemization reaction of aspartic acid and its use in dating fossil bones. *Natl. Acad. Sci., Proc.*, 70: 1331-1334.
- Bailey, W.J., Jobson, A.M. and Rogers, M.A., 1973. Bacterial degradation of crude oil; comparison of field and experimental data. *Chem. Geol.*, 11: 203-221.
- Bailey, W.J.L. and Krouse, H.R., 1970. Chemical aspects of crude oil preservation. *Am. Assoc. Pet. Geol. - Soc. Econ. Paleontol. Mineral.*, annual meeting Calgary, Alberta.
- Bailey, W.J., Krouse, H.R., Evans, C.R. and Rogers, M.A., 1973. Alteration of crude oil by waters and bacterial evidence from geochemical and isotope studies. *Am. Assoc. Pet. Geol., Bull.*, 57: 1276-1290.
- Bailler, D.R. and Claypool, G.E., 1970. Effects of incipient metamorphism on organic matter in mudrock. *Am. Assoc. Pet. Geol., Bull.*, 54: 456-468.
- Bajor, M., Roquebert, M.H. and Weide, B.M. van der., 1969. Transformation de la matière organique sous l'influence de la température. *Cent. Rech. Pau. Bull.*, 3: 113-124.

- Bannister, F.A., 1943. Brammallite (sodium illite), a new mineral from Llandebie, South Wales. *Mineral. Mag.*, 26: 304-307.
- Berkowitz, N., 1967. The coal-carbon transformation: basic mechanisms. Symposium on the science and technology of coal, Dept. Energy, Mines and Resources, Ottawa.
- Berner, R.A., 1969. Migration of iron and sulphur within anaerobic sediments during early diagenesis. *Am. J. Sci.*, 267: 19-42.
- Berner, R.A., 1971. *Principles of Chemical Sedimentology*. McGraw-Hill, New York, 240 pp.
- Bertin, A.P., 1970. *Principles and Practice of X-ray Spectrometric Analysis*. Plenum Press, New York, 679 pp.
- Black, R.H., 1953. Analysis of bauxite exploration samples: an X-ray diffraction method. *Anal. Chem.*, 25: 743-748.
- Blyth, F.G., 1949. The sheared porphyrite dykes of South Galloway. *Quart. Jl. Geol. Soc. London*, 105: 393-423.
- Boar, P.L. and Ingram, L.K., 1970. Comprehensive analysis of coal ash and silicate rocks by atomic absorption spectroscopy by a fusion technique. *Analyst.*, 95: 124-130.
- Bostick, N.H., 1971. Thermal alteration of clastic organic particles as an indicator of contact and burial metamorphism in sedimentary rocks. In: B.F. Perkins (Editor) *Geoscience and Man*. Am. Assoc. Stratigr. Palynol., Annu. Mtg., 3, Baton Rouge, pp. 83-92.
- Boström, K., 1970. Submarine volcanism as a source for iron. *Earth Planet. Sci. Lett.*, 9: 348-354.
- Boström, K., Joensuu, O., Valdes, S. and Riera, M. 1972. Geochemical history of South Atlantic ocean sediments since late Cretaceous. *Mar. Geol.*, 2: 85-121.

- Boström, K., Kraemer, T. and Gartner, S., 1973. Provenance and accumulation rates of opaline silica, aluminium, titanium, iron, manganese, copper, nickel and cobalt in Pacific pelagic sediments. *Chem. Geol.*, 11: 123-148.
- Brace, W.F. and Orange, A.S., 1968. Further studies on the effects of pressure on the electrical resistivity of rocks. *J. Geophys. Res.*, 73: 5407-5420.
- Bradley, W.F. and Grim, R.E., 1961. Mica clay minerals. In: G. Brown (Editor), *The X-ray Identification and Crystal Structures of Clay Minerals*. Min. Soc. London, pp. 208-241.
- Bray, F.E. and Evans, E.D., 1961. Distribution of n-paraffins as a clue to the recognition of source beds. *Geochim. Cosmochim. Acta*, 22: 2-15.
- Bray, F.E. and Evans, E.O., 1965. Hydrocarbons in non reservoir rock source beds. *Am. Assoc. Pet. Geol., Bull.*, 49: 248-257.
- Breger, I.A., 1963. Origin and classification of naturally occurring carbonaceous substances. In: I.A. Breger (Editor), *Organic Geochemistry*, MacMillan and Co., New York, pp. 50-86.
- Breger, I.A., 1963. Coal. In: R.O. Bolt and J.G. Carroll (Editors), *Radiation Effects on Organic Materials*. Academic Press, New York, pp. 509-518.
- Breger, I.A. and Deul, M., 1959. Association of uranium and carbonaceous materials with special references to Dimple Mountain Region. *U.S. Geol. Surv., Prof. Pap.*, 320: 139-156.
- Bridgman, P.W., 1946. Recent work in the field of high pressures. *Rev. Mod. Physics*, 18: 1-93.

- Brindley, G.W., 1961. Chlorite minerals. In: G. Brown (Editor), The X-ray Identification and Crystal Structures of Clay Minerals. Min. Soc. London, pp. 242-296.
- Brindley, G.W. and Youell, R.F., 1953. Ferrous and ferric chamosite. Min. Mag. 30: 57-70.
- Bristol, C.C., 1968. The quantitative determination of minerals in metamorphosed volcanic rocks by X-ray powder diffraction. Can. J. Earth Sci., 5: 235-242.
- Brooks, J.D. and Smith, J.W., 1967. The diagenesis of plant lipids during the formation of coal, petroleum and natural gas, I. Changes in the n-paraffin hydrocarbons. Geochim. Cosmochim. Acta, 31: 2389-2397.
- Brown, G., 1961. Other minerals. In: G. Brown (Editor), The X-ray Identification and Crystal Structures of Clay Minerals. Min. Soc. London, pp. 467-488.
- Brown, H.R., 1956. The decomposition of coal in relation to the plastic layer. Coke and Gas, October: p.390.
- Buckley, D.E. and Cranston, R.F., 1971. Atomic absorption spectroscopy analyses of 18 elements from a single decomposition of aluminosilicate. Chem. Geol., 7: 273-284.
- Bulman, O.M.B., 1970. Graptolithina. In: R.C.Moore (Editor), Treatise on Invertebrate Palaeontology, Part V, 2nd edition. Geological Society of America, Boulder, Colorado.
- Caillère, S. and Hémin, S., 1957. The chlorite and serpentine minerals. In: R.C.Mackenzie (Editor), Differential Thermal Investigation of clays. Min. Soc. London, pp. 207-230.
- Cattell, R.B., 1965. Factor analysis, an introduction to essentials. Biometrics, 21: 190-215.

- Chandra, D., 1963. Reflectance of thermally metamorphosed coals. *Fuel*, 4: 69-74.
- Chandra, D., 1965. Reflectance of coals carbonized under pressure. *Econ. Geol.*, 60: 621-630.
- Chatterjee, N.N., Chandra, D. and Ghosh, T.K., 1964. Reflectance of Ponaiti seam affected by a mica-peridotite dyke. *J. Mines. Met. Fuels.*, 12: 346-360.
- Chave, K.E. and Mackenzie, F.T., 1961. A statistical technique applied to the geochemistry of pelagic muds. *J. Geol.*, 69: 572-582.
- Chayes, F. 1954. The lognormal distribution of the elements - a discussion. *Geochim. Cosmochim. Acta*, 6: 119-120.
- Chayes, F., 1971. *Ratio Correlation*. University of Chicago Press, Chicago, 99 pp.
- Clarke, R.H., 1967. Amino acids in recent sediments (S.E.Devon). *Nature*, 213: 1003-1005.
- Cobbing, E.J., 1964. The Highland Boundary Fault in East Tyrone. *Geol. Mag.*, 101: 496-501.
- Cocks, L.R.M., Holland, C.H., Rickards, R.B. and Strachan, I., 1971. A correlation of Silurian rocks in the British Isles. *Jl. Geol. Soc. London*, 127: 103-136.
- Cole, A.J., 1969. An iterative approach to the fitting of trend surfaces. *Univ. Kansas, Comp. Contrib.*, No.37.
- Cole, A.J. and Adamson, P.G., 1969. A simple method for drawing molecules using a digital plotter. *Acta Crystallogr., Sect. A*, 25: 535-539.

- Collier, A., 1953. Titanium and zirconium in bloom of Gniodinium brevis Davis. *Science*, 118: 329.
- Combaz, A., 1971. Thermal degradation of sporopollenin and genesis of hydrocarbons. In: J. Brooks, P.R. Grant, M.Muir, P. van Giyzel and G. Shaw (Editors), *Sporopollenin*, New York Academic Press, New York, pp. 621-653.
- Connan, J., 1972. Laboratory simulation and natural diagenesis, 1. Thermal evolution of asphalts from the Aquitaine Basin (S.W.France). *Cent. Rech. Pau, Bull.*, 3: 195-214.
- Connan, J. and Orgeval, J.J., 1973. Les bitumens des minéralisation barytiques et sulfurées de St. Privat. *Cent. Rech. Pau, Bull.*, 7: 557-585.
- Cook, A.C., Murchison, D.G. and Scott, E., 1972a. Optically biaxial anthracitic vitrinites. *Fuel*, 51: 180-184.
- Cook, A.C., Murchison, D.G. and Scott E., 1972b. A British meta-anthracite of Devonian age. *J. Geol.*, 8: 83-94.
- Cook, M.G. and Rich, C.I., 1962. Weathering of sodium-potassium micas in soils of the Virginia piedmont. *Soil Sci. Soc. Am., Proc.*, 26: 591-595.
- Cooley, W.W. and Lohnes, P.R., 1962. *Multivariate Procedures for the Behavioural Sciences*. J. Wiley and Sons Inc., New York, 343 pp.
- Cooper, B.S., Coleman, S.H., Barnard, P.C. and Butterworth, J.S., 1974. Palaeotemperatures in the North Sea Basin. In: A. W. Woodland (Editor), *Petroleum and the Continental Shelf of North West Europe, Vol.1., Geology*. Applied Science Publishers, London, pp. 487-493.
- Cooper, J.E. and Bray, E.E., 1963. A postulated role of fatty acids in petroleum formation. *Geochim. Cosmochim. Acta*, 27: 1113-1127.

- Cosgrove, M.E., 1973. The geochemistry and mineralogy of the red beds of south-east England. *Chem. Geol.*, 11: 31-47.
- Craig, G.Y. and Walton, E.K., 1959. Sequence and structure in the Silurian rocks of Kircudbrightshire. *Geol. Mag.*, 96: 209-220.
- Cronin, J.R. and Moore, C.B., 1971. Amino acid analyses of the Murchison and Allende carbonaceous chondrites. *Science*, 172: 1327-1328.
- Chester, R. and Green, R.N., 1968. The infra-red determination of quartz in sediments and sedimentary rocks. *Chem. Geol.*, 3: 199-212.
- Dapples, E.C., 1967. Diagenesis in sandstones. In: *Diagenesis in Sediments, Developments in Sedimentology, Vol.8.*, pp. 91-95.
- Dapples, E.C. and Rominger, J.F., 1945. Analysis of fine grained clastic sediments. *J. Geol.*, 53: 246-261.
- Darbre, A. and Islam, A., 1968. Gas-liquid chromatography of trifluoroacetylated amino acid methyl esters. *J. Biochem.*, 106: 923-925.
- Davis, J.C., 1973. *Statistics and Data Analysis in Geology*. Wiley, New York, 550 pp.
- Deer, W.A., Howie, R.A. and Zussman, J., 1962. *Rock-Forming Minerals, Vol.3., Sheet Silicates; and Vol.5., Non-Silicates*, Longmans, London.
- Dembicki, H., Meinschein, W.G. and Hattin, D.E., 1976. Possible ecological and environmental significance of the predominance of even-carbon number $C_{20} - C_{30}$ n-alkanes. *Geochim. Cosmochim. Acta*, 40: 203-208.

- Dewey, J.F., 1961. A note concerning the age of the metamorphism of the Dalradian rocks of western Ireland. *Geol. Mag.*, 98: 209-220.
- Dewey, J.F., 1963. The Lower Palaeozoic stratigraphy of central Murrisk, County Mayo, Ireland. *Jl. Geol. Soc., London*, 119: 313-314.
- Dewey, J.F., 1969. Evolution of the Appalachian/Caledonian orogen. *Nature*, 222: 124-129.
- Dewey, J.F., 1971. A model for the Lower Palaeozoic evolution of the early Caledonides of Scotland and Ireland. *Scot. J. Geol.*, 7: 219-240.
- Dewey, J.F., McKerrow, W.S. and Moorbath, S., 1970. The relationship between isotopic ages, uplift and sedimentation during Ordovician times in western Ireland. *Scot. J. Geol.*, 6: 133-145.
- Douglas, A.G. and Eglinton, G., 1966. The distribution of alkanes. In: T. Swain (Editor), *Comparative Phytochemistry*. Academic Press, London, pp. 57-77.
- Douglas, A.G. and Grantham, P.J., 1973. Fingerprint chromatography in the analysis of some native bitumens, asphalts and related substances. In: B. Tissot and P. Bierner (Editors), *Advances in Organic Geochemistry*. Pergamon, Oxford, pp. 261-276.
- Duff, P. McL.D., Hallam, A. and Walton, E.K., 1967. Nomenclature of cycles. In: *Cyclic Sedimentation. Developments in Sedimentology*, Vol. 10., Elsevier, Amsterdam, pp. 1-20.
- Dungworth, G., 1972. The organic geochemistry of the Marl Slate and associated sediments. Ph.D. Thesis, University of Newcastle upon Tyne.

- Dungworth, G., 1976. Optical configuration and the racemisation of amino acids in sediments and in fossils - a review. *Chem. Geol.*, 17: 135-153.
- Dutta, A.K., 1947. Electrical conductivity of molybdenite crystals. *Nature*, 159: 447.
- Eames, T.D., 1974. Coal rank and gas source relationships - Rotliegendes reservoirs. In: A.W.Woodland (Editor), *Petroleum and the Continental Shelf of North West Europe, Vol.1., Geology.* Science Publishers, London, pp. 191-204.
- Eisma, E. and Jurg, J.W., 1969. Fundamental aspects of the generation of petroleum. In: G. Eglinton and M.T. Murphy (Editors), *Organic Geochemistry: Methods and Results.* Springer-Verlag, Berlin, pp. 676-698.
- Eglinton, G. and Hamilton, R.J., 1963. The distribution of alkanes. In: T. Swain (Editor), *Chemical Plant Taxonomy.* Academic Press, London, pp. 187-217.
- Elles, G.L. and Wood, E.M.R., 1901-1918. *A Monograph of British Graptolites.* Palaeontogr. Soc., Monogr.
- Emery, K.O., 1964. Amino acids of the Santa Barbara basin. *J. Sediment. Petrol.*, 34: 433-437.
- Ergun, S., O'Donnel, H.T. and Parks, B.C., 1959. Microscopic studies of rate of decomposition of petrographic components of coal. *Fuel*, 38: 205-210.
- Ergun, S. and McCartney, J.T., 1960. Reflectance of coals, graphite and diamond. *Fuel*, 39: 449-454.
- Eugster, H.P. and Yoder, H.S., 1954. Paragonite. *Carnegie Inst. Wash. Yearb.*, 53: 111-114.

- Eugster, H.P. and Yoder, H.S., 1955. The join muscovite-paragonite. *Inst. Wash. Yearb.*, 54: 124-126.
- Fatt, I., 1957. Effect of overburden and reservoir pressure on electric logging formation factor. *Am. Assoc. Pet. Geol.*, 41: 2456-2466.
- Flaig, W., 1968. Biochemical factors in coal formation. In: D.G. Murchison and T.S. Westoll (Editors), *Coal and Coal-Bearing Strata*. Oliver and Boyd, Edinburgh, pp. 197-227.
- Forsman, J.P. and Hunt, J.M., 1958. Insoluble organic matter (kerogen) in sedimentary rocks. *Geochim. Cosmochim. Acta* 15: 170-182.
- Foucart, M.F., Bricteux-Grégoire, S., Jeuniaux, Ch. and Florkin, M., 1965. Fossil proteins of graptolites. *Life Sci.*, 4: 467-471.
- Francis, W., 1954. *Coal*. Edward Arnold Ltd., London, 567 pp.
- French, B.M., 1964. Graphitization of organic material in a progressively metamorphosed Precambrian iron formation. *Science*, 146: 917-918.
- Friedel, R.A., 1966. Infra-red spectroscopy in coal structure research. In: D.W. Kendal (Editor), *Applied Infra-red Spectroscopy*. Reinhold, New York, pp. 312-343.
- Friedel, R.A. and Carlson, G.L., 1972. Difficult carbonaceous materials and their infra-red and Raman spectra: reassignments for coal spectra. *Fuel*, 51: 193-198.
- Fyfe, T.B. and Weir, J.A., 1976. The Ettrick Valley Thrust and the upper limit of the Moffat Shales in Craigmichan Scaurs (Dumfries and Galloway Region; Annandale and Eskdale District). *Scot. J. Geol.*, 12: 93-102.

- Fyfe, W.S. and Turner, F.J., 1966. Reappraisal of the metamorphic facies concept. *Contrib. Mineral. Petrol.*, 12: 354-364.
- Gehrke, C.W., Lamkin, W. and Stalling, D.L., 1965. Quantitative chromatography of amino acids. *Biochem. Biophys. Res. Comm.*, 19: 328-335.
- Gehrke, C.W. and Leimer, K., 1971. Trimethylsilylation of amino acids-derivitization and chromatography. *J. Chromatogr.*, 57: 219-238.
- Gehrke, C.W. and Shahrokhi, F., 1966. Chromatographic separation of n-butyl N-trifluoroacetyl esters of amino acids. *Anal. Biochem.*, 15: 97-108.
- Gehrke, C.W. and Stalling, D.L., 1967. Quantitative analysis of the twenty natural protein amino acids by gas-liquid chromatography. *Separation Sci.*, 2: 101-138.
- Gelpi, E., Noonan, D.W. and Oró, J., 1969. Isoprenoids and other hydrocarbons in terrestrial graphite. *Geochim. Cosmochim. Acta*, 33: 959-972.
- George, T.N., 1960. The stratigraphical evolution of the Midland Valley. *Geol. Soc. Glasg., Trans.*, 24: 32-107.
- Gilbert, L.A., 1960. The reflectivity spectra of coal vitrains in the visible and the ultraviolet. *Fuel*, 39: 393-400.
- Gilbert, L.A., 1962. Refractive indices and absorption coefficients of coal in bulk measured in the range 6000 to 2400 Å by a polarised light technique. *Fuel*, 41: 351-358.
- Glanville, C.R., 1959. Laboratory study indicates significant effect of pressure on resistivity of reservoir rocks. *J. Petrol. Technol.*, 11: 20-26.

- Glasstone, S. and Lewis, D., 1966. Elements of Physical Chemistry. Macmillan and Co. Ltd., London, 758 pp.
- Goldberg, E.D. and Arrhenius, G.O.S., 1958. Chemistry of Pacific pelagic sediments. *Geochim. Cosmochim. Acta*, 13: 153-212.
- Goodarzi, F. and Murchison, D.G., 1972. Optical properties of carbonized vitrinites. *Fuel*, 51: 322-328.
- Gordon, A.J., 1962. The Lower Palaeozoic rocks around Glenluce, Wigtownshire. Ph.D. Thesis, University of Edinburgh.
- Grasselly, G.Y., Agocs, M. and Nagy, R., 1972. Characterization of insoluble organic substances of sediments by thermal and infrared investigation. *Mineral. Petrogr. Acta*, 20: 241-253.
- Gray, J. and Boucot, A.J., 1975. Colour changes in pollen and spores - a review. *Geol. Soc. Am., Bull.*, 86: 1019-1033.
- Gutjahr, C.C.M., 1966. Carbonization measurements on pollen-grains and spores and their application. *Leidse Geol. Meded.*, 38: 1-29.
- Hacquebard, P.A. and Donaldson, J.R., 1970. Coal metamorphism and hydrocarbon potential in the Upper Palaeozoic of the Atlantic Provinces, Canada. *Can. J. Earth Sci.*, 7: 1139-1158.
- Hare, P.E., 1969. Geochemistry of proteins, and amino acids. In: G. Eglinton and M.T. Murphy (Editors), *Organic Geochemistry - Methods and Results*. Springer-Verlag, Berlin, pp. 438-452.
- Harkness, R. 1851. On the Silurian rocks of Dumfriesshire and Kircudbrightshire. *Quart. Jl. Geol. Soc. London*, 7: 46-58.
- Hayes, J.M., 1967. Organic constituents of meteorites - a review. *Geochim. Cosmochim. Acta*, 31: 1359-1394.

- Heslop, W.P., 1899. The coalfields of Natal. *Inst. Min. Eng., Trans.*, 18: 410-450.
- Hietanen, A., 1967. On the facies series in various types of metamorphism. *J. Geol.*, 75: 187-214.
- Himus, G.W., 1951. Observations on the composition of kerogen rocks and the chemical constituents of kerogen. In: G. Sell (Editor), *Oil shale and Cannel coal*, Inst. Petrol. London, 216 pp.
- Hinxman, I.W., Anderson, E.M. and Caruthers, R.G., 1920. The economic geology of the central coalfield of Scotland: area 4. *Mem. Geol. Surv. Scotland*.
- Hirsch, I.B., 1954. X-ray scattering of coals. *R. Soc. London, Proc., Ser. A*, 226: 143-169.
- Hirst, D.M. and Kaye, M.J., 1971. Factors controlling the mineralogy and chemistry of an upper Viséan sequence from Rookhope, County Durham. *Chem. Geol.*, 8: 37-69.
- Howarth, R.J., 1967. Trend surface fitting to random data - an experimental test. *Am. J. Sci.*, 265: 619-625.
- Hubbard, A.B., Smith, H.W., Heady, H.H. and Robinson, W.E., 1952. Method of concentrating kerogen in Colorado oil shale by treatment with acid and gravity separation. *U.S. Bur. Mines, Rep. Invest.*, 4872.
- Huck, G. and Karweil, J., 1955. Physikalisch-chemische probleme der inkohlung. *Brennstoff-Chemie*, 36: 1-32.
- Hunt, J.M., 1961. Distribution of hydrocarbons in sedimentary rocks. *Geochim. Cosmochim. Acta*, 22: 37-49.

- Hunt, J.M. and Jamieson, G.M., 1956. Oil and organic matter in source rocks of petroleum. *Am. Assoc. Pet. Geol. Bull.*, 40: 477-483.
- Jaeger, J.C., 1959. Temperatures outside a cooling intrusive sheet. *Am. J. Sci.*, 257: 44-54.
- Jaeger, J.C., 1964. Thermal effects of intrusions. *Reviews of Geophysics*, 2: 443-466.
- Jain, S., 1964. Electrical resistivity of the crust and upper mantle at Eskdalemuir, South Scotland. *Nature*, 203: 631-632.
- Jeanroy, E., 1972. Analyse totale des silicates naturels par photometrie d'absorption atomique. *Chimie Analitique*, 54: 159-166.
- Jenkins, R. and De Vries, D.L., 1967. *Practical X-ray Spectroscopy*. Philips Technical Library, Eindhoven, 181 pp.
- Johns, R.B., Belsky, T., McCarthy, E.D., Burlingame, A.L., Haug, P., Schones, H.K., Richter, W. and Calvin, M., 1966. The organic geochemistry of ancient sediments - Part II. *Geochim. Cosmochim. Acta*, 30: 1191-1222.
- Johnson, V.H., Gray, R.J. and Schapiro, N., 1963. Effect of igneous intrusions on the chemical, physical and optical properties of Somerset coal. *Am. Chem. Soc. Div. of Fuel Chem.*, 1: 110-124.
- Jones, J.M., 1961. The measurement of some of the physical properties of the coal macerals and their variation with rank. Ph.D. Thesis, University of Durham.
- Jones, J.M., Murchison, D.G. and Saleh, S.A., 1971. Variation of vitrinite reflectivity in relation to lithology. In: H.R. van Gaertner and H. Wehner (Editors), *Advances in Organic Geochemistry*. Pergamon, Oxford, pp. 601-612.

- Jones, J.M., Murchison, D.G., Scott, E. and Pickles, S., 1968.
Apparatus for reflectivity measurement of reactive and radioactive materials. *J. R. Microsc. Soc.*, 88: 503-512.
- Jurg, J.W. and Eisma, E., 1964. Petroleum hydrocarbons - generation from fatty acids. *Science*, 144: 1451-1452.
- Karpov, P.A., Stepanova, A.F., Solovyeva, N.V., Agulov, A.P., Gozhaya, A.L., Golikov, V.A. and Chaitskiy, V.P., 1976.
Quantitative estimation of temperature and geological time as factors in carbonification of disseminated coal residues and possible applications in oil geology. *Int. Geol. Rev.*, 18: 397-405.
- Kaye, M.J., Dunham, A.C. and Hirst, D.M., 1968. A comparison of two methods of quantitative mineralogical analysis of sedimentary rocks. *J. Sed. Pet.*, 38: 675-679.
- Kelling, G., 1961. The stratigraphy and structure of the Ordovician rocks of the Rhinns of Galloway. *Quart. Jl. Geol. Soc., London*, 17: 37-75.
- Kennedy, W.Q., 1958. The tectonic evolution of the Midland Valley of Scotland. *Trans. Geol. Soc. Glasg.*, 23: 106-133.
- Kesler, S.E. and Heath, S.A., 1968. The effect of dissolved volatiles on magmatic heat sources at intrusive contacts. *Am. J. Sci.*, 266: 824-839.
- Kisch, H.J., 1966. Carbonization of semi-anthracite vitrinite by an analcime-basanite sill. *Econ. Geol.*, 61: 1043-1063.
- Kisch, H.J., 1968. Coal rank and lowest grade regional metamorphism in the Southern Bowen Basin, Queensland, Australia. *Geol. Mijnbouw*, 47: 28-36.

- Kisch, H.J., 1968. Coal rank and burial metamorphic mineral facies. In: P.A. Schenk and I. Havenaar (Editors). *Advances in Organic Geochemistry*. Pergamon, Oxford, pp. 407-424.
- Kisch, H.J., 1974. Anthracite and meta-anthracite coal ranks associated with 'anchimetamorphism' and 'very low stage metamorphism'. *Ned. Akad. Wet., Proc., Ser. B*, 77: 81-118.
- Kisch, H.T. and Taylor, G.H., 1966. Metamorphism and alteration near an intrusive-coal contact. *Econ. Geol.*, 61: 343-361.
- Klug, H.P. and Alexander, L., 1954. *X-ray Diffraction Procedures*. J. Wiley and Sons, Inc., New York, pp. 410-416.
- Koch, G.S. and Link, R.F., 1970. *Statistical Analysis of Geological Data*. J. Wiley and Sons, New York, 375 pp.
- Koenig, W.A., Parr, W., Lichtenstein, H.A., Bayer, E. and Oró, J., 1970. Gas chromatographic separation of amino acids and their enantiomers - non polar stationary phases and a new optically active phase. *J. Chromatogr. Sci.*, 8: 183-186.
- Kossovskaya, A.G. and Shutov, V.D., 1961. The correlation of zones of regional epigenesis and metagenesis in terrigenous and volcanic rocks. *Acad. Sci. USSR, Dokl., Earth Sci. Sect.*, 139: 732-736.
- kossovskaya, A.G. and Shutov, V.D., 1970. Main aspects of the epigenesis problem. *Sedimentology* 15: 11-40.
- Krevelen, D.W. van, 1961. *Coal*. Elsevier, Amsterdam, 514 pp.
- Krevelen, D.W. van and Schuyer, J., 1957. *Coal Science; Aspects of Coal Constitution*. Elsevier, Amsterdam, 352 pp.

- Krishnan, K.S. and Ganguli, N., 1939. Large anisotropy of the electrical conductivity of graphite. *Nature*, 144: 667.
- Krumbein, W.C. and Graybill, F.A., 1965. *An Introduction to Statistical Methods in Geology*. McGraw-Hill Book Co., New York, 475 pp.
- Kubler, B., 1968. Evaluation quantitative du métamorphisme par la cristallinité de l'illite. *Cent. Rech. Pau, Bull.*, 2: 385-397.
- Kuyf, O.S., Muller, J. and Waterbolk, H.T., 1955. The application of palynology to oil geology with reference to western Venezuela. *Geol. Mijnbouw*, 17: 49-76.
- Kvenvolden, K.A., 1963. Normal paraffin hydrocarbons in sediments from San Francisco Bay, California. *Am. Assoc. Pet. Geol., Bull.*, 46: 1643-1652.
- Kvenvolden, K.A., 1966. Molecular distributions of normal fatty acids and paraffins in some lower Cretaceous sediments. *Nature*, 209: 573-577.
- Kvenvolden, K.A., 1973. Criteria for distinguishing biogenic and abiogenic amino acids - preliminary considerations. *Space Life Sciences*, 4: 60-68.
- Kvenvolden, K.A., Lawless, J.G. and Ponnampereuma, C., 1971. Non protein amino acids in the Murchison meteorite. *Natl. Acad. Sci., Proc.*, 68: 486-490.
- Kvenvolden, K.A., Lawless, J.G., Pering, K., Peterson, E., Flores, J., Ponnampereuma, C., Kaplan, I.R. and Moore, C., 1970. Evidence for extraterrestrial amino-acids and hydrocarbons in the Murchison meteorite. *Nature*, 228: 923-926.

- Kvenvolden, K.A. and Peterson, J., 1969. Optical configuration of amino acids in Precambrian Fig Tree Chert. *Nature*, 221: 141-143.
- Kvenvolden, K.A., Peterson, E. and Brown, F.S., 1970. Racemization of amino acids in sediments from Saanich inlet, British Columbia. *Science*, 169: 1079-1082.
- Lam, J. and Pederson, K.R., 1968. Precambrian organic compounds from the Ketilidian of south-west Greenland, Part 2. *Medd. Groenland*, 185, Number 6.
- Landis, C.A., 1971. Graphitization of dispersed carbonaceous material in metamorphic rocks. *Contrib. Mineral. Petrol.*, 30: 34-45.
- Landis, C.A. and Coombs, D.S., 1967. Metamorphic belts and orogenesis in southern New Zealand. *Tectonophysics*, 4: 501-518.
- Laplante, R.E., 1974. Hydrocarbon generation in Gulf coast Tertiary sediments. *Am. Soco. Petrol. Geol., Bull.*, 58: 1281-1289.
- Lapworth, C., 1878. The Moffat Series. *Quart. J. Geol. Soc. Lond.*, 34: 240-346.
- Lawless, J.G., Kvenvolden, K.A., Peterson, E., Ponnampuruma, C. and Moore, C., 1971. Amino acids indigenous to the Murray meteorite. *Science*, 173: 626-627.
- Le Maitre, R.W., 1968. Chemical variation within and between volcanic rock series - a statistical approach. *J. Petrol.*, 9: 220-252.
- Le Tran, K., Connan, J. and Weide, B. van der., 1974. Diagenesis of organic matter and occurrence of hydrocarbons and hydrogen sulphide in the South-west Aquitaine Basin. *Cent. Rech. Pau, Bull.*, 8: 111-137.

- Long, G., Neglia, S. and Favretto, L., 1968. The metamorphism of the kerogen from Triassic black shales, south-east Sicily. *Geochim. Cosmochim. Acta*, 32: 647-656.
- Loon, J.C. van and Parissis, C., 1969. Scheme of silicate analysis based on the lithium metaborate fusion followed by atomic absorption spectroscopy. *Analyst*, 94: 1057-1062.
- Love, L.G., 1964. Early diagenetic pyrite in fine grained sediments. In: G.C. Amstutz (Editor), *Sedimentology and Ore Genesis*. Elsevier, Amsterdam, pp. 11-17.
- Mackowsky, M. Th., 1961. Recent investigations into the basic principles of the reflectivity of coal. Conference at Le Touquet, Paper 61. National Coal Board translation A/2026/18.
- Mackowsky, M. Th., 1968. European Carboniferous coalfields and Permian Gondwana coalfields. In: D.G. Murchison and T.S. Westoll (Editors), *Coal and Coal Bearing Strata*. Oliver and Boyd, Edinburgh, pp. 325-345.
- Marmorshstein, I.M., 1962. Effect of pressure on the physical properties of rocks. *Tr. Inst. Geologii Artika*, 132: 152-162.
- Marsh, H., 1973. Carbonization and liquid crystal (mesophase) development, Part 1. The significance of the mesophase during carbonization of coking coals. *Fuel*, 52: 205-212.
- Marsh, H., Akitt, J.W., Hurley, J.M., Melvin, J. and Warburton, A.P., 1971. Formation of graphitisable carbons from gillsonite pitch and polyvinyl chloride - a mass spectrometric and N.M.R. study. *J. Appl. Chem. Biotechnol.*, 21: 251-260.
- Marshall, C.E., 1936. Alteration of coal seams by the intrusion of some igneous dykes in Northumberland and Durham. *Inst. Min. Eng., Trans.*, 91: 235-260.

- Marshall, C.E., 1945. The petrology of natural coke. *Fuel in Science and Practice*, 24: 120-126.
- Marshall, R.J. and Murchison, D.G., 1971. Dispersion of the optical properties of carbonised vitrinites. *Fuel*, 50: 4-22.
- Martin, R.T., 1955. The X-ray characteristics of chlorites. In: W.O. Milligan (Editor), *Clays and Clay Minerals*. National Academy of Science, Natural Research Council, Washington, Publ. 395, pp. 117-145.
- McCartney, J.T. and Teichmüller, M., 1972. Classification of coals according to degree of coalification and reflectance of the vitrinite component. *Fuel*, 51: 64-68.
- McCartney, J.T., Yasinsky, J.B. and Ergun, S., 1965. Optical constants of coal by reflectance measurement in the ultraviolet and visible spectrum. *Fuel*, 44: 349-354.
- McGregor, M. and Anderson, E.M., 1923. The economic geology of the central coalfields of Scotland: area 4. *Mem. Geol. Surv. Scotland*.
- McIntyre, D.J., 1972. Effect of experimental metamorphism on pollen in a lignite. *Geosci. Man*, 4: 111-117.
- McIver, K.D., 1967. Composition of kerogen: clue to its role in the origin of petroleum. In: 7th World Petrol. Cong. Proc., Mexico, Vol.2., pp. 25-36.
- Medlin, J.H., Suhr, W.H. and Bodkin, J.B., 1969. Atomic absorption analysis of silicates using lithium metaborate fusion. *Atomic Absorption Newsletter*, 8: 25-29.

- Melvin, J.N., 1967. Optical properties of vitrinite in a coal seam intruded by a tholeiite dyke. M.Sc. Thesis, University of Newcastle upon Tyne.
- Melvin, J.N., 1973. Thermal metamorphism and carbonisation of coals in relation to petrology. Ph.D. Thesis, University of Newcastle upon Tyne.
- Miesch, A.T., 1962. Computing mineral composition of sedimentary rocks from chemical analysis. *J. Sed. Pet.*, 32: 217-225.
- Miesch, A.T., 1969. Critical review of some multivariate procedures in the analysis of geochemical data. *Int. Assoc. Math. Geol.*, J., 1: 171-184.
- Miller, R.L. and Kahn, J.S., 1962. *Statistical Analysis in the Geological Sciences*. J. Wiley and Sons Inc., New York, 367 pp.
- Millson, M.F., 1970. Chromatography of sulphur: separation from hydrocarbons. *J. Chromatogr.*, 50: 155-159.
- Mitchell, A.H.G., 1974. Flysch-ophiolite successions: polarity indicators in arc and collision-type orogens. *Nature*, 248: 747-749.
- Mitchell, A.H.G. and McKerrow, W.S., 1975. Analogous evolution of the Burma Orogen and the Scottish Caledonides. *Geol. Soc. Am.*, Bull., 86: 305-315.
- Mitchell, W.A., 1960. A method of quantitative mineralogical analysis by X-ray powder diffraction. *Mineral. Mag.*, 32: 492-499.
- Moore, R.C., 1955. *Treatise on Invertebrate Palaeontology, Part V, Graptolithina*. Geological Society of America, Boulder, Colorado.

- Moss, C.W., Lambert, M.A. and Diaz, F.J., 1971. Gas-liquid chromatography of twenty protein amino acids on a single column. *J. Chromatogr.* 60: 134-137.
- Müller, C., 1967. Diagenesis in argillaceous sediments. In: *Diagenesis in Sediments. Developments in Sedimentology, Vol.8.* Elsevier, Amsterdam, pp. 127-177.
- Nakaparksin, S., Birrell, P., Gil-Av, E. and Oró, J., 1970. Gas chromatography with optically active stationary phases: resolution of amino acids. *J. Chromatogr. Sci.*, 8: 177-182.
- Nicholls, G.D., 1962. A scheme for recalculating the chemical analysis of argillaceous rocks for comparative purposes. *Am. Mineral.*, 47: 34-46.
- Nooner, D.W. and Oró, J., 1967. Organic compounds in meteorites, I: aliphatic hydrocarbons. *Geochim. Cosmochim. Acta*, 31: 1359-1394.
- Norrish, K. and Chappel, B., 1967. X-ray fluorescence spectroscopy. In: J. Zussman (Editor), *Physical Methods in Determinative Mineralogy.* Academic Press, Oxford, pp. 161-214.
- Norrish, K. and Hutton, J.T., 1969. An accurate X-ray spectrographic method for the analysis of a wide range of geological samples. *Geochim. Cosmochim. Acta*, 33: 431-453.
- Nuffield, E.W., 1966. *X-ray Diffraction Methods.* J. Wiley and Sons Inc., New York, pp. 157-147.
- Oró, J., Nakaparksin, S., Lichtenstein, H. and Gil-Av, E., 1971. Configuration of amino acids in carbonaceous chondrites and a Precambrian chert. *Nature*, 230: 107-108.
- Oró, J. and Skenes, H.B., 1965. Free amino acids on human fingers: the question of contamination in microanalysis. *Nature*, 207: 1042.

- Oró, J., Tornabene, T.G., Nooner, D.W. and Gelpi, E., 1967. Aliphatic hydrocarbons and fatty acids of some marine and freshwater micro-organisms. *J. Bacteriol.*, 93: 1811-1818.
- Otalórra, G. and Hess, H.H., 1969. Modal analysis of igneous rocks by X-ray diffraction with examples from St. Pauls Rock and an olivine nodule. *Am. J. Sci.*, 267: 822-840.
- Paproth, E. and Wolf, M., 1973. Some palaeogeographic interpretations of the carbonification in the Devonian and Carboniferous of the northern Rhenish Schiefergebirge. *Geol. Palaeontol.*, 8: 469-493. ^{Abh.}
- Pareek, H.S., 1964. Petrological characteristics of Saraker coal, metamorphosed by a lamprophyre sill, in Jharia coalfield India. *Econ. Geol.*, 59: 926-929.
- Parkhomenko, E.I., 1967. *Electrical Properties of Rocks*. Plenum Press, New York, 463 pp.
- Parkhomenko, E.I. and Bondarenko, A.T., 1960. Effect of uniaxial pressure on the electrical resistivity of rocks. *Akad. Nauk. SSSR, Izv., Ser. Geophys.*, 2: 214-219.
- Peach, B.N. and Horne, J., 1899. *The Silurian rocks of Britain, Vol.1, Scotland*. Mem. Geol. Survey, U.K.
- Peake, E., Baker, B.L. and Hodgson, B.L., 1970. The contribution of amino acids and chlorins to the Beaufort Sea by the McKenzie river. *Geol. Soc. Am., Abstr.*, 2: 646.
- Plumb, R.C. and Hornig, D.F., 1955. Infra-red spectrum, X-ray diffraction pattern and structure of ammonium fluoride. *J. Chem. Phys.* 23: 947-953.

- Pollock, G.E. and Miyamoto, A.K., 1971. A desalting technique for amino acid analysis of use in soil and geochemistry. *J. Agr. Food Chem.*, 19: 104-107.
- Powell, D.W., 1972. Letter: a model for the Lower Palaeozoic evolution of the southern margin of the early Caledonides of Scotland and Ireland. *Scot. J. Geol.*, 7: 369-372.
- Quass, F.W., 1939. The analysis of kerogen in oil shales. *J. Inst. Petrol. Geol.*, 25: 813-819.
- Quin, A.W. and Glass, H.D., 1958. Rank of coal and metamorphic grade of rocks of the Narragansett Basin of Rhode Island. *Econ. Geol.*, 53: 563-576.
- Rast, N., 1963. Structure and metamorphism in the Dalradian rocks of Scotland. In: M.R.W. Johnson and F.H. Stewart (Editors), *The British Caledonides*, Oliver and Boyd, Edinburgh, pp. 123-175.
- Reid, H.H., 1961. Aspects of Caledonian magmatism in Britain. *L'pool, Manchr. Geol. J.*, 2: 653-683.
- Reif, P., 1966. Identification et dosage par diffraction dans une chambre à haut température. Rapport Interne du Centre de Recherches des Ciments Lafarge, 25 pp.
- Ring, D., Wolman, Y., Friedman, N. and Miller, S.L., 1972. Prebiotic synthesis of hydrophobic and protein amino acids. *Natl. Acad. Sci., Proc.*, 69: 765-768.
- Robinson, R., 1966. The origin of petroleum. *Nature*, 212: 1291-1295.
- Rosenfield, J.R., Thompson, J.B. and Zen, E-An., 1958. Data on coexistent muscovite and paragonite. *Geol. Soc. Am., Bull.*, 69: 1637.

- Rusnak, G.A., 1957. Study of the Pleasantview sandstones. *J. Sed. Pet.*, 27: 41-55.
- Russel, A., 1904. The coalfields of Cape Colony. *Inst. Min. Eng., Trans.*, 29: 228-259.
- Salch, S.A., 1968. Optical properties of vitrinites in relation to differing lithologies. Ph.D. Thesis, University of Newcastle upon Tyne.
- Saxby, J.D., 1970. Isolation of kerogen from sediments by chemical methods. *Chem. Geol.*, 6: 173-184.
- Scalan, R.S. and Smith, J.E., 1970. An improved measure of the odd-even predominance in the normal alkanes of sediment extracts and petroleum. *Geochim. Cosmochim. Acta*, 34: 611-620.
- Schapiro, L., 1973. Rapid determination of sulphur in rocks. *J. Res. U.S. Geol. Surv.*, 1: 81-84.
- Schapiro, N. and Grey, R.J., 1966. Physical variations in highly metamorphosed Antarctic coals. In: *Coal Science, Advances in Chemistry Series, No. 55*. Am. Chem. Soc., Washington, pp.196-217.
- Schroll, E. 1968. Abundance of the chemical elements in the main rock types of the lithosphere in relation to a system of correlation. In: L.H. Ahrens (Editor), *Origin and Distribution of the Elements*. Pergamon, Oxford, pp. 599-639.
- Shibaoka, M., Bennet, A.J.R. and Gould, K.W., 1973. Diagenesis of organic matter and occurrence of hydrocarbons in Australian sedimentary basins. *Aust. Petrol. Expl., J.*, 13: 73-80.
- Shillaber, C.P., 1949. Spectral energy distribution of a tungsten filament lamp. In: *Photomicrography in Theory and Practice*. J. Wiley and Sons Inc., New York, 775 pp.

- Siegel, S., 1956. Nonparametric Statistics for the Behavioural Sciences, McGraw-Hill Book Co., Inc., New York, 312 pp.
- Smaltz, R.F. and Zen, E-An., 1959. Quantitative modal analysis of sediments by X-ray diffraction. In: M. Sears (Editor), International Oceanographic Congress, Proc., Washington. Amer. Assoc. Adv. Sci., pp. 485-486.
- Smith, H.W., 1961. Ultimate composition of organic material in Green River oil shale. U.S. Bur. Mines, Rep. Invest., 4872.
- Sokatch, J.R., 1969. Chemical composition of bacteria. In: Bacterial Physiology and Metabolism. Academic Press, London, pp. 25-51.
- Sowden, R., 1969. Effect of hydrolysis time and iron and aluminium removal on the determination of amino compounds in soils. Soil Sci., 107: 364-371.
- Spencer, D.W., 1966. Factors affecting element distribution in a Silurian graptolite band. Chem. Geol., 1: 221-249.
- Stach, E., 1952. Mikroskopie Naturlicher Kokse. In: H. Freund (Editor), Handbuch der Mikroskopie in der Technik, Vol.2, Umschau-Verlag, Frankfurt, pp. 413-442.
- Stach, E., 1975. In: E. Stach, G.H. Taylor, M.Th. Mackowsky, M. Teichmüller, R. Teichmüller and D. Chandra (Editors), Stach's Textbook of Coal Petrology. Translation and English revision by D.G. Murchison, G.H. Taylor and F. Zierke. Gebrüder Borntraeger, Berlin, 428 pp.
- Staplin, F.L., 1969. Sedimentary organic matter, organic metamorphism, and oil and gas occurrence. Can. Petrol. Geol., Bull., 17: 47-66.

- Stephens, W.E., 1972. The geochemistry of the Dalbeattie granodiorite complex and associated rocks. Ph.D. Thesis, University of Aberystwyth.
- Stephens, W.E., 1975. The Display of 3-factor models, (in litt.).
- Stephens, W.E., Watson, S.W., Philip, P.R. and Weir, J.A., 1975. Element associations and distributions through a Lower Palaeozoic graptolitic shale sequence in the Southern Uplands of Scotland. *Chem. Geol.*, 16: 269-294.
- Stevens, N.P., Bray, E.E. and Evans, E.D., 1956. Hydrocarbons in sediments of Gulf of Mexico. *Am. Assoc. Pet. Geol., Bull.*, 38: 377-404.
- Taylor, G.H., 1957. The behaviour of the petrological components of coal on carbonization. *Fuel*, 36: 221-235.
- Teichmüller, M. and Teichmüller, R., 1949. Inkohlungsfragen in Ruhrcarbon. *Dtsch. Geol. Ges., Z.*, 99 : 40-77.
- Teichmüller, M. and Teichmüller, R., 1958. Inkohlungsuntersuchungen und ihre nutzanwendung. *Geol. Mijnbouw*, 20: 41-66.
- Teichmüller, M. and Teichmüller, R. 1966. Geological Causes of Coalification. In: *Coal Science, Advances in Chemistry Series*, No. 55. *Am. Chem. Soc., Washington*, pp. 133-155.
- Teichmüller, M. and Teichmüller, R., 1968. Geological Aspects of Coal Metamorphism. In: D.G. Murchison and T.S. Westoll (Editors), *Coal and Coal Bearing Strata*. Oliver and Boyd, Edinburgh, pp. 233-267.
- Tissot, B., Califet, D., Deroo, G. and Oudin, J.L., 1971. Origin and evolution of hydrocarbons in early Toarcian Shales, Paris Basin, France. *Am. Assoc. Pet. Geol., Bull.*, 55: 2177-2193.

- Tissot, B., Durand, B., Espitalie, J. and Combaz, A., 1974. Influence of nature and diagenesis of organic matter in formation of petroleum. *Am. Assoc. Petrol. Geol., Bull.*, 58: 499-506.
- Toghill, P., 1968. The graptolite assemblages and zones of the Birkhill Shales (Lower Silurian) at Dobb's Linn. *Palaeontology*, 11: 654-658.
- Toghill, P., 1970a. Highest Ordovician (Hartfell Shales) graptolite faunas from the Moffat area, south Scotland. *Br. Mus. (Nat. Hist.), Bull., Geol.*, 19: 1-26.
- Toghill, P., 1970b. The south-east limit of the Moffat Shales in the upper Ettrick Valley region, Selkirkshire. *Scot. J. Geol.*, 6: 233-242.
- Tourtelot, E.B., 1970. A selected annotated bibliography of minor-element content of black shales and related sedimentary rocks, 1930-65. *U.S. Geol. Surv., Bull.*, 1293, 118 pp.
- Towe, K.M. and Urbanek, A., 1972. Collagen-like substances in Ordovician graptolite periderm. *Nature*, 237: 443-445.
- Trotter, F.M., 1948. The devolatilization of coal seams in South Wales. *Quart. Jl. Geol. Soc.*, 104: 387-437.
- Trotter, F.M., 1954. The genesis of high rank coals. *Yorkshire Geol. Soc., Proc.*, 29: 267-303.
- Vallentyne, J.R., 1964. Biogeochemistry of organic matter, II. Thermal reaction kinetics and transformation products of amino compounds. *Geochim. Cosmochim. Acta*, 28: 157-188.
- Vine, J.D. and Tourtelot, E.B., 1970. Geochemistry of black shale deposits - a summary report. *Econ. Geol.*, 65: 253-272.

- Vistefius, A.B., 1967. *Studies in Mathematical Geology*. Consultants Bureau, New York, 165 pp.
- Vologdin, A.G., Sergiyenko, I.Z. and Yegorov, I.A., 1971. Discovery of amino acids and sugars in Precambrian rocks. *Acad. Sci. USSR, Dokl., Earth Sci. Sect.*, 191: 206-208.
- Wahlstedt, W.C. and Davis, J.C., 1968. Fortran IV program for computation and display of principal components. *Univ. Kansas, Comp. Centr., No. 21*.
- Walton, E.K., 1963. Sedimentation and Structure in the Southern Uplands. In: M.R.W. Johnson and F.H. Stewart (Editors), *The British Caledonides*, Oliver and Boyd, Edinburgh, pp. 161-227.
- Walton, E.K., 1965. Lower Palaeozoic rocks - palaeogeography and structure. In: G.Y. Craig, (Editor), *Geology of Scotland*. Oliver and Boyd, Edinburgh, pp. 201-227.
- Watson, S.W., 1971. An introduction to the organic geochemistry of the Hartfell Shales. B.Sc. Research Essay, University of St. Andrews.
- Weaver, C.E., 1967. Potassium, illite and the ocean. *Geochim. Cosmochim. Acta*, 31: 281-296.
- Weaver, C.E. and Pollard, L.D., 1973. *The Chemistry of Clay Minerals*. Elsevier, Amsterdam, 213 pp.
- Wedepohl, K.H., 1974. Biogeochemistry of sulphur. In: K.H. Wedepohl (Editor), *Handbook of Geochemistry*, Vol. 11-4. Springer-Verlag, Berlin, Sect. 16L, pp. 1-19.
- Weir, J.A., 1962. Geology of the Lower Palaeozoic inliers of Slieve Bernagh and the Cratloe Hills. *R. Dublin Soc., Sci. Proc., Ser. A*, 1: 253-263.

- Weir, J.A., 1968. Structural history of the Silurian rocks of the coast west of Gatehouse, Kircudbrightshire. *Scot. J. Geol.*, 4: 31-52.
- Weir, J.A., 1973. Lower Palaeozoic graptolite facies in Ireland and Scotland; review, correlation and palaeogeography. *R. Dublin Soc., Sci. Proc., Ser. A*, 4: 439-460.
- Weir, J.A., 1974. Tectonic style in Lower Palaeozoic rocks: the Clare - south Galway area and the Southern Uplands contrasted. *R. Dublin Soc., Sci. Proc., Ser. A*, 5: 107-112.
- Weir, J.A., 1975. The sedimentology and diagenesis of the Silurian rocks east of Gatehouse, Kircudbrightshire. *Scot. J. Geol.*, 10: 165-186.
- Weir, J.A., 1976. A modified synthesis of the evolution of the paratectonic zone B of the Caledonides in Scotland and Ireland, (in litt.).
- Weiskirchner, W., 1960. Untersuchungen zur Quantitaven Bestimmung der Phasen mit Hilfe von Röntgenstrahlen. *Soc. Ital. Mineral. Petrol., Rend.*, 16: 363-378.
- Welte, D.H. and Ehardt, G., 1968. Distribution of long chain n-paraffins and n-fatty acids in sediments from the Persian Gulf. *Geochim. Cosmochim. Acta*, 32: 465-466.
- White, D., 1913. The origin of coal. *U.S. Bur. Mines, Bull.*, 38: 105-130.
- Whitehead, J.J., 1904. Notes on the coal in the Transvaal. *Inst. Min. Eng., Trans.*, 28: 380-394.
- Wilson, L.R., 1971. Palynological techniques in deep basin stratigraphy. *Shale Shaker*, 21: 124-139.

- Williams, A., 1959. A structural history of the Girvan district, south-west Ayrshire. *R. Soc. Edinb., Trans.*, 63: 629-667.
- Williams, A., 1962. The Barr and Lower Ardmillan Series (Carradoc) of the Girvan district, south-western Ayrshire with descriptions of the Brachiopoda. *Geol. Soc. Lond., Memoir.*, 3, 267 pp.
- Williams, A., Strachan, I., Basset, D.A., Dean, W.T., Ingham, J.K., Wright, A.D. and Whittington, H.B., 1972. A correlation of Ordovician rocks in the British Isles. *Geol. Soc. Lond., Spec. Rept.*, 3: 1-77.
- Williams, J.A. and Winters, J.C., 1969. Microbial alteration of crude oil in the reservoir. In: *Petroleum transformation in geologic environments*. Am. Chem. Soc. 158th Nat. Meeting, Proc.
- Winkler, H.G.F., 1967. *Die Genese der Metamorphen Gesteine*. Springer-Verlag, Berlin, 218 pp.
- Winkler, H.G.F., 1970. Abolition of metamorphic facies, introduction of the four divisions of metamorphic stage, and a classification based on isograds in common rocks. *N. JI. Mineral.*, 5: 189-248.
- Wolf, M., 1972. Relations between carbonification and geotectonics in the northern part of the Rheinisches Schiefergebirge. *N. JI. Geol. Palaeont. Abh.*, 141: 222-257.
- Wolman, Y., Haverland, W.J. and Millar, S.L., 1972. Nonprotein amino acids from spark discharges and their comparison with the Murchison Meteorite amino acids. *Natl. Acad. Sci., Proc.*, 69: 809-811.
- Wyable, D., 1958. Effect of applied pressure on the conductivity of sandstones. *J. Petrol. Technol.*, 10: 57-59.

- Yule, J.W. and Swanson, G.A., 1969. A rapid method for decomposition and the analysis of silicates and carbonates by atomic absorption spectroscopy. *Atomic Absorption Newsletter*, 8: 30-33.
- Zen, E-An and Albee, A.L., 1964. Coexistent muscovite and paragonite in pelitic schists. *Am. Mineral.*, 49: 904-925.
- Ziegler, A.M., 1970. Geosynclinal development of the British Isles during the Silurian period. *J. Geol.*, 78: 445-479.
- Zimmerman, J.L., 1970. Contribution à l'étude de la déshydratation et de la libération de l'argon des micas. *Geochim. Cosmochim. Acta*, 34: 1327-1358.
- Zumwalt, R.W., Kuo, K. and Gehrke, C.W., 1971a. Applications of a gas-liquid chromatographic method for amino acid analysis:- a system for analysis of nanogram amounts. *J. Chromatogr.*, 55: 267-280.
- Zumwalt, R.W., Kuo, K. and Gehrke, C.W., 1971b. A nanogram and picogram method for amino acid analysis by gas-liquid chromatography. *J. Chromatogr.*, 57: 193-208.
- Zumwalt, R.M., Roach, D. and Gehrke, C.W., 1970. Gas-liquid chromatography of amino acids in biological substances. *J. Chromatogr.*, 53: 171-194.

THE SEDIMENTARY GEOCHEMISTRY OF THE
MOFFAT SHALES : A CARBONACEOUS SEQUENCE
IN THE SOUTHERN UPLANDS OF SCOTLAND

by

STEWART W. WATSON, BSc.

VOLUME 2 APPENDICES

Thesis presented for the degree of Doctor of Philosophy of
the University of St. Andrews in the Faculty of Science.

1976.



Th 8943

CONTENTS

| | Page |
|---|------|
| APPENDIX A. <u>SUMMARY OF STRATIGRAPHY</u> | A1 |
| 1. DOBB'S LINN | A2 |
| 2. HARTFELL | A6 |
| 3. CLANYARD BAY | A8 |
| APPENDIX B. <u>ANALYTICAL METHODS</u> | B1 |
| 1. INTRODUCTION | B2 |
| 2. INORGANIC CHEMISTRY | B2 |
| a) Analysis of major elements | B2 |
| b) Analysis of sulphur | B4 |
| c) Analysis of trace elements | B7 |
| 3. ORGANIC CHEMISTRY | B11 |
| a) Desalting of amino acid hydrolyzates | B11 |
| b) Test for the presence of amino acids | B12 |
| c) Separation of amino acids by gas-liquid chromatography | B13 |
| d) Separation of amino acid enantiomers by gas-liquid chromatography | B15 |
| e) Removal of sulphur from organic extracts | B18 |
| f) Isolation of kerogen | B19 |
| 4. REFLECTIVITY | B22 |
| a) The microreflectivity equipment | B22 |
| b) Reflectivity standards | B26 |
| c) Sample preparation | B28 |

| | Page |
|--|------|
| APPENDIX C. <u>STATISTICAL METHODS</u> | C1 |
| 1. INTRODUCTION | C2 |
| 2. THE DISTRIBUTION LAWS | C2 |
| 3. LINEAR CORRELATION | C4 |
| a) The simple linear model | C4 |
| b) The Kendall rank order correlation coefficient | C4 |
| c) Polynomial regression | C5 |
| 4. CLASSIFICATION OF SAMPLES | C5 |
| a) Introduction | C5 |
| b) Principal components analysis | C6 |
| c) Factor analysis | C7 |
| d) Comparison of principal components and factor analysis | C7 |
| 5. TREND SURFACE ANALYSIS | C8 |
| 6. COMPUTATIONAL METHODS | C10 |
| a) Introduction | C10 |
| b) Descriptive statistics | C10 |
| c) The simple linear model | C11 |
| d) Multivariate statistics | C12 |
| APPENDIX D. <u>DESCRIPTION OF THE SPECTRAL VARIATION IN</u> <u>OPTICAL PROPERTIES OF GRAPTOLITE FRAGMENTS</u> | D1 |
| 1. SPECTRAL VARIATION OF REFLECTANCE VALUES | D2 |
| 2. SPECTRAL VARIATION IN REFRACTIVE INDICES | D4 |
| 3. SPECTRAL VARIATION IN ABSORPTIVE INDICES | D7 |

| | Page |
|--|------|
| APPENDIX E. <u>ANALYTICAL RESULTS</u> | E1 |
| 1. INTRODUCTION | E2 |
| 2. ANALYTICAL RESULTS | E3 |
| 3. STANDARD DEVIATION VALUES FOR GRAPTOLITE REFLECTIVITY MEASUREMENTS | E97 |

A P P E N D I X A

SUMMARY OF STRATIGRAPHY

In this Appendix the stratigraphical successions in the Moffat Shale inliers at Dobb's Linn, Hartfell and Clanyard Bay will be described.

1. DOBB'S LINN

The stratigraphy of Dobb's Linn, located about 17 km northeast of Moffat, has been described in detail (Toghill 1968, 1970a).

Pleurograptus linearis Zone, 4.9 m.

Black pyritic mudstones, lowest 2.8 m affected by strike faulting. Lowest fossiliferous horizon ca. 3.4 m from assumed base: P. linearis (Carruthers), Leptogr. flaccidus (Hall), Orthogr. quadrimucronatus (Hall) and Orthogr. truncatus (Lapworth). Succeeding 0.6 m: Orthogr. truncatus pauperatus Elles and Wood, Leptogr. capillaris (Carruthers) and Climacogr. styloideus Elles and Wood. Overlying 0.6 m sparsely fossiliferous: Orthogr. quadrimucronatus (Hall), Climacogr. scalaris miserabilis Elles and Wood, Dicellogr. pumilus Lapworth and Dicellogr. carruthersi Toghill. Highest 0.3 m: Dicellogr. pumilus Lapworth, and Dicellogr. morrisoni Hopkinson together on a bedding plane and Orthogr. truncatus pauperatus Elles and Wood, Orthogr. truncatus socialis (Lapworth), Plegmatogr. nebula Elles and Wood, Dicellogr. moffatensis (Carruthers), Dicellogr. elegans (Carruthers) and Dicellogr. carruthersi Toghill.

Dicellograptus complanatus Zone, 9.5 m

Grey and greyish-green mudstones, shaley towards base and more massive towards top. 40 mm black shale band 1.5 - 1.8 m from base

- 'the complanatus Band' - with Dicellogr. complanatus Lapworth, Orthogr. truncatus socialis (Lapworth) and Climacogr. scalaris miserabilis Elles and Wood.

Dicellograptus anceps Zone, 4.6 m.

Barren grey carbonate rich mudstones with thin units of black mudstones and claystones. Lowest 1.5 m: 5 rusty weathered black mudstones, respectively 50, 152, 25, 102 and 55 mm thick with Dicellogr. anceps (Nicholson), Climacogr. supernus Elles and Wood, Climacogr. scalaris miserabilis Elles and Wood and Orthogr. truncatus abbreviatus Elles and Wood. Overlying 3.1 m barren with thin soft claystones.

Glyptograptus persculptus Zone, 1.06 m.

Black mudstone with thin claystones. 20 mm thick fossiliferous band at base with Climacogr. scalaris normalis Lapworth. Throughout the zone: Glyptogr. persculptus (Salter), Climacogr. medius Törnquist, Climacogr. scalaris miserabilis Elles and Wood and Diplogr. modestus Lapworth.

Akidograptus acuminatus Zone, 5.0 m.

Grey-black mudstones with common thin claystones. Base of zone marked by appearance of Akidogr. acuminatus (Nicholson). Glyptogr. persculptus (Salter) is common in the lower part, Climacogr. trifilis Manck in the middle and Cystogr. vesiculosus (Nicholson) at the top of the zone.

Cystograptus vesiculosus Zone, 1.3 m.

Massive black mudstone with few claystones. Base is marked by the appearance of the Monograptidae together with Dimorphogr. and Rhapidogr. extenuatis (Elles and Wood). Particularly common towards the base are Monogr. cyphus praematurus Toghill and Monogr. atavus Jones. Climacogr. innotatus Nicholson, and Diplograptus modestus Lapworth occur throughout.

Monograptus cyphus Zone, 7.3 m.

Massively bedded black mudstones with yellow and orange claystones common towards top. Base of zone characterized by the appearance of dimorphograptids with short uniserial portions eg. D. confertus (Nicholson), D. confertus swanstoni Lapworth and D. erectus Elles and Wood. Monogr. cyphus Lapworth is rare towards the base but soon becomes more abundant and ranges through the zone. Top bounded by 300 mm thick nodular claystone.

Monograptus gregarius Zone, 7.9 m.

Black mudstones with characteristic thick nodular claystones in lower 5 m. Towards the top occur banded grey and black mudstones with many claystones. Appearance of Monogr. triangulatus (Harkness) marks the base with Monogr. sandersoni Lapworth, Monogr. incommodus Törnquist and Monogr. atavus Jones limited to lower part of zone. Rastrites longispinus Perner and R. peregrinus Barr appear in the middle of the zone and Monogr. communis Lapworth is characteristic of the upper part.

Monograptus convolutus Zone, 5.35 m.

Lower and upper highly fossiliferous black mudstones with claystones separated by barren grey mudstones also with claystones. The base of the zone is marked by the prolific occurrence of Monogr. lobiferus (McCoy) in association with Monogr. convolutus (Hisinger). Lower mudstones yield Petalogr. folium (Hisinger), and Cephalogr. tubaliformis (Nicholson). The upper group yields Monogr. clingani (Carruthers), Monogr. limatulus Törnquist, Monogr. convolutus and Monogr. crenularis Lapworth.

Monograptus sedgwickii Zone, 8.4 m.

Basal 2 m of barren grey mudstones with claystones, middle section of 1.8 m with fossiliferous black mudstones and claystones and an upper group of 4.6 m with grey mudstones, claystones and a few fossiliferous seams of black shale. Middle unit characterized by abundant Monogr. sedgwickii (Portlock), Monogr. regularis Törnquist and Monogr. jaculum Lapworth. Upper unit similar but with Monogr. attenuatus (Hopkinson).

Rastrites maximus Zone, 6.55 m.

Predominantly grey mudstones and claystones with black mudstones restricted to the lowest 3 m. Basal beds yield Monogr. sedgwickii (Portlock), Monogr. regularis Törnquist, Monogr. nudus Lapworth and Monogr. circularis. Top of zone is taken at base of first greywacke bed.

2. HARTFELL

The stratigraphy and fauna of the Hartfell Scaur section which lies 2.5 km northeast of Moffat have not been formally reviewed since the work of Lapworth (1878) and the Monograph of Elles and Wood (1901-18). The description which follows deals only with the North cliff (Watson 1971).

The standard Moffat Shale succession of Glenkiln Shales followed by the wilsoni, clingani, linearis and complanatus Zones is nowhere seen in its entirety in the North cliff at Hartfell Scaur, but various combinations are brought to the surface by reverse strike faulting and to a lesser extent by small scale folding. The order of succession is illustrated in Fig.6.

Glenkiln Shales

A maximum of 6.45 m outcrop. The beds lie in faulted contact with either the clingani or complanatus Zones. Basal 1.5 m is crumbly yellow mudstone apparently devoid of fossils; 2.05 m grey, yellow and black 'shivery' shales and grey black mudstones succeed: Glossograptids and Didymograptus superstes (Elles and Wood). Top of unit consists of 2.9 m of unfossiliferous, hard, cherty, orange-weathered grey mudstone which forms a prominent cornice along the cliff.

Climacograptus wilsoni Zone.

Outcrops of 2.6, 4.1 and 1.4 m yield coarser ribs of shale which swarm with graptolites extensively preserved in semi-relief. Basal unit of 0.5 m of soft, flaky, black shales speckled

with organic flakes and terminating in a coarser rib with abundant Corynoides calycularis (Nicholson). Middle unit of 0.8 m with black shales devoid of fossils and dirty to touch. Upper 1.3 , consist of cherty mudstones and black shales: Climacogr. wilsoni (Elles and Wood), Climacogr. bicornis (Hall) and Orthogr. truncatus Lapworth.

Dicranograptus clingani Zone.

Cherty black mudstone weathering to a characteristic bright orange colour. Two thin (ca. 30 mm) ash bands form marker horizons. The lower, occurring between 0.8 and 1.3 m yields Orthogr. pageanus Elles and Wood whereas the upper, occurring between 4.8 and 5.2 m is not fossiliferous. Lower and middle divisions of zone are indicated by Climacogr. caudatus Elles and Wood and Dicellogr. caduceus respectively. Graptolites occurring include: Dicranogr. clingani Elles and Wood, D. nicholsoni Hopkinson, D. ramosus Elles and Wood, Climacogr. scalaris miserabilis Elles and Wood, C. bicornis (Hall), Dicellogr. moffatensis Lapworth, Orthogr. truncatus Lapworth, Corynoides calycularis (Nicholson)

Pleurograptus linearis Zone.

Black pyritic mudstones with several thin (20 mm) ash bands. Seven marker horizons are recognised. The lowest 0.25 m from the base, yields Leptogr. flaccidus (Hall), Orthogr. truncatus (Lapworth), Climacogr. minimus Elles and Wood, C. tubuliferus Elles and Wood and C. scalaris miserabilis Elles and Wood. The next 0.80 m from the base yields only Orthogr. quadrimucronatus (Hall) and the third, 1.40 m from the base Orthogr. truncatus (Lapworth) and Dicellogr. pumilus Lapworth. 1.80 m from the base Orthogr. truncatus

occurs together with abundant Climacogr. bicornis (Hall). The presence of Climacogr. caudatus Elles and Wood and C. styloideus Elles and Wood at 2.60 m from the base indicates the fifth horizon. The next, at 3.30 m, yields good samples of Pleurogr. linearis (Carruthers) and the final at 4.50 m from the base yields abundant specimens of Dicellogr. morrisoni Hopkinson.

Dicellograptus complanatus Zone.

9.1 m of highly weathered grey mudstones, massively bedded in the top 3.0 m but more shaley in the lower part. About 1.5 m from the base of the lowest exposed outcrop, a 35 mm thick band of black shale occurs. This band is badly cleaved and shattered and although the lithology and position correspond with that of the 'complanatus Band' at Dobb's Linn it must only remain a tentative suggestion that this horizon is indeed the 'complanatus Band' until the characteristic fossil assemblage is found.

3. CLANYARD BAY

The stratigraphic succession at the north end of Clanyard Bay [NX 101381] is summarised in Table A-1. Igneous dykes have affected the originally present graptolite remnants to such an extent that in most cases accurate zonation based on fossil assemblages is not possible. Nevertheless, several horizons have yielded sufficient graptolitic fragments to indicate the presence of the C. vesiculosus, M. cyphus, M. gregarius and R. maximus Zones.

1.6 m above the 9.18 m wide dyke, the following species

indicating the Cystogr. vesiculosus Zone have been found; Monogr. atavus Jones, Cystogr. vesiculosus (Nicholson) and Monogr. cyphus praematurus Toghill. The succeeding 7.4 m although yielding fossil fragments cannot be accurately located but the lithology resembles that of the Monogr. cyphus Zone at Dobb's Linn. The incoming of abundant nodular claystones above, heralds the Monogr. gregarius Zone. This is confirmed by the presence of the zone fossil in association with Monogr. sandersoni Lapworth, Monogr. revolutus Kurck and Monogr. triangulatus (Harkness).

To the north of the fault which bounds the upper part of the M. gregarius Zone, fossils have only been detected in the 2.3 m thick unit of grey-black shales and mudstones which is bounded on both sides by thin dykes. The presence of Rastrites maximus Carruthers, Monogr. regularis Törnquist and Monogr. circularis Elles and Wood indicates a horizon in the lower part of the Monogr. turriculatus Zone.

| Thickness (metres) | Lithology | Zone |
|-----------------------|--|-----------------------------|
| undefined | jointed greywacke | |
| 2.2 | dyke | |
| 2.3 | grey-black shale and mudstone | <u>R.maximus</u> (sub-zone) |
| 1.4 | dyke | |
| 3.0 | blue-black shale and mudstone | |
| <u>fault</u> ----- | | |
| 4.11 | black fossiliferous shale with nodular claystones | <u>M.gregarius</u> |
| 3.59 | sheared black mudstone | <u>M.cyphus</u> |
| <u>fault</u> ----- | | |
| 3.80 | black mudstone | <u>M.cyphus</u> |
| <u>fault</u> ----- | | |
| 0.7 | fossiliferous black mudstones | <u>C.vesiculosus</u> |
| <u>fault</u> ----- | | |
| 0.91 | sheared, qtz-veined black shale | |
| 9.18 | porphyrite dyke | |
| 6.5 | grey mudstone | <u>D.complanatus</u> |
| 5.8 | black blocky mudstone with thin claystones | <u>P.linearis</u> ? |
| 0.35 | hard, light grey mudstone | |
| <u>fault ?</u> | 1.72 beach debris | |
| 0.71 | black blocky mudstone | |
| 0.76 | black shale | |
| 13.73 | fissile platy grey shale and mudstone | |

TABLE A-1 Stratigraphic succession at the north end of Clanyard Bay.

A P P E N D I X B

ANALYTICAL METHODS

1. INTRODUCTION

The contents of this appendix are intended to amplify those experimental methods which have been named without description in the text. It is not intended to give a detailed appraisal of each method but merely to give a brief account of the procedures used.

2. INORGANIC CHEMISTRY

a) Analysis of major elements

Introduction

The method used to analyse for the major component elements of the rocks is an adaptation of a number of published techniques. The procedure is dependant upon contributions from the following:- Medlin et al., (1969), van Loon and Parissis (1969), Yule and Swanson (1969), Boar and Ingram (1970), Buckley and Cranston (1971) and Jeanroy (1972).

Reagents

Anhydrous lithium metaborate.

Lanthanum chloride solution (10% La w/v).

Nitric acid (4% v/v prepared by diluting 80 ml "Aristar" nitric acid to 2 litres).

Method

Approximately 0.5 g of -200 mesh rock powder was weighed accurately into a clean 25% gold/palladium alloy crucible of 30 ml capacity and roasted over a Meker burner for 10 minutes. This step was repeated until constant weight was obtained after cooling in a dessicator. Roasting of the powder was found to be necessary because

experience showed that fusion of samples containing carbonaceous material had an adverse effect on the life of the crucibles.

Approximately 0.1 g of the roasted powder was then weighed accurately into another similar crucible to which was added exactly 0.500 g of lithium metaborate flux. The sample and the flux were then thoroughly mixed using a P.T.F.E. coated wire to avoid scratching the crucible.

After fusing the mixture until a clear melt was obtained (approximately 10 minutes depending on the amount of iron present in the sample) the resulting bead was allowed to cool and then transferred into a clean 250 ml beaker containing 50 ml of 4% v/v nitric acid. The dissolution of the bead was aided by stirring with a magnetic stirrer for about 20 minutes. The solution was then transferred to a 100 ml volumetric flask, 10 ml of lanthanum chloride solution was added and the flask made up to volume with distilled water.

A blank was taken through the same procedure with the exception that lanthanum chloride was not added. This was not considered to be necessary because impurities in the lanthanum chloride were compensated by their presence in standard solutions.

The rock solutions were aspirated directly into an atomic absorption spectrophotometer and the elements Si, Ti, Al, Fe, Mn, Mg, Ca, Na and K analysed. Instrumental conditions for each element are given in Table B-1.

Calculation of results

The concentration of a particular element was calculated from the following:-

$$\mu\text{g/ml element oxide} = \frac{(x - y)(a + b)}{(h + l)}$$

$$\text{and \% element oxide} = \frac{\mu\text{g/ml element oxide} \times \text{dilution} \times 10^2}{\text{weight of sample in g} \times 10^6}$$

where x = sample absorption

y = blank absorption

h = absorption of high standard containing a $\mu\text{g/ml}$

l = absorption of low standard containing b $\mu\text{g/ml}$

dilution = total volume (ml) into which the sample is dissolved.

The final result is reported after correcting for loss on ignition due to roasting of the sample.

Reproducibility

Replicate analyses are presented for the standard rock BMS, which was supplied by the University of Southampton, in Table B-2. Elementary statistics for the variation about the mean value are given in Table B-3.

b) Analysis of sulphur

Introduction

The method used for the rapid determination of sulphur is dependent upon the measurement of the optical absorbance of a turbid solution containing precipitated sulphate ions (Schapiro 1973). Most sulphur bearing minerals yield to the treatment involved in the

preparation of the solution but it has been suggested that organic material is best decomposed by an oxidising fusion (Schapiro 1973). This was not found to be necessary in this work. Instead, a slightly more oxidising acid mixture was employed.

Reagents

Barium chloride (crushed crystals)

Calcium chloride (5% w/v solution in water)

Ammonia (50% v/v solution in water)

Concentrated nitric acid

Concentrated hydrochloric acid

Stock standard sulphur solution (1000 µg/ml) prepared by dissolving 5.4342 g of potassium sulphate in distilled water and diluting to 1 litre.

Stock standard sulphur solution (100 µg/ml) prepared by diluting above solution in water.

Method

Approximately 0.1 g of rock powder was weighed accurately in a watch glass and then transferred to a glass centrifuge tube. 0.2 ml of concentrated nitric acid followed by 0.6 ml of concentrated hydrochloric acid were then added to the powder. Double quantities of acid were added to powders containing sulphur in excess of 5%. The mixture in the tube was heated until boiling and then removed from the flame and cooled.

After cooling, 1.0 ml of the calcium chloride solution and 5 ml of water were added. The mixture was boiled for 30 secs and after cooling, 3 ml of the ammonia solution added. Insoluble

residues were then settled by centrifuging.

The supernatant liquid was decanted into a volumetric flask and the insoluble residue washed with distilled water. The washings were transferred to the volumetric flask and after diluting to volume, an estimate of the background turbidity was measured in comparison to a distilled water blank. An aliquot of the solution was placed in a 20 mm spectrometer cell and 0.03 ± 0.01 g of powdered barium chloride added. The optical density of the turbid solution was then measured at 651 nm after two minutes of gentle agitation.

Standard solutions

A series of standard solutions was prepared from the 100 µg/ml standard stock solution by pipetting 2.5, 5.0 and 10.0 ml of solution into three centrifuge tubes and precipitating the sulphate ion in the same manner as described above. The resultant supernatant liquids were made up to 50 ml to yield standard solutions containing 5, 10 and 20 µg/ml of sulphur respectively.

In order to equate matrices, another series of standards again with 5, 10 and 20 µg/ml of sulphur was prepared for use with samples of higher than 1% sulphur concentration. This series was prepared by pipetting 2.5, 5.0 and 10.0 ml of the 1000 µg/ml standard stock solution into three centrifuge tubes and precipitating the sulphate ion. In this case the resultant supernatant liquids were diluted to 500 ml.

Calculation of results

Both sets of standards yielded straight lines which pass through the origin. The weight per unit volume of sulphur in a

sample is calculated from :-

$$\mu\text{g/ml sulphur} = \frac{\text{Abs. sample } (\mu\text{g/ml Std 1} + \mu\text{g/ml Std 2})}{\text{Abs. Std 1} + \text{Abs. Std 2}}$$

where Abs. is the absorbance

and Std is the standard solution

The percentage sulphur in a sample is then calculated from :-

$$\%S = \frac{\mu\text{g/ml sulphur in sample} \times \text{dilution} \times 10^2}{\text{weight sample in g} \times 10^6}$$

where dilution is the total volume in which the original sample is dissolved.

Reproducibility

Replicate analyses and elementary statistics for the variation in the amount of sulphur found in the standard rock BMS (University of Southampton) are presented in Tables B-2 and B-3 respectively.

c) Analysis of trace elements

Introduction

The trace elements Cu, Pb, Zn, Rb, Sr, Y and Zr were analysed by X-ray fluorescence (XRF). The principles of this technique are given in detail by Jenkins and De Vries (1967), Norrish and Chappel (1967) and Bertin (1970). Briefly, the principle of analysis by XRF is that the element to be analysed is excited by a source of energy (the X-ray tube) and in response gives off a characteristic radiation. The amount of radiation given off is normally in proportion to the concentration of the element in a sample. In all cases, some of the

emitted radiation is absorbed within the sample. This is compensated for by use of mass absorption coefficients.

Wavelengths of the radiation to be measured are selected so that the analyte line and adjacent backgrounds are not interfered with by other elements or the X-ray tube. Comments pertaining to the choice of spectral lines for the elements under consideration are given in Table B-4.

Method

Analysis of the Moffat Shale samples was conducted on borax discs containing approximately 2.7 g of -200 mesh rock powder. The equipment used was manually operated, and incorporated a Philips standard generator (PW 1540), a tungsten tube (PW 2144) and a scintillation detector probe (PW 1964). The analysing crystal was LiF-220.

The emitted radiation was measured by counting for 100 secs over peaks and backgrounds at a current of 18 mA at 36 kV. Instrumental conditions are given for each element in Table B-5. The standard black marine shale, BMS (University of Southampton), was used as the standard. Details of the mineralogy and chemistry of this secondary standard are given in Table B-6.

Calculation of results

The standard equation for the calculation of the concentration of an element in a sample (x) is :-

$$\text{Conc. (x)} = \text{Conc. (std.)} \times \frac{\text{count rate (x)} \times \text{TMAC (x)}}{\text{count rate (std)} \text{ TMAC (std)}}$$

where std. is the standard and TMAC is the total mass absorption coefficient. This latter parameter is calculated as the sum of the products of the weight per cent of each major element multiplied by the absorption coefficient for the absorption by that major element of the characteristic radiation of the trace element under analysis. Mass absorption coefficients are found in tables of emitted radiation wavelength versus absorbing major elements (eg. in Jenkins and De Vries 1967).

If a major element analysis is not available then TMAC of a sample can be estimated in one of three ways:-

- 1) By graphing TMAC of analysed rocks against percentage of the heaviest absorber. TMAC of unanalysed rocks may then be estimated from an estimate of the amount of the heaviest absorber present.
- 2) By assuming that the ratio of the background counts for the sample and the standard is equal to the ratio of the TMAC of the standard to the TMAC of the sample.
- 3) By plotting TMAC of analysed rocks against the ratio of the background counts in the sample to the background counts in the standard.

In this study the third method has been used to estimate TMAC of unanalysed rocks.

Precision of accuracy

The equipment used in this study gives very precise results, the absolute precision of which is only limited by the convenience of reasonably short counting times. Counting times of

100 secs per angular position gives counts which are within 3 per cent of the mean, and final results which are always within 5 per cent of the mean and usually within 3 per cent. Consequently, elements such as Rb, Sr and Zn, which are free from interference, give good calibration curves and yield results for International Standards which are in agreement with the results of other laboratories.

Precision depends only on the reliability of the equipment but accuracy is controlled by the use to which the raw data is put. In the context of analysis by XRF, inaccuracy is introduced in the estimation of TMAC and in the choice of a value for the concentration of a particular element in the standard. For calibration purposes the use of 'average' values is not recommended but the use of one particular laboratory's results for a set of rocks is usually satisfactory. With this in mind, calibrations were usually established from a series of standards supplied and analysed by the University of Southampton.

Replicate estimates of TMAC derived using the third method cited above are given in Table B-7. The computed elementary statistics for the variation in TMAC about the mean value are given in Table B-8. Replicate analyses for the amount of Cu, Pb, Zn, Rb, Sr, Y and Zr in the standard rock BMS are given in Table B-9. Elementary statistics for the results are given in Table B-10.

5. ORGANIC CHEMISTRY

a) Desalting of amino acid hydrolyzates

Introduction

The method used for the extraction of amino acids from sediments involves hydrolysis in 6M HCl followed by evaporation of the solution to dryness. After evaporation, there are usually large quantities of inorganic salts associated with the organic extract. These salts are unwanted and the method used in their removal can bring about the introduction of contaminants into the extract. The desalting technique employed in this work uses acid hydrolysis followed by precipitation of most cations as fluorides (Pollock and Miyamoto 1971). Ferric iron was removed by adjustment of the pH of the filtrate to between 8 and 8.5 and sodium chloride was removed by saturating the solution with HCl gas. Trace quantities of salt were finally removed on a strong cation exchange column.

Reagents

Hydrofluoric acid

Sodium hydroxide solutions (0.5N, 2N, 4N)

Hydrogen chloride gas

Water saturated with HCl gas

Ion exchange resin (AG 50 W x 8H⁺, 100 mesh)

Ammonium hydroxide solution (2N)

Method

The desalting method is represented schematically in Table B-11. After hydrolysis and cooling, the hydrolyzate was filtered

through Whatman GF/A paper and the insoluble residue washed with deionised and distilled water. HCl was then removed by evaporation and the mixture dissolved in water and diluted to a known volume. The amount of HF necessary for precipitation of the salts was calculated by titrating a small aliquot of the hydrolyzate to pH 8 with 0.5N NaOH. Twice the calculated ml-equivalent of HF was added to the ice-cold sample and the solution stirred continuously for 5 mins. The cations Na^+ , K^+ , Ca^{2+} , Mg^{2+} and Al^{3+} were precipitated and the slurry filtered through a special 10 μ millipore 'Teflon' filter disc. The ml-equivalent of 4N NaOH was added and the pH re-adjusted to 8 over a period of about 90 mins in order to precipitate iron. The suspension was filtered through a fine porosity sintered glass funnel and washed with a little water. The filtrate was adjusted to pH 1 and concentrated on a rotary evaporator until salt crystals began to form. The flask was removed from the evaporator and when ice-cold, the solution was saturated with HCl gas. After saturation, the salt crystals were filtered off and washed with a small amount of water saturated with HCl gas. The pH of the sample was then adjusted to between 4.5 and 6 and placed on an ion-exchange column filled with 25 ml of AG 50 W x 8H⁺ resin. Residual salt was removed and neutral species and anions were washed off the column with water. The desalted amino acids were finally removed from the column by elution with 100 ml of 2N NH_4OH .

b) Test for the presence of amino acids

Introduction

After desalting a hydrolyzate, the presence of amino acids

may be checked by means of a ninhydrin test. This involves treating a solution of the hydrolyzate with a few drops of ninhydrin (Triketohydrindene hydrate) in the presence of an acetate buffer.

Reagents

Ninhydrin (8.88% w/v in 2-methoxy-ethanol)

Citrate buffer (pH 5 containing 0.16% w/v stannous chloride).

The buffer was prepared from a 1:2 volume ratio of 0.1M citric acid and 0.1M sodium citrate solutions. 0.16 g stannous chloride was then added per 100 ml of solution.

Method

Immediately prior to the test, equal volumes of buffer and ninhydrin solution were mixed. 1 ml of the hydrolyzate solution was mixed with 1 ml of the ninhydrin-buffer solution and heated at 100°C for 5 minutes. A blue colouration indicates the presence of amino acids.

c) Separation of amino acids by gas-liquid chromatography

Introduction

A gas-liquid chromatographic (GLC) technique based on that of Moss et al., (1971) was adopted for the analysis of amino acids. Separation of individual acids was achieved with the N-heptafluorobutyl n-propyl derivatives using a siloxane column (OV-1) as the liquid phase. It is necessary to derivitize amino acids because the polar nature of these compounds prohibits their direct analysis by GLC. Extensive studies have been made to develop methods

for preparing suitable derivatives and to develop GLC column materials for their separation eg. Gehrke et al., (1965) Gehrke et al., (1966), Gehrke and Stalling (1967), Darbre and Islam (1968), Zumwalt et al., (1970), Zumwalt et al., (1971a, 1971b) and Gehrke and Leimer (1971).

The method of Moss et al., (1971) was chosen for use in this work for three reasons. Firstly, the derivative was relatively easily prepared, secondly, separation of the derivatives was achieved on a single column and thirdly, OV-1 was a suitable phase, this being the column packing used in the analysis of hydrocarbons.

Reagents

Standard amino acid solution

Hydrochloric acid (0.1M)

Dry nitrogen

HCl gas

Propanol

Heptafluorobutyric anhydride

Ethyl acetate

Preparation of the derivative

A standard series of 19 protein amino acids (supplied by Shandon Ltd.) was dissolved in 0.1M HCl to a concentration of 10 μ moles/litre. The amino acid mixture was then dried under a vigorous stream of dry nitrogen. 0.4 ml of propanol-HCl was then run into the reaction vial which was heated at 100°C for 10 mins. The vial contents were then evaporated to dryness and the propylation step repeated. The N-heptafluorobutyl n-propyl esters of the amino acids were prepared by adding 0.2 ml heptafluorobutyric anhydride and 0.1 ml ethyl acetate

to the mixture of propyl esters. The reaction vial was sealed and heated in an oil bath at 150°C for 10 mins. The derivative was then dried at 80°C under a steady stream of nitrogen.

Chromatographic conditions and results

After preparation of the derivative, the contents of the vial were dissolved in 0.1 ml ethyl acetate and 2 µl of standard solution with 2 µl of acetic anhydride was injected onto a 10' x 1/16" glass column containing 3% OV-1 on 100-120 mesh Varaport-30. The injection port temperature of the Varian 1400 chromatograph was 230°C and the detector temperature was 290°C. The column was maintained at 70°C for 15 mins after injection of the sample and then temperature-programmed to 260°C at 4°C/min. Nitrogen was used as the carrier gas at a flow rate of approximately 35 ml/min.

A typical chromatogram illustrating the separation of the amino acid derivatives is given in Fig.194. It may be noted that methionine is not resolved from aspartic acid and that there is poor resolution between leucine and isoleucine. The resolution between isoleucine and leucine can be improved by judicious temperature control but always at the expense of the alanine-glycine resolution.

d) Separation of amino acid enantiomers by gas-liquid chromatography

Introduction

With the knowledge that the presence of recent biological contamination can be detected in amino acid extracts from the enantiomeric distribution of the constituent amino acids (Rast et al., 1972), a GLC technique was developed to separate individual isomers.

This has previously been performed by using optically active stationary phases. The compound N-TFA (trifluoroacetyl) - L - valyl - L - valine cyclohexyl ester has been shown to be of use for the separation of the enantiomers of a wide variety of amino acid derivatives. (Nakaparksin et al., 1970). This phase however is limited by its low thermal stability. In order to overcome this limitation, the N - TFA - L - phenylalanine - L - leucine cyclohexyl ester was developed as a stationary phase (Koenig et al., 1970).

One major disadvantage in using optically active stationary phases to resolve amino acid enantiomers is that capillary columns must be used to achieve satisfactory resolution. The coating of capillary columns is a highly specialized technique which requires much practice before consistently good results are obtained. In order to alleviate this difficulty, an optically active derivative capable of separation on a column packed with the common siloxane phase OV-1 was sought. The derivative chosen was the L - menthol N - TFA (trifluoro-acetyl) ester of the amino acids.

Reagents

Methanol

HCl gas

Dry nitrogen

L - menthol crystals

Petroleum ether (BP 40-60°C)

Dichloromethane

Trifluoroacetic anhydride.

Preparation of the optically active derivative

The method which follows is that of G. Dungworth (pers. comm). A racemic mixture containing a total of 5 mg of amino acids was dissolved in a methanol-anhydrous HCl gas mixture. The 'Pyrex' tube containing the amino acid mixture was then sealed with a teflon lined screw cap and heated for 2 hours at 50°C. The solvent was then removed under a stream of dry nitrogen and 500 mg of L - menthol crystals added to the tube. Anhydrous HCl gas was blown onto the surface of the crystals until a syrupy liquid formed. This liquid was heated for 2 hours at 50°C. At the end of this period 5 ml of methanol in the presence of HCl gas was passed into the tube until complete dissolution was evident.

The solution was left overnight and then transferred to a sublimation flask before removal of the solvent under a stream of nitrogen. Excess menthol was then removed by vacuum sublimation at 100°C and at a pressure of approximately 10^{-1} mm Hg. This was repeated until no frosting of the cold finger occurred. The residue was finally washed with 2 x 5 ml portions of petroleum ether to remove traces of menthol.

After evaporation of the petroleum ether, 1 ml of dichloromethane and 0.5 ml of trifluoro- acetic anhydride was added and the solution left standing at room temperature for 30 mins. The solvent was evaporated off and the derivative was ready for analysis by gas-liquid chromatography.

Chromatographic conditions and results

The optically active derivative was dissolved in a small quantity of dichloromethane (50 μ l), and 1 μ l of the solution injected onto a 10' x 1/8" glass column containing 3% OV-1 on 100-120 mesh Varaport-30. The injection port temperature of the Varian 1400 chromatograph was 210°C and the detector temperature was 260°C. The column was maintained at 140°C for 5 mins after injection of the sample and then temperature programmed to 260°C at 4°/min. Nitrogen was used as the carrier gas at a flow rate of approximately 40ml/min.

A typical chromatogram is illustrated in Fig.195. It may be observed that although great care was taken to remove any excess menthol, there is still evidence of its incomplete removal. Peaks have been assigned to amino acids and their enantiomers after coinjection with derivatives prepared from simple two-component mixtures. The method, at this stage in its development, only satisfactorily separates the enantiomers of valine, threonine, leucine and phenylalanine. This is however sufficient to indicate the presence of recent biological contamination in amino acid extracts from ancient sediments.

e) Removal of sulphur from organic extracts

Introduction

Extraction of the Moffat Shale samples with organic solvent resulted in the release of large quantities of sulphur into solution. This was separated from the organic extract by treatment with freshly precipitated copper.

Reagents

Zinc granules

Copper sulphate

Acetone

Dichloromethane

Method

Before each separation, copper was freshly precipitated by adding 15 g of zinc granules to a solution containing 25 g of copper sulphate in 500 ml of water. Agitation released the copper which was decanted into a glass tube and washed repeatedly with distilled water, acetone and dichloromethane. A solution of the organic extract in dichloromethane was passed through the column to remove the sulphur.

f) Isolation of kerogen

Introduction

Most sedimentary rocks contain some organic matter. This can be divided into two general groups; the soluble organic matter i.e. that which can be extracted from sediments by organic solvents and in general accounts for 5-15% of the total (Hunt and Jamieson 1956), and the insoluble material left after extraction, known as kerogen. In this study, kerogen is formally defined as the bitumen-free biotic remains disseminated in a rock.

Various physical methods have been used for the separation of kerogen (Quass 1939 and Hubbard et al., 1952), but the most common method is acid digestion using hydrochloric acid or hydrofluoric acid, or combinations of these acids (Smith 1961, Saxby 1970). The

advantages of the chemical method are threefold:-

- 1) Most minerals, except pyrite and zircon, are readily removed.
- 2) There is little opportunity for fractionation of the organic material.
- 3) The method is reasonably fast.

The one main disadvantage of the chemical method is the possible alteration of the kerogen by the action of strong mineral acids.

Reagents

Methanol

Hydrochloric acid (1:9 v/v solution in water)

Hydrochloric acid (1:1 v/v solution in water)

Hydrofluoric/hydrochloric acid mixture (1:1 v/v)

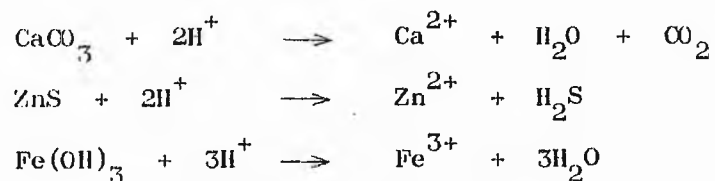
Boric acid solution.

Method

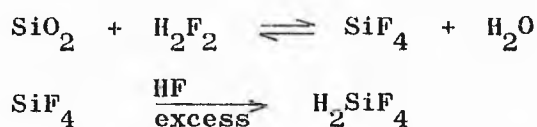
The method used in this study is essentially that of Saxby (1970). Approximately 60 g of rock powder previously extracted with solvent was suspended in the minimum quantity of methanol (ca. 25 ml) in a polypropylene beaker. The purpose of the alcohol treatment is to wet the sample so that good contact between acid and rock is achieved.

Mineral carbonates, sulphides, basic oxides and hydroxides were removed by treating the powder with 100 ml of a 1:9 mixture of concentrated hydrochloric acid and water at room temperature for 15 mins. This was followed by treatment with 150 ml of a 1:1 mixture of hydrochloric acid and water at room temperature for two hours. The

chemical reactions may be represented by the following :-



The suspension was then filtered and washed with hot (75°C) deionised water and the residue treated with 150 ml of a 1:1 mixture of concentrated hydrochloric acid (37%) and hydrofluoric acid (48%). The mixture was then evaporated to dampness at 100°C to volatilise the reaction products of the silicates. The HF/HCl treatment was repeated five times and is represented by the following formulae:-



It was at this stage that the insoluble fluorides may have formed eg. CaF_2 ; $\text{MgAlF}_5 \cdot \text{H}_2\text{O}$; $\text{NaAlF}_4 \cdot x \text{H}_2\text{O}$ and $\text{Fe}^{2+} [\text{AlFe}^{3+}]_5 \text{F}_5 \cdot x \text{H}_2\text{O}$. Excess hydrofluoric acid was neutralised with saturated boric acid solution.

The residue was then filtered, suspended in hot (75°C) water and repeatedly washed with deionised water to remove chloride ions. The isolate was then dried slowly at 80°C.

No attempt was made in this study to separate pyrite from the kerogen because as yet, no general method has been developed which can separate pyrite without chemically altering the kerogen.

1. REFLECTIVITY

a) The microreflectivity equipment

Introduction

In recent years there has been gradual development of sensitive reflectivity-measuring equipment for use in the fields of ore mineralogy and coal petrology. Of the many systems devised, the most successful and the one very widely used in applied coal petrology is a system in which a photomultiplier is fitted to an incident light microscope and connected to either a sensitive galvanometer or to a fast response pen-recorder sometimes with auxiliary amplification after the detector.

Description of apparatus

Fig. 196 is a schematic diagram indicating the important elements that comprise the equipment used in this study. This is based on the Leitz MPV microscope photometer connected to a Philips model PM 8220 pen-recorder. The microscope (Fig.197) is better understood by reference to a diagram of the light beam path for incident light (Fig.198). Light from the 6 volt 15 watt tungsten lamp passes through an aperture diaphragm and a field diaphragm to enter the vertical illuminator which consists of two components; the Berek prism and a plane glass reflector. The light is deflected through 90° by one of these components and passes through the objective before hitting the sample. That portion of the light which is reflected from the specimen returns back through the objective and enters the body tube of the microscope where it is deflected into the

binocular eyepiece by means of a prism. When a reflectivity measurement is made this prism is removed from the optical train, allowing the light to pass upwards through an auxiliary magnifying system and photometer viewing arrangement to the measuring diaphragm. This diaphragm is of the four-leaf type and allows the field of measurement to be varied. After passing through the diaphragm the light traverses a replaceable Schott interference filter before striking the cathode of the photo-multiplier tube. The photo-multiplier is activated by a H.T. supply provided by a Rank-Cintel high stability power-pack. The output from the photo-multiplier is fed through a D.C. amplifier and thence to the pen-recorder which is of variable speed and attenuation.

The illumination system

The tungsten lamp required very little attention during operation, but occasionally a strongly erratic signal would appear on the pen-recorder chart which could in most cases be traced to a faulty contact between the terminals of the lamp and those of its socket. This fault was caused by oxidation from the heat generated by the lamp and was rectified by cleansing the terminals with fine emery-paper. Rarer cases of instability occurred when the lamp reached the last stages of life. Vibrations of the filament were responsible.

The vertical illuminator

As previously stated two alternative types of reflector are incorporated in the microscope to provide vertical illumination.

- 1) A plane-glass reflector in the form of a coated coverslip. With this device in use the polar is adjusted so that the light incident on the coverslip is horizontally polarised. This arrangement ensures that the light is plane-polarised after reflection through 90° .
- 2) A Berek prism reflector. In this case the polariser is set so that the light incident on the prism is plane-polarised at 45° to the horizontal. This arrangement, besides retaining plane-polarised light after the 90° reflection, also reduces the error in the reflectivity due to the measurable angle of incidence by the objective.

The light path for each of the two reflectors is illustrated in Fig.199.

In this study the coverslip was used when measuring the reflectance of graptolite fragments in air because this device gives a much sharper image which results in easier focusing. It was more practical however to use the Berek prism when measuring in oil because at low reflectance levels there is considerable loss of light when using the coverslip.

Interference filters

Optical measurements on the samples were carried out at seven wavelengths in the visible part of the spectrum viz. 410, 442, 502, 546, 590, 651 and 710 nm. Approximately monochromatic light of each of these wavelengths was produced by using a series of Schott single line filters.

The photomultiplier tube and its spectral response

Most photomultipliers are unsuitable for use with a tungsten lamp because they have a maximum response between 400 and 500 nm with a total cut-off at 600 nm. This is the region in which the spectral response of the lamp is low although it does increase appreciably with increasing wavelength (Fig.200). In the Leitz system this difficulty is overcome by using an EMI 9592B photomultiplier. This is a high gain, small-diameter photo-multiplier with 11 dynodes, maximum sensitivity at 400 nm and with cut-offs at 200 nm in the ultra-violet and at 800 nm in the infra-red. The general spectral response of the photo-multiplier as described by the manufacturer is illustrated in Fig.201.

Spectral response of the apparatus

To assess the overall response of the apparatus at each of the seven wavelengths, a diamond standard was placed on the microscope stage and the 502 nm filter placed in position. This filter was found to result in maximum response for a given signal with fixed optical conditions and amplification. The recorder deflection and back reflection were then noted. Each of the interference filters was then placed in turn in the filter slot and the corresponding signals and back reflections recorded while keeping the experimental conditions constant. The relative signal strengths at each wavelength were then calculated as a percentage of the signal at 502 nm after correction for the dispersion of the diamond standard (Fig.202).

b) Reflectivity standards

The primary standards used in this work for the measurement of reflectivity were optical glass, diamond and silicon carbide. These exhibit values in oil at 546 nm of the order of 1.4, 5.3 and 7.5 per cent respectively.

The optical glass standard was only occasionally used as most graptolite samples examined displayed reflectance values in excess of 3 per cent in oil at 546 nm. Glass standards are specially manufactured and contain rare-earth metal oxides to give them a higher reflectivity than common soda glass. A general disadvantage of such standards which is directly related to their particular chemical formulation is a tendency for the polished surfaces to tarnish rapidly when exposed to moist air.

The diamond standard was the most frequently used in the measurement of the graptolite fragments. This is mounted in the form of a small, 4° wedge in the centre of a clear 'Bakelite' disc, which is 20 mm in diameter and 10 mm deep. The polished surface of the diamond measures 3 x 4 mm. The wedge form is essential in order to restrict the amount of light re-entering the microscope lens to that from either the diamond/oil or the diamond/air interface.

Diamond as a reflectivity standard has certain advantages over almost all other standard materials. It is extremely hard and very poorly chemically reactive hence it has surface properties which cannot be matched by any other mineral. In addition, because diamond belongs to the cubic crystallographic system, any section through the crystal is isotropic and therefore alignment of the standard is not critical. Another important attribute of diamond as

a standard is that because of its chemical and crystallographic form there is little freedom in the crystal matrix for atomic substitution. This is in contrast to many other crystalline compounds which can exhibit molecular interchange between similar sized molecules to form a solid solution series.

The third standard used in this work was a mounted basal section of synthetic silicon carbide. This is a crystalline compound which is physically hard and shows very little chemical reactivity. Unfortunately, unlike the diamond and the optical glass, silicon carbide is opaque and as such its reflectivity is only known by reference to that of other standards.

It is obvious from the foregoing that there is a large gap in the reflectance values of the standards between the glass (1.4%) and the diamond (5.3%). It has been suggested (Melvin 1973) that this might be overcome by introducing a single high stability primary standard of high reflectivity, for example diamond, and by using a series of neutral density filters the apparent reflectivity of the standard could be reduced to any value between 0 and 5 per cent in oil. Although appealing, this idea is yet to be accepted.

It is essential that if consideration is to be given to spectral variations in reflectance values of samples, the exact manner in which the reflectance of the standard varies with wavelength must be computed. This is achieved by utilising the Fresnel equation, the general form of which is :-

$$R = \frac{(n - n_0)^2}{(n + n_0)^2}$$

where R is the reflectivity at normal incidence, n is the refractive

index of the material and n_o is the refractive index of the medium in which the material is situated.

In this work, the standard was either measured in air or in Zeiss immersion oil. The variation of refractive index with wavelength for the diamond was obtained from Dana's Mineralogy while that of the oil was supplied by the manufacturer. Tables B-12 and B-13 and Figs. 203 and 204 illustrate the spectral variation for the diamond and for the oil. The spectral variation of oil and air reflectivities is given in Table B-14 and illustrated in Figs. 205 and 206.

c) Sample preparation

Mounting

The field-collected sample was cut on a diamond saw to obtain a block of suitable size for mounting. This was normally of the order of a 10-mm cube but at times due to the friable nature of some samples the block was much smaller. The block was placed in a plastic mould which was then filled with resin. In this study 'Metset' resin type SW was normally used. This has a relatively slow setting time of between 10 and 15 hours but has the advantage of a low exotherm temperature of 40°C. For speedier preparation of moulds, the 'Metset' resin type FT was occasionally used. This hardens in 15 minutes but has a maximum exotherm of 130°C.

After hardening, the cylindrical cast measuring 30 mm in diameter by 20 mm deep was gently removed from the mould and the name of the sample inscribed with a 'Vibrotool'.

Polishing

Prior to the main polishing process the sample mould was ground flat on a revolving diamond lap and all but the finest scratches removed by grinding on successively finer grades of corundum paper, backed with thick plate-glass and flushed continuously with running water.

The main polishing process was performed on a series of 'Selvyt' covered brass laps using graded alumina powders. Three grades were used; 5/20, 3/50 and gamma. The technique employed was to hold the sample firmly onto the outer edge of the slowly revolving lap. Small additions of alumina and water were made at intervals to maintain the polishing fluid as a thin creamy liquid. The routine established for polishing graptolite fragments was to rotate the sample for 300 turns on a revolving 5/20 alumina lap, 200 turns on a revolving 3/50 alumina lap and 100 turns on a stationary gamma alumina lap.

After completion of the gamma stage the sample was washed with weak soap solution and flushed with a jet of water before placing in an ultrasonic tank for 2 minutes to remove any remaining polishing powder from the crevices. The sample was then dried by pressing it lightly against a folded piece of tissue and stored in a dust free box prior to measurement.

Mounting the sample onto the microscope stage

The polished samples were mounted onto a plasticine pad resting on a glass microscope slide by means of a press. To ensure that the mount was level, two mutually perpendicular traverses were

made over the surface of the specimen. If adjustment of the microscope focus was necessary during the traverse, the position of the mount was altered and checked again.

| Element | Lamp current mA | Wave-length nm | Slit width μ | Flame | Burner alignment | Burner depth mm | Limit of Detection $\mu\text{g/ml}$ |
|-----------|--------------------|-------------------|---------------------|---|---------------------|--------------------|--|
| Aluminium | 10 | 309.3 | 100 | $\text{N}_2\text{O}/\text{C}_2\text{H}_2$ | Inclined 20° | 2 | 0.5 |
| Calcium | 4 | 422.7 | 100 | $\text{N}_2\text{O}/\text{C}_2\text{H}_2$ | \perp | 2 | 0.05 |
| Iron | 5 | 371.9 | 50 | $\text{Air}/\text{C}_2\text{H}_2$ | // | 2 | 0.4 |
| Magnesium | 4 | 285.2 | 100 | $\text{N}_2\text{O}/\text{C}_2\text{H}_2$ | \perp | 2 | 0.025 |
| Manganese | 5 | 279.5 | 50 | $\text{Air}/\text{C}_2\text{H}_2$ | // | 2 | 0.02 |
| Potassium | 5 | 766.5 | 300 | $\text{Air}/\text{C}_2\text{H}_2$ | \perp | 2 | 0.1 |
| Silicon | 15 | 251.6 | 50 | $\text{N}_2\text{O}/\text{C}_2\text{H}_2$ | Inclined 20° | 2 | 2.0 |
| Sodium | 5 | 589.6 | 50 | $\text{Air}/\text{C}_2\text{H}_2$ | \perp | 2 | 0.1 |
| Titanium | 8 | 364.9 | 50 | $\text{N}_2\text{O}/\text{C}_2\text{H}_2$ | // | 2 | 0.5 |

TABLE B-1 Instrumental conditions for the analysis of major elements by atomic absorption spectroscopy.

| SiO ₂ | TiO ₂ | Al ₂ O ₃ | Fe ₂ O ₃ | MnO | MgO | CaO | Na ₂ O | K ₂ O | LOI | S |
|------------------|------------------|--------------------------------|--------------------------------|--------|--------|--------|-------------------|------------------|-------|--------|
| 43.8 | 0.58 | 14.78 | 10.22 | 0.09 | 2.56 | 6.00 | 0.55 | 2.49 | 19.92 | 4.54 |
| 44.0 | 0.51 | 14.34 | 10.10 | 0.09 | 2.60 | 5.98 | 0.54 | 2.47 | 20.34 | 4.94 |
| 43.5 | 0.59 | 15.00 | 10.01 | 0.10 | 2.61 | 6.16 | 0.54 | 2.53 | 19.94 | 4.71 |
| 44.2 | 0.58 | 14.67 | 10.02 | 0.09 | 2.63 | 6.04 | 0.55 | 2.49 | 19.66 | 4.54 |
| 43.2 | 0.59 | 15.34 | 10.21 | 0.09 | 2.69 | 6.09 | 0.57 | 2.52 | 19.68 | 4.49 |
| (46.5) | (0.50) | (15.20) | (10.10) | (0.10) | (2.10) | (6.20) | (0.40) | (2.70) | - | (3.65) |

TABLE B-2 Replicate analyses of major elements in standard rock BMS.

(Values in per cent. Values in brackets are those quoted in report No. 1, Geochemistry Laboratory, University of Southampton, 1971).

| Variable | Mean | Std. Dev. | Maximum | Minimum | Range |
|--------------------------------|-------|-----------|---------|---------|-------|
| SiO ₂ | 43.74 | 0.40 | 44.20 | 43.20 | 1.00 |
| TiO ₂ | 0.57 | 0.05 | 0.59 | 0.51 | 0.08 |
| Al ₂ O ₃ | 14.82 | 0.58 | 15.34 | 14.34 | 1.00 |
| Fe ₂ O ₃ | 10.11 | 0.10 | 10.22 | 10.01 | 0.21 |
| MnO | 0.09 | 0.00 | 0.10 | 0.09 | 0.01 |
| MgO | 2.62 | 0.05 | 2.69 | 2.56 | 0.13 |
| CaO | 6.05 | 0.07 | 6.16 | 5.98 | 0.18 |
| Na ₂ O | 0.55 | 0.01 | 0.57 | 0.54 | 0.03 |
| K ₂ O | 2.50 | 0.02 | 2.53 | 2.47 | 0.06 |
| LOI | 19.91 | 0.27 | 20.34 | 19.66 | 0.68 |
| S | 4.64 | 0.24 | 4.94 | 4.49 | 0.45 |

TABLE B-3 Elementary statistics for replicate analyses of major elements in standard rock BMS.

(Values in per cent).

| Element | Line | Remarks |
|-----------|-----------------|---|
| Rubidium | Ka | Very precise and accurate |
| Strontium | Ka | " " " " |
| Yttrium | Ka | Interference from RbKb |
| " | Kb1 | Not useful because levels are usually too low |
| Zirconium | Ka | Interference from SrKb |
| " | Kb1 | Useful since Zr usually occurs in fairly high levels |
| Niobium | Ka | Background may be interfered with by a small Thorium peak |
| Lead | Lb ₁ | Good calibration but low sensitivity due to heavy element and small peak. Some difficulty obtaining good standard |
| Copper | Ka | Good sensitivity and response but small impurity in the Tungsten tube makes analysis consistently inaccurate. An attempt is made in Program ZGXRF5 to remove the influence of the impurity. |
| Zinc | Ka | Precise and accurate |
| Nickel | Ka | High absorption by Iron makes accurate determination difficult |
| Cobalt | Ka | SEVERE interference by FeKb makes determination of cobalt no more than qualitative |

TABLE B-4 Comments pertaining to the choice of analytical lines in the analysis of trace elements by X-ray fluorescence.

| Element | Position of peak (two-theta) | Backgrounds (two-theta) | Lower limit | Window | EHT |
|---------|---------------------------------|----------------------------|-------------|--------|-----|
| Cu | 45.00 | 44.70 \approx 45.50 | 139 | 442 | 150 |
| Pb | 41.76 | 41.00 \approx 42.20 | 215 | 330 | 145 |
| Zn | 28.20 | 27.70 \approx 28.75 | 214 | 213 | 150 |
| Rb | 26.55 | 25.80 \approx 27.20 | 240 | 320 | 155 |
| Sr | 25.10 | 24.40 \approx 25.80 | 242 | 316 | 155 |
| Y | 23.79 | 23.25 \approx 24.40 | 245 | 250 | 150 |
| Zr | 22.50 | 22.00 \approx 23.25 | 241 | 238 | 145 |

TABLE B-5 Instrumental conditions for the analysis of trace elements by X-ray fluorescence.

GEOCHEMISTRY LABORATORY - STANDARD ROCK BMS

BMS - Black Marine Shale, Samlesbury, Lancs.

Minerals include - illite, kaolinite, calcite, dolomite, quartz, felspar and some carbonaceous material.

Chemical analysis (provisional)

| | % | | ppm | | ppm |
|--------------------------------|------|----|-------|----|------|
| SiO ₂ | 46.5 | P | 740 | Y | 40 |
| TiO ₂ | 0.5 | S | 36500 | Zr | 87 |
| Al ₂ O ₃ | 15.2 | Cl | 160 | Nb | 12 |
| Fe ₂ O ₃ | 10.0 | V | 170 | Mo | 74 |
| MgO | 2.1 | Mn | 830 | Sn | 7 |
| CaO | 6.2 | Ni | 130 | I | n.d. |
| Na ₂ O | 0.4 | Cu | 190 | Ba | 400 |
| K ₂ O | 2.7 | Zn | 120 | La | 36 |
| H ₂ O | 6.4 | Ga | 19 | Ce | 75 |
| CO ₂ | 6.1 | As | 64 | Nd | 29 |
| C | 3.7 | Br | n.d. | Pb | 22 |
| less O | 1.4 | Rb | 120 | Th | 7 |
| for S | | Sr | 190 | U | 13 |

n.d. = not detected

All analyses by X-ray Spectrometry on rock-powder pellets (except H₂O, CO₂ and C).

TABLE B-6 Mineralogy and chemistry of the standard rock BMS.

(University of Southampton, 1971).

| Cu | Pb | Zn | Rb | Sr | Y | Zr |
|---------|---------|---------|---------|---------|--------|--------|
| 55.12 | 31.30 | 45.32 | 13.15 | 11.52 | 9.60 | 8.78 |
| 54.18 | 31.28 | 45.37 | 13.36 | 11.50 | 9.63 | 8.75 |
| 54.97 | 31.07 | 44.89 | 13.13 | 11.43 | 9.62 | 8.76 |
| 54.60 | 31.62 | 45.08 | 13.26 | 11.52 | 9.59 | 8.81 |
| 54.83 | 31.09 | 45.02 | 13.26 | 11.58 | 9.63 | 8.80 |
| (55.27) | (31.32) | (45.45) | (13.23) | (11.57) | (9.56) | (8.75) |

TABLE B-7 Replicate estimates of mass absorption coefficients for standard rock BMS.

(Values in brackets are those derived from analytical data quoted in Report No.1, Geochemistry Laboratory, University of Southampton, 1971).

| Variable | Mean | Std.Dev. | Maximum | Minimum | Range |
|----------|-------|----------|---------|---------|-------|
| Cu | 54.74 | 0.37 | 55.12 | 54.18 | 0.94 |
| Pb | 31.27 | 0.22 | 31.62 | 31.07 | 0.55 |
| Zn | 45.14 | 0.20 | 45.37 | 44.89 | 0.48 |
| Rb | 13.23 | 0.09 | 13.36 | 13.13 | 0.23 |
| Sr | 11.51 | 0.05 | 11.58 | 11.43 | 0.15 |
| Y | 9.61 | 0.02 | 9.63 | 9.59 | 0.04 |
| Zr | 8.78 | 0.03 | 8.81 | 8.75 | 0.06 |

TABLE B-8 Elementary statistics for replicate estimates of mass absorption coefficients in standard rock BMS.

| | | | | | | |
|-------|------|-------|-------|-------|------|------|
| Cu | Pb | Zn | Rb | Sr | Y | Zr |
| 191 | 21 | 119 | 114 | 188 | 38 | 84 |
| 185 | 24 | 122 | 120 | 188 | 40 | 84 |
| 190 | 19 | 119 | 116 | 189 | 43 | 90 |
| 185 | 24 | 122 | 120 | 190 | 40 | 91 |
| 186 | 22 | 123 | 116 | 198 | 40 | 90 |
| (190) | (22) | (120) | (120) | (190) | (40) | (87) |

TABLE B-9 Replicate analyses of trace elements in standard rock BMS.

(Values in ppm. Values in brackets are those quoted in report No. 1, Geochemistry Laboratory, University of Southampton, 1971).

| Variable | Mean | Std.Dev. | Maximum | Minimum | Range |
|----------|-------|----------|---------|---------|-------|
| Cu | 187.4 | 2.9 | 191 | 185 | 6 |
| Pb | 22.0 | 2.1 | 24 | 19 | 5 |
| Zn | 121.0 | 1.9 | 123 | 119 | 4 |
| Rb | 117.2 | 2.7 | 120 | 114 | 6 |
| Sr | 190.6 | 4.2 | 198 | 188 | 10 |
| Y | 40.2 | 1.8 | 43 | 38 | 5 |
| Zr | 87.8 | 3.5 | 91 | 84 | 7 |

TABLE B-10 Elementary statistics for replicate analyses of trace elements in standard rock BMS.

(Values in ppm).

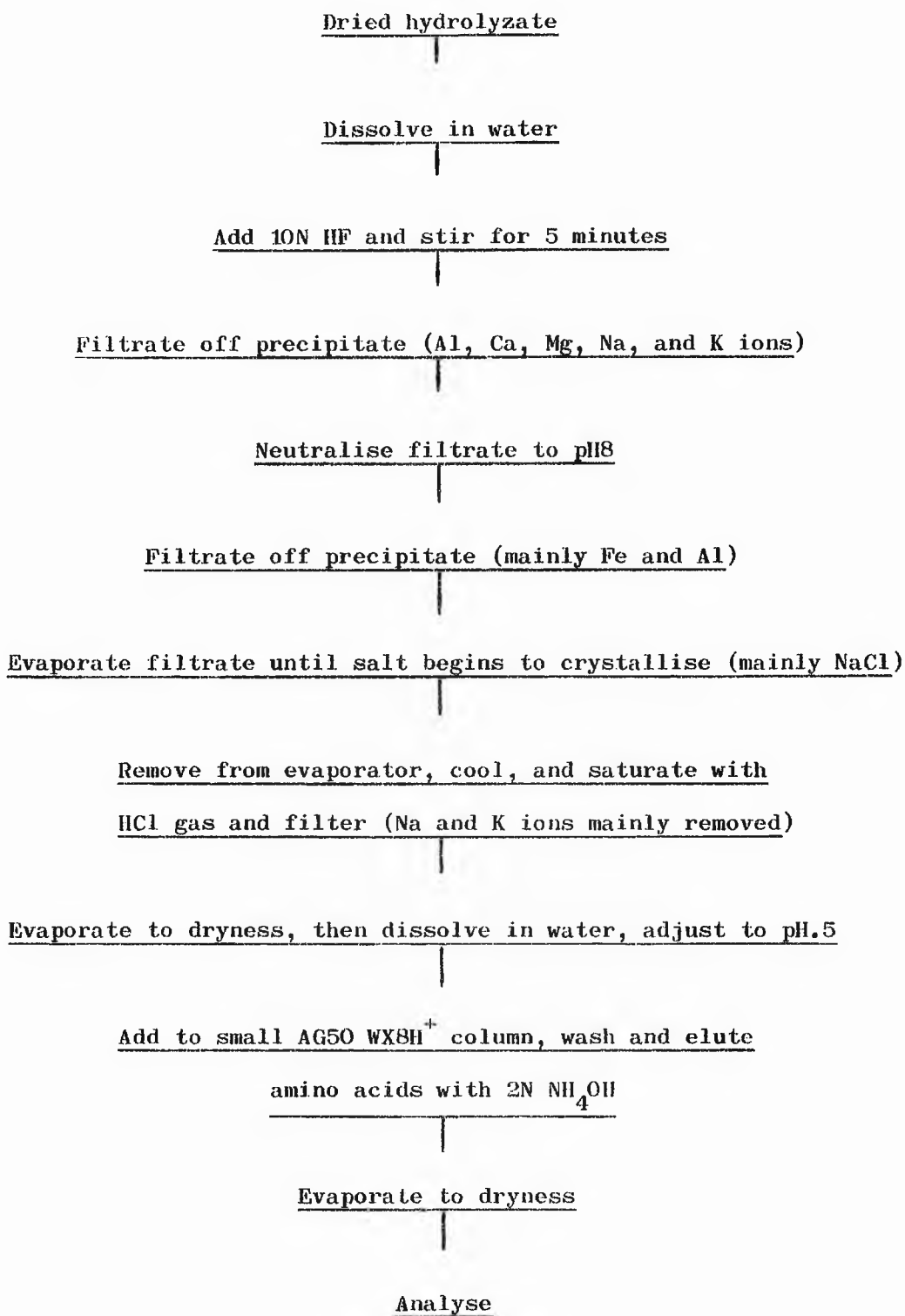


TABLE B-11 Desalting method scheme.

| Wavelength (nm) | Refractive index |
|-----------------|------------------|
| 410 | 2.4599 |
| 442 | 2.4472 |
| 502 | 2.4318 |
| 546 | 2.4238 |
| 590 | 2.4176 |
| 651 | 2.4106 |
| 710 | 2.4056 |

TABLE B-12 Variation in the refractive index of diamond with wavelength.

| Wavelength (nm) | Refractive index |
|-----------------|------------------|
| 410 | 1.5319 |
| 442 | 1.5265 |
| 502 | 1.5193 |
| 546 | 1.5160 |
| 590 | 1.5134 |
| 651 | 1.5106 |
| 710 | 1.5081 |

TABLE B-13 Variation in the refractive index of Zeiss immersion oil with wavelength.

| Wavelength (nm) | R(oil)% | R(air)% |
|-----------------|---------|---------|
| 410 | 5.397 | 17.793 |
| 442 | 5.375 | 17.635 |
| 502 | 5.334 | 17.420 |
| 546 | 5.307 | 17.290 |
| 590 | 5.289 | 17.200 |
| 651 | 5.271 | 17.110 |
| 710 | 5.262 | 17.039 |

TABLE B-11 Variation in reflectance values of diamond in oil and in air with wavelength.

A P P E N D I X C

STATISTICAL METHODS

1. INTRODUCTION

The most useful texts describing the application of statistics to geology are those of Miller and Kahn (1962), Krumbein and Graybill (1965), Koch and Link (1970) and Davis (1973). The last mentioned not only serves as an introduction to statistical terms and their application, but also describes the composition of computer programs written in Fortran IV. No attempt will be made in this appendix to review recent advances in the application of statistics to geology, but instead descriptions will be given of the techniques used, or considered for use, in this study.

2. THE DISTRIBUTION LAWS

Any measurements taken from a set of random samples comprising a single population will tend to form a simple frequency distribution i.e. more samples have values near the mean than those with values far removed from the mean. In this way, the frequency distribution tends to be peaked in form and can either be symmetrical or skewed in a positive or negative direction. The most familiar symmetrical distribution, and the one most commonly assumed in statistical techniques, is the normal distribution. This is mathematically simple and can be applied to many natural populations. The simplicity of this distribution is such that many statistical techniques have been formulated around it and it is often assumed to have universal applicability.

A similar dogmatic approach has been taken by some geochemists when describing the distribution of chemical elements in

nature. In this case, following the work of Ahrens (1954), a positively skewed lognormal distribution is often assumed. Vistelius (1967) for example, states 'The joint probability distribution function of the concentration of the minor chemical elements deposited by natural chemical reactions has a large positive skewness'. This he describes as 'a fundamental law of the geochemical process'.

Frequency distributions of data are of interest for two reasons. The first is that if data can be shown to be normally distributed, more advanced statistical techniques can often be applied and inferences made from the results. If however, the data are not found to be normally distributed, a decision has to be made as to whether or not subsequent tests would be of any real value. It is at this point that non-parametric, distribution free, statistics become useful. Non-parametric statistics are relatively new and are only now beginning to be used in geological studies. They have been applied in two ways in this work. Firstly, a non-parametric test known as the Kolmogorov - Smirnov test (Siegel 1956) has been employed to test for normal and lognormal distributions. Secondly, a non-parametric correlation coefficient (Kendall rank order correlation coefficient) has been calculated in order to avoid the assumption of a normal distribution.

The second reason for studying frequency distributions is often the desire to demonstrate the universality of the geochemical 'lognormal law'. This study shows that the chemical elements in the Moffat Shales are not lognormally distributed (Chapter III).

3. LINEAR CORRELATION

The techniques of linear correlation are those most familiar to the geologist. In general, simple linear correlation, normally represented in the form of a diagonal correlation matrix, aims to define the relationship between pairs of variables.

a) The simple linear model

The linear relationship between any two variables can be described by three parameters. These are the regression coefficient and the intercept, both of which define the line, and the correlation coefficient which is an estimate of the degree of fit of that line. The calculation procedure is described in Krumbein and Graybill (1965).

In Table 3-10, both the Pearson product moment and the Kendall rank order correlation coefficients are presented. The calculation of the latter was considered necessary because the product moment correlation coefficient can only be used with confidence when the scores on each variable are normally distributed. As was demonstrated above, this is not the case for the Moffat Shale geochemical data. In this work the product moment correlation coefficient is included in order to conform with standard procedures.

b) The Kendall rank order correlation coefficient

The rank order correlation coefficient is based on the transformation of the raw data to ranks ie. the data is first ordered from lowest to highest for each variable and then the orders of samples are compared. Almost invariably it is found that the rank order correlation coefficient is numerically lower than the product moment

correlation coefficient. There is however no change in sign between the two coefficients for significant correlations. Thus, the two coefficients differ in terms of magnitude with the rank order being a more conservative and a more significant estimate of the degree of correlation between two variables.

c) Polynomial regression

In many instances in this study it was found that a simple linear regression did not explain a significant amount of sums of squares. Where this occurred, progressively higher orders of polynomial curves were fitted to the data until no improvement in the sums of squares resulted between one order and the next. In all cases the F-value was calculated from the analyses of variance. This parameter is an estimate of the significance of the computation.

4. CLASSIFICATION OF SAMPLES

a) Introduction

The techniques of classification which are now used by the geologist were developed primarily for use in psychological research (Cattell 1965). The two main techniques employed are principal components analysis and factor analysis. Both methods produce similar types of results with factor analysis being a mathematical extension of principal components analysis. Each technique has both advantageous and undesirable qualities and therefore a comparison of both methods is not superfluous.

b) Principal components analysis

Le Maitre (1969) first demonstrated the power of this technique over other forms of petrochemical analysis. In general terms, the method involves a mathematical manipulation of the data contained in a matrix of correlation or covariance coefficients to reduce the data to a new set of variables defined in terms of proportions of the old variables. The technique has two advantages. The first is that all the new 'variables' or vectors are mutually orthogonal or uncorrelated which makes the technique desirable for use in the analysis of highly correlated data. The second advantage is that the number of significant vectors is normally smaller than the original number of variables. These are thus easier to handle. The object of the analysis is the recognition of these vectors as geological processes.

Mathematically, the technique consists of the extraction of latent roots or eigenvalues from a correlation or covariance matrix. There is associated with each eigenvalue an eigenvector which is the principal component. The first principal component is the vector which explains most of the variance and so on through the set. It is usually found that most of the variation is explained by the first few eigenvalues. The method of computation applied in this study is that of Wahlstedt and Davis (1968).

Principal components analysis can be considered by the use of a three dimensional analogy. Given a three dimensional system with three mutually orthogonal axes (such as the cubic system of crystallography) all the data points can be represented in the space defined within these axes. If all variables are equally important and perfectly correlated, the data will define a sphere. More commonly

however, the shape of the data envelope will be ellipsoidal and in this case the first principal component is the long axis of the ellipsoid defined in terms of the three orthogonal axes.

c) Factor analysis

Factor analysis is a mathematical extension of principal components analysis. Again the first step is the extraction of eigenvectors. Subsequent varimax rotation produces a new set of vectors which are defined as factors. This technique has been applied to the classification of geological data by Spencer (1966) and Cosgrove (1973). Factor analysis has not been used in this study because of the limitations outlined below.

d) Comparison of principal components and factor analyses

Rotation of the principal components to factors can only be satisfactorily accomplished if the original data is normally distributed. This has already been demonstrated to be an invalid assumption for the parameters measured in this study and therefore the use of factor analysis is not justified. Miesch (1969) in a study of the use of multivariate procedures in the analysis of geochemical data, concludes that after varimax rotation, further rotation is necessary to produce a factor that is consistent with the geological information. Though the relationships between variables are similar for both techniques, it is found that the loadings of factors and components appear to be erroneous when considered from a purely mathematical point of view. The lack of normality in a data set can be overcome by mathematical transformation but interpretation of the factors resulting after such a manipulation is difficult.

Stephens (1972), when comparing the results of both types of analyses from a set of non-normally distributed geochemical values, concludes that the results of both techniques are very similar for the first factor and the first component. Thereafter the differences between the two techniques become greater so that by the third factor and the third component there is little resemblance between the results of factor and principal component analysis. From this it is implied that the use of factor analysis in this present study would have confused the interpretation of the geological processes responsible for the observed distribution of results.

5. TREND SURFACE ANALYSIS

The technique of trend surface analysis has been employed throughout this work. This is a statistical method which aims to reduce areally distributed data to three maps. The first map consists of a 'smoothed' regional trend, the second of a contoured map of the data while the third indicates the deviation of the observed data from the computed trend. Two general methods exist for the calculation of the trend maps. These are Fourier series analysis and the least-squares fitting of polynomial functions.

Polynomial fitting is the basis of the technique used in this study. In general terms, the areal data is considered to be three-dimensional with each datum point being defined by two geographic coordinates 'u' and 'v', and a third coordinate 'w' which corresponds to the variable being studied. This third parameter can be considered as 'height' on a relief map.

The method of Cole (1969) has been used throughout the present study. This is a two-stage process, the first of which involves the computation of the 'best-fit' polynomial surface. In this case 'best-fit' is unfortunately defined as the surface that explains the largest percentage of the sums of squares in contrast to the method proposed by Allen and Krumbain (1962) which uses the analysis of variance as an estimate of the degree of fit. The use of the former technique always results in the highest possible order of polynomial surface being chosen. As the program of Cole (1969) only has facilities for the first three orders it is inevitable that the cubic surface is chosen. There is however an option within the program that provides the facility of displaying all three polynomial surfaces. Judicious use of this facility ensures that the amount of information lost by only computing the cubic surface is kept to a minimum. It is anticipated that in the near future an F-test will be built into the program (Cole pers. comm.). This will give a more accurate guide as to the significance of each computed surface.

The second stage of the process is to modify the chosen surface until after a prescribed number of iterations the fit of the data to the new surface (iterative fit surface) is considerably improved. The original surface has by this time lost much of its original form. The difference map is then computed by comparing the iterative and trend surface maps.

In summary, the iterative map can be considered as a slightly smoothed objectively contoured map with any non-significant deviations filtered out. The polynomial surface is a highly smoothed representation of the data and can be considered as illustrating the

main trend in the data. Since the global fit surface is mathematically simple it can often be used in a predictive mode but this facility is of little value in the present work.

6. COMPUTATIONAL METHODS

a) Introduction

The computation of the various required parameters was performed using an IBM 360/44 computer. All programs were written in Fortran IV and the output plotted where necessary by means of a UCC digital incremental drum plotter.

Some programs, and in particular those involving the use of the Scientific Subroutine package (IBM application program system 360), output results in an E14.7 format. This format has not been transposed in some of the tables presented, because it was felt that by so doing some valuable information may have been lost. The form of the data in this format is either 0.1234567Eb02 or -0.1234567E-02 (b = space) which if transposed equals 12.34567 and -0.001234567 respectively.

b) Descriptive statistics

In the interests of completeness some of the mathematically simpler statistics will be described. Symbols are defined in Table C-2.

The mean

This is the simplest descriptive statistic and is defined as:-

$$\bar{X} = \frac{1}{N} \sum_{i=1}^N x_i$$

The standard deviation

This is a generally useful statistic but it loses much of its significance when the data distribution is not normal. It is calculated in the following way:-

$$\sigma = \sqrt{\frac{1}{N - 1} \sum_{i = 1}^N (X_i - \bar{X})^2}$$

Histograms

These were drawn by computer by first calculating the minimum maximum and standard deviation. The class interval is then made equal to one half of the standard deviation.

c) The simple linear model

Regression

The standard form of the regression equation is :-

$$Y = a + bX$$

where b is the slope of the line, and a the intercept. The slope is calculated as follows:-

$$b = \frac{\sum XY - \frac{(\sum X)(\sum Y)}{N}}{\sum X^2 - \frac{(\sum X)^2}{N}}$$

and $a = \bar{Y} - b\bar{X}$

The Pearson product moment correlation coefficient

This again is generally useful but it is only meaningful when the distribution is normal.

It is calculated as follows:-

$$r = \frac{N \sum XY - (\sum X)(\sum Y)}{\left[\overline{N \sum X^2 - (\sum X)^2} \right] \left[\overline{N \sum Y^2 - (\sum Y)^2} \right]}$$

The Kendall rank order correlation coefficient

This is a non-parametric coefficient, not bound by the requirement of a normal distribution. It is based on a ranking procedure where Nr is the number of pairs of ranks and Dr is the difference between a pair of ranks. It is calculated in the following way:-

$$pr = 1 - \frac{6 \sum Dr^2}{Nr(Nr^2 - 1)}$$

d) Multivariate statistics

Principal components analysis

The mathematics involved in this technique are more complex than can be described here. Principal components were calculated from the correlation coefficient matrix using the computational method of Cooley and Lohnes (1962).

| NAME | PURPOSE | AUTHOR |
|---------|--|--|
| JCMAP 1 | To perform an iterative trend surface analysis on irregularly spaced data | A.J.COLE (1969) |
| SWUNIX | To calculate and draw univariate statistics incorporating a KOLMOGOROV-SMIRNOV test for normal and lognormal distributions | W.E.STEPHENS adapted by J.B.FOWLER and S.W.W. |
| ESBIVAR | To calculate bivariate statistics such as the Pearson product moment correlation coefficient and the Kendall rank order correlation coefficient and also to plot scatter diagrams with superimposed regression lines | W.E.STEPHENS |
| ESSTRAT | To calculate and plot polynomial regression curves for the stratigraphic variation of parameters up the type Moffat Shales succession | W.E.STEPHENS |
| SWHART | To calculate and plot polynomial regression curves for the variation of parameters up the north cliff at Hartfell | adapted from ESSTRAT by S.W.W. |
| ESPCA | To perform a principal components analysis | W.C.WAHLSTEDT and J.C.DAVIS (1968) |

/continued

TABLE C-1 List of computer programs used during the study.

TABLE C-1 Continued

| NAME | PURPOSE | AUTHOR |
|---------|--|---|
| PAMOLE | To draw a molecule using three mutually perpendicular axes | A.J.COILE and P.ADAMSON (1969) adapted by W.E. STEPHENS to display principal components |
| ZGTMAC | To calculate total mass absorption coefficient from major element analysis | P.R.PHILIP |
| ZGXRF 4 | To calculate concentrations of Cu or Pb or Zn and estimate mass absorption coefficients from spectrometer counts | P.R.PHILIP and S.W.W. |
| ZGXRF 7 | To calculate concentration of Rb,Sr,Y and Zr and estimate mass absorption coefficients from spectrometer counts | P.R.PHILIP and S.W.W. |
| SWPO | To calculate the dependant variable given polynomial regression equations | S.W.W. |
| SWNK | To calculate refractive and absorptive indices from reflectivity data | S.W.W. |

| NAME | PURPOSE | AUTHOR |
|--------|---|--------|
| SWXRAY | To calculate two-theta values from d-spacings and plot templates to aid in the identification of minerals by X-ray diffraction analysis | S.W.W. |
| SWXR 1 | To calculate the modal mineral composition from X-ray diffraction data | S.W.W. |
| SWOEP | To calculate odd-even predominance values of alkanes from GLC information | S.W.W. |
| CLST 1 | To give facilities for editing data, transforming data, calculating elementary statistics and drawing histograms and scatter diagrams | RSP |
| CLST 2 | To give facilities for the calculation of linear and polynomial regressions | RSP |

All programs are housed at the Computer Laboratory, University of St. Andrews. Listings are available either from the present author or in the form of publications where cited.

SWW = Stewart W. Watson

RSP = RAX system statistical package which is based on the IBM program number 360D 13.0.003.

TABLE C-1 Continued.

| | | |
|-----------|---|--|
| X_i | = | value of sample i for variable X |
| Y_i | = | value of sample i for variable Y |
| \bar{X} | = | mean value for variable X |
| \bar{Y} | = | mean value for variable Y |
| $\sum X$ | = | the sum of all samples in variable X |
| $\sum Y$ | = | the sum of all samples in variable Y |
| N | = | total number of samples |
| σ | = | standard deviation |
| a | = | intercept of a regression line |
| b | = | slope of a regression line |
| r | = | Pearson product moment correlation coefficient |
| r_r | = | Kendall rank order correlation coefficient |
| D_r | = | difference between pairs of ranks |
| N_r | = | number of pairs of ranks |

TABLE C-2 Glossary of statistical and mathematical terms.

A P P E N D I X D

DESCRIPTION OF THE SPECTRAL VARIATION IN
OPTICAL PROPERTIES OF GRAPTOLITE FRAGMENTS

1. SPECTRAL VARIATION OF REFLECTANCE VALUES

Moving towards the 9.18 m wide dyke at Clanyard Bay from the south, the following observations pertaining to the spectral variation of oil and air reflectivities of carbonized graptolites may be made.

Sample LB-12 (Fig.152)

There is very little dispersion in reflectance values in this sample. In oil there is a slight increase in values from blue to the red in the visible spectrum. Computed values increase from 1.90 per cent at 410 nm to 1.96 per cent at 710 nm. In air, the increase in values from the blue to the red, although more noticeable, is still slight with values ranging from 8.79 per cent at 410 nm to 9.49 per cent at 710 nm.

Sample LB-13 (Fig.153)

The computed trends show a general increase in values both in oil and in air from the blue to the red. Between 410 and 546 nm values decrease in oil from 1.87 to 1.78 per cent whereas in air values increase from 5.78 to 10.01 per cent.

Sample LB-14 (Fig.154)

Although organic material was relatively abundant within this sample, visual inspection revealed unusually large differences in reflectivities between fragments. There was no reason to believe that the fragments were not of graptolitic origin, therefore it was decided not to measure the reflectance values of the customary ten fragments but instead to choose only two fragments and measure ten values at

each wavelength over each of them. These fragments have been designated LB-14 (1) and LB-14 (2). The former is a long narrow fragment of relatively low reflectivity, while the latter is semi-quadrant and of higher reflectivity. The enhanced reflectivity of LB-14 (2) may be due wholly or partly to the fact that it lies in juxtaposition with a haematitic fragment.

LB-14 (1)

Both oil and air reflectance values decrease towards the red. Values range from 2.72 per cent at 410 nm to 1.42 per cent at 710 nm in oil and from 10.31 per cent at 410 nm to 9.61 per cent at 710 nm in air.

LB-14 (2)

The actual values are considerably higher in this fragment than in LB-14 (1) and the computed trends show an increase in values in both air and oil from the blue to the red. Only slight dispersion is evident between 410 and 546 nm but the slope of the curves increase to give significant differences in values between 590 and 710 nm.

Sample LB-15 (Fig.153)

Both oil and air reflectivities increase towards the red. In oil, values increase linearly with wavelength while in air they first rise sharply and then level off at wavelengths greater than 590 nm.

Sample LB-16 (Fig.152)

A simple linear trend with values increasing from the blue to the red is computed for this sample. Values range from 4.51 per

cent at 410 nm to 5.55 per cent at 710 nm in oil and from 10.46 per cent at 410 nm to 13.97 per cent at 710 nm in air.

Sample LB-17A (Fig.153)

The computed trend for the spectral variation of reflectivity in oil for this sample which was collected at 1.40 metres from the dyke contact, appears to differ from that of the preceding samples in that the curve is computed to have a negative slope with values decreasing towards the red. Values in oil range from 6.10 per cent at 410 nm to 5.71 per cent at 710 nm. Values in air show a slight tendency to increase towards the red.

Sample LB-18 (Fig.155)

The trend described for the spectral variation of reflectivity in oil for the previous sample is now enhanced so that in both air and oil, reflectance values plunge steeply towards the red. The measured values indicate that in each of the two media the reflectivity first increases to a maximum at 442 nm and then falls rapidly towards higher wavelengths.

2. SPECTRAL VARIATION IN REFRACTIVE INDICES

Spectral trends for the variation of refractive index in the samples from Clanyard Bay are illustrated in Figs.161 - 166. These trends will now be briefly described for each sample in order of decreasing distance from the dyke.

Sample LB-12 (Fig.161)

There is no dispersion of refractive index with wavelength

between 410 nm and 546 nm. Thereafter, values increase with increasing wavelength to attain a maximum of 1.78 at 710 nm.

Sample LB-13 (Fig.162)

In contrast to the previous sample there is a sharp increase in refractive indices at lower wavelengths with values increasing from a minimum of 1.44 at 410 nm to a maximum of 1.86 at 546 nm. Values then fall towards the red attaining 1.73 at 710 nm.

Sample LB-14 (Fig.163)

Both LB-14 (1) and LB-14 (2) show comparable dispersions between the blue and the red of the visible spectrum, with the former displaying values which increase from 1.78 to 1.88 and the latter values which increase from 1.69 to 1.85. Thus the marked differences in the refractive indices are clearly not related to the marked differences in the reflectivities of the two particles.

Sample LBR-9 (Fig.164)

Superimposed upon a general increase from the blue to the red, the dispersion trend follows a sigmoidal curve which rises to a maximum value of 1.71 at 502 nm and falls to a secondary minimum of 1.69 at 651 nm.

Sample LBR-3 (Fig.165)

A similar curve to that of sample LBR-9 is drawn for the variation in refractive index with wavelength of this sample. Values range from 1.49 at 410 nm to 1.82 at 710 nm in contrast to those of the previous sample which range from 1.56 to 1.74.

Sample LB-15 (Fig. 162)

Although there is pronounced dispersion between 410 nm (1.56) and 502 nm (1.70) values thereafter increase only slowly with wavelength to reach a maximum of around 1.75 at 651 nm.

Sample LBR-7 (Fig.165)

There appears to be very little dispersion of refractive index when only the extreme ends of the visible spectrum are considered. Values however rise from a minimum of 1.68 at 410 nm to a maximum of 1.83 in the vicinity of 520 nm before falling to 1.73 at 710 nm.

Sample LB-16 (Fig.161)

The refractive index of the organic material within this sample increases linearly with wavelength with values of 1.52 and 1.79 being computed at wavelengths of 410 and 710 nm respectively.

Sample LBR-13 (Fig.164)

The dispersion curve of refractive index with wavelength is similar in both trend and magnitude to that of sample LB-16. Refractive index increases from 1.55 at 410 nm to 1.78 at 710 nm.

Sample LBR-8 (Fig.165)

This sample, estimated to have been closer to the dyke at the time of intrusion than samples LBR-3 and LBR-7, displays values of refractive index between 410 and 546 nm which are intermediate. Values, however, rise between 546 and 710 nm to reach a maximum of 1.82.

Sample LB-17A (Fig.162)

Some of the highest refractive index values have been calculated for the organic material in this sample. Values increase in an almost linear fashion from 1.72 at 410 nm to 1.83 at 710 nm.

Sample LB-18 (Fig.166)

This sample, collected nearest to the dyke, exhibits a comparable trend of refractive index with wavelength to that of sample LBR-7. The computed values however are considerably higher with a maximum of 2.30 at 546 nm.

3. SPECTRAL VARIATION IN ABSORPTIVE INDICES

The dispersion trends of absorptive index with wavelength indicate that for samples close to the dyke values decrease with increasing wavelength, whereas for samples further away there is a more complex spectral relationship. This observation is now amplified by describing in order of decreasing distance from the dyke the spectral variation in the absorptive index of the Clanyard Bay samples.

Sample LB-12 (Fig.161)

There is only slight dispersion of absorptive index with wavelength. Values decrease almost linearly from 0.25 at 410 nm to 0.21 at 710 nm.

Sample LB-13 (Fig.162)

The trend of the absorptive index with wavelength for the organic material in this sample is complementary to that of the

refractive index trend. Values decrease from 0.28 at 410 nm to a minimum of 0.16 at 546 nm before increasing towards the extreme red of the visible spectrum.

Sample LB-14 (Fig.163)

Although there is a pronounced decrease in absorptive index values toward the red in particle LB-14 (1), there is virtually no dispersion of the index in particle LB-14 (2). It is therefore now evident that it is the variation in absorptive index and not that of the refractive index that is causing the disparity in the reflectance spectral trends of the two particles.

Sample LBR-9 (Fig.164)

There is only slight dispersion of the index between 546 and 710 nm. Values remain almost stationary at 0.35 between 410 and 546 nm and then increase to 0.39 in the extreme red.

Sample LBR-3 (Fig.165)

Absorptive index values although slightly higher at any one wavelength than those of sample LBR-9 follow a similar spectral trend. The main difference in the two trends is that whereas sample LBR-9 displays a slight increase in values towards the red, sample LBR-3 displays a slight increase towards the blue.

Sample LB-15 (Fig.162)

There is virtually no dispersion of the absorptive index between the two extreme ends of the spectrum but there is a slight indication of a drop in values in the green. Values calculated for this sample range from 0.41 at 410 nm to 0.39 at 546 nm.

Sample LBR-7 (Fig.165)

After a slight drop from 0.40 at 410 nm to 0.39 at 502 nm the absorptive index increase steadily into the red with a value of 0.49 being calculated at 710 nm.

Sample LB-16 (Fig.161)

Values appear to remain stationary at 0.44 between 410 and 590 nm. Thereafter they decrease towards the red.

Sample LBR-13 (Fig.164)

Again, as for samples LBR-9 and LB-16, there is little dispersion of the absorptive index between 410 and 590 nm. Values then increase from 0.40 at 546 nm to 0.42 at 710 nm.

Sample LBR-8 (Fig.165)

The absorptive index first increases from 0.45 at 410 nm to 0.49 at 502 nm and then decreases to 0.47 at 590 nm. Thereafter values increase to a maximum of 0.51 at 710 nm.

Sample LB-17A (Fig.162)

Values decrease linearly from the blue to the red in the visible spectrum with absorptive indices of 0.47 and 0.41 being computed at wavelengths of 410 and 710 nm respectively.

Sample LB-18 (Fig.166)

Absorptive index values for the organic material in this sample which was collected nearest to the dyke show a pronounced increase towards the blue. Values rise from 0.39 at 651 nm to 0.60 at 410 nm.

| | | | | |
|------|----------------|----------------|----------------|----------------|
| Samp | LB-12 | | | |
| Cep | 0.1823390E 01 | | | |
| Rc | 0.1911862E-03 | | | |
| LoS | 25.0 | | | |
| | | | | |
| Samp | LB-13 | | | |
| Cep | 0.6159985E 01 | | | |
| Rc | -0.1786629E-01 | 0.1802770E-04 | | |
| LoS | 15.0 | | | |
| | | | | |
| Samp | LB-14(1) | | | |
| Cep | 0.7493586E 01 | | | |
| Rc | -0.1585631E-01 | 0.1027936E-04 | | |
| LoS | 2.5 | | | |
| | | | | |
| Samp | LB-14(2) | | | |
| Cep | 0.7141187E 01 | | | |
| Rc | -0.6925203E-02 | -0.3441774E-04 | 0.1100378E-06 | -0.7576305E-10 |
| LoS | 2.5 | | | |
| | | | | |
| Samp | LB-15 | | | |
| Cep | 0.4419889E 01 | | | |
| Rc | -0.1094979E-01 | 0.3648447E-04 | -0.3121407E-07 | 0.4889527E-11 |
| LoS | 5.0 | | | |
| | | | | |
| Samp | LB-16 | | | |
| Cep | 0.6567338E 01 | | | |
| Rc | -0.1536361E-01 | 0.2950145E-04 | -0.5989733E-08 | -0.1173107E-10 |
| LoS | 5.0 | | | |
| | | | | |
| Samp | LB-17A | | | |
| Cep | 0.6637597E 01 | | | |
| Rc | -0.1312190E-02 | | | |
| LoS | 25.0 | | | |

/continued

TABLE D-1 Regression line parameters for the dispersion of mean reflectance values of graptolite fragments in oil with wavelength for selected samples from Clanyard Bay.

Samp LB-18
Cep 0.2748044E 02
Rc -0.4087120E-01 0.1844722E-04
LoS 10.0

Samp LBR-3
Cep 0.1865566E 01
Rc 0.4513372E-02
LoS 0.1

Samp LBR-7
Cep 0.3502066E 01
Rc -0.6370142E-02 0.2674952E-04 -0.1569909E-07
LoS 1.0

Samp LBR-8
Cep -0.2709515E 02
Rc 0.1665543E 00 -0.2786987E-03 0.1611160E-06
LoS 2.5

Samp LBR-9
Cep 0.8352737E 00
Rc 0.5534418E-02
LoS 0.1

Samp LBR-13
Cep 0.2798978E 02
Rc -0.1395972E 00 0.2588802E-03 -0.1503817E-06
LoS 5.0

Samp = sample number
Cep = intercept
Rc = regression coefficients
LoS = level of significance of computed curve (%)

TABLE D-1 Continued

Samp LB-12
Cep 0.1240246E 02
Rc -0.1526096E-01 0.1571194E-04
LoS 15.0

Samp LB-13
Cep -0.1487049E 03
Rc 0.8022627E 00 -0.1341540E-02 0.7410248E-06
LoS 5.0

Samp LB-14(1)
Cep 0.1127618E 02
Rc -0.2348310E-02
LoS 15.0

Samp LB-14(2)
Cep 0.1934564E 02
Rc -0.3932111E-01 0.4157893E-04 0.3864045E-07 -0.4859584E-10
LoS 1.0

Samp LB-15
Cep -0.3086043E 02
Rc 0.2011406E 00 -0.3156541E-03 0.1709095E-06
LoS 2.5

Samp LB-16
Cep 0.7492409E 00
Rc 0.4246716E-01 -0.7533329E-04 0.9005237E-07 -0.4403258E-10
LoS 2.5

Samp LB-17A
Cep 0.1432764E 02
Rc 0.3859999E-03
LoS 25.0

/continued

TABLE D-2 Regression line parameters for the dispersion of mean reflectance values of graptolite fragments in air with wavelength for selected samples from Clanyard Bay.

Samp LB-18

Cep 0.3648511E 02

Rc -0.2480028E-01

LoS 5.0

Samp LBR-3

Cep -0.9696130E 02

Rc 0.5554028E 00 -0.9452133E-02 0.5388875E-06

LoS 1.0

Samp LBR-7

Cep -0.4108530E 02

Rc 0.2643244E 00 -0.4247313E-03 0.2315117E-06

LoS 5.0

Samp LBR-8

Cep -0.1188559E 01

Rc 0.4583618E-01 -0.2641376E-04

LoS 5.0

Samp LBR-9

Cep -0.6526373E 02

Rc 0.3877321E 00 -0.6578690E-03 0.3755533E-06

LoS 5.0

Samp LBR-13

Cep 0.2273576E 02

Rc -0.8976126E-01 0.1892108E-03 -0.1127672E-06

LoS 2.5

Samp = sample number

Cep = intercept

Rc = regression coefficients

LoS = level of significance of computed curve (%)

TABLE D-2 Continued.

Samp HCL-16
 Cep -0.1479603E 02
 Rc 0.7372893E-01 -0.6291363E-04 -0.4636456E-07 0.6480104E-10
 LoS 2.5

Samp HCL-26
 Cep 0.1192274E 02
 Rc -0.4620264E-01 0.7797204E-04 -0.2745598E-07 -0.1391136E-10
 LoS 2.5

Samp HCL-26A
 Cep 0.7226565E 01
 Rc 0.3583431E-02 -0.6644086E-04 0.1600299E-06 -0.1045928E-09
 LoS 10.0

Samp HCL-29
 Cep 0.3260362E 01
 Rc -0.3028169E-02 0.1094222E-04
 LoS 1.0

Samp HCL-31
 Cep -0.1891749E 01
 Rc 0.2465914E-01 -0.2322561E-04 -0.9547339E-08 0.2031862E-10
 LoS 1.0

Samp HL-4
 Cep 0.2719832E 02
 Rc -0.9680271E-01 0.9024533E-04 0.9076700E-07 -0.1178381E-09
 LoS 1.0

Samp HL-13
 Cep -0.1168791E 02
 Rc 0.7018518E-01 -0.6184966E-04 -0.6504155E-07 0.8910864E-10
 LoS 1.0

/continued

TABLE D-3 Regression line parameters for the dispersion of mean reflectance values of graptolite fragments in oil with wavelength for selected samples from Hartfell.

Samp III-14
Cep 0.8132166E 01
Rc -0.3026818E-01 0.7626746E-04 -0.6994480E-07 0.2149896E-10
LoS 10.0

Samp III-15
Cep -0.3373857E 02
Rc 0.1973194E 00 -0.2462955E-03 -0.2988554E-07 0.1377700E-09
LoS 5.0

Samp = sample
Cep = intercept
Rc = regression coefficients
LoS = level of significance of computed curve (%)

TABLE D-3 Continued.

| | | | | | |
|------|----------------|----------------|----------------|----------------|--|
| Samp | HCL-16 | | | | |
| Cep | -0.5727811E 01 | | | | |
| Rc | 0.4851241E-01 | -0.2707342E-04 | -0.1249205E-08 | -0.4618634E-11 | |
| LoS | 1.0 | | | | |
| Samp | HCL-26 | | | | |
| Cep | 0.6669416E 01 | | | | |
| Rc | -0.1099539E-01 | 0.7300258E-04 | -0.5371274E-07 | -0.7981402E-11 | |
| LoS | 1.0 | | | | |
| Samp | HCL-26A | | | | |
| Cep | 0.4269073E 01 | | | | |
| Rc | -0.1274025E-01 | 0.1126832E-03 | -0.1192220E-06 | 0.2349590E-10 | |
| LoS | 2.5 | | | | |
| Samp | HCL-29 | | | | |
| Cep | 0.8731723E 01 | | | | |
| Rc | 0.9010103E-02 | | | | |
| LoS | 15.0 | | | | |
| Samp | HCL-31 | | | | |
| Cep | 0.1031754E 02 | | | | |
| Rc | -0.2577462E-01 | 0.7877260E-04 | -0.5421125E-07 | 0.1588185E-11 | |
| LoS | 1.0 | | | | |
| Samp | HL-4 | | | | |
| Cep | 0.8593943E 01 | | | | |
| Rc | 0.2099548E-01 | -0.3453050E-04 | 0.2587820E-07 | 0.3199578E-11 | |
| LoS | 1.0 | | | | |
| Samp | HL-13 | | | | |
| Cep | 0.9456737E 01 | | | | |
| Rc | -0.1007283E-01 | 0.8285613E-04 | -0.1340480E-06 | 0.8069602E-10 | |
| LoS | 2.5 | | | | |

/continued

TABLE D-4 Regression line parameters for the dispersion of mean reflectance values of graptolite fragments in air with wavelength for selected samples from Hartfell.

Samp III-14
Cep 0.7613865E 01
Rc 0.6057028E-02 0.4980657E-05 -0.4189566E-08
LoS 10.0

Samp III-15
Cep -0.1124362E 03
Rc 0.7282063E 00 -0.1305979E-02 0.7609302E-06
LoS 15.0

Samp = sample

Cep = intercept

Rc = regression coefficients

LoS = level of significance of computed curve (%)

TABLE D-4 Continued.

A P P E N D I X E

ANALYTICAL RESULTS

1. INTRODUCTION

In the compilation of results which follows, the symbols and units of the measured parameters are:

| <u>parameter measured</u> | <u>symbol</u> | <u>unit</u> |
|---------------------------|--------------------------------|-------------|
| silicon oxide | SiO ₂ | % |
| titanium oxide | TiO ₂ | % |
| aluminium oxide | Al ₂ O ₃ | % |
| ferric oxide | Fe ₂ O ₃ | % |
| manganese oxide | MnO | % |
| magnesium oxide | MgO | % |
| calcium oxide | CaO | % |
| sodium oxide | Na ₂ O | % |
| potassium oxide | K ₂ O | % |
| loss-on-ignition | LOI | % |
| copper | Cu | ppm |
| lead | Pb | ppm |
| zinc | Zn | ppm |
| rubidium | Rb | ppm |
| strontium | Sr | ppm |
| yttrium | Y | ppm |
| zirconium | Zr | ppm |
| carbon | C | % |
| mean reflectance in oil | Ro | % |
| logarithm of resistivity | log Rv | - |
| modal albite | albite | % |
| modal chlorite | chlorite | % |
| modal sericite | sericite | % |
| modal pyrite | pyrite | % |
| modal quartz | quartz | % |

Samples were collected by the author (SWW), J.A.Weir (JAW), W.E.Stephens (WES) and T.B.Fyfe (TBF). Analyses were performed either at Exeter University (EX) or by the author at St. Andrews University. Reflectivity determinations were made at the Organic Geochemistry Unit, University of Newcastle upon Tyne.

2. ANALYTICAL RESULTS

Sample HRC-1
 Locality Hartfell
 Grid Reference NT 094115
 Stratigraphic unit Glenkiln Shales
 Zone
 Collected by SWW
 Analysed by SWW
 Description Radiolarian chert

| | | | | | |
|--------------------------------|-------|--------|-------|----------|----------|
| SiO ₂ | 85.39 | Cu | 75 | Albite | 2.5 |
| TiO ₂ | 0.54 | Pb | 22 | Chlorite | 4.8 |
| Al ₂ O ₃ | 7.64 | Zn | 2 | Sericite | 6.0 |
| Fe ₂ O ₃ | 1.48 | Rb | 63 | Pyrite | 4.8 |
| MnO | 0.01 | Sr | 29 | Quartz | 81.8 |
| MgO | 0.34 | Y | 15 | | |
| CaO | 0.02 | Zr | 78 | | |
| Na ₂ O | 0.45 | C | 0.49 | Organics | analysed |
| K ₂ O | 1.15 | Ro | 4.83 | | |
| LOI | 2.98 | log Rv | 7.656 | | |

Sample HW-1
 Locality Hartfell
 Grid Reference NT 094115
 Stratigraphic unit Lower Hartfell Shales
 Zone wilsoni
 Collected by SWW
 Analysed by SWW
 Description Black graptolitic blocky mudstone

| | | | | | |
|--------------------------------|-------|--------|-------|----------|----------|
| SiO ₂ | 75.94 | Cu | 138 | Albite | 3.3 |
| TiO ₂ | 0.71 | Pb | 44 | Chlorite | 4.2 |
| Al ₂ O ₃ | 11.24 | Zn | 19 | Sericite | 12.6 |
| Fe ₂ O ₃ | 2.39 | Rb | 121 | Pyrite | 6.3 |
| MnO | 0.03 | Sr | 36 | Quartz | 73.7 |
| MgO | 0.99 | Y | 45 | | |
| CaO | 0.02 | Zr | 163 | | |
| Na ₂ O | 0.48 | C | 1.29 | Organics | analysed |
| K ₂ O | 2.13 | Ro | 1.71 | | |
| LOI | 5.95 | log Rv | 7.749 | | |

Sample HG-1

Locality Hartfell

Grid Reference NT 094115

Stratigraphic unit Glenkiln Shales

Zone

Collected by SWW

Analysed by SWW

Description Massive siliceous mudstone

| | | | | | |
|--------------------------------|-------|--------|-------|----------|----------|
| SiO ₂ | 86.60 | Cu | 79 | Albite | 1.9 |
| TiO ₂ | 0.71 | Pb | 16 | Chlorite | 3.5 |
| Al ₂ O ₃ | 5.62 | Zn | 3 | Sericite | 7.8 |
| Fe ₂ O ₃ | 3.57 | Rb | 57 | Pyrite | 4.5 |
| MnO | 0.01 | Sr | 26 | Quartz | 82.4 |
| MgO | 0.29 | Y | 15 | | |
| CaO | 0.03 | Zr | 62 | | |
| Na ₂ O | 0.36 | C | 0.35 | Organics | analysed |
| K ₂ O | 0.92 | Ro | 4.87 | | |
| LOI | 1.61 | log Rv | 7.723 | | |

Sample HG-2

Locality Hartfell

Grid reference NT 094115

Stratigraphic unit Glenkiln Shales

Zone

Collected by SWW

Analysed by SWW

Description Grey chert

| | | | | | |
|--------------------------------|-------|--------|-------|----------|----------|
| SiO ₂ | 84.38 | Cu | 91 | Albite | 0.7 |
| TiO ₂ | 0.41 | Pb | 18 | Chlorite | 4.7 |
| Al ₂ O ₃ | 7.02 | Zn | 14 | Sericite | 11.7 |
| Fe ₂ O ₃ | 3.18 | Rb | 43 | Pyrite | 4.7 |
| MnO | 0.07 | Sr | 13 | Quartz | 78.1 |
| MgO | 0.64 | Y | 21 | | |
| CaO | 0.02 | Zr | 62 | | |
| Na ₂ O | 0.33 | C | 0.33 | Organics | analysed |
| K ₂ O | 0.92 | Ro | 1.87 | | |
| LOI | 3.03 | log Rv | 7.624 | | |

Sample HW-4

Locality Hartfell

Grid reference NT 094115

Stratigraphic unit Lower Hartfell Shales

Zone wilsoni

Collected by SWW

Analysed by SWW

Description Blocky black mudstone

| | | | | | |
|--------------------------------|-------|--------|-------|----------|----------|
| SiO ₂ | 83.71 | Cu | 53 | Albite | 3.6 |
| TiO ₂ | 0.70 | Pb | 20 | Chlorite | 2.1 |
| Al ₂ O ₃ | 7.58 | Zn | 3 | Sericite | 12.0 |
| Fe ₂ O ₃ | 0.74 | Rb | 91 | Pyrite | 4.6 |
| MnO | 0.01 | Sr | 75 | Quartz | 77.8 |
| MgO | 0.52 | Y | 21 | | |
| CaO | 0.03 | Zr | 89 | | |
| Na ₂ O | 0.34 | C | 2.40 | Organics | analysed |
| K ₂ O | 1.54 | Ro | | | |
| LOI | 4.75 | log Rv | 4.731 | | |

Sample HW-5

Locality Hartfell

Grid reference NT 094115

Stratigraphic unit Lower Hartfell Shales

Zone wilsoni

Collected by SWW

Analysed by SWW

Description Blocky black graptolitic mudstone

| | | | | | |
|--------------------------------|-------|--------|-------|----------|----------|
| SiO ₂ | 75.62 | Cu | 113 | Albite | 4.0 |
| TiO ₂ | 0.61 | Pb | 42 | Chlorite | 4.4 |
| Al ₂ O ₃ | 10.80 | Zn | 17 | Sericite | 14.9 |
| Fe ₂ O ₃ | 2.30 | Rb | 115 | Pyrite | 5.1 |
| MnO | 0.03 | Sr | 41 | Quartz | 71.6 |
| MgO | 1.02 | Y | 47 | | |
| CaO | 0.03 | Zr | 147 | | |
| Na ₂ O | 0.46 | C | 1.17 | Organics | analysed |
| K ₂ O | 2.45 | Ro | 5.07 | | |
| LOI | 6.60 | log Rv | 7.829 | | |

Sample HCL-1

Locality Hartfell

Grid reference NT 094115

Stratigraphic unit Lower Hartfell Shales

Zone clingani

Collected by SWW

Analysed by SWW

Description Ashy textured black shale

| | | | | | |
|--------------------------------|-------|--------|-------|-------------------|------|
| SiO ₂ | 81.91 | Cu | 17 | Albite | 4.2 |
| TiO ₂ | 0.81 | Pb | 42 | Chlorite | 4.3 |
| Al ₂ O ₃ | 8.25 | Zn | 5 | Sericite | 11.9 |
| Fe ₂ O ₃ | 0.55 | Rb | 85 | Pyrite | 5.2 |
| MnO | 0.00 | Sr | 128 | Quartz | 74.4 |
| MgO | 0.53 | Y | 46 | | |
| CaO | 0.02 | Zr | 105 | | |
| Na ₂ O | 0.62 | C | 1.68 | Organics analysed | |
| K ₂ O | 1.69 | Ro | 4.84 | | |
| LOI | 5.55 | log Rv | 4.039 | | |

Sample HCL-2

Locality Hartfell

Grid reference NT 094115

Stratigraphic unit Lower Hartfell Shales

Zone clingani

Collected by SWW

Analysed by SWW

Description Platy black graptolitic shale

| | | | | | |
|--------------------------------|-------|--------|-------|-------------------|------|
| SiO ₂ | 83.60 | Cu | 34 | Albite | 1.2 |
| TiO ₂ | 1.08 | Pb | 34 | Chlorite | 3.9 |
| Al ₂ O ₃ | 5.44 | Zn | 2 | Sericite | 7.6 |
| Fe ₂ O ₃ | 0.48 | Rb | 53 | Pyrite | 6.5 |
| MnO | 0.01 | Sr | 49 | Quartz | 80.8 |
| MgO | 0.38 | Y | 14 | | |
| CaO | 0.01 | Zr | 56 | | |
| Na ₂ O | 0.33 | C | 3.78 | Organics analysed | |
| K ₂ O | 1.50 | Ro | 4.67 | | |
| LOI | 7.11 | log Rv | 3.096 | | |

Sample HCL-3

Locality Hartfell

Grid reference NT 094115

Stratigraphic unit Lower Hartfell Shales

Zone clingani

Collected by SWW

Analysed by SWW

Description Cleaved black cherty mudstone

| | | | | |
|--------------------------------|-------|--------|-------|-------------------|
| SiO ₂ | 85.03 | Cu | 40 | Albite |
| TiO ₂ | | Pb | 48 | Chlorite |
| Al ₂ O ₃ | 5.49 | Zn | 2 | Sericite |
| Fe ₂ O ₃ | | Rb | 65 | Pyrite |
| MnO | | Sr | 55 | Quartz |
| MgO | | Y | 2 | |
| CaO | | Zr | 65 | |
| Na ₂ O | | C | 4.01 | Organics analysed |
| K ₂ O | | Ro | 5.07 | |
| LOI | | log Rv | 3.204 | |

Sample HCL-4

Locality Hartfell

Grid reference NT 094115

Stratigraphic unit Lower Hartfell Shales

Zone clingani

Collected by SWW

Analysed by SWW

Description Blocky black mudstone

| | | | | | |
|--------------------------------|-------|--------|-------|-------------------|------|
| SiO ₂ | 82.43 | Cu | 62 | Albite | 4.3 |
| TiO ₂ | 0.30 | Pb | 31 | Chlorite | 2.0 |
| Al ₂ O ₃ | 6.48 | Zn | 2 | Sericite | 12.4 |
| Fe ₂ O ₃ | 0.55 | Rb | 74 | Pyrite | 4.9 |
| MnO | 0.00 | Sr | 48 | Quartz | 76.5 |
| MgO | 0.38 | Y | 25 | | |
| CaO | 0.02 | Zr | 86 | | |
| Na ₂ O | 0.50 | C | 3.66 | Organics analysed | |
| K ₂ O | 1.69 | Ro | | | |
| LOI | 7.54 | log Rv | 3.816 | | |

Sample HCL-5

Locality Hartfell

Grid reference NT 094115

Stratigraphic unit Lower Hartfell Shales

Zone clingani

Collected by SWW

Analysed by SWW

Description Platy black shale

| | | | | | |
|--------------------------------|-------|--------|-------|-------------------|------|
| SiO ₂ | 85.72 | Cu | 18 | Albite | 3.0 |
| TiO ₂ | 0.29 | Pb | 39 | Chlorite | 2.5 |
| Al ₂ O ₃ | 4.74 | Zn | 0 | Sericite | 7.5 |
| Fe ₂ O ₃ | 0.53 | Rb | 62 | Pyrite | 4.6 |
| MnO | 0.00 | Sr | 29 | Quartz | 85.4 |
| MgO | 0.36 | Y | 18 | | |
| CaO | 0.02 | Zr | 61 | | |
| Na ₂ O | 0.34 | C | 3.40 | Organics analysed | |
| K ₂ O | 0.98 | Ro | 4.80 | | |
| LOI | 6.87 | log Rv | 3.333 | | |

Sample HCL-6

Locality Hartfell

Grid reference NT 094115

Stratigraphic unit Lower Hartfell Shales

Zone clingani

Collected by SWW

Analysed by SWW

Description Pyritised cleaved black mudstone

| | | | | | |
|--------------------------------|-------|--------|-------|-------------------|--|
| SiO ₂ | 85.53 | Cu | 3 | Albite | |
| TiO ₂ | 0.42 | Pb | 32 | Chlorite | |
| Al ₂ O ₃ | 6.82 | Zn | 1 | Sericite | |
| Fe ₂ O ₃ | 0.54 | Rb | 61 | Pyrite | |
| MnO | 0.00 | Sr | 160 | Quartz | |
| MgO | 0.37 | Y | 29 | | |
| CaO | 0.03 | Zr | 75 | | |
| Na ₂ O | 0.41 | C | 1.85 | Organics analysed | |
| K ₂ O | 1.22 | Ro | 4.97 | | |
| LOI | 4.35 | log Rb | 5.622 | | |

Sample HCL-7

Locality Hartfell

Grid reference NT 094115

Stratigraphic unit Lower Hartfell Shales

Zone clingani

Collected by SWW

Analysed by SWW

Description Thin intercalations of black graptolitic shale within black mudstone

| | | | | | |
|--------------------------------|-------|--------|-------|----------|------|
| SiO ₂ | 84.12 | Cu | 36 | Albite | 1.9 |
| TiO ₂ | | Pb | 26 | Chlorite | 3.8 |
| Al ₂ O ₃ | 6.52 | Zn | 2 | Sericite | 14.3 |
| Fe ₂ O ₃ | | Rb | 56 | Pyrite | 5.7 |
| MnO | | Sr | 47 | Quartz | 74.4 |
| MgO | 0.53 | Y | 30 | | |
| CaO | | Zr | 85 | | |
| Na ₂ O | | C | 1.72 | Organics | |
| K ₂ O | | Ro | 3.82 | | |
| LOI | | log Rv | 4.000 | | |

Sample HCL-8

Locality Hartfell

Grid reference NT 094115

Stratigraphic unit Lower Hartfell Shales

Zone clingani

Collected by SWW

Analysed by SWW

Description Blocky black mudstone

| | | | | | |
|--------------------------------|-------|--------|-------|----------|------|
| SiO ₂ | 87.47 | Cu | 30 | Albite | 0.6 |
| TiO ₂ | | Pb | 21 | Chlorite | 3.1 |
| Al ₂ O ₃ | 4.79 | Zn | 0 | Sericite | 8.5 |
| Fe ₂ O ₃ | | Rb | 53 | Pyrite | 4.3 |
| MnO | | Sr | 42 | Quartz | 83.6 |
| MgO | 0.36 | Y | 13 | | |
| CaO | | Zr | 62 | | |
| Na ₂ O | | C | 3.63 | Organics | |
| K ₂ O | | Ro | 4.01 | | |
| LOI | | log Rv | 3.635 | | |

Sample HCL-9
 Locality Hartfell
 Grid reference NT 094115
 Stratigraphic unit Lower Hartfell Shales
 Zone clingani
 Collected by SWW
 Analysed by SWW
 Description Cherty graphitic mudstone

| | | | | | |
|--------------------------------|-------|--------|-------|----------|------|
| SiO ₂ | 87.79 | Cu | 27 | Albite | 1.4 |
| TiO ₂ | | Pb | 18 | Chlorite | 4.1 |
| Al ₂ O ₃ | 4.56 | Zn | 0 | Sericite | 8.9 |
| Fe ₂ O ₃ | | Rb | 47 | Pyrite | 5.0 |
| MnO | | Sr | 25 | Quartz | 80.7 |
| MgO | 0.33 | Y | 5 | | |
| CaO | | Zr | 47 | | |
| Na ₂ O | | C | 1.52 | Organics | |
| K ₂ O | | Ro | 4.47 | | |
| LOI | | log Rv | 5.195 | | |

Sample HCL-10
 Locality Hartfell
 Grid reference NT 094115
 Stratigraphic unit Lower Hartfell Shales
 Zone clingani
 Collected by SWW
 Analysed by SWW
 Description Cherty black mudstone with comminuted graptolite fragments

| | | | | | |
|--------------------------------|-------|--------|-------|----------|------|
| SiO ₂ | 87.26 | Cu | 28 | Albite | 2.4 |
| TiO ₂ | | Pb | 17 | Chlorite | 3.2 |
| Al ₂ O ₃ | 5.68 | Zn | 1 | Sericite | 7.4 |
| Fe ₂ O ₃ | | Rb | 56 | Pyrite | 5.1 |
| MnO | | Sr | 21 | Quartz | 82.0 |
| MgO | 0.44 | Y | 11 | | |
| CaO | | Zr | 61 | | |
| Na ₂ O | | C | 2.23 | Organics | |
| K ₂ O | | Ro | 4.10 | | |
| LOI | | log Rv | 4.806 | | |

Sample HCL-11

Locality Hartfell

Grid reference NT 094115

Stratigraphic unit Lower Hartfell Shales

Zone clingani

Collected by SWW

Analysed by SWW

Description Blocky black graptolitic mudstone

| | | | | | |
|--------------------------------|-------|--------|-------|----------|----------|
| SiO ₂ | 87.59 | Cu | 29 | Albite | 1.7 |
| TiO ₂ | | Pb | 22 | Chlorite | 2.3 |
| Al ₂ O ₃ | 5.51 | Zn | 1 | Sericite | 8.0 |
| Fe ₂ O ₃ | | Rb | 60 | Pyrite | 4.7 |
| MnO | | Sr | 20 | Quartz | 83.3 |
| MgO | 0.43 | Y | 12 | | |
| CaO | | Zr | 60 | | |
| Na ₂ O | | C | 2.11 | Organics | analysed |
| K ₂ O | | Ro | 2.42 | | |
| LOI | | log Rv | 5.013 | | |

Sample HCL-12

Locality Hartfell

Grid reference NT 094115

Stratigraphic unit Lower Hartfell Shales

Zone clingani

Collected by SWW

Analysed by SWW

Description Laminated pyritous black mudstone

| | | | | | |
|--------------------------------|-------|--------|-------|----------|------|
| SiO ₂ | 89.18 | Cu | 29 | Albite | 1.5 |
| TiO ₂ | | Pb | 21 | Chlorite | 3.6 |
| Al ₂ O ₃ | 5.50 | Zn | 1 | Sericite | 7.3 |
| Fe ₂ O ₃ | | Rb | 25 | Pyrite | 4.6 |
| MnO | | Sr | 26 | Quartz | 83.0 |
| MgO | 0.38 | Y | 0 | | |
| CaO | | Zr | 64 | | |
| Na ₂ O | | C | 1.48 | Organics | |
| K ₂ O | | Ro | 4.10 | | |
| LOI | | log Rv | 6.351 | | |

Sample HCL-13

Locality Hartfell

Grid reference NT 094115

Stratigraphic unit Lower Hartfell Shales

Zone clingani

Collected by SWW

Analysed by SWW

Description Black mudstone with intercalations of black graptolitic shale

| | | | | | |
|--------------------------------|-------|--------|-------|----------|------|
| SiO ₂ | 84.66 | Cu | 32 | Albite | 3.0 |
| TiO ₂ | | Pb | 29 | Chlorite | 2.4 |
| Al ₂ O ₃ | 5.75 | Zn | 0 | Sericite | 10.4 |
| Fe ₂ O ₃ | | Rb | 64 | Pyrite | 4.8 |
| MnO | | Sr | 59 | Quartz | 79.4 |
| MgO | 0.46 | Y | 39 | | |
| CaO | | Zr | 80 | | |
| Na ₂ O | | C | 2.68 | Organics | |
| K ₂ O | | Ro | 4.32 | | |
| LOI | | log Rv | 3.977 | | |

Sample HCL-14

Locality Hartfell

Grid reference NT 094115

Stratigraphic unit Lower Hartfell Shales

Zone clingani

Collected by SWW

Analysed by SWW

Description Black mudstone with intercalations of black graptolitic shale

| | | | | | |
|--------------------------------|-------|--------|-------|----------|------|
| SiO ₂ | 82.10 | Cu | 33 | Albite | 2.2 |
| TiO ₂ | | Pb | 27 | Chlorite | 3.0 |
| Al ₂ O ₃ | 6.94 | Zn | 3 | Sericite | 12.5 |
| Fe ₂ O ₃ | | Rb | 78 | Pyrite | 4.3 |
| MnO | | Sr | 85 | Quartz | 78.0 |
| MgO | 0.57 | Y | 16 | | |
| CaO | | Zr | 94 | | |
| Na ₂ O | | C | 3.99 | Organics | |
| K ₂ O | | Ro | 4.09 | | |
| LOI | | log Rv | 3.507 | | |

Sample HCL-15

Locality Hartfell

Grid reference NT 094115

Stratigraphic unit Lower Hartfell Shales

Zone clingani

Collected by SWW

Analysed by SWW

Description Laminated black graptolitic mudstone

| | | | | | |
|--------------------------------|-------|--------|-------|----------|------|
| SiO ₂ | 88.98 | Cu | 36 | Albite | 1.0 |
| TiO ₂ | | Pb | 22 | Chlorite | 3.6 |
| Al ₂ O ₃ | 4.76 | Zn | 0 | Sericite | 5.5 |
| Fe ₂ O ₃ | | Rb | 54 | Pyrite | 5.2 |
| MnO | | Sr | 31 | Quartz | 84.7 |
| MgO | 0.40 | Y | 13 | | |
| CaO | | Zr | 67 | | |
| Na ₂ O | | C | 1.23 | Organics | |
| K ₂ O | | Ro | 3.95 | | |
| LOI | | log Rv | 4.281 | | |

Sample HCL-16

Locality Hartfell

Grid reference NT 094115

Stratigraphic unit Lower Hartfell Shales

Zone clingani

Collected by SWW

Analysed by SWW

Description Badly cleaved graptolitic mudstone

| | | | | | |
|--------------------------------|-------|--------|-------|----------|------|
| SiO ₂ | 89.10 | Cu | 33 | Albite | 0.1 |
| TiO ₂ | | Pb | 28 | Chlorite | 2.8 |
| Al ₂ O ₃ | 4.55 | Zn | 1 | Sericite | 6.3 |
| Fe ₂ O ₃ | | Rb | 50 | Pyrite | 5.4 |
| MnO | | Sr | 58 | Quartz | 85.4 |
| MgO | 0.45 | Y | 10 | | |
| CaO | | Zr | 63 | | |
| Na ₂ O | | C | 2.40 | Organics | |
| K ₂ O | | Ro | 4.51 | | |
| LOI | | log Rv | 3.708 | | |

Sample HCL-17

Locality Hartfell

Grid reference NT 094115

Stratigraphic unit Lower Hartfell Shales

Zone clingani

Collected by SWW

Analysed by SWW

Description Cherty black mudstone rich in sulphur

| | | | | | |
|--------------------------------|-------|--------|-------|----------|------|
| SiO ₂ | 71.46 | Cu | 56 | Albite | 0.4 |
| TiO ₂ | | Pb | 25 | Chlorite | 2.1 |
| Al ₂ O ₃ | 4.06 | Zn | 2 | Sericite | 8.3 |
| Fe ₂ O ₃ | | Rb | 51 | Pyrite | 4.9 |
| MnO | | Sr | 63 | Quartz | 84.3 |
| MgO | 0.36 | Y | 7 | | |
| CaO | | Zr | 64 | | |
| Na ₂ O | | C | 2.00 | Organics | |
| K ₂ O | | Ro | 4.51 | | |
| LOI | | log Rv | 6.441 | | |

Sample HCL-18

Locality Hartfell

Grid reference NT 094115

Stratigraphic unit Lower Hartfell Shales

Zone clingani

Collected by SWW

Analysed by SWW

Description Badly cleaved cherty black mudstone

| | | | | | |
|--------------------------------|-------|--------|-------|----------|------|
| SiO ₂ | 87.13 | Cu | 30 | Albite | 0.8 |
| TiO ₂ | | Pb | 27 | Chlorite | 3.8 |
| Al ₂ O ₃ | 5.39 | Zn | 0 | Sericite | 7.4 |
| Fe ₂ O ₃ | | Rb | 57 | Pyrite | 4.4 |
| MnO | | Sr | 56 | Quartz | 83.6 |
| MgO | 0.47 | Y | 6 | | |
| CaO | | Zr | 71 | | |
| Na ₂ O | | C | 1.18 | Organics | |
| K ₂ O | | Ro | 4.20 | | |
| LOI | | log Rv | 5.777 | | |

Sample HCL-19

Locality Hartfell

Grid reference NT 094115

Stratigraphic unit Lower Hartfell Shales

Zone clingani

Collected by SWW

Analysed by SWW

Description Cleaved black graptolitic mudstone

| | | | | | |
|--------------------------------|-------|--------|-------|----------|------|
| SiO ₂ | 85.24 | Cu | 0 | Albite | 0.5 |
| TiO ₂ | | Pb | 22 | Chlorite | 4.5 |
| Al ₂ O ₃ | 5.42 | Zn | 2 | Sericite | 7.2 |
| Fe ₂ O ₃ | | Rb | 56 | Pyrite | 5.8 |
| MnO | | Sr | 88 | Quartz | 81.9 |
| MgO | 0.39 | Y | 12 | | |
| CaO | | Zr | 65 | | |
| Na ₂ O | | C | 2.39 | Organics | |
| K ₂ O | | Ro | 4.76 | | |
| LOI | | log Rv | 5.806 | | |

Sample HCL-20

Locality Hartfell

Grid reference NT 094115

Stratigraphic unit Lower Hartfell Shales

Zone clingani

Collected by SWW

Analysed by SWW

Description Pyritised cherty black mudstone

| | | | | | |
|--------------------------------|-------|--------|-------|----------|------|
| SiO ₂ | 90.21 | Cu | 35 | Albite | 0.7 |
| TiO ₂ | | Pb | 27 | Chlorite | 4.4 |
| Al ₂ O ₃ | 5.19 | Zn | 1 | Sericite | 8.6 |
| Fe ₂ O ₃ | | Rb | 53 | Pyrite | 5.2 |
| MnO | | Sr | 53 | Quartz | 81.1 |
| MgO | 0.36 | Y | 4 | | |
| CaO | | Zr | 60 | | |
| Na ₂ O | | C | 1.19 | Organics | |
| K ₂ O | | Ro | 4.89 | | |
| LOI | | log Rv | 7.308 | | |

Sample HCL-21

Locality Hartfell

Grid reference NT 094115

Stratigraphic unit Lower Hartfell Shales

Zone clingani

Collected by SWW

Analysed by SWW

Description Badly cleaved cherty black mudstone

| | | | | | |
|--------------------------------|-------|--------|-------|----------|------|
| SiO ₂ | 87.62 | Cu | 41 | Albite | 0.0. |
| TiO ₂ | | Pb | 26 | Chlorite | 2.5 |
| Al ₂ O ₃ | 4.97 | Zn | 0 | Sericite | 6.3 |
| Fe ₂ O ₃ | | Rb | 59 | Pyrite | 4.9 |
| MnO | | Sr | 59 | Quartz | 86.4 |
| MgO | 0.38 | Y | 11 | | |
| CaO | | Zr | 60 | | |
| Na ₂ O | | C | 3.11 | Organics | |
| K ₂ O | | Ro | | | |
| LOI | | log Rv | 3.968 | | |

Sample HCL-22

Locality Hartfell

Grid reference NT 094115

Stratigraphic unit Lower Hartfell Shales

Zone clingani

Collected by SWW

Analysed by SWW

Description Pyritised blocky black mudstone

| | | | | | |
|--------------------------------|-------|--------|-------|----------|------|
| SiO ₂ | 86.70 | Cu | 51 | Albite | 1.3 |
| TiO ₂ | | Pb | 29 | Chlorite | 5.0 |
| Al ₂ O ₃ | 4.94 | Zn | 2 | Sericite | 8.5 |
| Fe ₂ O ₃ | | Rb | 52 | Pyrite | 5.9 |
| MnO | | Sr | 98 | Quartz | 79.3 |
| MgO | 0.33 | Y | 17 | | |
| CaO | | Zr | 65 | | |
| Na ₂ O | | C | 2.53 | Organics | |
| K ₂ O | | Ro | 4.75 | | |
| LOI | | log Rv | 4.248 | | |

Sample HCL-23

Locality Hartfell

Grid reference NT 094115

Stratigraphic unit Lower Hartfell Shales

Zone clingani

Collected by SWW

Analysed by SWW

Description Pyritised black shale with partings of ash

| | | | | | |
|--------------------------------|-------|--------|-------|----------|------|
| SiO ₂ | 63.62 | Cu | 42 | Albite | 4.6 |
| TiO ₂ | | Pb | 87 | Chlorite | 5.4 |
| Al ₂ O ₃ | 15.11 | Zn | 8 | Sericite | 15.4 |
| Fe ₂ O ₃ | | Rb | 119 | Pyrite | 10.5 |
| MnO | | Sr | 474 | Quartz | 64.2 |
| MgO | 0.94 | Y | 89 | | |
| CaO | | Zr | 278 | | |
| Na ₂ O | | C | 0.73 | Organics | |
| K ₂ O | | Ro | | | |
| LOI | | log Rv | 7.528 | | |

Sample HCL-24

Locality Hartfell

Grid reference NT 094115

Stratigraphic unit Lower Hartfell Shales

Zone clingani

Collected by SWW

Analysed by SWW

Description Cleaved platy black graptolitic shale

| | | | | | |
|--------------------------------|-------|--------|-------|----------|------|
| SiO ₂ | 85.78 | Cu | 39 | Albite | 0.8 |
| TiO ₂ | | Pb | 31 | Chlorite | 3.5 |
| Al ₂ O ₃ | 4.77 | Zn | 0 | Sericite | 7.2 |
| Fe ₂ O ₃ | | Rb | 54 | Pyrite | 5.3 |
| MnO | | Sr | 68 | Quartz | 83.2 |
| MgO | 0.36 | Y | 11 | | |
| CaO | | Zr | 58 | | |
| Na ₂ O | | C | 2.44 | Organics | |
| K ₂ O | | Ro | | | |
| LOI | | log Rv | 4.231 | | |

Sample HCL-25

Locality Hartfell

Grid reference NT 094115

Stratigraphic unit Lower Hartfell Shales

Zone clingani

Collected by SWW

Analysed by SWW

Description Slickensided and crushed cherty black mudstone

| | | | | | |
|--------------------------------|-------|--------|-------|----------|------|
| SiO ₂ | 86.27 | Cu | 39 | Albite | 0.1 |
| TiO ₂ | | Pb | 23 | Chlorite | 4.6 |
| Al ₂ O ₃ | 5.86 | Zn | 1 | Sericite | 9.0 |
| Fe ₂ O ₃ | | Rb | 62 | Pyrite | 4.8 |
| MnO | | Sr | 78 | Quartz | 81.5 |
| MgO | 0.42 | Y | 13 | | |
| CaO | | Zr | 70 | | |
| Na ₂ O | | C | 2.29 | Organics | |
| K ₂ O | | Ro | 4.98 | | |
| LOI | | log Rv | 4.838 | | |

Sample HCL-26

Locality Hartfell

Grid reference NT 094115

Stratigraphic unit Lower Hartfell Shales

Zone clingani

Collected by SWW

Analysed by SWW

Description Pyritised cherty black mudstone

| | | | | | |
|--------------------------------|-------|--------|-------|----------|------|
| SiO ₂ | 88.84 | Cu | 38 | Albite | 0.0 |
| TiO ₂ | | Pb | 26 | Chlorite | 4.7 |
| Al ₂ O ₃ | 3.81 | Zn | 0 | Sericite | 6.6 |
| Fe ₂ O ₃ | | Rb | 42 | Pyrite | 4.8 |
| MnO | | Sr | 60 | Quartz | 84.1 |
| MgO | 0.28 | Y | 6 | | |
| CaO | | Zr | 56 | | |
| Na ₂ O | | C | 2.17 | Organics | |
| K ₂ O | | Ro | 5.20 | | |
| LOI | | log Rv | 3.297 | | |

Sample HCL-27

Locality Hartfell

Grid reference NT 094115

Stratigraphic unit Lower Hartfell Shales

Zone clingani

Collected by SWW

Analysed by SWW

Description Blocky cherty black mudstone

| | | | | | |
|--------------------------------|-------|--------|-------|----------|------|
| SiO ₂ | 89.70 | Cu | 37 | Albite | 0.0 |
| TiO ₂ | | Pb | 22 | Chlorite | 2.6 |
| Al ₂ O ₃ | 5.94 | Zn | 1 | Sericite | 7.4 |
| Fe ₂ O ₃ | | Rb | 61 | Pyrite | 1.8 |
| MnO | | Sr | 67 | Quartz | 88.3 |
| MgO | 0.44 | Y | 12 | | |
| CaO | | Zr | 107 | | |
| Na ₂ O | | C | 1.91 | Organics | |
| K ₂ O | | Ro | 4.54 | | |
| LOI | | log Rv | 4.732 | | |

Sample HCL-28

Locality Hartfell

Grid reference NT 094115

Stratigraphic unit Lower Hartfell Shales

Zone clingani

Collected by SWW

Analysed by SWW

Description Thin parting of ash with fragments of black shale

| | | | | | |
|--------------------------------|-------|--------|-------|----------|------|
| SiO ₂ | 47.18 | Cu | 86 | Albite | 2.0 |
| TiO ₂ | | Pb | 88 | Chlorite | 3.2 |
| Al ₂ O ₃ | 15.57 | Zn | 10 | Sericite | 24.6 |
| Fe ₂ O ₃ | | Rb | 174 | Pyrite | 24.0 |
| MnO | | Sr | 141 | Quartz | 46.2 |
| MgO | 1.36 | Y | 135 | | |
| CaO | | Zr | 298 | | |
| Na ₂ O | | C | 0.55 | Organics | |
| K ₂ O | | Ro | | | |
| LOI | | log Rv | 7.763 | | |

Sample HCL-29

Locality Hartfell

Grid reference NT 094115

Stratigraphic unit Lower Hartfell Shales

Zone clingani

Collected by SWW

Analysed by SWW

Description Badly cleaved pyritised black mudstone

| | | | | | |
|--------------------------------|-------|--------|-------|----------|------|
| SiO ₂ | 84.64 | Cu | 36 | Albite | 1.8 |
| TiO ₂ | | Pb | 40 | Chlorite | 3.0 |
| Al ₂ O ₃ | 4.20 | Zn | 2 | Sericite | 7.6 |
| Fe ₂ O ₃ | | Rb | 92 | Pyrite | 5.1 |
| MnO | | Sr | 29 | Quartz | 82.6 |
| MgO | 0.38 | Y | 1 | | |
| CaO | | Zr | 70 | | |
| Na ₂ O | | C | 2.55 | Organics | |
| K ₂ O | | Ro | 4.41 | | |
| LOI | | log Rv | 3.846 | | |

Sample HCL-30

Locality Hartfell

Grid reference NT 094115

Stratigraphic unit Lower Hartfell Shales

Zone clingani

Collected by SWW

Analysed by SWW

Description Black mudstone with abundant pyrite crystals

| | | | | | |
|--------------------------------|-------|--------|-------|----------|------|
| SiO ₂ | 87.87 | Cu | 36 | Albite | 3.5 |
| TiO ₂ | | Pb | 33 | Chlorite | 1.6 |
| Al ₂ O ₃ | 4.84 | Zn | 1 | Sericite | 5.2 |
| Fe ₂ O ₃ | | Rb | 18 | Pyrite | 5.0 |
| MnO | | Sr | 119 | Quartz | 84.8 |
| MgO | 0.43 | Y | 18 | | |
| CaO | | Zr | 70 | | |
| Na ₂ O | | C | 2.17 | Organics | |
| K ₂ O | | Ro | 3.59 | | |
| LOI | | log Rv | 5.049 | | |

Sample HCL-31

Locality Hartfell

Grid reference NT 094115

Stratigraphic unit Lower Hartfell Shales

Zone clingani

Collected by SWW

Analysed by SWW

Description Pyritised cherty black mudstone

| | | | | | |
|--------------------------------|-------|--------|-------|----------|------|
| SiO ₂ | 88.38 | Cu | 38 | Albite | 0.0 |
| TiO ₂ | | Pb | 29 | Chlorite | 1.8 |
| Al ₂ O ₃ | 3.98 | Zn | 6 | Sericite | 5.6 |
| Fe ₂ O ₃ | | Rb | 48 | Pyrite | 4.8 |
| MnO | | Sr | 43 | Quartz | 87.9 |
| MgO | 0.35 | Y | 12 | | |
| CaO | | Zr | 63 | | |
| Na ₂ O | | C | 3.52 | Organics | |
| K ₂ O | | Ro | 4.72 | | |
| LOI | | log Rv | 6.785 | | |

Sample HCL-32

Locality Hartfell

Grid reference NT 094115

Stratigraphic unit Lower Hartfell Shales

Zone clingani

Collected by SWW

Analysed by SWW

Description Cherty black graptolitic mudstone rich in sulphur

| | | | | | |
|--------------------------------|-------|--------|-------|----------|------|
| SiO ₂ | 84.04 | Cu | 31 | Albite | 0.9 |
| TiO ₂ | | Pb | 26 | Chlorite | 3.0 |
| Al ₂ O ₃ | 6.33 | Zn | 3 | Sericite | 6.2 |
| Fe ₂ O ₃ | | Rb | 81 | Pyrite | 5.9 |
| MnO | | Sr | 42 | Quartz | 84.0 |
| MgO | 0.44 | Y | 26 | | |
| CaO | | Zr | 94 | | |
| Na ₂ O | | C | 2.60 | Organics | |
| K ₂ O | | Ro | 2.97 | | |
| LOI | | log Rv | 5.692 | | |

Sample HCL-33
 Locality Hartfell
 Grid reference NT 094115
 Stratigraphic unit Lower Hartfell Shales
 Zone clingani
 Collected by SWW
 Analysed by SWW
 Description Blocky black mudstone

| | | | | | |
|--------------------------------|-------|--------|-------|----------|------|
| SiO ₂ | 84.46 | Cu | 28 | Albite | 2.6 |
| TiO ₂ | | Pb | 23 | Chlorite | 2.8 |
| Al ₂ O ₃ | 5.98 | Zn | 0 | Sericite | 3.2 |
| Fe ₂ O ₃ | | Rb | 67 | Pyrite | 6.1 |
| MnO | | Sr | 39 | Quartz | 85.2 |
| MgO | 0.50 | Y | 21 | | |
| CaO | | Zr | 77 | | |
| Na ₂ O | | C | 2.07 | Organics | |
| K ₂ O | | Ro | 3.53 | | |
| LOI | | log Rv | 4.812 | | |

Sample HCL-34
 Locality Hartfell
 Grid reference NT 094115
 Stratigraphic unit Lower Hartfell Shales
 Zone clingani
 Collected by SWW
 Analysed by SWW
 Description Cleaved cherty black mudstone

| | | | | | |
|--------------------------------|-------|--------|-------|----------|------|
| SiO ₂ | 85.22 | Cu | 35 | Albite | 2.7 |
| TiO ₂ | | Pb | 24 | Chlorite | 3.5 |
| Al ₂ O ₃ | 6.07 | Zn | 1 | Sericite | 0.3 |
| Fe ₂ O ₃ | | Rb | 69 | Pyrite | 5.0 |
| MnO | | Sr | 41 | Quartz | 79.5 |
| MgO | 0.42 | Y | 18 | | |
| CaO | | Zr | 80 | | |
| Na ₂ O | | C | 3.67 | Organics | |
| K ₂ O | | Ro | 3.65 | | |
| LOI | | log Rv | 3.675 | | |

Sample HL-1

Locality Hartfell

Grid reference NT 094115

Stratigraphic unit Upper Hartfell Shales

Zone linearis

Collected by SWW

Analysed by SWW

Description Platy black graptolitic shale

| | | | | | |
|--------------------------------|-------|--------|-------|----------|----------|
| SiO ₂ | 92.30 | Cu | 33 | Albite | 2.3 |
| TiO ₂ | | Pb | 34 | Chlorite | 3.1 |
| Al ₂ O ₃ | 6.21 | Zn | 83 | Sericite | 8.1 |
| Fe ₂ O ₃ | | Rb | 63 | Pyrite | 5.7 |
| MnO | | Sr | 36 | Quartz | 80.8 |
| MgO | 0.55 | Y | 14 | | |
| CaO | | Zr | 75 | | |
| Na ₂ O | | C | 2.88 | Organics | analysed |
| K ₂ O | | Ro | 5.50 | | |
| LOI | | log Rv | 3.135 | | |

Sample HL-2

Locality Hartfell

Grid reference NT 094115

Stratigraphic unit Upper Hartfell Shales

Zone linearis

Collected by SWW

Analysed by SWW

Description Badly cleaved black mudstone

| | | | | | |
|--------------------------------|-------|--------|-------|----------|------|
| SiO ₂ | 80.79 | Cu | 36 | Albite | 1.7 |
| TiO ₂ | | Pb | 30 | Chlorite | 3.9 |
| Al ₂ O ₃ | 4.99 | Zn | 5 | Sericite | 12.4 |
| Fe ₂ O ₃ | | Rb | 70 | Pyrite | 4.8 |
| MnO | | Sr | 57 | Quartz | |
| MgO | 0.43 | Y | 16 | | |
| CaO | | Zr | 85 | | |
| Na ₂ O | | C | 3.44 | Organics | |
| K ₂ O | | Ro | | | |
| LOI | | log Rv | 3.438 | | |

Sample HL-3

Locality Hartfell

Grid reference NT 094115

Stratigraphic unit Upper Hartfell Shales

Zone linearis

Collected by SWW

Analysed by SWW

Description Blocky black mudstone

| | | | | | |
|--------------------------------|-------|--------|-------|----------|----------|
| SiO ₂ | 81.01 | Cu | 43 | Albite | 5.0 |
| TiO ₂ | | Pb | 58 | Chlorite | 5.0 |
| Al ₂ O ₃ | 8.89 | Zn | 6 | Sericite | 8.1 |
| Fe ₂ O ₃ | | Rb | 100 | Pyrite | 6.5 |
| MnO | | Sr | 33 | Quartz | 75.3 |
| MgO | 0.68 | Y | 33 | | |
| CaO | | Zr | 142 | | |
| Na ₂ O | | C | 4.73 | Organics | analysed |
| K ₂ O | | Ro | 4.50 | | |
| LOI | | log Rv | 4.007 | | |

Sample HL-4

Locality Hartfell

Grid reference NT 094115

Stratigraphic unit Upper Hartfell Shales

Zone linearis

Collected by SWW

Analysed by SWW

Description Badly cleaved black shale

| | | | | | |
|--------------------------------|-------|--------|-------|----------|------|
| SiO ₂ | 81.93 | Cu | 37 | Albite | 1.7 |
| TiO ₂ | | Pb | 27 | Chlorite | 4.9 |
| Al ₂ O ₃ | 8.36 | Zn | 1 | Sericite | 12.3 |
| Fe ₂ O ₃ | | Rb | 45 | Pyrite | 5.1 |
| MnO | | Sr | 25 | Quartz | 76.1 |
| MgO | 0.59 | Y | 11 | | |
| CaO | | Zr | 53 | | |
| Na ₂ O | | C | 3.54 | Organics | |
| K ₂ O | | Ro | 5.70 | | |
| LOI | | log Rv | 3.790 | | |

Sample HL-5
 Locality Hartfell
 Grid reference NT 094115
 Stratigraphic unit Upper Hartfell Shales
 Zone linearis
 Collected by SWW
 Analysed by SWW
 Description Badly cleaved black shale

| | | | | | |
|--------------------------------|-------|--------|-------|----------|------|
| SiO ₂ | 88.79 | Cu | 43 | Albite | 1.2 |
| TiO ₂ | | Pb | 22 | Chlorite | 4.0 |
| Al ₂ O ₃ | 5.19 | Zn | 2 | Sericite | 11.1 |
| Fe ₂ O ₃ | | Rb | 47 | Pyrite | 4.5 |
| MnO | | Sr | 102 | Quartz | 79.3 |
| MgO | 0.42 | Y | 16 | | |
| CaO | | Zr | 59 | | |
| Na ₂ O | | C | 1.92 | Organics | |
| K ₂ O | | Ro | 4.99 | | |
| LOI | | log Rv | 3.804 | | |

Sample HL-6
 Locality Hartfell
 Grid reference NT 094115
 Stratigraphic unit Upper Hartfell Shales
 Zone linearis
 Collected by SWW
 Analysed by SWW
 Description Friable black shale

| | | | | | |
|--------------------------------|-------|--------|-------|-------------------|------|
| SiO ₂ | 75.47 | Cu | 26 | Albite | 5.1 |
| TiO ₂ | 0.47 | Pb | 37 | Chlorite | 3.2 |
| Al ₂ O ₃ | 7.66 | Zn | 4 | Sericite | 11.4 |
| Fe ₂ O ₃ | 3.75 | Rb | 96 | Pyrite | 8.4 |
| MnO | 0.01 | Sr | 72 | Quartz | 71.9 |
| MgO | 0.54 | Y | 28 | | |
| CaO | 0.03 | Zr | 104 | | |
| Na ₂ O | 0.64 | C | 3.28 | Organics analysed | |
| K ₂ O | 1.44 | Ro | 4.48 | | |
| LOI | 9.89 | log Rv | 3.171 | | |

Sample HL-7
 Locality Hartfell
 Grid reference NT 094115
 Stratigraphic unit Upper Hartfell Shales
 Zone linearis
 Collected by SWW
 Analysed by SWW
 Description Friable graphitic shale

| | | | | | |
|--------------------------------|-------|--------|-------|----------|----------|
| SiO ₂ | 85.00 | Cu | 45 | Albite | 2.3 |
| TiO ₂ | 0.42 | Pb | 22 | Chlorite | 3.2 |
| Al ₂ O ₃ | 5.69 | Zn | 1 | Sericite | 2.0 |
| Fe ₂ O ₃ | 0.87 | Rb | 58 | Pyrite | 6.6 |
| MnO | 0.00 | Sr | 230 | Quartz | 85.9 |
| MgO | 0.36 | Y | 23 | | |
| CaO | 0.03 | Zr | 82 | | |
| Na ₂ O | 0.28 | C | 1.08 | Organics | analysed |
| K ₂ O | 1.31 | Ro | 5.24 | | |
| LOI | 5.68 | log Rv | 3.852 | | |

Sample HL-8
 Locality Hartfell
 Grid reference NT 094115
 Stratigraphic unit Upper Hartfell Shales
 Zone linearis
 Collected by SWW
 Analysed by SWW
 Description Friable graphitic shale

| | | | | | |
|--------------------------------|-------|--------|-------|----------|----------|
| SiO ₂ | 83.71 | Cu | 41 | Albite | 2.7 |
| TiO ₂ | | Pb | 21 | Chlorite | 4.8 |
| Al ₂ O ₃ | 9.05 | Zn | 5 | Sericite | 17.2 |
| Fe ₂ O ₃ | | Rb | 90 | Pyrite | 3.8 |
| MnO | | Sr | 314 | Quartz | 71.5 |
| MgO | 0.66 | Y | 27 | | |
| CaO | | Zr | 128 | | |
| Na ₂ O | | C | 1.87 | Organics | analysed |
| K ₂ O | | Ro | 4.92 | | |
| LOI | | log Rv | 7.255 | | |

Sample HL-9

Locality Hartfell

Grid reference NT 094115

Stratigraphic unit Upper Hartfell Shales

Zone linearis

Collected by SWW

Analysed by SWW

Description Badly cleaved friable black shale

| | | | | | |
|--------------------------------|-------|--------|-------|----------|----------|
| SiO ₂ | 84.53 | Cu | 55 | Albite | 2.6 |
| TiO ₂ | 0.51 | Pb | 15 | Chlorite | 5.0 |
| Al ₂ O ₃ | 8.25 | Zn | 3 | Sericite | 11.8 |
| Fe ₂ O ₃ | 0.51 | Rb | 87 | Pyrite | 4.2 |
| MnO | 0.00 | Sr | 201 | Quartz | 76.5 |
| MgO | 0.44 | Y | 21 | | |
| CaO | 0.03 | Zr | 140 | | |
| Na ₂ O | 0.18 | C | 1.97 | Organics | analysed |
| K ₂ O | 1.41 | Ro | 4.70 | | |
| LOI | 3.84 | log Rv | 7.593 | | |

Sample HL-10

Locality Hartfell

Grid reference NT 094115

Stratigraphic unit Upper Hartfell Shales

Zone linearis

Collected by SWW

Analysed by SWW

Description Platy pyritised black shale

| | | | | | |
|--------------------------------|-------|--------|------|----------|----------|
| SiO ₂ | 87.42 | Cu | 61 | Albite | 2.6 |
| TiO ₂ | 0.50 | Pb | 31 | Chlorite | 3.1 |
| Al ₂ O ₃ | 4.54 | Zn | 0 | Sericite | 9.2 |
| Fe ₂ O ₃ | 0.67 | Rb | 51 | Pyrite | 4.3 |
| MnO | 0.00 | Sr | 22 | Quartz | 80.8 |
| MgO | 0.30 | Y | 10 | | |
| CaO | 0.02 | Zr | 55 | | |
| Na ₂ O | 0.30 | C | 3.02 | Organics | analysed |
| K ₂ O | 1.04 | Ro | 4.36 | | |
| LOI | 4.91 | log Rv | 3.54 | | |

Sample HL-11

Locality Hartfell

Grid reference NT 094115

Stratigraphic unit Upper Hartfell Shales

Zone linearis

Collected by SWW

Analysed by SWW

Description Platy black shale

| | | | | | |
|--------------------------------|-------|--------|-------|----------|----------|
| SiO ₂ | 83.30 | Cu | 52 | Albite | 4.2 |
| TiO ₂ | 0.36 | Pb | 41 | Chlorite | 3.8 |
| Al ₂ O ₃ | 6.88 | Zn | 3 | Sericite | 10.6 |
| Fe ₂ O ₃ | 0.45 | Rb | 77 | Pyrite | 4.1 |
| MnO | 0.00 | Sr | 45 | Quartz | 77.3 |
| MgO | 0.42 | Y | 23 | | |
| CaO | 0.02 | Zr | 91 | | |
| Na ₂ O | 0.34 | C | 3.40 | Organics | analysed |
| K ₂ O | 1.30 | Ro | 4.95 | | |
| LOI | 6.91 | log Rv | 3.235 | | |

Sample HL-12

Locality Hartfell

Grid reference NT 094115

Stratigraphic unit Upper Hartfell Shales

Zone linearis

Collected by SWW

Analysed by SWW

Description Badly cleaved black mudstone

| | | | | | |
|--------------------------------|-------|--------|-------|----------|----------|
| SiO ₂ | 83.59 | Cu | 55 | Albite | 3.9 |
| TiO ₂ | 0.25 | Pb | 32 | Chlorite | 1.6 |
| Al ₂ O ₃ | 4.24 | Zn | 0 | Sericite | 9.1 |
| Fe ₂ O ₃ | 0.50 | Rb | 43 | Pyrite | 4.2 |
| MnO | 0.00 | Sr | 30 | Quartz | 81.3 |
| MgO | 0.22 | Y | 11 | | |
| CaO | 0.01 | Zr | 51 | | |
| Na ₂ O | 0.01 | C | 2.66 | Organics | analysed |
| K ₂ O | 5.75 | Ro | 5.62 | | |
| LOI | 5.35 | log Rv | 3.364 | | |

Sample HL-13

Locality Hartfell

Grid reference NT 094115

Stratigraphic unit Upper Hartfell Shales

Zone linearis

Collected by SWW

Analysed by SWW

Description Cleaved blocky black mudstone

| | | | | | |
|--------------------------------|-------|--------|-------|----------|----------|
| SiO ₂ | 85.80 | Cu | 28 | Albite | 4.6 |
| TiO ₂ | | Pb | 31 | Chlorite | 3.9 |
| Al ₂ O ₃ | 5.13 | Zn | 0 | Sericite | 2.3 |
| Fe ₂ O ₃ | | Rb | 63 | Pyrite | 5.2 |
| MnO | | Sr | 70 | Quartz | 84.0 |
| MgO | 0.35 | Y | 18 | | |
| CaO | | Zr | 67 | | |
| Na ₂ O | | C | 5.43 | Organics | analysed |
| K ₂ O | | Ro | 4.59 | | |
| LOI | | log Rv | 3.176 | | |

Sample HL-15

Locality Hartfell

Grid reference NT 094115

Stratigraphic unit Upper Hartfell Shales

Zone linearis

Collected by SWW

Analysed by SWW

Description Blocky black mudstone

| | | | | | |
|--------------------------------|-------|--------|-------|----------|----------|
| SiO ₂ | 81.75 | Cu | 22 | Albite | 3.8 |
| TiO ₂ | 0.51 | Pb | 46 | Chlorite | 3.0 |
| Al ₂ O ₃ | 5.30 | Zn | 0 | Sericite | 7.2 |
| Fe ₂ O ₃ | 0.45 | Rb | 64 | Pyrite | 4.5 |
| MnO | 0.00 | Sr | 95 | Quartz | 81.5 |
| MgO | 0.27 | Y | 22 | | |
| CaO | 0.00 | Zr | 79 | | |
| Na ₂ O | 0.01 | C | 5.28 | Organics | analysed |
| K ₂ O | 6.47 | Ro | 4.76 | | |
| LOI | 5.24 | log Rv | 3.825 | | |

Sample HL-16

Locality Hartfell

Grid reference NT 094115

Stratigraphic unit Upper Hartfell Shales

Zone linearis

Collected by SWW

Analysed by SWW

Description Platy pyritised black graptolitic shale

| | | | | | |
|--------------------------------|-------|--------|-------|----------|------|
| SiO ₂ | 72.00 | Cu | 47 | Albite | 3.4 |
| TiO ₂ | 0.46 | Pb | 57 | Chlorite | 4.7 |
| Al ₂ O ₃ | 8.21 | Zn | 7 | Sericite | 12.8 |
| Fe ₂ O ₃ | 0.55 | Rb | 95 | Pyrite | 4.0 |
| MnO | 0.00 | Sr | 31 | Quartz | 75.2 |
| MgO | 0.48 | Y | 29 | | |
| CaO | 0.01 | Zr | 114 | | |
| Na ₂ O | 0.14 | C | 2.74 | Organics | |
| K ₂ O | 10.29 | Ro | 4.55 | | |
| LOI | 7.86 | log Rv | 3.229 | | |

Sample HL-17

Locality Hartfell

Grid reference NT 094115

Stratigraphic unit Upper Hartfell Shales

Zone linearis

Collected by SWW

Analysed by SWW

Description Blocky black mudstone rich in sulphur

| | | | | | |
|--------------------------------|-------|--------|-------|----------|------|
| SiO ₂ | 85.77 | Cu | 41 | Albite | 0.7 |
| TiO ₂ | | Pb | 39 | Chlorite | 3.1 |
| Al ₂ O ₃ | 4.10 | Zn | 0 | Sericite | 3.4 |
| Fe ₂ O ₃ | | Rb | 44 | Pyrite | 5.4 |
| MnO | | Sr | 20 | Quartz | 87.4 |
| MgO | 0.29 | Y | 8 | | |
| CaO | | Zr | 49 | | |
| Na ₂ O | | C | 2.84 | Organics | |
| K ₂ O | | Ro | 3.38 | | |
| LOI | | log Rv | 3.561 | | |

Sample HC-1

Locality Hartfell

Grid reference NT 094115

Stratigraphic unit Upper Hartfell Shales

Zone complanatus

Collected by SWW

Analysed by SWW

Description Dark grey shale within dominant grey mudstone

| | | | | | |
|--------------------------------|-------|--------|-------|----------|----------|
| SiO ₂ | 69.04 | Cu | 90 | Albite | |
| TiO ₂ | | Pb | 26 | Chlorite | |
| Al ₂ O ₃ | 14.63 | Zn | 7 | Sericite | |
| Fe ₂ O ₃ | | Rb | 144 | Pyrite | |
| MnO | | Sr | 127 | Quartz | |
| MgO | 0.82 | Y | 47 | | |
| CaO | | Zr | 142 | | |
| Na ₂ O | | C | 0.88 | Organics | analysed |
| K ₂ O | | Ro | 5.59 | | |
| LOI | | log Rv | 7.851 | | |

Sample HC-2

Locality Hartfell

Grid reference NT 094115

Stratigraphic unit Upper Hartfell Shales

Zone complanatus

Collected by SWW

Analysed by SWW

Description Grey mudstone with intercalations of grey shale

| | | | | | |
|--------------------------------|-------|--------|-------|----------|------|
| SiO ₂ | 81.55 | Cu | 46 | Albite | 5.8 |
| TiO ₂ | | Pb | 27 | Chlorite | 4.2 |
| Al ₂ O ₃ | 11.54 | Zn | 4 | Sericite | 17.0 |
| Fe ₂ O ₃ | | Rb | 90 | Pyrite | 3.7 |
| MnO | | Sr | 80 | Quartz | 69.2 |
| MgO | 0.65 | Y | 48 | | |
| CaO | | Zr | 91 | | |
| Na ₂ O | | C | 0.16 | Organics | |
| K ₂ O | | Ro | | | |
| LOI | | log Rv | 7.714 | | |

Sample HC-3

Locality Hartfell

Grid reference NT 094115

Stratigraphic unit Upper Hartfell Shales

Zone complanatus

Collected by SWW

Analysed by SWW

Description Badly cleaved grey mudstone

| | | | | | |
|--------------------------------|-------|--------|-------|----------|------|
| SiO ₂ | 78.47 | Cu | 78 | Albite | 8.9 |
| TiO ₂ | | Pb | 12 | Chlorite | 4.4 |
| Al ₂ O ₃ | 10.25 | Zn | 4 | Sericite | 14.6 |
| Fe ₂ O ₃ | | Rb | 77 | Pyrite | 3.7 |
| MnO | | Sr | 79 | Quartz | 68.4 |
| MgO | 0.51 | Y | 25 | | |
| CaO | | Zr | 85 | | |
| Na ₂ O | | C | 0.08 | Organics | |
| K ₂ O | | Ro | | | |
| LOI | | log Rv | 7.547 | | |

Sample HC-4

Locality Hartfell

Grid reference NT 094115

Stratigraphic unit Upper Hartfell Shales

Zone complanatus

Collected by SWW

Analysed by SWW

Description Badly cleaved grey mudstone

| | | | | | |
|--------------------------------|-------|--------|-------|----------|------|
| SiO ₂ | 79.43 | Cu | 56 | Albite | 7.5 |
| TiO ₂ | | Pb | 23 | Chlorite | 3.9 |
| Al ₂ O ₃ | 9.44 | Zn | 5 | Sericite | 11.5 |
| Fe ₂ O ₃ | | Rb | 50 | Pyrite | 4.0 |
| MnO | | Sr | 51 | Quartz | 73.1 |
| MgO | 0.55 | Y | 31 | | |
| CaO | | Zr | 77 | | |
| Na ₂ O | | C | 0.11 | Organics | |
| K ₂ O | | Ro | | | |
| LOI | | log Rv | 7.578 | | |

Sample DCL-1

Locality Dobb's Linn

Grid reference NT 198159

Stratigraphic unit Lower Hartfell Shales

Zone clingani

Collected by SWW

Analysed by SWW

Description Blocky iron-stained black mudstone

| | | | | | |
|--------------------------------|-------|--------|-------|----------|----------|
| SiO ₂ | 82.95 | Cu | 38 | Albite | 1.6 |
| TiO ₂ | 0.31 | Pb | 29 | Chlorite | 3.0 |
| Al ₂ O ₃ | 4.89 | Zn | 7 | Sericite | 6.3 |
| Fe ₂ O ₃ | 1.84 | Rb | 72 | Pyrite | 5.4 |
| MnO | 0.01 | Sr | 35 | Quartz | 83.8 |
| MgO | 0.37 | Y | 31 | | |
| CaO | 0.04 | Zr | 86 | | |
| Na ₂ O | 1.81 | C | 1.81 | Organics | analysed |
| K ₂ O | 1.70 | Ro | 2.27 | | |
| LOI | 5.73 | log Rv | 7.534 | | |

Sample DL-1

Locality Dobb's Linn

Grid reference NT 198159

Stratigraphic unit Upper Hartfell Shales

Zone linearis

Collected by SWW

Analysed by SWW

Description Platy black graptolitic shale

| | | | | | |
|--------------------------------|-------|--------|-------|----------|--|
| SiO ₂ | 80.26 | Cu | 55 | Albite | |
| TiO ₂ | 0.72 | Pb | 45 | Chlorite | |
| Al ₂ O ₃ | 7.79 | Zn | 16 | Sericite | |
| Fe ₂ O ₃ | 0.97 | Rb | 125 | Pyrite | |
| MnO | 0.01 | Sr | 41 | Quartz | |
| MgO | 0.64 | Y | 35 | | |
| CaO | 0.03 | Zr | 137 | | |
| Na ₂ O | 0.56 | C | | Organics | |
| K ₂ O | 2.52 | Ro | | | |
| LOI | 6.20 | log Rv | 7.680 | | |

Sample DL-2

Locality Dobb's Linn

Grid reference NT 198159

Stratigraphic unit Upper Hartfell Shales

Zone linearis

Collected by SWW

Analysed by SWW

Description Platy black graptolitic shale

| | | | | |
|--------------------------------|-------|--------|-------|----------|
| SiO ₂ | 78.59 | Cu | 59 | Albite |
| TiO ₂ | 0.73 | Pb | 46 | Chlorite |
| Al ₂ O ₃ | 8.92 | Zn | 28 | Sericite |
| Fe ₂ O ₃ | 1.09 | Rb | 128 | Pyrite |
| MnO | 0.01 | Sr | 41 | Quartz |
| MgO | 0.69 | Y | 30 | |
| CaO | 0.07 | Zr | 143 | |
| Na ₂ O | 0.69 | C | 1.92 | Organics |
| K ₂ O | 2.46 | Ro | 2.60 | |
| LOI | 6.52 | log Rv | 7.817 | |

Sample DL-4

Locality Dobb's Linn

Grid reference NT 198159

Stratigraphic unit Upper Hartfell Shales

Zone linearis

Collected by SWW

Analysed by SWW

Description Platy black shale

| | | | | | |
|--------------------------------|-------|--------|-------|----------|----------|
| SiO ₂ | 81.85 | Cu | 34 | Albite | 2.0 |
| TiO ₂ | 0.62 | Pb | 42 | Chlorite | 3.3 |
| Al ₂ O ₃ | 6.96 | Zn | 10 | Sericite | 8.4 |
| Fe ₂ O ₃ | 0.85 | Rb | 98 | Pyrite | 4.8 |
| MnO | 0.01 | Sr | 37 | Quartz | 81.6 |
| MgO | 0.58 | Y | 33 | | |
| CaO | 0.03 | Zr | 125 | | |
| Na ₂ O | 0.50 | C | 3.29 | Organics | analysed |
| K ₂ O | 2.29 | Ro | 2.80 | | |
| LOI | 5.90 | log Rv | 7.064 | | |

Sample DL-5

Locality Dobb's Linn

Grid reference NT 198159

Stratigraphic unit Upper Hartfell Shales

Zone linearis

Collected by SWW

Analysed by SWW

Description Platy black graptolitic shale

| | | | | | |
|--------------------------------|-------|--------|-------|----------|------|
| SiO ₂ | 77.17 | Cu | 32 | Albite | 3.6 |
| TiO ₂ | 0.60 | Pb | 35 | Chlorite | 3.8 |
| Al ₂ O ₃ | 10.42 | Zn | 0 | Sericite | 12.3 |
| Fe ₂ O ₃ | 0.76 | Rb | 99 | Pyrite | 5.3 |
| MnO | 0.01 | Sr | 37 | Quartz | 75.1 |
| MgO | 0.93 | Y | 40 | | |
| CaO | 0.03 | Zr | 124 | | |
| Na ₂ O | 0.42 | C | 2.48 | Organics | |
| K ₂ O | 2.60 | Ro | 3.00 | | |
| LOI | 6.84 | log Rv | 7.911 | | |

Sample DC-1

Locality Dobb's Linn

Grid reference NT 198159

Stratigraphic unit Upper Hartfell Shales

Zone complanatus

Collected by SWW

Analysed by SWW

Description Grey mudstone

| | | | | | |
|--------------------------------|-------|--------|-------|-------------------|--|
| SiO ₂ | 58.61 | Cu | 103 | Albite | |
| TiO ₂ | 0.90 | Pb | 30 | Chlorite | |
| Al ₂ O ₃ | 16.87 | Zn | 102 | Sericite | |
| Fe ₂ O ₃ | 7.68 | Rb | 162 | Pyrite | |
| MnO | 0.26 | Sr | 88 | Quartz | |
| MgO | 3.60 | Y | 27 | | |
| CaO | 1.29 | Zr | 204 | | |
| Na ₂ O | 1.18 | C | 0.65 | Organics analysed | |
| K ₂ O | 3.80 | Ro | 4.65 | | |
| LOI | 5.68 | log Rv | 7.653 | | |

Sample DC-2

Locality Dobb's Linn

Grid reference NT 198159

Stratigraphic unit Upper Hartfell Shales

Zone complanatus

Collected by SWW

Analysed by SWW

Description Thin band of graptolitic black shale
(The complanatus Band)

| | | | | | |
|--------------------------------|--|--------|------|----------|----------|
| SiO ₂ | | Cu | 66 | Albite | 10.5 |
| TiO ₂ | | Pb | 75 | Chlorite | 4.1 |
| Al ₂ O ₃ | | Zn | 78 | Sericite | 19.1 |
| Fe ₂ O ₃ | | Rb | 134 | Pyrite | 7.9 |
| MnO | | Sr | 63 | Quartz | 58.4 |
| MgO | | Y | 19 | | |
| CaO | | Zr | 200 | | |
| Na ₂ O | | C | 1.56 | Organics | analysed |
| K ₂ O | | Ro | 3.20 | | |
| LOI | | log Rv | | | |

Sample DA-0

Locality Dobb's Linn

Grid reference NT 198159

Stratigraphic unit Upper Hartfell Shales

Zone anceps

Collected by SWW

Analysed by SWW

Description Thin band of black graptolitic shale at base of zone

| | | | | | |
|--------------------------------|-------|--------|-------|----------|------|
| SiO ₂ | 65.90 | Cu | 58 | Albite | 7.3 |
| TiO ₂ | 0.83 | Pb | 83 | Chlorite | 4.0 |
| Al ₂ O ₃ | 16.68 | Zn | 82 | Sericite | 18.0 |
| Fe ₂ O ₃ | 3.70 | Rb | 155 | Pyrite | 6.4 |
| MnO | 0.02 | Sr | 47 | Quartz | 64.2 |
| MgO | 1.72 | Y | 37 | | |
| CaO | 0.01 | Zr | 249 | | |
| Na ₂ O | 1.07 | C | 2.38 | Organics | |
| K ₂ O | 3.32 | Ro | | | |
| LOI | 6.69 | log Rv | 7.574 | | |

Sample DA-1

Locality Dobb's Linn

Grid reference NT 198159

Stratigraphic unit Upper Hartfell Shales

Zone anceps

Collected by SWW

Analysed by SWW

Description Thin band of black graptolitic shale. Next band up from DA-0

| | | | |
|--------------------------------|--------|------|----------|
| SiO ₂ | Cu | 47 | Albite |
| TiO ₂ | Pb | 94 | Chlorite |
| Al ₂ O ₃ | Zn | 83 | Sericite |
| Fe ₂ O ₃ | Rb | 151 | Pyrite |
| MnO | Sr | 45 | Quartz |
| MgO | Y | 23 | |
| CaO | Zr | 215 | |
| Na ₂ O | C | 2.70 | Organics |
| K ₂ O | Ro | 2.78 | |
| LOI | log Rv | | |

Sample DA-3

Locality Dobb's Linn

Grid reference NT 198159

Stratigraphic unit Upper Hartfell Shales

Zone anceps

Collected by SWW

Analysed by SWW

Description Blocky black mudstone from next band above DA-2

| | | | | | |
|--------------------------------|-------|--------|-------|----------|------|
| SiO ₂ | 62.26 | Cu | 19 | Albite | 6.1 |
| TiO ₂ | 0.69 | Pb | 128 | Chlorite | 4.6 |
| Al ₂ O ₃ | 13.67 | Zn | 90 | Sericite | 17.5 |
| Fe ₂ O ₃ | 6.02 | Rb | 150 | Pyrite | 10.8 |
| MnO | 0.03 | Sr | 46 | Quartz | 61.0 |
| MgO | 2.05 | Y | 31 | | |
| CaO | 0.04 | Zr | 182 | | |
| Na ₂ O | 1.26 | C | 0.16 | Organics | |
| K ₂ O | 2.67 | Ro | | | |
| LOI | 11.02 | log Rv | 7.786 | | |

Sample DA-4

Locality Dobb's Linn

Grid reference NT 198159

Stratigraphic unit Upper Hartfell Shales

Zone anceps

Collected by SWW

Analysed by SWW

Description Black graptolitic shale from next black band above DA-3

| | | | | | |
|--------------------------------|-------|--------|-------|----------|------|
| SiO ₂ | 61.30 | Cu | 77 | Albite | 13.4 |
| TiO ₂ | 0.77 | Pb | 154 | Chlorite | 2.3 |
| Al ₂ O ₃ | 19.47 | Zn | 46 | Sericite | 22.9 |
| Fe ₂ O ₃ | 2.52 | Rb | 199 | Pyrite | 4.1 |
| MnO | 0.01 | Sr | 55 | Quartz | 57.3 |
| MgO | 1.42 | Y | 38 | | |
| CaO | 0.04 | Zr | 228 | | |
| Na ₂ O | 1.73 | C | 2.32 | Organics | |
| K ₂ O | 4.14 | Ro | | | |
| LOI | 8.40 | log Rv | 7.735 | | |

Sample DPE-1

Locality Dobb's Linn

Grid reference NT 198159

Stratigraphic unit Lower Birkhill Shales

Zone persculptus

Collected by SWW

Analysed by SWW

Description Blocky black mudstone

| | | | | | |
|--------------------------------|-------|--------|-------|----------|------|
| SiO ₂ | 56.96 | Cu | 125 | Albite | 6.9 |
| TiO ₂ | 0.82 | Pb | 41 | Chlorite | 3.5 |
| Al ₂ O ₃ | 14.41 | Zn | 47 | Sericite | 15.6 |
| Fe ₂ O ₃ | 8.63 | Rb | 131 | Pyrite | 21.3 |
| MnO | 0.03 | Sr | 45 | Quartz | 52.7 |
| MgO | 2.26 | Y | 37 | | |
| CaO | 0.03 | Zr | 209 | | |
| Na ₂ O | 1.14 | C | 2.32 | Organics | |
| K ₂ O | 2.60 | Ro | 3.65 | | |
| LOI | 12.70 | log Rv | 7.673 | | |

Sample DPE-2

Locality Dobb's Linn

Grid reference NT 198159

Stratigraphic unit Lower Birkhill Shales

Zone perseulptus

Collected by SWW

Analysed by SWW

Description Blocky black mudstone

| | | | | | |
|--------------------------------|-------|--------|------|----------|----------|
| SiO ₂ | 69.00 | Cu | 35 | Albite | 8.0 |
| TiO ₂ | 0.77 | Pb | 118 | Chlorite | 4.1 |
| Al ₂ O ₃ | 14.84 | Zn | 56 | Sericite | 16.8 |
| Fe ₂ O ₃ | 2.93 | Rb | 144 | Pyrite | 6.5 |
| MnO | 0.02 | Sr | 42 | Quartz | 64.7 |
| MgO | 1.27 | Y | 35 | | |
| CaO | 0.02 | Zr | 242 | | |
| Na ₂ O | 1.37 | C | 1.51 | Organics | analysed |
| K ₂ O | 3.18 | Ro | 3.26 | | |
| LOI | 6.60 | log Rv | | | |

Sample DAC-1

Locality Dobb's Linn

Grid reference NT 198159

Stratigraphic unit Lower Birkhill Shales

Zone acuminatus

Collected by SWW

Analysed by SWW

Description Black graptolitic mudstone

| | | | | | |
|--------------------------------|-------|--------|-------|----------|----------|
| SiO ₂ | 68.35 | Cu | 75 | Albite | 14.6 |
| TiO ₂ | 0.78 | Pb | 30 | Chlorite | 3.8 |
| Al ₂ O ₃ | 11.12 | Zn | 35 | Sericite | 14.4 |
| Fe ₂ O ₃ | 4.85 | Rb | 136 | Pyrite | 9.1 |
| MnO | 0.02 | Sr | 50 | Quartz | 58.1 |
| MgO | 1.44 | Y | 20 | | |
| CaO | 0.05 | Zr | 183 | | |
| Na ₂ O | 1.03 | C | 0.72 | Organics | analysed |
| K ₂ O | 2.75 | Ro | 2.89 | | |
| LOI | 9.50 | log Rv | 7.418 | | |

Sample DVE-1

Locality Dobb's Linn

Grid reference NT 198159

Stratigraphic unit Lower Birkhill Shales

Zone vesciculosus

Collected by SWW

Analysed by SWW

Description Flaggy black mudstone

| | | | | | |
|--------------------------------|-------|--------|-------|----------|----------|
| SiO ₂ | 71.29 | Cu | 72 | Albite | 5.0 |
| TiO ₂ | 0.58 | Pb | 34 | Chlorite | 4.3 |
| Al ₂ O ₃ | 8.50 | Zn | 48 | Sericite | 10.7 |
| Fe ₂ O ₃ | 6.54 | Rb | 94 | Pyrite | 16.9 |
| MnO | 0.03 | Sr | 39 | Quartz | 63.2 |
| MgO | 2.61 | Y | 21 | | |
| CaO | 0.04 | Zr | 163 | | |
| Na ₂ O | 0.75 | C | 1.07 | Organics | analysed |
| K ₂ O | 1.85 | Ro | 3.39 | | |
| LOI | 7.80 | log Rv | 7.767 | | |

Sample DVE-2

Locality Dobb's Linn

Grid reference NT 198159

Stratigraphic unit Lower Birkhill Shales

Zone vesciculosus

Collected by SWW

Analysed by SWW

Description Black graptolitic mudstone

| | | | | | |
|--------------------------------|-------|--------|-------|----------|----------|
| SiO ₂ | 64.24 | Cu | 83 | Albite | |
| TiO ₂ | 0.76 | Pb | 37 | Chlorite | |
| Al ₂ O ₃ | 11.30 | Zn | 51 | Sericite | |
| Fe ₂ O ₃ | 7.59 | Rb | 106 | Pyrite | |
| MnO | 0.03 | Sr | 42 | Quartz | |
| MgO | 2.86 | Y | 22 | | |
| CaO | 0.02 | Zr | 177 | | |
| Na ₂ O | 1.65 | C | 1.48 | Organics | analysed |
| K ₂ O | 2.63 | Ro | 3.65 | | |
| LOI | 8.70 | log Rv | 7.551 | | |

Sample DCYP-1

Locality Dobb's Linn

Grid reference NT 198159

Stratigraphic unit Lower Birkhill Shales

Zone cyphus

Collected by SWW

Analysed by SWW

Description Blocky black mudstone

| | | | | | |
|--------------------------------|-------|--------|-------|----------|----------|
| SiO ₂ | 51.55 | Cu | 106 | Albite | 4.4 |
| TiO ₂ | 0.77 | Pb | 38 | Chlorite | 3.8 |
| Al ₂ O ₃ | 12.61 | Zn | 71 | Sericite | 16.7 |
| Fe ₂ O ₃ | 16.55 | Rb | 103 | Pyrite | 25.5 |
| MnO | 0.18 | Sr | 49 | Quartz | 49.7 |
| MgO | 3.02 | Y | 43 | | |
| CaO | 0.07 | Zr | 161 | | |
| Na ₂ O | 0.99 | C | 1.28 | Organics | analysed |
| K ₂ O | 2.87 | Ro | 4.04 | | |
| LOI | 11.14 | log Rv | 7.650 | | |

Sample DCYP-3A

Locality Dobb's Linn

Grid reference NT 198159

Stratigraphic unit Lower Birkhill Shales

Zone cyphus

Collected by SWW

Analysed by SWW

Description Bleached white soft crumbly material from 'claystone'
band

| | | | | | |
|--------------------------------|-------|--------|-------|----------|--|
| SiO ₂ | 46.40 | Cu | 99 | Albite | |
| TiO ₂ | | Pb | 36 | Chlorite | |
| Al ₂ O ₃ | 23.67 | Zn | 48 | Sericite | |
| Fe ₂ O ₃ | | Rb | 170 | Pyrite | |
| MnO | | Sr | 57 | Quartz | |
| MgO | 2.49 | Y | 139 | | |
| CaO | | Zr | 652 | | |
| Na ₂ O | | C | 0.26 | Organics | |
| K ₂ O | | Ro | | | |
| LOI | | log Rv | 7.642 | | |

Sample DCYP-3

Locality Dobb's Linn

Grid reference NT 198159

Stratigraphic unit Lower Birkhill Shales

Zone cyphus

Collected by SWW

Analysed by SWW

Description Pyritised black mudstone

| | | | | | |
|--------------------------------|-------|--------|-------|----------|------|
| SiO ₂ | 69.71 | Cu | 89 | Albite | 4.6 |
| TiO ₂ | | Pb | 29 | Chlorite | 4.3 |
| Al ₂ O ₃ | 10.11 | Zn | 35 | Sericite | 11.9 |
| Fe ₂ O ₃ | | Rb | 92 | Pyrite | 17.8 |
| MnO | | Sr | 38 | Quartz | 61.4 |
| MgO | 2.40 | Y | 16 | | |
| CaO | | Zr | 180 | | |
| Na ₂ O | | C | 1.95 | Organics | |
| K ₂ O | | Ro | 2.91 | | |
| LOI | | log Rv | 7.779 | | |

Sample DCYP-4

Locality Dobb's Linn

Grid reference NT 198159

Stratigraphic unit Lower Birkhill Shales

Zone cyphus

Collected by SWW

Analysed by SWW

Description Pyritised black mudstone rich in sulphur

| | | | | | |
|--------------------------------|-------|--------|-------|----------|------|
| SiO ₂ | 70.63 | Cu | 83 | Albite | 4.2 |
| TiO ₂ | | Pb | 33 | Chlorite | 4.4 |
| Al ₂ O ₃ | 10.47 | Zn | 42 | Sericite | 7.6 |
| Fe ₂ O ₃ | | Rb | 45 | Pyrite | 17.4 |
| MnO | | Sr | 16 | Quartz | 66.5 |
| MgO | 2.45 | Y | 40 | | |
| CaO | | Zr | 170 | | |
| Na ₂ O | | C | 0.86 | Organics | |
| K ₂ O | | Ro | 4.02 | | |
| LOI | | log Rv | 7.665 | | |

Sample DCYP-5

Locality Dobb's Linn

Grid reference NT 198159

Stratigraphic unit Lower Birkhill Shales

Zone cyphus

Collected by SWW

Analysed by SWW

Description Cleaved black graptolitic mudstone

| | | | | | |
|--------------------------------|-------|--------|-------|----------|------|
| SiO ₂ | 69.35 | Cu | 93 | Albite | 4.8 |
| TiO ₂ | | Pb | 34 | Chlorite | 4.3 |
| Al ₂ O ₃ | 10.22 | Zn | 38 | Sericite | 12.1 |
| Fe ₂ O ₃ | | Rb | 92 | Pyrite | 19.2 |
| MnO | | Sr | 39 | Quartz | 59.6 |
| MgO | 2.61 | Y | 20 | | |
| CaO | | Zr | 185 | | |
| Na ₂ O | | C | 0.95 | Organics | |
| K ₂ O | | Ro | 2.75 | | |
| LOI | | log Rv | 7.730 | | |

Sample DCYP-6

Locality Dobb's Linn

Grid reference NT 198159

Stratigraphic unit Lower Birkhill Shales

Zone cyphus

Collected by SWW

Analysed by SWW

Description Blocky black graptolitic mudstone

| | | | | | |
|--------------------------------|-------|--------|-------|----------|------|
| SiO ₂ | 61.10 | Cu | 107 | Albite | 6.8 |
| TiO ₂ | | Pb | 51 | Chlorite | 4.0 |
| Al ₂ O ₃ | 12.87 | Zn | 43 | Sericite | 13.1 |
| Fe ₂ O ₃ | | Rb | 114 | Pyrite | 21.3 |
| MnO | | Sr | 41 | Quartz | 54.7 |
| MgO | 3.08 | Y | 38 | | |
| CaO | | Zr | 301 | | |
| Na ₂ O | | C | 1.33 | Organics | |
| K ₂ O | | Ro | 3.59 | | |
| LOI | | log Rv | 7.679 | | |

Sample DCYP-7

Locality Dobb's Linn

Grid reference NT 198159

Stratigraphic unit Lower Birkhill Shales

Zone cyphus

Collected by SWW

Analysed by SWW

Description Black graptolitic mudstone below 'claystone' band

| | | | | | |
|--------------------------------|-------|--------|-------|----------|------|
| SiO ₂ | 63.77 | Cu | 72 | Albite | 7.3 |
| TiO ₂ | | Pb | 21 | Chlorite | 4.2 |
| Al ₂ O ₃ | 14.83 | Zn | 40 | Sericite | 13.9 |
| Fe ₂ O ₃ | | Rb | 109 | Pyrite | 16.9 |
| MnO | | Sr | 70 | Quartz | 57.8 |
| MgO | 3.13 | Y | 45 | | |
| CaO | | Zr | 331 | | |
| Na ₂ O | | C | 1.61 | Organics | |
| K ₂ O | | Ro | 2.58 | | |
| LOI | | log Rv | 7.778 | | |

Sample DCYP-8

Locality Dobb's Linn

Grid reference NT 198159

Stratigraphic unit Lower Birkhill Shales

Zone cyphus

Collected by SWW

Analysed by SWW

Description Blocky black mudstone

| | | | | | |
|--------------------------------|-------|--------|-------|----------|------|
| SiO ₂ | 62.95 | Cu | 93 | Albite | 5.4 |
| TiO ₂ | | Pb | 40 | Chlorite | 5.2 |
| Al ₂ O ₃ | 15.21 | Zn | 50 | Sericite | 20.2 |
| Fe ₂ O ₃ | | Rb | 125 | Pyrite | 11.9 |
| MnO | | Sr | 44 | Quartz | 57.4 |
| MgO | 3.47 | Y | 25 | | |
| CaO | | Zr | 285 | | |
| Na ₂ O | | C | 2.15 | Organics | |
| K ₂ O | | Ro | 3.33 | | |
| LOI | | log Rv | 7.648 | | |

Sample DCYP-9

Locality Dobb's Linn

Grid reference NT 198159

Stratigraphic unit Lower Birkhill Shales

Zone cyphus

Collected by SWW

Analysed by SWW

Description Pyritised blocky black mudstone

| | | | | |
|--------------------------------|-------|--------|-------|----------|
| SiO ₂ | 60.50 | Cu | 110 | Albite |
| TiO ₂ | | Pb | 55 | Chlorite |
| Al ₂ O ₃ | 13.10 | Zn | 38 | Sericite |
| Fe ₂ O ₃ | | Rb | 114 | Pyrite |
| MnO | | Sr | 46 | Quartz |
| MgO | 2.75 | Y | 39 | |
| CaO | | Zr | 262 | |
| Na ₂ O | | C | 3.41 | Organics |
| K ₂ O | | Ro | 3.67 | |
| LOI | | log Rv | 7.792 | |

Sample DCYP-9A

Locality Dobb's Linn

Grid reference NT 198159

Stratigraphic unit Lower Birkhill Shales

Zone cyphus

Collected by SWW

Analysed by SWW

Description Bleached white soft material from 'claystone' band

| | | | | |
|--------------------------------|-------|--------|-------|----------|
| SiO ₂ | 54.66 | Cu | 157 | Albite |
| TiO ₂ | | Pb | 52 | Chlorite |
| Al ₂ O ₃ | 17.96 | Zn | 17 | Sericite |
| Fe ₂ O ₃ | | Rb | 153 | Pyrite |
| MnO | | Sr | 40 | Quartz |
| MgO | 2.72 | Y | 79 | |
| CaO | | Zr | 466 | |
| Na ₂ O | | C | 1.55 | Organics |
| K ₂ O | | Ro | | |
| LOI | | log Rv | 7.828 | |

Sample DCYP-10

Locality Dobb's Linn

Grid reference NT 198159

Stratigraphic unit Lower Birkhill Shales

Zone cyphus

Collected by SWW

Analysed by SWW

Description Pyritised blocky black mudstone

| | | | | | |
|--------------------------------|-------|--------|-------|----------|------|
| SiO ₂ | 63.77 | Cu | 81 | Albite | 4.3 |
| TiO ₂ | | Pb | 33 | Chlorite | 4.3 |
| Al ₂ O ₃ | 13.07 | Zn | 44 | Sericite | 15.5 |
| Fe ₂ O ₃ | | Rb | 106 | Pyrite | 14.8 |
| MnO | | Sr | 43 | Quartz | 61.1 |
| MgO | 3.11 | Y | 29 | | |
| CaO | | Zr | 253 | | |
| Na ₂ O | | C | 1.41 | Organics | |
| K ₂ O | | Ro | 3.24 | | |
| LOI | | log Rv | 7.723 | | |

Sample DCYP-11

Locality Dobb's Linn

Grid reference NT 198159

Stratigraphic unit Lower Birkhill Shales

Zone cyphus

Collected by SWW

Analysed by SWW

Description Pyritised black graptolitic mudstone

| | | | | | |
|--------------------------------|-------|--------|-------|----------|------|
| SiO ₂ | 52.45 | Cu | 142 | Albite | 5.3 |
| TiO ₂ | | Pb | 47 | Chlorite | 6.6 |
| Al ₂ O ₃ | 12.48 | Zn | 57 | Sericite | 15.6 |
| Fe ₂ O ₃ | | Rb | 90 | Pyrite | 28.3 |
| MnO | | Sr | 34 | Quartz | 44.2 |
| MgO | 3.08 | Y | 17 | | |
| CaO | | Zr | 171 | | |
| Na ₂ O | | C | 1.53 | Organics | |
| K ₂ O | | Ro | 3.82 | | |
| LOI | | log Rv | 7.691 | | |

Sample DCYP-12

Locality Dobb's Linn

Grid reference NT 198159

Stratigraphic unit Lower Birkhill Shales

Zone cyphus

Collected by SWW

Analysed by SWW

Description Pyritised blocky black mudstone rich in sulphur

| | | | | |
|--------------------------------|--------|-------|----------|------|
| SiO ₂ | Cu | 143 | Albite | 4.2 |
| TiO ₂ | Pb | 46 | Chlorite | 3.7 |
| Al ₂ O ₃ | Zn | 45 | Sericite | 12.6 |
| Fe ₂ O ₃ | Rb | 91 | Pyrite | 29.9 |
| MnO | Sr | 31 | Quartz | 49.7 |
| MgO | Y | 24 | | |
| CaO | Zr | 185 | | |
| Na ₂ O | C | 0.72 | Organics | |
| K ₂ O | Ro | 2.72 | | |
| LOI | log Rv | 7.679 | | |

Sample DCYP-13

Locality Dobb's Linn

Grid reference NT 198159

Zone cyphus

Collected by SWW

Analysed by SWW

Description Pyritised black mudstone

| | | | | |
|--------------------------------|--------|-------|----------|--|
| SiO ₂ | Cu | 90 | Albite | |
| TiO ₂ | Pb | 45 | Chlorite | |
| Al ₂ O ₃ | Zn | 79 | Sericite | |
| Fe ₂ O ₃ | Rb | 127 | Pyrite | |
| MnO | Sr | 43 | Quartz | |
| MgO | Y | 38 | | |
| CaO | Zr | 214 | | |
| Na ₂ O | C | 1.91 | Organics | |
| K ₂ O | Ro | 2.77 | | |
| LOI | log Rv | 7.793 | | |

Sample DGR-1

Locality Dobb's Linn

Grid reference NT 198159

Stratigraphic unit Upper Birkhill Shales

Zone gregarius

Collected by SWW

Analysed by SWW

Description Blocky black mudstone

| | | | | | |
|--------------------------------|-------|--------|-------|----------|----------|
| SiO ₂ | 51.89 | Cu | 115 | Albite | 6.9 |
| TiO ₂ | 0.64 | Pb | 81 | Chlorite | 4.4 |
| Al ₂ O ₃ | 14.94 | Zn | 126 | Sericite | 19.2 |
| Fe ₂ O ₃ | 15.25 | Rb | 106 | Pyrite | 21.0 |
| MnO | 0.06 | Sr | 43 | Quartz | 48.5 |
| MgO | 3.73 | Y | 25 | | |
| CaO | 0.30 | Zr | 201 | | |
| Na ₂ O | 0.87 | C | 1.99 | Organics | analysed |
| K ₂ O | 2.50 | Ro | 2.60 | | |
| LOI | 9.80 | log Rv | 7.611 | | |

Sample DCV-1

Locality Dobb's Linn

Grid reference NT 198159

Stratigraphic unit Upper Birkhill Shales

Zone convolutus

Collected by SWW

Analysed by SWW

Description Black mudstone

| | | | | | |
|--------------------------------|-------|--------|-------|----------|------|
| SiO ₂ | 53.66 | Cu | 126 | Albite | 8.0 |
| TiO ₂ | 0.84 | Pb | 54 | Chlorite | 4.4 |
| Al ₂ O ₃ | 16.97 | Zn | 85 | Sericite | 19.3 |
| Fe ₂ O ₃ | 10.53 | Rb | 126 | Pyrite | 21.1 |
| MnO | 0.16 | Sr | 47 | Quartz | 47.2 |
| MgO | 3.39 | Y | 33 | | |
| CaO | 0.12 | Zr | 242 | | |
| Na ₂ O | 1.14 | C | 3.02 | Organics | |
| K ₂ O | 3.76 | Ro | 3.51 | | |
| LOI | 9.11 | log Rv | 6.976 | | |

Sample DCV-2

Locality Dobb's Linn

Grid reference NT 198159

Stratigraphic unit Upper Birkhill Shales

Zone convolutus

Collected by SWW

Analysed by SWW

Description Black graptolitic mudstone

| | | | | | |
|--------------------------------|-------|--------|-------|----------|----------|
| SiO ₂ | 49.06 | Cu | 162 | Albite | |
| TiO ₂ | 0.93 | Pb | 60 | Chlorite | |
| Al ₂ O ₃ | 18.33 | Zn | 78 | Sericite | |
| Fe ₂ O ₃ | 11.82 | Rb | 131 | Pyrite | |
| MnO | 0.05 | Sr | 52 | Quartz | |
| MgO | 3.11 | Y | 45 | | |
| CaO | 0.05 | Zr | 259 | | |
| Na ₂ O | 1.50 | C | 1.46 | Organics | analysed |
| K ₂ O | 3.09 | Ro | 4.64 | | |
| LOI | 11.36 | log Rv | 7.650 | | |

Sample DCV-3

Locality Dobb's Linn

Grid reference NT 198159

Stratigraphic unit Upper Birkhill Shales

Zone convolutus

Collected by SWW

Analysed by SWW

Description Pyritised grey mudstone

| | | | | | |
|--------------------------------|-------|--------|-------|----------|------|
| SiO ₂ | 61.53 | Cu | 50 | Albite | 9.2 |
| TiO ₂ | 0.77 | Pb | 20 | Chlorite | 7.1 |
| Al ₂ O ₃ | 15.70 | Zn | 99 | Sericite | 18.1 |
| Fe ₂ O ₃ | 9.04 | Rb | 116 | Pyrite | 7.9 |
| MnO | 0.31 | Sr | 54 | Quartz | 57.8 |
| MgO | 4.45 | Y | 47 | | |
| CaO | 0.32 | Zr | 274 | | |
| Na ₂ O | 0.89 | C | 0.89 | Organics | |
| K ₂ O | 2.41 | Ro | | | |
| LOI | 4.65 | log Rv | 7.564 | | |

Sample DSE-1

Locality Dobb's Linn

Grid reference NT 198159

Stratigraphic unit Upper Birkhill Shales

Zone sedgwickii

Collected by SWW

Analysed by SWW

Description Grey mudstone

| | | | | | |
|--------------------------------|-------|--------|-------|----------|----------|
| SiO ₂ | 47.64 | Cu | 106 | Albite | 3.3 |
| TiO ₂ | 0.45 | Pb | 244 | Chlorite | 2.2 |
| Al ₂ O ₃ | 11.73 | Zn | 105 | Sericite | 7.5 |
| Fe ₂ O ₃ | 18.37 | Rb | 72 | Pyrite | 5.0 |
| MnO | 0.05 | Sr | 42 | Quartz | 82.0 |
| MgO | 2.73 | Y | 15 | | |
| CaO | 0.25 | Zr | 127 | | |
| Na ₂ O | 0.85 | C | 1.76 | Organics | analysed |
| K ₂ O | 2.00 | Ro | 3.68 | | |
| LOI | 15.93 | log Rv | 7.310 | | |

Sample DMAX-1

Locality Dobb's Linn

Grid reference NT 198159

Stratigraphic unit Upper Birkhill Shales

Zone maximus

Collected by SWW

Analysed by SWW

Description Hard grey mudstone

| | | | | | |
|--------------------------------|-------|--------|-------|----------|----------|
| SiO ₂ | 56.86 | Cu | 211 | Albite | 9.9 |
| TiO ₂ | 0.84 | Pb | 104 | Chlorite | 7.7 |
| Al ₂ O ₃ | 20.19 | Zn | 113 | Sericite | 17.7 |
| Fe ₂ O ₃ | 7.26 | Rb | 147 | Pyrite | 4.1 |
| MnO | 0.28 | Sr | 64 | Quartz | 60.7 |
| MgO | 3.72 | Y | 26 | | |
| CaO | 0.59 | Zr | 230 | | |
| Na ₂ O | 2.06 | C | 0.59 | Organics | analysed |
| K ₂ O | 3.05 | Ro | 4.21 | | |
| LOI | 5.10 | log Rv | 7.805 | | |

Sample 1E-1

Locality Dobb's Linn

Grid reference NT 198159

Stratigraphic unit Lower Birkhill Shales

Zone persculptus

Collected by WES and JAW

Analysed by EX and SWW

Description Grey mudstone

| | | | | |
|--------------------------------|-------|--------|-------|-------------------|
| SiO ₂ | 56.93 | Cu | 46 | Albite |
| TiO ₂ | 0.82 | Pb | 47 | Chlorite |
| Al ₂ O ₃ | 12.67 | Zn | 174 | Sericite |
| Fe ₂ O ₃ | 7.45 | Rb | 118 | Pyrite |
| MnO | 0.33 | Sr | 101 | Quartz |
| MgO | 5.32 | Y | 35 | |
| CaO | 4.27 | Zr | 194 | |
| Na ₂ O | 1.08 | C | 0.99 | Organics analysed |
| K ₂ O | 2.81 | Ro | 2.45 | |
| LOI | 8.06 | log Rv | 7.547 | |

Sample 2-1

Locality Dobb's Linn

Grid reference NT 198159

Stratigraphic unit Upper Hartfell Shales

Zone complanatus

Collected by WES and JAW

Analysed by EX and SWW

Description Black graptolitic shale from complanatus Band

| | | | | |
|--------------------------------|-------|--------|------|----------|
| SiO ₂ | 53.99 | Cu | 198 | Albite |
| TiO ₂ | 0.77 | Pb | 92 | Chlorite |
| Al ₂ O ₃ | 14.62 | Zn | 93 | Sericite |
| Fe ₂ O ₃ | 8.55 | Rb | 121 | Pyrite |
| MnO | 0.05 | Sr | 42 | Quartz |
| MgO | 3.19 | Y | 35 | |
| CaO | 0.15 | Zr | 174 | |
| Na ₂ O | 0.98 | C | 3.61 | Organics |
| K ₂ O | 3.06 | Ro | 2.67 | |
| LOI | 14.36 | log Rv | | |

Sample GK-4

Locality Glenkiln

Grid reference NY 006895

Stratigraphic unit Glenkiln Shales

Zone

Collected by WES, SWW and JAW

Analysed by EX and SWW

Description Black mudstone

| | | | | | |
|--------------------------------|-------|--------|----|----------|------|
| SiO ₂ | 84.42 | Cu | 32 | Albite | 3.2 |
| TiO ₂ | 0.42 | Pb | 33 | Chlorite | 1.6 |
| Al ₂ O ₃ | 7.45 | Zn | 4 | Sericite | 7.3 |
| Fe ₂ O ₃ | 1.13 | Rb | 78 | Pyrite | 4.9 |
| MnO | 0.02 | Sr | 31 | Quartz | 83.0 |
| MgO | 0.39 | Y | 30 | | |
| CaO | 0.02 | Zr | 73 | | |
| Na ₂ O | 0.87 | C | | Organics | |
| K ₂ O | 1.91 | Ro | | | |
| LOI | | log Rv | | | |

Sample GK-5

Locality Glenkiln

Grid reference NY 006895

Stratigraphic unit Glenkiln Shales

Zone

Collected by WES, SWW and JAW

Analysed by EX and SWW

Description Black mudstone

| | | | | | |
|--------------------------------|-------|--------|----|----------|------|
| SiO ₂ | 81.10 | Cu | 35 | Albite | 4.2 |
| TiO ₂ | 0.43 | Pb | 34 | Chlorite | 2.9 |
| Al ₂ O ₃ | 8.90 | Zn | 4 | Sericite | 11.3 |
| Fe ₂ O ₃ | 0.71 | Rb | 91 | Pyrite | 4.5 |
| MnO | 0.02 | Sr | 35 | Quartz | 77.1 |
| MgO | 0.68 | Y | 40 | | |
| CaO | 0.03 | Zr | 90 | | |
| Na ₂ O | 1.80 | C | | Organics | |
| K ₂ O | 2.40 | Ro | | | |
| LOI | | log Rv | | | |

Sample B-1

Locality Dobb's Linn

Grid reference NT 198159

Stratigraphic unit

Zone

Collected by WES and JAW

Analysed by EX and SWW

Description Cleaved black shale

| | | | | | |
|--------------------------------|-------|--------|----|----------|------|
| SiO ₂ | 87.62 | Cu | 45 | Albite | 0.1 |
| TiO ₂ | 0.36 | Pb | 39 | Chlorite | 2.8 |
| Al ₂ O ₃ | 6.72 | Zn | 9 | Sericite | 6.3 |
| Fe ₂ O ₃ | 0.98 | Rb | 61 | Pyrite | 5.2 |
| MnO | 0.02 | Sr | 36 | Quartz | 85.6 |
| MgO | 0.55 | Y | 35 | | |
| CaO | 0.02 | Zr | 80 | | |
| Na ₂ O | 1.74 | C | | | |
| K ₂ O | 1.77 | Ro | | | |
| LOI | | log Rv | | | |

Sample GK-1

Locality Glenkiln

Grid reference NT 006895

Stratigraphic unit Lower Hartfell Shales

Zone wilsoni

Collected by WES, SWW and JAW

Analysed by EX and SWW

Description Black mudstone

| | | | | | |
|--------------------------------|-------|--------|-----|----------|------|
| SiO ₂ | 72.06 | Cu | 167 | Albite | 7.3 |
| TiO ₂ | 0.46 | Pb | 145 | Chlorite | 4.3 |
| Al ₂ O ₃ | 8.90 | Zn | 166 | Sericite | 8.4 |
| Fe ₂ O ₃ | 6.61 | Rb | 76 | Pyrite | 14.7 |
| MnO | 0.07 | Sr | 50 | Quartz | 65.4 |
| MgO | 1.41 | Y | 51 | | |
| CaO | 0.31 | Zr | 121 | | |
| Na ₂ O | 1.56 | C | | Organics | |
| K ₂ O | 1.75 | Ro | | | |
| LOI | | log Rv | | | |

Sample GK-2
 Locality Glenkiln
 Grid reference NY 006895
 Stratigraphic unit Lower Hartfell Shales
 Zone wilsoni
 Collected by WES, SWW and JAW
 Analysed by EX and SWW
 Description Grey chert

| | | | | | |
|--------------------------------|-------|--------|----|----------|------|
| SiO ₂ | 78.53 | Cu | 53 | Albite | 3.3 |
| TiO ₂ | 0.32 | Pb | 22 | Chlorite | 5.3 |
| Al ₂ O ₃ | 7.17 | Zn | 27 | Sericite | 7.4 |
| Fe ₂ O ₃ | 6.24 | Rb | 50 | Pyrite | 6.2 |
| MnO | 0.36 | Sr | 64 | Quartz | 77.9 |
| MgO | 2.62 | Y | 40 | | |
| CaO | 1.28 | Zr | 63 | | |
| Na ₂ O | 1.74 | C | | Organics | |
| K ₂ O | 1.15 | Ro | | | |
| LOI | | log Rv | | | |

Sample GK-3
 Locality Glenkiln
 Grid reference NY 006895
 Stratigraphic unit Lower Hartfell Shales
 Zone wilsoni
 Collected by WES, SWW and JAW
 Analysed by EX and SWW
 Description Black mudstone

| | | | | | |
|--------------------------------|-------|--------|----|----------|------|
| SiO ₂ | 77.07 | Cu | 85 | Albite | 3.4 |
| TiO ₂ | 0.31 | Pb | 94 | Chlorite | 4.5 |
| Al ₂ O ₃ | 6.83 | Zn | 20 | Sericite | 9.4 |
| Fe ₂ O ₃ | 6.89 | Rb | 54 | Pyrite | 15.5 |
| MnO | 0.18 | Sr | 54 | Quartz | 67.2 |
| MgO | 1.40 | Y | 35 | | |
| CaO | 0.69 | Zr | 75 | | |
| Na ₂ O | 6.89 | C | | Organics | |
| K ₂ O | 1.25 | Ro | | | |
| LOI | | log Rv | | | |

Sample H-2

Locality Hartfell

Grid reference NT 094115

Stratigraphic unit Lower Hartfell Shales

Zone wilsoni

Collected by WES, SWW and JAW

Analysed by EX and SWW

Description Black mudstone

| | | | | | |
|--------------------------------|-------|--------|-----|----------|------|
| SiO ₂ | 81.08 | Cu | 29 | Albite | 3.2 |
| TiO ₂ | 0.62 | Pb | 31 | Chlorite | 4.2 |
| Al ₂ O ₃ | 9.25 | Zn | 8 | Sericite | 5.2 |
| Fe ₂ O ₃ | 0.80 | Rb | 108 | Pyrite | 6.9 |
| MnO | 0.04 | Sr | 47 | Quartz | 80.4 |
| MgO | 0.91 | Y | 21 | | |
| CaO | 0.04 | Zr | 125 | | |
| Na ₂ O | 1.45 | C | | Organics | |
| K ₂ O | 2.50 | Ro | | | |
| LOI | | log Rv | | | |

Sample H-5

Locality Hartfell

Grid reference NT 094115

Stratigraphic unit Lower Hartfell Shales

Zone clingani

Collected by WES, SWW and JAW

Analysed by EX and SWW

Description Hard black mudstone rich in sulphur

| | | | | | |
|--------------------------------|-------|--------|-----|----------|------|
| SiO ₂ | 86.32 | Cu | 53 | Albite | 0.0 |
| TiO ₂ | 0.33 | Pb | 39 | Chlorite | 3.2 |
| Al ₂ O ₃ | 5.96 | Zn | 4 | Sericite | 9.0 |
| Fe ₂ O ₃ | 1.53 | Rb | 59 | Pyrite | 7.0 |
| MnO | 0.02 | Sr | 122 | Quartz | 80.0 |
| MgO | 0.55 | Y | 23 | | |
| CaO | 0.04 | Zr | 74 | | |
| Na ₂ O | 1.84 | C | | Organics | |
| K ₂ O | 1.58 | Ro | | | |
| LOI | | log Rv | | | |

Sample MB-1

Locality Mountbenger

Grid reference NT 316259

Stratigraphic unit Upper Hartfell Shales

Zone linearis

Collected by WES and JAW

Analysed by EX and SWW

Description Black mudstone

| | | | | | |
|--------------------------------|-------|--------|-----|----------|------|
| SiO ₂ | 82.59 | Cu | 113 | Albite | 4.3 |
| TiO ₂ | 0.36 | Pb | 62 | Chlorite | 3.3 |
| Al ₂ O ₃ | 6.80 | Zn | 17 | Sericite | 6.9 |
| Fe ₂ O ₃ | 2.25 | Rb | 67 | Pyrite | 7.9 |
| MnO | 0.03 | Sr | 50 | Quartz | 77.7 |
| MgO | 0.68 | Y | 33 | | |
| CaO | 0.04 | Zr | 84 | | |
| Na ₂ O | 2.20 | C | | Organics | |
| K ₂ O | 1.55 | Ro | | | |
| LOI | | log Rv | | | |

Sample MB-2

Locality Mountbenger

Grid reference NT 316259

Stratigraphic unit Upper Hartfell Shales

Zone linearis

Collected by WES and JAW

Analysed by EX and SWW

Description Black mudstone

| | | | | | |
|--------------------------------|-------|--------|-----|----------|------|
| SiO ₂ | 72.62 | Cu | 149 | Albite | 7.0 |
| TiO ₂ | 0.52 | Pb | 54 | Chlorite | 4.1 |
| Al ₂ O ₃ | 10.14 | Zn | 30 | Sericite | 9.7 |
| Fe ₂ O ₃ | 4.20 | Rb | 92 | Pyrite | 13.0 |
| MnO | 0.04 | Sr | 58 | Quartz | 66.3 |
| MgO | 1.17 | Y | 39 | | |
| CaO | 0.04 | Zr | 121 | | |
| Na ₂ O | 3.59 | C | | Organics | |
| K ₂ O | 2.11 | Ro | | | |
| LOI | | log Rv | | | |

Sample H-1

Locality Hartfell

Grid reference NT 094115

Stratigraphic unit Upper Hartfell Shales

Zone linearis

Collected by WES, SWW and JAW

Analysed by EX and SWW

Description Blocky black mudstone

| | | | | | |
|--------------------------------|-------|--------|----|----------|------|
| SiO ₂ | 91.60 | Cu | 27 | Albite | 2.5 |
| TiO ₂ | 0.40 | Pb | 35 | Chlorite | 1.8 |
| Al ₂ O ₃ | 4.48 | Zn | 0 | Sericite | 7.7 |
| Fe ₂ O ₃ | 0.13 | Rb | 43 | Pyrite | 4.7 |
| MnO | 0.02 | Sr | 46 | Quartz | 83.3 |
| MgO | 0.30 | Y | 32 | | |
| CaO | 0.01 | Zr | 52 | | |
| Na ₂ O | 0.84 | C | | Organics | |
| K ₂ O | 1.00 | Ro | | | |
| LOI | | log Rv | | | |

Sample H-6

Locality Hartfell

Grid reference NT 094115

Stratigraphic unit Upper Hartfell Shales

Zone linearis

Collected by WES, SWW and JAW

Analysed by EX and SWW

Description Blocky black mudstone

| | | | | | |
|--------------------------------|-------|--------|----|----------|------|
| SiO ₂ | 88.84 | Cu | 30 | Albite | 3.2 |
| TiO ₂ | 0.40 | Pb | 33 | Chlorite | 2.6 |
| Al ₂ O ₃ | 5.78 | Zn | 2 | Sericite | 6.7 |
| Fe ₂ O ₃ | 0.81 | Rb | 52 | Pyrite | 5.2 |
| MnO | 0.02 | Sr | 75 | Quartz | 82.4 |
| MgO | 0.63 | Y | 14 | | |
| CaO | 0.02 | Zr | 75 | | |
| Na ₂ O | 0.69 | C | | Organics | |
| K ₂ O | 1.35 | Ro | | | |
| LOI | | log Rv | | | |

Sample C-1

Locality Carrifran

Grid reference NT 151131

Stratigraphic unit Upper Hartfell Shales

Zone linearis

Collected by WES and JAW

Analysed by EX and SWW

Description Black mudstone

| | | | | | |
|--------------------------------|-------|--------|----|----------|------|
| SiO ₂ | 95.08 | Cu | 26 | Albite | 0.0 |
| TiO ₂ | 0.13 | Pb | 38 | Chlorite | 2.0 |
| Al ₂ O ₃ | 2.68 | Zn | 0 | Sericite | 5.5 |
| Fe ₂ O ₃ | 0.13 | Rb | 27 | Pyrite | 4.9 |
| MnO | 0.02 | Sr | 9 | Quartz | 87.7 |
| MgO | 0.22 | Y | 10 | | |
| CaO | 0.02 | Zr | 34 | | |
| Na ₂ O | 1.88 | C | | Organics | |
| K ₂ O | 0.79 | Ro | | | |
| LOI | | log Rv | | | |

Sample ID-3

Locality Dobb's Linn

Grid reference NT 198159

Stratigraphic unit Upper Hartfell Shales

Zone anceps

Collected by WES and JAW

Analysed by EX and SWW

Description Grey mudstone

| | | | | | |
|--------------------------------|-------|--------|-----|----------|------|
| SiO ₂ | 70.04 | Cu | 43 | Albite | 1.2 |
| TiO ₂ | 0.88 | Pb | 61 | Chlorite | 0.8 |
| Al ₂ O ₃ | 16.11 | Zn | 20 | Sericite | 17.0 |
| Fe ₂ O ₃ | 1.43 | Rb | 157 | Pyrite | 4.7 |
| MnO | 0.02 | Sr | 37 | Quartz | 76.3 |
| MgO | 0.77 | Y | 36 | | |
| CaO | 0.02 | Zr | 177 | | |
| Na ₂ O | 0.90 | C | | Organics | |
| K ₂ O | 4.71 | Ro | | | |
| LOI | | log Rv | | | |

Sample ID-4

Locality Dobb's Linn

Grid reference NT 198159

Stratigraphic unit Upper Hartfell Shales

Zone anceps

Collected by WES and JAW

Analysed by EX and SWW

Description Grey mudstone (same bed, same locality as ID-3)

| | | | | | |
|--------------------------------|-------|--------|-----|----------|------|
| SiO ₂ | 50.42 | Cu | 79 | Albite | 5.3 |
| TiO ₂ | 0.68 | Pb | 29 | Chlorite | 4.9 |
| Al ₂ O ₃ | 12.35 | Zn | 89 | Sericite | 19.4 |
| Fe ₂ O ₃ | 4.92 | Rb | 107 | Pyrite | 6.7 |
| MnO | 0.84 | Sr | 146 | Quartz | 63.7 |
| MgO | 7.12 | Y | 46 | | |
| CaO | 8.73 | Zr | 217 | | |
| Na ₂ O | 1.05 | C | | Organics | |
| K ₂ O | 2.97 | Ro | | | |
| LOI | | log Rv | | | |

Sample ID-5

Locality Dobb's Linn

Grid reference NT 198159

Stratigraphic unit Upper Hartfell Shales

Zone anceps

Collected by WES and JAW

Analysed by EX and SWW

Description Grey mudstone (same bed along strike from ID-4)

| | | | | | |
|--------------------------------|-------|--------|-----|----------|------|
| SiO ₂ | 50.77 | Cu | 81 | Albite | 6.0 |
| TiO ₂ | 0.68 | Pb | 56 | Chlorite | 4.6 |
| Al ₂ O ₃ | 12.39 | Zn | 89 | Sericite | 17.1 |
| Fe ₂ O ₃ | 5.05 | Rb | 104 | Pyrite | 6.0 |
| MnO | 0.84 | Sr | 159 | Quartz | 66.3 |
| MgO | 6.96 | Y | 38 | | |
| CaO | 8.83 | Zr | 216 | | |
| Na ₂ O | 1.77 | C | | Organics | |
| K ₂ O | 2.91 | Ro | | | |
| LOI | | log Rv | | | |

Sample ID-6

Locality Dobb's Linn

Grid reference NT 198159

Stratigraphic unit Upper Hartfell Shales

Zone anceps

Collected by WES and JAW

Analysed by EX and SWW

Description Grey mudstone (same bed still further along strike from ID-4)

| | | | | | |
|--------------------------------|-------|--------|-----|----------|------|
| SiO ₂ | 50.32 | Cu | 99 | Albite | 7.3 |
| TiO ₂ | 0.68 | Pb | 39 | Chlorite | 4.9 |
| Al ₂ O ₃ | 12.11 | Zn | 100 | Sericite | 15.1 |
| Fe ₂ O ₃ | 5.09 | Rb | 100 | Pyrite | 6.7 |
| MnO | 0.82 | Sr | 141 | Quartz | 66.1 |
| MgO | 7.63 | Y | 51 | | |
| CaO | 9.06 | Zr | 214 | | |
| Na ₂ O | 1.92 | C | | Organics | |
| K ₂ O | 2.94 | Ro | | | |
| LOI | | log Rv | | | |

Sample ID-7

Locality Dobb's Linn

Grid reference NT 198159

Stratigraphic unit Upper Hartfell Shales

Zone anceps

Collected by WES and JAW

Analysed by EX and SWW

Description Black graptolitic mudstone

| | | | | | |
|--------------------------------|-------|--------|-----|----------|------|
| SiO ₂ | 62.56 | Cu | 52 | Albite | 8.8 |
| TiO ₂ | 0.90 | Pb | 192 | Chlorite | 3.5 |
| Al ₂ O ₃ | 16.39 | Zn | 49 | Sericite | 18.7 |
| Fe ₂ O ₃ | 4.56 | Rb | 157 | Pyrite | 6.1 |
| MnO | 0.03 | Sr | 37 | Quartz | 62.9 |
| MgO | 1.70 | Y | 28 | | |
| CaO | 0.03 | Zr | 285 | | |
| Na ₂ O | 2.24 | C | | Organics | |
| K ₂ O | 4.30 | Ro | | | |
| LOI | | log Rv | | | |

Sample 1E-3

Locality Dobb's Linn

Grid reference NT 198159

Stratigraphic unit Lower Birkhill Shales

Zone persculptus

Collected by WES and JAW

Analysed by EX and SWW

Description Bleached white 'claystone'

| | | | | | |
|--------------------------------|-------|--------|-----|----------|------|
| SiO ₂ | 64.10 | Cu | 61 | Albite | 5.8 |
| TiO ₂ | 0.83 | Pb | 145 | Chlorite | 4.0 |
| Al ₂ O ₃ | 14.17 | Zn | 54 | Sericite | 16.0 |
| Fe ₂ O ₃ | 5.30 | Rb | 135 | Pyrite | 9.9 |
| MnO | 0.02 | Sr | 33 | Quartz | 64.3 |
| MgO | 1.48 | Y | 33 | | |
| CaO | 0.02 | Zr | 221 | | |
| Na ₂ O | 1.60 | C | | Organics | |
| K ₂ O | 3.84 | Ro | | | |
| LOI | | log Rv | | | |

Sample 1F-5

Locality Dobb's Linn

Grid reference NT 198159

Stratigraphic unit Lower Birkhill Shales

Zone acuminatus

Collected by WES and JAW

Analysed by EX and SWW

Description Blocky black mudstone

| | | | | | |
|--------------------------------|-------|--------|-----|----------|------|
| SiO ₂ | 59.10 | Cu | 120 | Albite | 7.5 |
| TiO ₂ | 0.80 | Pb | 55 | Chlorite | 2.9 |
| Al ₂ O ₃ | 14.80 | Zn | 60 | Sericite | 13.5 |
| Fe ₂ O ₃ | 9.29 | Rb | 136 | Pyrite | 19.8 |
| MnO | 0.03 | Sr | 38 | Quartz | 56.3 |
| MgO | 1.73 | Y | 31 | | |
| CaO | 0.02 | Zr | 216 | | |
| Na ₂ O | 1.95 | C | | Organics | |
| K ₂ O | 3.68 | Ro | | | |
| LOI | | log Rv | | | |

Sample 2A-2

Locality Dobb's Linn

Grid reference NT 198159

Stratigraphic unit Lower Birkhill Shales

Zone acuminatus

Collected by WES and JAW

Analysed by EX and SWW

Description Massive blocky black mudstone

| | | | | | |
|--------------------------------|-------|--------|-----|----------|------|
| SiO ₂ | 66.15 | Cu | 91 | Albite | 5.4 |
| TiO ₂ | 0.66 | Pb | 52 | Chlorite | 4.1 |
| Al ₂ O ₃ | 12.76 | Zn | 67 | Sericite | 13.9 |
| Fe ₂ O ₃ | 8.24 | Rb | 108 | Pyrite | 19.0 |
| MnO | 0.04 | Sr | 48 | Quartz | 57.7 |
| MgO | 2.70 | Y | 0 | | |
| CaO | 0.08 | Zr | 180 | | |
| Na ₂ O | 2.20 | C | | Organics | |
| K ₂ O | 2.87 | Ro | | | |
| LOI | | log Rv | | | |

Sample 2C-5

Locality Dobb's Linn

Grid reference NT 198159

Stratigraphic unit Lower Birkhill Shales

Zone cyphus

Collected by WES and JAW

Analysed by EX and SWW

Description Blocky black mudstone

| | | | | | |
|--------------------------------|-------|--------|-----|----------|------|
| SiO ₂ | 59.09 | Cu | 121 | Albite | 6.7 |
| TiO ₂ | 0.78 | Pb | 38 | Chlorite | 4.7 |
| Al ₂ O ₃ | 14.95 | Zn | 67 | Sericite | 19.3 |
| Fe ₂ O ₃ | 8.87 | Rb | 119 | Pyrite | 16.9 |
| MnO | 0.05 | Sr | 36 | Quartz | 52.4 |
| MgO | 3.97 | Y | 14 | | |
| CaO | 0.07 | Zr | 202 | | |
| Na ₂ O | 2.28 | C | | Organics | |
| K ₂ O | 3.25 | Ro | | | |
| LOI | | log Rv | | | |

Sample 2C-6

Locality Dobb's Linn

Grid reference NT 198159

Stratigraphic unit Lower Birkhill Shales

Zone cyphus

Collected by WES and JAW

Analysed by EX and SWW

Description Massive black mudstone

| | | | | | |
|--------------------------------|-------|--------|-----|----------|------|
| SiO ₂ | 55.12 | Cu | 126 | Albite | 4.3 |
| TiO ₂ | 0.64 | Pb | 93 | Chlorite | 3.6 |
| Al ₂ O ₃ | 12.14 | Zn | 70 | Sericite | 12.1 |
| Fe ₂ O ₃ | 14.61 | Rb | 91 | Pyrite | 28.0 |
| MnO | 0.05 | Sr | 31 | Quartz | 52.1 |
| MgO | 3.10 | Y | 42 | | |
| CaO | 0.09 | Zr | 184 | | |
| Na ₂ O | 2.31 | C | | Organics | |
| K ₂ O | 2.74 | Ro | | | |
| LOI | | log Rv | | | |

Sample MB-3

Locality Mountbenger

Grid reference NT 316259

Stratigraphic unit Upper Birkhill Shales

Zone convolutus

Collected by WES and JAW

Analysed by EX and SWW

Description Black mudstone

| | | | | | |
|--------------------------------|-------|--------|-----|----------|--|
| SiO ₂ | 48.20 | Cu | 168 | Albite | |
| TiO ₂ | 0.61 | Pb | 440 | Chlorite | |
| Al ₂ O ₃ | 12.58 | Zn | 76 | Sericite | |
| Fe ₂ O ₃ | 19.39 | Rb | 80 | Pyrite | |
| MnO | 0.06 | Sr | 38 | Quartz | |
| MgO | 2.07 | Y | 23 | | |
| CaO | 0.03 | Zr | 114 | | |
| Na ₂ O | 4.49 | C | | Organics | |
| K ₂ O | 2.43 | Ro | | | |
| LOI | | log Rv | | | |

Sample 2E-6

Locality Dobb's Linn

Grid reference NT 198159

Stratigraphic unit Upper Birkhill Shales

Zone convolutus

Collected by WES and JAW

Analysed by EX and SWW

Description Bleached white 'claystone'

| | | | | | |
|--------------------------------|-------|--------|-----|----------|------|
| SiO ₂ | 51.51 | Cu | 88 | Albite | 6.6 |
| TiO ₂ | 0.68 | Pb | 31 | Chlorite | 4.8 |
| Al ₂ O ₃ | 12.27 | Zn | 96 | Sericite | 15.3 |
| Fe ₂ O ₃ | 4.97 | Rb | 110 | Pyrite | 6.5 |
| MnO | 0.82 | Sr | 132 | Quartz | 66.8 |
| MgO | 7.41 | Y | 30 | | |
| CaO | 8.96 | Zr | 223 | | |
| Na ₂ O | 1.59 | C | | Organics | |
| K ₂ O | 3.06 | Ro | | | |
| LOI | | log Rv | | | |

Sample 2F-10

Locality Dobb's Linn

Grid reference NT 198159

Stratigraphic unit Upper Birkhill Shales

Zone sedgwickii

Collected by WES and JAW

Analysed by EX and SWW

Description Greywacke

| | | | | | |
|--------------------------------|-------|--------|-----|----------|------|
| SiO ₂ | 52.06 | Cu | 58 | Albite | 23.7 |
| TiO ₂ | 0.82 | Pb | 45 | Chlorite | 3.4 |
| Al ₂ O ₃ | 17.35 | Zn | 94 | Sericite | 16.0 |
| Fe ₂ O ₃ | 3.71 | Rb | 61 | Pyrite | 10.6 |
| MnO | 1.22 | Sr | 338 | Quartz | 46.4 |
| MgO | 2.59 | Y | 45 | | |
| CaO | 11.86 | Zr | 294 | | |
| Na ₂ O | 6.29 | C | | Organics | |
| K ₂ O | 2.22 | Ro | | | |
| LOI | | log Rv | | | |

Sample 2F-11

Locality Dobb's Linn

Grid reference NT 198159

Stratigraphic unit Upper Birkhill Shales

Zone sedgwickii

Collected by WES and JAW

Analysed by EX and SWW

Description Massive graptolitic mudstone

| | | | | | |
|--------------------------------|-------|--------|-----|----------|------|
| SiO ₂ | 59.29 | Cu | 116 | Albite | 9.7 |
| TiO ₂ | 0.69 | Pb | 29 | Chlorite | 6.1 |
| Al ₂ O ₃ | 16.81 | Zn | 96 | Sericite | 18.5 |
| Fe ₂ O ₃ | 7.04 | Rb | 112 | Pyrite | 4.2 |
| MnO | 0.36 | Sr | 91 | Quartz | 61.5 |
| MgO | 4.65 | Y | 19 | | |
| CaO | 1.12 | Zr | 209 | | |
| Na ₂ O | 1.95 | C | | Organics | |
| K ₂ O | 3.16 | Ro | | | |
| LOI | | log Rv | | | |

Sample 2G-10

Locality Dobb's Linn

Grid reference NT 198159

Stratigraphic unit Upper Birkhill Shales

Zone maximus

Collected by WES and JAW

Analysed by EX and SWW

Description Grey mudstone

| | | | | | |
|--------------------------------|-------|--------|-----|----------|------|
| SiO ₂ | 59.75 | Cu | 61 | Albite | 5.7 |
| TiO ₂ | 0.75 | Pb | 26 | Chlorite | 9.1 |
| Al ₂ O ₃ | 15.88 | Zn | 104 | Sericite | 16.2 |
| Fe ₂ O ₃ | 9.01 | Rb | 115 | Pyrite | 7.2 |
| MnO | 0.36 | Sr | 63 | Quartz | 61.8 |
| MgO | 4.40 | Y | 34 | | |
| CaO | 1.37 | Zr | 209 | | |
| Na ₂ O | 2.38 | C | | Organics | |
| K ₂ O | 3.11 | Ro | | | |
| LOI | | log Rv | | | |

Sample 2G-11

Locality Dobb's Linn

Grid reference NT 198159

Stratigraphic unit Upper Birkhill Shales

Zone maximus

Collected by WES and JAW

Analysed by EX and SWW

Description Grey mudstone

| | | | | | |
|--------------------------------|-------|--------|-----|----------|------|
| SiO ₂ | 57.94 | Cu | 32 | Albite | 15.5 |
| TiO ₂ | 0.80 | Pb | 20 | Chlorite | 7.9 |
| Al ₂ O ₃ | 19.16 | Zn | 61 | Sericite | 14.9 |
| Fe ₂ O ₃ | 7.62 | Rb | 158 | Pyrite | 5.9 |
| MnO | 0.12 | Sr | 77 | Quartz | 55.9 |
| MgO | 3.70 | Y | 33 | | |
| CaO | 0.65 | Zr | 221 | | |
| Na ₂ O | 2.10 | C | | Organics | |
| K ₂ O | 3.99 | Ro | | | |
| LOI | | log Rv | | | |

Sample GL-GL1

Locality Glenkiln

Grid reference NY 006895

Stratigraphic unit Glenkiln Shales

Zone gracilis

Collected by SWW

Analysed by SWW

Description Black mudstone

| | | | | | |
|--------------------------------|-------|--------|-------|----------|------|
| SiO ₂ | 80.70 | Cu | 35 | Albite | 2.7 |
| TiO ₂ | 0.43 | Pb | 54 | Chlorite | 2.3 |
| Al ₂ O ₃ | 7.76 | Zn | 3 | Sericite | 6.8 |
| Fe ₂ O ₃ | 1.21 | Rb | 77 | Pyrite | 4.8 |
| MnO | 0.01 | Sr | 38 | Quartz | 83.5 |
| MgO | 0.65 | Y | 26 | | |
| CaO | 0.03 | Zr | 75 | | |
| Na ₂ O | 0.50 | C | 3.14 | Organics | |
| K ₂ O | 1.77 | Ro | 2.40 | | |
| LOI | 6.67 | log Rv | 7.508 | | |

Sample GL-W1
 Locality Glenkiln
 Grid reference NY 006895
 Stratigraphic unit Lower Hartfell Shales
 Zone wilsoni
 Collected by SWW
 Analysed by SWW
 Description Black mudstone

| | | | | | |
|--------------------------------|-------|--------|-------|----------|----------|
| SiO ₂ | 68.36 | Cu | 107 | Albite | 6.5 |
| TiO ₂ | 0.50 | Pb | 163 | Chlorite | 3.3 |
| Al ₂ O ₃ | 9.90 | Zn | 28 | Sericite | 12.4 |
| Fe ₂ O ₃ | 7.29 | Rb | 110 | Pyrite | 26.6 |
| MnO | 0.02 | Sr | 51 | Quartz | 51.1 |
| MgO | 0.79 | Y | 36 | | |
| CaO | 0.02 | Zr | 136 | | |
| Na ₂ O | 0.53 | C | 3.01 | Organics | analysed |
| K ₂ O | 1.46 | Ro | 2.20 | | |
| LOI | 11.11 | log Rv | 7.372 | | |

Sample GL-W2
 Locality Glenkiln
 Grid reference NY 006895
 Stratigraphic unit Lower Hartfell Shales
 Zone wilsoni
 Collected by SWW
 Analysed by SWW
 Description Black mudstone

| | | | | | |
|--------------------------------|-------|--------|-------|----------|----------|
| SiO ₂ | 70.41 | Cu | 75 | Albite | 5.9 |
| TiO ₂ | 0.53 | Pb | 148 | Chlorite | 2.0 |
| Al ₂ O ₃ | 10.54 | Zn | 13 | Sericite | 14.3 |
| Fe ₂ O ₃ | 4.56 | Rb | 123 | Pyrite | 9.7 |
| MnO | 0.02 | Sr | 65 | Quartz | 68.2 |
| MgO | 0.78 | Y | 51 | | |
| CaO | 0.01 | Zr | 138 | | |
| Na ₂ O | 0.52 | C | 2.61 | Organics | analysed |
| K ₂ O | 1.85 | Ro | 1.86 | | |
| LOI | 10.68 | log Rv | 7.519 | | |

Sample GL-Cl.1
Locality Glenkiln
Grid reference NY 006895
Stratigraphic unit Lower Hartfell Shales
Zone clingani
Collected by SWW
Analysed by SWW
Description Black mudstone

| | | | | | |
|--------------------------------|-------|--------|-------|----------|----------|
| SiO ₂ | 71.85 | Cu | 111 | Albite | 5.4 |
| TiO ₂ | 0.45 | Pb | 127 | Chlorite | 2.4 |
| Al ₂ O ₃ | 9.26 | Zn | 20 | Sericite | 14.5 |
| Fe ₂ O ₃ | 5.59 | Rb | 103 | Pyrite | 9.3 |
| MnO | 0.02 | Sr | 56 | Quartz | 68.5 |
| MgO | 0.86 | Y | 42 | | |
| CaO | 0.02 | Zr | 119 | | |
| Na ₂ O | 0.42 | C | 2.39 | Organics | analysed |
| K ₂ O | 1.29 | Ro | 1.95 | | |
| LOI | 10.14 | log Rv | 7.577 | | |

Sample MG-1
Locality Entertrona Burn
Grid reference NT 183081
Stratigraphic unit Upper Birkhill Shales
Zone
Collected by SWW
Analysed by SWW
Description Cherty black mudstone

| | | | | | |
|--------------------------------|-------|--------|-------|----------|--|
| SiO ₂ | 51.89 | Cu | 69 | Albite | |
| TiO ₂ | 0.12 | Pb | 20 | Chlorite | |
| Al ₂ O ₃ | 4.78 | Zn | 26 | Sericite | |
| Fe ₂ O ₃ | 1.96 | Rb | 48 | Pyrite | |
| MnO | 0.09 | Sr | 25 | Quartz | |
| MgO | 0.73 | Y | 23 | | |
| CaO | 0.10 | Zr | 35 | | |
| Na ₂ O | 0.72 | C | 0.35 | Organics | |
| K ₂ O | 0.73 | Ro | 2.10 | | |
| LOI | 1.40 | log Rv | 7.510 | | |

Sample MG-2

Locality Range Cleuch

Grid reference NT 193107

Stratigraphic unit Gala Greywackes

Zone

Collected by SWW

Analysed by SWW

Description Fine grained greywacke

| | | | | |
|--------------------------------|-------|--------|-------|----------|
| SiO ₂ | 55.85 | Cu | 71 | Albite |
| TiO ₂ | 0.76 | Pb | 31 | Chlorite |
| Al ₂ O ₃ | 20.60 | Zn | 129 | Sericite |
| Fe ₂ O ₃ | 9.19 | Rb | 160 | Pyrite |
| MnO | 0.12 | Sr | 48 | Quartz |
| MgO | 3.91 | Y | 33 | |
| CaO | 0.02 | Zr | 148 | |
| Na ₂ O | 0.84 | C | 0.10 | Organics |
| K ₂ O | 4.09 | Ro | 1.89 | |
| LOI | 4.60 | log Rv | 7.649 | |

Sample MG-3

Locality Range Cleuch

Grid reference NT 193107

Stratigraphic unit Upper Hartfell Shales

Zone linearis

Collected by SWW

Analysed by SWW

Description Graptolitic black shale

| | | | | |
|--------------------------------|-------|--------|-------|----------|
| SiO ₂ | 79.79 | Cu | 82 | Albite |
| TiO ₂ | 0.15 | Pb | 59 | Chlorite |
| Al ₂ O ₃ | 7.30 | Zn | 16 | Sericite |
| Fe ₂ O ₃ | 3.76 | Rb | 63 | Pyrite |
| MnO | 0.02 | Sr | 18 | Quartz |
| MgO | 1.24 | Y | 18 | |
| CaO | 0.00 | Zr | 83 | |
| Na ₂ O | 0.58 | C | 0.52 | Organics |
| K ₂ O | 2.31 | Ro | 2.88 | |
| LOI | 4.70 | log Rv | 7.523 | |

Sample MG-4

Locality Ettrick Water

Grid reference NT 213117

Stratigraphic unit Lower Birkhill Shales

Zone

Collected by SWW

Analysed by SWW

Description Graptolitic black shale

| | | | | |
|--------------------------------|-------|--------|-------|----------|
| SiO ₂ | 61.84 | Cu | 121 | Albite |
| TiO ₂ | 0.64 | Pb | 45 | Chlorite |
| Al ₂ O ₃ | 13.67 | Zn | 58 | Sericite |
| Fe ₂ O ₃ | 7.70 | Rb | 123 | Pyrite |
| MnO | 0.03 | Sr | 54 | Quartz |
| MgO | 1.90 | Y | 33 | |
| CaO | 0.00 | Zr | 131 | |
| Na ₂ O | 1.11 | C | 1.74 | Organics |
| K ₂ O | 2.41 | Ro | 2.81 | |
| LOI | 10.30 | log Rv | 7.581 | |

Sample MG-5

Locality Glendearg Burn

Grid reference NT 212105

Zone

Collected by SWW

Analysed by SWW

Description Grey mudstone

| | | | | |
|--------------------------------|-------|--------|-------|----------|
| SiO ₂ | 55.58 | Cu | 94 | Albite |
| TiO ₂ | 0.74 | Pb | 34 | Chlorite |
| Al ₂ O ₃ | 18.54 | Zn | 98 | Sericite |
| Fe ₂ O ₃ | 9.94 | Rb | 163 | Pyrite |
| MnO | 0.05 | Sr | 46 | Quartz |
| MgO | 5.61 | Y | 59 | |
| CaO | 0.14 | Zr | 138 | |
| Na ₂ O | 0.72 | C | 0.18 | Organics |
| K ₂ O | 3.34 | Ro | 2.04 | |
| LOI | 5.20 | log Rv | 7.664 | |

Sample MG-5A
Locality Coomb Burn
Grid reference NT 212105
Stratigraphic unit Upper Birkhill Shales
Zone
Collected by SWW
Analysed by SWW
Description Flaggy grey mudstone

| | | | | |
|--------------------------------|-------|--------|-------|----------|
| SiO ₂ | 54.67 | Cu | 97 | Albite |
| TiO ₂ | 0.76 | Pb | 34 | Chlorite |
| Al ₂ O ₃ | 19.48 | Zn | 114 | Sericite |
| Fe ₂ O ₃ | 9.16 | Rb | 163 | Pyrite |
| MnO | 0.04 | Sr | 42 | Quartz |
| MgO | 5.69 | Y | 44 | |
| CaO | 0.12 | Zr | 161 | |
| Na ₂ O | 0.54 | C | 0.53 | Organics |
| K ₂ O | 3.34 | Ro | 3.99 | |
| LOI | 6.10 | log Rv | 7.534 | |

Sample MG-6
Locality Coomb Burn
Grid reference NT 206096
Stratigraphic unit Upper Birkhill Shales
Zone
Collected by SWW
Analysed by SWW
Description Greywacke

| | | | | |
|--------------------------------|-------|--------|-------|----------|
| SiO ₂ | 71.08 | Cu | 95 | Albite |
| TiO ₂ | 0.50 | Pb | 34 | Chlorite |
| Al ₂ O ₃ | 8.09 | Zn | 106 | Sericite |
| Fe ₂ O ₃ | 3.84 | Rb | 172 | Pyrite |
| MnO | 0.08 | Sr | 35 | Quartz |
| MgO | 2.68 | Y | 41 | |
| CaO | 5.68 | Zr | 134 | |
| Na ₂ O | 1.00 | C | 0.50 | Organics |
| K ₂ O | 0.89 | Ro | | |
| LOI | 5.80 | log Rv | 7.517 | |

Sample MG-7

Locality Coomb Burn

Grid reference NT 296096

Stratigraphic unit Gala Greywackes

Zone

Collected by SWW

Analysed by SWW

Description Grey mudstone (interbedded with greywacke)

| | | | | |
|--------------------------------|-------|--------|-------|----------|
| SiO ₂ | 55.20 | Cu | 63 | Albite |
| TiO ₂ | 0.89 | Pb | 21 | Chlorite |
| Al ₂ O ₃ | 19.93 | Zn | 44 | Sericite |
| Fe ₂ O ₃ | 8.89 | Rb | 51 | Pyrite |
| MnO | 0.04 | Sr | 104 | Quartz |
| MgO | 5.27 | Y | 21 | |
| CaO | 0.13 | Zr | 228 | |
| Na ₂ O | 0.82 | C | 0.51 | Organics |
| K ₂ O | 3.51 | Ro | 2.56 | |
| LOI | 5.30 | log Rv | 7.535 | |

Sample MG-8

Locality Ettrick Water

Grid reference NT 212133

Stratigraphic unit Birkhill Shales

Zone

Collected by SWW

Analysed by SWW

Description Black shale rich in sulphur

| | | | | |
|--------------------------------|-------|--------|-------|----------|
| SiO ₂ | 55.64 | Cu | 102 | Albite |
| TiO ₂ | 0.70 | Pb | 73 | Chlorite |
| Al ₂ O ₃ | 17.38 | Zn | 71 | Sericite |
| Fe ₂ O ₃ | 9.53 | Rb | 143 | Pyrite |
| MnO | 0.04 | Sr | 56 | Quartz |
| MgO | 2.69 | Y | 39 | |
| CaO | 0.01 | Zr | 127 | |
| Na ₂ O | 0.72 | C | 1.77 | Organics |
| K ₂ O | 2.94 | Ro | 2.27 | |
| LOI | 9.30 | log Rv | 7.517 | |

Sample MG-9

Locality Brockhope Burn

Grid reference NT 212133

Stratigraphic unit Birkhill Shales

Zone

Collected by SWW

Analysed by SWW

Description Black graptolitic shale

| | | | | |
|--------------------------------|-------|--------|-------|----------|
| SiO ₂ | 69.55 | Cu | 105 | Albite |
| TiO ₂ | 0.37 | Pb | 146 | Chlorite |
| Al ₂ O ₃ | 10.44 | Zn | 38 | Sericite |
| Fe ₂ O ₃ | 7.86 | Rb | 95 | Pyrite |
| MnO | 0.02 | Sr | 24 | Quartz |
| MgO | 1.46 | Y | 25 | |
| CaO | 0.00 | Zr | 91 | |
| Na ₂ O | 0.45 | C | 1.05 | Organics |
| K ₂ O | 2.45 | Ro | 2.56 | |
| LOI | 7.40 | log Rv | 7.478 | |

Sample MG-10

Locality Back Grain

Grid reference NT 225134

Stratigraphic unit Upper Birkhill Shales

Zone

Collected by SWW

Analysed by SWW

Description Dark grey mudstone

| | | | | |
|--------------------------------|-------|--------|-------|----------|
| SiO ₂ | 54.50 | Cu | 92 | Albite |
| TiO ₂ | 0.90 | Pb | 37 | Chlorite |
| Al ₂ O ₃ | 19.03 | Zn | 110 | Sericite |
| Fe ₂ O ₃ | 10.66 | Rb | 160 | Pyrite |
| MnO | 0.07 | Sr | 44 | Quartz |
| MgO | 5.38 | Y | 44 | |
| CaO | 0.20 | Zr | 139 | |
| Na ₂ O | 0.79 | C | 0.18 | Organics |
| K ₂ O | 2.93 | Ro | 2.32 | |
| LOI | 5.60 | log Rv | 7.510 | |

Sample MG-11

Locality South side of Loch Skeen

Grid reference NT 165164

Stratigraphic unit Upper Birkhill Shales

Zone gregarius

Collected by SWW

Analysed by SWW

Description Black mudstone

| | | | | |
|--------------------------------|-------|--------|-------|----------|
| SiO ₂ | 63.56 | Cu | 80 | Albite |
| TiO ₂ | 0.76 | Pb | 31 | Chlorite |
| Al ₂ O ₃ | 16.35 | Zn | 78 | Sericite |
| Fe ₂ O ₃ | 7.46 | Rb | 132 | Pyrite |
| MnO | 0.07 | Sr | 27 | Quartz |
| MgO | 4.47 | Y | 38 | |
| CaO | 0.11 | Zr | 211 | |
| Na ₂ O | 0.13 | C | | Organics |
| K ₂ O | 2.84 | Ro | 6.50 | |
| LOI | 3.80 | log Rv | 7.505 | |

Sample MG-12

Locality South side of Loch Skeen

Grid reference NT 165164

Stratigraphic unit Upper Hartfell Shales

Zone linearis

Collected by SWW

Analysed by SWW

Description Black mudstone rich in sulphur

| | | | | |
|--------------------------------|-------|--------|-------|----------|
| SiO ₂ | 75.31 | Cu | 90 | Albite |
| TiO ₂ | 0.42 | Pb | 98 | Chlorite |
| Al ₂ O ₃ | 9.29 | Zn | 46 | Sericite |
| Fe ₂ O ₃ | 5.47 | Rb | 96 | Pyrite |
| MnO | 0.07 | Sr | 11 | Quartz |
| MgO | 1.57 | Y | 25 | |
| CaO | 0.01 | Zr | 94 | |
| Na ₂ O | 0.12 | C | 0.84 | Organics |
| K ₂ O | 2.10 | Ro | 2.27 | |
| LOI | 5.20 | log Rv | 7.515 | |

Sample MG-13

Locality Muckra

Grid reference NT 226168

Stratigraphic unit Upper Hartfell Shales

Zone linearis

Collected by SWW

Analysed by SWW

Description Blocky pyritised black mudstone

| | | | | |
|--------------------------------|-------|--------|-------|----------|
| SiO ₂ | 74.92 | Cu | 111 | Albite |
| TiO ₂ | 0.41 | Pb | 45 | Chlorite |
| Al ₂ O ₃ | 7.98 | Zn | 27 | Sericite |
| Fe ₂ O ₃ | 6.16 | Rb | 76 | Pyrite |
| MnO | 0.02 | Sr | 26 | Quartz |
| MgO | 1.30 | Y | 17 | |
| CaO | 1.00 | Zr | 79 | |
| Na ₂ O | 0.32 | C | 0.50 | Organics |
| K ₂ O | 1.47 | Ro | 2.16 | |
| LOI | 7.20 | log Rv | 7.323 | |

Sample MG-14

Locality Crosscleuch

Grid reference NF 248203

Stratigraphic unit Lower Hartfell Shales

Zone clingani

Collected by SWW

Analysed by SWW

Description Blocky black graptolitic mudstone

| | | | | |
|--------------------------------|-------|--------|-------|----------|
| SiO ₂ | 87.59 | Cu | 58 | Albite |
| TiO ₂ | 0.21 | Pb | 44 | Chlorite |
| Al ₂ O ₃ | 4.04 | Zn | 14 | Sericite |
| Fe ₂ O ₃ | 0.89 | Rb | 63 | Pyrite |
| MnO | 0.01 | Sr | 36 | Quartz |
| MgO | 0.27 | Y | 23 | |
| CaO | 0.01 | Zr | 55 | |
| Na ₂ O | 0.64 | C | 3.71 | Organics |
| K ₂ O | 0.95 | Ro | 1.68 | |
| LOI | 4.60 | log Rv | 7.454 | |

Sample MG-15

Locality Eldinhope Burn

Grid reference NT 305238

Stratigraphic unit Upper Birkhill Shales

Zone maximus?

Collected by SWW

Analysed by SWW

Description Grey mudstone

| | | | | |
|--------------------------------|-------|--------|-------|----------|
| SiO ₂ | 57.78 | Cu | 111 | Albite |
| TiO ₂ | 0.71 | Pb | 41 | Chlorite |
| Al ₂ O ₃ | 17.89 | Zn | 94 | Sericite |
| Fe ₂ O ₃ | 7.73 | Rb | 123 | Pyrite |
| MnO | 0.28 | Sr | 62 | Quartz |
| MgO | 6.55 | Y | 39 | |
| CaO | 0.08 | Zr | 180 | |
| Na ₂ O | 0.58 | C | 0.48 | Organics |
| K ₂ O | 2.51 | Ro | 1.44 | |
| LOI | 5.26 | log Rv | 7.572 | |

Sample MG-16

Locality Berrybush Burn

Grid reference NT 270192

Stratigraphic unit Glenkiln Shales

Zone gracilis

Collected by SWW

Analysed by SWW

Description Black graptolitic shale

| | | | | |
|--------------------------------|-------|--------|-------|----------|
| SiO ₂ | 83.66 | Cu | 133 | Albite |
| TiO ₂ | 0.55 | Pb | 72 | Chlorite |
| Al ₂ O ₃ | 4.22 | Zn | 50 | Sericite |
| Fe ₂ O ₃ | 5.53 | Rb | 57 | Pyrite |
| MnO | 0.02 | Sr | 38 | Quartz |
| MgO | 0.27 | Y | 21 | |
| CaO | 0.03 | Zr | 56 | |
| Na ₂ O | 0.11 | C | 2.04 | Organics |
| K ₂ O | 0.59 | Ro | 1.54 | |
| LOI | 7.10 | log Rv | 7.557 | |

Sample MG-17
Locality Graigierig Burn
Grid reference NT 208232
Stratigraphic unit Upper Birkhill
Zone sedgwickii?
Collected by SWW
Analysed by SWW
Description

| | | | | |
|--------------------------------|-------|--------|-------|----------|
| SiO ₂ | 55.65 | Cu | 182 | Albite |
| TiO ₂ | 0.70 | Pb | 160 | Chlorite |
| Al ₂ O ₃ | 13.85 | Zn | 37 | Sericite |
| Fe ₂ O ₃ | 11.05 | Rb | 140 | Pyrite |
| MnO | 0.08 | Sr | 31 | Quartz |
| MgO | 2.18 | Y | 37 | |
| CaO | 0.03 | Zr | 168 | |
| Na ₂ O | 0.45 | C | 1.63 | Organics |
| K ₂ O | 2.98 | Ro | 4.36 | |
| LOI | 12.85 | log Rv | 7.662 | |

Sample MG-18
Locality Dead Burn
Grid reference NT 045097
Stratigraphic unit Lower Birkhill Shales
Zone vesiculosus
Collected by SWW
Analysed by SWW
Description Flaggy grey mudstone

| | | | | |
|--------------------------------|-------|--------|-------|----------|
| SiO ₂ | 62.99 | Cu | 77 | Albite |
| TiO ₂ | 0.75 | Pb | 21 | Chlorite |
| Al ₂ O ₃ | 16.45 | Zn | 145 | Sericite |
| Fe ₂ O ₃ | 9.00 | Rb | 175 | Pyrite |
| MnO | 0.07 | Sr | 21 | Quartz |
| MgO | 2.76 | Y | 40 | |
| CaO | 0.07 | Zr | 150 | |
| Na ₂ O | 0.02 | C | 0.05 | Organics |
| K ₂ O | 5.14 | Ro | 6.67 | |
| LOI | 4.63 | log Rv | 7.667 | |

Sample MG-19

Locality Ruttonside

Grid reference NT 041079

Stratigraphic unit Birkhill Shales

Zone cyphus?

Collected by SWW

Analysed by SWW

Description Blocky black graptolitic mudstone

| | | | | |
|--------------------------------|-------|--------|-------|----------|
| SiO ₂ | 66.04 | Cu | 175 | Albite |
| TiO ₂ | 0.43 | Pb | 148 | Chlorite |
| Al ₂ O ₃ | 8.72 | Zn | 33 | Sericite |
| Fe ₂ O ₃ | 12.74 | Rb | 91 | Pyrite |
| MnO | 0.03 | Sr | 32 | Quartz |
| MgO | 1.83 | Y | 24 | |
| CaO | 0.01 | Zr | 127 | |
| Na ₂ O | 0.01 | C | 1.01 | Organics |
| K ₂ O | 1.57 | Ro | 3.14 | |
| LOI | 8.52 | log Rv | 7.437 | |

Sample MG-20

Locality Garpol Water

Grid reference NT 067031

Stratigraphic unit Upper Birkhill Shales

Zone gregarius

Collected by SWW

Analysed by SWW

Description Graptolitic shale

| | | | | |
|--------------------------------|-------|--------|-------|----------|
| SiO ₂ | 52.98 | Cu | 223 | Albite |
| TiO ₂ | 0.84 | Pb | 23 | Chlorite |
| Al ₂ O ₃ | 18.68 | Zn | 95 | Sericite |
| Fe ₂ O ₃ | 13.73 | Rb | 124 | Pyrite |
| MnO | 0.39 | Sr | 45 | Quartz |
| MgO | 3.90 | Y | 44 | |
| CaO | 0.22 | Zr | 203 | |
| Na ₂ O | 0.22 | C | 0.85 | Organics |
| K ₂ O | 2.50 | Ro | 1.78 | |
| LOI | 6.45 | log Rv | 7.543 | |

Sample MG-21

Locality Selcoth Burn

Grid reference NT 155064

Stratigraphic unit Upper Birkhill Shales

Zone convolutus

Collected by TBF

Analysed by SWW

Description Black graptolitic shale

| | | | | |
|--------------------------------|-------|--------|-------|----------|
| SiO ₂ | 64.54 | Cu | 85 | Albite |
| TiO ₂ | 0.80 | Pb | 156 | Chlorite |
| Al ₂ O ₃ | 15.18 | Zn | 21 | Sericite |
| Fe ₂ O ₃ | 6.63 | Rb | 137 | Pyrite |
| MnO | 0.03 | Sr | 55 | Quartz |
| MgO | 1.33 | Y | 41 | |
| CaO | 0.01 | Zr | 212 | |
| Na ₂ O | 0.74 | C | 1.52 | Organics |
| K ₂ O | 2.76 | Ro | | |
| LOI | 7.87 | log Rv | 7.786 | |

Sample MG-22

Locality South side of Capel Fell

Grid reference NT 165065

Stratigraphic unit Lower Birkhill Shales

Zone persculptus?

Collected by TBF

Analysed by SWW

Description Black shale

| | | | | |
|--------------------------------|-------|--------|-------|-------------------|
| SiO ₂ | 73.00 | Cu | 63 | Albite |
| TiO ₂ | 0.70 | Pb | 38 | Chlorite |
| Al ₂ O ₃ | 14.66 | Zn | 42 | Sericite |
| Fe ₂ O ₃ | 2.18 | Rb | 146 | Pyrite |
| MnO | 0.02 | Sr | 47 | Quartz |
| MgO | 1.01 | Y | 36 | |
| CaO | 0.02 | Zr | 134 | |
| Na ₂ O | 0.35 | C | | Organics analysed |
| K ₂ O | 2.40 | Ro | 0.75 | |
| LOI | 5.64 | log Rv | 7.667 | |

Sample MG-23

Locality Cornal Burn

Grid reference NT 143037

Stratigraphic unit Upper Hartfell Shales

Zone complanatus

Collected by SWW

Analysed by SWW

Description Grey mudstone

| | | | | |
|--------------------------------|-------|--------|-------|----------|
| SiO ₂ | 62.84 | Cu | 128 | Albite |
| TiO ₂ | 0.76 | Pb | 23 | Chlorite |
| Al ₂ O ₃ | 16.86 | Zn | 132 | Sericite |
| Fe ₂ O ₃ | 7.96 | Rb | 142 | Pyrite |
| MnO | 0.07 | Sr | 62 | Quartz |
| MgO | 3.01 | Y | 40 | |
| CaO | 0.04 | Zr | 159 | |
| Na ₂ O | 0.26 | C | 0.99 | Organics |
| K ₂ O | 2.47 | Ro | 2.50 | |
| LOI | 5.59 | log Rv | 7.798 | |

Sample MG-24

Locality Frenchland Burn

Grid reference NT 102052

Stratigraphic unit Lower Hartfell Shales

Zone wilsoni

Collected by SWW

Analysed by SWW

Description Platy black graptolitic shale

| | | | | |
|--------------------------------|-------|--------|-------|----------|
| SiO ₂ | 73.94 | Cu | 115 | Albite |
| TiO ₂ | 0.45 | Pb | 197 | Chlorite |
| Al ₂ O ₃ | 8.15 | Zn | 9 | Sericite |
| Fe ₂ O ₃ | 4.12 | Rb | 72 | Pyrite |
| MnO | 0.01 | Sr | 116 | Quartz |
| MgO | 0.43 | Y | 62 | |
| CaO | 0.01 | Zr | 158 | |
| Na ₂ O | 0.48 | C | 0.72 | Organics |
| K ₂ O | 1.24 | Ro | | |
| LOI | 10.59 | log Rv | 7.786 | |

Sample MG-25

Locality Scabcleuch Burn

Grid reference NT 242158

Stratigraphic unit Upper Hartfell Shales

Zone linearis

Collected by SWW

Analysed by SWW

Description Blocky black graptolitic mudstone

| | | | | |
|--------------------------------|-------|--------|-------|----------|
| SiO ₂ | 74.04 | Cu | 101 | Albite |
| TiO ₂ | 0.41 | Pb | 130 | Chlorite |
| Al ₂ O ₃ | 8.68 | Zn | 66 | Sericite |
| Fe ₂ O ₃ | 6.03 | Rb | 77 | Pyrite |
| MnO | 0.02 | Sr | 42 | Quartz |
| MgO | 1.46 | Y | 20 | |
| CaO | 0.01 | Zr | 89 | |
| Na ₂ O | 0.47 | C | 1.11 | Organics |
| K ₂ O | 1.27 | Ro | 2.37 | |
| LOI | 6.87 | log Rv | 7.763 | |

Sample MG-26

Locality Moffat Well

Grid reference NT 094076

Stratigraphic unit Lower Hartfell Shales

Zone clingani

Collected by SWW

Analysed by SWW

Description Platy black graptolitic shale

| | | | | |
|--------------------------------|-------|--------|-------|----------|
| SiO ₂ | 82.00 | Cu | 60 | Albite |
| TiO ₂ | 0.41 | Pb | 47 | Chlorite |
| Al ₂ O ₃ | 5.59 | Zn | 2 | Sericite |
| Fe ₂ O ₃ | 0.67 | Rb | 84 | Pyrite |
| MnO | 0.01 | Sr | 17 | Quartz |
| MgO | 0.32 | Y | 29 | |
| CaO | 0.01 | Zr | 85 | |
| Na ₂ O | 0.00 | C | | Organics |
| K ₂ O | 1.27 | Ro | 5.63 | |
| LOI | 9.72 | log Rv | 4.998 | |

Sample MG-27

Locality Ettrickbridgend

Grid reference NT 390242

Stratigraphic unit Lower Birkhill Shales

Zone cyphus

Collected by WES and JAW

Analysed by SWW

Description Blocky black mudstone rich in pyrite

| | | | | |
|--------------------------------|-------|--------|-------|----------|
| SiO ₂ | 67.24 | Cu | 135 | Albite |
| TiO ₂ | 0.55 | Pb | 111 | Chlorite |
| Al ₂ O ₃ | 10.41 | Zn | 40 | Sericite |
| Fe ₂ O ₃ | 9.32 | Rb | 104 | Pyrite |
| MnO | 0.03 | Sr | 19 | Quartz |
| MgO | 1.52 | Y | 23 | |
| CaO | 0.02 | Zr | 93 | |
| Na ₂ O | 0.48 | C | | Organics |
| K ₂ O | 1.73 | Ro | 3.42 | |
| LOI | 8.59 | log Rv | 7.654 | |

Sample MB4X

Locality Mountbenger

Grid reference NT 318258

Stratigraphic unit Upper Birkhill Shales

Zone convolutus

Collected by SWW

Analysed by SWW

Description Black graptolitic shale

| | | | | |
|--------------------------------|-------|--------|-------|-------------------|
| SiO ₂ | 55.64 | Cu | 131 | Albite |
| TiO ₂ | 0.67 | Pb | 81 | Chlorite |
| Al ₂ O ₃ | 16.52 | Zn | 49 | Sericite |
| Fe ₂ O ₃ | 5.61 | Rb | 114 | Pyrite |
| MnO | 0.04 | Sr | 69 | Quartz |
| MgO | 1.72 | Y | 42 | |
| CaO | 0.01 | Zr | 219 | |
| Na ₂ O | 1.44 | C | 1.69 | Organics analysed |
| K ₂ O | 2.08 | Ro | 1.39 | |
| LOI | 16.12 | log Rv | 7.722 | |

Sample LB-1

Locality East coast of Luce Bay

Grid reference NX 275505

Stratigraphic unit Upper Hartfell Shales

Zone complanatus

Collected by SWW

Analysed by SWW

Description Grey mudstone

| | | | | |
|--------------------------------|-------|--------|-------|----------|
| SiO ₂ | 62.81 | Cu | 104 | Albite |
| TiO ₂ | 0.77 | Pb | 15 | Chlorite |
| Al ₂ O ₃ | 16.64 | Zn | 100 | Sericite |
| Fe ₂ O ₃ | 7.93 | Rb | 146 | Pyrite |
| MnO | 0.21 | Sr | 34 | Quartz |
| MgO | 3.21 | Y | 35 | |
| CaO | 0.00 | Zr | 165 | |
| Na ₂ O | 0.25 | C | 0.24 | Organics |
| K ₂ O | 4.02 | Ro | 1.31 | |
| LOI | 3.98 | log Rv | 7.607 | |

Sample LB-2

Locality Garheugh

Grid reference NX 277502

Stratigraphic unit Lower Hartfell Shales

Zone clingani

Collected by SWW

Analysed by SWW

Description Fissile black shale

| | | | | |
|--------------------------------|-------|--------|-------|----------|
| SiO ₂ | 80.71 | Cu | 55 | Albite |
| TiO ₂ | 0.33 | Pb | 56 | Chlorite |
| Al ₂ O ₃ | 5.82 | Zn | 3 | Sericite |
| Fe ₂ O ₃ | 0.69 | Rb | 74 | Pyrite |
| MnO | 0.00 | Sr | 18 | Quartz |
| MgO | 0.46 | Y | 24 | |
| CaO | 0.01 | Zr | 78 | |
| Na ₂ O | 0.01 | C | 0.74 | Organics |
| K ₂ O | 9.43 | Ro | 3.03 | |
| LOI | 2.54 | log Rv | 7.566 | |

Sample LB-3

Locality Culshabben

Grid reference NX 306512

Stratigraphic unit Lower Hartfell Shales

Zone clingani

Collected by SWW

Analysed by SWW

Description Black shale

| | | | | |
|--------------------------------|-------|--------|-------|----------|
| SiO ₂ | 84.62 | Cu | 65 | Albite |
| TiO ₂ | 0.25 | Pb | 42 | Chlorite |
| Al ₂ O ₃ | 4.50 | Zn | 3 | Sericite |
| Fe ₂ O ₃ | 0.88 | Rb | 49 | Pyrite |
| MnO | 0.00 | Sr | 18 | Quartz |
| MgO | 0.26 | Y | 18 | |
| CaO | 0.00 | Zr | 45 | |
| Na ₂ O | 0.01 | C | 1.69 | Organics |
| K ₂ O | 6.22 | Ro | 2.10 | |
| LOI | 2.96 | log Rv | 7.340 | |

Sample LB-4

Locality Malzie Water

Grid reference NX 327519

Stratigraphic unit Upper Hartfell Shales

Zone linearis

Collected by SWW

Analysed by SWW

Description Siliceous Black Shale

| | | | | |
|--------------------------------|-------|--------|-------|----------|
| SiO ₂ | 84.14 | Cu | 55 | Albite |
| TiO ₂ | 0.27 | Pb | 47 | Chlorite |
| Al ₂ O ₃ | 4.53 | Zn | 2 | Sericite |
| Fe ₂ O ₃ | 0.37 | Rb | 58 | Pyrite |
| MnO | 0.00 | Sr | 43 | Quartz |
| MgO | 0.22 | Y | 14 | |
| CaO | 0.00 | Zr | 55 | |
| Na ₂ O | 0.01 | C | 0.99 | Organics |
| K ₂ O | 6.07 | Ro | 4.40 | |
| LOI | 3.96 | log Rv | 7.317 | |

Sample LB-5

Locality Ballaird

Grid reference NX 359548

Stratigraphic unit Lower Birkhill Shales

Zone

Collected by SWW

Analysed by SWW

Description Black graptolitic mudstone

| | | | | |
|--------------------------------|-------|--------|-------|----------|
| SiO ₂ | 64.29 | Cu | 100 | Albite |
| TiO ₂ | 0.76 | Pb | 28 | Chlorite |
| Al ₂ O ₃ | 16.45 | Zn | 88 | Sericite |
| Fe ₂ O ₃ | 6.99 | Rb | 141 | Pyrite |
| MnO | 0.08 | Sr | 65 | Quartz |
| MgO | 3.37 | Y | 34 | |
| CaO | 0.00 | Zr | 145 | |
| Na ₂ O | 0.41 | C | 2.26 | Organics |
| K ₂ O | 3.51 | Ro | 3.26 | |
| LOI | 3.64 | log Rv | 7.568 | |

Sample LB-5A

Locality Ballaird

Grid reference NX 364548

Stratigraphic unit Lower Birkhill Shales

Zone

Collected by SWW

Analysed by SWW

Description Pyritised black shale

| | | | | |
|--------------------------------|-------|--------|-------|----------|
| SiO ₂ | 59.61 | Cu | 99 | Albite |
| TiO ₂ | 0.64 | Pb | 60 | Chlorite |
| Al ₂ O ₃ | 15.90 | Zn | 59 | Sericite |
| Fe ₂ O ₃ | 7.77 | Rb | 149 | Pyrite |
| MnO | 0.05 | Sr | 55 | Quartz |
| MgO | 3.00 | Y | 54 | |
| CaO | 0.14 | Zr | 157 | |
| Na ₂ O | 0.45 | C | 1.61 | Organics |
| K ₂ O | 3.58 | Ro | 3.26 | |
| LOI | 7.93 | log Rv | 7.467 | |

Sample LB-6

Locality Ballaird

Grid reference NX 366544

Stratigraphic unit Lower Birkhill Shales

Zone

Collected by SWW

Analysed by SWW

Description Pyritised black shale

| | | | | |
|--------------------------------|-------|--------|-------|----------|
| SiO ₂ | 66.09 | Cu | 85 | Albite |
| TiO ₂ | 0.79 | Pb | 23 | Chlorite |
| Al ₂ O ₃ | 15.70 | Zn | 64 | Sericite |
| Fe ₂ O ₃ | 6.40 | Rb | 144 | Pyrite |
| MnO | 0.18 | Sr | 57 | Quartz |
| MgO | 2.90 | Y | 32 | |
| CaO | 0.00 | Zr | 141 | |
| Na ₂ O | 0.12 | C | 0.15 | Organics |
| K ₂ O | 3.75 | Ro | | |
| LOI | 4.04 | log Rv | 7.527 | |

Sample LB-8

Locality South east of Whitefield Loch

Grid reference NX 242548

Stratigraphic unit Upper Birkhill Shales

Zone

Collected by SWW

Analysed by SWW

Description Grey shale

| | | | | |
|--------------------------------|-------|--------|-------|----------|
| SiO ₂ | 63.42 | Cu | 84 | Albite |
| TiO ₂ | 0.84 | Pb | 51 | Chlorite |
| Al ₂ O ₃ | 16.39 | Zn | 94 | Sericite |
| Fe ₂ O ₃ | 7.09 | Rb | 131 | Pyrite |
| MnO | 0.04 | Sr | 83 | Quartz |
| MgO | 3.33 | Y | 43 | |
| CaO | 0.00 | Zr | 168 | |
| Na ₂ O | 0.50 | C | 0.58 | Organics |
| K ₂ O | 3.46 | Ro | 1.83 | |
| LOI | 4.62 | log Rv | 7.578 | |

Sample LB-9

Locality Gillespie Burn

Grid reference NX 258540

Stratigraphic unit Upper Hartfell Shales

Zone linearis

Collected by SWW

Analysed by SWW

Description Platy pyritised black shale

| | | | | |
|--------------------------------|-------|--------|-------|----------|
| SiO ₂ | 87.19 | Cu | 59 | Albite |
| TiO ₂ | 0.17 | Pb | 34 | Chlorite |
| Al ₂ O ₃ | 3.83 | Zn | 1 | Sericite |
| Fe ₂ O ₃ | 0.49 | Rb | 48 | Pyrite |
| MnO | 0.01 | Sr | 15 | Quartz |
| MgO | 0.17 | Y | 14 | |
| CaO | 0.01 | Zr | 35 | |
| Na ₂ O | 0.01 | C | 1.09 | Organics |
| K ₂ O | 5.46 | Ro | 4.54 | |
| LOI | 2.31 | log Rv | 7.429 | |

Sample LB-10

Locality Culroy

Grid reference NX 253542

Stratigraphic unit Lower Birkhill Shales

Zone

Collected by SWW

Analysed by SWW

Description Black mudstone with abundant pyrite grains

| | | | | |
|--------------------------------|-------|--------|------|----------|
| SiO ₂ | 63.88 | Cu | 100 | Albite |
| TiO ₂ | 0.75 | Pb | 44 | Chlorite |
| Al ₂ O ₃ | 15.71 | Zn | 72 | Sericite |
| Fe ₂ O ₃ | 7.14 | Rb | 115 | Pyrite |
| MnO | 0.04 | Sr | 53 | Quartz |
| MgO | 2.51 | Y | 33 | |
| CaO | 0.00 | Zr | 158 | |
| Na ₂ O | 0.67 | C | 1.22 | Organics |
| K ₂ O | 2.71 | Ro | 2.54 | |
| LOI | 6.22 | log Rv | 7.06 | |

Sample LB-11

Locality Near Barhaskine

Grid reference NX 268542

Stratigraphic unit Upper Birkhill Shales

Zone

Collected by SWW

Analysed by SWW

Description Grey mudstone

| | | | | |
|--------------------------------|-------|--------|-------|----------|
| SiO ₂ | 60.91 | Cu | 81 | Albite |
| TiO ₂ | 0.75 | Pb | 35 | Chlorite |
| Al ₂ O ₃ | 15.04 | Zn | 49 | Sericite |
| Fe ₂ O ₃ | 8.80 | Rb | 121 | Pyrite |
| MnO | 0.04 | Sr | 61 | Quartz |
| MgO | 3.45 | Y | 30 | |
| CaO | 0.00 | Zr | 178 | |
| Na ₂ O | 0.52 | C | 0.27 | Organics |
| K ₂ O | 2.82 | Ro | 1.89 | |
| LOI | 7.58 | log Rv | 7.490 | |

Sample LB-12

Locality Clanyard Bay

Grid reference NX 101381

Stratigraphic unit Upper Hartfell Shales

Zone complanatus

Collected by SWW

Analysed by SWW

Description Badly cleaved grey mudstone

| | | | | | |
|--------------------------------|--|--------|-------|----------|------|
| SiO ₂ | | Cu | 77 | Albite | 3.9 |
| TiO ₂ | | Pb | 21 | Chlorite | 9.3 |
| Al ₂ O ₃ | | Zn | 124 | Sericite | 19.5 |
| Fe ₂ O ₃ | | Rb | 162 | Pyrite | 14.6 |
| MnO | | Sr | 109 | Quartz | 52.7 |
| MgO | | Y | 37 | | |
| CaO | | Zr | 137 | | |
| Na ₂ O | | C | 0.11 | Organics | |
| K ₂ O | | Ro | 3.29 | | |
| LOI | | log Rv | 7.297 | | |

Sample LB-13

Locality Clanyard Bay

Grid reference NX 101381

Stratigraphic unit Upper Hartfell Shales

Zone complanatus

Collected by SWW

Analysed by SWW

Description Badly cleaved grey mudstone

| | | | | |
|--------------------------------|--------|-------|----------|------|
| SiO ₂ | Cu | 80 | Albite | 3.9 |
| TiO ₂ | Pb | 22 | Chlorite | 7.8 |
| Al ₂ O ₃ | Zn | 94 | Sericite | 22.7 |
| Fe ₂ O ₃ | Rb | 200 | Pyrite | 11.6 |
| MnO | Sr | 77 | Quartz | 54.0 |
| MgO | Y | 46 | | |
| CaO | Zr | 143 | | |
| Na ₂ O | C | 0.21 | Organics | |
| K ₂ O | Ro | 3.38 | | |
| LOI | log Rv | 7.413 | | |

Sample LB-14

Locality Clanyard Bay

Grid reference NX 101381

Stratigraphic unit Upper Hartfell Shales

Zone

Collected by SWW

Analysed by SWW

Description Hard, dark grey mudstone with some pyrite present

| | | | | |
|--------------------------------|--------|-------|----------|------|
| SiO ₂ | Cu | 74 | Albite | 0.0 |
| TiO ₂ | Pb | 23 | Chlorite | 15.4 |
| Al ₂ O ₃ | Zn | 64 | Sericite | 15.8 |
| Fe ₂ O ₃ | Rb | 58 | Pyrite | 7.7 |
| MnO | Sr | 51 | Quartz | 61.1 |
| MgO | Y | 35 | | |
| CaO | Zr | 94 | | |
| Na ₂ O | C | 0.71 | Organics | |
| K ₂ O | Ro | 3.89 | | |
| LOI | log Rv | 7.118 | | |

Sample LB-15

Locality Clanyard Bay

Grid reference NX 101381

Stratigraphic unit Upper Hartfell Shales

Zone

Collected by SWW

Analysed by SWW

Description Blocky black mudstone with pyrite and free sulphur present

| | | | | | |
|--------------------------------|-------|--------|-------|----------|------|
| SiO ₂ | 80.11 | Cu | 121 | Albite | 4.1 |
| TiO ₂ | 0.44 | Pb | 49 | Chlorite | 4.0 |
| Al ₂ O ₃ | 8.77 | Zn | 25 | Sericite | 12.3 |
| Fe ₂ O ₃ | 4.34 | Rb | 75 | Pyrite | 5.3 |
| MnO | 0.02 | Sr | 57 | Quartz | 74.3 |
| MgO | 0.05 | Y | 20 | | |
| CaO | 0.01 | Zr | 93 | | |
| Na ₂ O | 0.05 | C | 0.87 | Organics | |
| K ₂ O | 1.35 | Ro | 3.98 | | |
| LOI | 4.62 | log Rv | 6.845 | | |

Sample LB-16

Locality Clanyard Bay

Grid reference NX 101381

Stratigraphic unit Upper Hartfell Shales

Zone

Collected by SWW

Analysed by SWW

Description Dark grey shale

| | | | | | |
|--------------------------------|--|--------|-------|----------|------|
| SiO ₂ | | Cu | 96 | Albite | 2.0 |
| TiO ₂ | | Pb | 36 | Chlorite | 3.4 |
| Al ₂ O ₃ | | Zn | 33 | Sericite | 7.4 |
| Fe ₂ O ₃ | | Rb | 77 | Pyrite | 9.2 |
| MnO | | Sr | 45 | Quartz | 78.1 |
| MgO | | Y | 19 | | |
| CaO | | Zr | 105 | | |
| Na ₂ O | | C | 0.36 | Organics | |
| K ₂ O | | Ro | 4.15 | | |
| LOI | | log Rv | 7.308 | | |

Sample LB-17

Locality Clanyard Bay

Grid reference NX 101381

Stratigraphic unit Upper Hartfell Shales

Zone

Collected by SWW

Analysed by SWW

Description Platy blue-grey shale

| | | | | |
|--------------------------------|--------|--------|----------|------|
| SiO ₂ | Cu | 65 | Albite | 6.1 |
| TiO ₂ | Pb | 20 | Chlorite | 21.7 |
| Al ₂ O ₃ | Zn | 70 | Sericite | 12.6 |
| Fe ₂ O ₃ | Rb | 177 | Pyrite | 5.2 |
| MnO | Sr | 46 | Quartz | 54.6 |
| MgO | Y | 45 | | |
| CaO | Zr | 143 | | |
| Na ₂ O | C | 0.16 | Organics | |
| K ₂ O | Ro | 4.60 | | |
| LOI | log Rv | 6.4331 | | |

Sample LB-18

Locality Clanyard Bay

Grid reference NX 101381

Stratigraphic unit Upper Hartfell Shales

Zone

Collected by SWW

Analysed by SWW

Description Very hard steel-grey shale

| | | | | |
|--------------------------------|--------|-------|----------|------|
| SiO ₂ | Cu | 125 | Albite | 8.5 |
| TiO ₂ | Pb | 24 | Chlorite | 19.4 |
| Al ₂ O ₃ | Zn | 70 | Sericite | 11.7 |
| Fe ₂ O ₃ | Rb | 87 | Pyrite | 4.4 |
| MnO | Sr | 65 | Quartz | 56.0 |
| MgO | Y | 27 | | |
| CaO | Zr | 137 | | |
| Na ₂ O | C | 0.29 | Organics | |
| K ₂ O | Ro | 7.60 | | |
| LOI | log Rv | 6.336 | | |

Sample LB-19
 Locality Clanyard Bay
 Grid reference NX 101381
 Stratigraphic unit
 Zone
 Collected by SWW
 Analysed by SWW
 Description Porphyrite dyke

| | | | |
|--------------------------------|--------|-----|----------|
| SiO ₂ | Cu | 82 | Albite |
| TiO ₂ | Pb | 26 | Chlorite |
| Al ₂ O ₃ | Zn | 76 | Sericite |
| Fe ₂ O ₃ | Rb | 56 | Pyrite |
| MnO | Sr | 965 | Quartz |
| MgO | Y | 19 | |
| CaO | Zr | 174 | |
| Na ₂ O | C | | Organics |
| K ₂ O | Ro | | |
| LOI | log Rv | | |

Sample LB-20
 Locality Clanyard Bay
 Grid reference NX 101381
 Stratigraphic unit Lower Birkhill Shales
 Zone
 Collected by SWW
 Analysed by SWW
 Description Baked, bleached shale with abundant quartz veins

| | | | | |
|--------------------------------|--------|-------|----------|------|
| SiO ₂ | Cu | 110 | Albite | 2.9 |
| TiO ₂ | Pb | 30 | Chlorite | 5.5 |
| Al ₂ O ₃ | Zn | 55 | Sericite | 12.9 |
| Fe ₂ O ₃ | Rb | 94 | Pyrite | 6.0 |
| MnO | Sr | 40 | Quartz | 72.7 |
| MgO | Y | 33 | | |
| CaO | Zr | 169 | | |
| Na ₂ O | C | 1.03 | Organics | |
| K ₂ O | Ro | 4.04 | | |
| LOI | log Rv | 6.496 | | |

Sample LB-21

Locality Clanyard Bay

Grid reference NX 101381

Stratigraphic unit Lower Birkhill Shales

Zone anceps?

Collected by SWW

Analysed by SWW

Description Blocky black mudstone rich in sulphur

| | | | | |
|--------------------------------|--------|-------|----------|------|
| SiO ₂ | Cu | 113 | Albite | 4.5 |
| TiO ₂ | Pb | 50 | Chlorite | 5.4 |
| Al ₂ O ₃ | Zn | 40 | Sericite | 0.9 |
| Fe ₂ O ₃ | Rb | 97 | Pyrite | 18.9 |
| MnO | Sr | 27 | Quartz | 70.3 |
| MgO | Y | 26 | | |
| CaO | Zr | 119 | | |
| Na ₂ O | C | 1.02 | Organics | |
| K ₂ O | Ro | 5.59 | | |
| LOI | log Rv | 7.677 | | |

Sample LB-22

Locality Clanyard Bay

Grid reference NX 101381

Stratigraphic unit Lower Birkhill Shales

Zone

Collected by SWW

Analysed by SWW

Description Blocky black mudstone with shale intercalations

| | | | | |
|--------------------------------|--------|-------|----------|------|
| SiO ₂ | Cu | 99 | Albite | 2.9 |
| TiO ₂ | Pb | 73 | Chlorite | 4.4 |
| Al ₂ O ₃ | Zn | 24 | Sericite | 13.1 |
| Fe ₂ O ₃ | Rb | 77 | Pyrite | 10.9 |
| MnO | Sr | 27 | Quartz | 68.8 |
| MgO | Y | 24 | | |
| CaO | Zr | 92 | | |
| Na ₂ O | C | 1.04 | Organics | |
| K ₂ O | Ro | 4.11 | | |
| LOI | log Rv | 7.009 | | |

Sample LB-24

Locality Clanyard Bay

Grid reference NX 101381

Stratigraphic unit Lower Birkhill Shales

Zone

Collected by SWW

Analysed by SWW

Description Black shale

| | | | | | |
|--------------------------------|--|--------|-------|----------|------|
| SiO ₂ | | Cu | 80 | Albite | 8.8 |
| TiO ₂ | | Pb | 12 | Chlorite | 14.6 |
| Al ₂ O ₃ | | Zn | 68 | Sericite | 24.8 |
| Fe ₂ O ₃ | | Rb | 137 | Pyrite | 4.5 |
| MnO | | Sr | 52 | Quartz | 47.3 |
| MgO | | Y | 37 | | |
| CaO | | Zr | 181 | | |
| Na ₂ O | | C | 1.13 | Organics | |
| K ₂ O | | Ro | 2.61 | | |
| LOI | | log Rv | 6.072 | | |

Sample LB-25

Locality Drumbreddan Bay

Grid reference NX 078038

Stratigraphic unit Upper Birkhill Shales

Zone gregarius

Collected by SWW

Analysed by SWW

Description Black shale

| | | | | | |
|--------------------------------|-------|--------|-------|----------|------|
| SiO ₂ | 58.56 | Cu | 142 | Albite | 7.2 |
| TiO ₂ | 0.86 | Pb | 56 | Chlorite | 6.5 |
| Al ₂ O ₃ | 17.29 | Zn | 105 | Sericite | 24.0 |
| Fe ₂ O ₃ | 7.64 | Rb | 155 | Pyrite | 13.8 |
| MnO | 0.07 | Sr | 92 | Quartz | 48.5 |
| MgO | 2.42 | Y | 40 | | |
| CaO | 0.16 | Zr | 199 | | |
| Na ₂ O | 0.32 | C | 1.40 | Organics | |
| K ₂ O | 4.19 | Ro | 2.94 | | |
| LOI | 7.04 | log Rv | 7.685 | | |

Sample LB-26

Locality Malzie Water

Grid reference NX 340522

Stratigraphic unit Upper Birkhill Shales

Zone

Collected by SWW

Analysed by SWW

Description Dark grey mudstone

| | | | | |
|--------------------------------|-------|--------|------|----------|
| SiO ₂ | 63.49 | Cu | 120 | Albite |
| TiO ₂ | 0.96 | Pb | 16 | Chlorite |
| Al ₂ O ₃ | 18.39 | Zn | 56 | Sericite |
| Fe ₂ O ₃ | 7.32 | Rb | 133 | Pyrite |
| MnO | 0.23 | Sr | 107 | Quartz |
| MgO | 1.75 | Y | 47 | |
| CaO | 0.00 | Zr | 276 | |
| Na ₂ O | 0.72 | C | 0.45 | Organics |
| K ₂ O | 3.19 | Ro | 3.17 | |
| LOI | 3.86 | log Rv | | |

| Sample | Sulphur % | Fe ₂ O ₃ % | Fe ³⁺ % | Modal pyrite % |
|--------|--------------|-------------------------------------|-----------------------|-------------------|
| 2A-2 | 3.17 | 8.24 | 5.76 | 18.95 |
| B-1 | nd | 0.98 | 0.69 | 5.24 |
| C-1 | nd | 0.13 | 0.09 | 4.85 |
| 2C-5 | 2.57 | 8.87 | 6.20 | 16.90 |
| 2C-6 | 6.04 | 14.61 | 10.22 | 27.97 |
| ID-3 | 0.45 | 1.43 | 1.00 | 4.72 |
| ID-4 | nd | 4.92 | 3.44 | 6.74 |
| ID-5 | 0.02 | 5.05 | 3.53 | 6.03 |
| ID-6 | nd | 5.09 | 3.56 | 6.66 |
| ID-7 | 0.97 | 4.56 | 3.19 | 6.13 |
| 1E-6 | 1.86 | 5.30 | 3.70 | 6.90 |
| 2E-6 | 0.02 | 4.97 | 3.48 | 6.51 |
| 1F-5 | 3.21 | 9.29 | 6.50 | 19.82 |
| 2F-10 | 1.24 | 3.71 | 2.59 | 10.61 |
| 2F-11 | nd | 7.04 | 4.92 | 4.18 |
| GK-1 | 1.71 | 6.60 | 4.62 | 14.67 |
| GK-2 | 0.15 | 6.20 | 4.36 | 6.18 |
| GK-3 | 2.02 | 6.90 | 4.82 | 15.52 |
| GK-4 | 0.05 | 1.10 | 0.79 | 4.87 |
| GK-5 | 0.15 | 0.70 | 0.50 | 4.50 |
| H-1 | nd | 0.10 | 0.09 | 4.68 |
| H-2 | 0.05 | 0.80 | 0.56 | 6.93 |
| H-5 | 0.52 | 1.50 | 1.07 | 7.02 |
| H-6 | 0.21 | 0.80 | 0.57 | 5.17 |
| MB-1 | 0.87 | 2.25 | 1.57 | 7.87 |
| MB-2 | 2.12 | 4.20 | 2.94 | 12.97 |
| MB-3 | 10.59 | 19.40 | 13.56 | - |

5. STANDARD DEVIATION VALUES FOR GRAPTOLITE REFLECTIVITY MEASUREMENTS

| Sample | Ro (mean) | n | s | Sample | Ro (mean) | n | s |
|--------|-----------|----|------|--------|-----------|----|------|
| HRC-1 | 4.85 | 5 | 0.45 | HCL-30 | 3.59 | 67 | 0.46 |
| HG-1 | 4.87 | 4 | 0.47 | HCL-31 | 4.72 | 37 | 0.69 |
| HG-2 | 1.87 | 3 | 0.13 | HCL-32 | 2.97 | 7 | 0.98 |
| IW-1 | 1.71 | 23 | 0.21 | HCL-33 | 3.53 | 8 | 0.18 |
| IW-3 | 4.92 | 34 | 0.52 | HCL-34 | 3.65 | 22 | 0.61 |
| IW-5 | 5.07 | 13 | 0.29 | HL-1 | 5.50 | 24 | 0.52 |
| HCL-1 | 4.84 | 27 | 0.49 | HL-3 | 4.50 | 19 | 0.47 |
| HCL-2 | 4.67 | 18 | 0.37 | HL-4 | 5.70 | 49 | 0.32 |
| HCL-3 | 5.07 | 24 | 0.34 | HL-5 | 4.99 | 31 | 0.39 |
| HCL-5 | 4.80 | 33 | 0.49 | HL-6 | 4.48 | 30 | 0.52 |
| HCL-6 | 4.97 | 48 | 0.58 | HL-7 | 5.24 | 29 | 0.42 |
| HCL-7 | 3.82 | 23 | 0.80 | HL-8 | 4.92 | 26 | 0.46 |
| HCL-8 | 4.01 | 16 | 0.41 | HL-9 | 4.70 | 38 | 0.33 |
| HCL-9 | 4.47 | 9 | 0.51 | HL-10 | 4.36 | 27 | 0.42 |
| HCL-10 | 4.10 | 15 | 0.37 | HL-11 | 4.95 | 24 | 0.70 |
| HCL-11 | 2.42 | 11 | 0.83 | HL-12 | 5.62 | 52 | 0.28 |
| HCL-12 | 4.10 | 23 | 0.37 | HL-13 | 4.59 | 28 | 0.72 |
| HCL-13 | 4.32 | 14 | 0.31 | HL-14 | 4.64 | 30 | 0.66 |
| HCL-14 | 4.09 | 16 | 0.37 | HL-15 | 4.76 | 27 | 0.49 |
| HCL-15 | 3.95 | 22 | 0.60 | HL-16 | 4.55 | 29 | 0.47 |
| HCL-16 | 4.51 | 29 | 0.54 | HL-17 | 3.38 | 26 | 0.41 |
| HCL-17 | 4.51 | 21 | 0.60 | HC-1 | 5.59 | 4 | 0.98 |
| HCL-18 | 4.20 | 10 | 0.47 | DCL-1 | 2.27 | 14 | 0.64 |
| HCL-19 | 4.76 | 5 | 1.27 | DL-2 | 2.60 | 21 | 0.51 |
| HCL-20 | 4.89 | 27 | 0.39 | DL-3 | 2.60 | 38 | 0.55 |
| HCL-22 | 4.75 | 18 | 0.64 | DL-4 | 2.80 | 17 | 0.34 |
| HCL-25 | 4.98 | 25 | 0.42 | DL-5 | 3.00 | 33 | 0.37 |
| HCL-26 | 5.20 | 47 | 0.87 | DC-1 | 4.65 | 11 | 0.79 |
| HCL-27 | 4.54 | 11 | 0.46 | DC-2 | 3.20 | 41 | 0.63 |
| HCL-29 | 4.41 | 33 | 0.43 | DA-1 | 2.78 | 43 | 0.80 |

Ro (mean) : mean reflectivity in oil at 546 nm

n : number of measurements

s : standard deviation

| Sample | Ro (mean) | n | s | Sample | Ro (mean) | n | s |
|---------|-----------|----|------|--------|-----------|----|------|
| DPE-1 | 3.65 | 18 | 0.39 | MG-3 | 2.88 | 19 | 0.39 |
| DPE-2 | 3.26 | 38 | 0.39 | MG-4 | 2.81 | 20 | 0.41 |
| DAC-1 | 2.89 | 19 | 0.33 | MG-5 | 2.04 | 9 | 0.45 |
| DVE-1 | 3.39 | 31 | 0.31 | MG-5A | 3.99 | 16 | 0.56 |
| DVE-2 | 3.65 | 15 | 0.38 | MG-7 | 2.56 | 3 | 0.26 |
| DCYP-1 | 4.04 | 18 | 0.49 | MG-8 | 2.27 | 8 | 0.61 |
| DCYP-3 | 2.91 | 12 | 0.41 | MG-9 | 2.56 | 15 | 0.49 |
| DCYP-4 | 4.02 | 23 | 0.56 | MG-10 | 2.32 | 16 | 0.56 |
| DCYP-5 | 2.75 | 16 | 0.68 | MG-11 | 6.50 | 21 | 0.38 |
| DCYP-6 | 3.59 | 43 | 0.44 | MG-12 | 2.27 | 24 | 0.56 |
| DCYP-7 | 2.58 | 28 | 0.69 | MG-13 | 2.16 | 6 | 0.41 |
| DCYP-8 | 3.33 | 14 | 0.49 | MG-14 | 1.68 | 31 | 0.23 |
| DCYP-9 | 3.67 | 21 | 0.64 | MG-15 | 1.44 | 16 | 0.46 |
| DCYP-10 | 3.24 | 12 | 0.39 | MG-16 | 1.54 | 16 | 0.38 |
| DCYP-11 | 3.82 | 45 | 0.38 | MG-17 | 4.36 | 25 | 0.75 |
| DCYP-12 | 2.72 | 23 | 0.31 | MG-18 | 6.67 | 15 | 0.77 |
| DCYP-13 | 2.77 | 19 | 0.71 | MG-19 | 3.14 | 10 | 0.69 |
| DGR-1 | 2.00 | 8 | 0.46 | MG-20 | 1.78 | 25 | 0.30 |
| DCV-1 | 3.51 | 17 | 0.56 | MG-23 | 2.50 | 14 | 0.23 |
| DCV-2 | 4.64 | 22 | 0.38 | MG-25 | 2.37 | 15 | 0.11 |
| DSE-1 | 3.68 | 16 | 0.39 | MG-26 | 5.63 | 35 | 0.34 |
| DMAX-1 | 4.21 | 5 | 0.31 | MG-27 | 3.42 | 18 | 0.50 |
| 1E-1 | 2.45 | 3 | 0.37 | MBAX | 1.39 | 30 | 0.22 |
| 2-1 | 2.67 | 32 | 0.36 | LB-1 | 1.31 | 5 | 0.05 |
| GL-GL1 | 2.40 | 19 | 0.38 | LB-2 | 3.03 | 18 | 0.30 |
| GL-W1 | 2.02 | 22 | 0.41 | LB-3 | 2.10 | 20 | 0.43 |
| GL-W2 | 1.86 | 18 | 0.31 | LB-4 | 1.40 | 24 | 0.64 |
| GL-CL1 | 1.95 | 28 | 0.36 | LB-5 | 3.26 | 19 | 0.43 |
| MG-1 | 2.10 | 8 | 0.47 | LB-5A | 3.26 | 21 | 0.36 |
| MG-2 | 1.89 | 7 | 0.49 | LB-7 | 4.12 | 21 | 0.58 |

Ro (mean) : mean reflectivity in oil at 516 nm

n : number of measurements

s : standard deviation

| Sample | Ro (mean) | n | s | Sample | Ro (mean) | n | s |
|---------|-----------|----|------|--------|-----------|----|------|
| LB-8 | 1.83 | 16 | 0.31 | MBL-1 | 2.20 | 23 | 0.43 |
| LB-9 | 4.54 | 18 | 0.61 | B-1 | 2.66 | 18 | 0.28 |
| LB-10 | 2.54 | 16 | 0.87 | LBR-1 | 3.31 | 20 | 0.48 |
| LB-11 | 1.89 | 17 | 0.66 | LBR-2 | 4.26 | 14 | 0.57 |
| LB-12 | 3.29 | 17 | 0.52 | LBR-3 | 3.88 | 31 | 0.52 |
| LB-13 | 3.38 | 22 | 0.53 | LBR-4 | 4.45 | 24 | 0.64 |
| LB-14 | 3.89 | 41 | 0.63 | LBR-5 | 4.64 | 29 | 0.51 |
| LB-15 | 3.98 | 27 | 0.55 | LBR-6 | 2.68 | 5 | 0.08 |
| LB-16 | 4.15 | 19 | 0.41 | LBR-7 | 4.68 | 35 | 0.49 |
| LB-17 | 4.60 | 13 | 0.38 | LBR-8 | 6.86 | 29 | 0.81 |
| LB-18 | 7.60 | 41 | 0.47 | LBR-9 | 3.52 | 40 | 0.74 |
| LB-20 | 4.04 | 25 | 0.57 | LBR-10 | 4.45 | 19 | 0.66 |
| LB-21 | 5.59 | 26 | 0.64 | LBR-11 | 4.62 | 20 | 0.19 |
| LB-22 | 4.11 | 17 | 0.63 | LBR-12 | 3.90 | 15 | 0.59 |
| LB-23 | 3.46 | 10 | 0.47 | LBR-13 | 6.50 | 20 | 0.63 |
| LB-24 | 2.61 | 23 | 0.39 | LBR-14 | 6.03 | 3 | 0.71 |
| LB-25 | 2.94 | 17 | 0.63 | LBR-15 | 4.55 | 22 | 0.71 |
| LB-26 | 3.17 | 16 | 0.59 | LBR-16 | 4.57 | 39 | 0.34 |
| DRC-455 | 6.18 | 16 | 0.59 | LBR-17 | 2.87 | 13 | 0.63 |
| DRC-457 | 4.51 | 27 | 0.74 | LBR-18 | 2.00 | 37 | 0.65 |
| DRC-459 | 1.93 | 11 | 0.58 | LBR-20 | 5.28 | 18 | 0.76 |
| DRC-462 | 7.23 | 17 | 0.49 | LBR-21 | 4.55 | 14 | 0.38 |
| LD-1 | 3.16 | 16 | 0.73 | LBR-22 | 4.99 | 16 | 0.24 |
| LD-2 | 5.55 | 15 | 0.78 | LBR-23 | 4.23 | 14 | 0.46 |
| LD-3 | 7.05 | 13 | 0.83 | LBR-24 | 4.00 | 23 | 0.37 |
| LD-4 | 1.90 | 20 | 0.46 | LBR-25 | 3.81 | 15 | 0.18 |
| C-1 | 3.24 | 33 | 0.61 | LBR-29 | 4.00 | 53 | 0.39 |

Ro (mean) : mean reflectivity in oil at 546 nm

n : number of measurements

s : standard deviation

THE SEDIMENTARY GEOCHEMISTRY OF THE
MOFFAT SHALES : A CARBONACEOUS SEQUENCE
IN THE SOUTHERN UPLANDS OF SCOTLAND

by

STEWART W. WATSON, BSc.

V O L U M E 3 F I G U R E S

Thesis presented for the degree of Doctor of Philosophy of
the University of St. Andrews in the Faculty of Science.

1976.



TH 8944

CONTENTS

- Fig.1. Simplified geological map of Southern Uplands of Scotland, showing disposition of facies belts.
- Fig.2. Key to Figure 3.
- Fig.3. Facies distribution at Dobb's Linn.
- Fig.4. Location of the Moffat Shales and sampled inliers.
- Fig.5. Sketch map indicating areas of study in the south-west of Scotland.
- Fig.6. Location of samples collected from the north cliff at Hartfell.
- Fig.7. Geological map of the Craigmichan Scaurs.
- Fig.8. Cross-sections along lines A-A', B-B', C-C' in Figure 7, with schematic interpretations of structures in depth.
- Fig.9. Structure of the north cliff at Hartfell.
- Fig.10. Structural and locality map of the Southern Uplands.
- Fig.11. Structural and locality map of Ireland.
- Fig.12. Evolution of Zone B of the Caledonian orogen-1.
- Fig.13. Evolution of Zone B of the Caledonian orogen-2.
- Fig.14. NNW-SSE sections to illustrate the structural evolution of the Southern Uplands.

- Fig.15. Reproduction of a computer drawn template used in the identification of X-ray diffractogram peaks.
- Fig.16. Stratigraphic location of samples.
- Fig.17. Plots illustrating the effects of glycerol and dilute hydrochloric acid on the X-ray reflections of sample DCYP-3.
- Fig.18. Plots illustrating the effects of temperature on the X-ray reflections of sample DCYP-3.
- Fig.19. Calibration curves for two component mixtures used in modal analysis by X-ray diffraction.
- Fig.20. Key to symbols used in stratigraphic variation diagrams.
- Fig.21. Plots illustrating the stratigraphic variation of albite and chlorite concentrations in the Moffat Shales.
- Fig.22. Plots illustrating the stratigraphic variation of sericite and pyrite concentrations in the Moffat Shales.
- Fig.23. Plot illustrating the stratigraphic variation of quartz concentration in the Moffat Shales.
- Fig.24. Comparison of profiles illustrated in Figures 21-23.
- Fig.25. Histograms of the variation in graptolite stipe orientations.
- Fig.26. Location map for samples collected from the eastern margin of Luce Bay.
- Fig.27. Mean values for the elements in the Moffat Shales compared with ranges from Vine and Tourtelot (1970).

- Fig.28. Histograms of the major element oxides in the Moffat Shales.
- Fig.29. Histograms of minor elements in the Moffat Shales.
- Fig.30. Global-fit and iterative surface maps for the variation of SiO_2 in the Moffat Shales.
- Fig.31. Global-fit and iterative surface maps for the variation of TiO_2 in the Moffat Shales.
- Fig.32. Global-fit and iterative surface maps for the variation of Al_2O_3 in the Moffat Shales.
- Fig.33. Global-fit and iterative surface maps for the variation of Fe_2O_3 in the Moffat Shales.
- Fig.34. Global-fit and iterative surface maps for the variation of MnO in the Moffat Shales.
- Fig.35. Global-fit and iterative surface maps for the variation of MgO in the Moffat Shales.
- Fig.36. Global-fit and iterative surface maps for the variation of CaO in the Moffat Shales.
- Fig.37. Global-fit and iterative surface maps for the variation of Na_2O in the Moffat Shales.
- Fig.38. Global-fit and iterative surface maps for the variation of K_2O in the Moffat Shales.
- Fig.39. Global-fit and iterative surface maps for the variation of loss on ignition in the Moffat Shales.

- Fig.40. Global-fit and iterative surface maps for the variation of copper in the Moffat Shales.
- Fig.41. Global-fit and iterative surface maps for the variation of lead in the Moffat Shales.
- Fig.42. Global-fit and iterative surface maps for the variation of zinc in the Moffat Shales.
- Fig.43. Global-fit and iterative surface maps for the variation of rubidium in the Moffat Shales.
- Fig.44. Global-fit and iterative surface maps for the variation of strontium in the Moffat Shales.
- Fig.45. Global-fit and iterative surface maps for the variation of yttrium in the Moffat Shales.
- Fig.46. Global-fit and iterative surface maps for the variation of zirconium in the Moffat Shales.
- Fig.47. Global-fit and iterative surface maps for the variation of carbon in the Moffat Shales.
- Fig.48. Plots illustrating the stratigraphic variation of SiO_2 and TiO_2 concentrations in the Moffat Shales.
- Fig.49. Plots illustrating the stratigraphic variation of Al_2O_3 and Fe_2O_3 concentrations in the Moffat Shales.
- Fig.50. Plots illustrating the stratigraphic variation of MnO and MgO concentrations in the Moffat Shales.
- Fig.51. Plots illustrating the stratigraphic variation of CaO and Na_2O concentrations in the Moffat Shales.

- Fig.52. Plots illustrating the stratigraphic variation of K_2O concentrations and loss on ignition values in the Moffat Shales.
- Fig.53. Plots illustrating the stratigraphic variation of copper and lead concentrations in the Moffat Shales.
- Fig.54. Plots illustrating the stratigraphic variation of zinc and rubidium concentrations in the Moffat Shales.
- Fig.55. Plots illustrating the stratigraphic variation of strontium and yttrium concentrations in the Moffat Shales.
- Fig.56. Plots illustrating the stratigraphic variation of zirconium concentration and muscovite basal-spacing values in the Moffat Shales.
- Fig.57. Plots illustrating the stratigraphic variation of carbon and sulphur concentrations in the Moffat Shales.
- Fig.58. Key to symbols used for various stratigraphic units at Hartfell.
- Fig.59. Plots illustrating the stratigraphic variation of the SiO_2 concentration in the sediments of the north cliff at Hartfell Scaur.
- Fig.60. Plot illustrating the stratigraphic variation of the TiO_2 concentration in the sediments of the north cliff at Hartfell Scaur.
- Fig.61. Plots illustrating the stratigraphic variation of the Al_2O_3 concentration in the sediments of the north cliff at Hartfell Scaur.

- Fig.62. Plots illustrating the stratigraphic variation of the Fe_2O_3 concentration in the sediments of the north cliff at Hartfell Scaur.
- Fig.63. Plots illustrating the stratigraphic variation of the MnO concentration in the sediments of the north cliff at Hartfell Scaur.
- Fig.64. Plots illustrating the stratigraphic variation of the MgO concentration in the sediments of the north cliff at Hartfell Scaur.
- Fig.65. Plots illustrating the stratigraphic variation of the Na_2O concentration in the sediments of the north cliff at Hartfell Scaur.
- Fig.66. Plots illustrating the stratigraphic variation of the CaO concentration in the sediments of the north cliff at Hartfell Scaur.
- Fig.67. Plots illustrating the stratigraphic variation of the K_2O concentration in the sediments of the north cliff at Hartfell Scaur.
- Fig.68. Plots illustrating the stratigraphic variation of the loss on ignition values in the sediments of the north cliff at Hartfell Scaur.
- Fig.69. Plots illustrating the stratigraphic variation of the copper concentration in the sediments of the north cliff at Hartfell Scaur.
- Fig.70. Plots illustrating the stratigraphic variation of the lead concentration in the sediments of the north cliff at Hartfell Scaur.

- Fig.71. Plots illustrating the stratigraphic variation of the zinc concentration in the sediments of the north cliff at Hartfell Scaur.
- Fig.72. Plots illustrating the stratigraphic variation of the rubidium concentration in the sediments of the north cliff at Hartfell Scaur.
- Fig.73. Plots illustrating the stratigraphic variation of the strontium concentration in the sediments of the north cliff at Hartfell Scaur.
- Fig.74. Plots illustrating the stratigraphic variation of the yttrium concentration in the sediments of the north cliff at Hartfell Scaur.
- Fig.75. Plots illustrating the stratigraphic variation of the zirconium concentration in the sediments of the north cliff at Hartfell Scaur.
- Fig.76. Plots illustrating the stratigraphic variation of the carbon concentration in the sediments of the north cliff at Hartfell Scaur.
- Fig.77. Scatter plots with linear regressions for element pairs.
- Fig.78. Scatter plots with linear regressions for element pairs.
- Fig.79. Scatter plots with linear regressions for element pairs.
- Fig.80. Scatter plots with linear regressions for element pairs.
- Fig.81. Scatter plots with linear regressions for element pairs.
- Fig.82. Scatter plots with linear regressions for element pairs.

- Fig.83. Scatter plots with linear regressions for element pairs.
- Fig.84. Scatter plots with linear regressions for element pairs.
- Fig.85. Scatter plots with linear regressions for element pairs.
- Fig.86.a. The 31 element pairs with Kendal rank order correlation coefficients greater than 0.50.
b. Simplified form of a.
c. Significant correlations between element-mineral and mineral-mineral pairs.
- Fig.87. Scatter plots with linear regressions for element-mineral pairs.
- Fig.88. Scatter plots with linear regressions for element-mineral pairs.
- Fig.89. Scatter plots with linear regressions for element-mineral pairs.
- Fig.90. Element loadings on the first three principal components.
- Fig.91. Projection of all elements over the three vector space of the first three principal components.
- Fig.92. Plots illustrating the stratigraphic variation of the scores of the first three principal components.
- Fig.93. Scatter plot of the extractability of organic material isolated from a silica gel column in the petroleum ether eluate against the combined extractabilities of the material in the benzene and methanol eluates.

- Fig.94. Plots illustrating the stratigraphic variation in the Moffat Shales of a) total amount of organic material eluted from a silica gel column, b) extractability of the total organic material eluted from a silica gel column, c) extractability of the total alkanes, d) extractability of the benzene eluate, e) extractability of the methanol eluate.
- Fig.95. Plots illustrating the variation in organic parameters with distance from the 9.18 m thick dyke at Clanyard Bay.
- Fig.96. Gas-liquid chromatograms of the total alkanes extracted from samples DCL-1, DL-4, DC-1.
- Fig.97. Gas-liquid chromatograms of the total alkanes extracted from samples DPE-2, DAC-1, DVE-2.
- Fig.98. Gas-liquid chromatograms of the total alkanes extracted from samples DCYP-1, DGR-1, DCV-2.
- Fig.99. Gas-liquid chromatograms of the total alkanes extracted from samples DMAX-1, DSE-1.
- Fig.100. Gas-liquid chromatograms of the total alkanes extracted from samples HL-9, HL-7, HC-1.
- Fig.101. Gas-liquid chromatograms of the total alkanes extracted from samples HRC-1, HL-11, HW-2.
- Fig.102. Gas-liquid chromatograms of the total alkanes extracted from samples HW-4, HCL-4, HG-1.
- Fig.103. Gas-liquid chromatograms of the total alkanes extracted from samples HW-3, HCL-1, HCL-2.

- Fig.104. Gas-liquid chromatograms of the total alkanes extracted from samples HCL-5, HCL-6, HCL-3.
- Fig.105. Gas-liquid chromatograms of the total alkanes extracted from samples HL-3, HL-14, HL-15.
- Fig.106. Gas-liquid chromatograms of the total alkanes extracted from samples HG-2, HW-1, HW-5.
- Fig.107. Gas-liquid chromatograms of the total alkanes extracted from samples CLAN-1, CLAN-2, CLAN-3.
- Fig.108. Gas-liquid chromatograms of the total alkanes extracted from samples CLAN-4, CLAN-5, CLAN-6.
- Fig.109. Gas-liquid chromatograms of the total alkanes extracted from samples CLAN-7, and from a contaminatory 'tar' found in a fracture at Clanyard Bay.
- Fig.110. Plot of the variation in odd-even predominance values with respect to carbon chain length for samples collected adjacent the dyke at Clanyard Bay.
- Fig.111. Plots illustrating the stratigraphic variation in the Moffat Shales of odd-even predominance values at various carbon chain lengths.
- Fig.112. Plots illustrating the stratigraphic variation in the Moffat Shales of odd-even predominance values at various carbon chain lengths.
- Fig.113. Triangular variation diagram illustrating the chemical variation (d.a.f.) of Moffat Shale kerogenous isolates.

- Fig.114. Plots illustrating the stratigraphic variation in the Moffat Shales of the elemental composition of Moffat Shale kerogen isolates.
- Fig.115. X-ray diffraction traces between 25.5 and 27.5° two-theta for Moffat Shale kerogen isolates.
- Fig.116. p - t - facies metamorphic grid, showing estimated conditions at which graphite and disordered graphite occur in nature.
- Fig.117. Infra-red spectra of sample HW-4 kerogen isolate recorded after crushing for different lengths of time.
- Fig.118. Infra-red spectra of the kerogen material isolated from samples DL-4, DGR-1, HL-8 and HL-6.
- Fig.119. Chart recoding of reflectivity-rotation measurements on graptolite particles in a block of mudstone cut parallel to the plane of the bedding.
- Fig.120. Plot of the variation in graptolite fragments of maximum and minimum air reflectivity with respect to the angle the measurement surface makes with the plane of the bedding.
- Fig.121. Plot of the variation in graptolite fragments of oil and air reflectivity with wavelength for particles cut at various angles to the plane of the bedding.
- Fig.122. Plot of the variation in graptolite fragments of the difference between maximum and minimum reflectivity with wavelength for particles cut at various angles to the plane of the bedding.
- Fig.123. Indicatrices of uniaxial and biaxial crystals.

- Fig.124. Histograms for the variation in reflectivity in sample LBR-29.
- Fig.125. Linear iterative surface map for the variation in reflectivity over the surface of a graptolite fragment.
- Fig.126. Linear surface global fit map for the variation in reflectivity over the surface of a graptolite fragment.
- Fig.127. Linear surface difference map for the variation in reflectivity over the surface of a graptolite fragment.
- Fig.128. Quadratic iterative surface map for the variation in reflectivity over the surface of a graptolite fragment.
- Fig.129. Quadratic surface global fit map for the variation in reflectivity over the surface of a graptolite fragment.
- Fig.130. Quadratic surface difference map for the variation in reflectivity over the surface of a graptolite fragment.
- Fig.131. Cubic iterative surface map for the variation in reflectivity over the surface of a graptolite fragment.
- Fig.132. Cubic surface global fit map for the variation in reflectivity over the surface of a graptolite fragment.
- Fig.133. Cubic surface difference map for the variation in reflectivity over the surface of a graptolite fragment.
- Fig.134. Linear iterative surface map for the variation in reflectance values produced at random over the surface of a graptolite fragment.

- Fig.135. Linear surface global fit map for the variation in reflectance values produced at random over the surface of a graptolite fragment.
- Fig.136. Linear surface difference map for the variation in reflectance values produced at random over the surface of a graptolite fragment.
- Fig.137. Quadratic iterative surface map for the variation in reflectance values produced at random over the surface of a graptolite fragment.
- Fig.138. Quadratic surface global fit map for the variation in reflectance values produced at random over the surface of a graptolite fragment.
- Fig.139. Quadratic surface difference map for the variation in reflectance values produced at random over the surface of a graptolite fragment.
- Fig.140. Cubic iterative surface map for the variation in reflectance values produced at random over the surface of a graptolite fragment.
- Fig.141. Cubic surface global fit map for the variation in reflectance values produced at random over the surface of a graptolite fragment.
- Fig.142. Cubic surface difference map for the variation in reflectance values produced at random over the surface of a graptolite fragment.
- Fig.143. Plot of the variation in reflectivity with focal length.
- Fig.144. Plan of sample collection points at Clanyard Bay.

- Fig.145. Plots of the variation in reflectivity, refractive and absorptive indices of graptolite fragments from the LB-series of samples from the south side of the dyke at Clanyard Bay.
- Fig.146. Representative chart recording obtained during the measurement of reflectivity of graptolite fragments.
- Fig.147. Plot illustrating the relationship for graptolite fragments from the south side of the dyke at Clanyard Bay between mean and mean-maximum reflectivities.
- Fig.148. Plot of the variation in reflectivity of graptolite fragments along a measured section at Clanyard Bay.
- Fig.149. Plot of the variation in reflectivity of graptolite fragments with distance for samples collected from the north of the dyke at Clanyard Bay.
- Fig.150. Plot of the variation in the bireflectance ratio of graptolite fragments with distance from an igneous dyke.
- Fig.151. Plot illustrating the variation in reflectivity at selected wavelengths of graptolite fragments adjacent to an igneous dyke.
- Fig.152. Plots illustrating the dispersion with wavelength of oil and air reflectivities in samples LB-12 and LB-16.
- Fig.153. Plots illustrating the dispersion with wavelength of oil and air reflectivities in samples LB-17A, LB-15 and LB-13.
- Fig.154. Plots illustrating the dispersion with wavelength of oil and air reflectivities in samples LB-14 (1) and LB-14 (2).

- Fig.155. Plots illustrating the dispersion with wavelength of oil and air reflectivities in sample LB-18.
- Fig.156. Plots illustrating the dispersion with wavelength of oil and air reflectivities in samples LBR-8, LBR-7 and LBR-3.
- Fig.157. Plots illustrating the dispersion with wavelength of oil and air reflectivities in samples LBR-13 and LBR-9.
- Fig.158. Composite plot illustrating the dispersion with wavelength of the reflectivity in samples from the LBR-series.
- Fig.159. Plot of linear regression lines for the spectral variation of graptolite reflectivity.
- Fig.160. Plot illustrating the variation with distance from an igneous dyke of the refractive index of graptolite fragments.
- Fig.161. Plots illustrating the dispersion with wavelength of the absorptive and refractive indices in samples LB-12 and LB-16.
- Fig.162. Plots illustrating the dispersion with wavelength of the absorptive and refractive indices in samples LB-17A, LB-15 and LB-13.
- Fig.163. Plots illustrating the dispersion with wavelength of the absorptive and refractive indices in samples LB-14 (1) and LB-14 (2).
- Fig.164. Plots illustrating the dispersion with wavelength of the absorptive and refractive indices in samples LBR-13 and LBR-9.

- Fig.165. Plots illustrating the dispersion with wavelength of the absorptive and refractive index in samples LBR-8, LBR-7 and LBR-3.
- Fig.166. Plots illustrating the dispersion with wavelength of the absorptive and refractive index of sample LB-18.
- Fig.167. Linear regression lines for the variation of absorptive index of graptolite fragments with distance from the dyke at Clanyard Bay.
- Fig.168. Plot of linear regression lines for various values of equivalent temperature (T_0^+) for the variation of reflectivity with temperature of graptolite fragments.
- Fig.169. Plot of 'best-fit' regression lines at various wavelengths for the variation of refractive index with temperature of graptolite fragments.
- Fig.170. Plot of the variation in refractive index with temperature of graptolite fragments.
- Fig.171. Plot of the variation of absorptive index with temperature for graptolite fragments.
- Fig.172. Global-fit surface map for the variation of reflectivity in an area along the eastern margin of Luce Bay.
- Fig.173. Global-fit and iterative surface maps for the variation of reflectivity in the Moffat Shales.
- Fig.174. Bouguer gravity map for part of the Moffat Region.
- Fig.175. Plot illustrating the stratigraphic variation of reflectivity in the Moffat Shales.

- Fig.176. Plots illustrating the stratigraphic variation in reflectivity in the sediments of the north cliff at Hartfell.
- Fig.177. Plots illustrating the dispersion with wavelength of oil and air reflectivities in samples HL-15, HL-13 and HL-14.
- Fig.178. Plots illustrating the dispersion with wavelength of oil and air reflectivities in samples HCL-26A, HCL-26 and HCL-31.
- Fig.179. Plots illustrating the dispersion with wavelength of oil and air reflectivities in samples HL-4 and HCL-16.
- Fig.180. Plots illustrating the dispersion with wavelength of the absorptive and refractive indices in samples HL-15, HL-13, HL-14.
- Fig.181. Plots illustrating the dispersion with wavelength of the absorptive and refractive indices in samples HCL-26A, HCL-26, HCL-31.
- Fig.182. Plots illustrating the dispersion with wavelength of the absorptive and refractive indices in samples HL-4 and HCL-6.
- Fig.183. Plot of the variation in reflectivity of graptolite fragments with distance from igneous plutons.
- Fig.184. Plot of the variation in reflectivity with temperature for graptolites in the vicinity of igneous plutons.
- Fig.185. Electrical circuit and apparatus used to measure the resistivity of powdered rock samples.
- Fig.186. Plots of the variation in resistivity with pressure for samples from Clanyard Bay.
- Fig.187. Plots of the variation in resistivity with pressure for samples from Clanyard Bay.

- Fig.188. Plot of the variation in resistivity with distance from the dyke at Clanyard Bay.
- Fig.189. Histograms illustrating the variation in resistivity and reflectivity in the Moffat Shales in the vicinity of Moffat.
- Fig.190. Global-fit and iterative surface maps for the variation in resistivity in the Moffat Shales.
- Fig.191. Plots illustrating the stratigraphic variation in reflectivity and resistivity in the Moffat Shales.
- Fig.192. Plots illustrating the stratigraphic variation in resistivity of the sediments of the north cliff at Hartfell Scaur.
- Fig.193. Plots of the variation in resistivity of two component mixtures of quartz with chlorite, muscovite, graphite and pyrite.
- Fig.194. Gas-liquid chromatogram of the N-heptafluoro-butyl n-propyl derivatives of a standard series of amino acids.
- Fig.195. Gas-liquid chromatogram of the N-trifluoro-acetyl L-valyl-L-valine cyclohexyl esters of a standard series of amino acids.
- Fig.196. Schematic flow diagram of important elements in the microphotometer system.
- Fig.197. Drawing illustrating the position of the important elements in the Leitz Orthoplan microphotometer system.
- Fig.198. Light beam path for incident light in the Leitz Orthoplan system.

- Fig.199. Diagrams of the light path in each of the two types of vertical illuminator which are incorporated in the Leitz Orthoplan system.
- Fig.200. Graph of the spectral response of a tungsten lamp.
- Fig.201. Graph of the spectral response of the EMI type 9592 photomultiplier.
- Fig.202. Plot of the spectral response of the Leitz Orthoplan microphotometer system.
- Fig.203. Plot of the dispersion with wavelength of the refractive index of diamond.
- Fig.204. Plot of the dispersion with wavelength of the refractive index of Zeiss immersion oil at 24°C.
- Fig.205. Plot of the dispersion with wavelength of the reflectivity of diamond in Zeiss immersion oil.
- Fig.206. Plot of the dispersion with wavelength of the reflectivity of diamond in air.

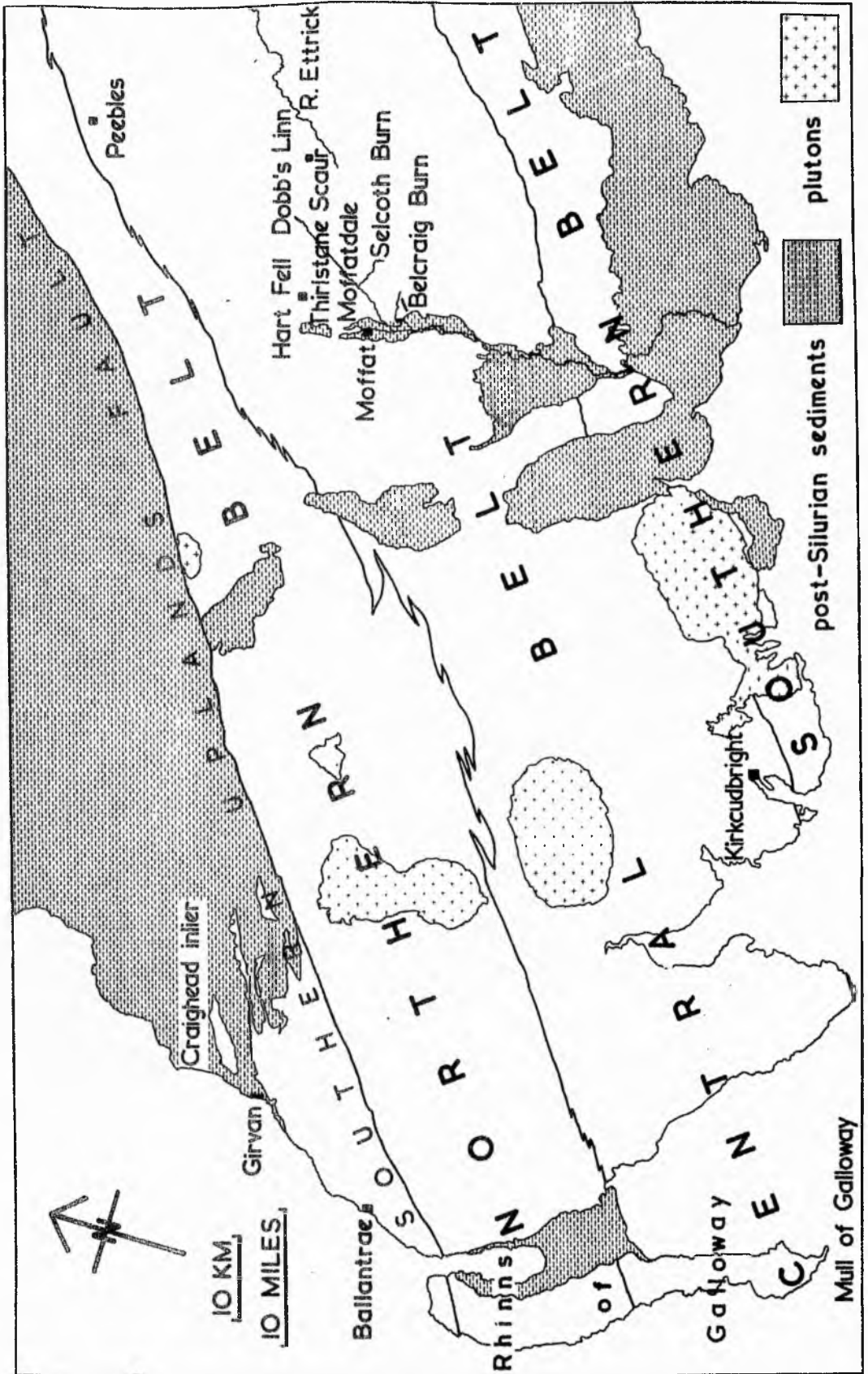


Figure 1. Simplified geological map of Southern Uplands of Scotland, showing disposition of facies belts, (after Weir 1973).

Thicknesses of stratigraphical units
expressed in metres

Diagram not to scale

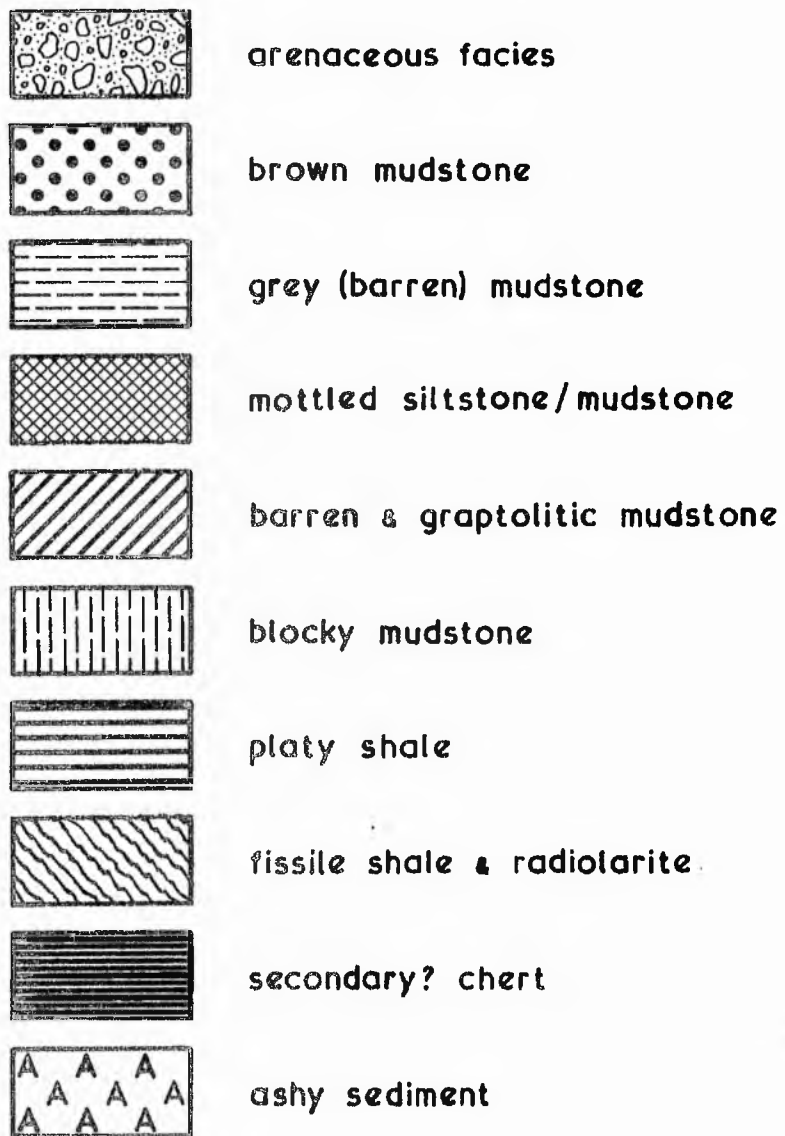


Figure 2. Key to Figure 3.

MOFFAT

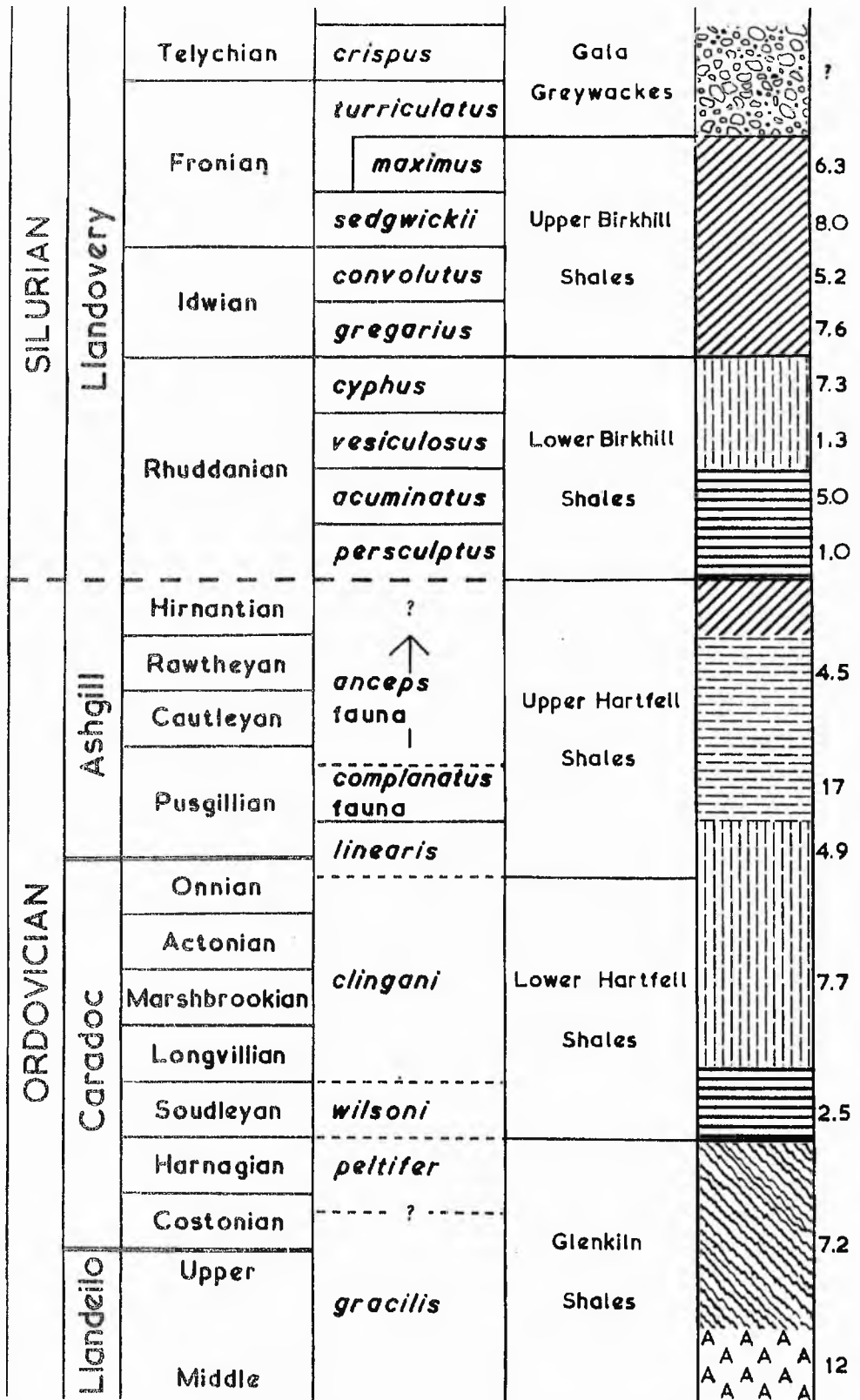


Figure 3. Facies distribution at Dobb's Linn, (after Weir 1973). Key illustrated in Figure 2.

Figure 1. Location of the Moffat Shales and sampled inliers.

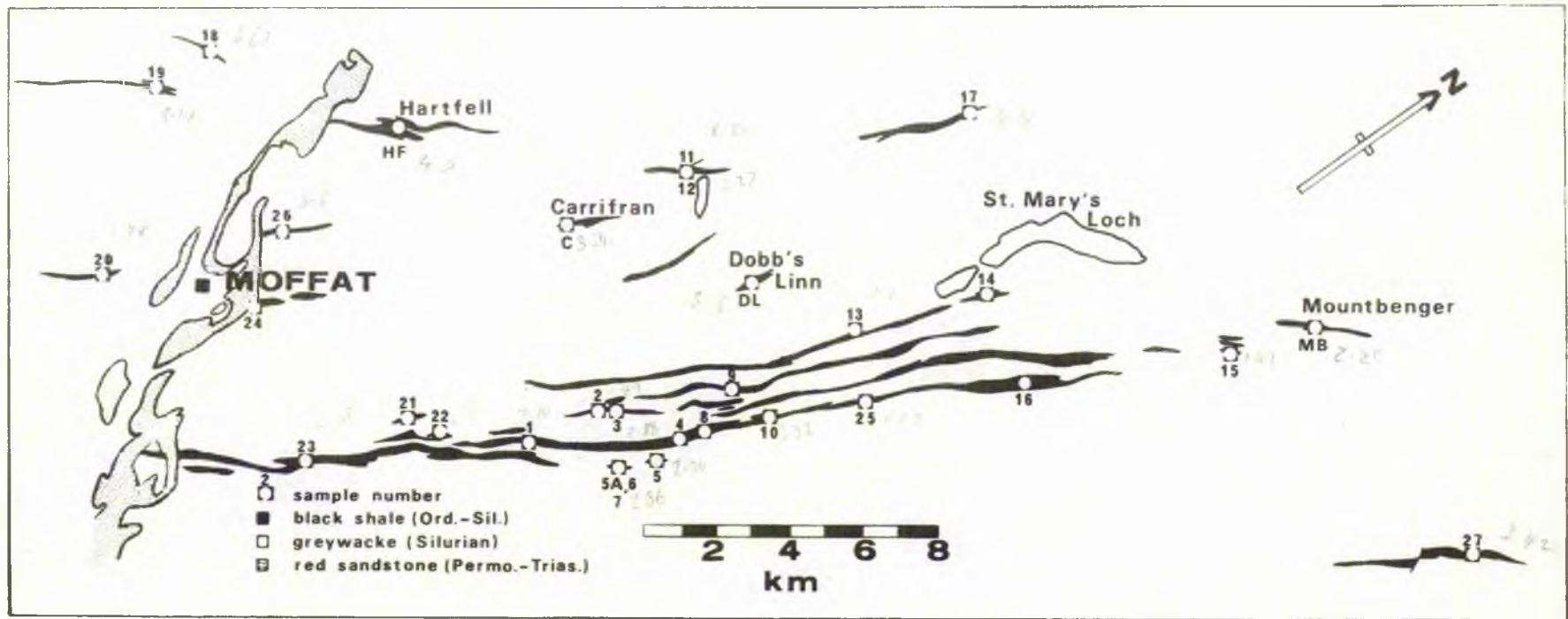
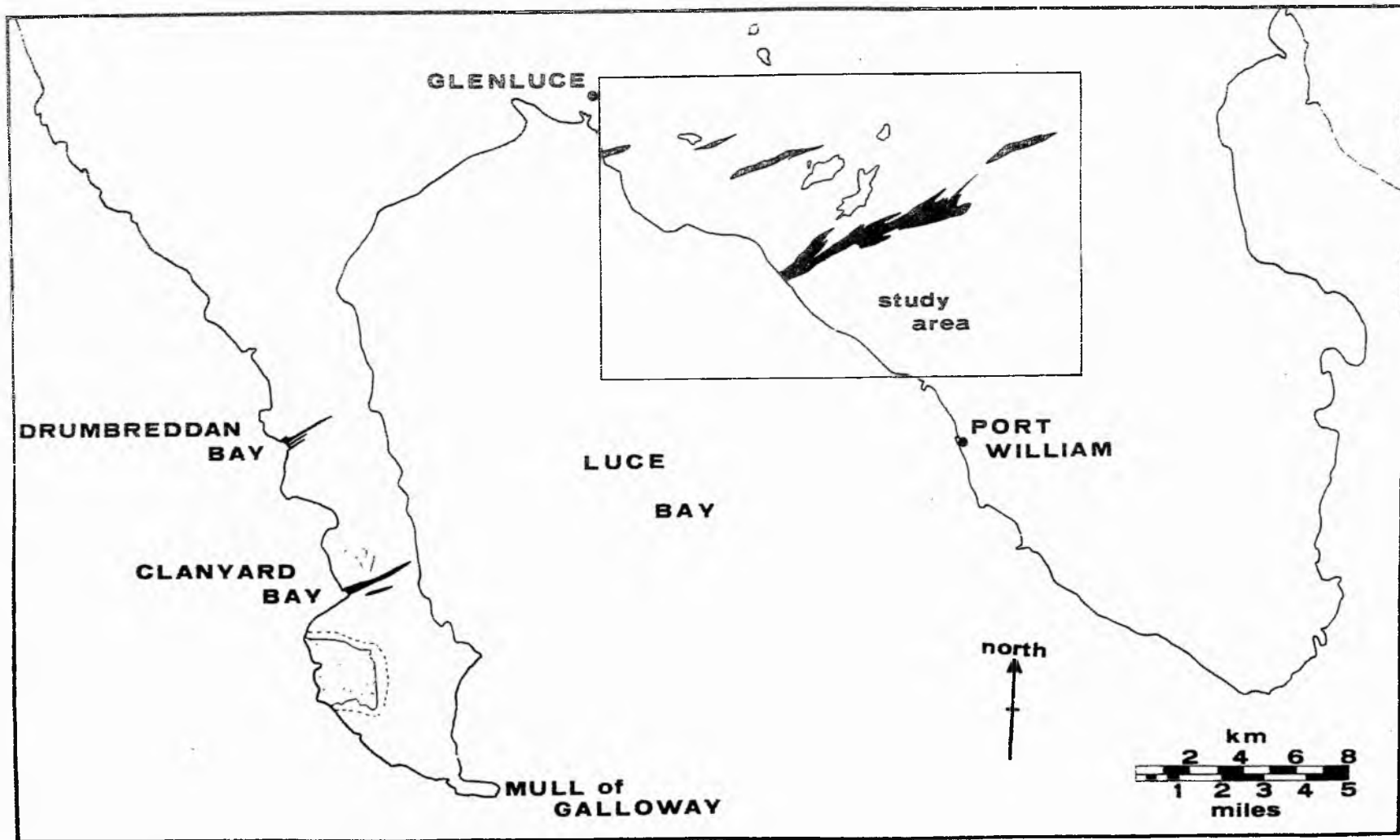


Figure 5. Sketch map indicating areas of study in the south-west of Scotland.



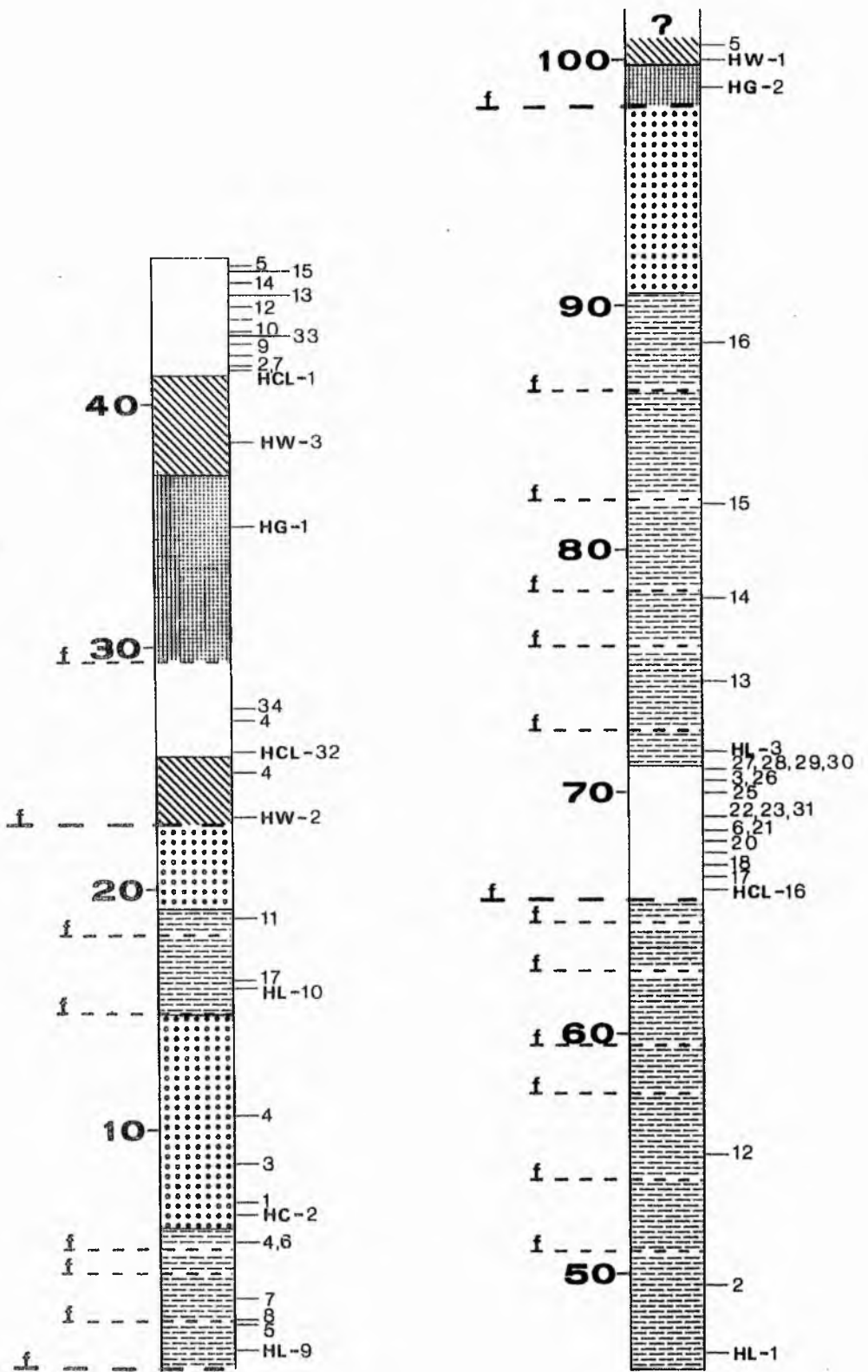
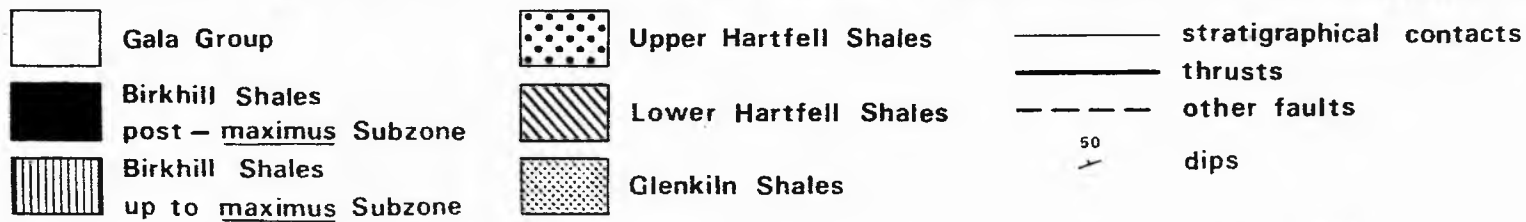
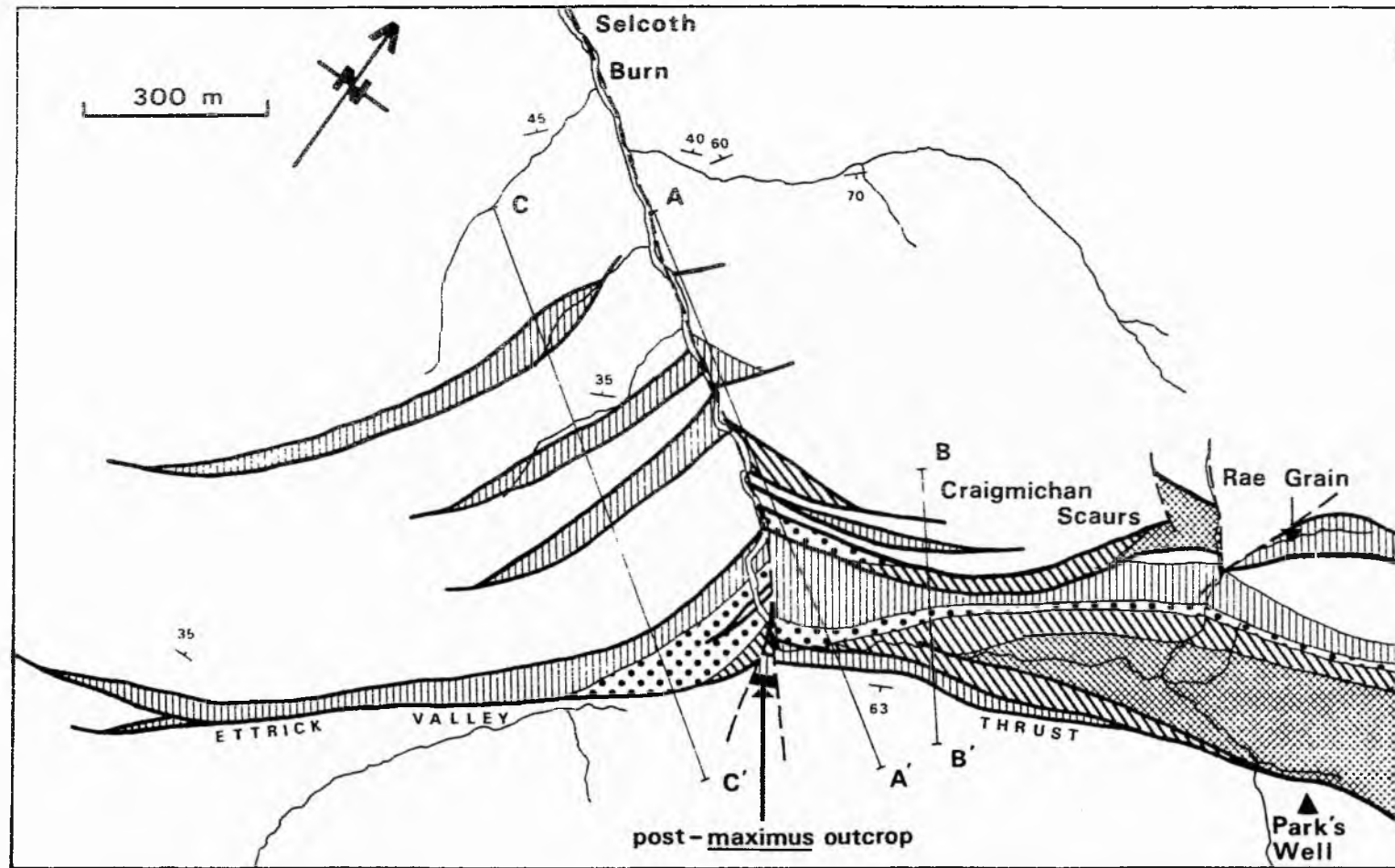


Figure 6. Location of samples collected from the north cliff at Hartfell. *f* indicates thrust-fault, stratigraphic-key same as Figure 9.

Figure 7. Geological map of the Craigmichan Scaurs - Selcoth Burn area, (after Fyfe and Weir 1976).



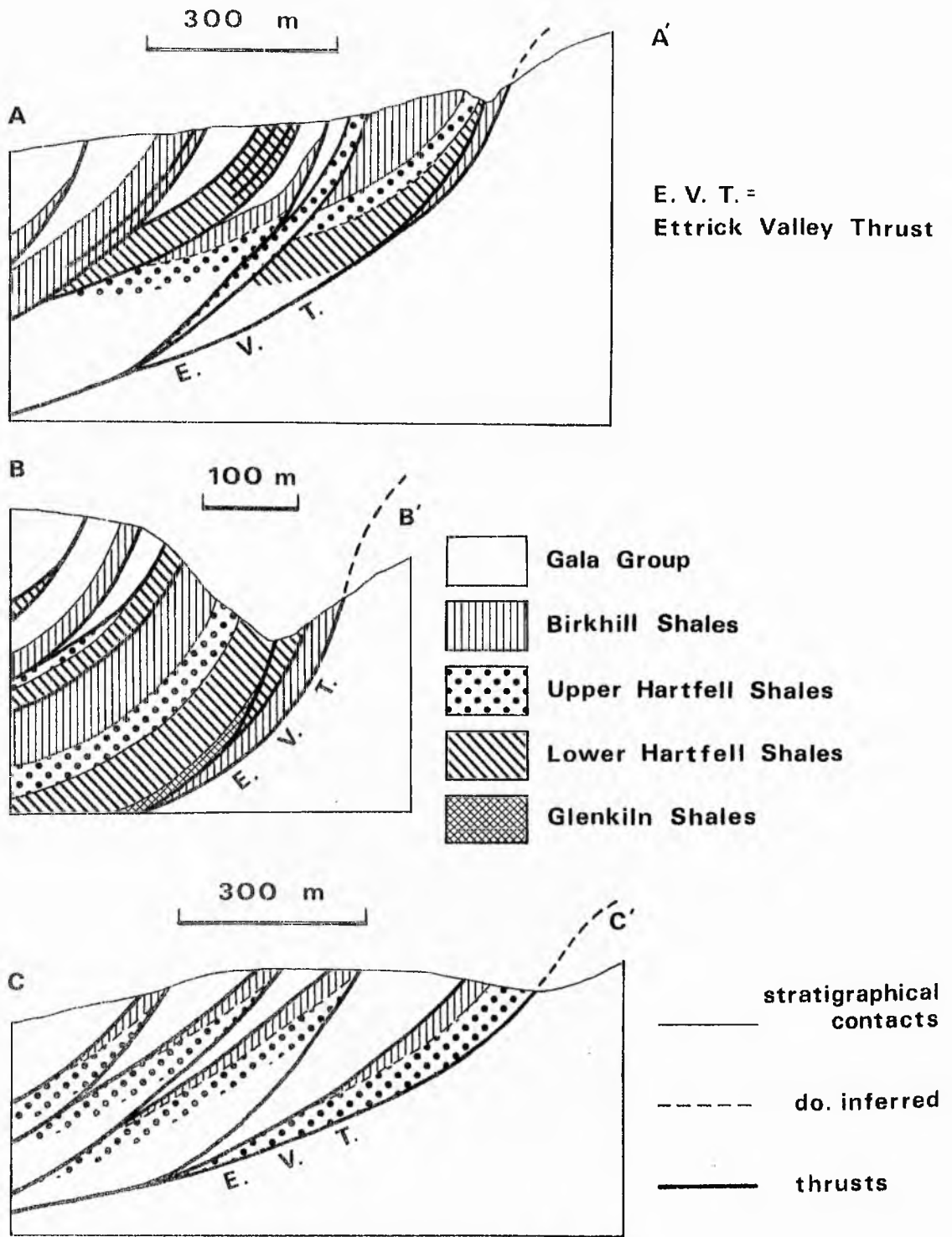
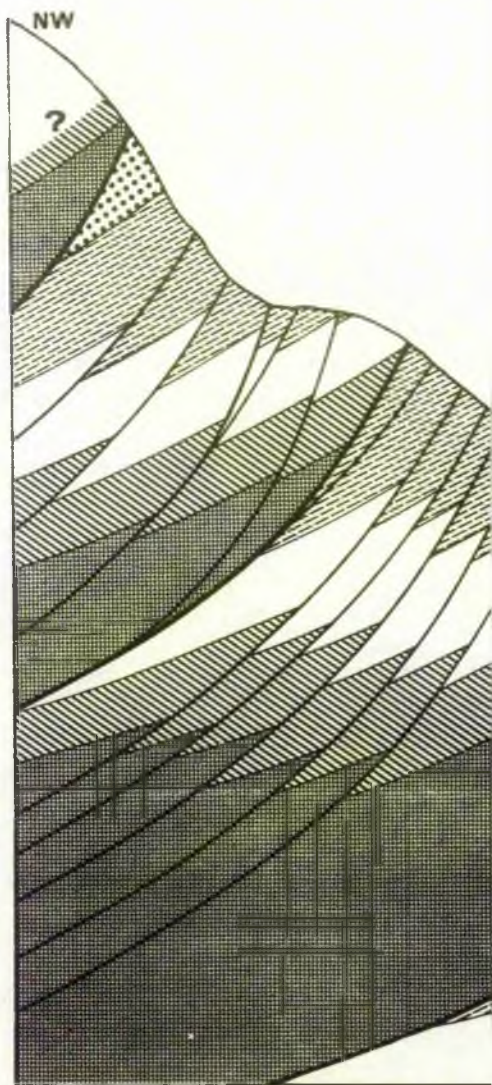


Figure 8. Cross-sections along lines A-A', B-B', C-C' in Figure 7, with schematic interpretations of structures in depth, (after Fyfe and Weir 1976).

Figure 9. Structure of the north cliff at Hartfell.





Barren Mudstone

P. linearis zone

D. clingani zone

C. wilsoni zone

Birkhill Shales

Hartfell Shales

Glenkiln Shales

- stratigraphical contacts
- thrusts with minor displacement
- thrusts with major displacement

20 metres

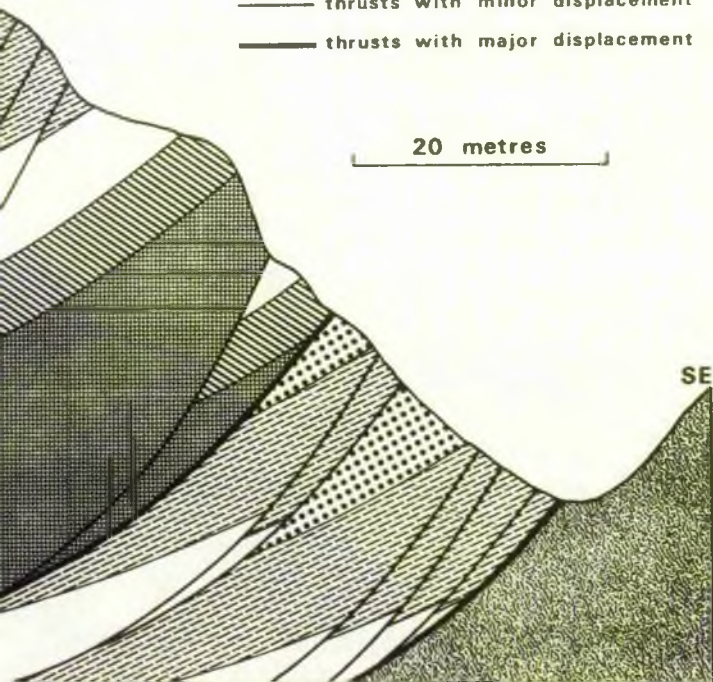
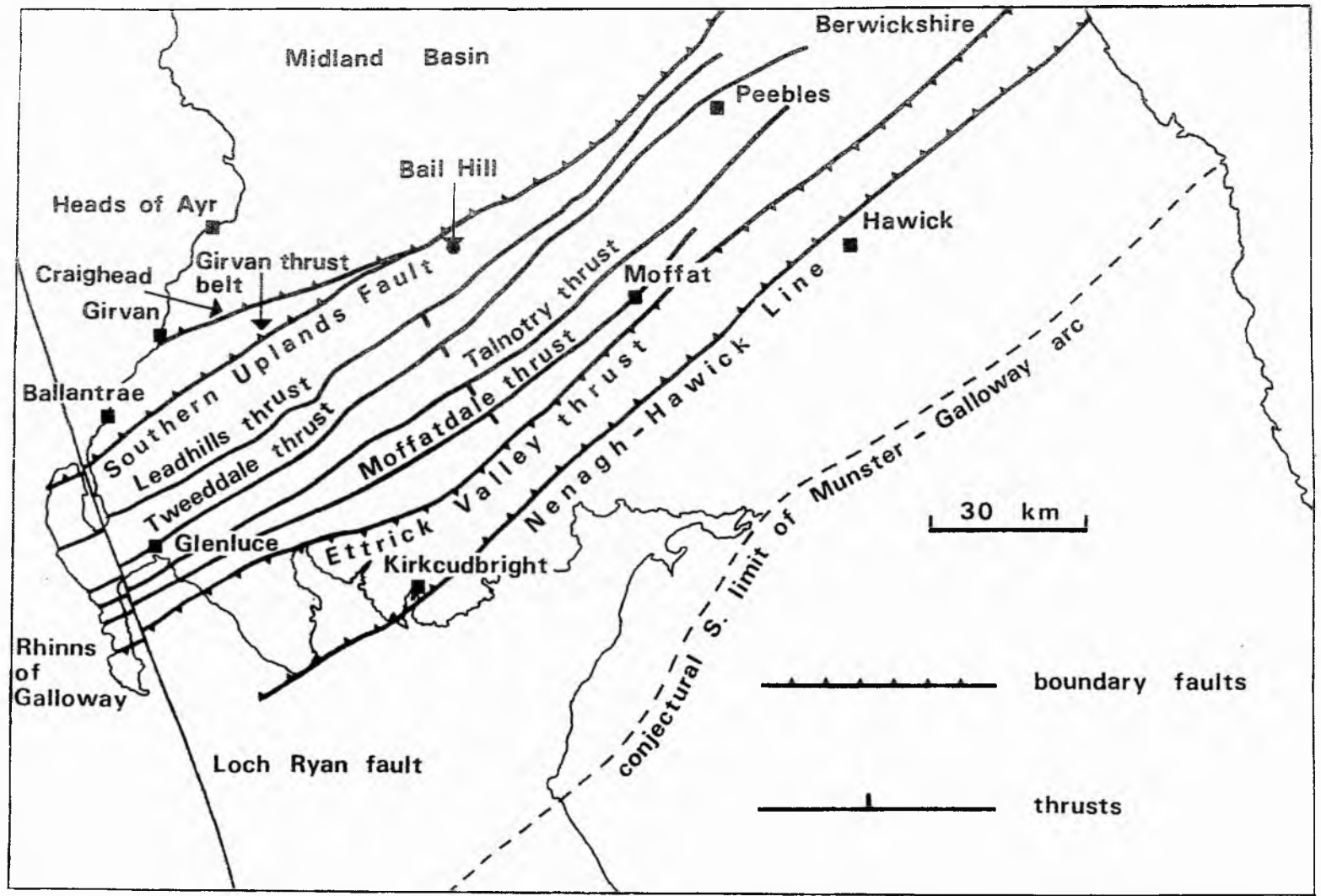


Figure 10. Structural and locality map of the Southern Uplands, (after Weir in litt).



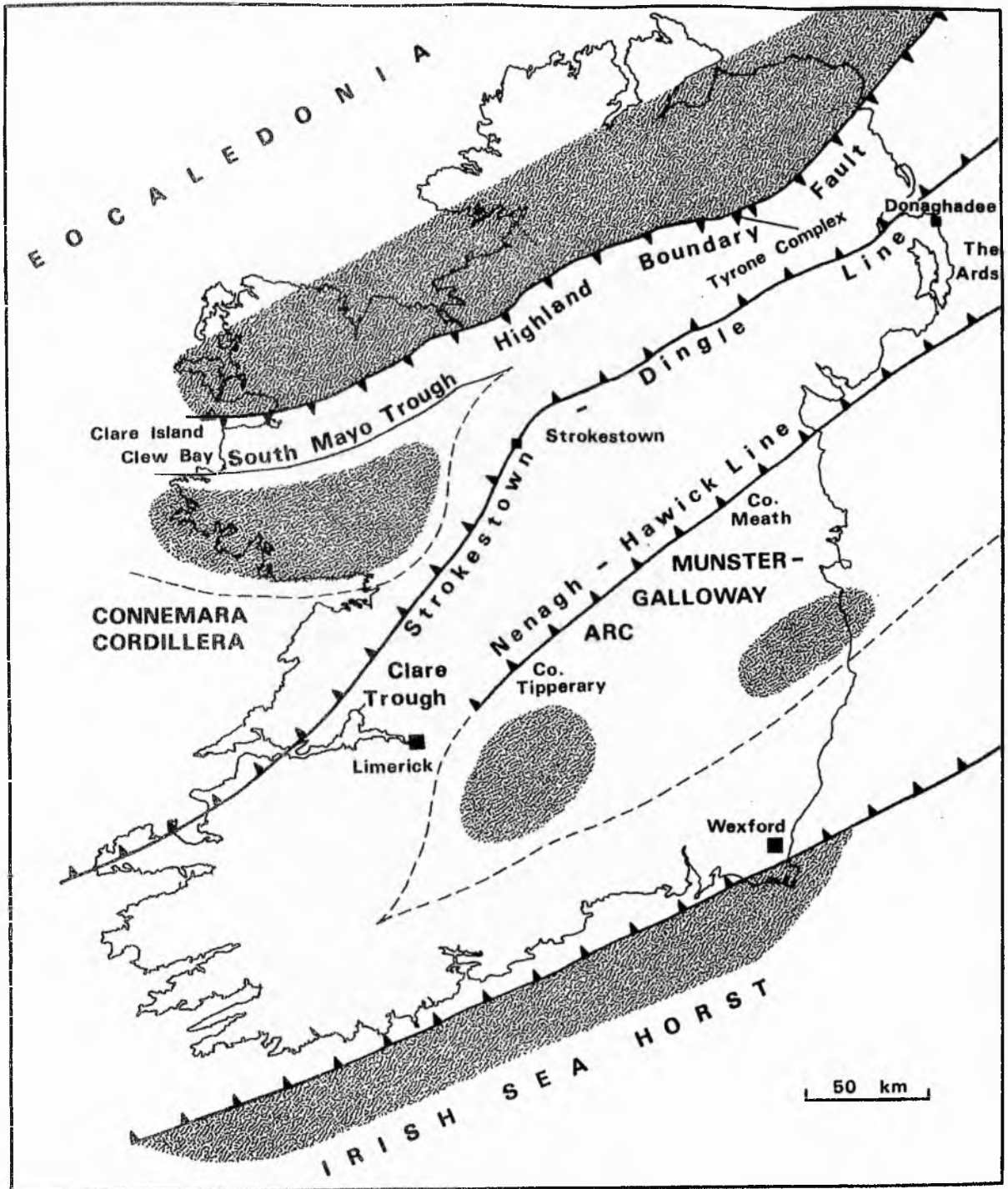


Figure 11. Structural and locality map of Ireland. Lower Palaeozoic landmasses shaded, (after Weir *in litt.*).

Figure 12. Evolution of Zone B of the Caledonian orogen-1. A, rifting and detachment of Munster-Galloway arc. Late Cambrian (immediately post-Grampian) B, pre-Arenig separation of Munster-Galloway arc; rifting and detachment of Connemara Cordillera. (Graptolitic shales of South Mayo Trough). C, Arenig-Caradoc establishment of Moffat-Clare axis as mid-oceanic ridge; formation of Highland Border (2), Glenn App (3) and Southern Uplands (5) Benioff zones in southward succession; generation of Tweedale volcanic arc (VVVV). Dalradian sectors shaded; ophiolitic mélange dots.

1, Connemara Cordillera; 4, conjectural limit of Balantrae mélange.

Scale hypothetical.

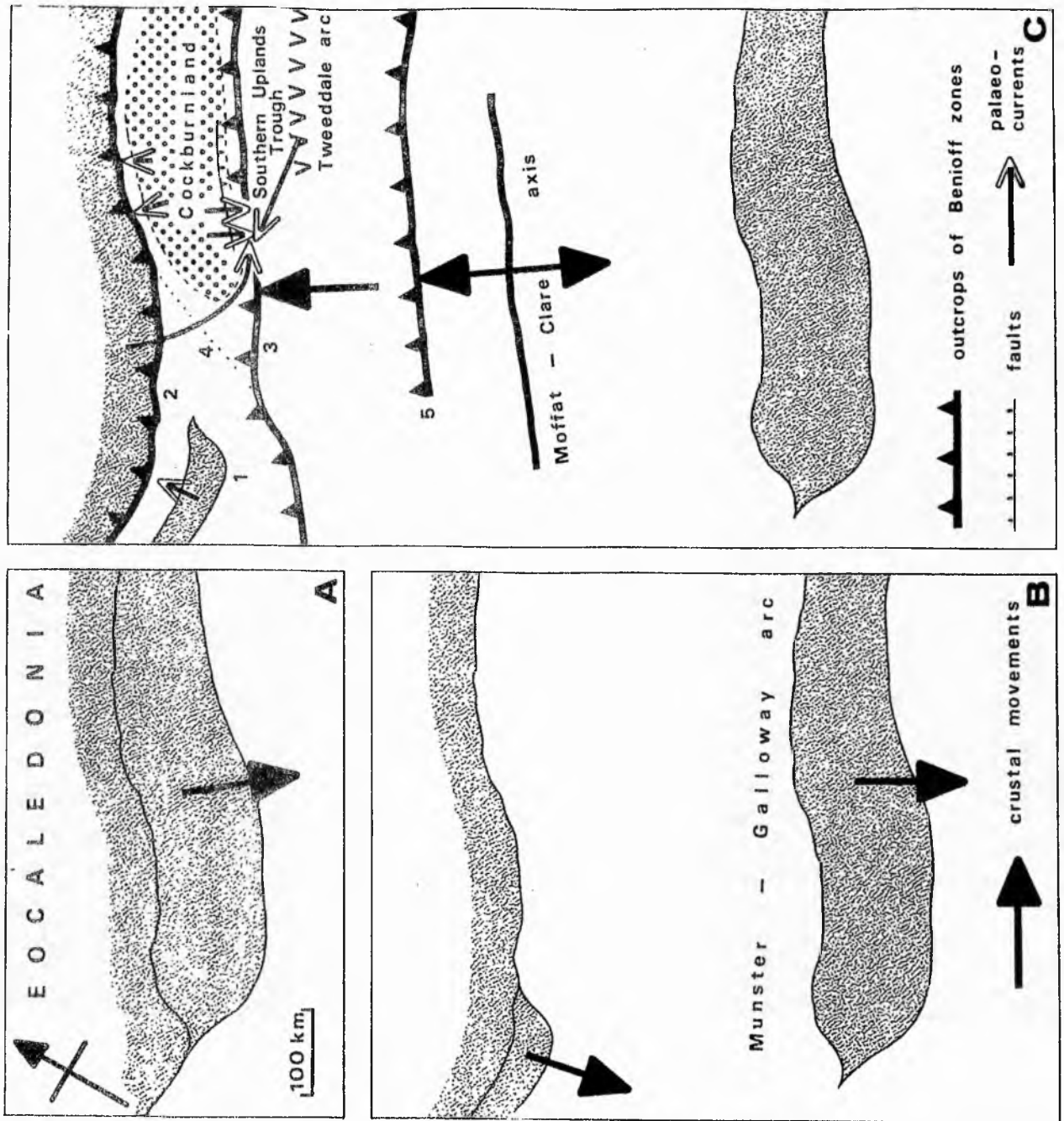


Figure 12. Evolution of Zone B of the Caledonian orogen-1, (after Weir *in litt.*).

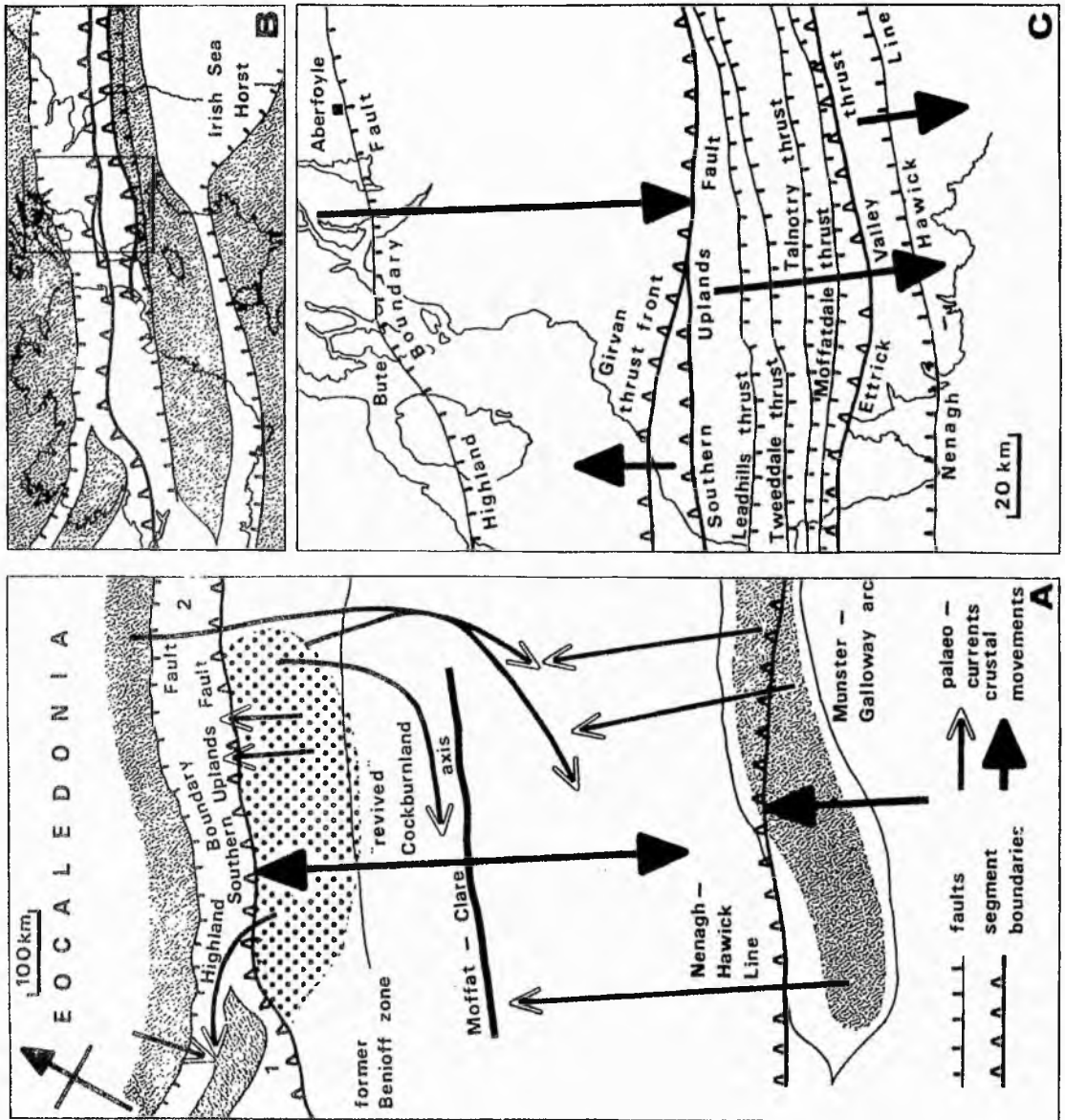


Figure 13. Evolution of Zone B of the Caledonian orogen-2. A, crustal segmentation with establishment of Southern Uplands Fault (late Llandovery) and Neagh-Hawick Line (? Late Llandovery-Wenlock). Shading, Dalradian tracts; dots, oceanic basement. 1, Connemara Cordillera; 2, Midland Basin. B, orogenesis of Zone B. Scale as in Figure 13A. C, insert in Figure 13B enlarged to show structural detail.

Figure 14. NNW-SSE sections to illustrate the structural evolution of the Southern Uplands. A, Caradoc, Glen App and Southern Upland Benioff zones lately active, latter giving rise to Tweeddale volcanics. B, late Llandovery and (? Wenlock). Establishment of Southern Uplands Fault along former Benioff zone, and of Nenagh-Hawick Line with upward wedging. C, main phase of orogeny, post-Wenlock. Southeastward movement of Eocaledonia; development of Moffat décollement, Girvan thrust belt and Southern Uplands thrust belt. 1, Leadhills thrust; 2, Tweeddale thrust; 3, Talnothy thrust; 4, Ettrick Valley thrust. Stipples, Dalradian/Precambrian; vertical lines, oceanic crust; black, Moffat Shales; hachures, volcanic arc rocks.

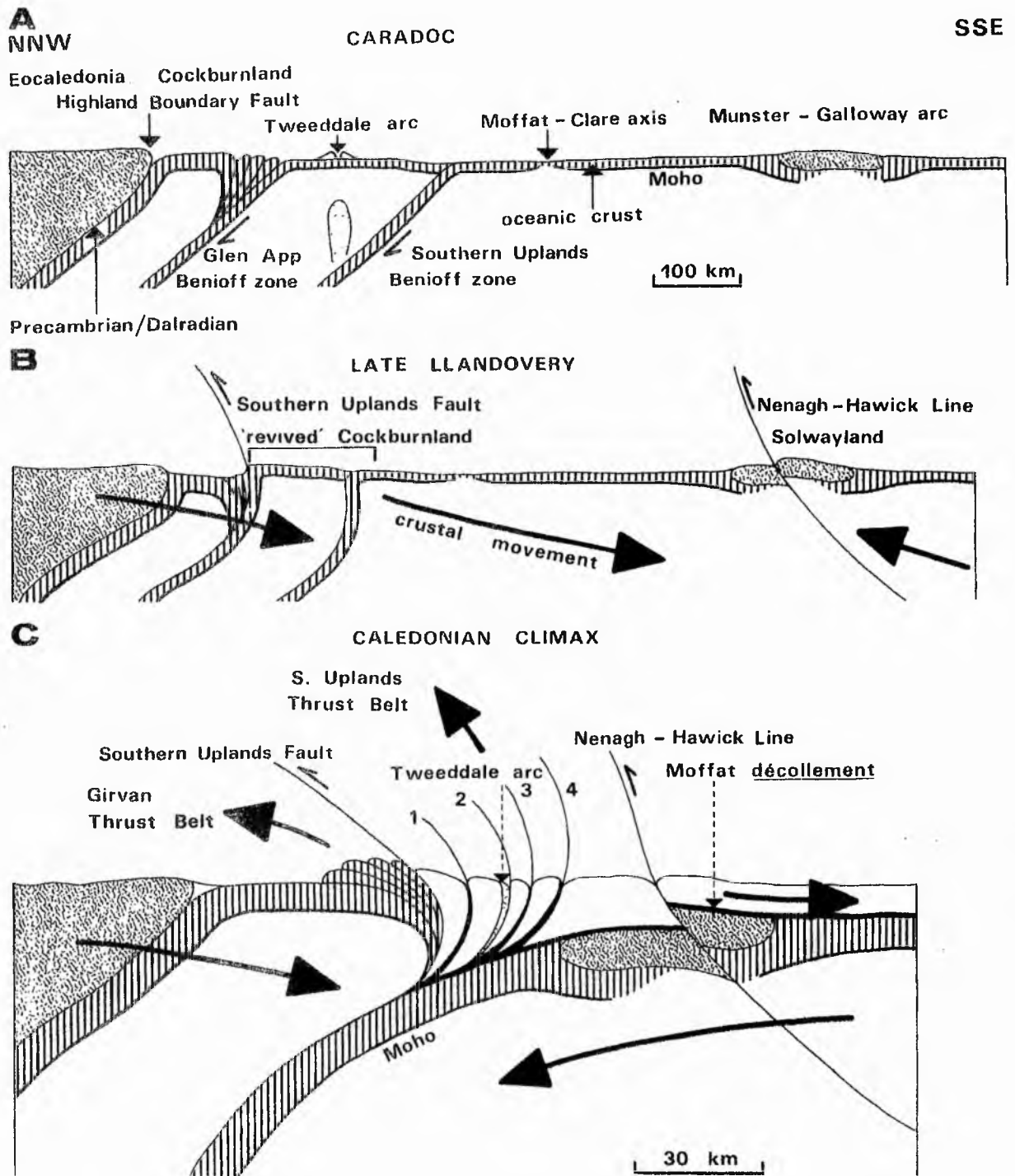


Figure 14. NNW-SSE sections to illustrate the structural evolution of the Southern Uplands, (after Weir *in litt.*).

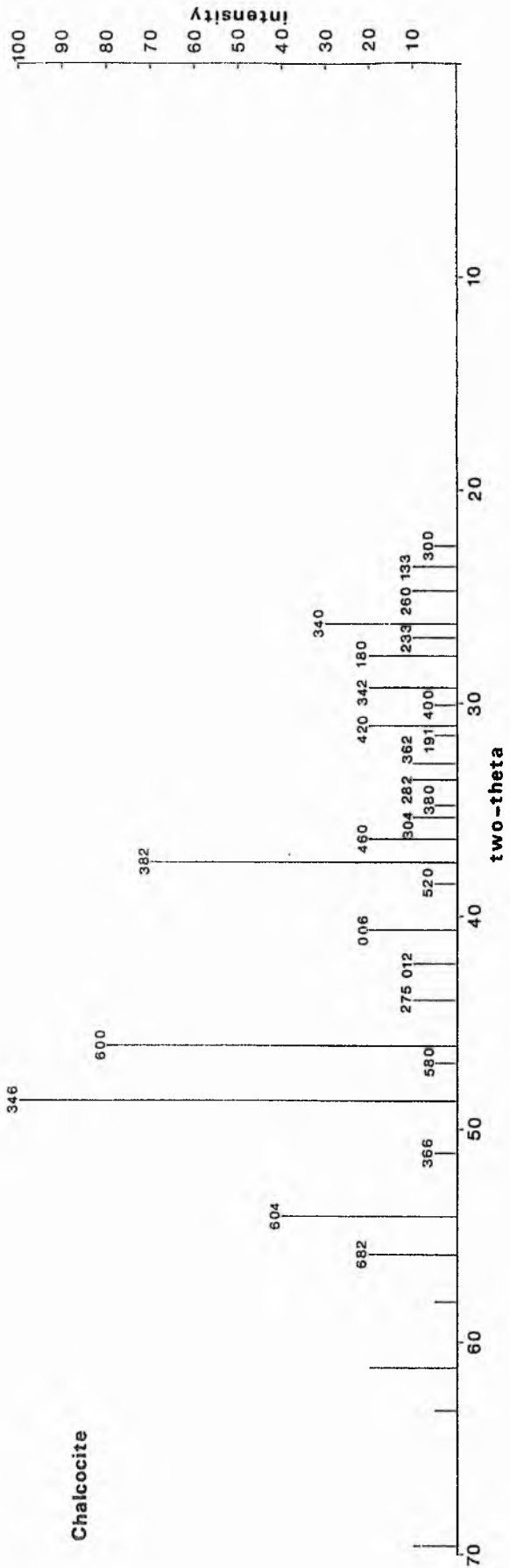


Figure 15. Reproduction of a computer drawn template used in the identification of X-ray diffractogram peaks.

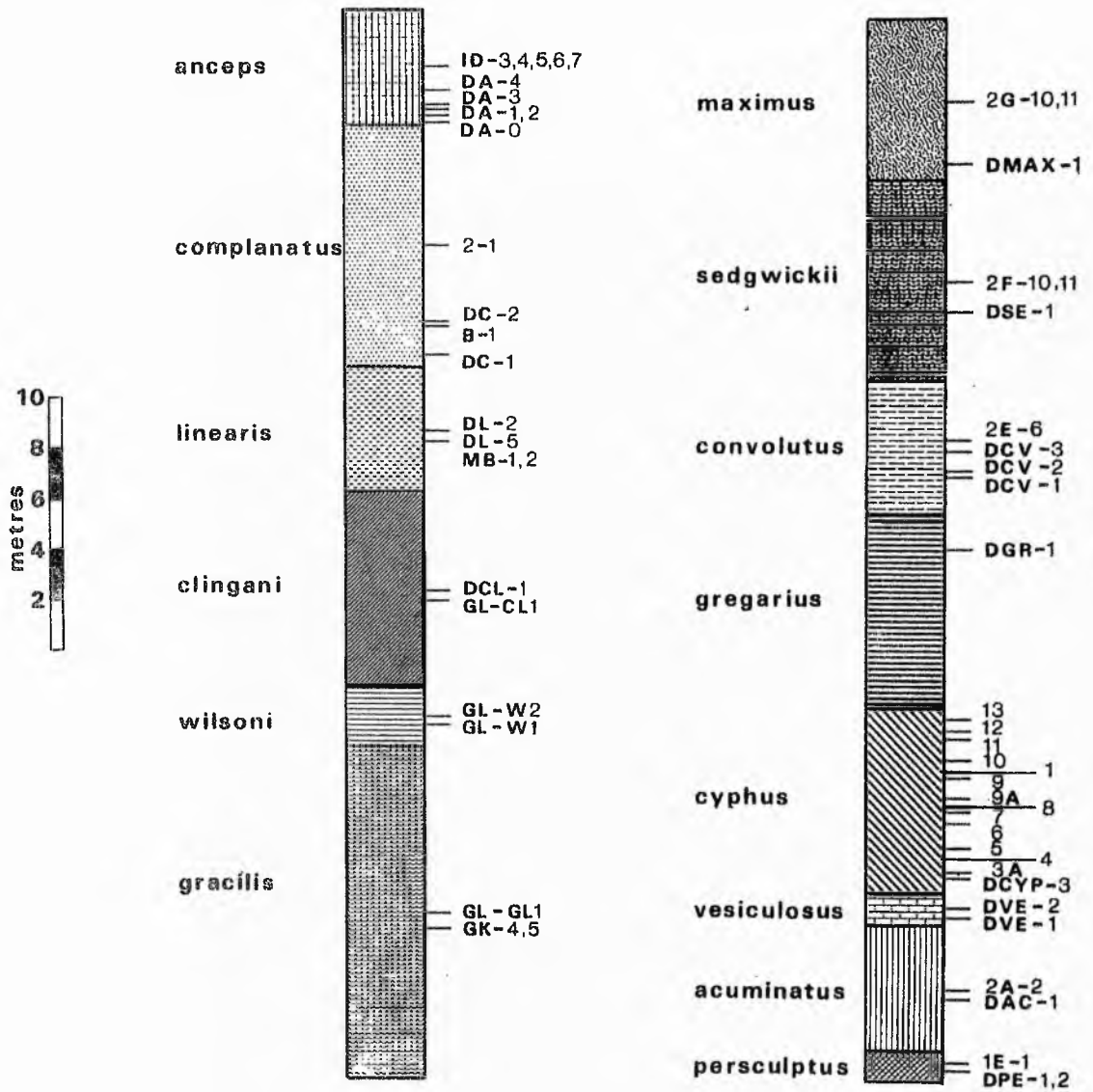


Figure 16. Stratigraphic location of samples.

Figure 17. Plots illustrating the effects of glycerol and dilute hydrochloric acid on the X-ray reflections of sample DCYP-3. Solid lines, chlorite reflections. Broken lines, sericite reflections.

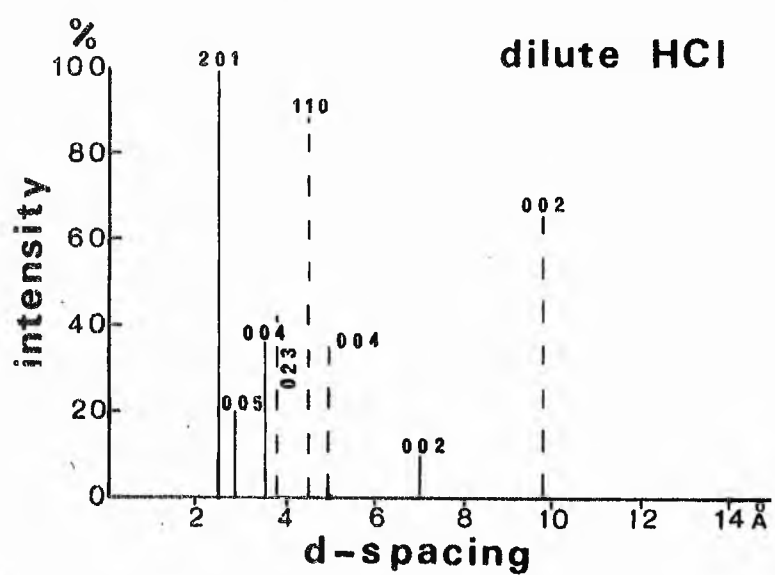
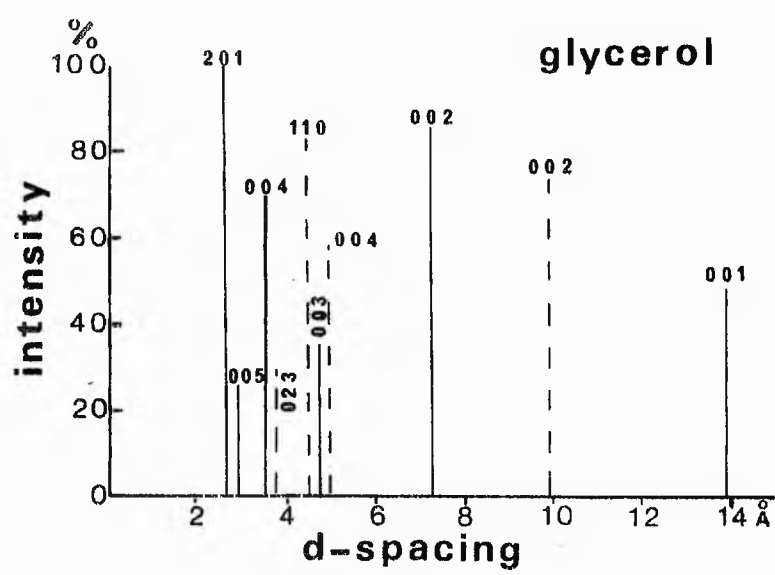
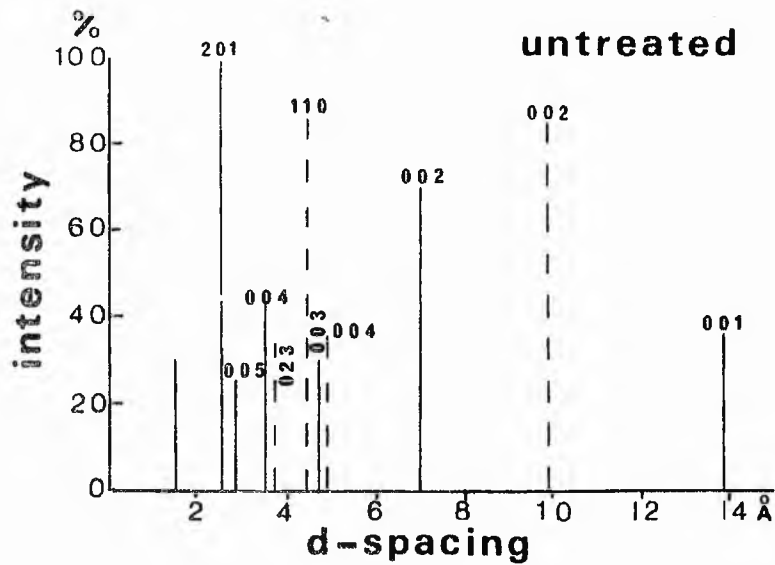


Figure 17.

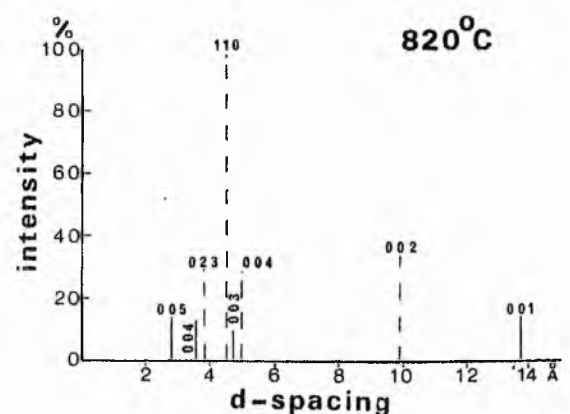
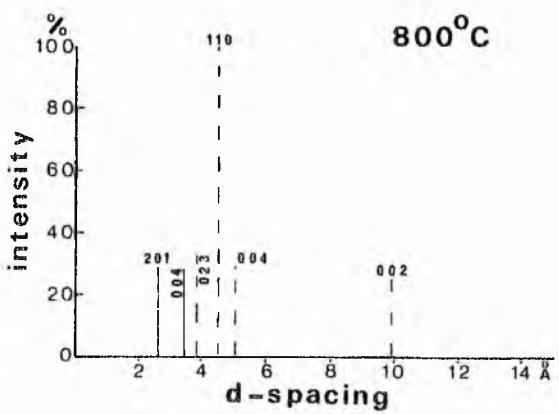
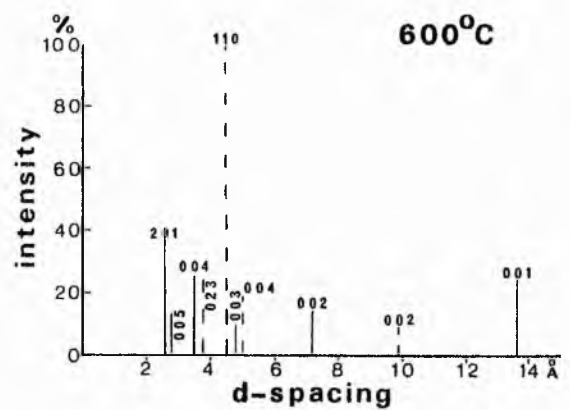
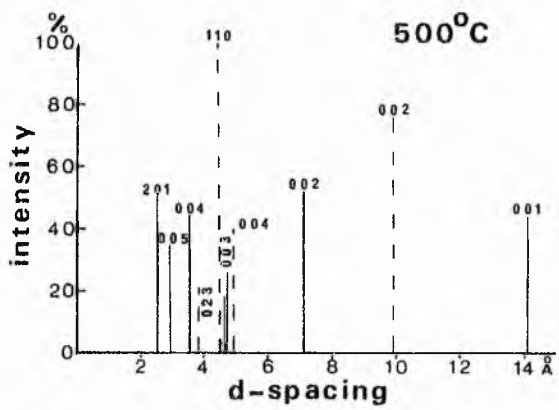
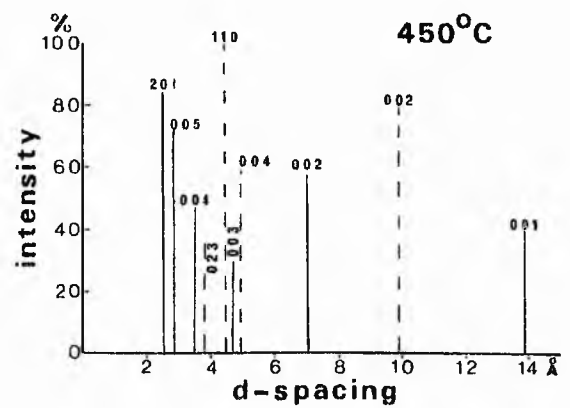
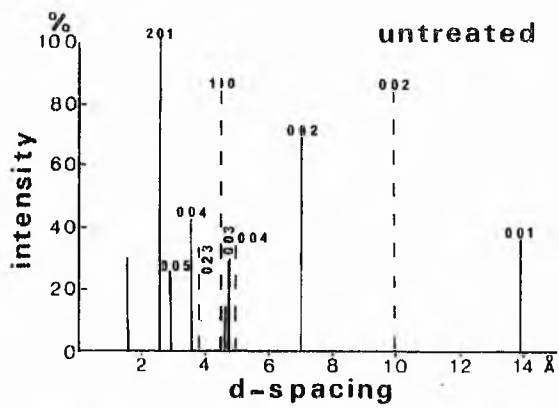
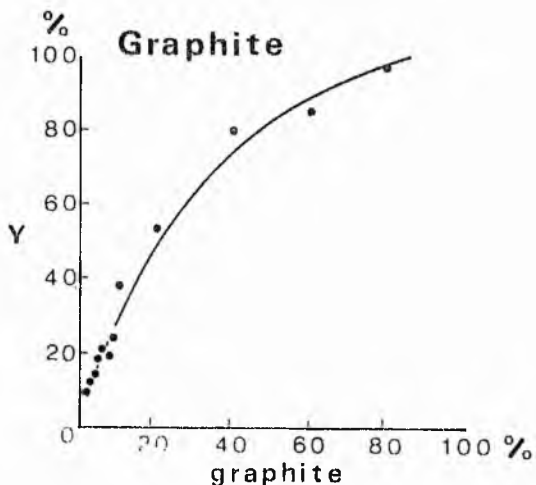
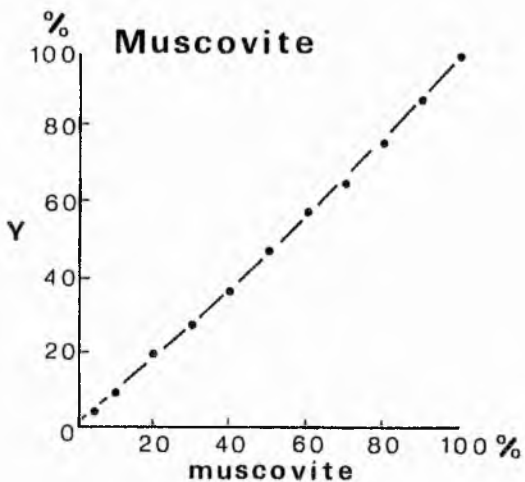
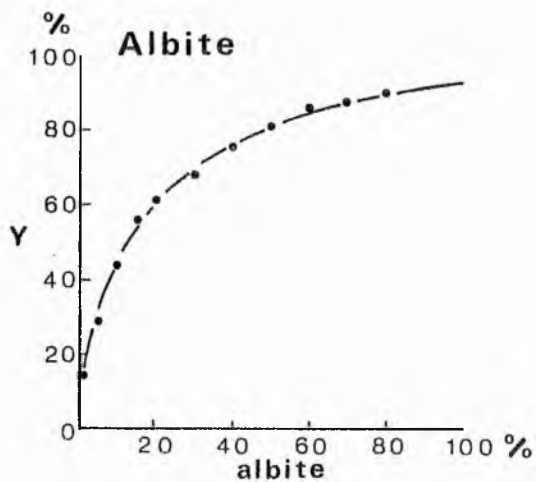
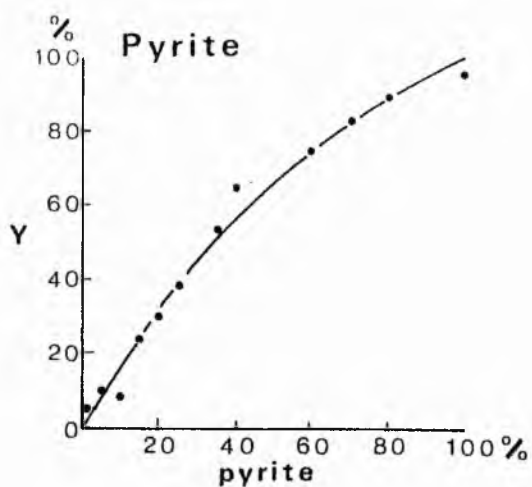
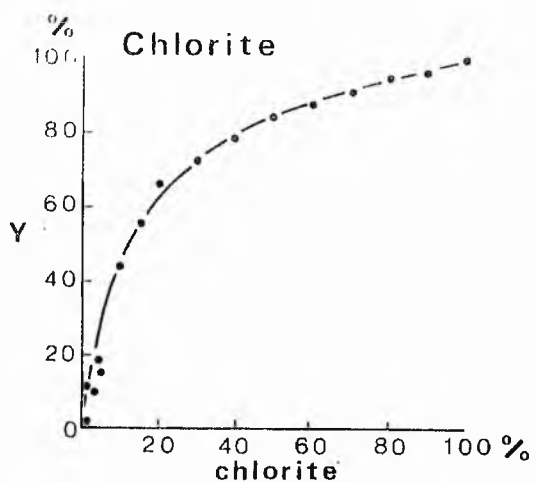


Figure 18. Plots illustrating the effects of temperature on the X-ray reflections of sample DCYP-3. Solid lines, chlorite reflections. Broken lines, sericite reflections.



$$Y = \frac{\text{ht. mineral}}{\text{ht. mineral} + \text{ht. quartz}}$$

Figure 19. Calibration curves for two component mixtures used in modal analysis by X-ray diffraction.

STRATIGRAPHIC DISTRIBUTION OF ELEMENTS IN BLACK SHALES

- HARTFELL
- ◇ CARRIFRAN BURN
- ◇ MOUNTBENGER
- ◇ GLENKILN
- + DOBB' S LINN

Figure 20. Key to symbols used in stratigraphic variation diagrams.

+

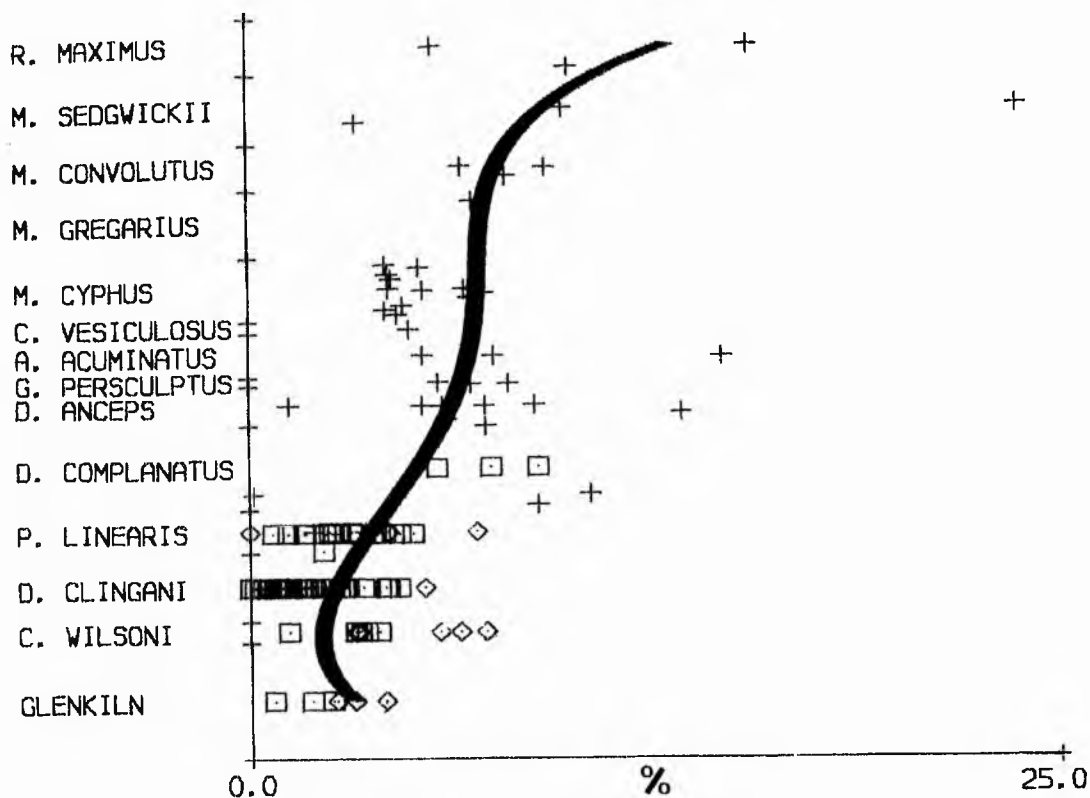
In Figures 21-23,

the divisions of ordinate are proportional to the zone thicknesses at the type section of Dobb's Linn, (Toghill 1968, 1970a).

Key to symbols for the inliers sampled is illustrated in Figure 20.

In each case, the best-fit polynomial regression curve is superimposed if significant at the 0.99 confidence level.

ALBITE 119 DATA POINTS



CHLORITE 119 DATA POINTS

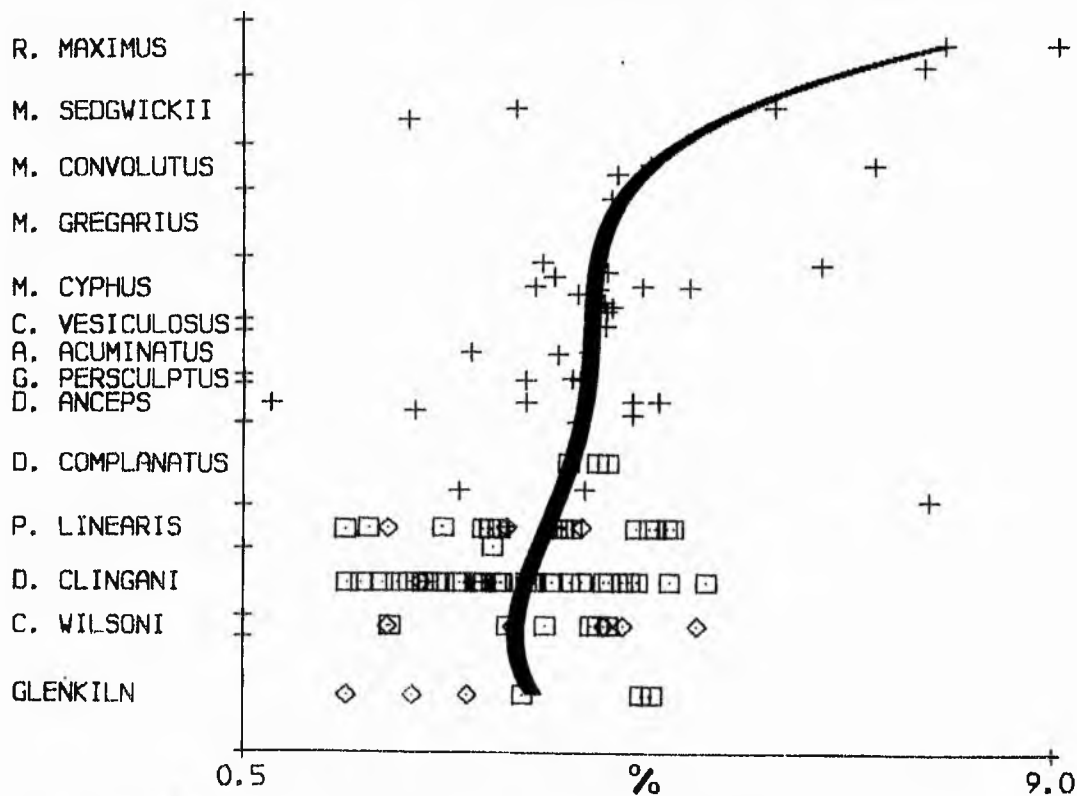
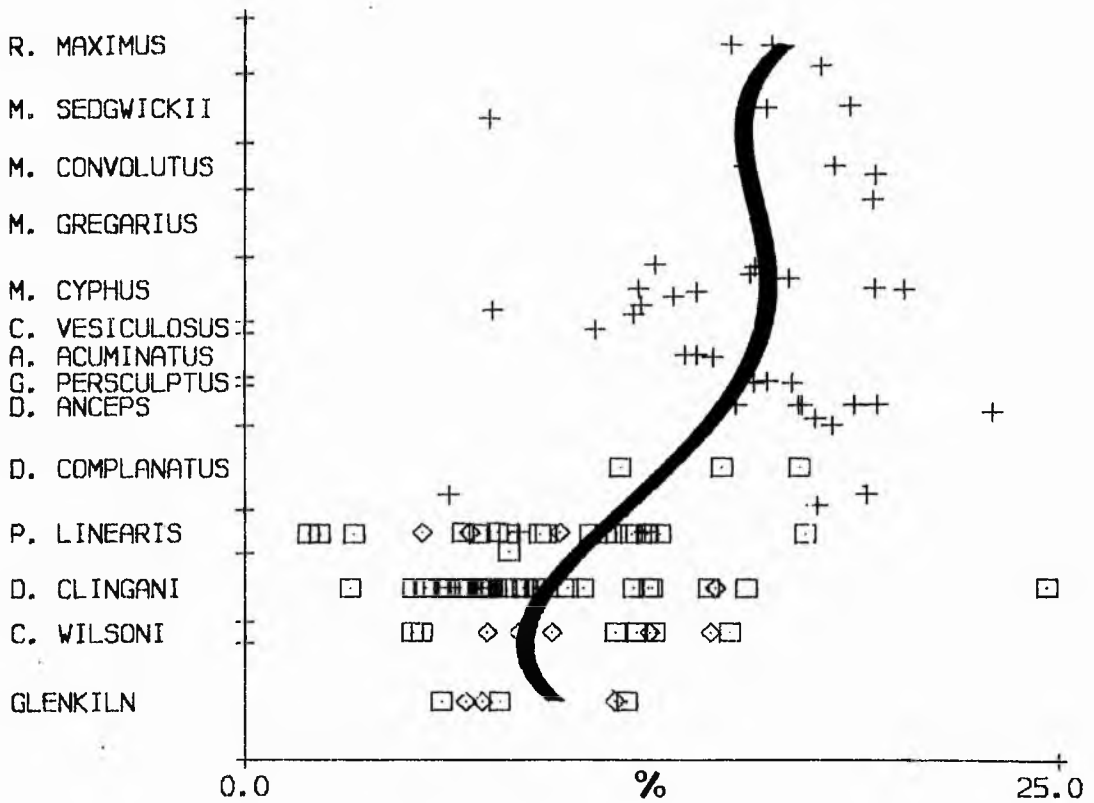


Figure 21.† Plots illustrating the stratigraphic variation of albite and chlorite concentrations in the Moffat Shales.

SERICITE 119 DATA POINTS



PYRITE 119 DATA POINTS

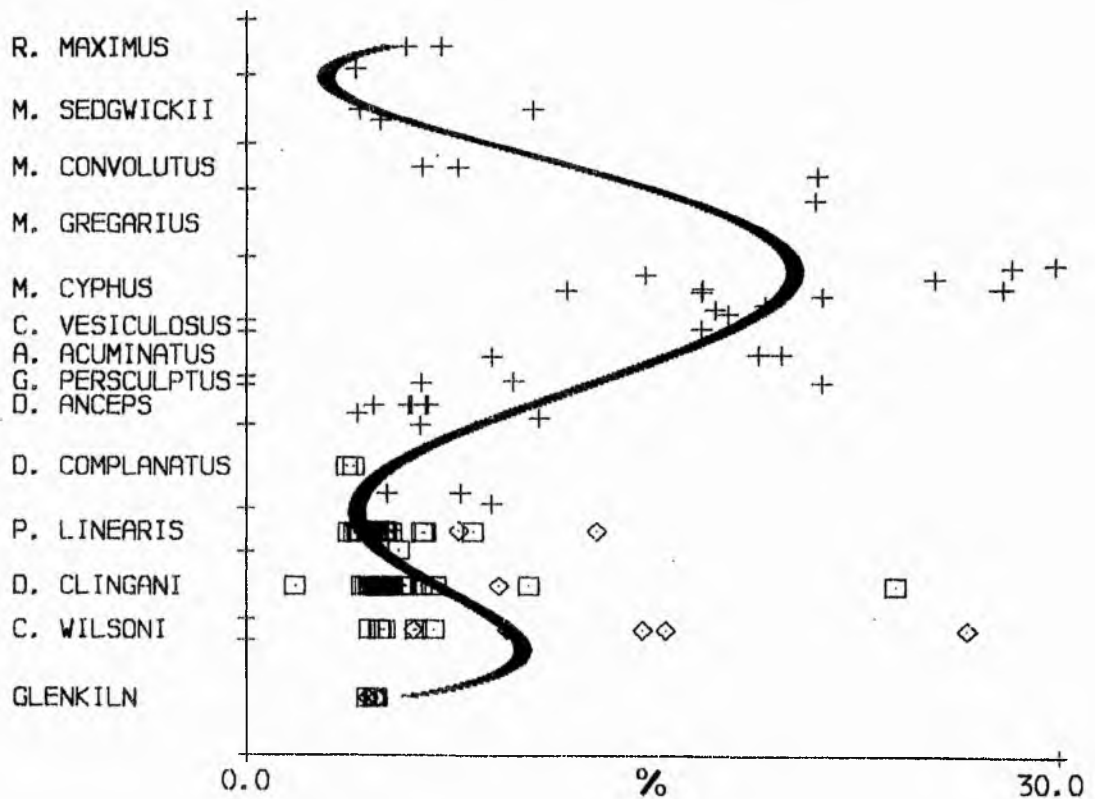


Figure 22. Plots illustrating the stratigraphic variation of sericite and pyrite concentrations in the Moffat Shales.

QUARTZ 119 DATA POINTS

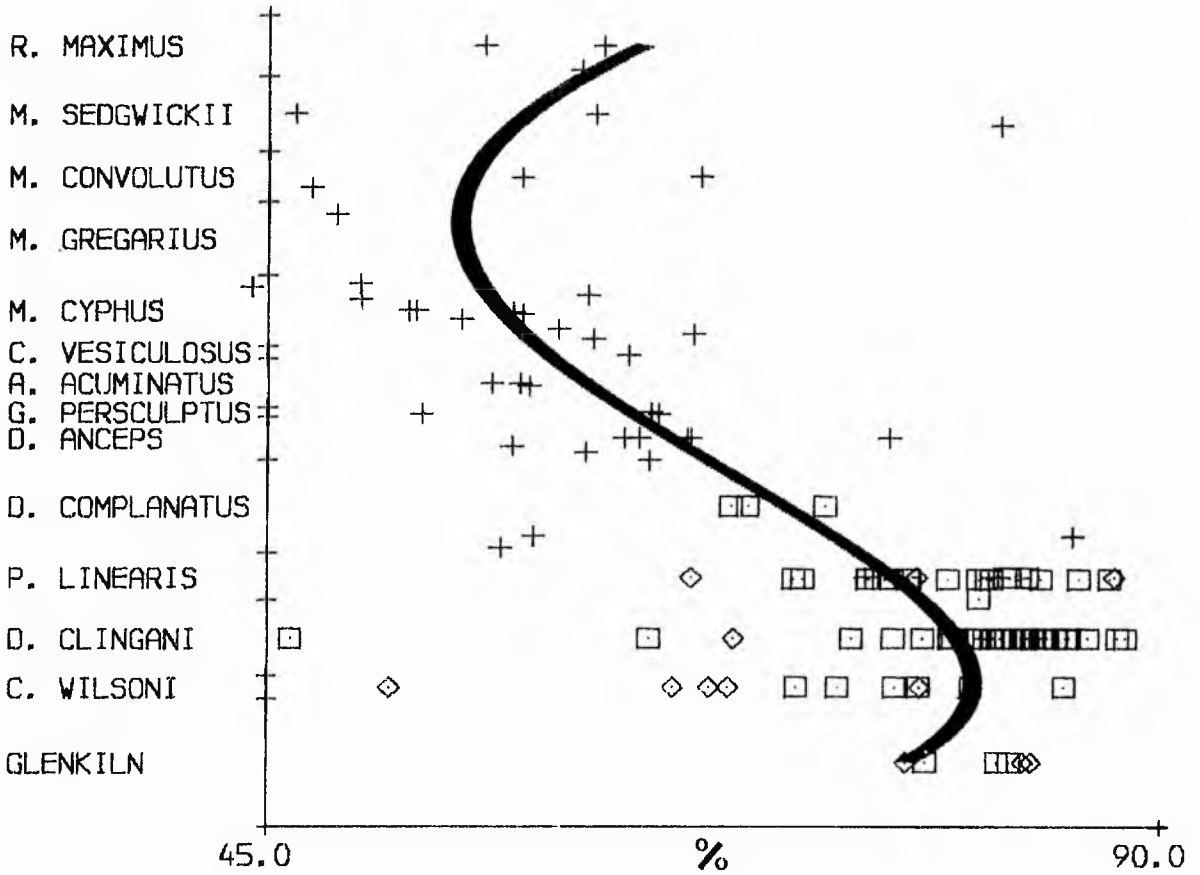


Figure 23. Plot illustrating the stratigraphic variation of quartz concentration in the Moffat Shales.

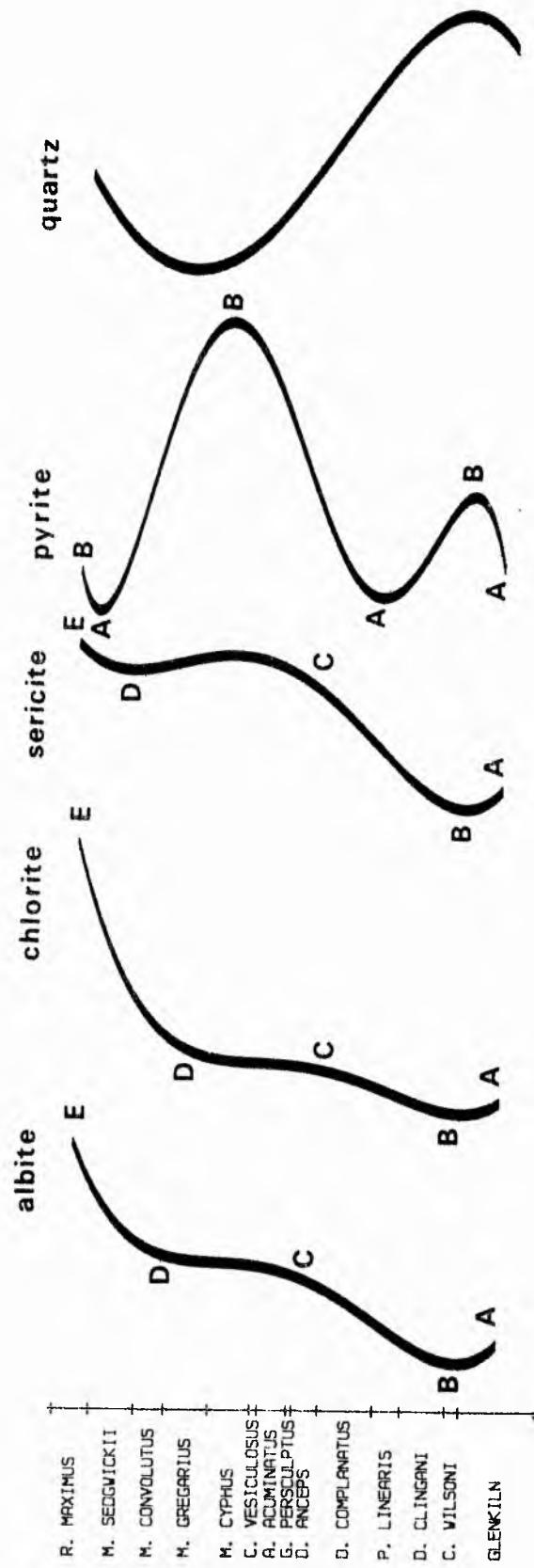


Figure 24. Comparison of profiles illustrated in Figures 21-23.

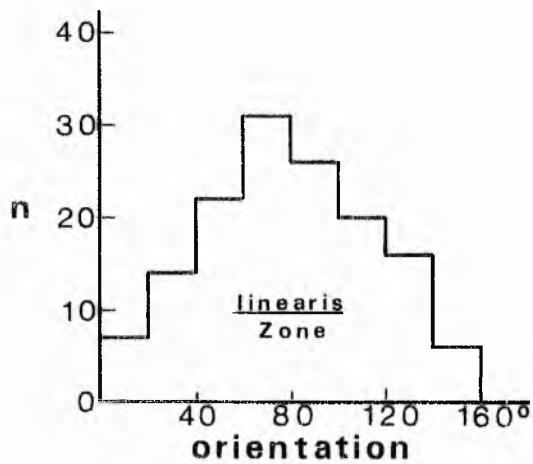
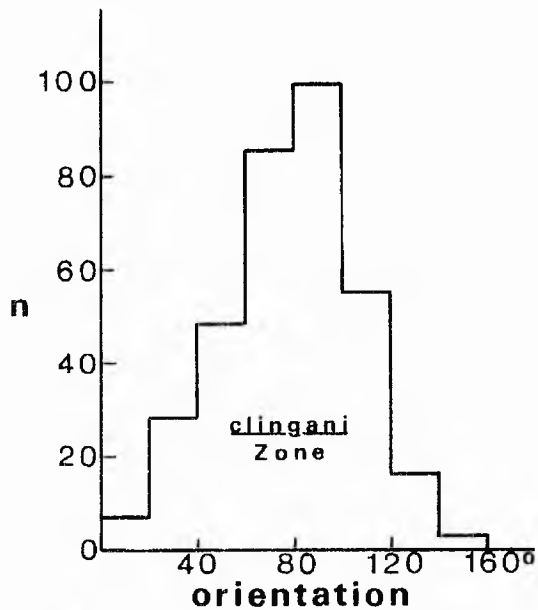
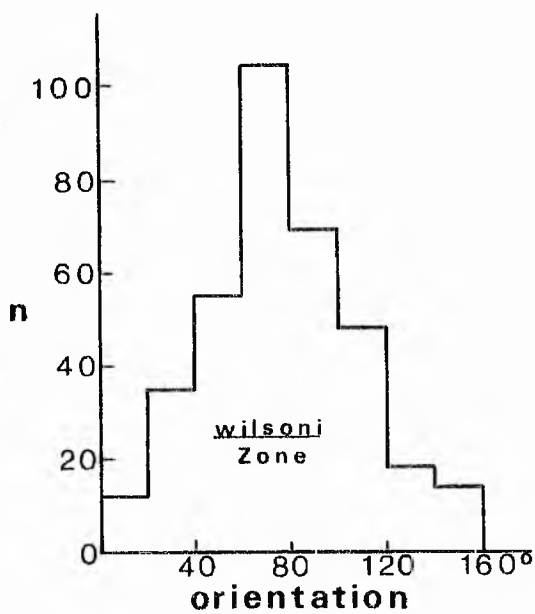


Figure 25. Histograms of the variation in graptolite stipe orientations, (after Watson 1971).

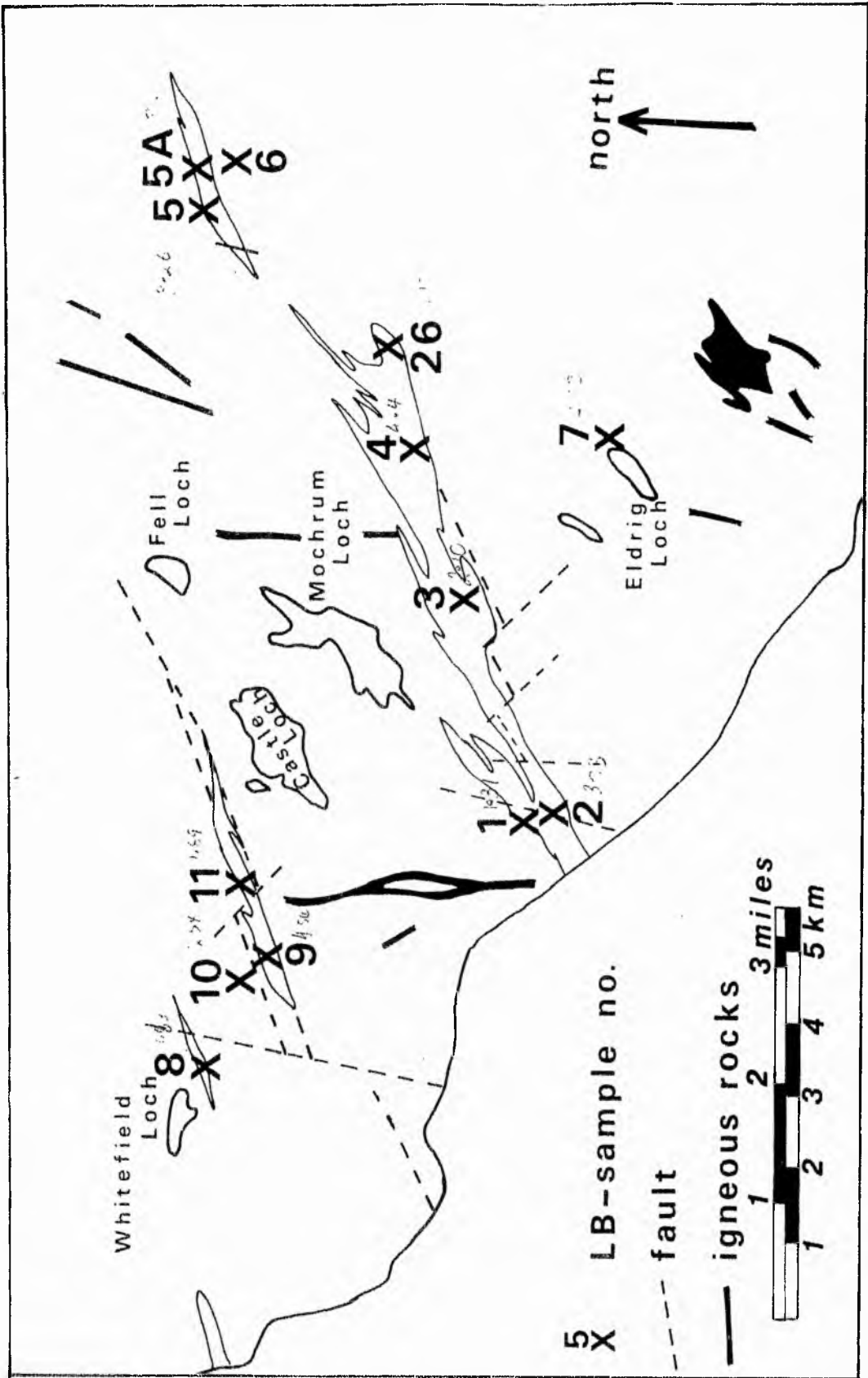


Figure 26. Location map for samples collected from the eastern margin of Luce Bay. For regional setting see Figure 5.

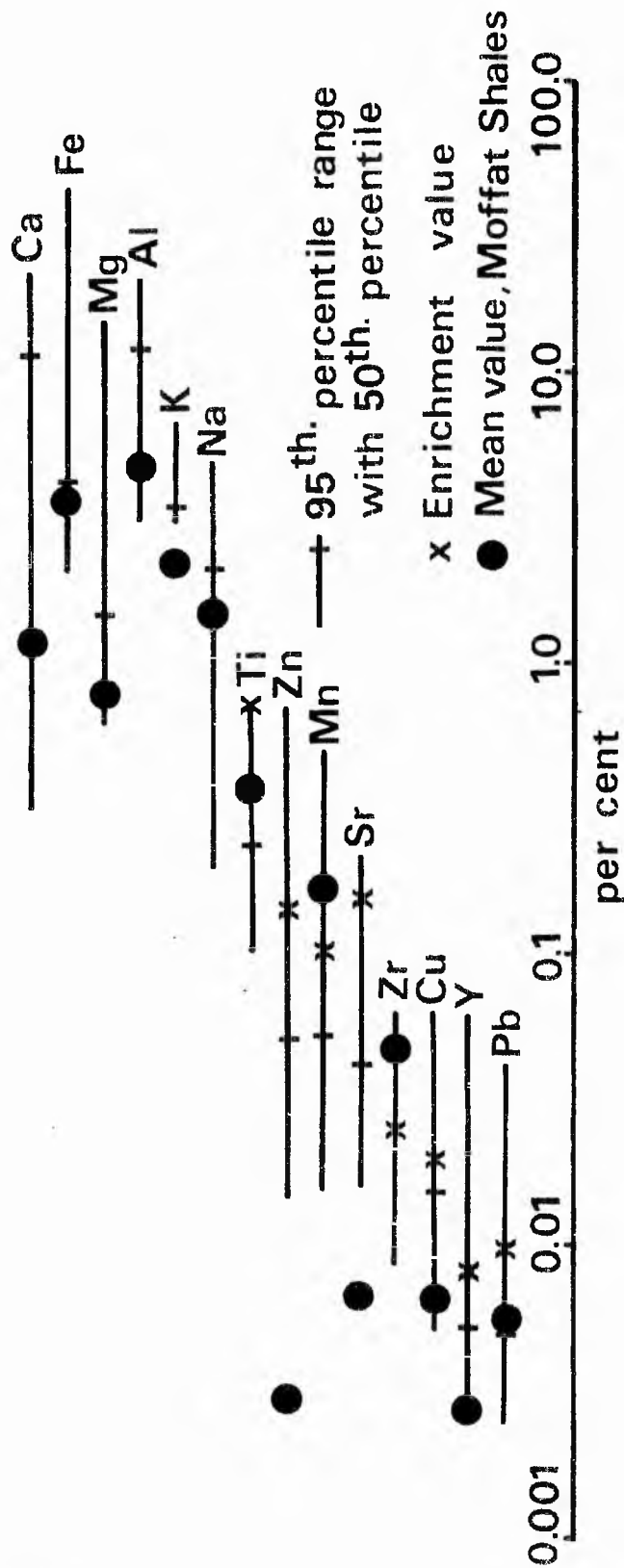


Figure 27. Mean values for the elements in the Moffat Shales compared with ranges from Vine and Tourtelot (1970).

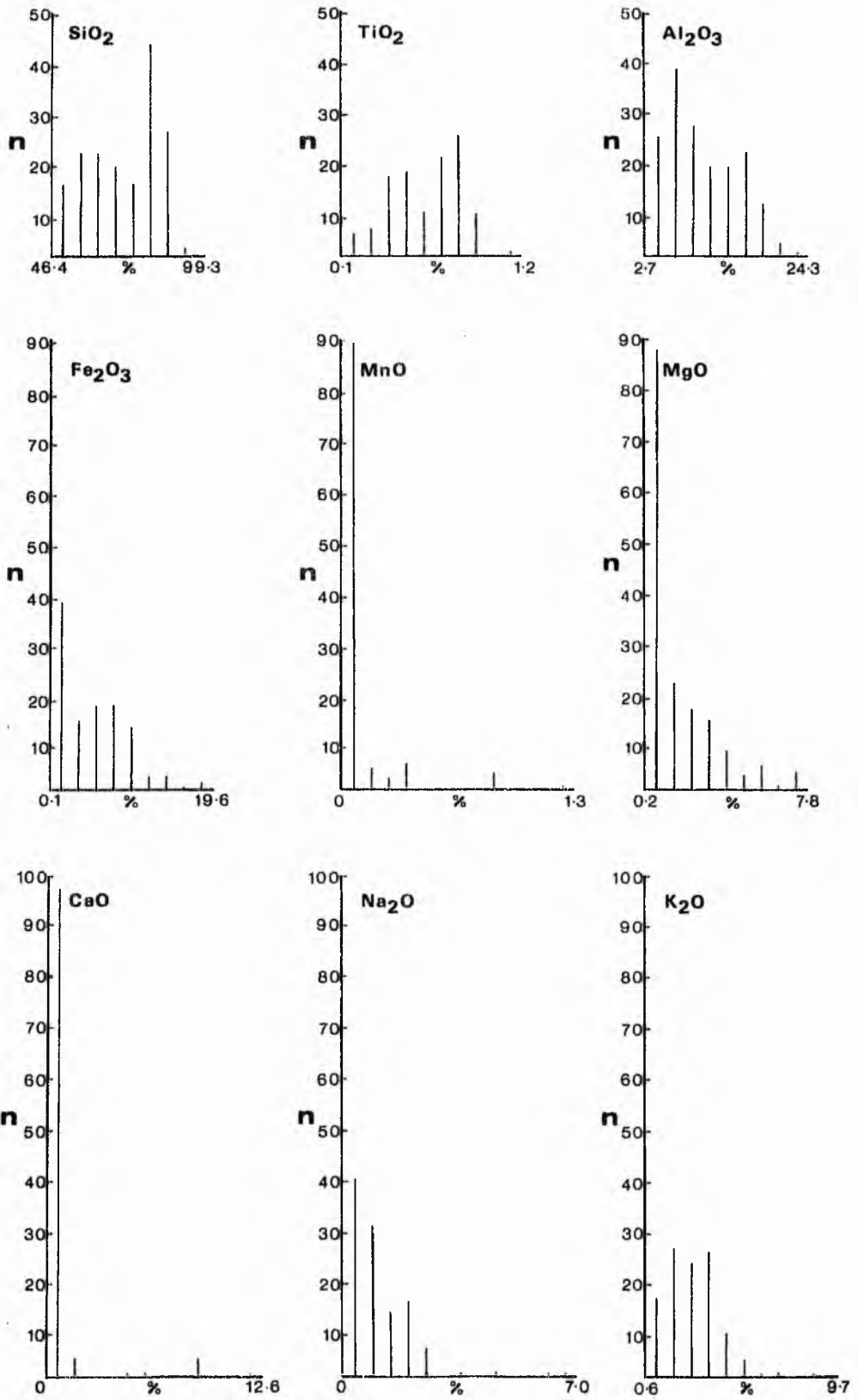


Figure 28. Histograms of the major element oxides in the Moffat Shales.

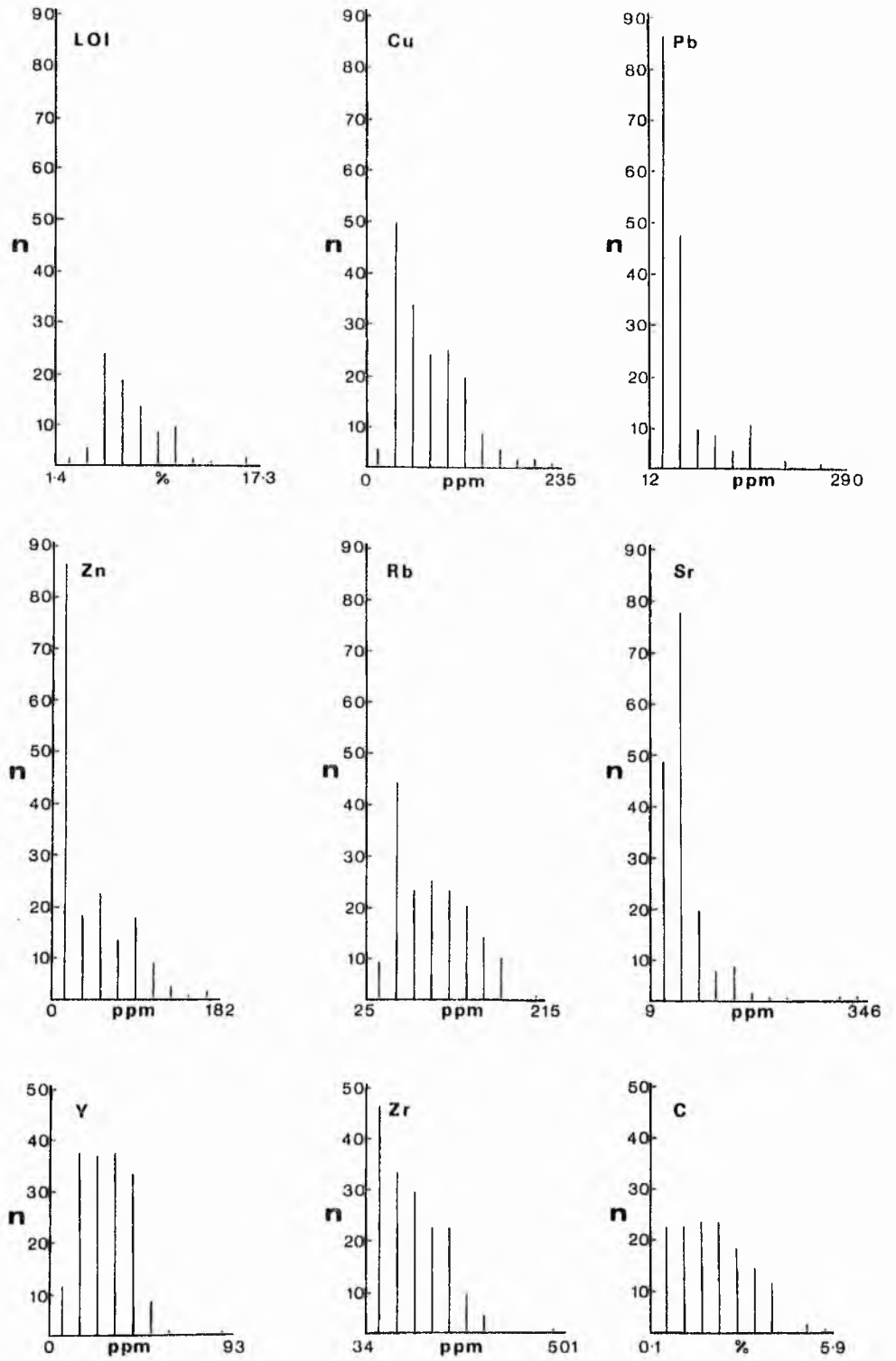
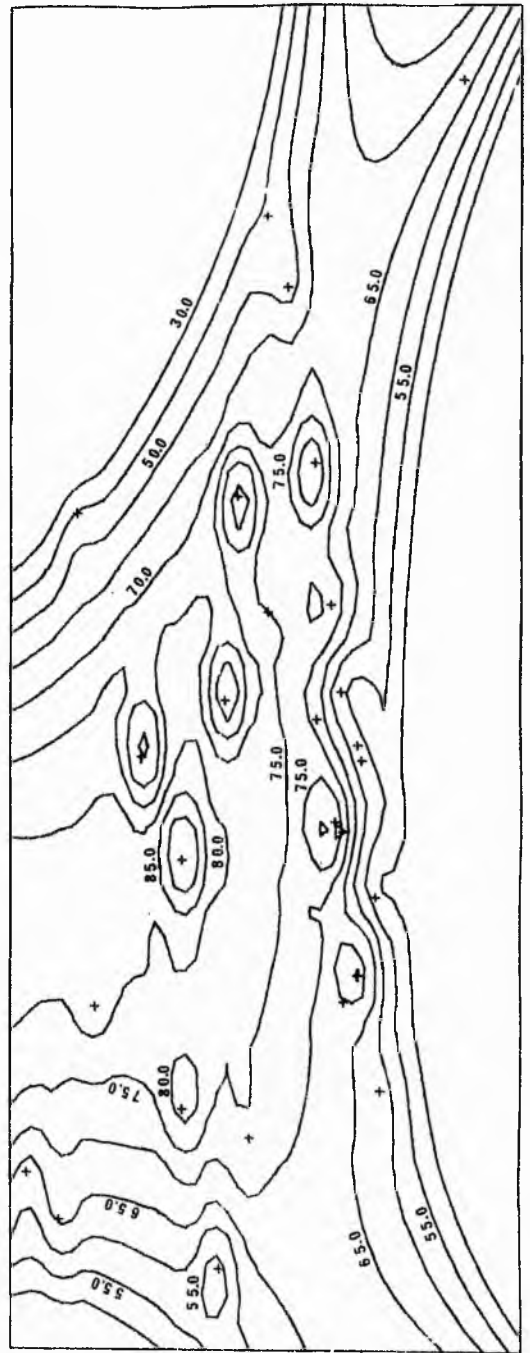


Figure 29. Histograms of minor elements in the Moffat Shales. LOI: loss on ignition.



GLOBAL FIT SURFACE PLOT

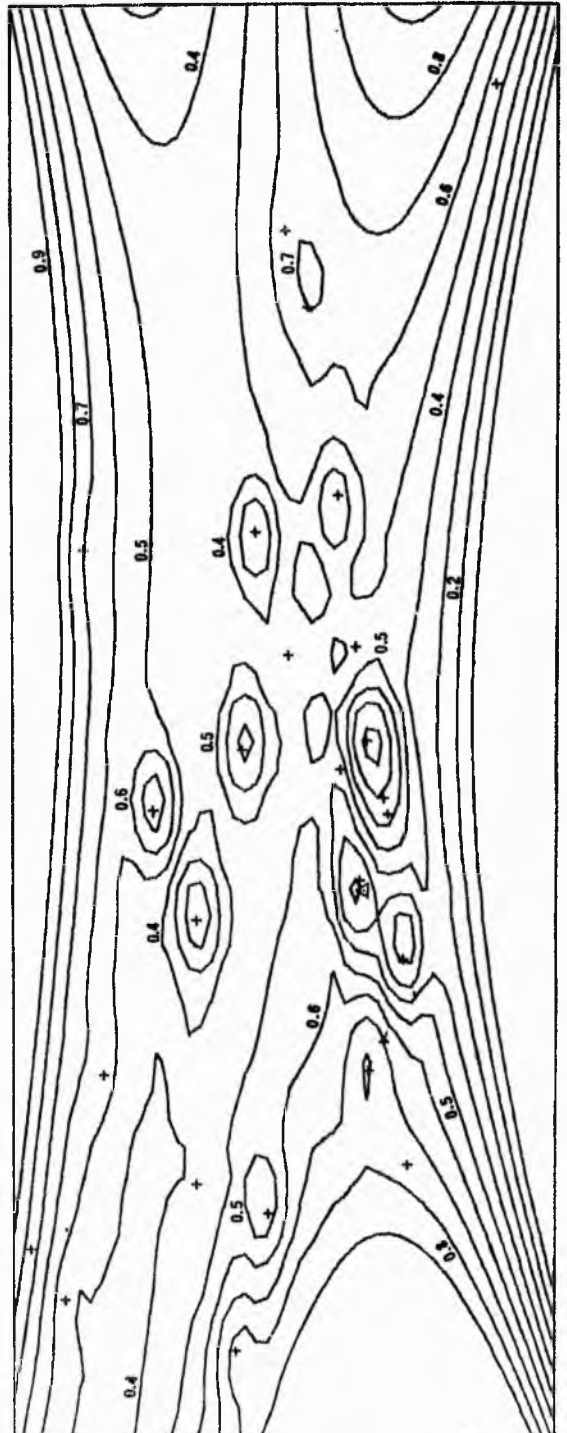


SiO₂ IN MOFFAT REGION

Figure 30. Global-fit and iterative surface maps for the variation of SiO_2 in the Moffat Shales. For scale and orientation, compare Figure 4. + , location of sample.

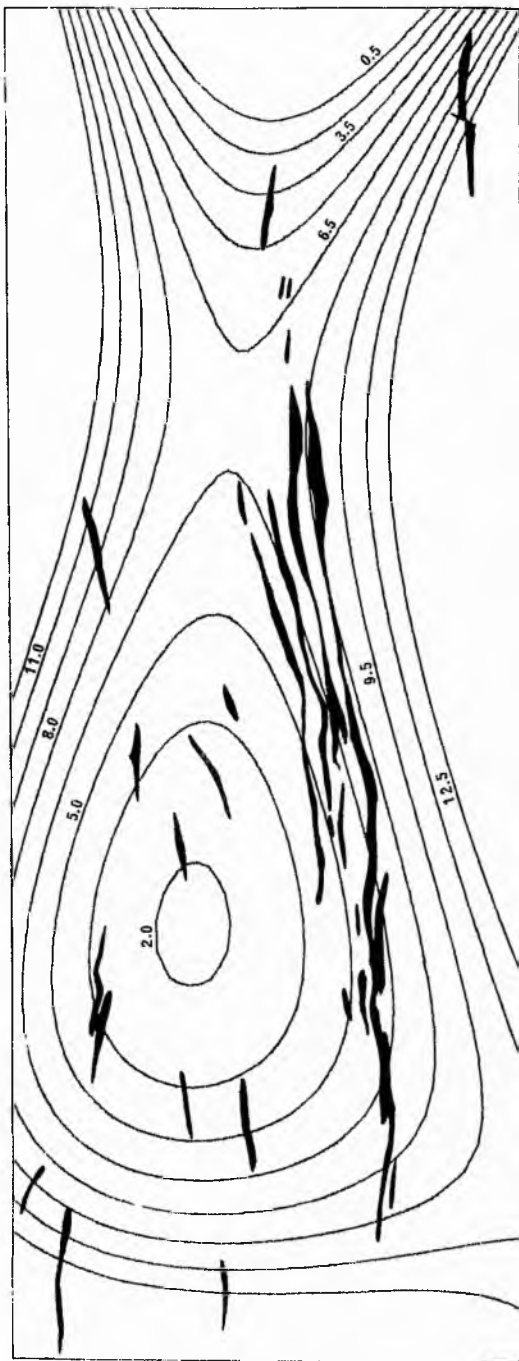


GLOBAL FIT SURFACE PLOT

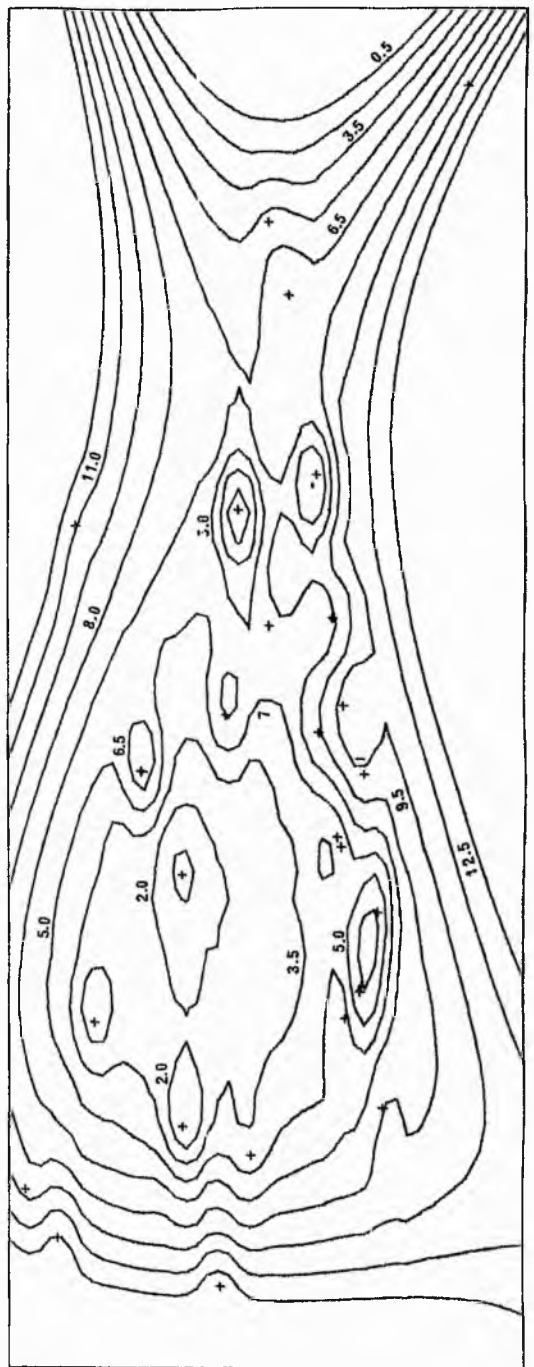


TiO₂ IN MOFFAT REGION

Figure 31. Global-fit and iterative surface maps for the variation of TiO_2 in the Moffat Shales. For scale and orientation, compare Figure 4. + , location of sample.

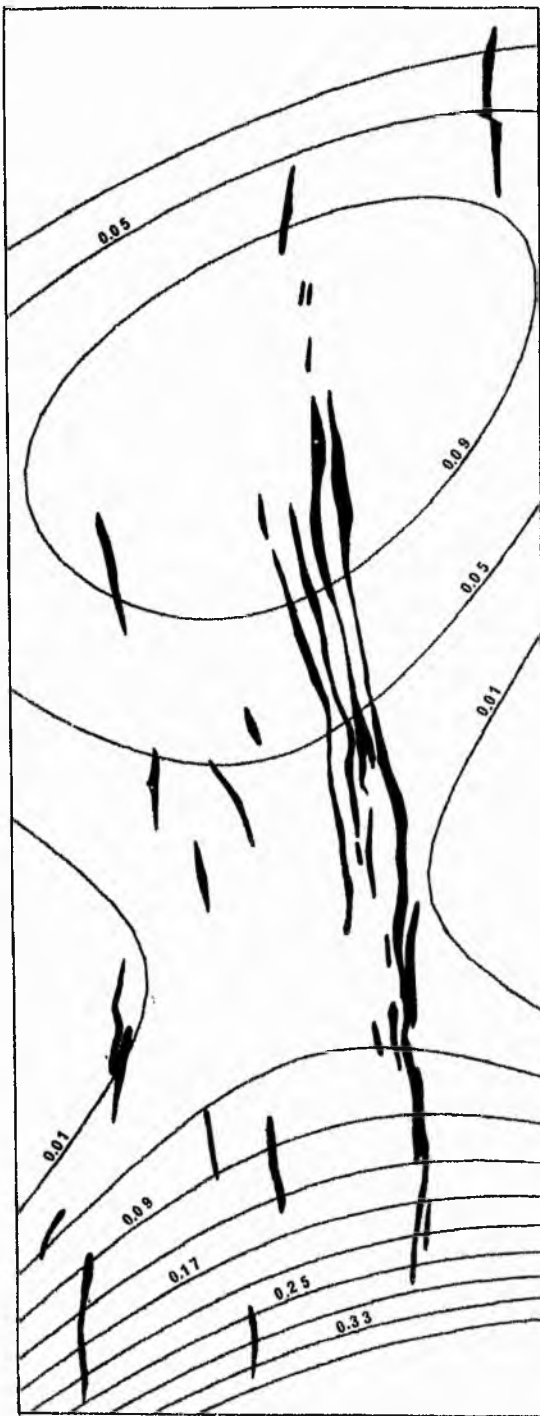


GLOBAL FIT SURFACE PLOT

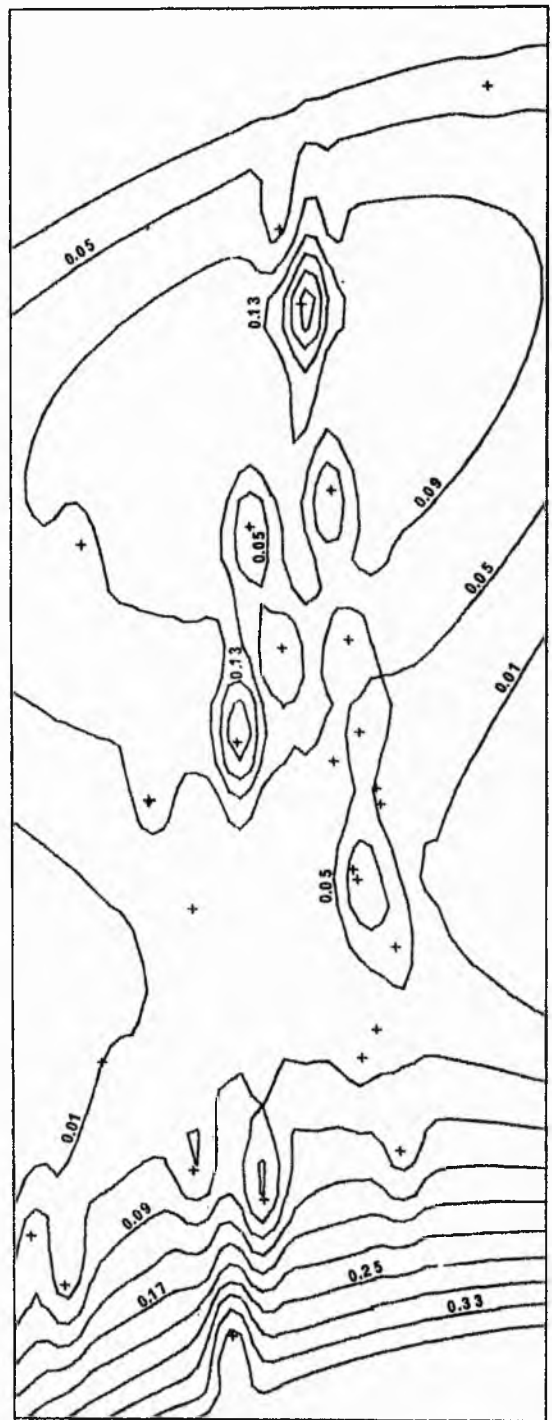


FE2O3 IN MOFFAT REGION

Figure 33. Global-fit and iterative surface maps for the variation of Fe_2O_3 in the Moffat Shales. For scale and orientation, compare Figure 4. + , location of sample.



GLOBAL FIT SURFACE PLOT

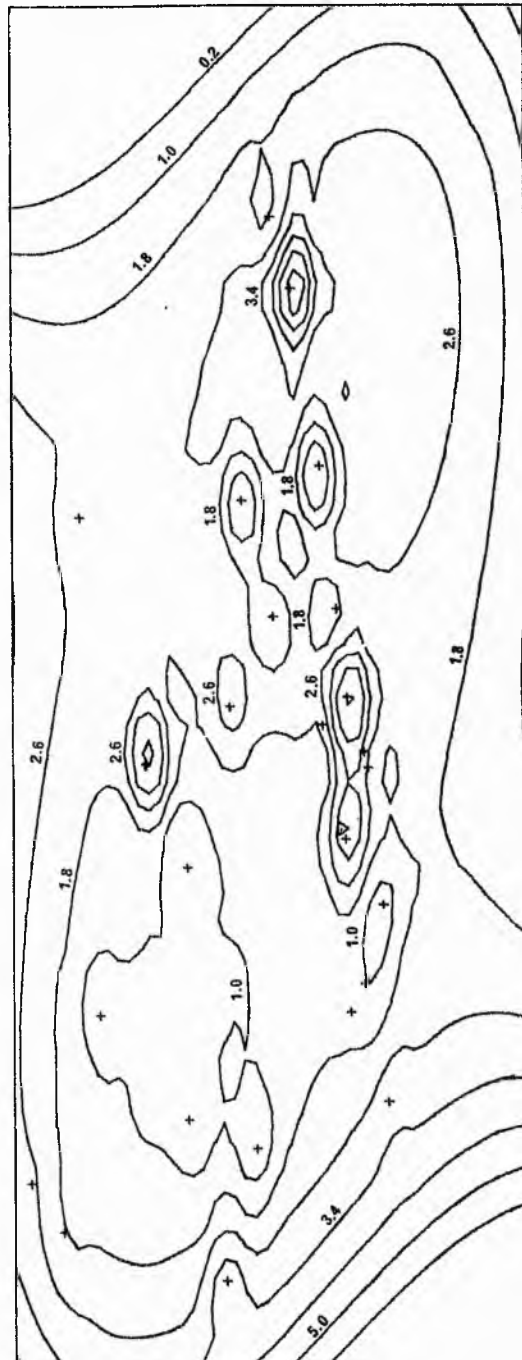


MNO IN MOFFAT REGION

Figure 34. Global-fit and iterative surface maps for the variation of MnO in the Moffat Shales. For scale and orientation, compare Figure 4. + , location of sample.



GLOBAL FIT SURFACE PLOT

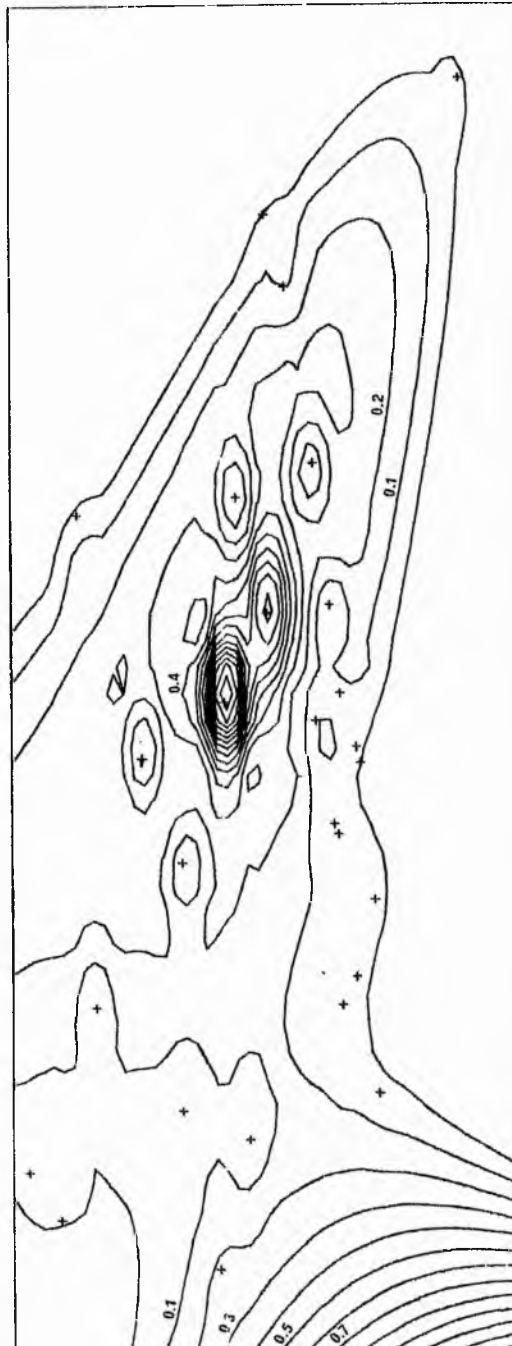


MGO IN MOFFAT REGION

Figure 35. Global-fit and iterative maps for the variation of MgO in the Moffat Shales. For scale and orientation, compare Figure 4. + , location of sample.



GLOBAL FIT SURFACE PLOT

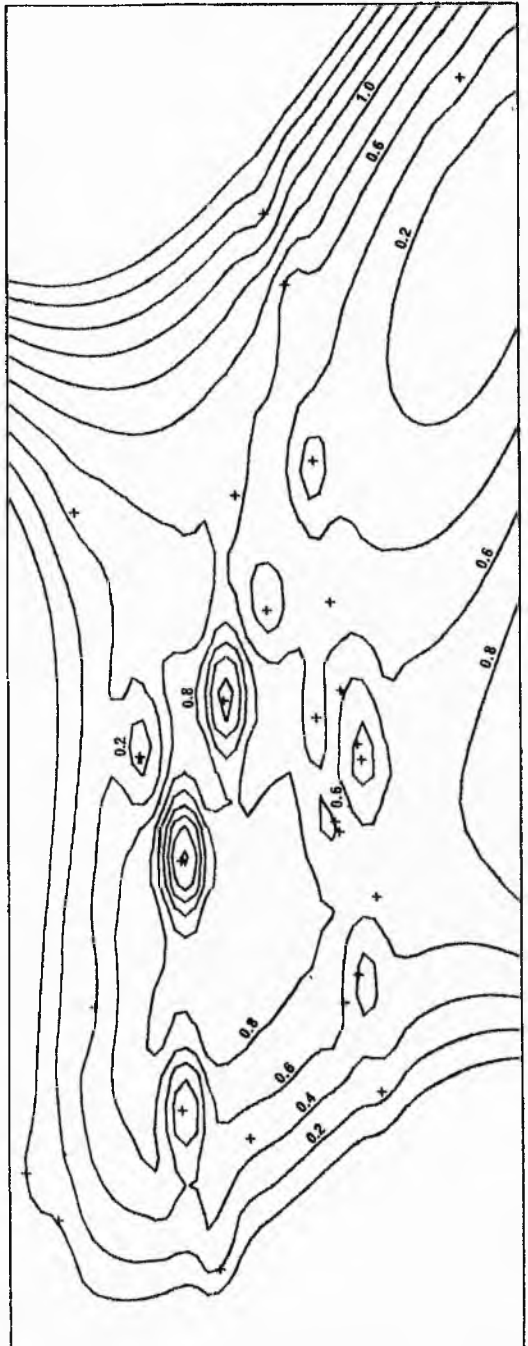


CaO IN MOFFAT REGION

Figure 36. Global-fit and iterative surface maps for the variation of CaO in the Moffat Shales. For scale and orientation, compare Figure 4. + , location of sample.

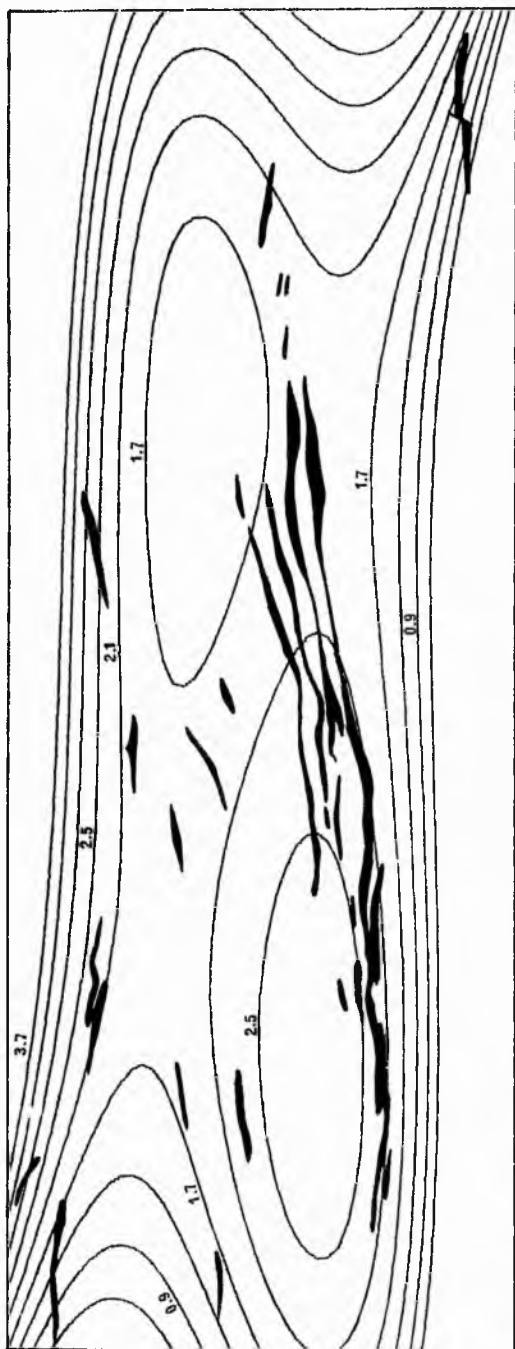


GLOBAL FIT SURFACE PLOT

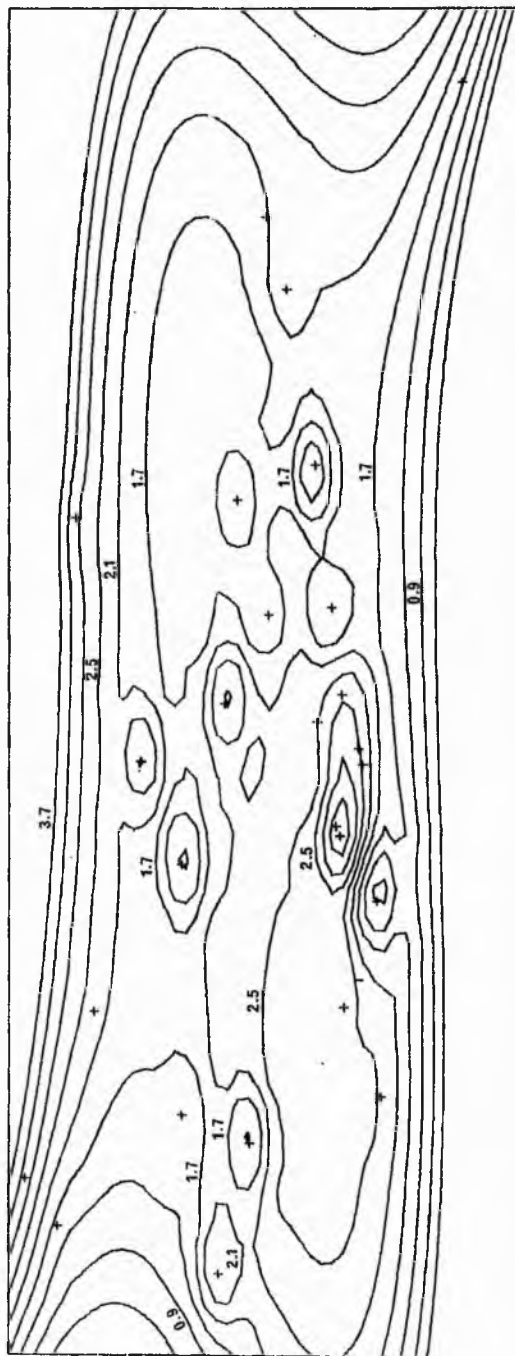


NA2O IN MOFFAT REGION

Figure 37. Global-fit and iterative surface maps for the variation of Na_2O in the Moffat Shales. For scale and orientation, compare Figure 4. + , location of sample.



GLOBAL FIT SURFACE PLOT

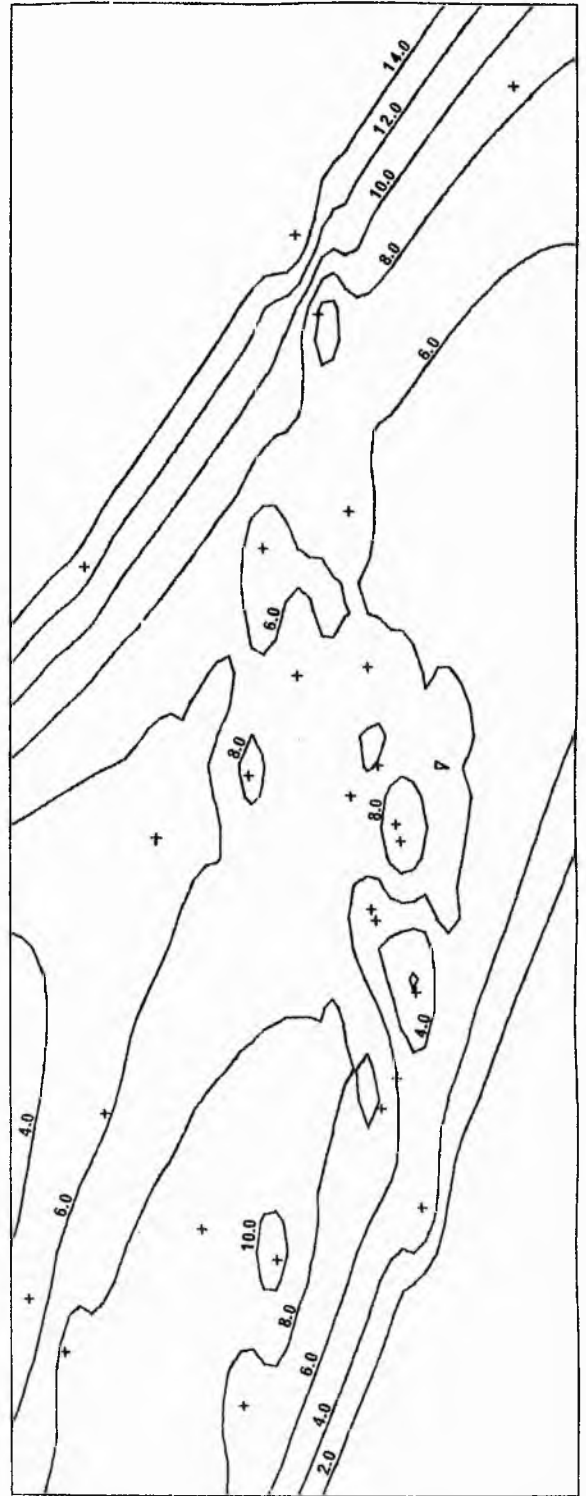


K2O IN MOFFAT REGION

Figure 38. Global-fit and iterative surface maps for the variation of K_2O in the Moffat Shales. For scale and orientation, compare Figure 4. + , location of sample.

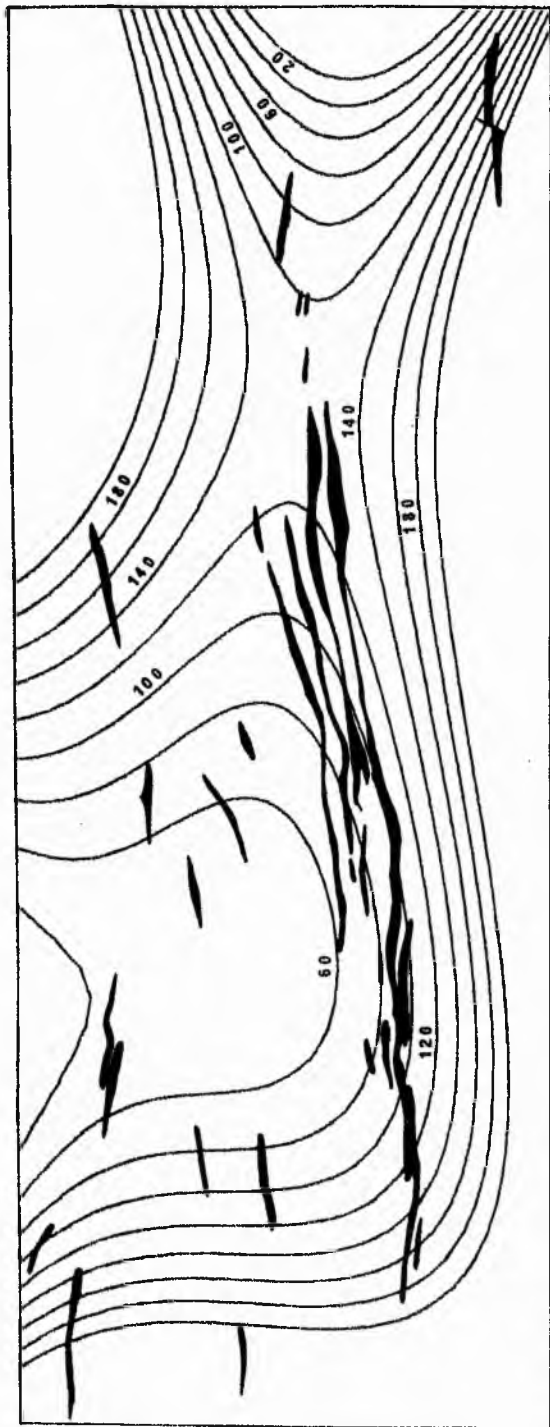


GLOBAL FIT SURFACE PLOT

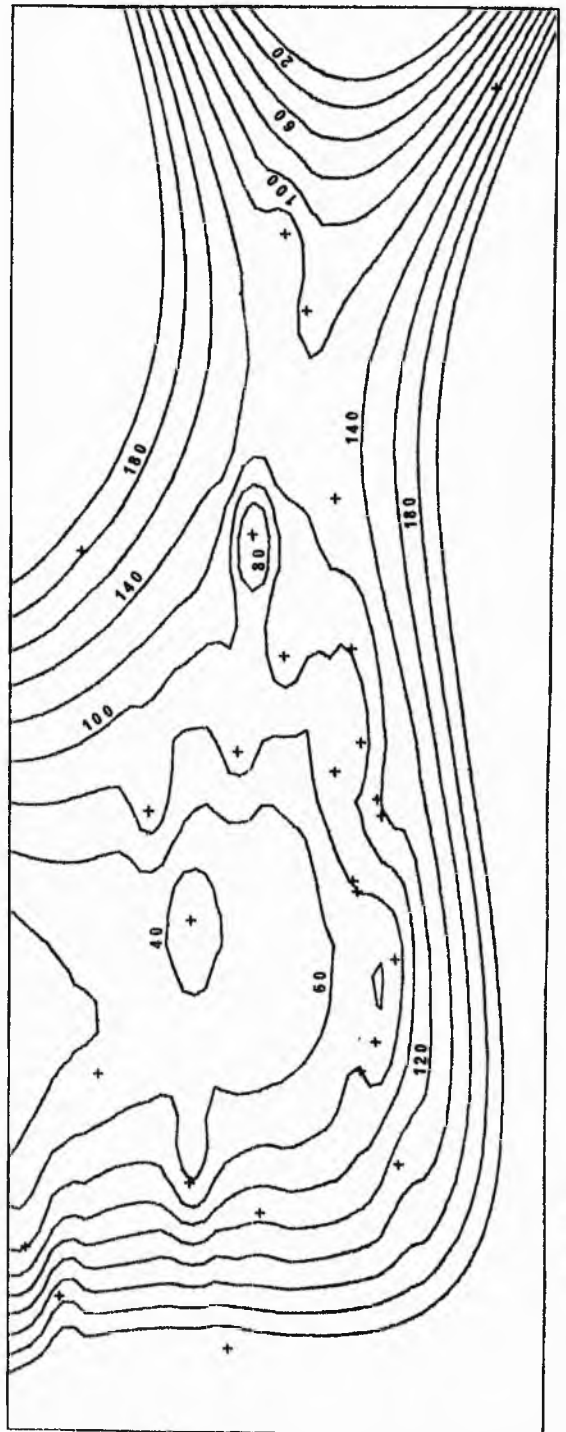


LOI IN MOFFAT REGION

Figure 39. Global-fit and iterative surface maps for the variation of loss on ignition in the Moffat Shales. For scale and orientation, compare Figure 4. + , location of sample.

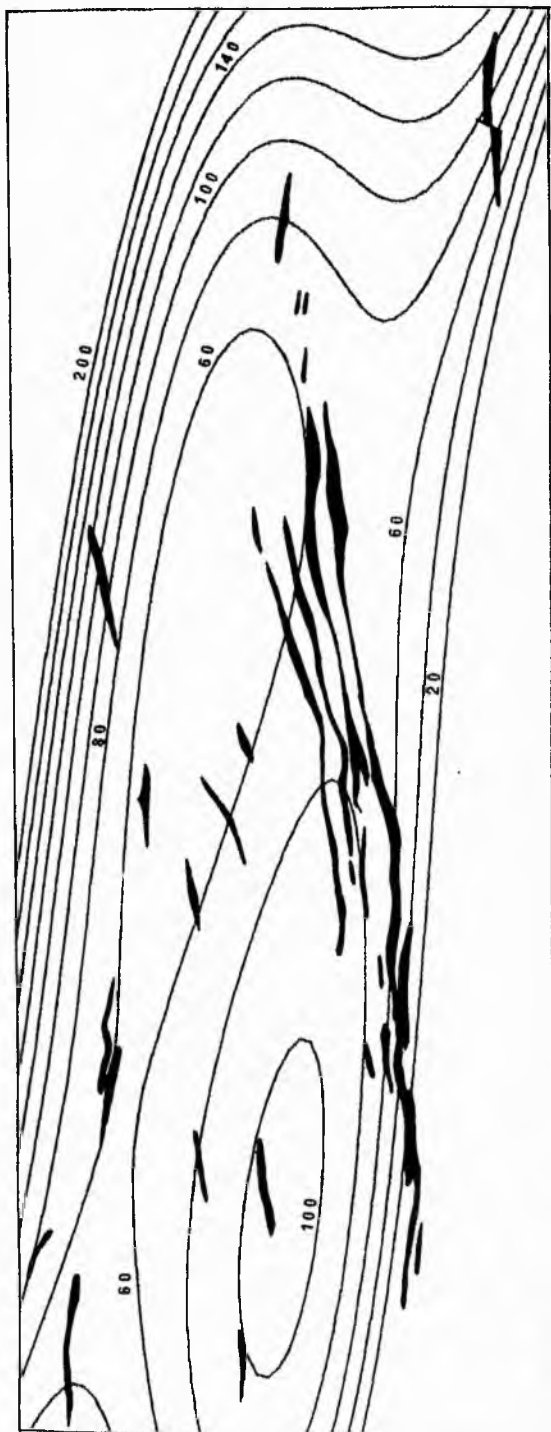


GLOBAL FIT SURFACE PLOT

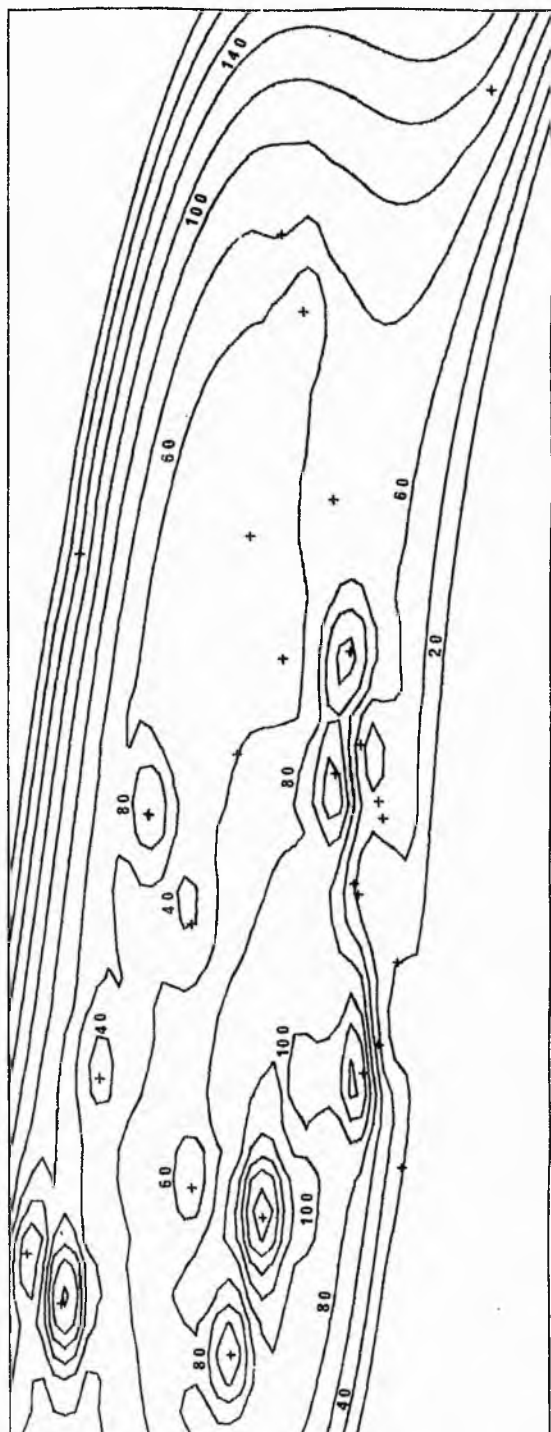


CU IN MOFFAT REGION

Figure 40. Global-fit and iterative surface maps for the variation of copper in the Moffat Shales. For scale and orientation, compare Figure 4. + , location of sample.

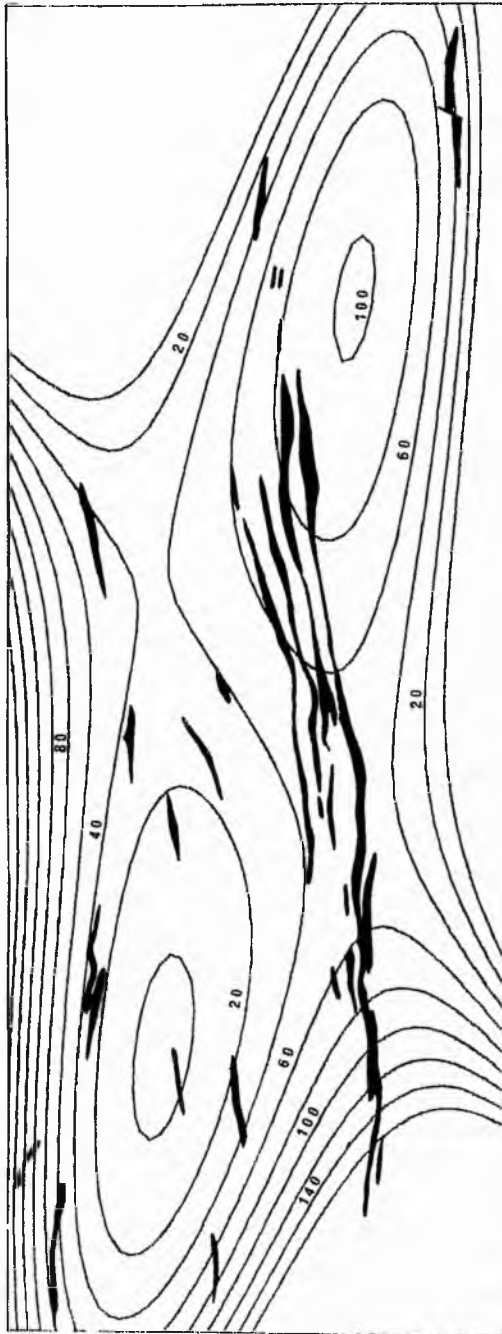


GLOBAL FIT SURFACE PLOT

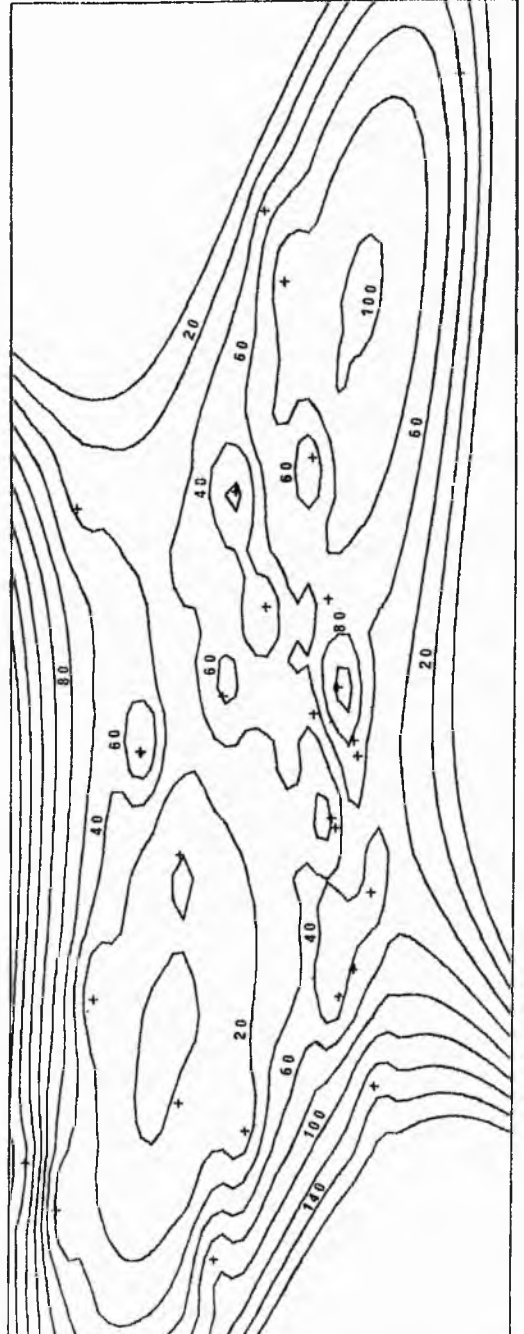


PB IN MOFFAT REGION

Figure 41. Global-fit and iterative surface maps for the variation of lead in the Moffat Shales. For scale and orientation, compare Figure 4. + , location of sample.



GLOBAL FIT SURFACE PLOT

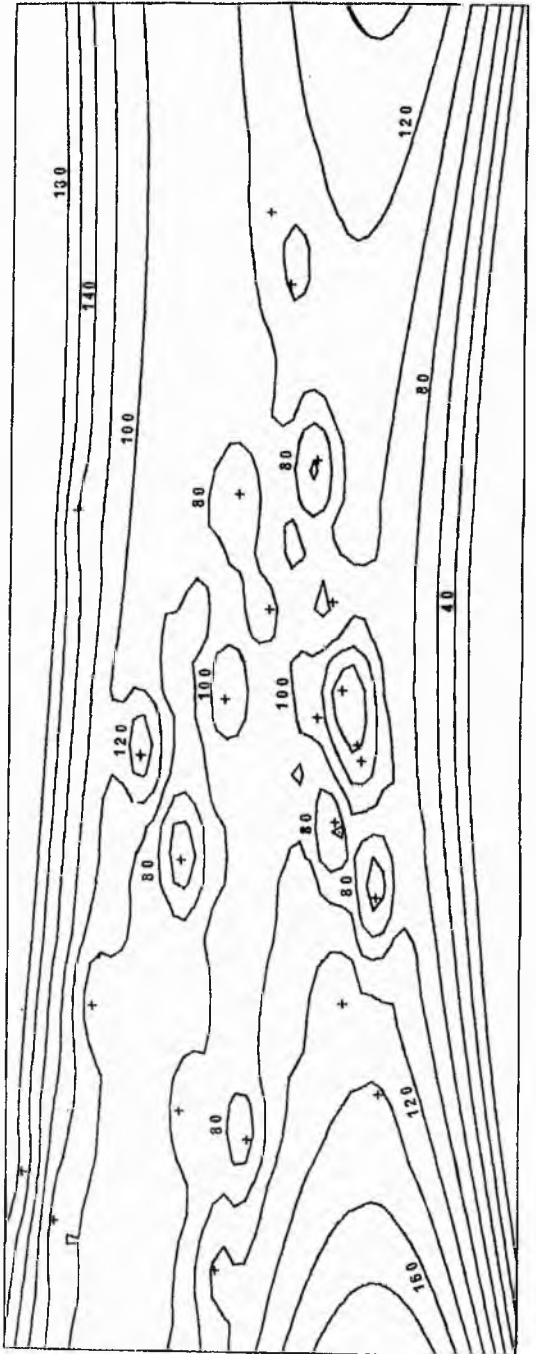


ZN IN MOFFAT REGION

Figure 42. Global-fit and iterative surface maps for the variation of zinc in the Moffat Shales. For scale and orientation, compare Figure 4. + , location of sample.

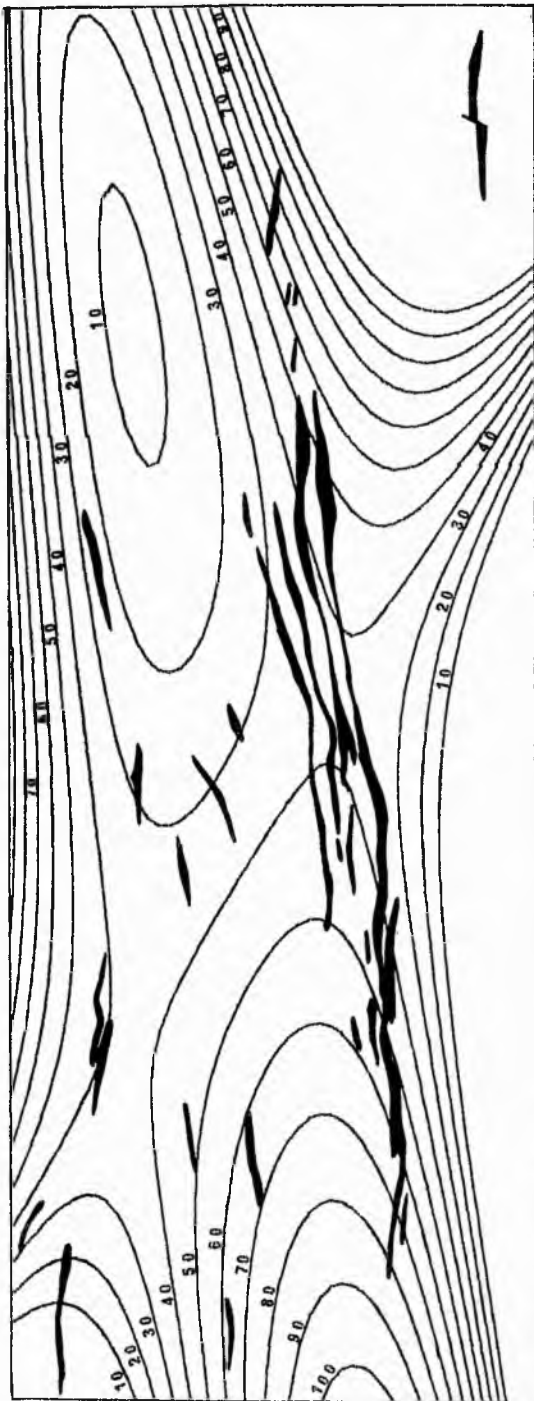


GLOBAL FIT SURFACE PLOT

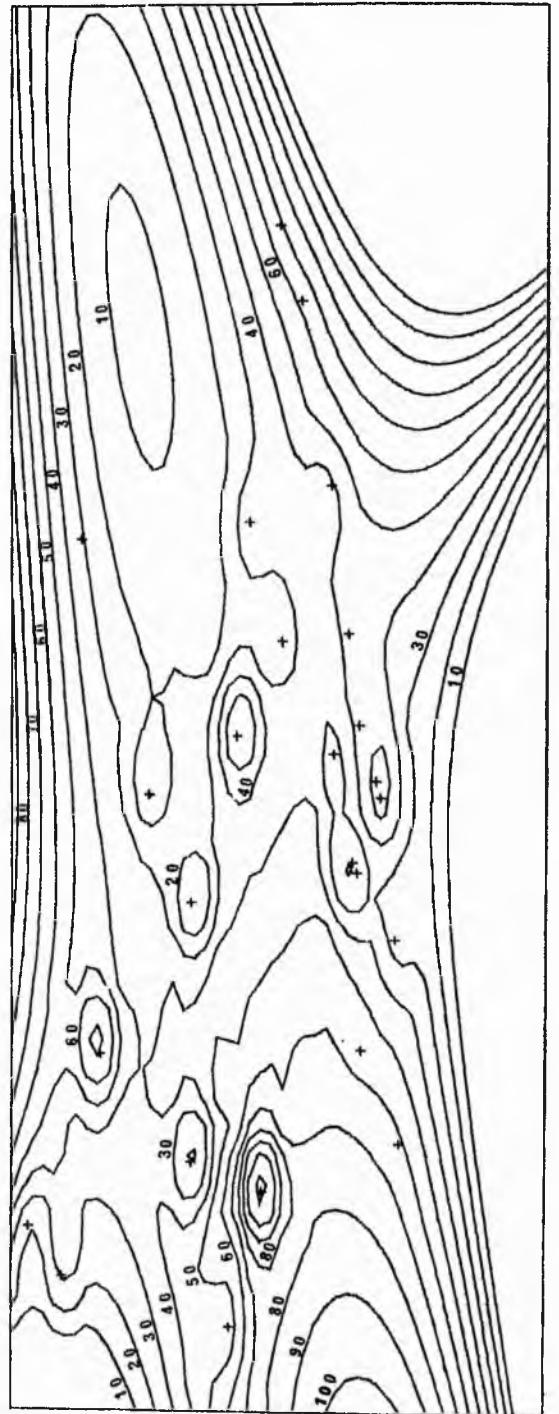


RB IN MOFFAT REGION

Figure 43. Global-fit and iterative surface maps for the variation of rubidium in the Moffat Shales. For scale and orientation, compare Figure 4. + , location of sample.



GLOBAL FIT SURFACE PLOT

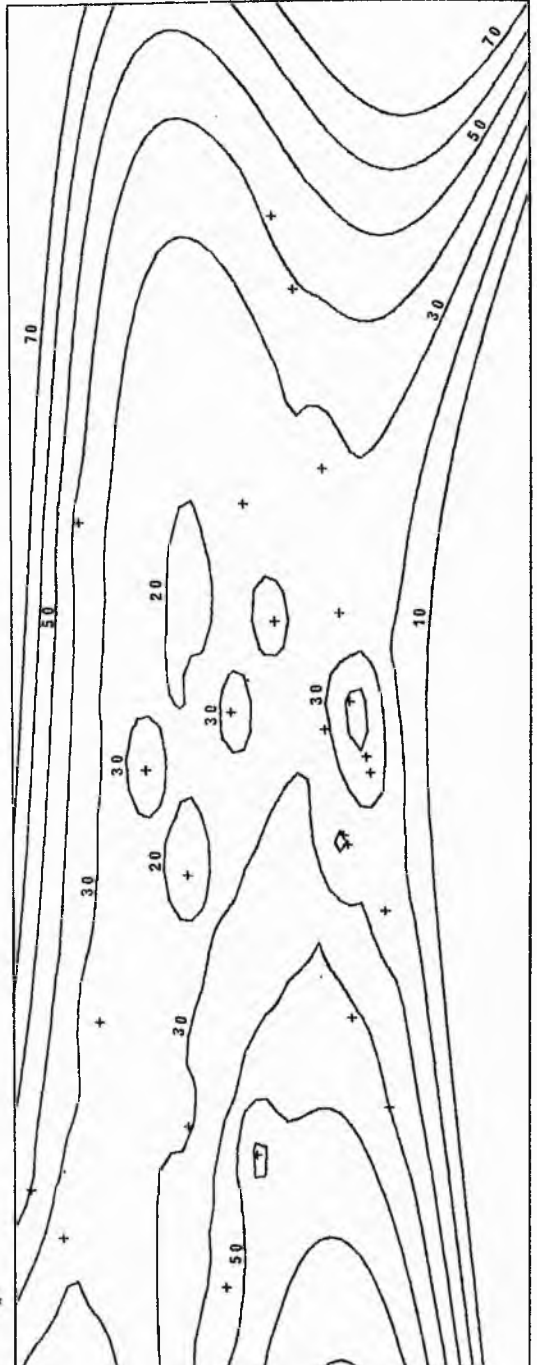


SR IN MOFFAT REGION

Figure 44. Global-fit and iterative surface maps for the variation of strontium in the Moffat Shales. For scale and orientation, compare Figure 4. + , location of sample.



GLOBAL FIT SURFACE PLOT

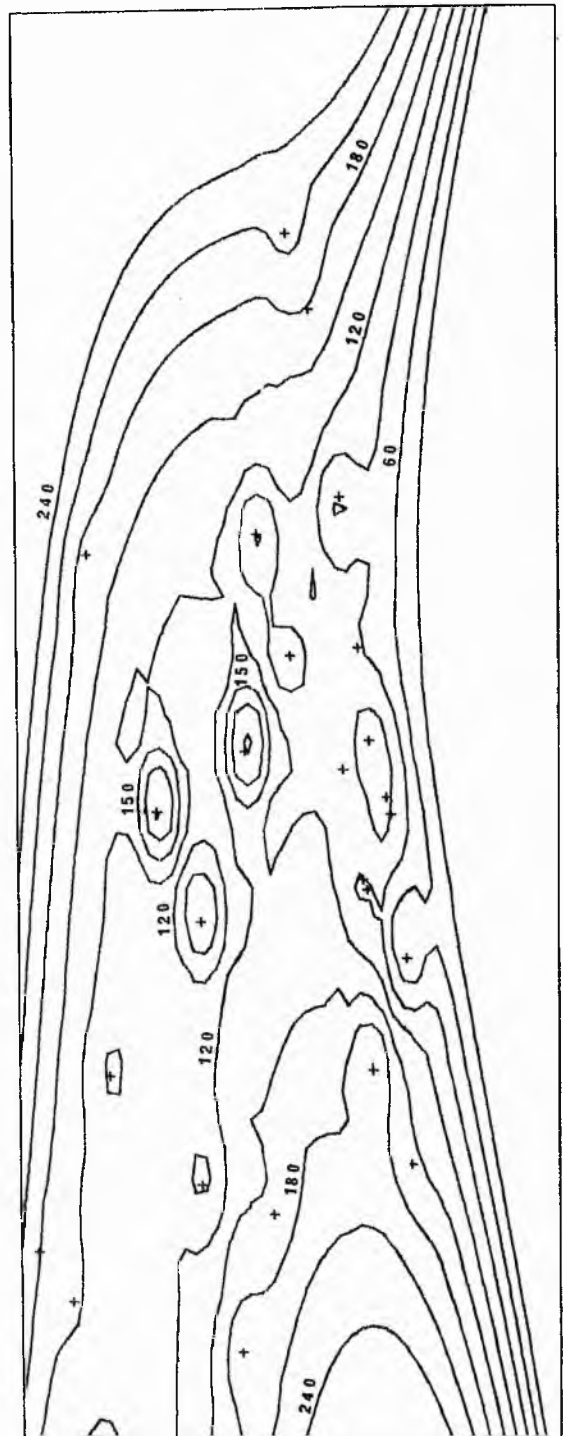


Y IN MOFFAT REGION

Figure 45. Global-fit and iterative surface maps for the variation of yttrium in the Moffat Shales. For scale and orientation, compare Figure 4. + , location of sample.



GLOBAL FIT SURFACE PLOT



ZR IN MOFFAT REGION

Figure 46. Global-fit and iterative surface maps for the variation of zirconium in the Moffat Shales. For scale and orientation, compare Figure 4, +, location of sample.

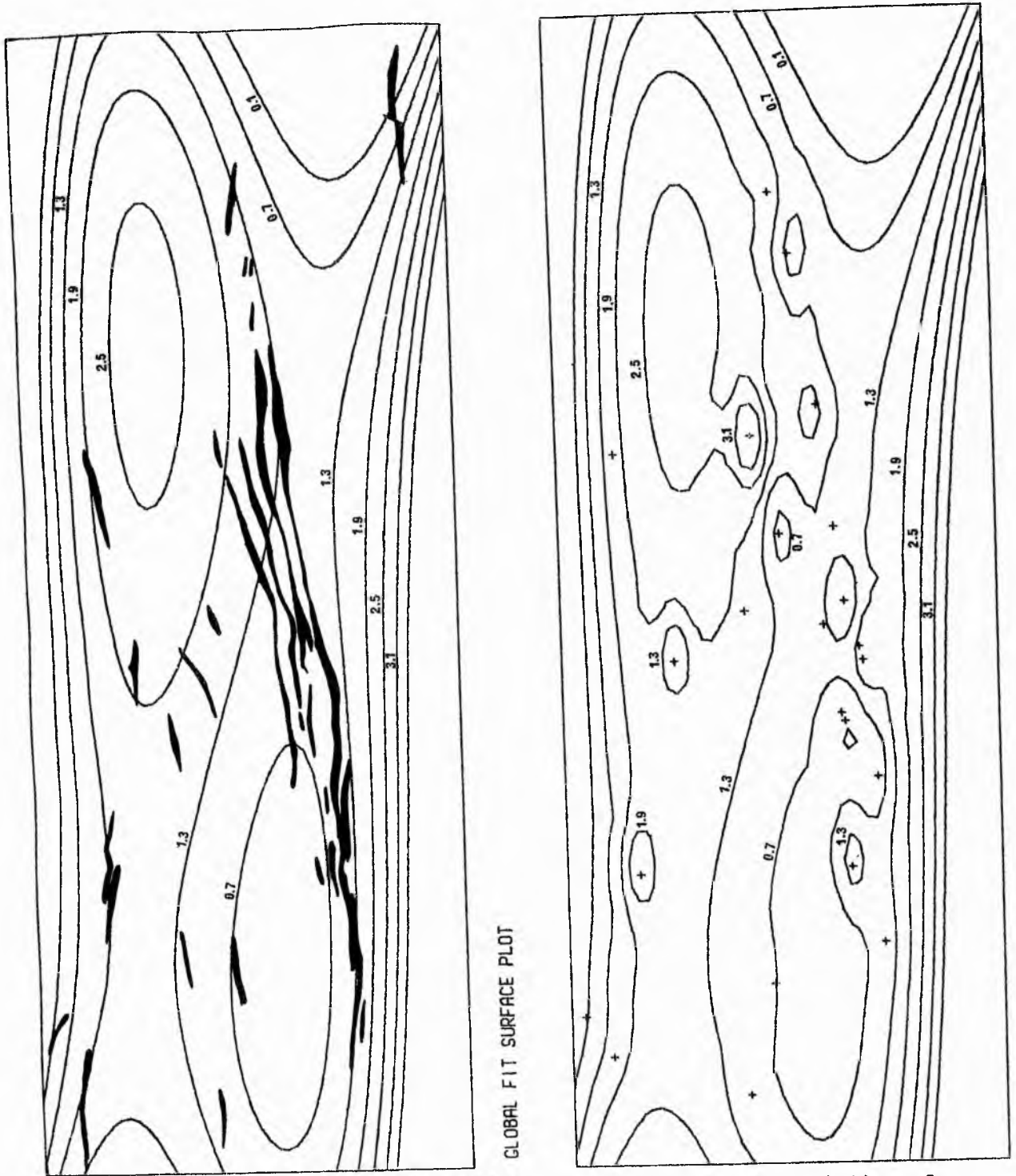


Figure 47. Global-fit and iterative surface maps of the variation of carbon in the Moffat Shales. For scale and orientation, compare Figure 4. + , location of sample.

CARBON IN MOFFAT REGION

+

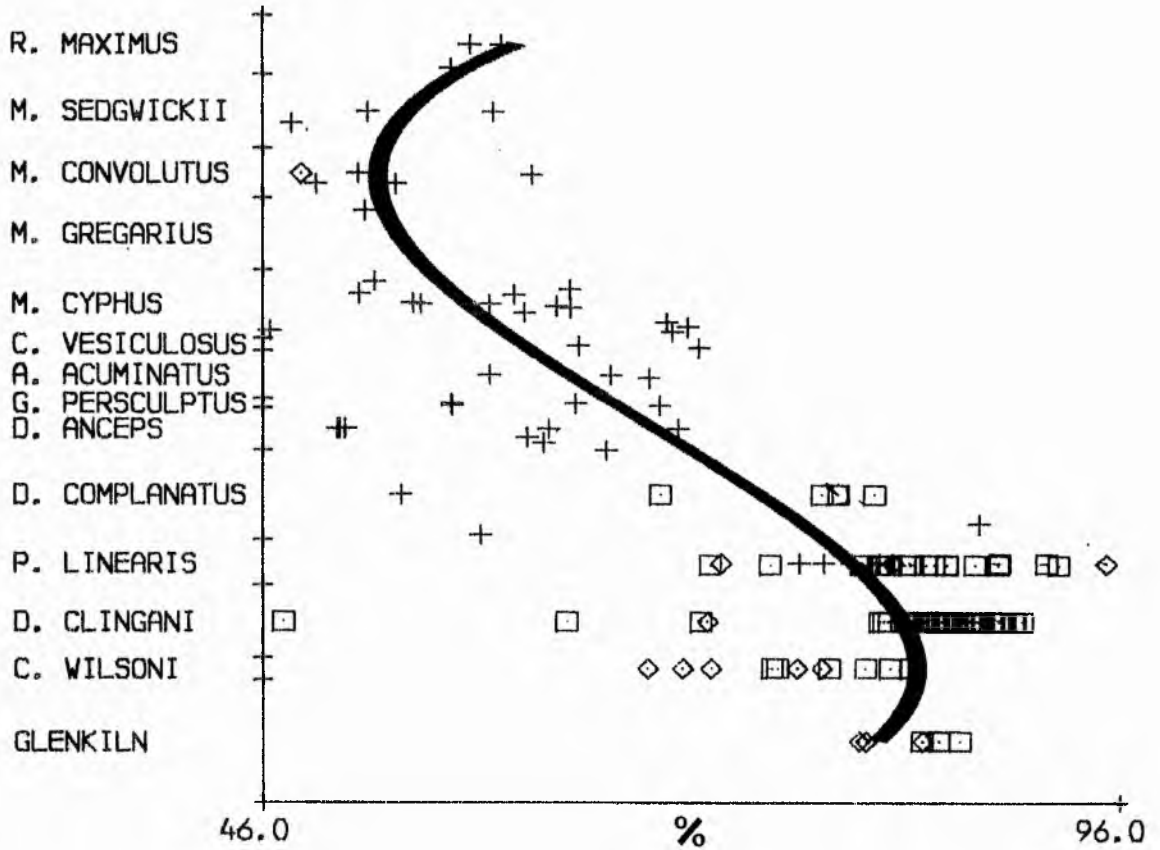
In Figures 48-57,

the divisions of ordinate are proportional to the zone thicknesses at the type section of Dobb's Linn (Toghill 1968, 1970a).

Key to symbols for the inliers sampled is illustrated in Figure 20.

In each case, the best-fit polynomial regression curve is superimposed if significant at the 0.99 confidence level.

SI02 129 DATA POINTS



TiO2 77 DATA POINTS

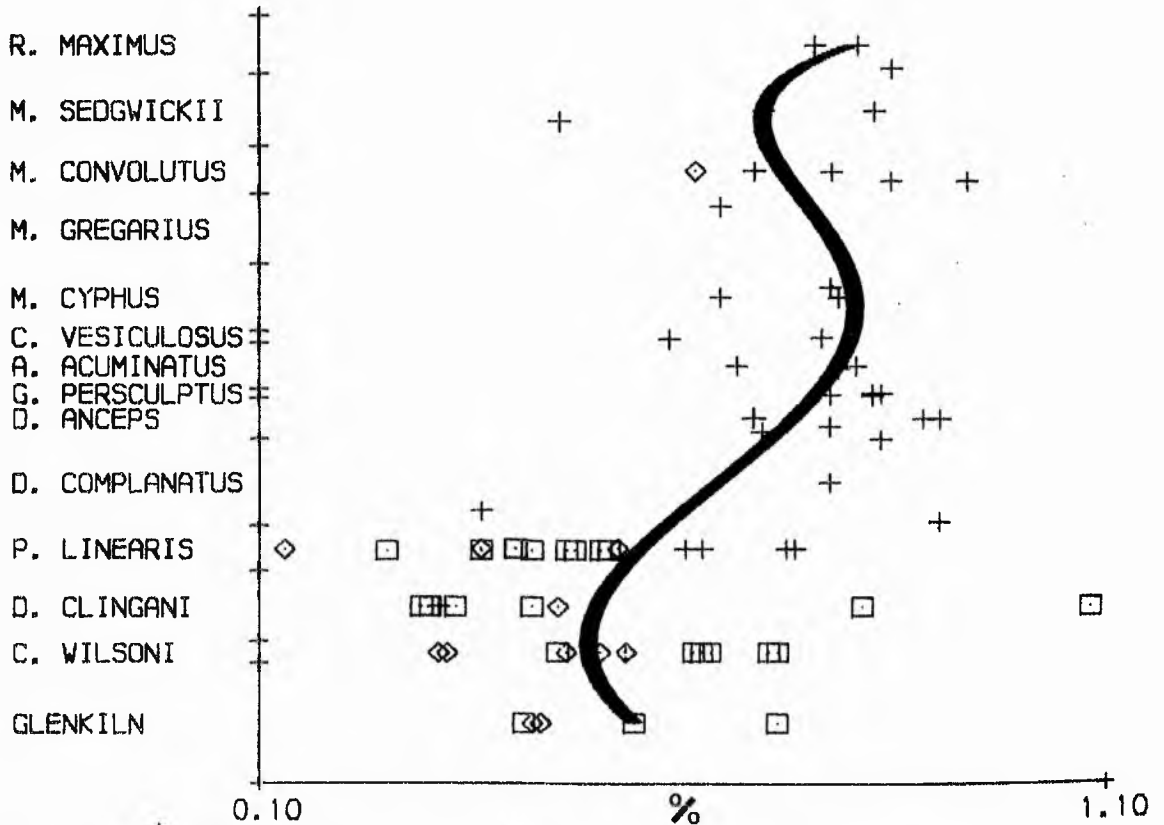
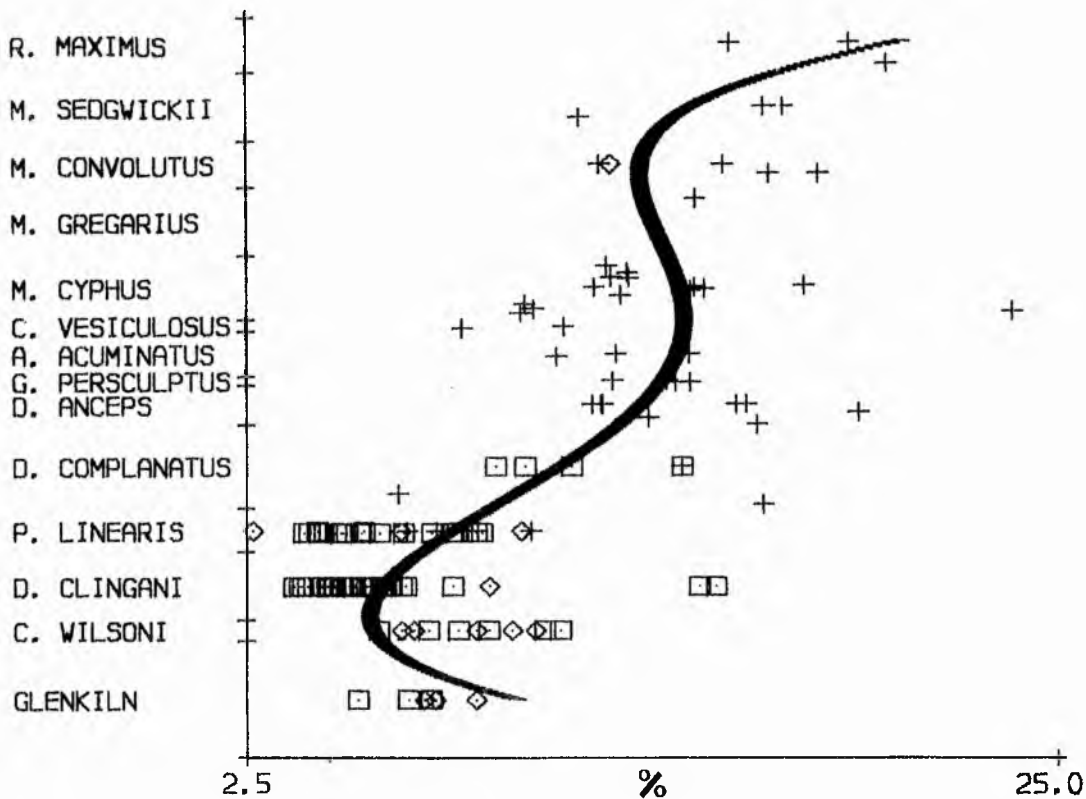


Figure 48⁺. Plots illustrating the stratigraphic variation of SiO₂ and TiO₂ concentrations in the Moffat Shales.

AL2O3 129 DATA POINTS



FE2O3 77 DATA POINTS

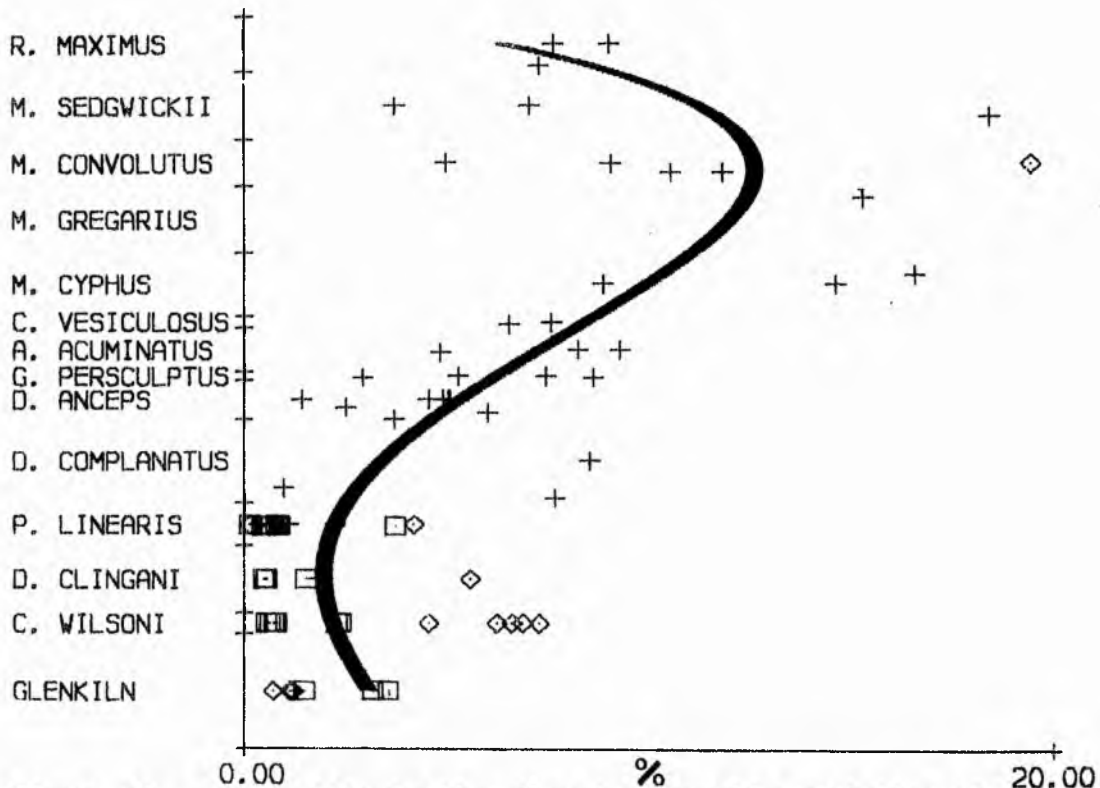


Figure 49. Plots illustrating the stratigraphic variation of Al_2O_3 and Fe_2O_3 concentrations in the Moffat Shales.

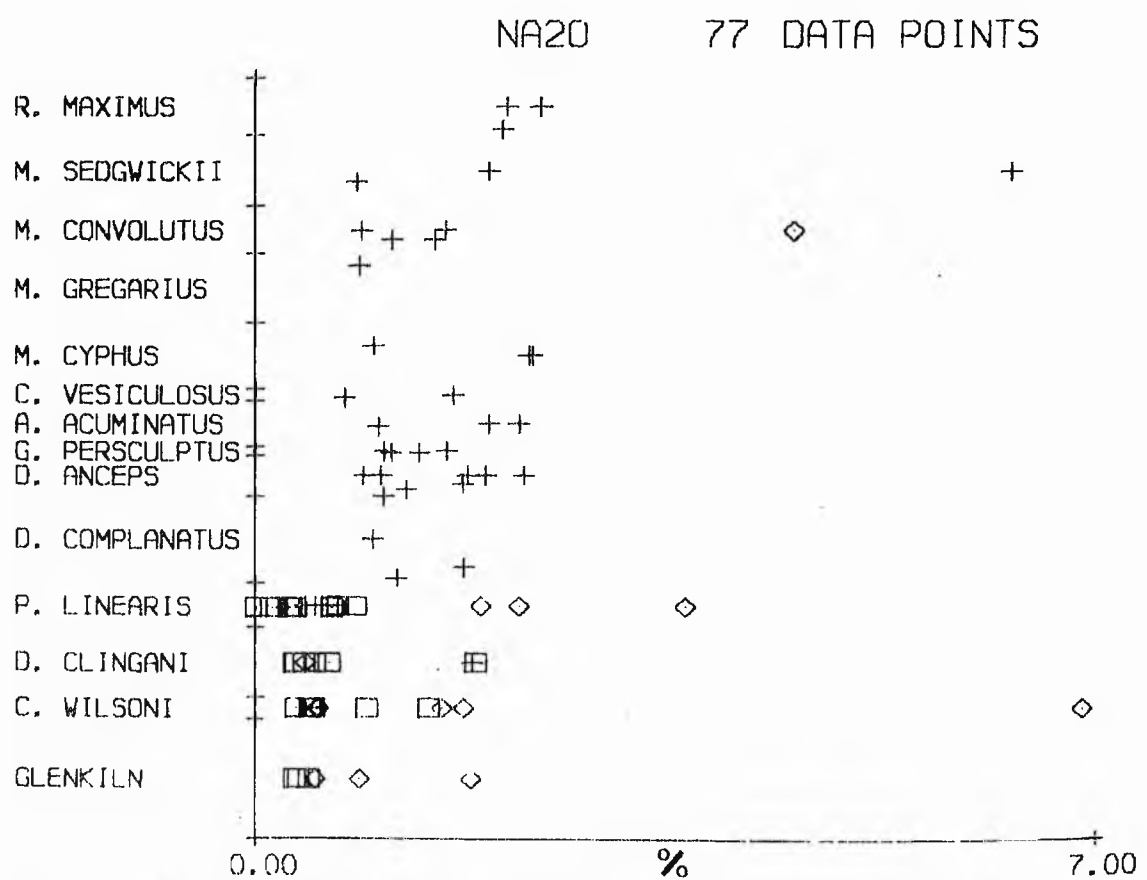
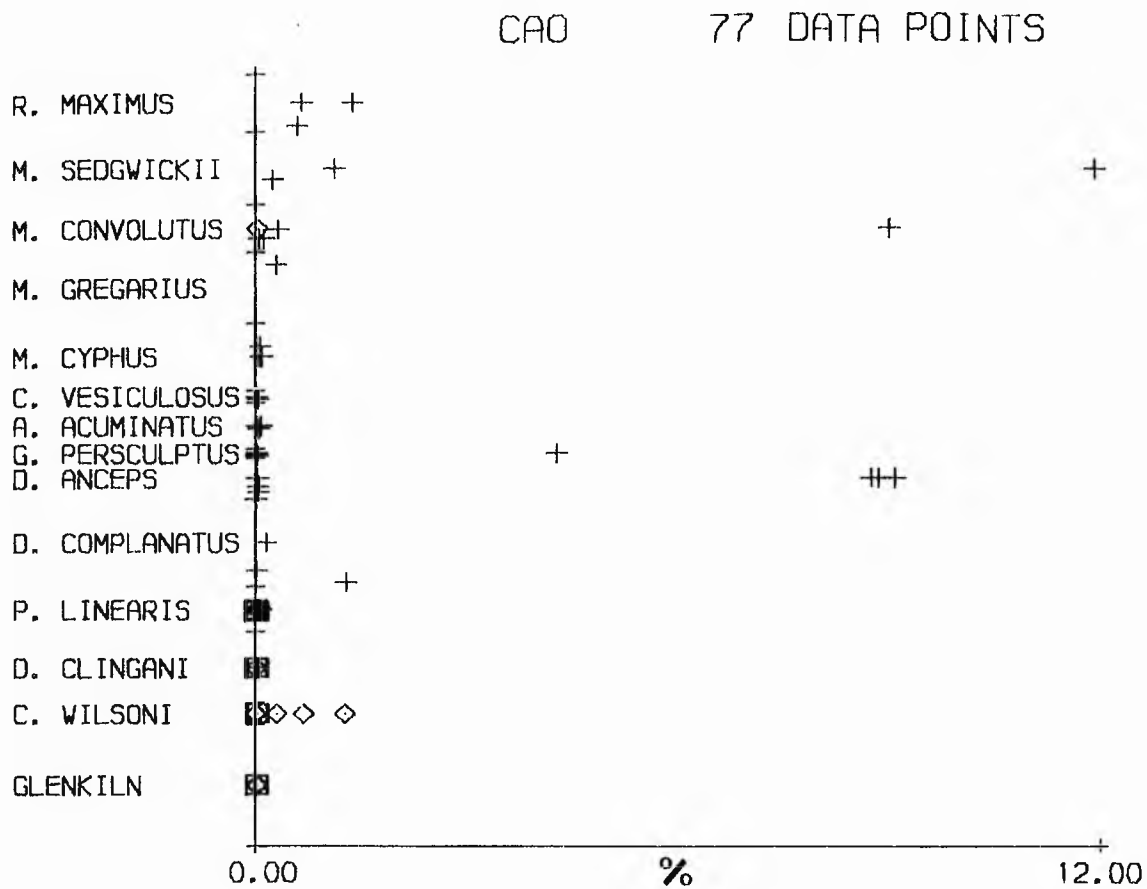


Figure 51. Plots illustrating the stratigraphic variation of CaO and Na₂O concentrations in the Moffat Shales.

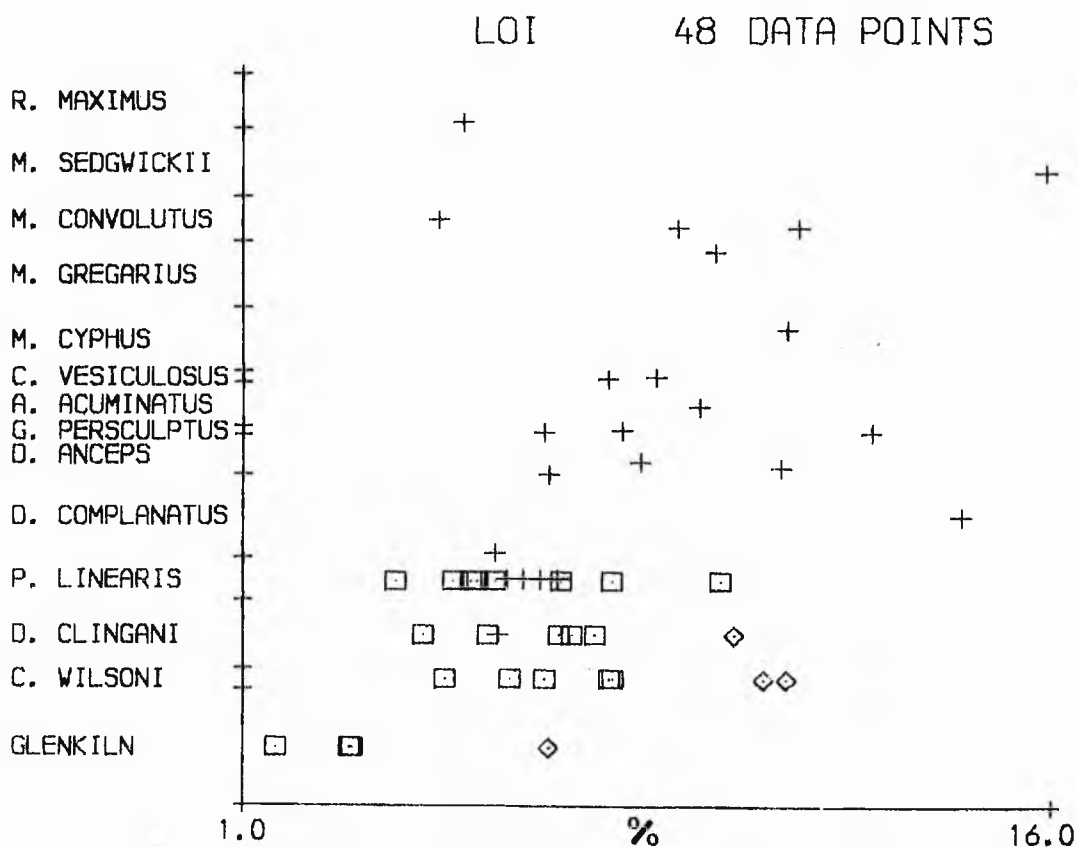
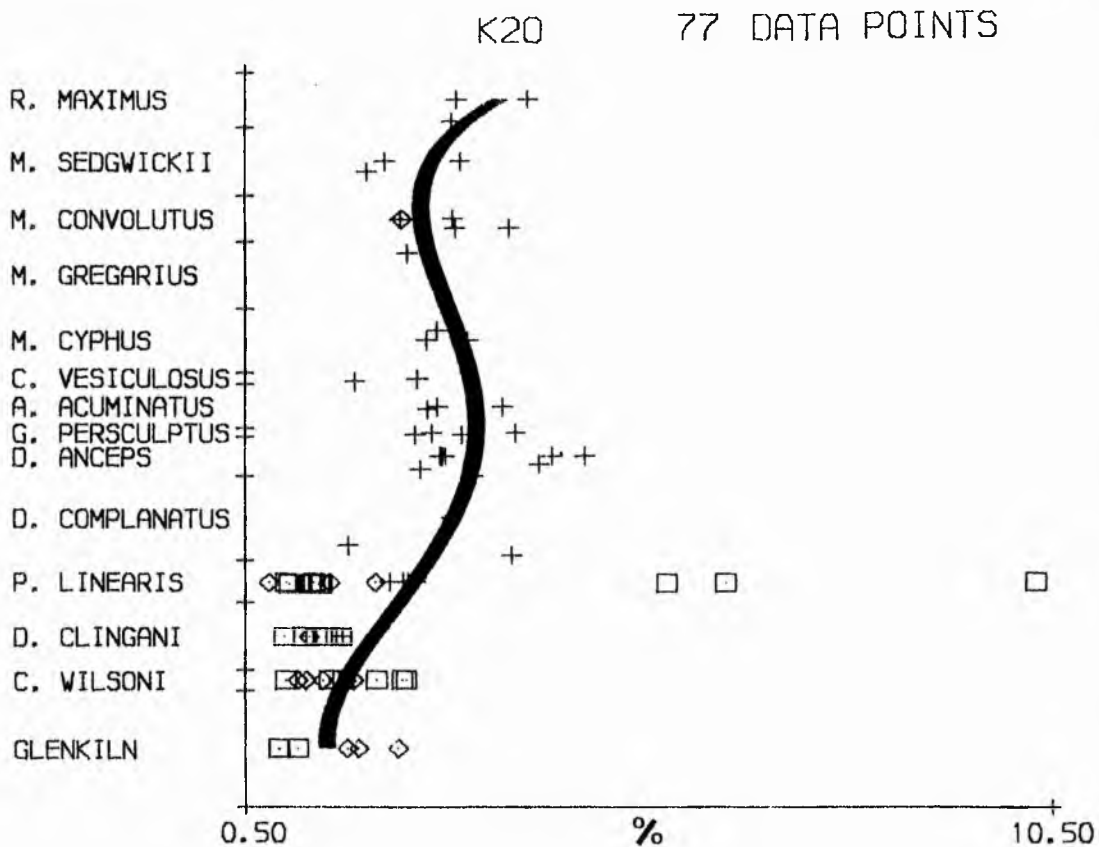


Figure 52. Plots illustrating the stratigraphic variation of K₂O concentration and loss on ignition values in the Moffat Shales.

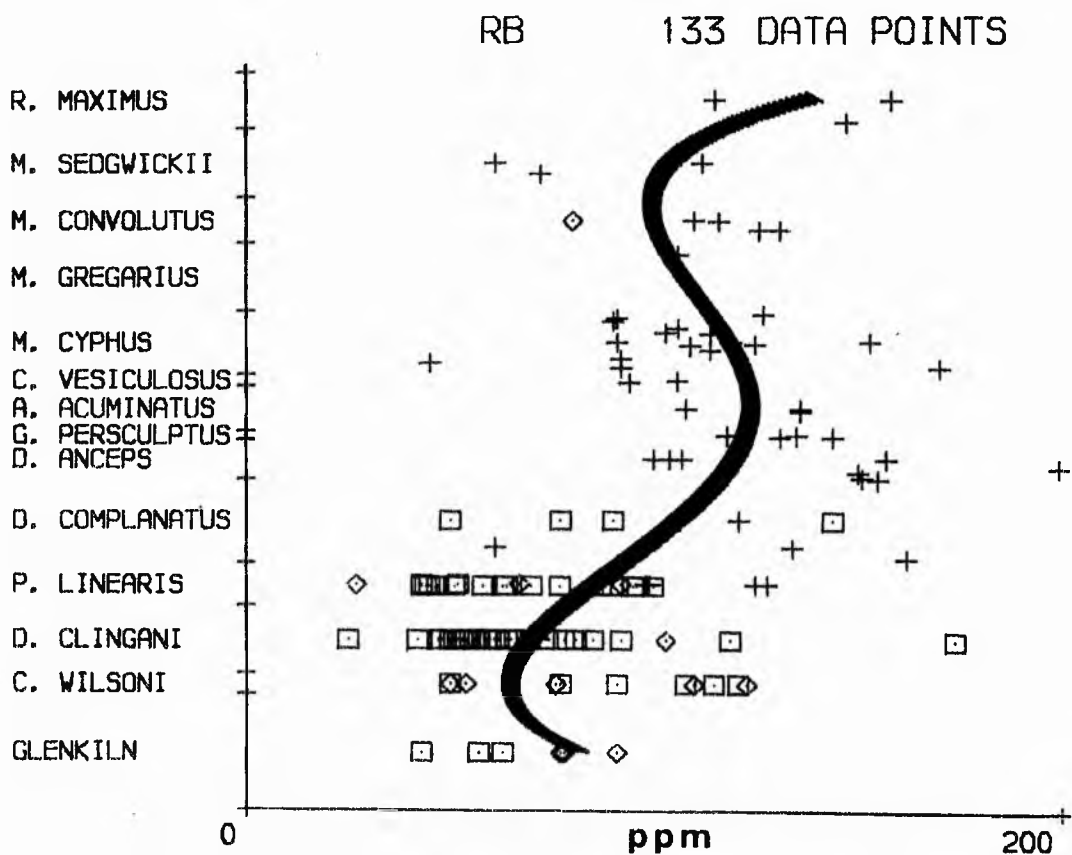
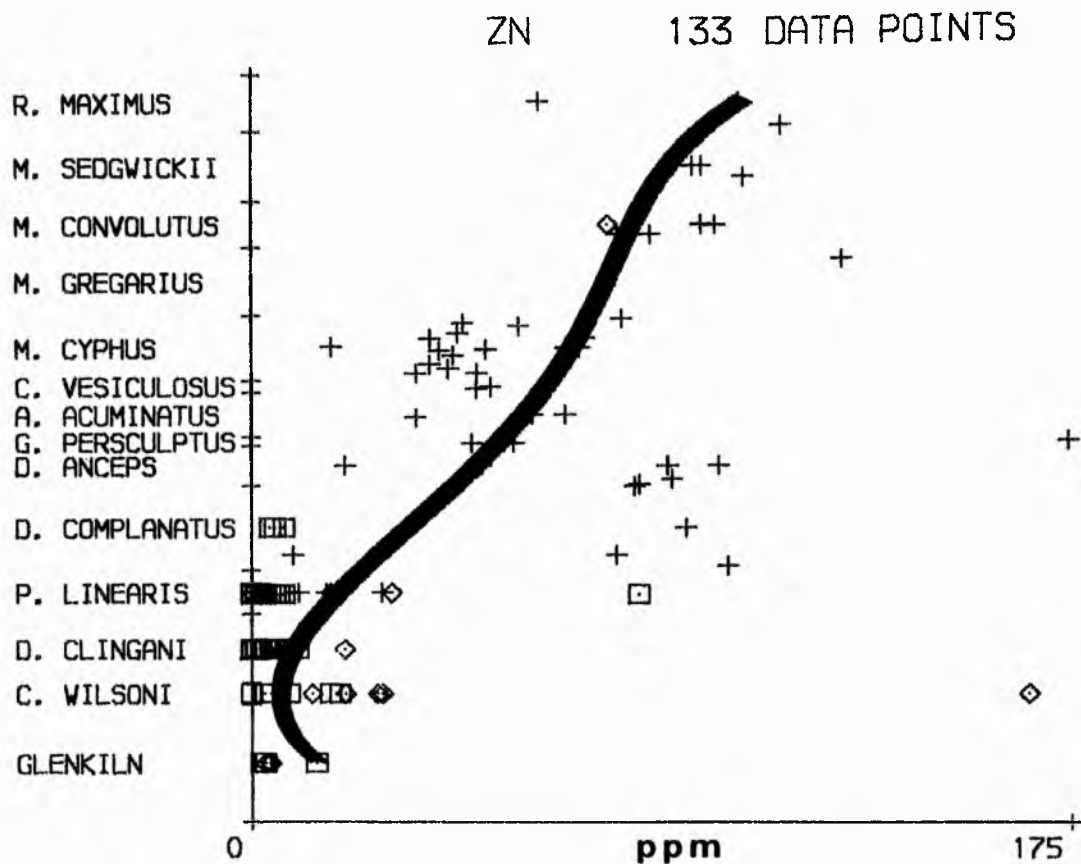


Figure 54. Plots illustrating the stratigraphic variation of zinc and rubidium concentrations in the Moffat Shales.

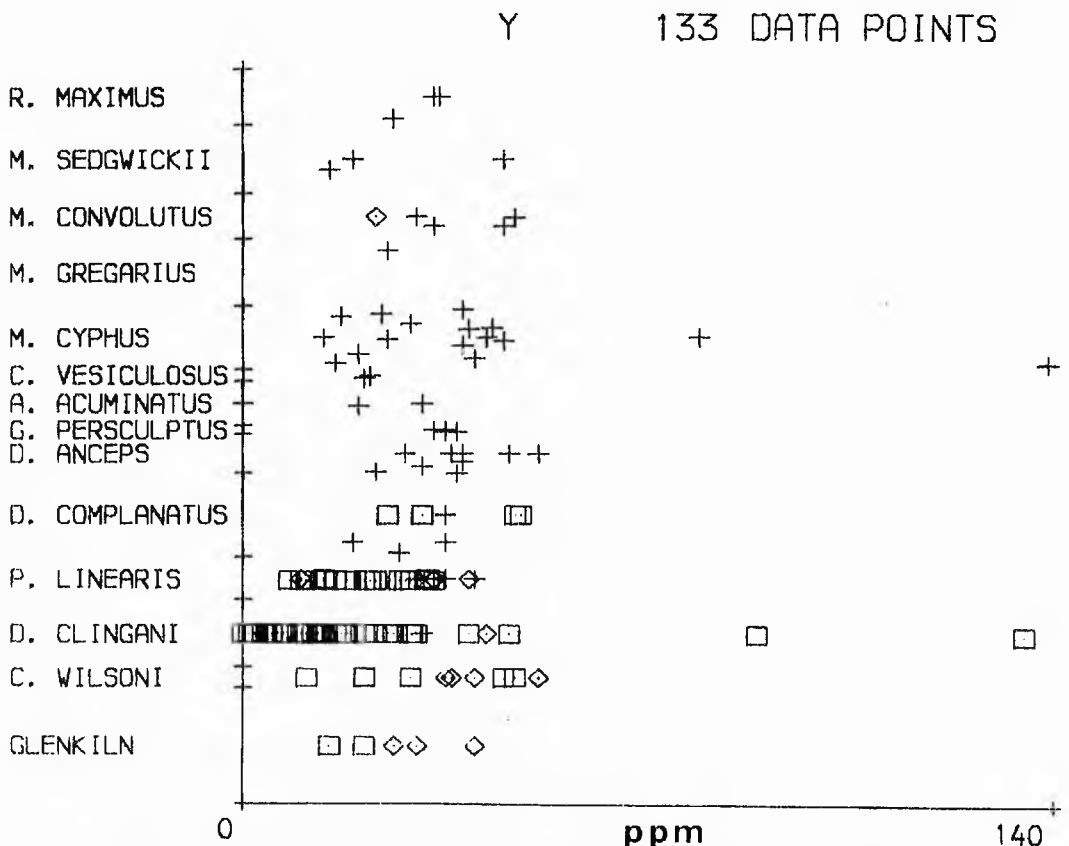
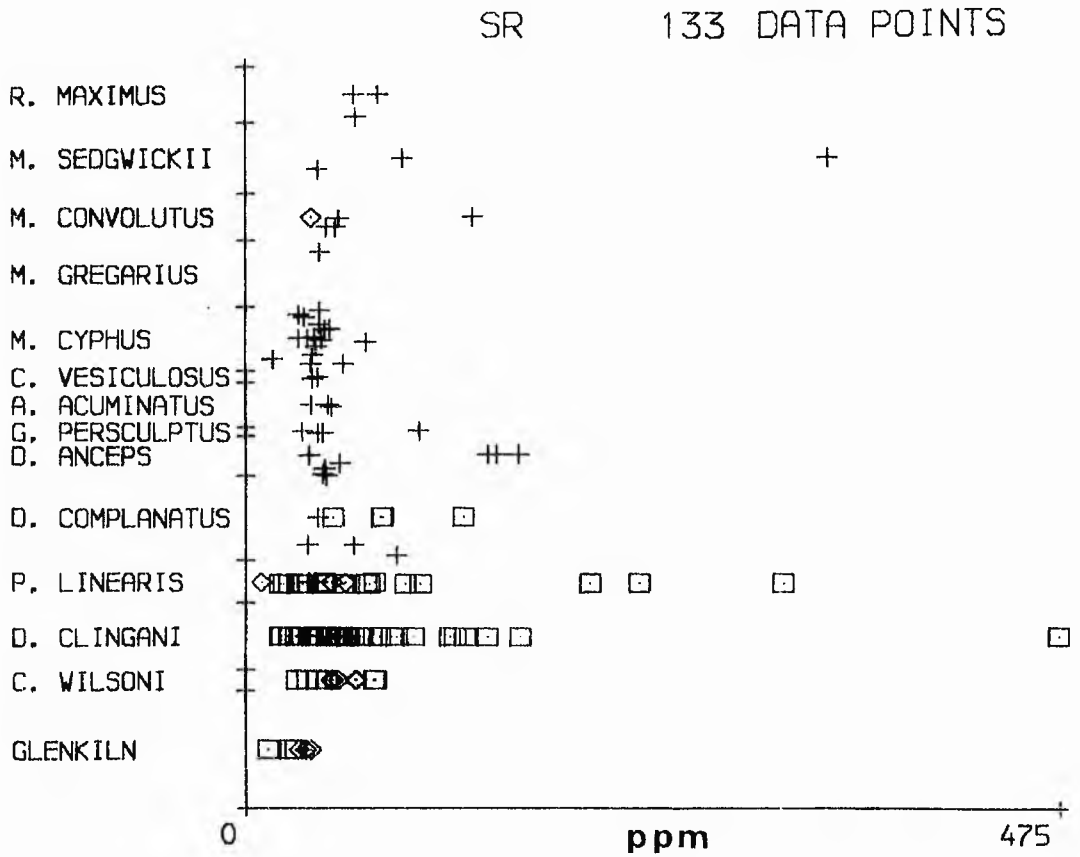
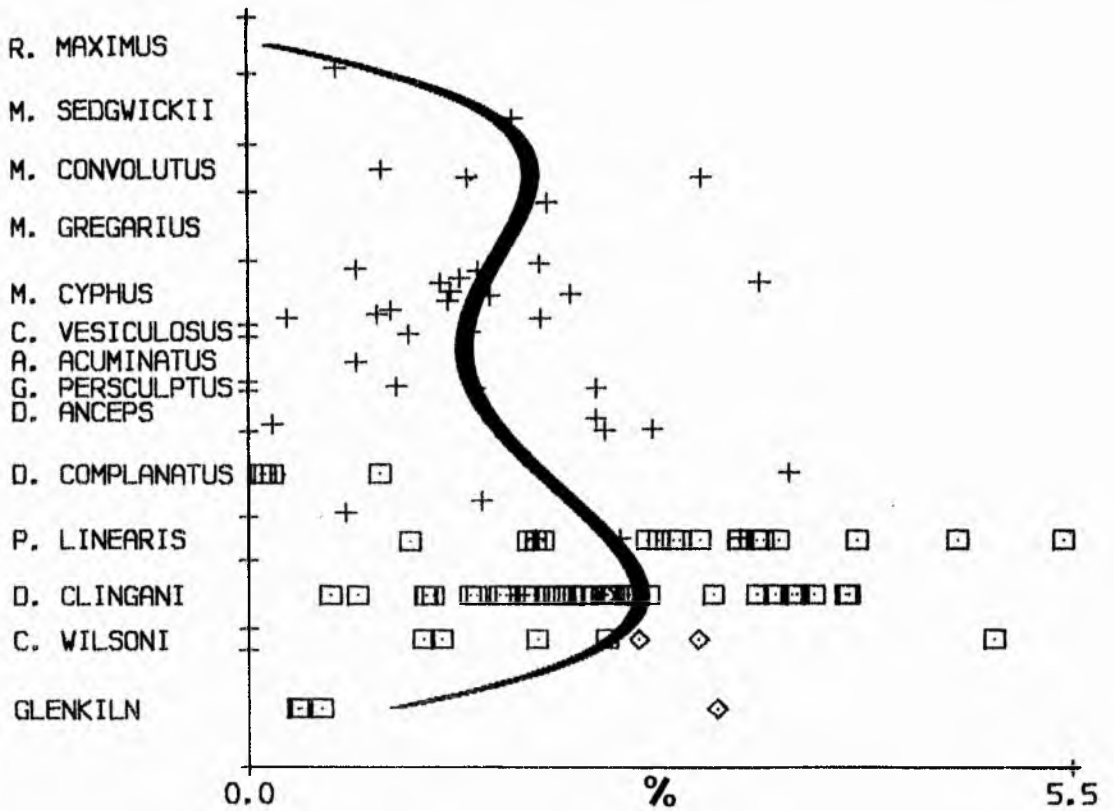


Figure 55. Plots illustrating the stratigraphic variation of strontium and yttrium concentrations in the Moffat Shales.

CARBON 104 DATA POINTS



SULPHUR 27 DATA POINTS

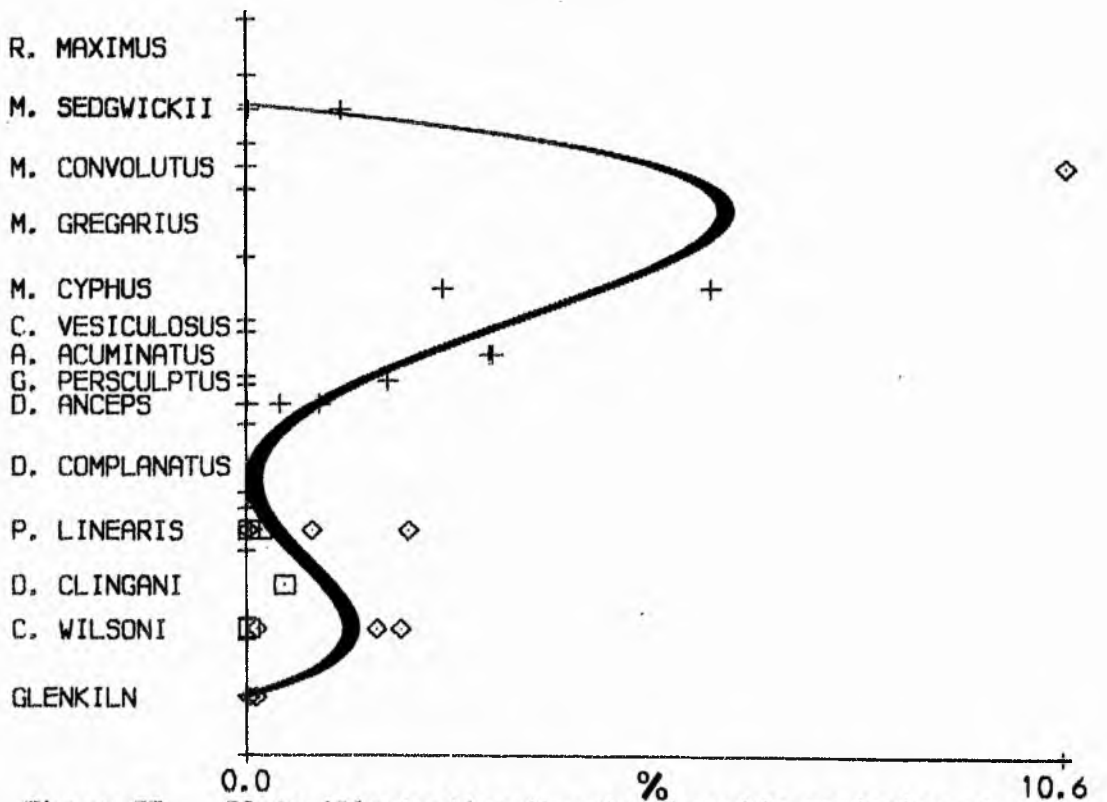


Figure 57. Plots illustrating the stratigraphic variation of carbon and sulphur concentrations in the Moffat Shales.

STRATIGRAPHIC DISTRIBUTION OF ELEMENTS IN BLACK SHALES

◇ D. COMPLANATUS

+ P. LINEARIS

□ D. CLINGANI

△ C. WILSONI

* GLENKILN

Figure 58. Key to symbols used for various stratigraphic units at Hartfell.

+

In Figures 59-76,

- a) samples plotted as a function of the observed distance up the cliff. For key, see Figure 58.

- b) samples plotted as a function of the calculated height up the stratigraphic succession after structural restoration of the cliff to its pre-fault and pre-fold position.

In each case the best-fit polynomial regression curve is superimposed if significant at the 0.95 confidence level.

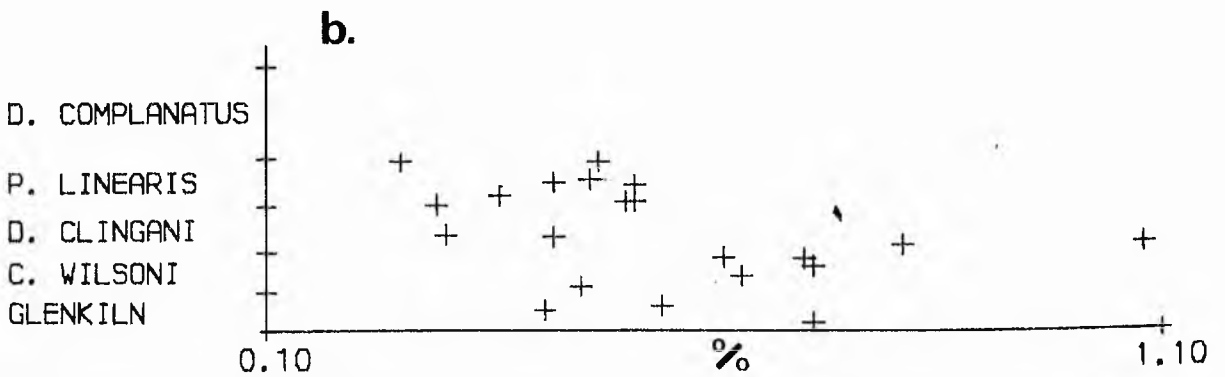
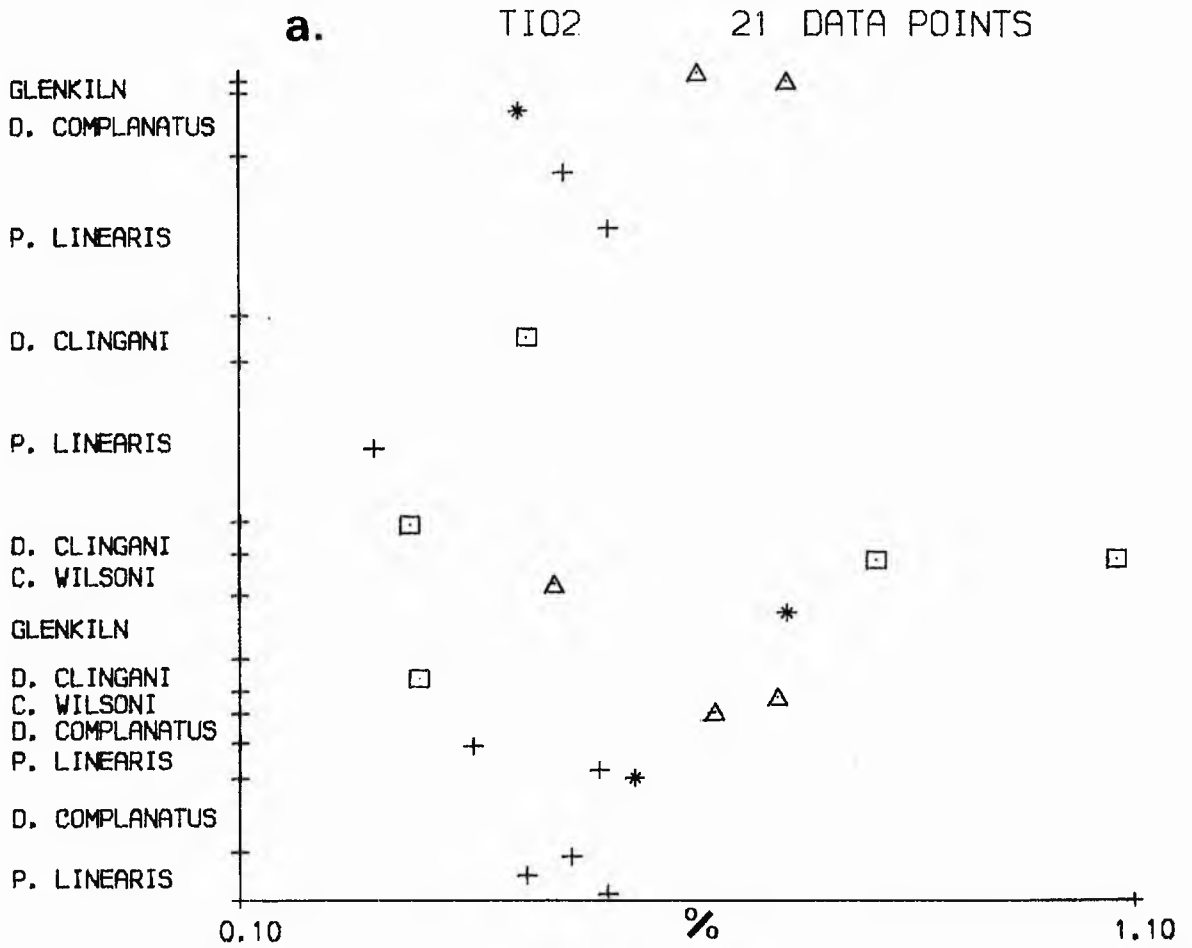


Figure 60. Plots illustrating the stratigraphic variation of the TiO_2 concentration in the sediments of the north cliff at Hartfell Scaur.

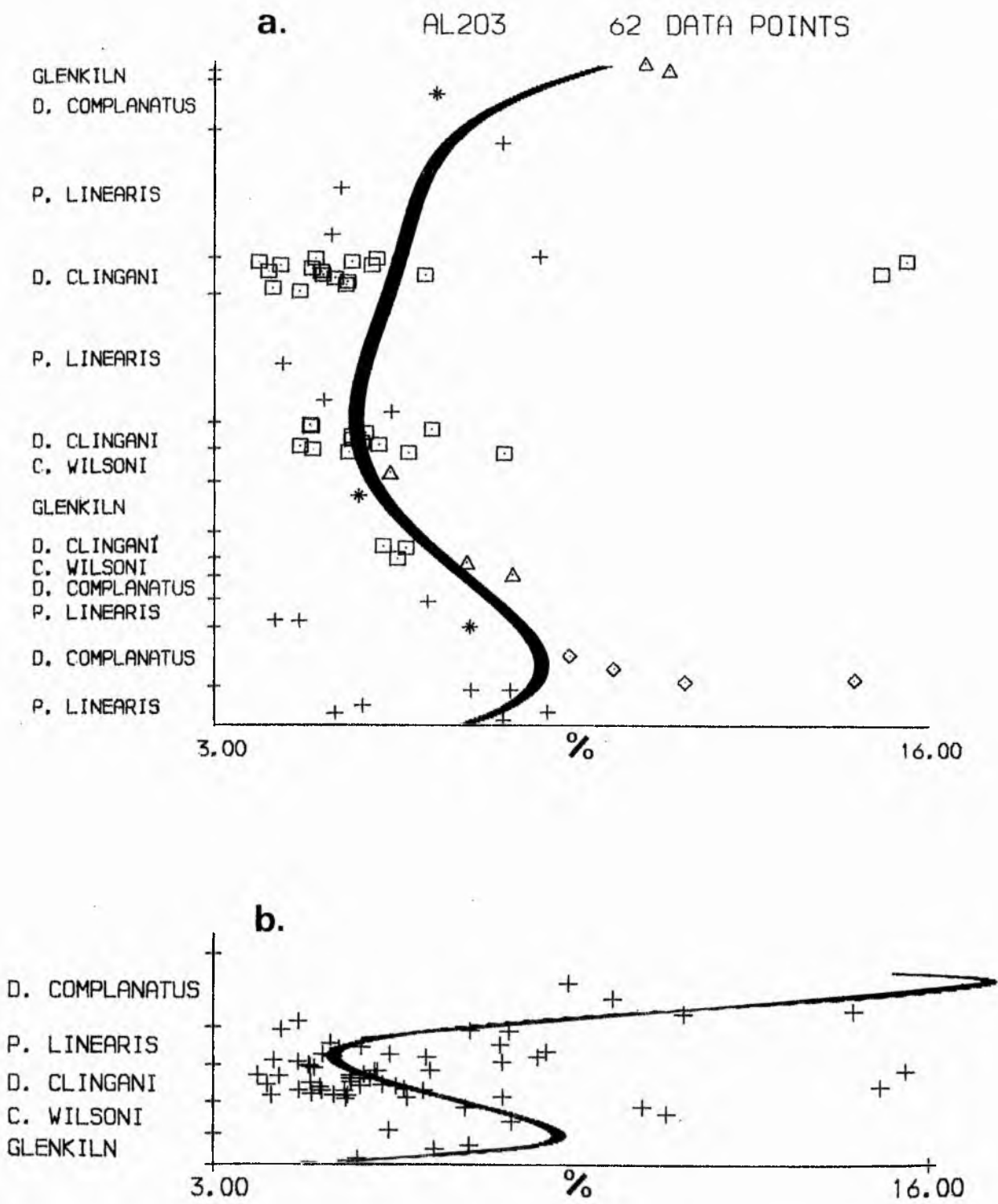


Figure 61. Plots illustrating the stratigraphic variation of the Al₂O₃ concentration in the sediments of the north cliff at Hartfell Scaur.

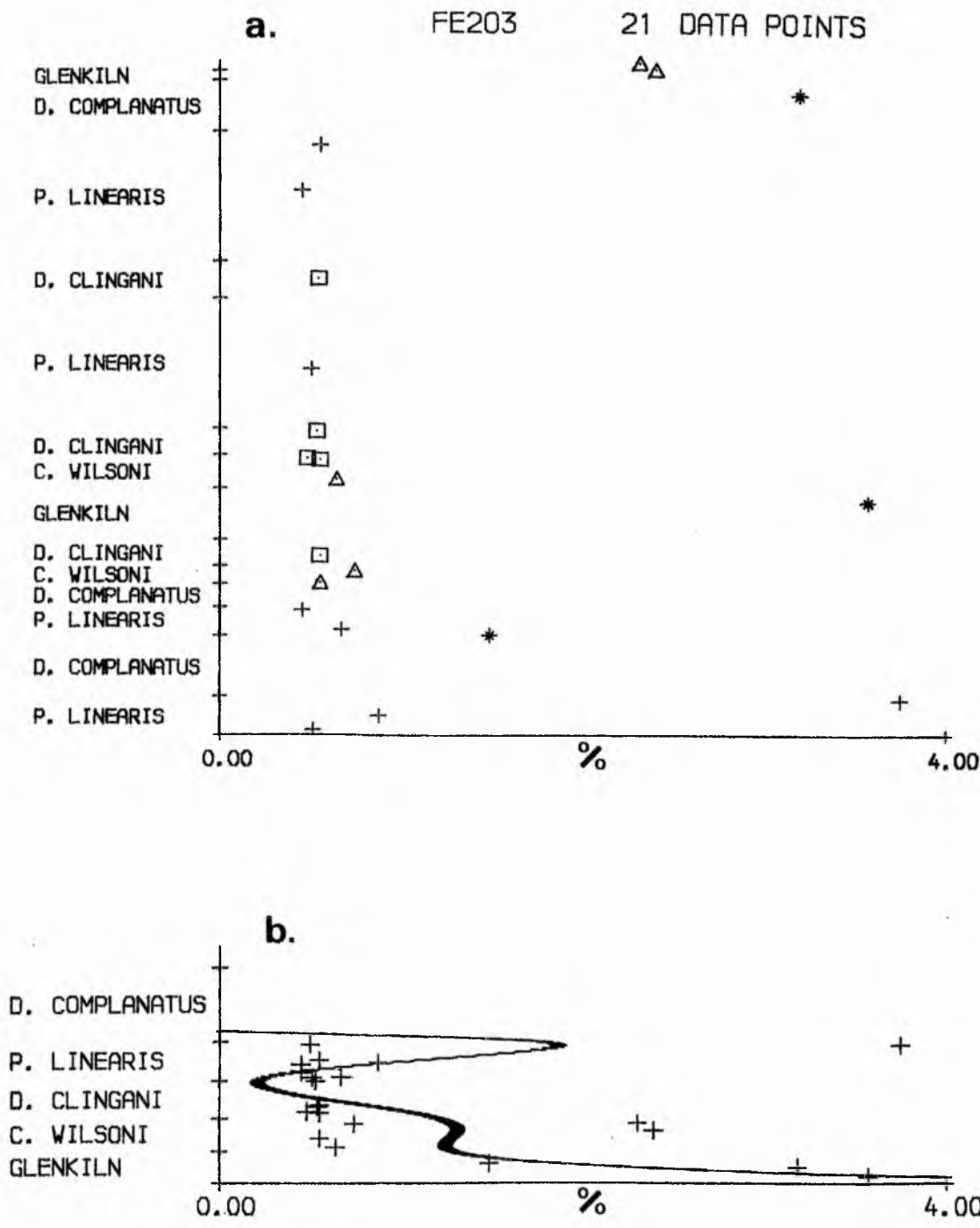


Figure 62. Plots illustrating the stratigraphic variation of the Fe₂O₃ concentration in the sediments of the north cliff at Hartfell Scaur.

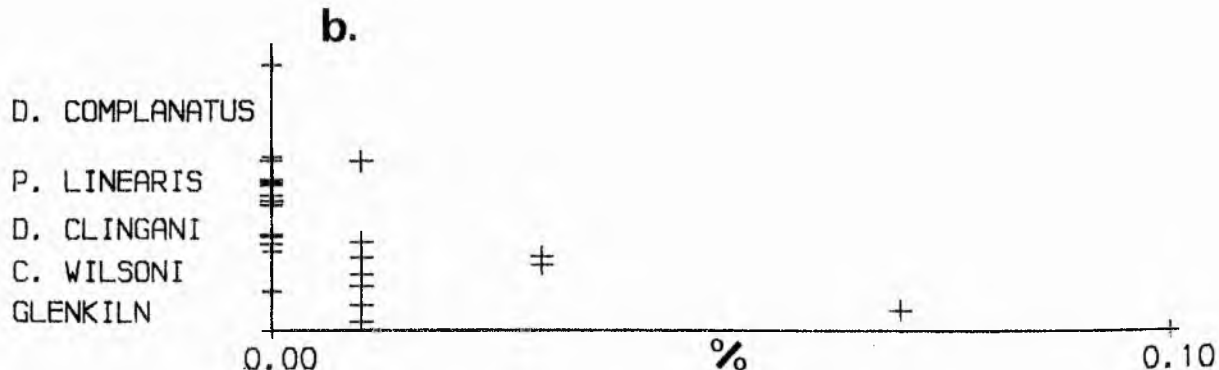
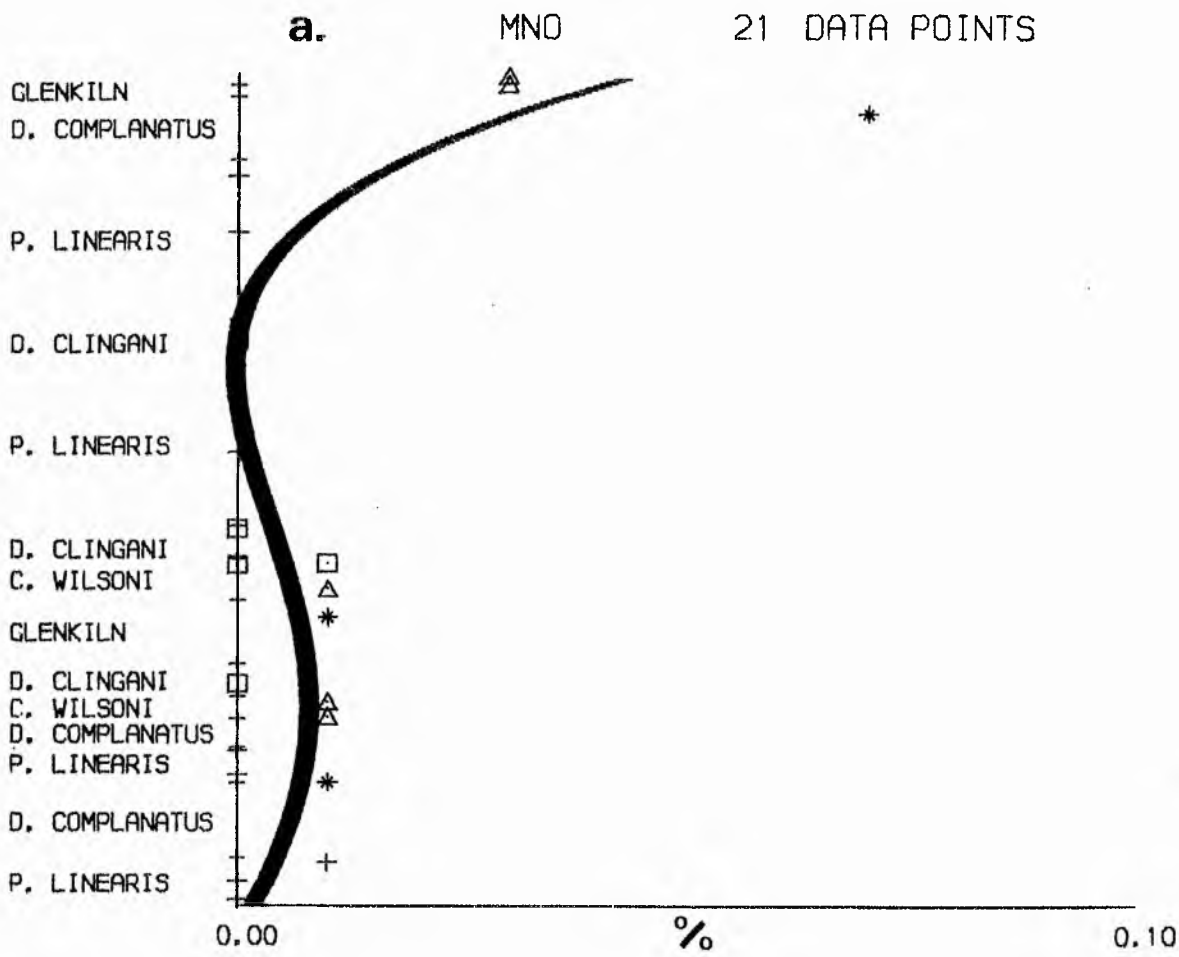


Figure 63. Plots illustrating the stratigraphic variation of the MnO concentration in the sediments of the north cliff at Hartfell Scaur.

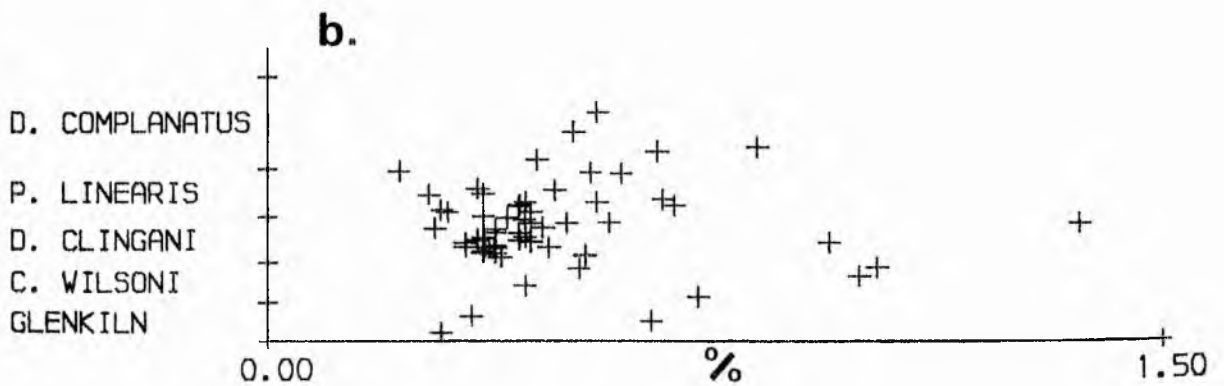
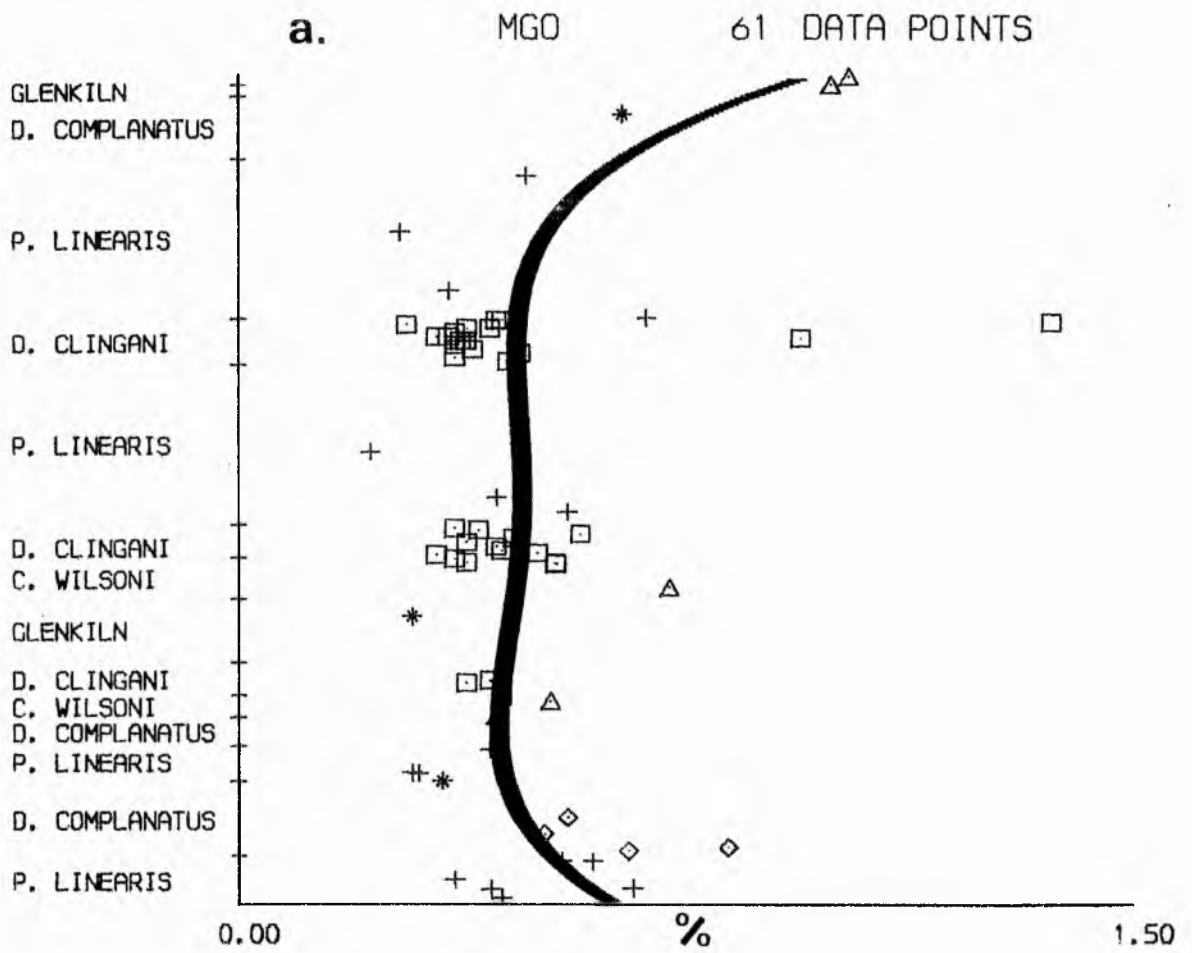


Figure 64. Plots illustrating the stratigraphic variation of the MgO concentration in the sediments of the north cliff at Hartfell Scaur.

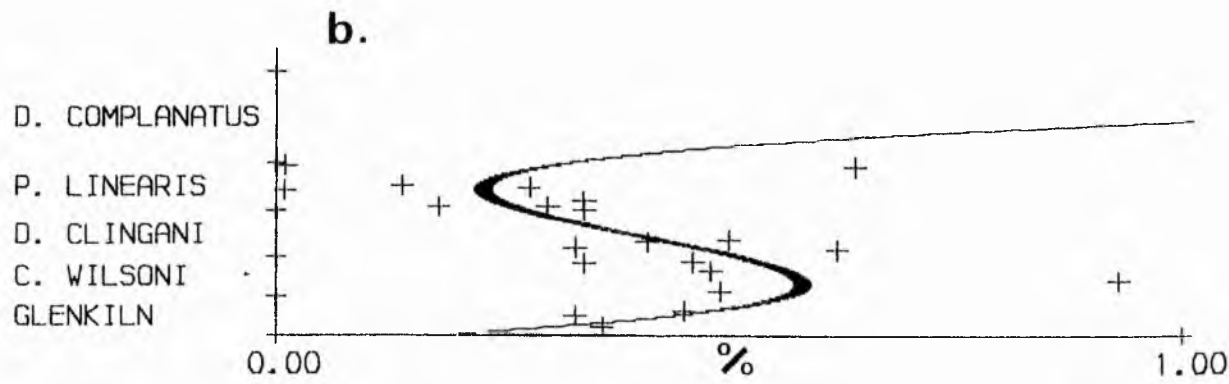
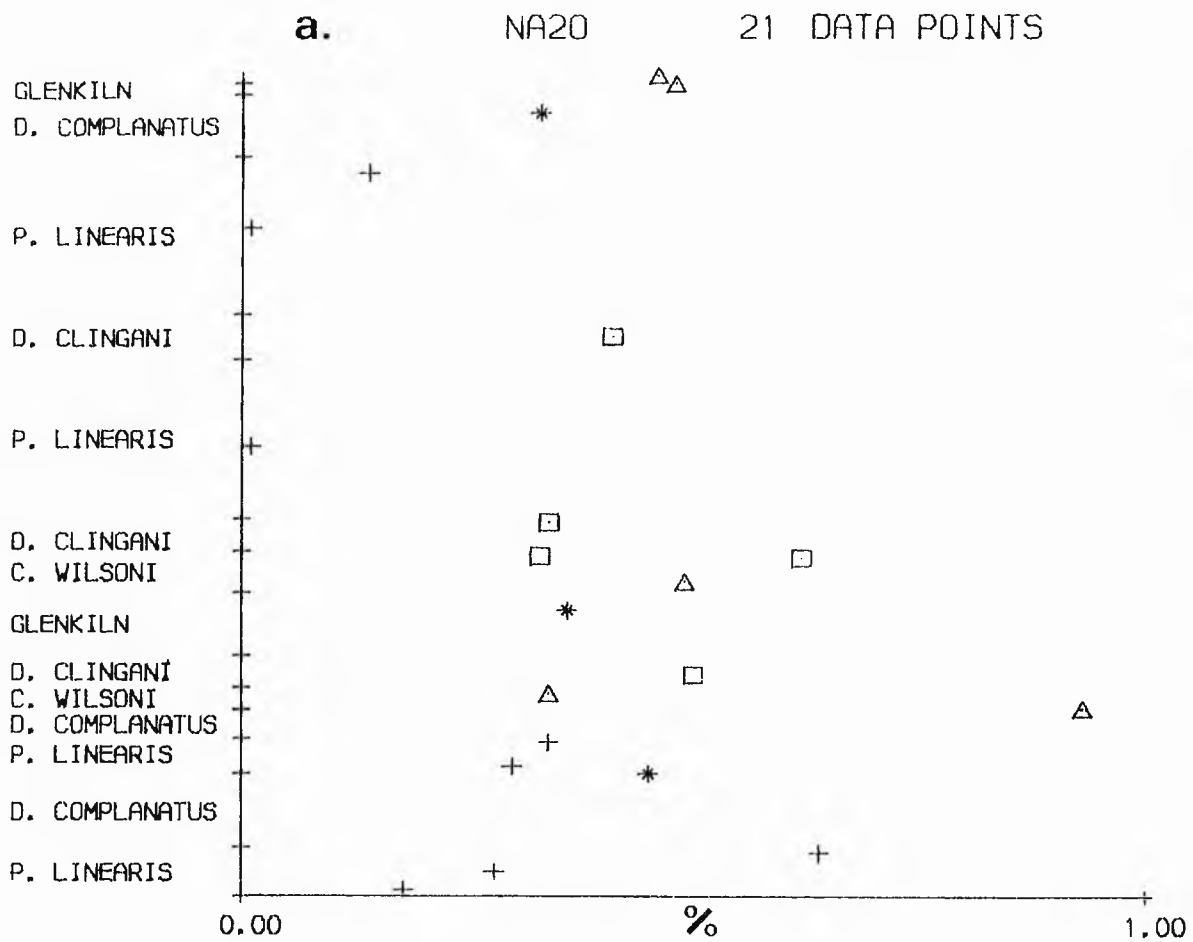


Figure 65. Plots illustrating the stratigraphic variation of the Na₂O concentration in the sediments of the north cliff at Hartfell Scaur.

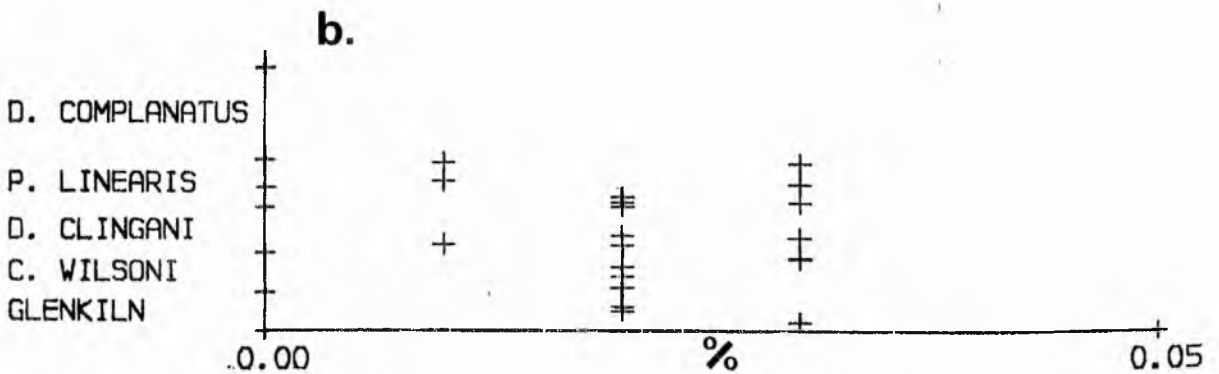
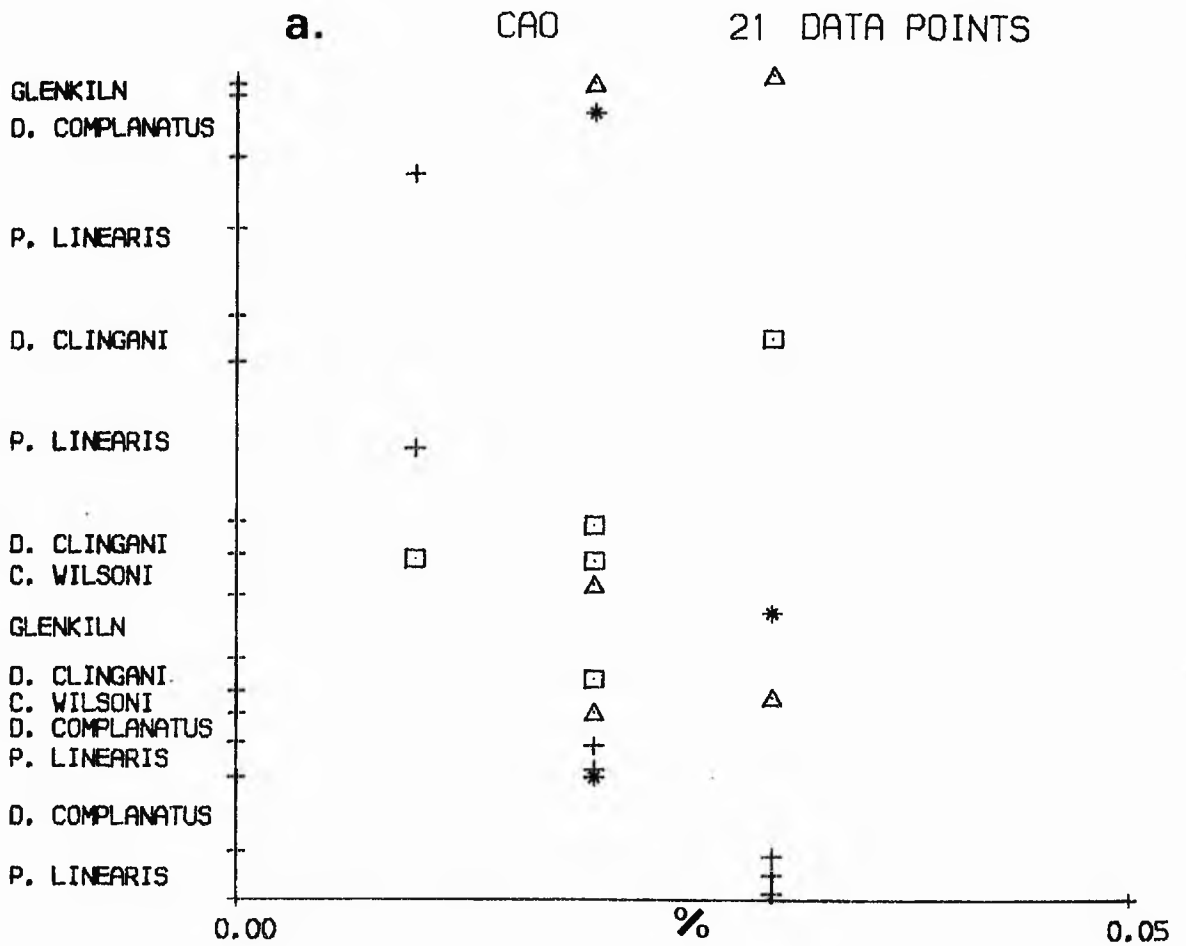


Figure 66. Plots illustrating the stratigraphic variation of the CaO concentration in the sediments of the north cliff at Hartfell Scaur.

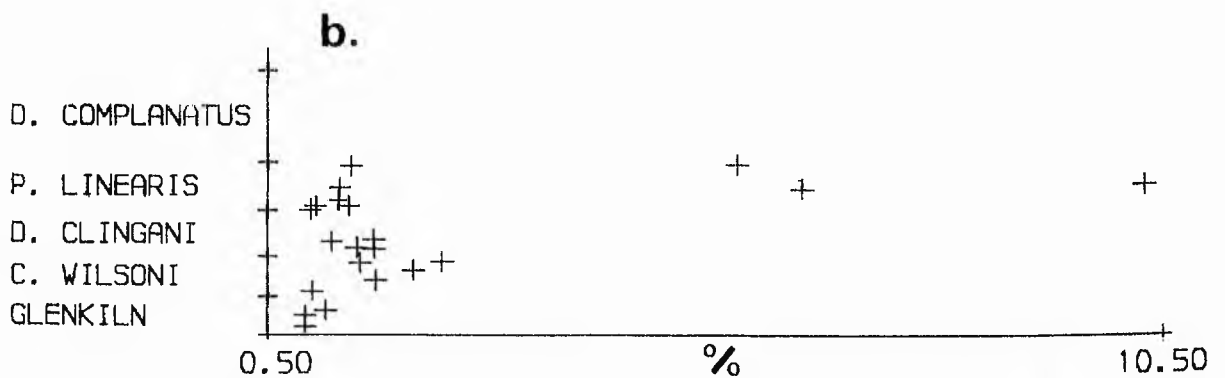
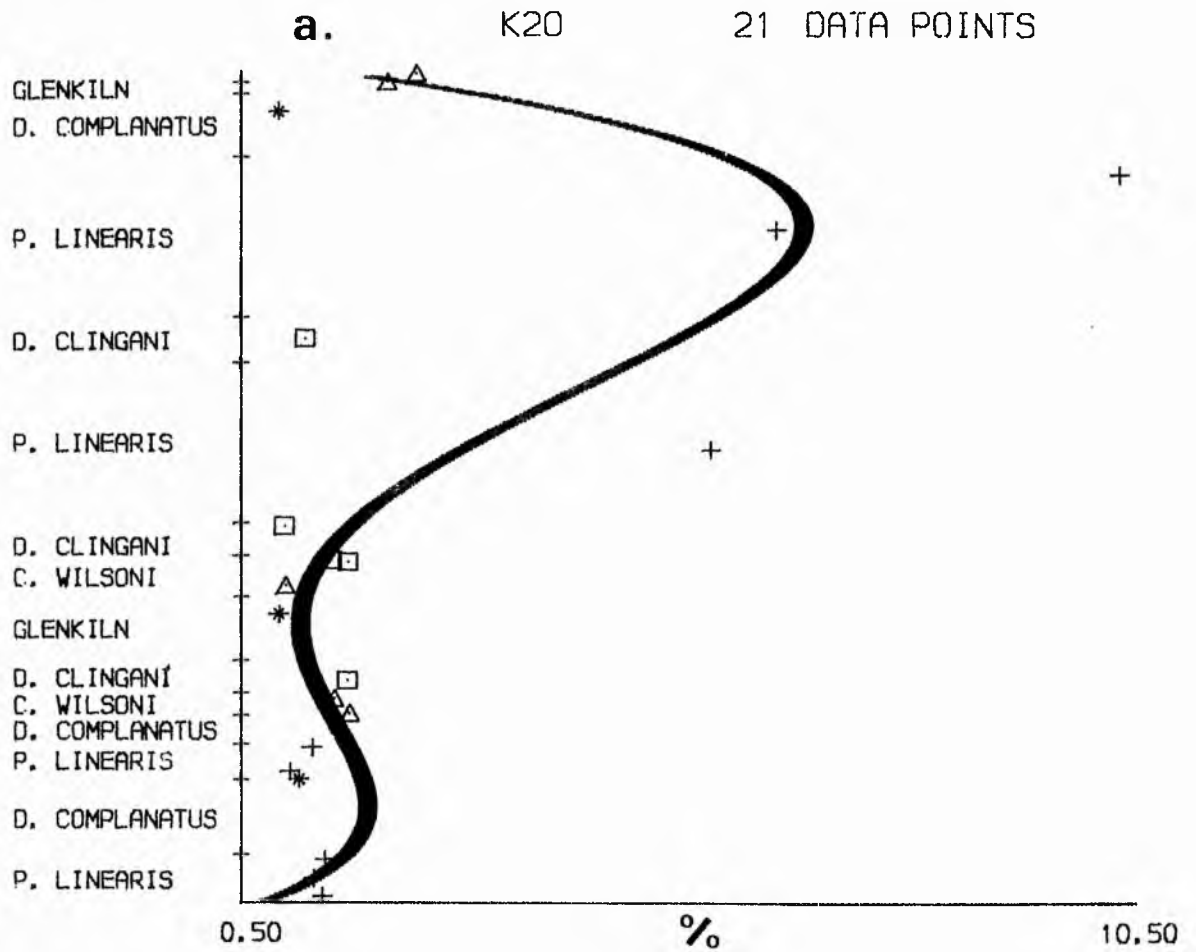


Figure 67. Plots illustrating the stratigraphic variation of the K₂O concentration in the sediments of the north cliff at Hartfell Scaur.

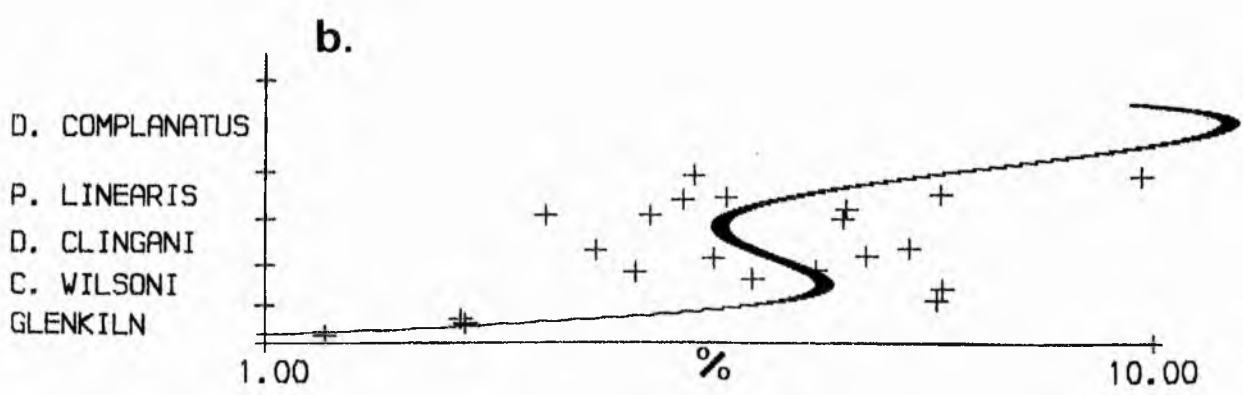
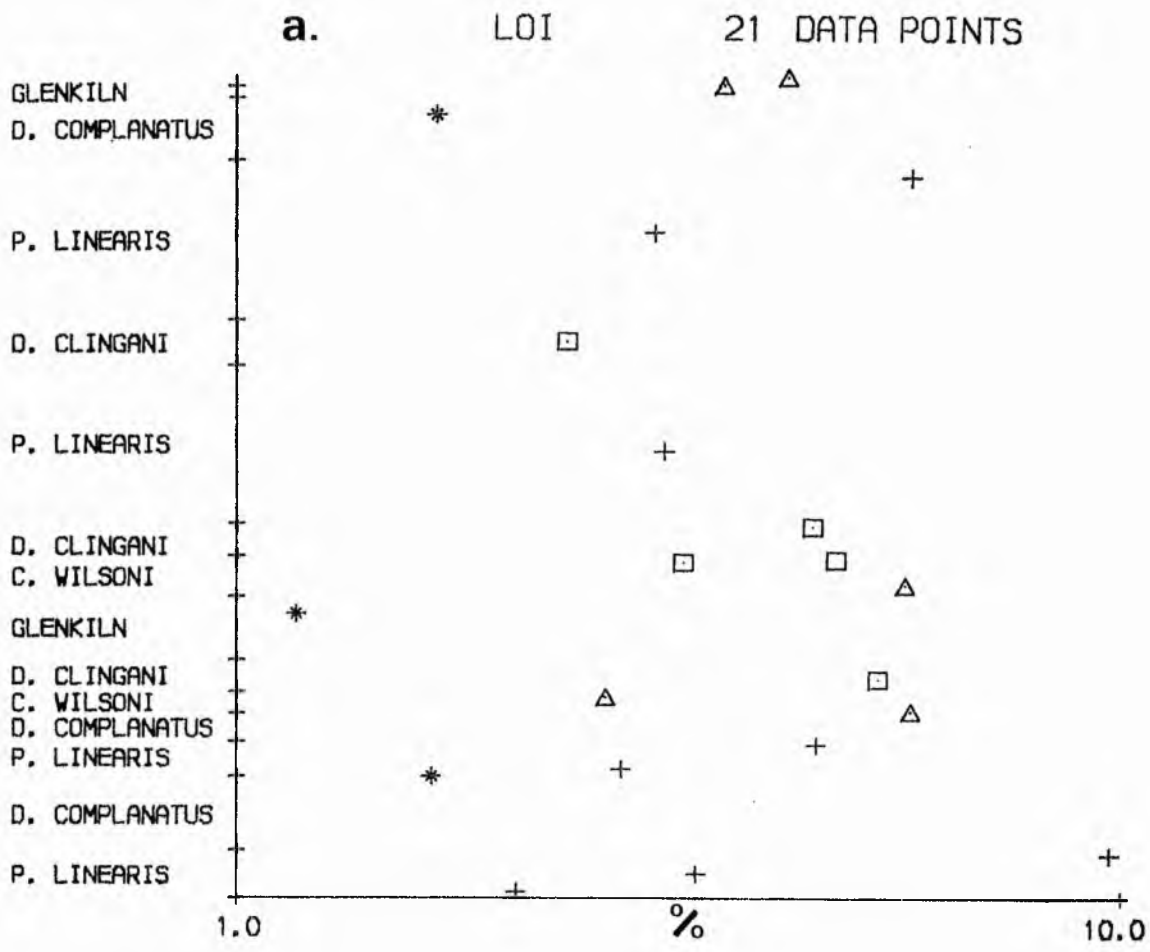


Figure 68. Plots illustrating the stratigraphic variation of the loss on ignition values in the sediments of the north cliff at Hartfell Scaur.

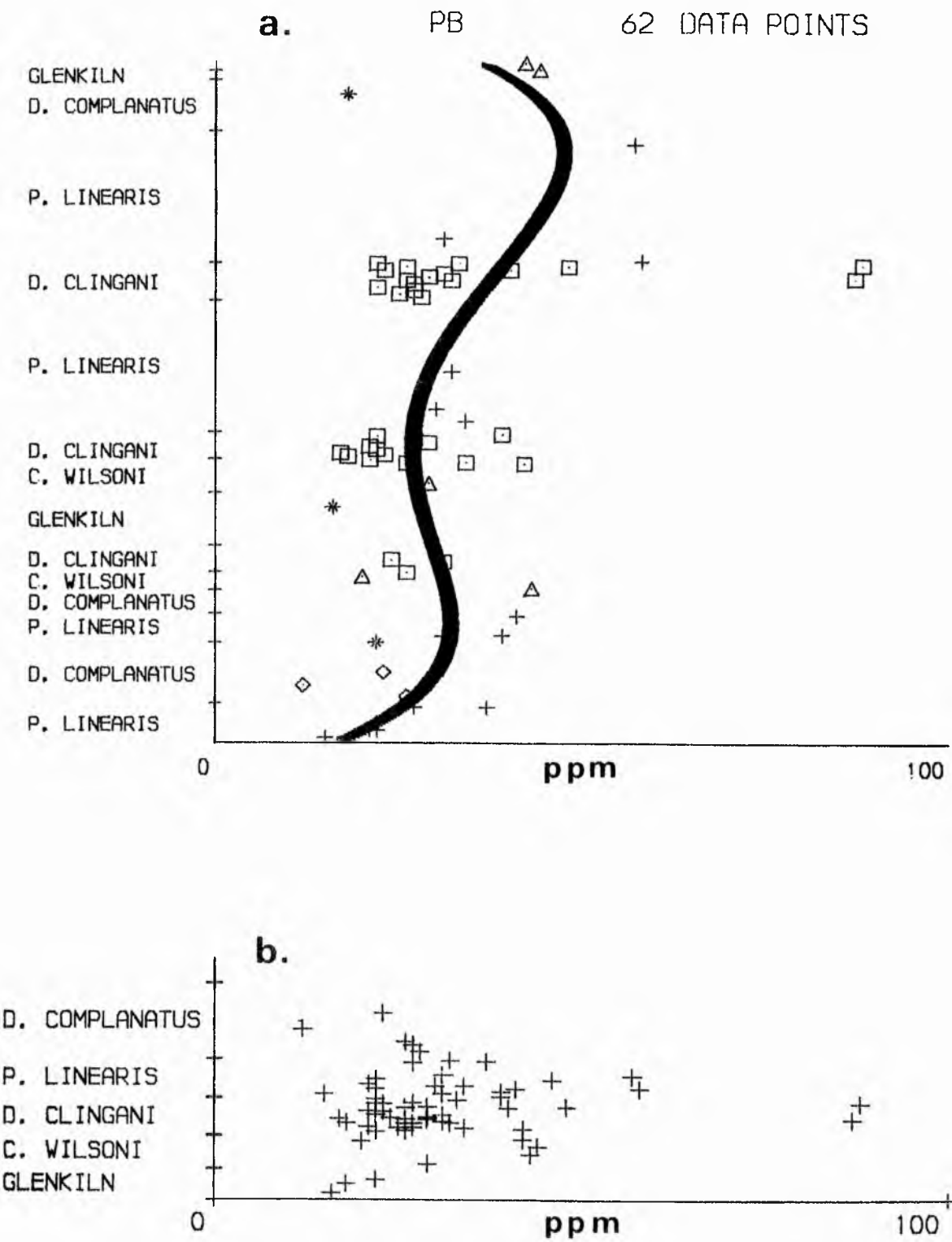


Figure 70. Plots illustrating the stratigraphic variation of the lead concentration in the sediments of the north cliff at Hartfell Scaur.

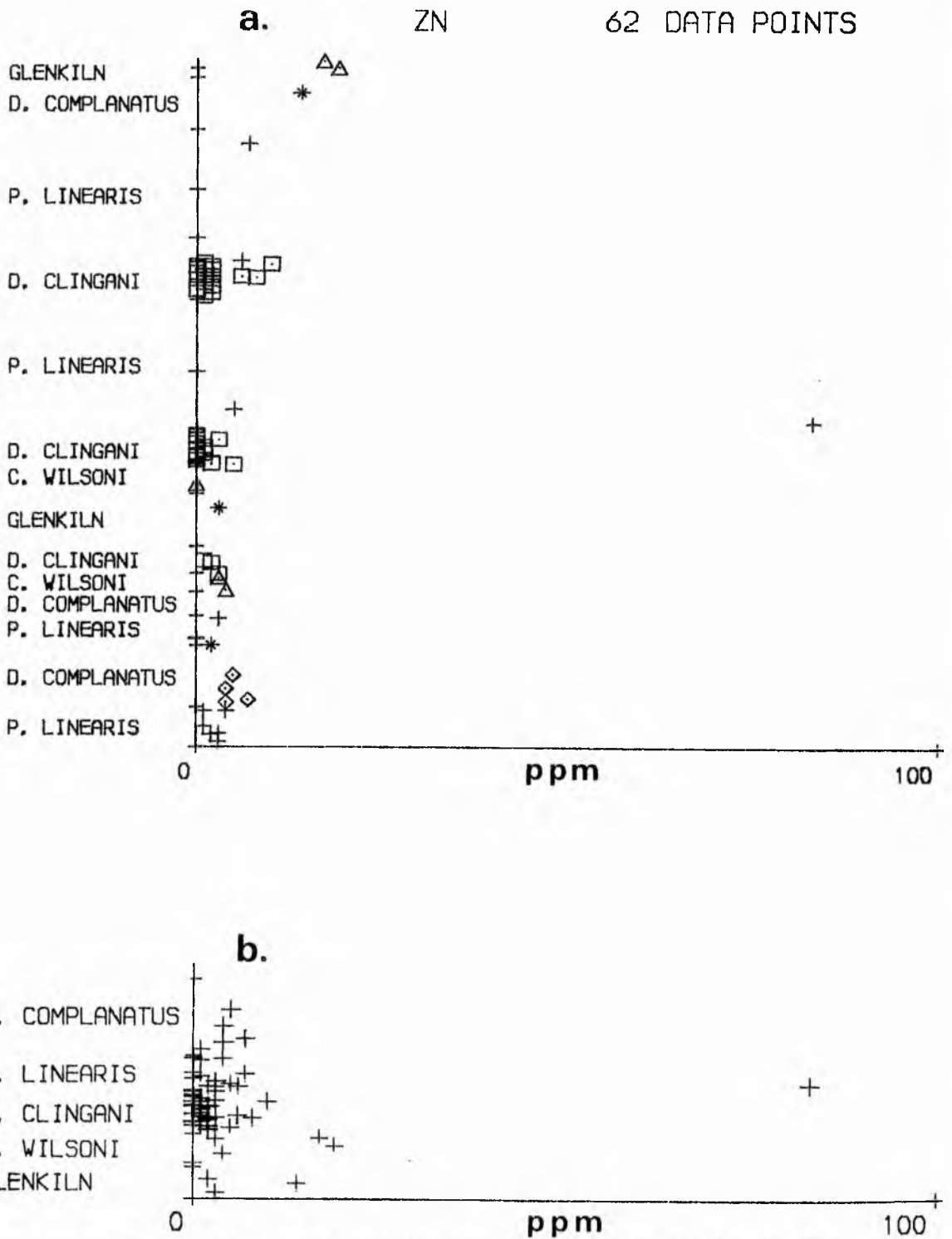


Figure 71. Plots illustrating the stratigraphic variation of the zinc concentration in the sediments of the north cliff at Hartfell Scaur.

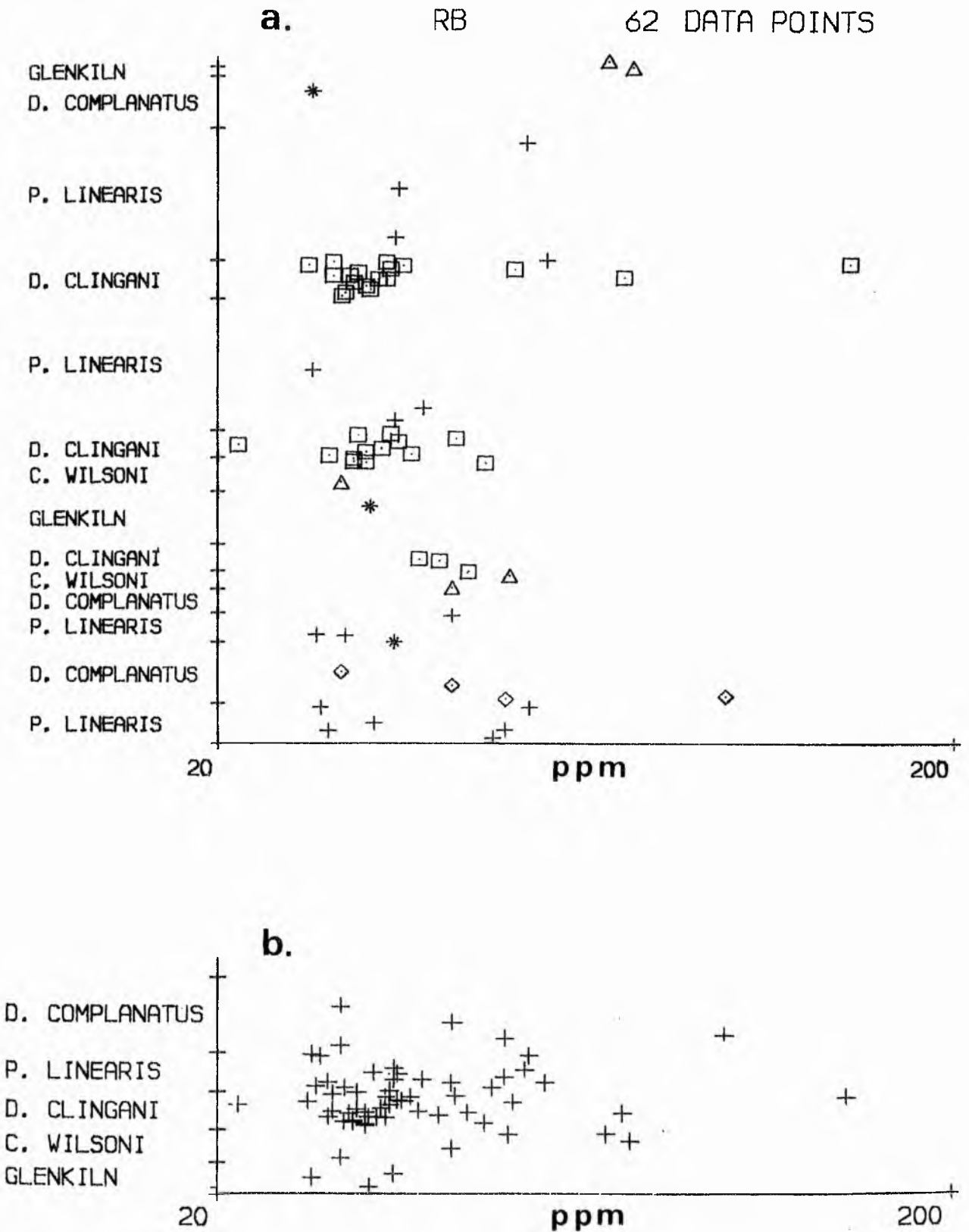


Figure 72. Plots illustrating the stratigraphic variation of the rubidium concentration in the sediments of the north cliff at Hartfell Scaur.

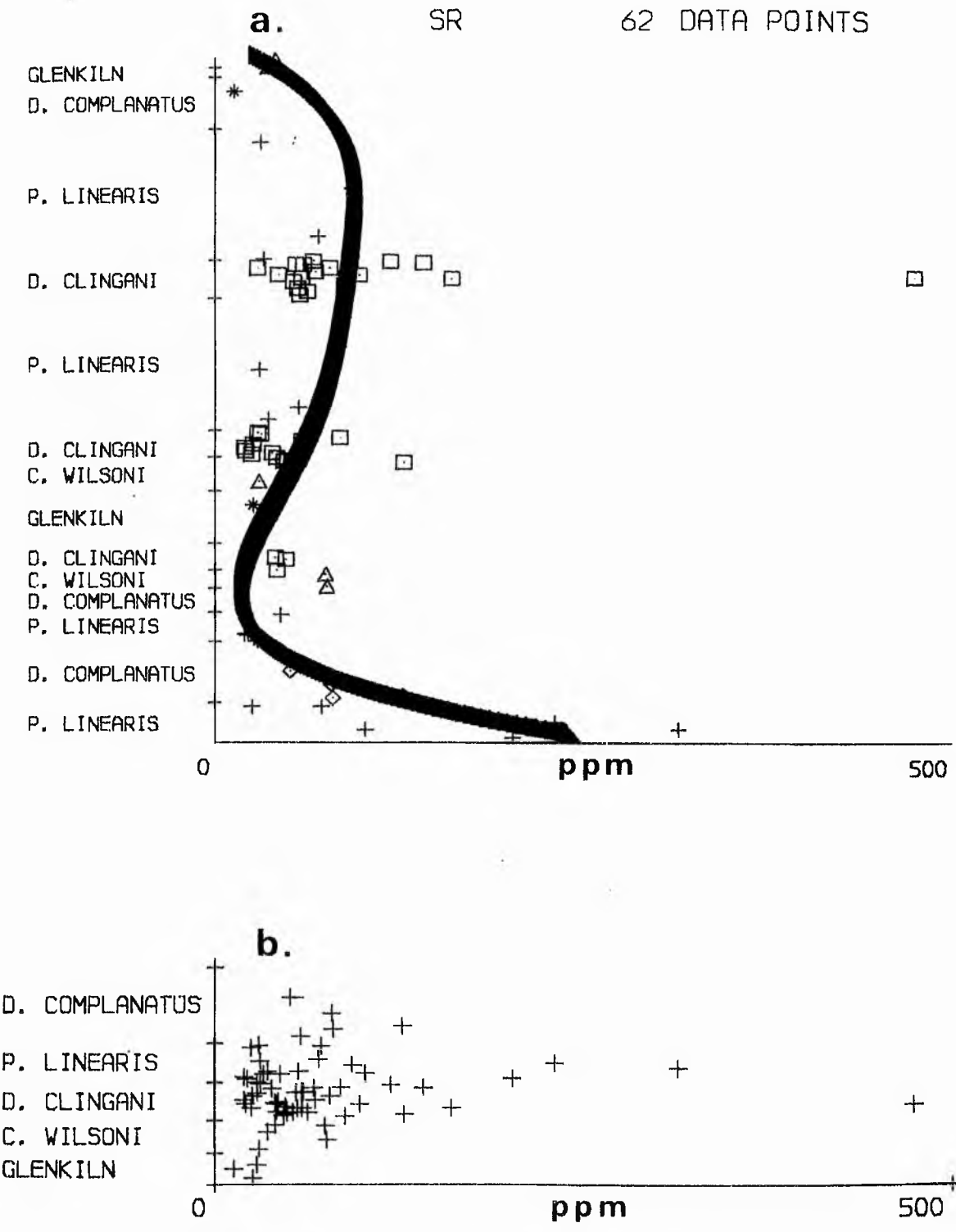


Figure 73. Plots illustrating the stratigraphic variation of the strontium concentration in the sediments of the north cliff at Hartfell Scaur.

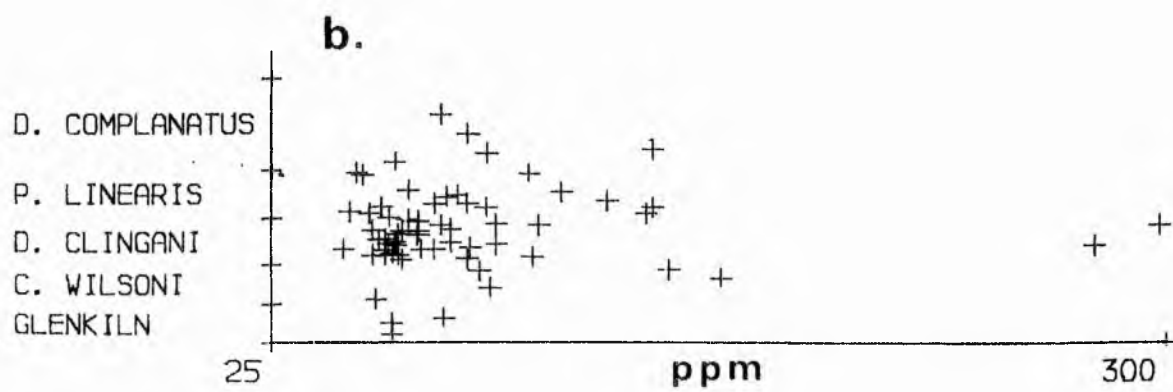
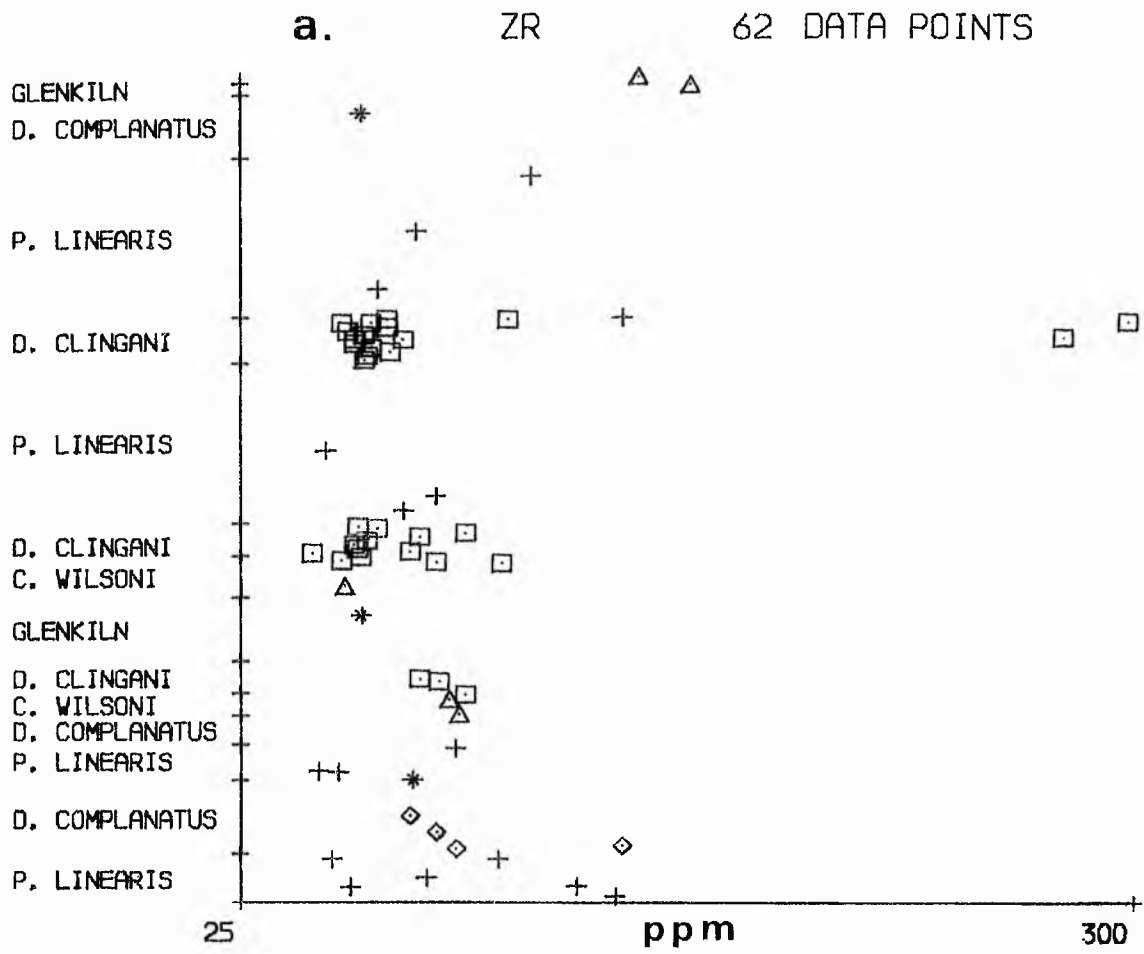


Figure 75. Plots illustrating the stratigraphic variation of the zirconium concentration in the sediments of the north cliff at Hartfell Scaur.

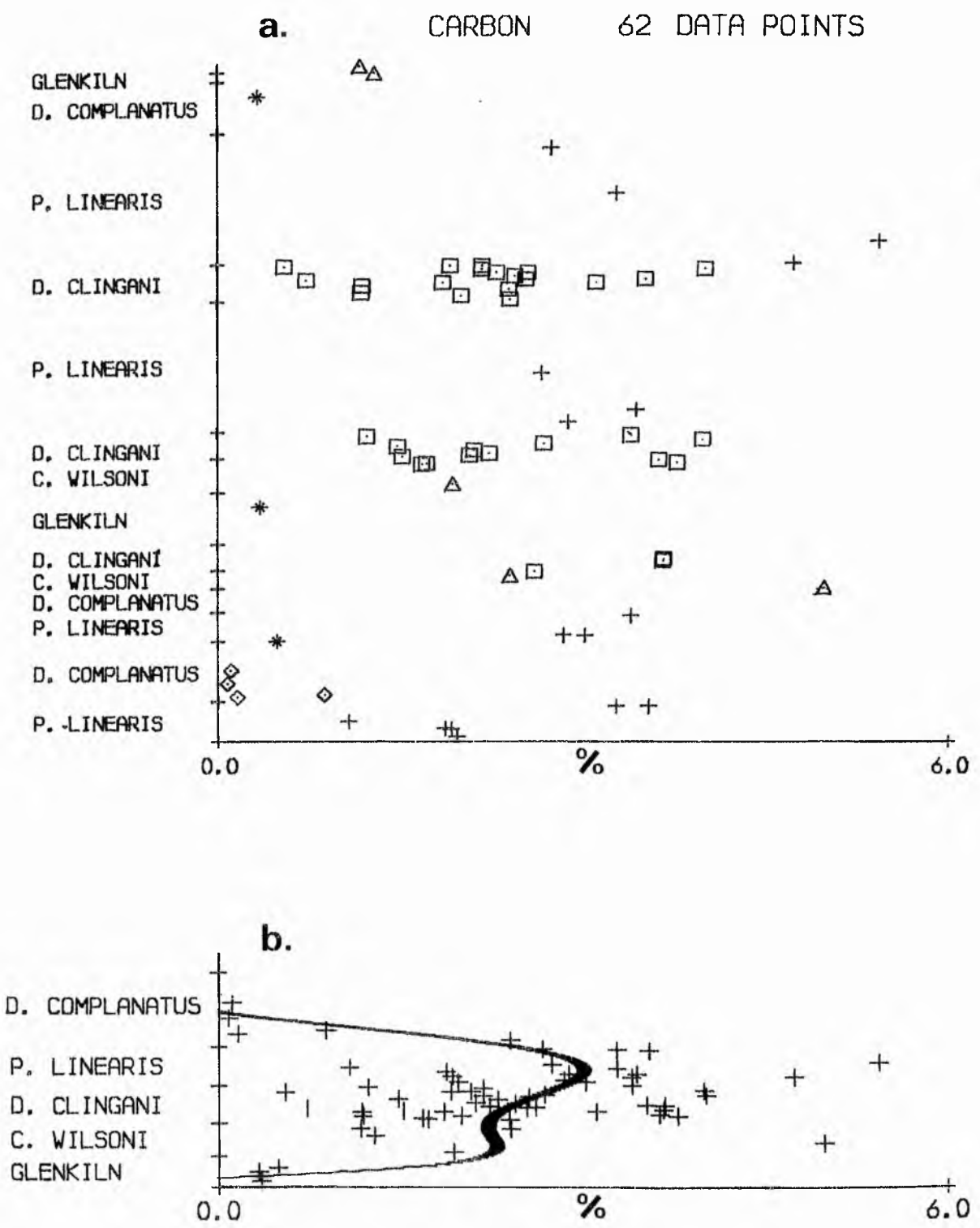


Figure 76. Plots illustrating the stratigraphic variation of the carbon concentration in the sediments of the north cliff at Hartfell Scaur.

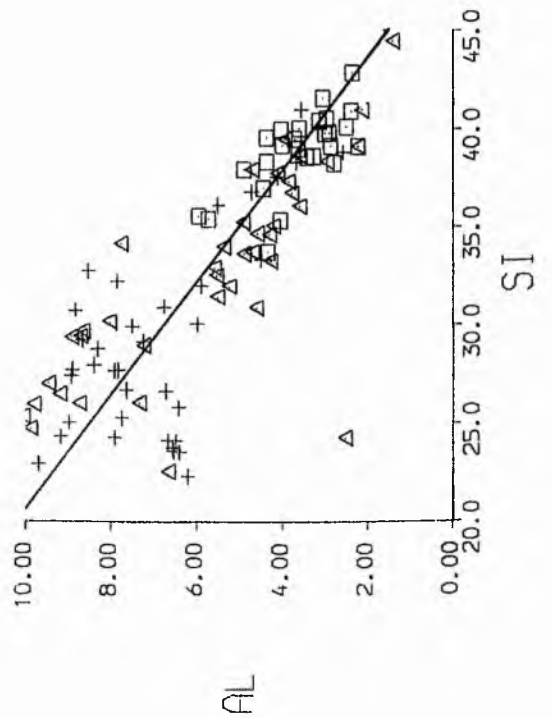
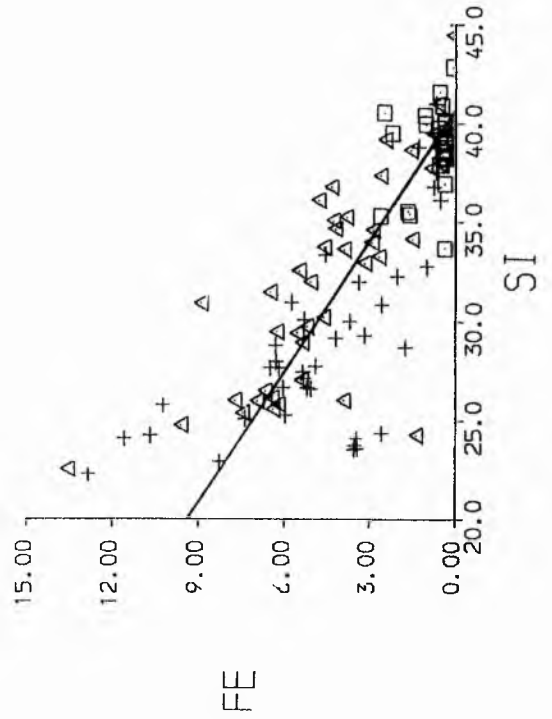
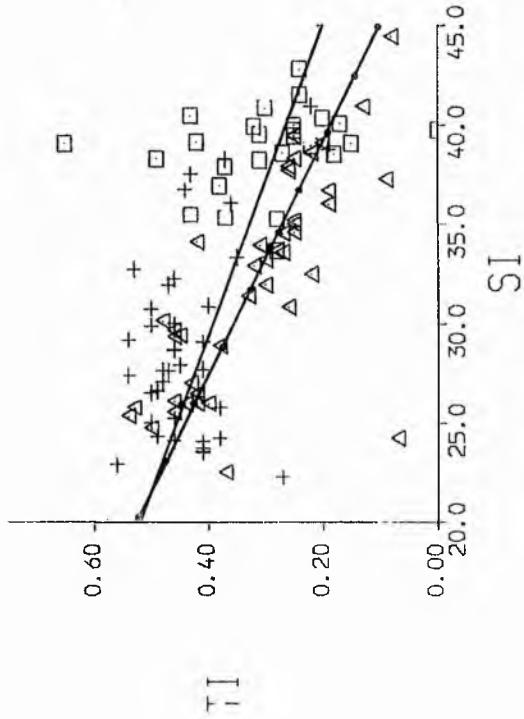
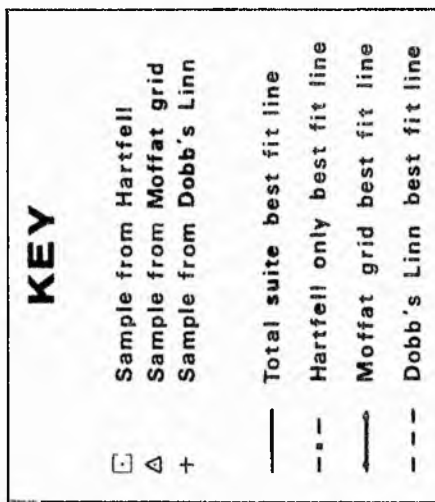


Figure 77. Scatter plots with linear regressions for element pairs.

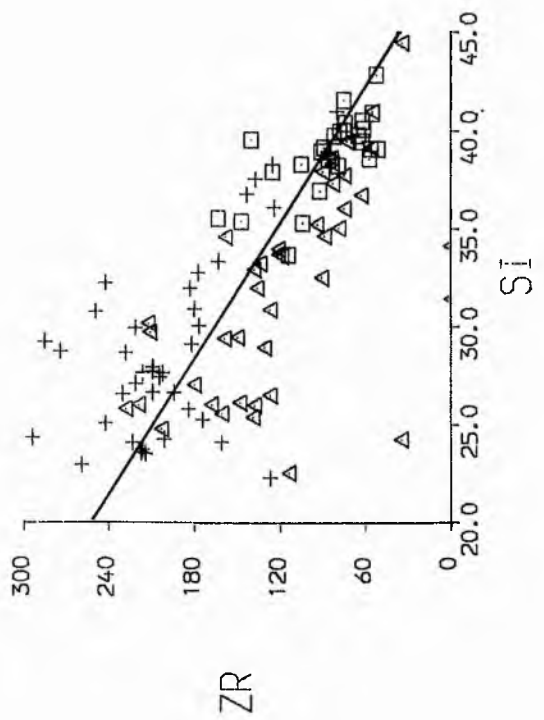
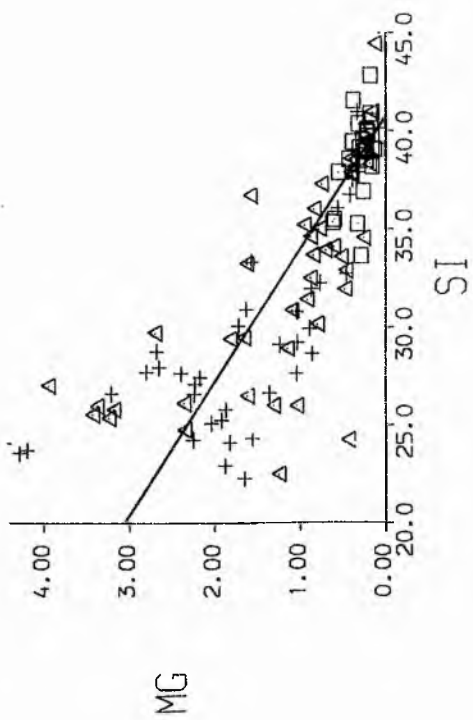
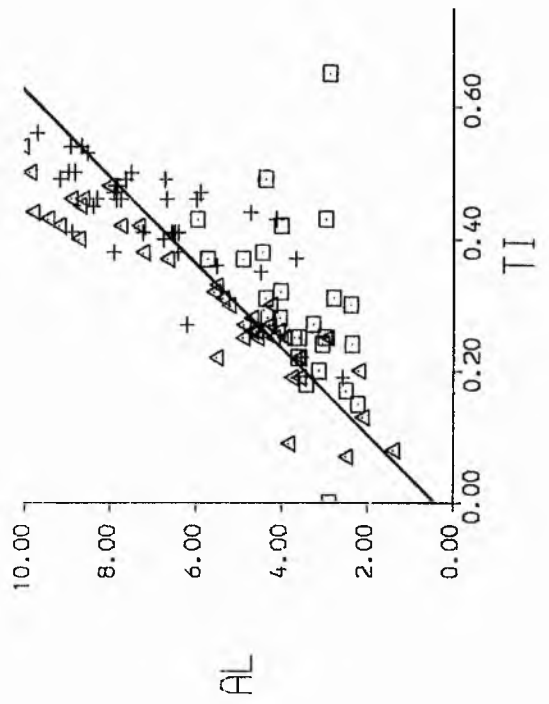
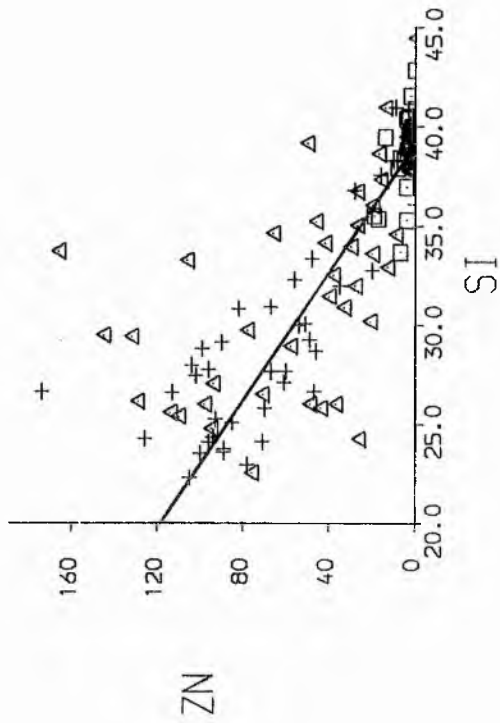


Figure 78. Scatter plots with linear regressions for element pairs.
For key, see Figure 77.

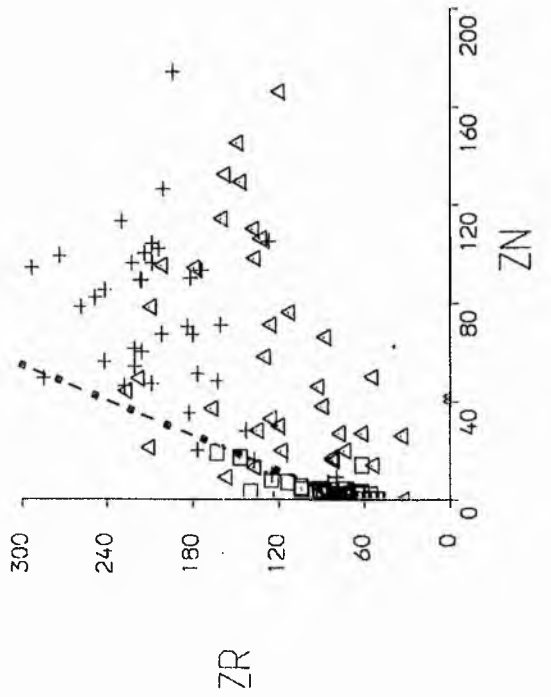
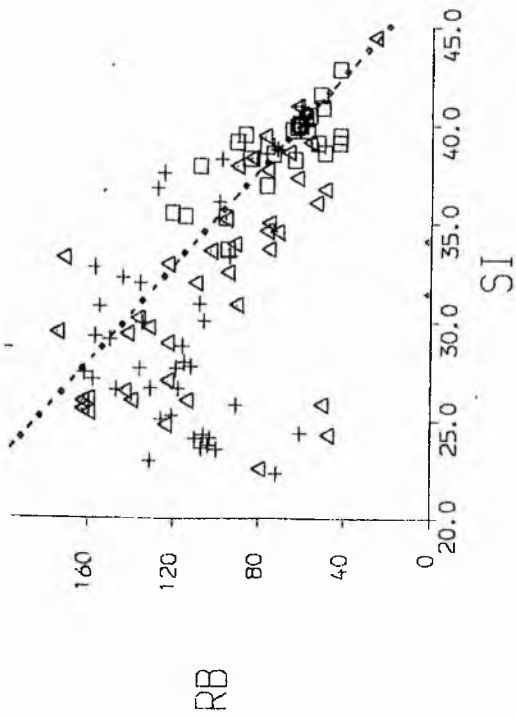
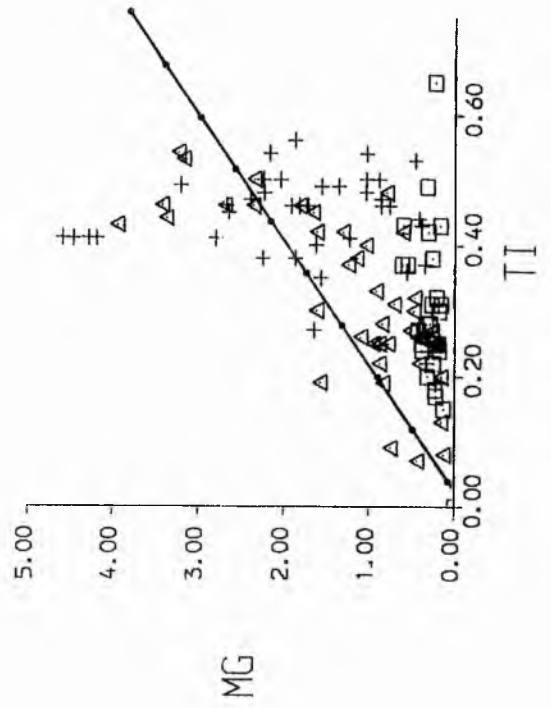
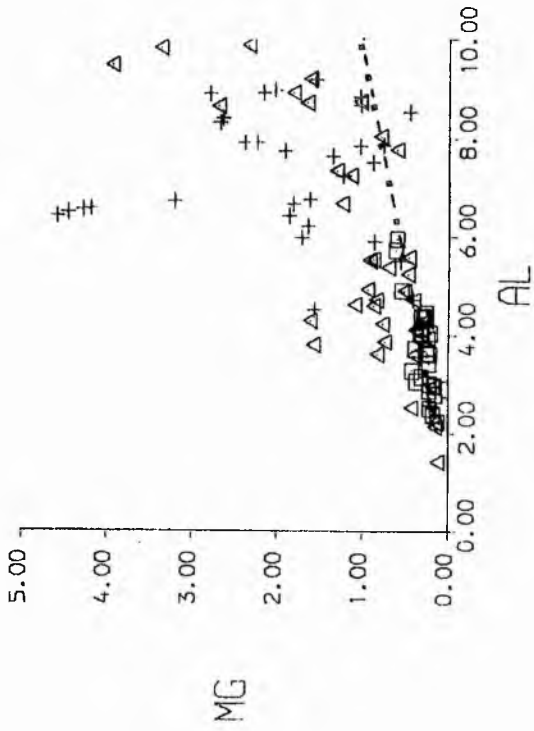


Figure 79. Scatter plots with linear regressions for element pairs.
For key, see Figure 77.

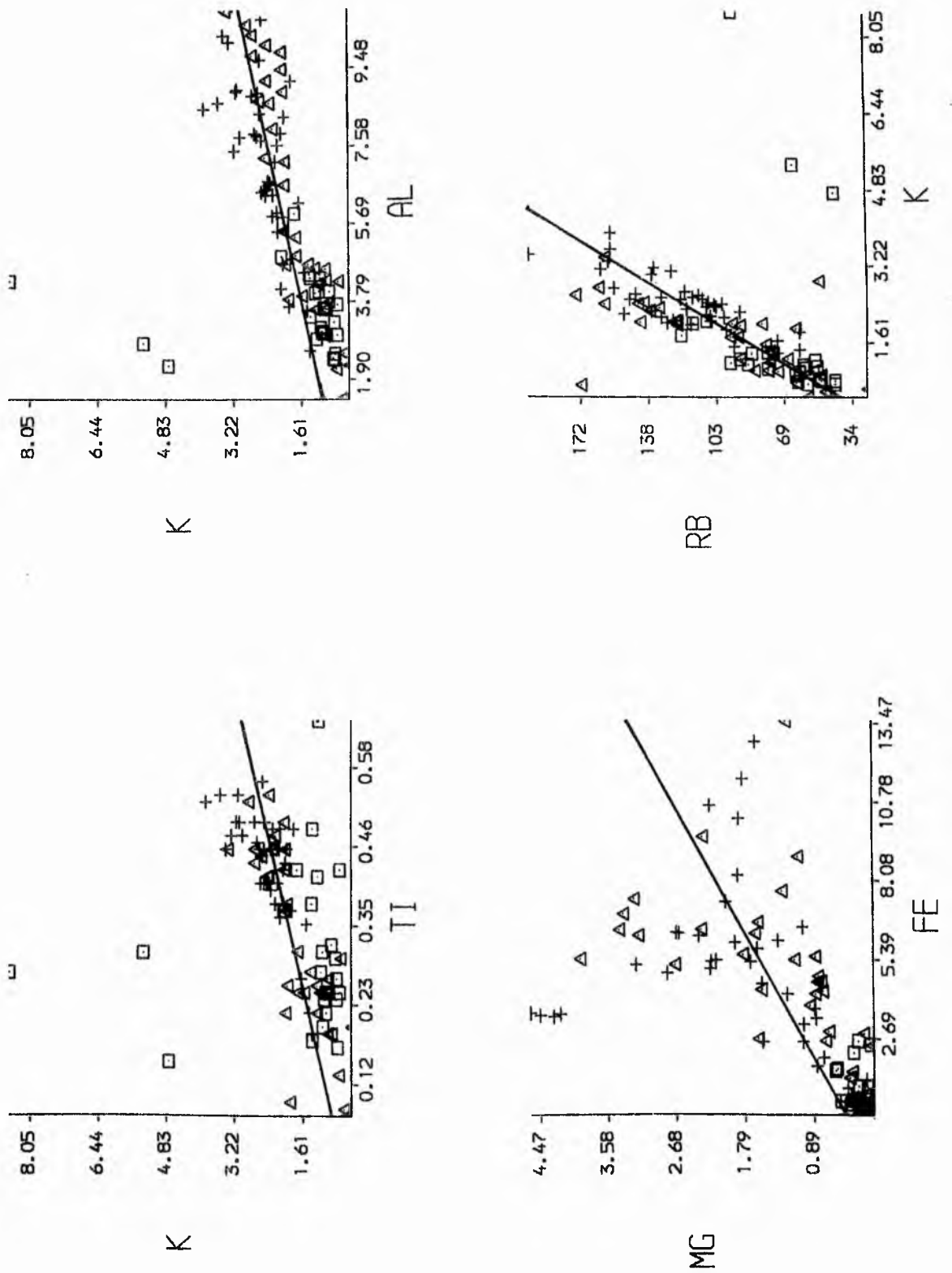


Figure 80. Scatter plots with linear regressions for element pairs. For key, see Figure 77.

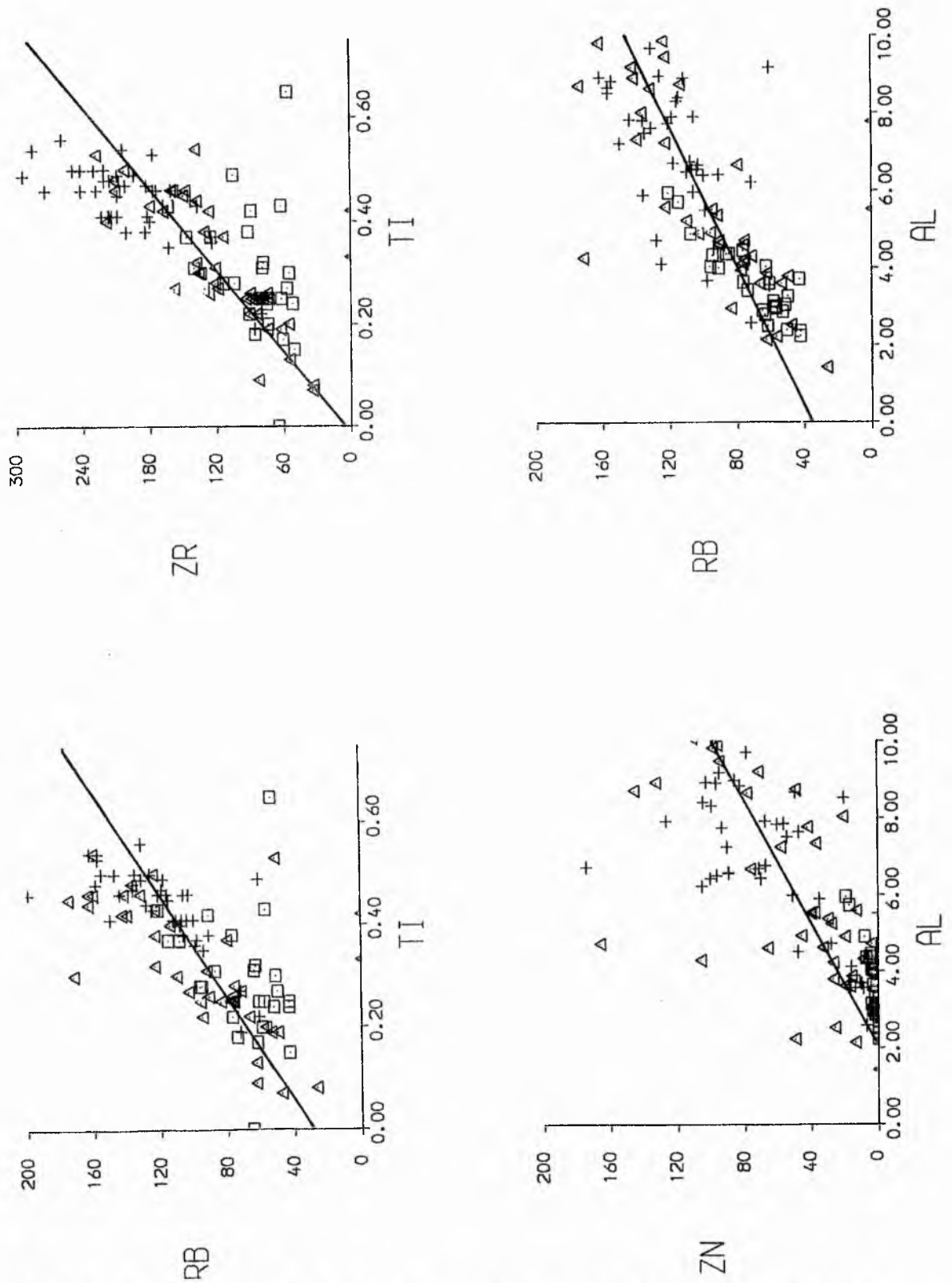


Figure 81. Scatter plots with linear regressions for element pairs.
 For key, see Figure 77.

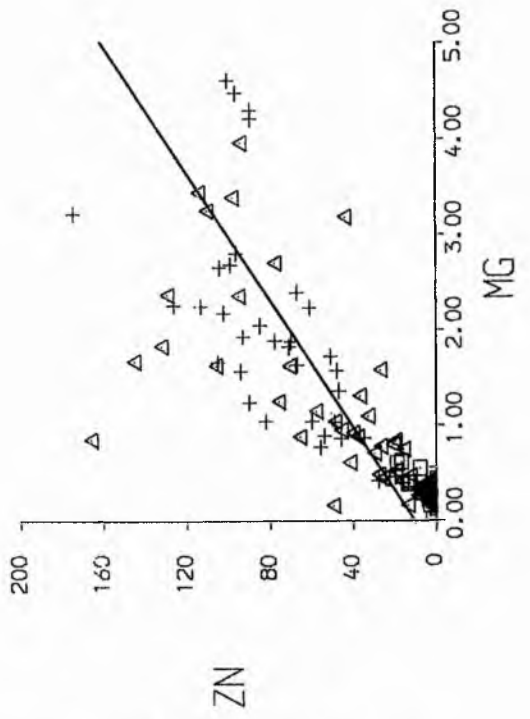
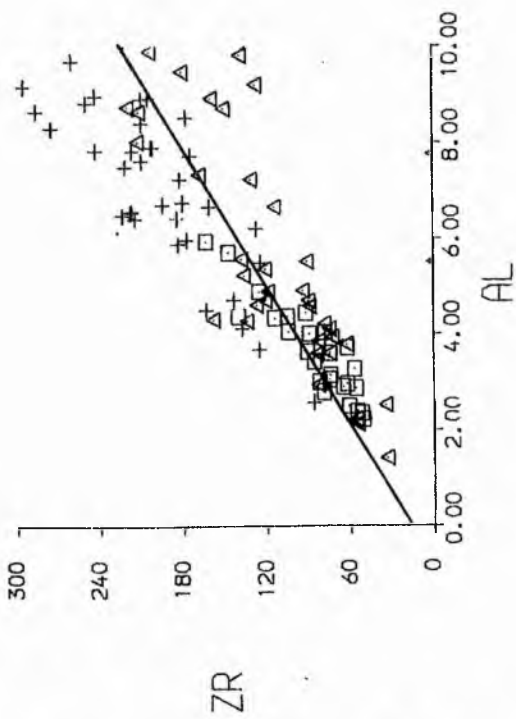
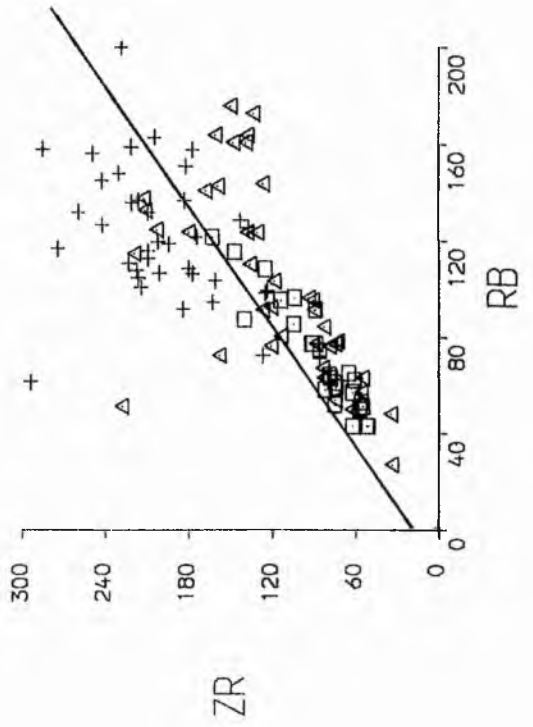
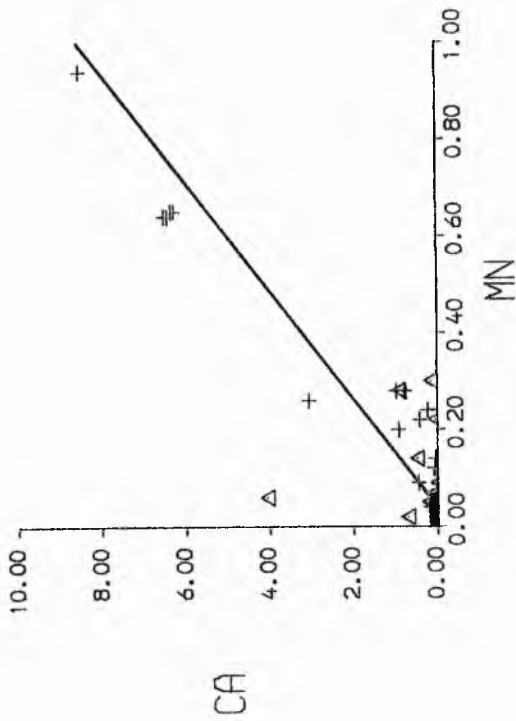


Figure 82. Scatter plots with linear regressions for element pairs.
For key, see Figure 77.

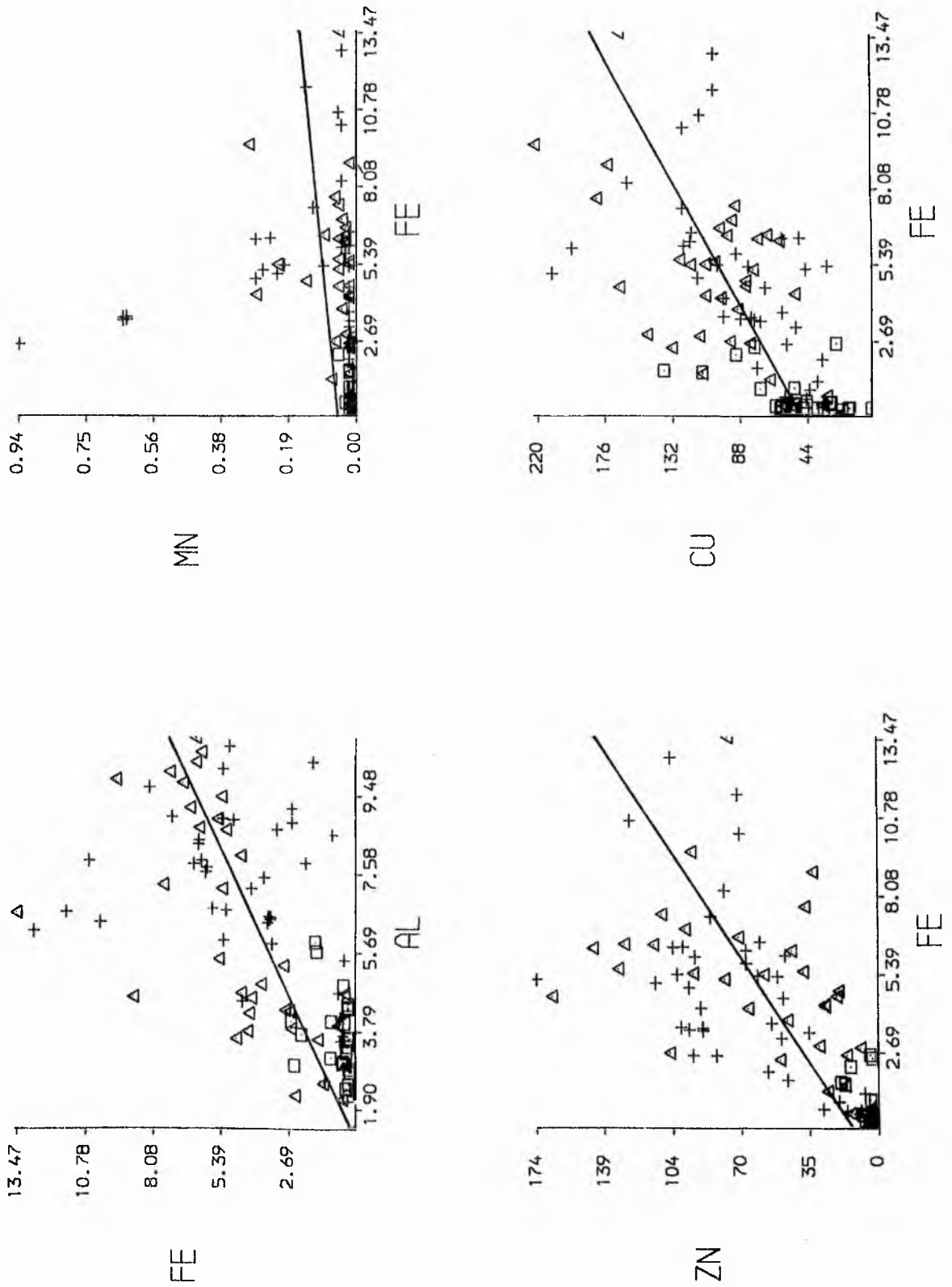


Figure 83. Scatter plots with linear regressions for element pairs. For key, see Figure 77.

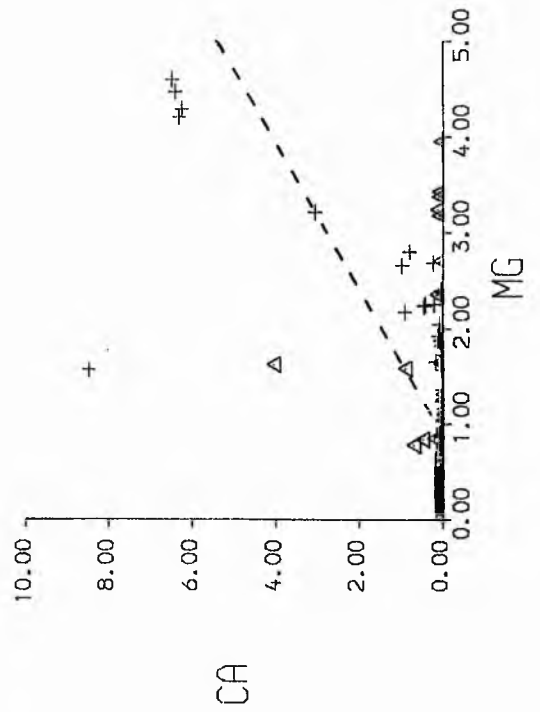
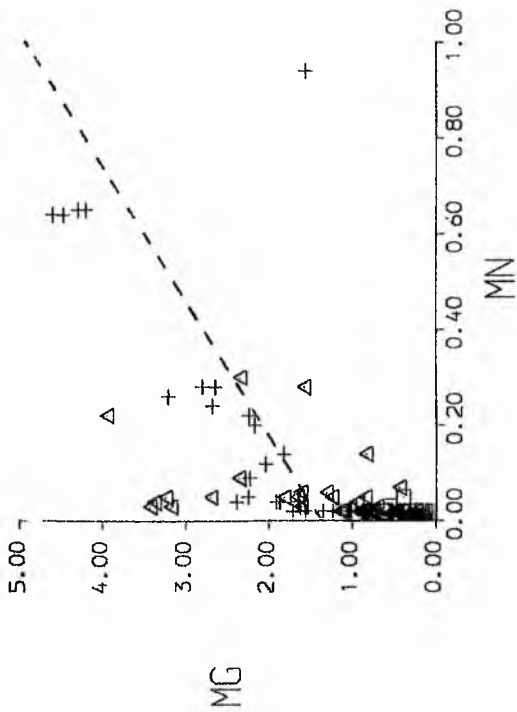
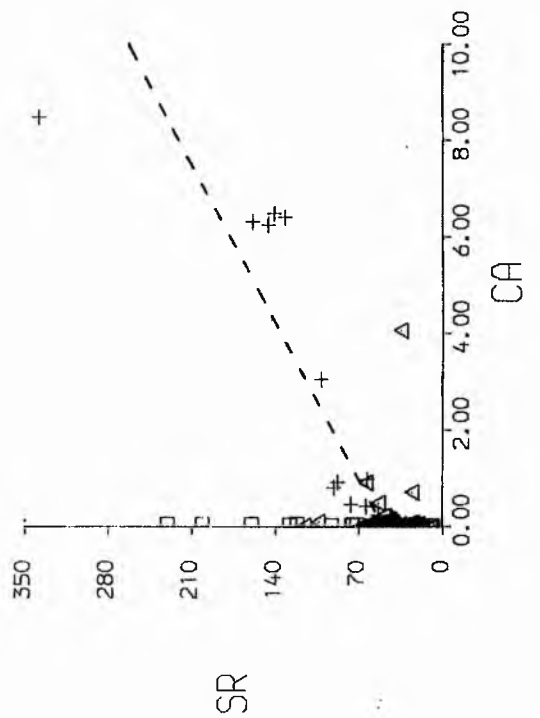
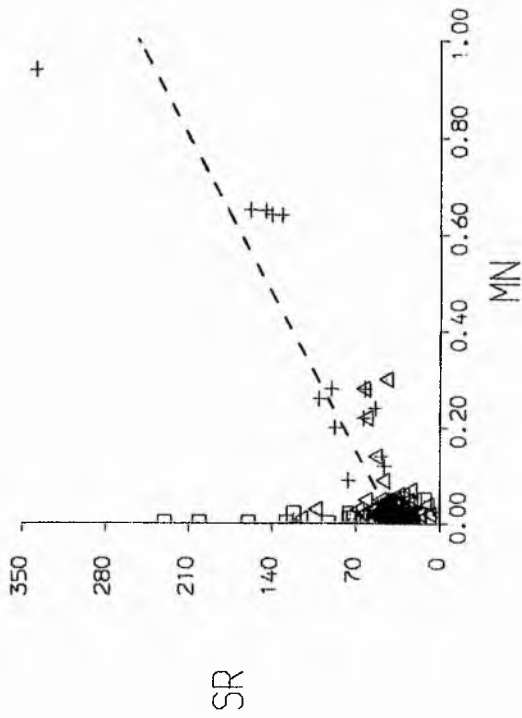


Figure 84. Scatter plots with linear regressions for element pairs.
For key, see Figure 77.

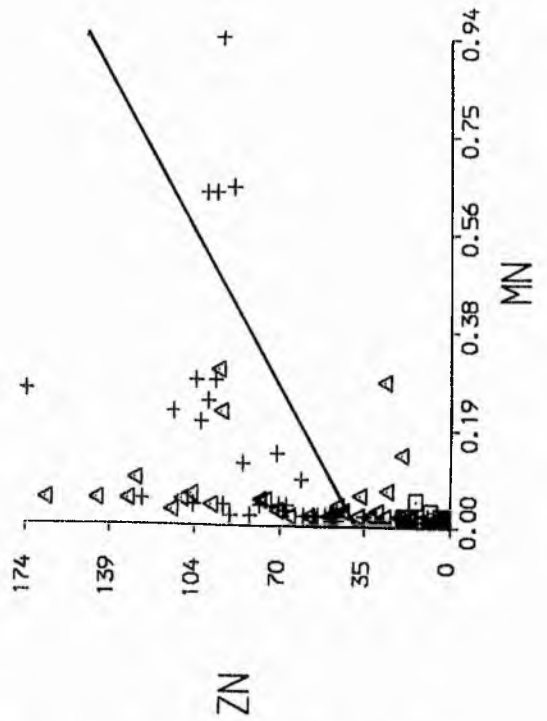
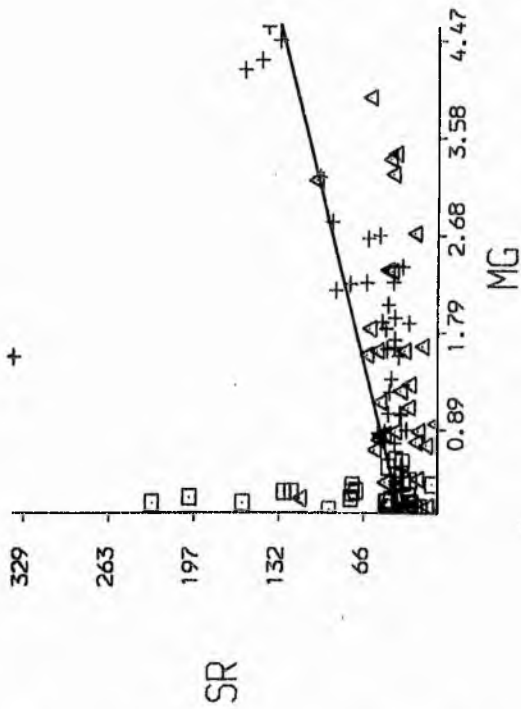
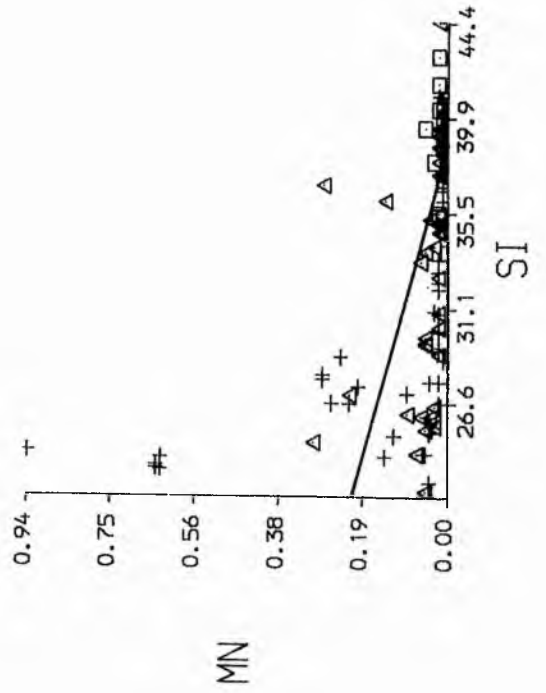
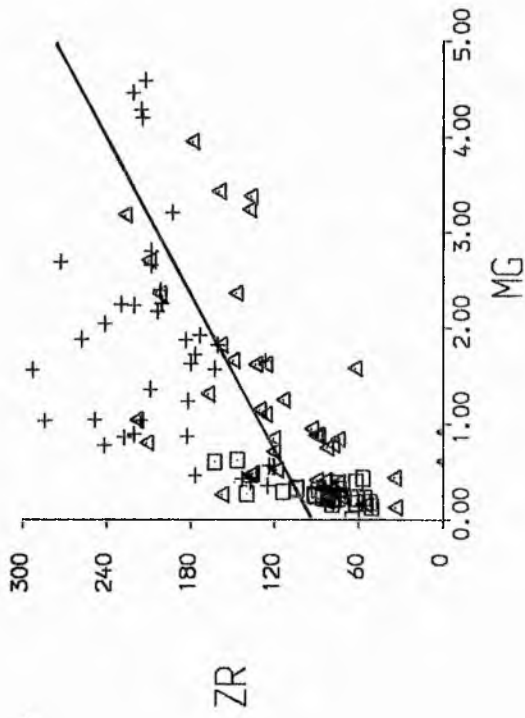


Figure 85. Scatter plots with linear regressions for element pairs. For key, see Figure 77.

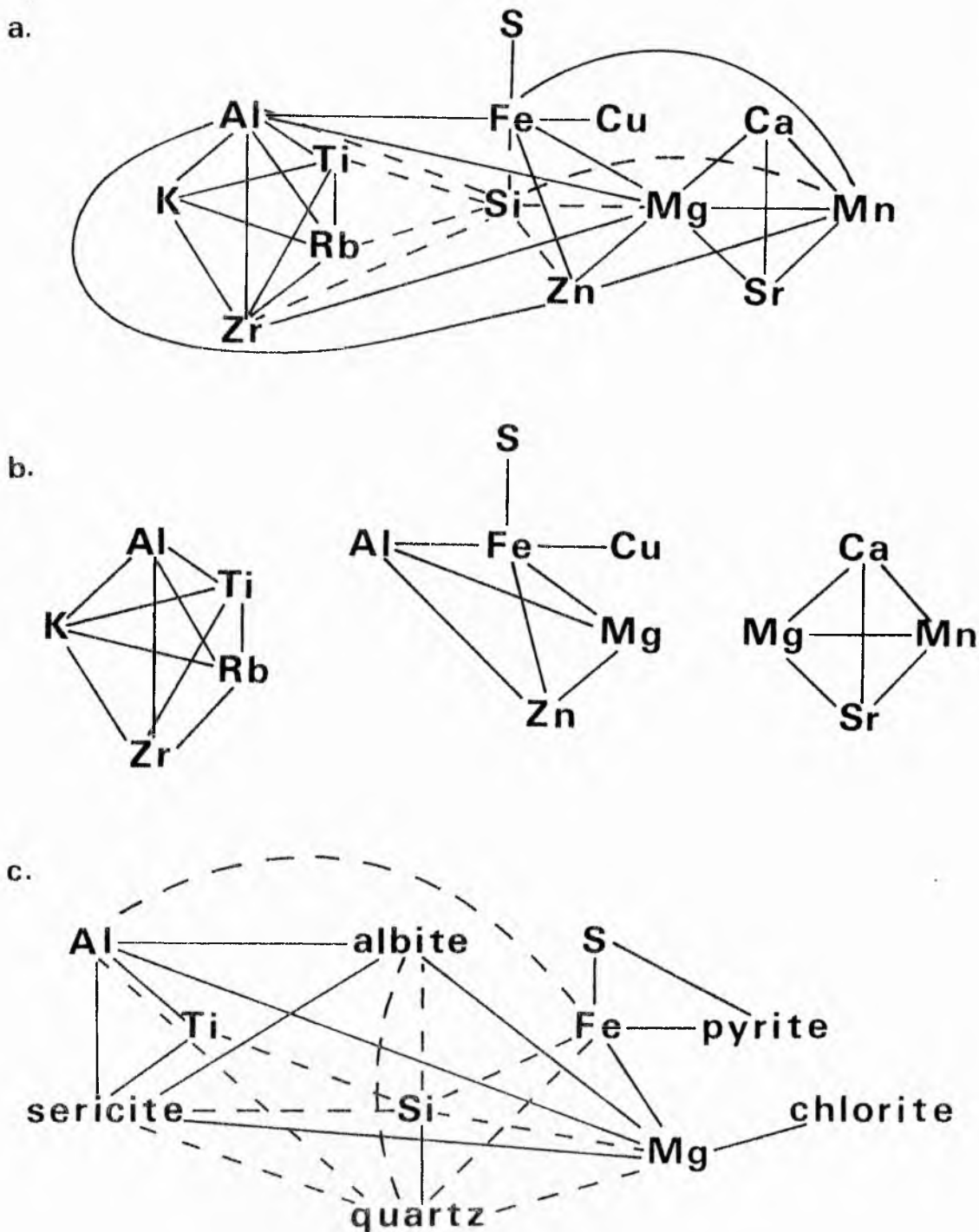


Figure 86. a, The 31 element pairs with Kendall rank order correlation coefficients greater than 0.50.
 b, Simplified form of a.
 c, Significant correlations between element-mineral and mineral-mineral pairs.
 Solid lines represent positive correlations and broken lines negative correlations.

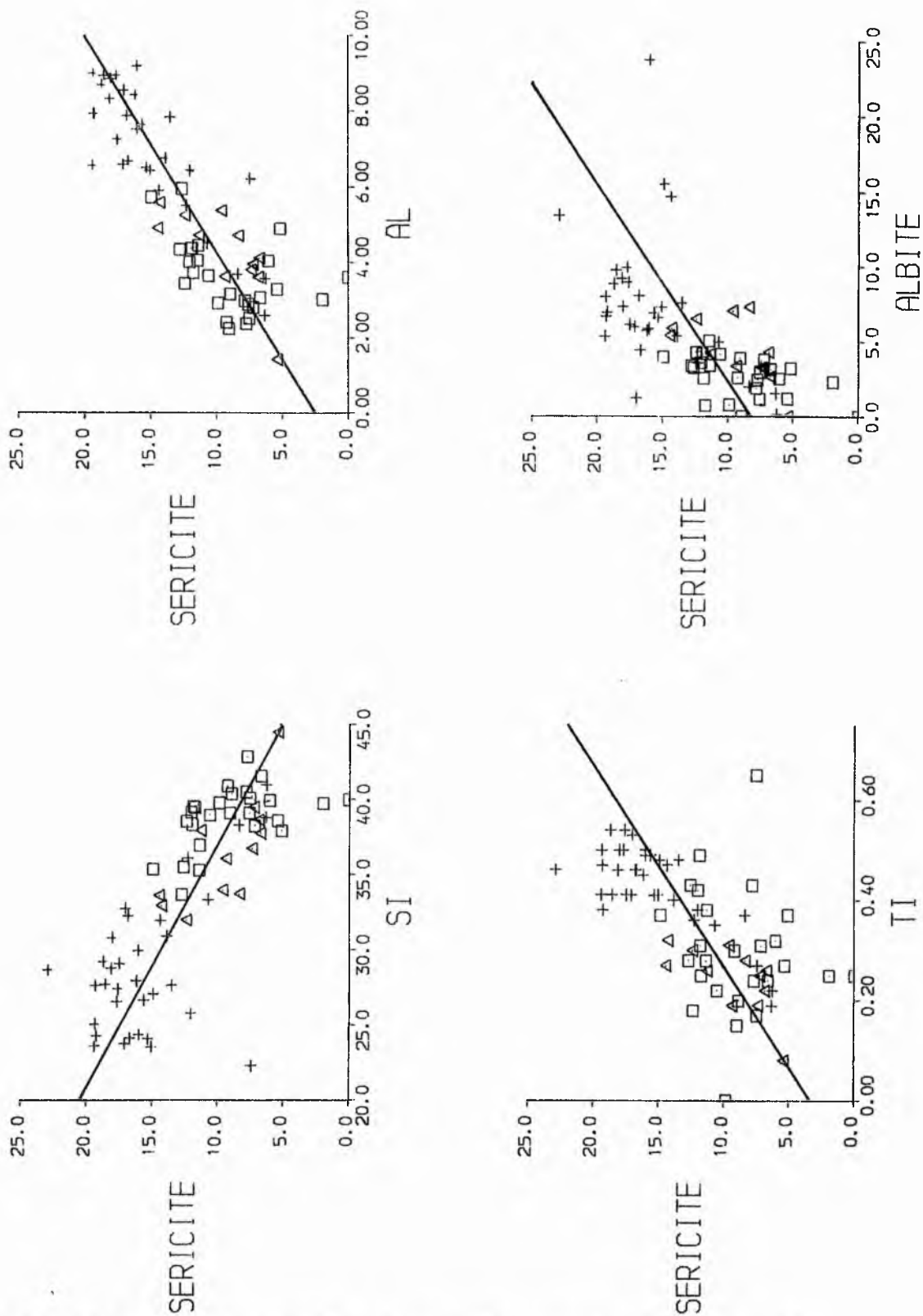
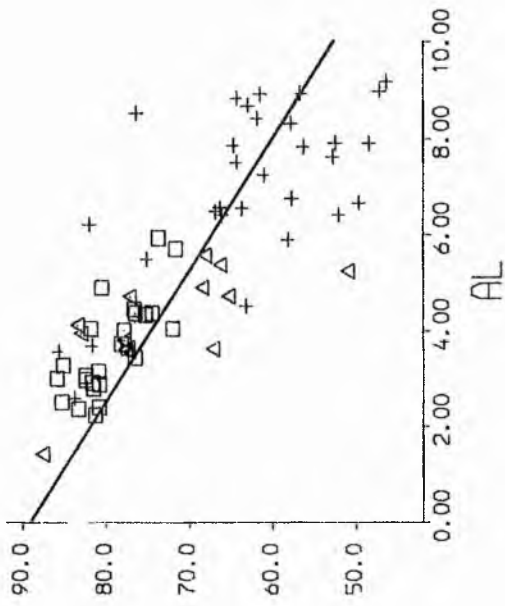
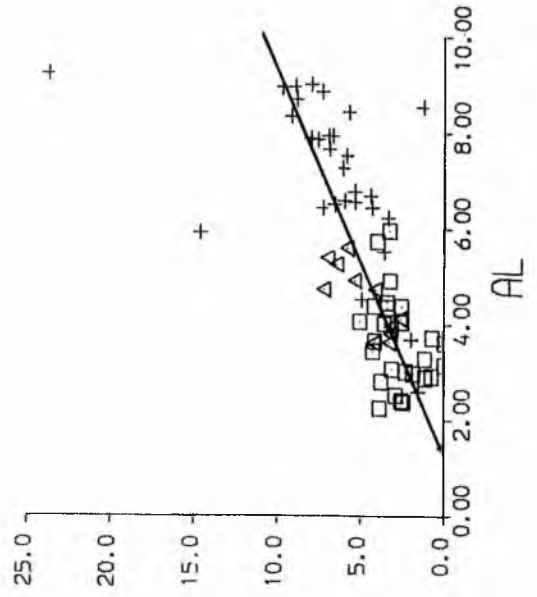


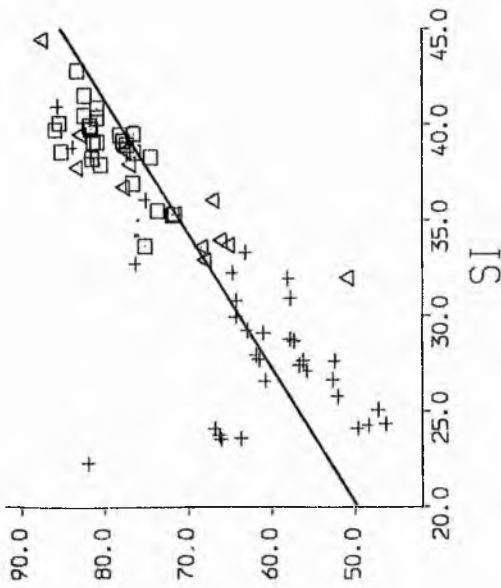
Figure 87. Scatter plots with linear regressions for element-mineral pairs. For key, see Figure 77.



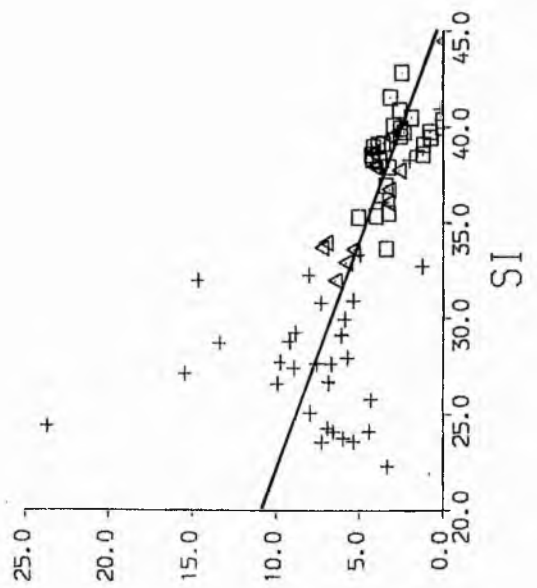
QUARTZ



ALBITE



QUARTZ

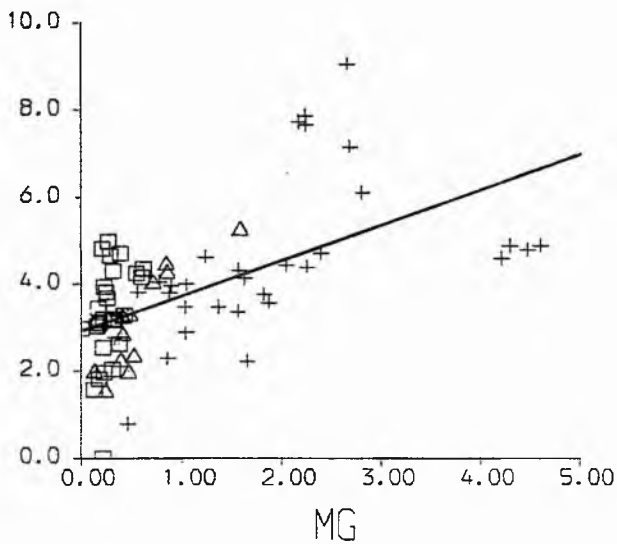


ALBITE

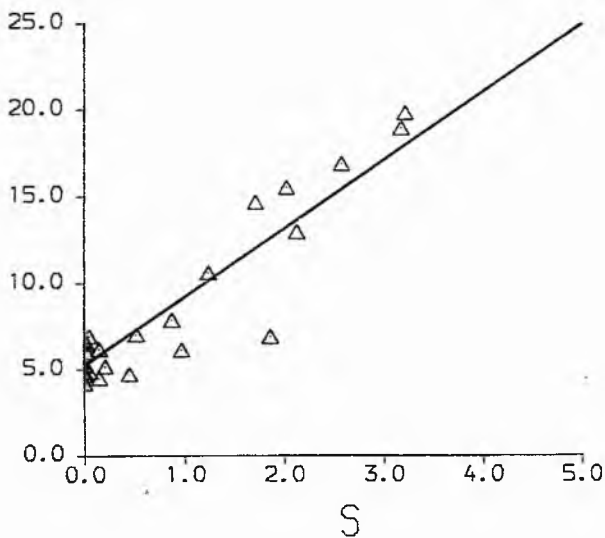
Figure 88. Scatter plots with linear regressions for element-mineral pairs. For key see Figure 77.

Figure 89. Scatter plots with linear regressions for element-mineral pairs. For key, see Figure 77.

CHLORITE



PYRITE



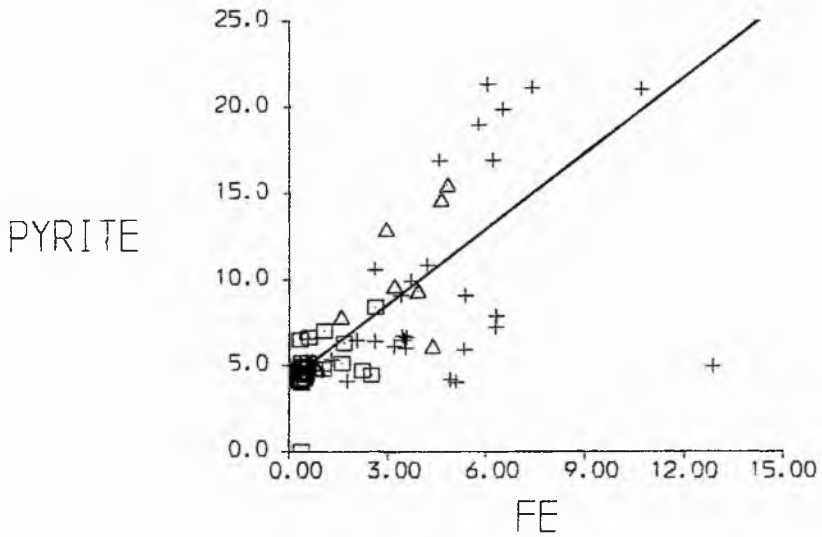
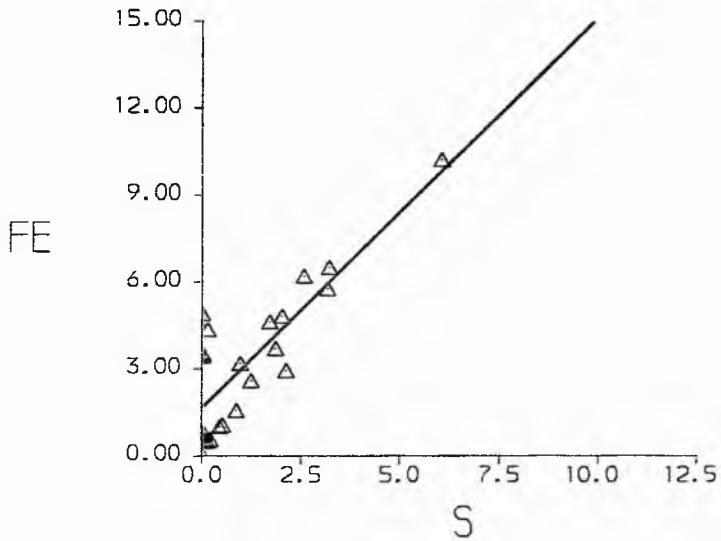
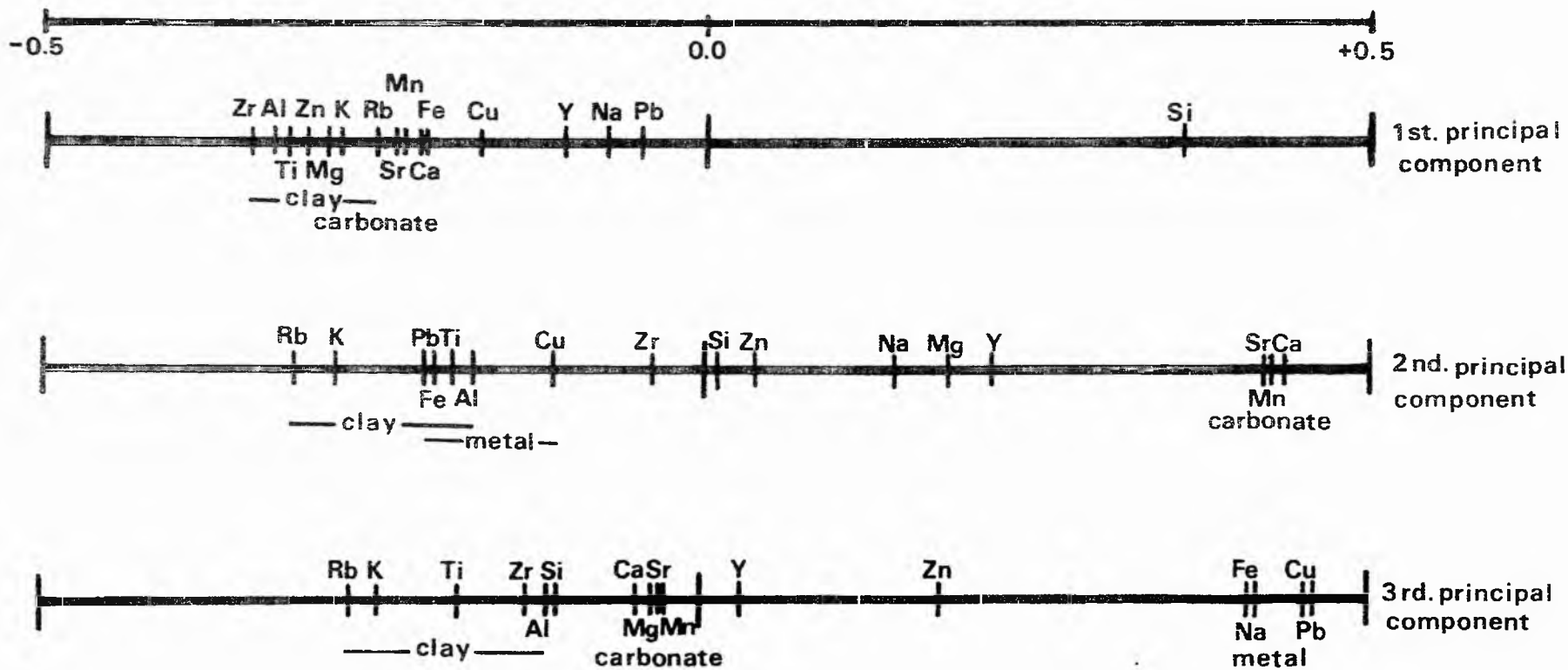


Figure 90. Element loadings on the first three principal components.



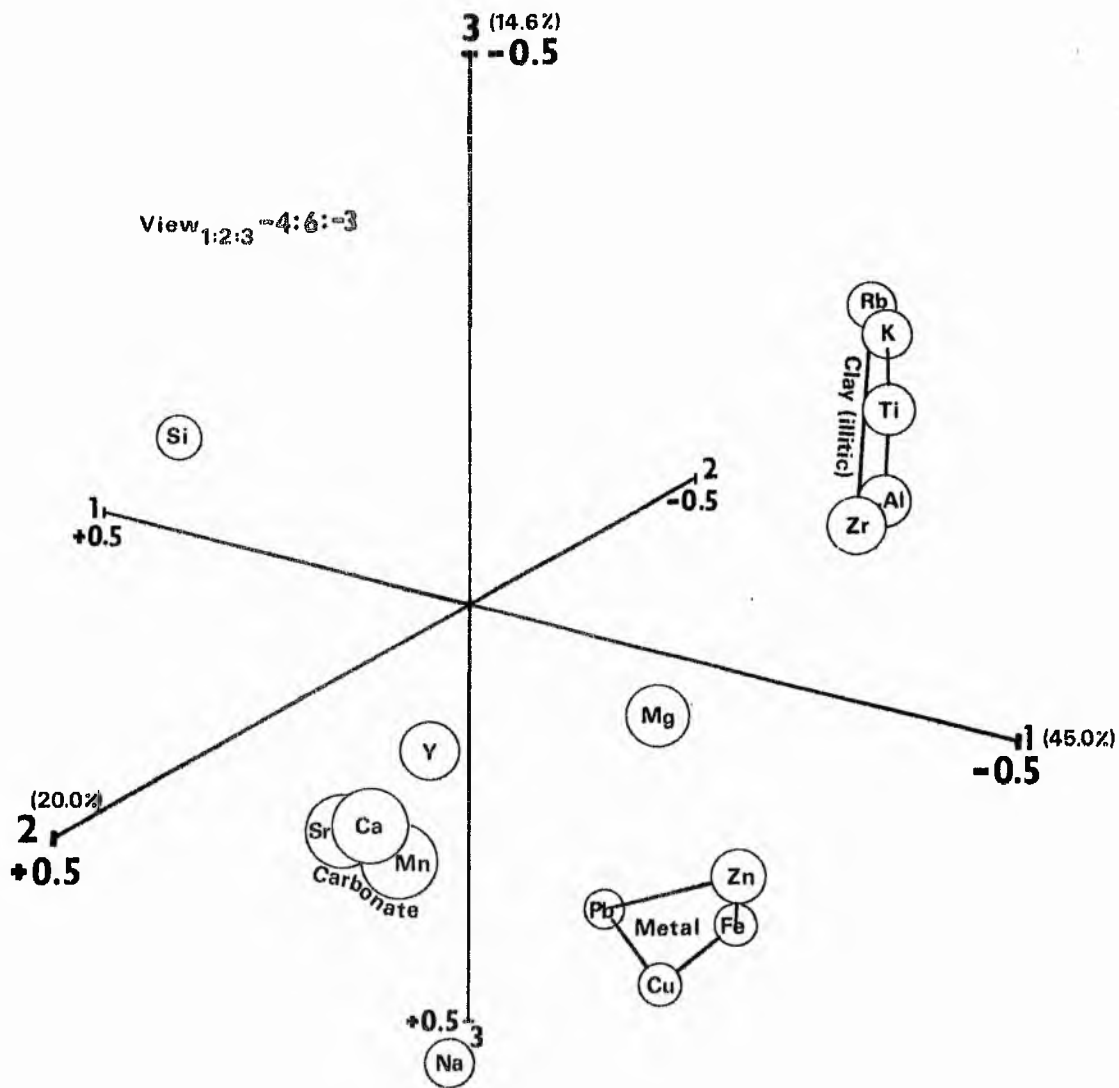


Figure 91. Projection of all elements over the three vector space of the first three principal components.

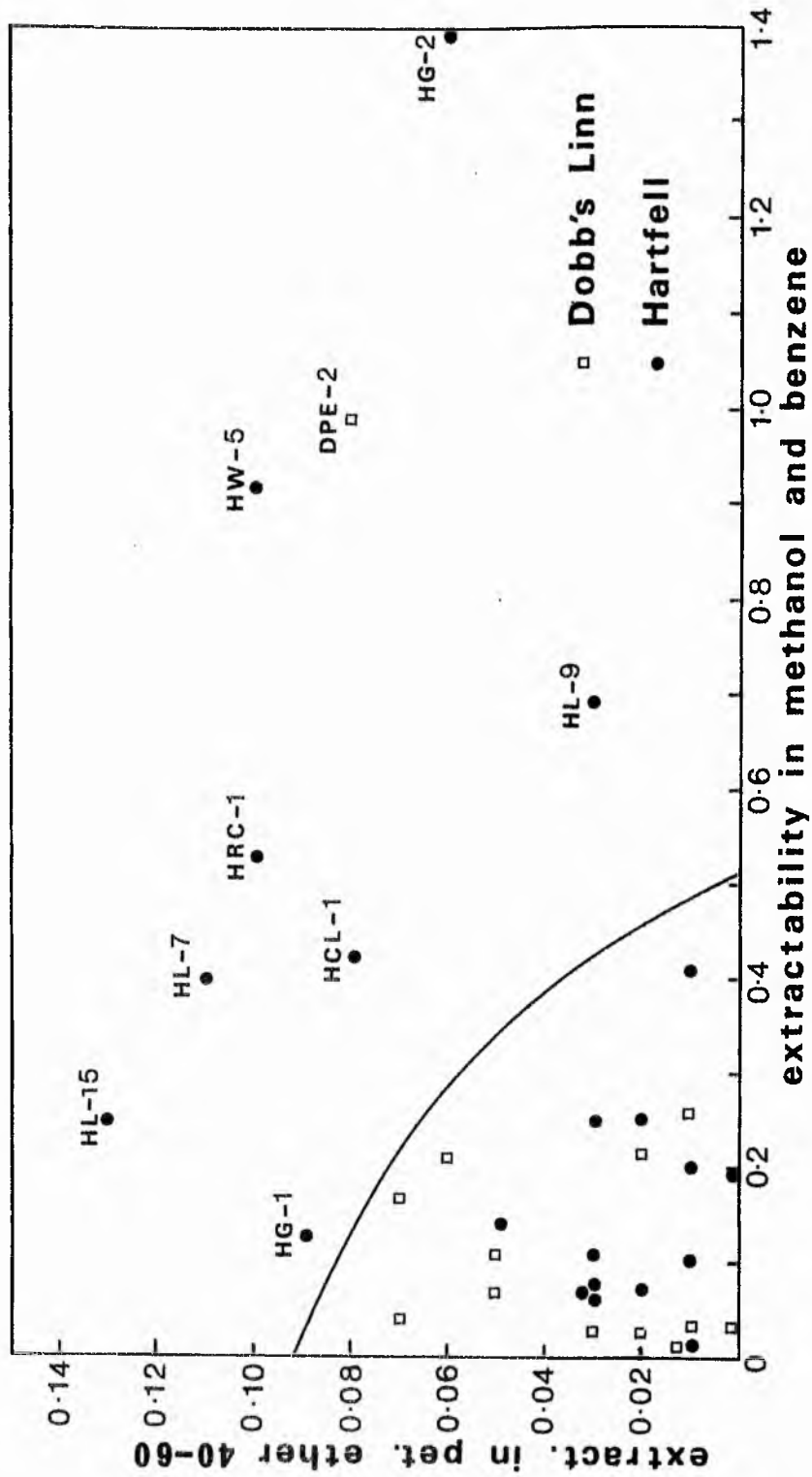


Figure 93. Scatter plot of the extractability of organic material isolated from a silica gel column in the petroleum ether eluate against the combined extractabilities of the material in the benzene and methanol eluates.

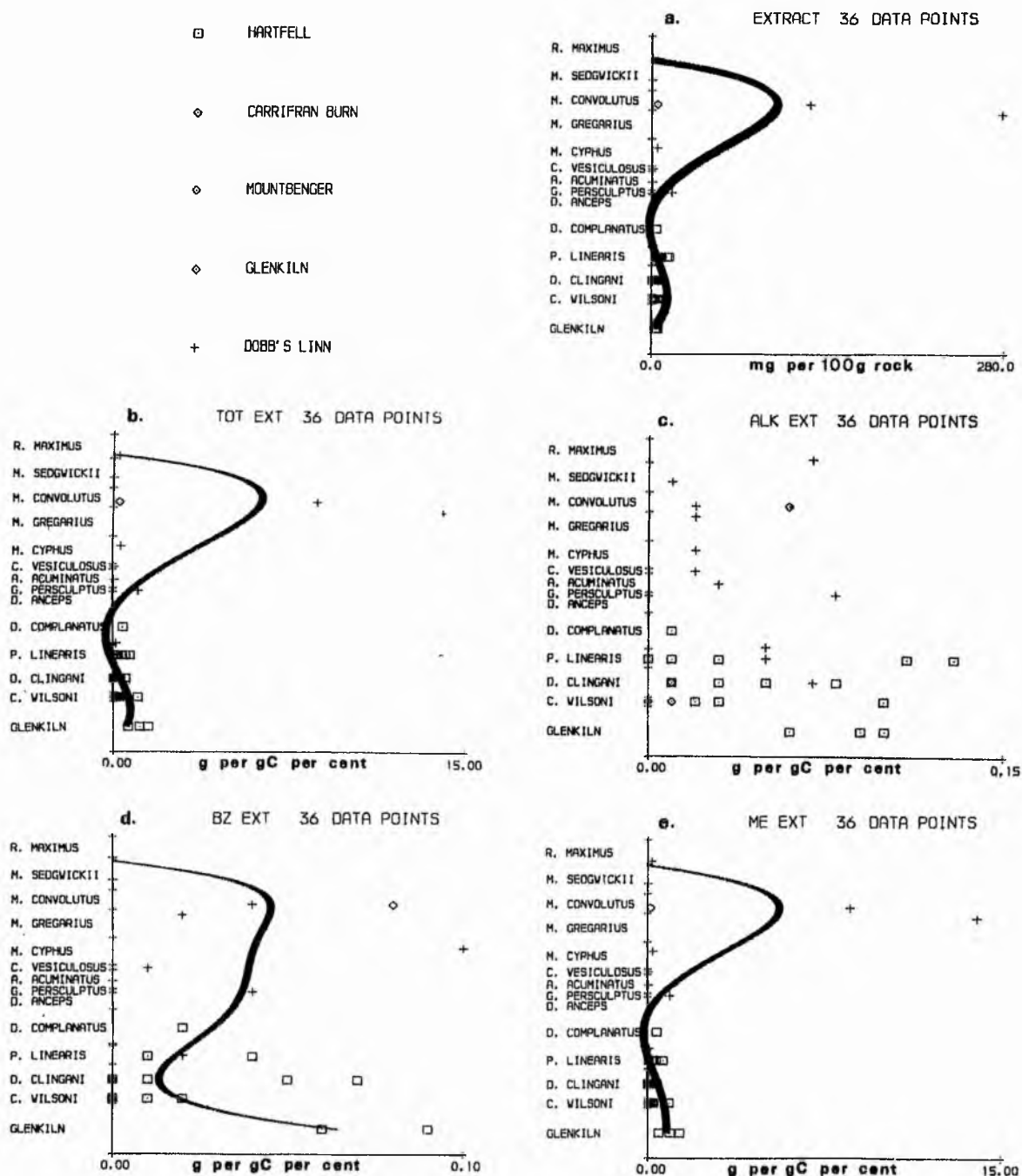


Figure 94. Plots illustrating the stratigraphic variation in the Moffat Shales of a) total amount of organic material eluted from a silica gel column, b) extractability of the total organic material eluted from a silica gel column, c) extractability of the total alkanes d) extractability of the benzene eluate, e) extractability of the methanol eluate.

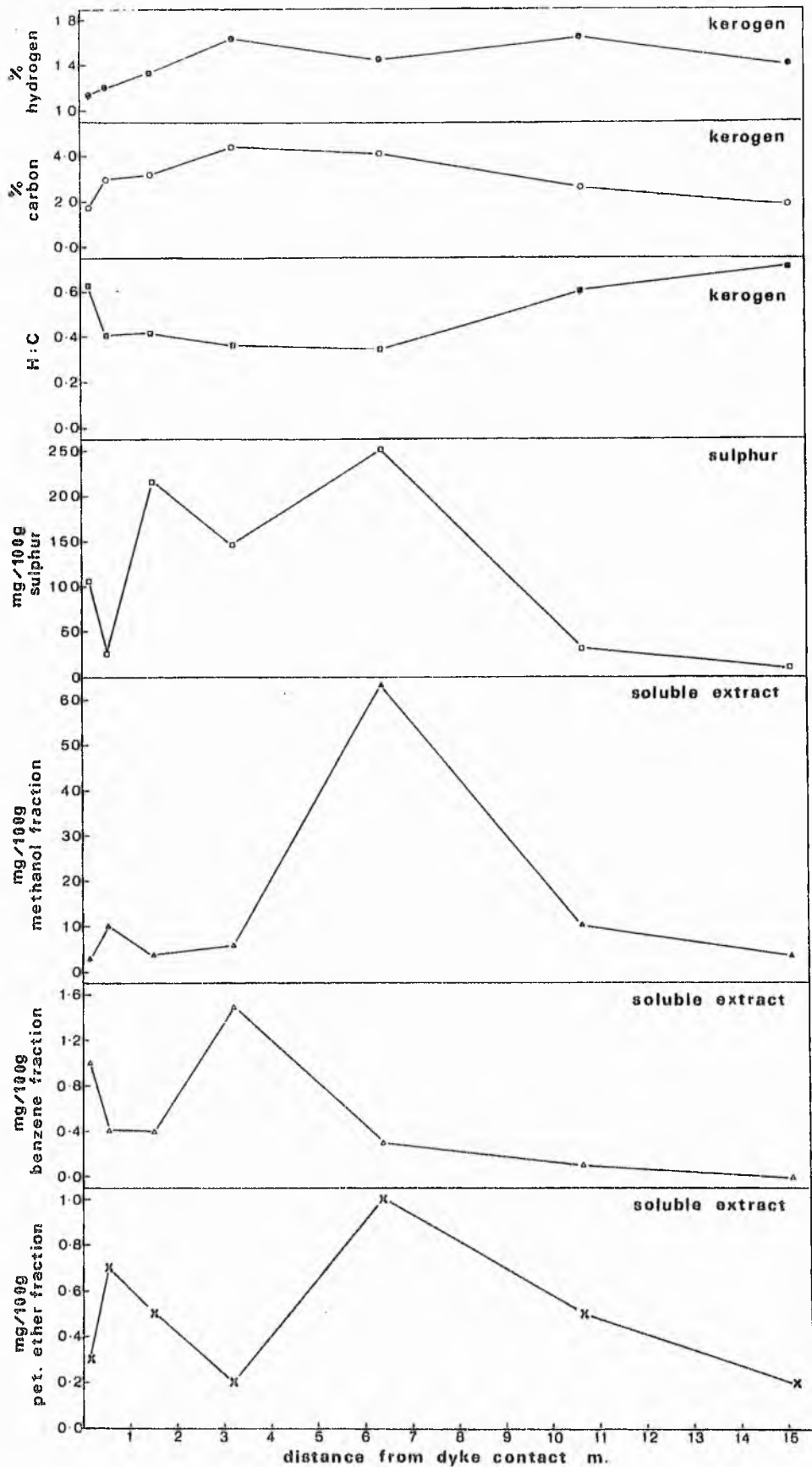


Figure 95. Plots illustrating the variation in organic parameters with distance from the 9.18 m thick dyke at Clanyard Bay.

Sample DCL-1

Model of chromatograph Varian 1400
Column 5' x 1/8"
Packing 3% OV-1 on 100-120 mesh Varaport 30
Column temp. 70-300°C 6°/min.
Detector temp. 300°C Injector temp. 300°C
Attenuation 8 x 10⁻¹⁰
Recorder 1 mV 12 in/hr.
Nitrogen 40 psi

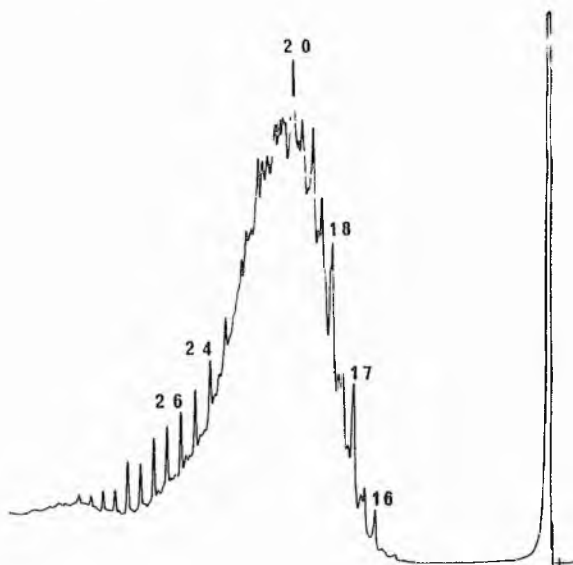
Sample DL-4

Model of chromatograph Varian 1400
Column 5' x 1/8"
Packing 3% OV-1 on 100-120 mesh Varaport 30
Column temp. 70-300°C 6°/min.
Detector temp. 300°C Injector temp. 300°C
Attenuation 64 x 10⁻¹¹
Recorder 1 mV 12 in/hr.
Nitrogen 40 psi

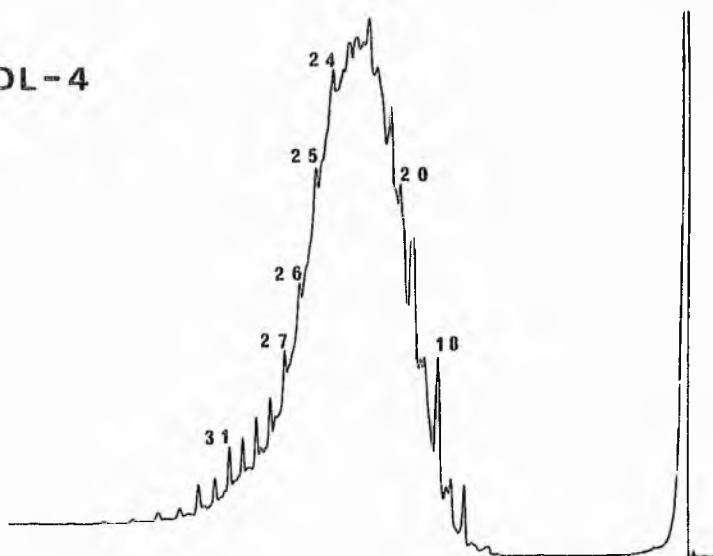
Sample DC-1

Model of chromatograph Varian 1400
Column 10' x 1/16"
Packing 5% OV-1 on 100-120 mesh Varaport 30
Column temp. 80-300°C 4°/min.
Detector temp. 300°C Injector temp. 300°C
Attenuation 32 x 10⁻¹¹
Recorder 1 mV 12 in/hr.
Nitrogen 40 psi

DCL-1



DL-4



DC-1

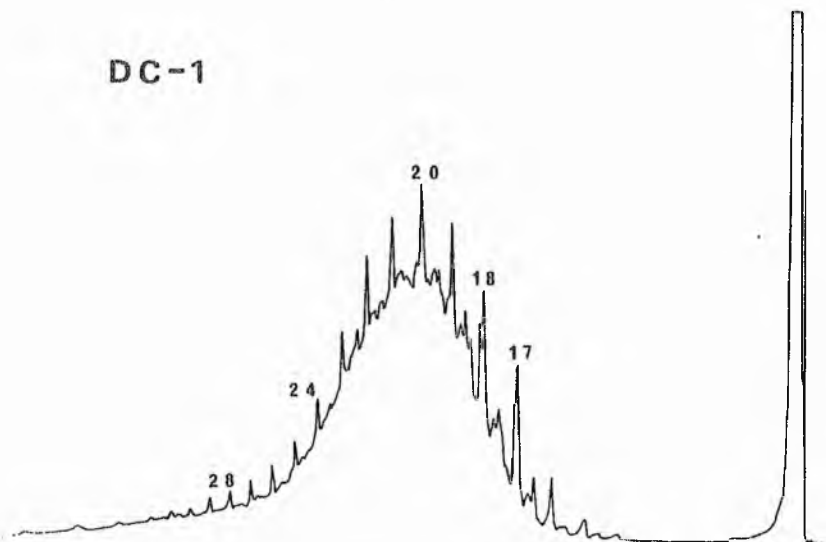


Figure 96. Gas-liquid chromatograms of the total alkanes extracted from samples DCL-1, DL-4, DC-1. Numbers above peaks are carbon chain lengths of coinjected n-alkanes.

Sample DPE-2

| | |
|------------------------|---------------------------------------|
| Model of chromatograph | Varian 1200 |
| Column | 5' x 1/8" |
| Packing | 3% OV-101 on 100-120 mesh Varaport 30 |
| Column temp. | 80-300°C 6°/min. |
| Detector temp. | 300°C Injector temp. 300°C |
| Attenuation | 1 x 64 |
| Recorder | 1 mV 12 in/hr. |
| Nitrogen | 40 psi |

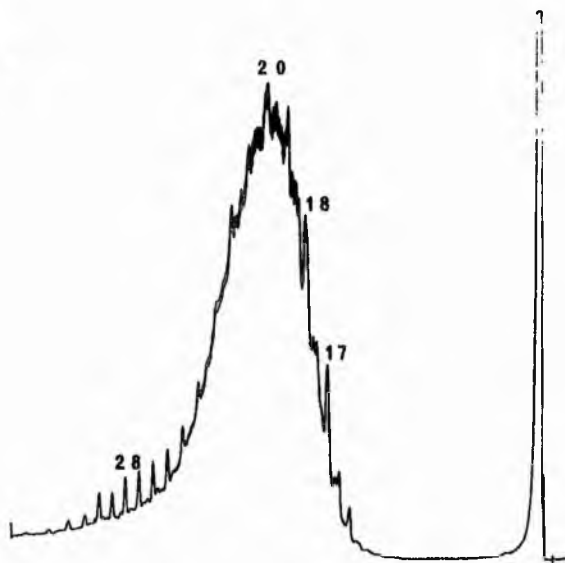
Sample DAC-1

| | |
|------------------------|---------------------------------------|
| Model of chromatograph | Varian 1200 |
| Column | 5' x 1/8" |
| Packing | 3% OV-101 on 100-120 mesh Varaport 30 |
| Column temp. | 80-300°C 6°/min. |
| Detector temp. | 300°C Injector temp. 300°C |
| Attenuation | 1 x 16 |
| Recorder | 1 mV 12 in/hr. |
| Nitrogen | 40 psi |

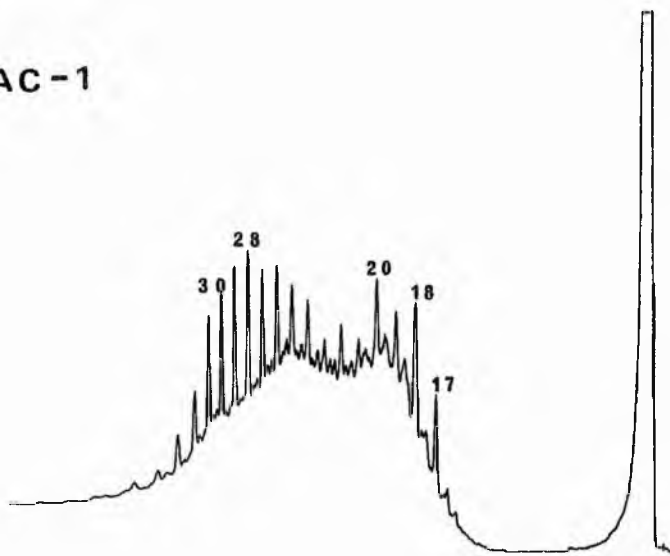
Sample DVE-2

| | |
|------------------------|---------------------------------------|
| Model of chromatograph | Varian 1200 |
| Column | 5' x 1/8" |
| Packing | 3% OV-101 on 100-120 mesh Varaport 30 |
| Column Temp. | 80-300°C 6°/min. |
| Detector temp. | 300°C Injector temp. 300°C |
| Attenuation | 1 x 16 |
| Recorder | 1 mV 12 in/hr. |
| Nitrogen | 40 psi |

DPE-2



DAC-1



DVE-2

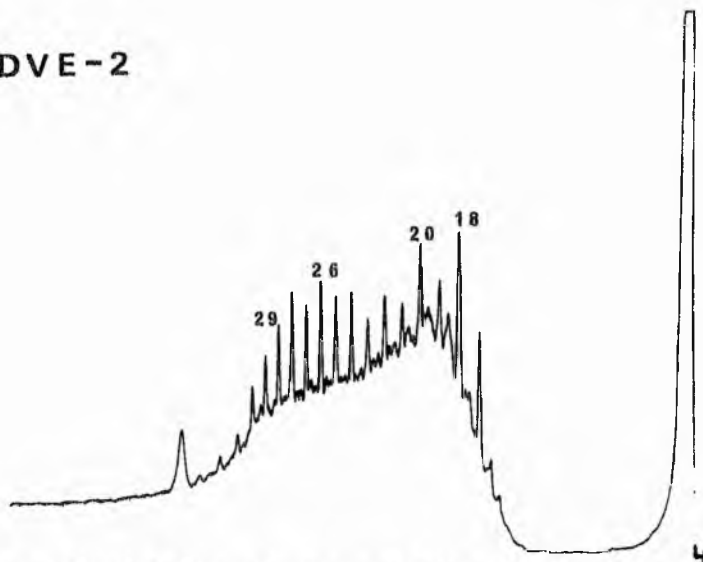


Figure 97. Gas-liquid chromatograms of the total alkanes extracted from samples DPE-2, DAC-1, DVE-2. Numbers above peaks are carbon chain lengths of coinjected n-alkanes.

Sample DCYP-1

Model of chromatograph Varian 1400
Column 10' x 1/16"
Packing 5% OV-1 on 100-120 mesh Varaport 30
Column temp. 80-300°C 4°/min.
Detector temp. 300°C Injector temp. 300°C
Attenuation 16 x 10⁻¹²
Recorder 1 mV 12 in/hr.
Nitrogen 40 psi

Sample DGR-1

Model of chromatograph Varian 1400
Column 5' x 1/8"
Packing 3% OV-101 on 100-120 mesh Varaport 30
Column temp. 80-300°C 6°/min.
Detector temp. 300°C Injector temp. 300°C
Attenuation 8 x 10⁻¹⁰
Recorder 1 mV 12 in/hr.
Nitrogen 40 psi

Sample DCV-2

Model of chromatograph Varian 1400
Column 5' x 1/8"
Packing 3% OV-101 on 100-120 mesh Varaport 30
Column temp. 80-300°C 6°/min.
Detector temp. 300°C Injector temp. 300°C
Attenuation 64 x 10⁻¹⁰
Recorder 1 mV 12 in/hr.
Nitrogen 40 psi

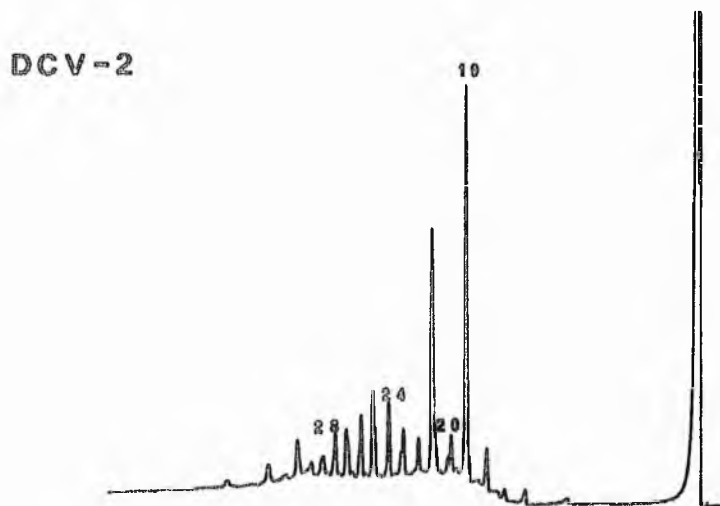
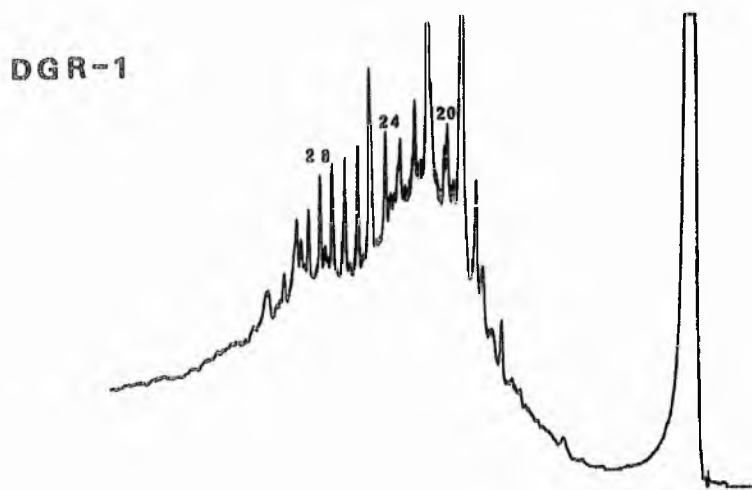
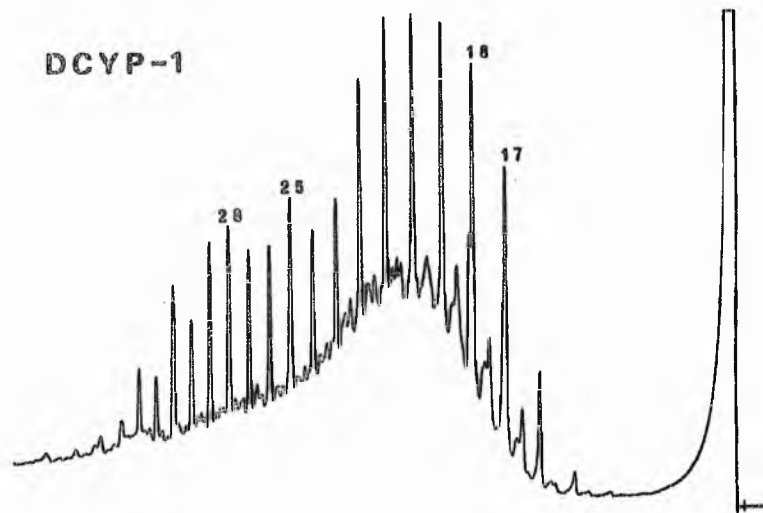


Figure 98. Gas-liquid chromatograms of the total alkanes extracted from samples DCYP-1, DGR-1, DCV-2. Numbers above peaks are carbon chain lengths of coinjected n-alkanes.

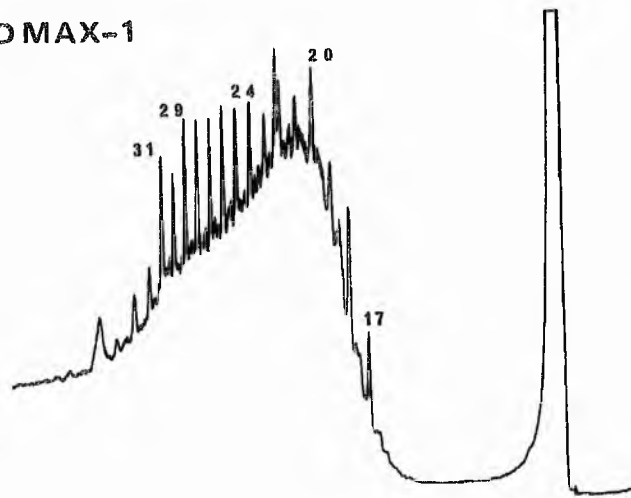
Sample DMAX-1

| | |
|------------------------|-------------------------------------|
| Model of chromatograph | Varian 1200 |
| Column | 5' x 1/8" |
| Packing | 3% OV-1 on 100-120 mesh Varaport 30 |
| Column temp. | 80-300°C 6°/min. |
| Detector temp. | 300°C Injector temp. 300°C |
| Attenuation | 8 x 1 |
| Recorder | 1 mV 12 in/hr. |
| Nitrogen | 40 psi |

Sample DSE-1

| | |
|------------------------|-------------------------------------|
| Model of chromatograph | Varian 1400 |
| Column | 5' x 1/8" |
| Packing | 3% OV-1 on 100-120 mesh Varaport 30 |
| Column temp. | 80-300°C 6°/min. |
| Detector temp. | 300°C Injector temp. 300°C |
| Attenuation | 32 x 10 ⁻¹¹ |
| Recorder | 1 mV 12 in/hr. |
| Nitrogen | 40 psi |

DMAX-1



DSE-1

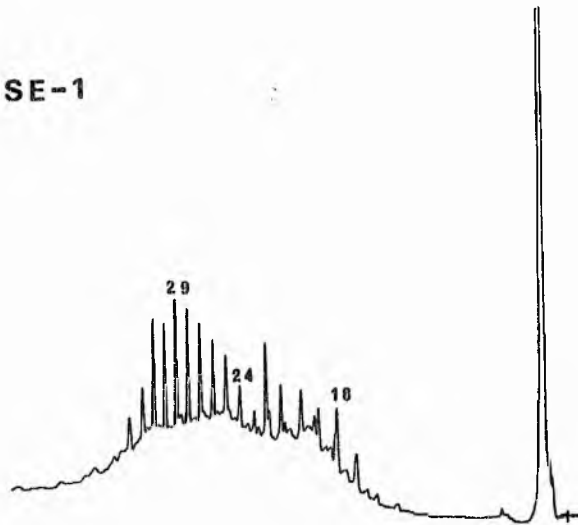


Figure 99. Gas-liquid chromatograms of the total alkanes extracted from samples DMAX-1, DSE-1. Numbers above peaks are carbon chain lengths of coinjected n-alkanes.

Sample HL-9

Model of chromatograph Varian 1400
Column 5' x 1/8"
Packing 3% OV-1 on 100-120 mesh Varaport 30
Column Temp. 70-300°C 6°/min.
Detector temp. 300°C Injector temp. 300°C
Attenuation 8 x 10⁻¹⁰
Recorder 1 mV 12 in/hr.
Nitrogen 40 psi

Sample HL-7

Model of chromatograph Varian 1400
Column 5' x 1/8"
Packing 3% OV-1 on 100-120 mesh Varaport 30
Column temp. 80-300°C 6°/min.
Detector temp. 300°C Injector temp. 300°C
Attenuation 32 x 10⁻¹¹
Recorder 1 mV 12 in/hr.
Nitrogen 40 psi

Sample HC-1

Model of chromatograph Varian 1400
Column 5' x 1/8"
Packing 3% OV-1 on 100-120 mesh Varaport 30
Column temp. 70-300°C 6°/min.
Detector temp. 300°C Injector temp. 300°C
Attenuation 8 x 10⁻¹⁰
Recorder 1 mV 12 in/hr.
Nitrogen 40 psi

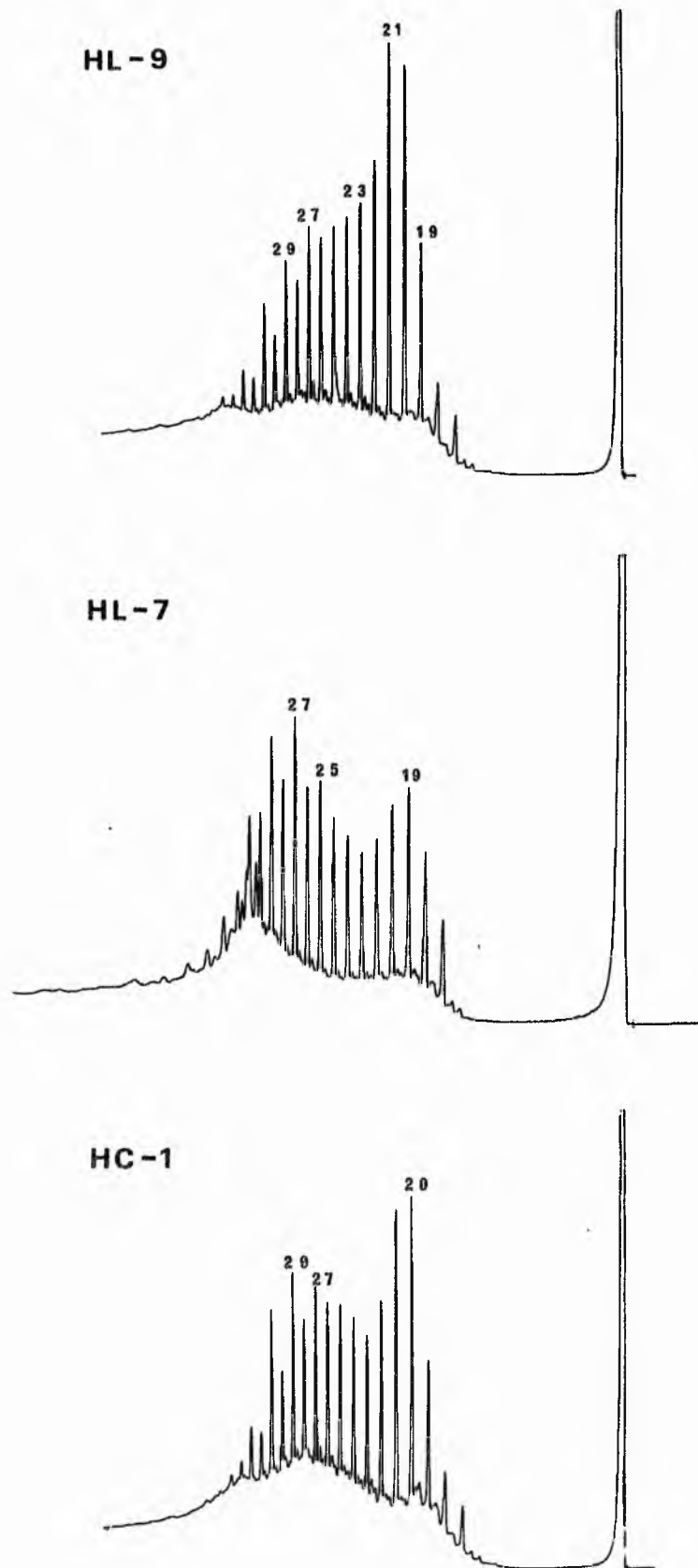


Figure 100. Gas-liquid chromatograms of the total alkanes extracted from samples HL-9, HL-7, HC-1. Numbers above peaks are carbon chain lengths of coinjected n-alkanes.

Sample HRC-1

| | | |
|------------------------|-------------------------------------|----------------------|
| Model of chromatograph | Varian 1400 | |
| Column | 5' x 1/8" | |
| Packing | 3% OV-1 on 100-120 mesh Varaport 30 | |
| Column temp. | 70-300°C | 6°/min. |
| Detector temp. | 300°C | Injector temp. 300°C |
| Attenuation | 8 x 10 ⁻¹⁰ | |
| Recorder | 1 mV | 12 in/hr. |
| Nitrogen | 40 psi | |

Sample III-11

| | | |
|------------------------|---------------------------------------|----------------------|
| Model of chromatograph | Varian 1400 | |
| Column | 5' x 1/8" | |
| Packing | 3% OV-101 on 100-120 mesh Varaport 30 | |
| Column temp. | 80-300°C | 6°/min. |
| Detector temp. | 300°C | Injector temp. 300°C |
| Attenuation | 32 x 10 ⁻¹¹ | |
| Recorder | 1 mV | 12 in/hr. |
| Nitrogen | 40 psi | |

Sample HW-2

| | | |
|------------------------|---------------------------------------|----------------------|
| Model of chromatograph | Varian 1200 | |
| Column | 5' x 1/8" | |
| Packing | 3% OV-101 on 100-120 mesh Varaport 30 | |
| Column temp. | 80-300°C | 6°/min. |
| Detector temp. | 300°C | Injector temp. 300°C |
| Attenuation | 32 x 1 | |
| Recorder | 1 mV | 12 in/hr. |
| Nitrogen | 40 psi | |

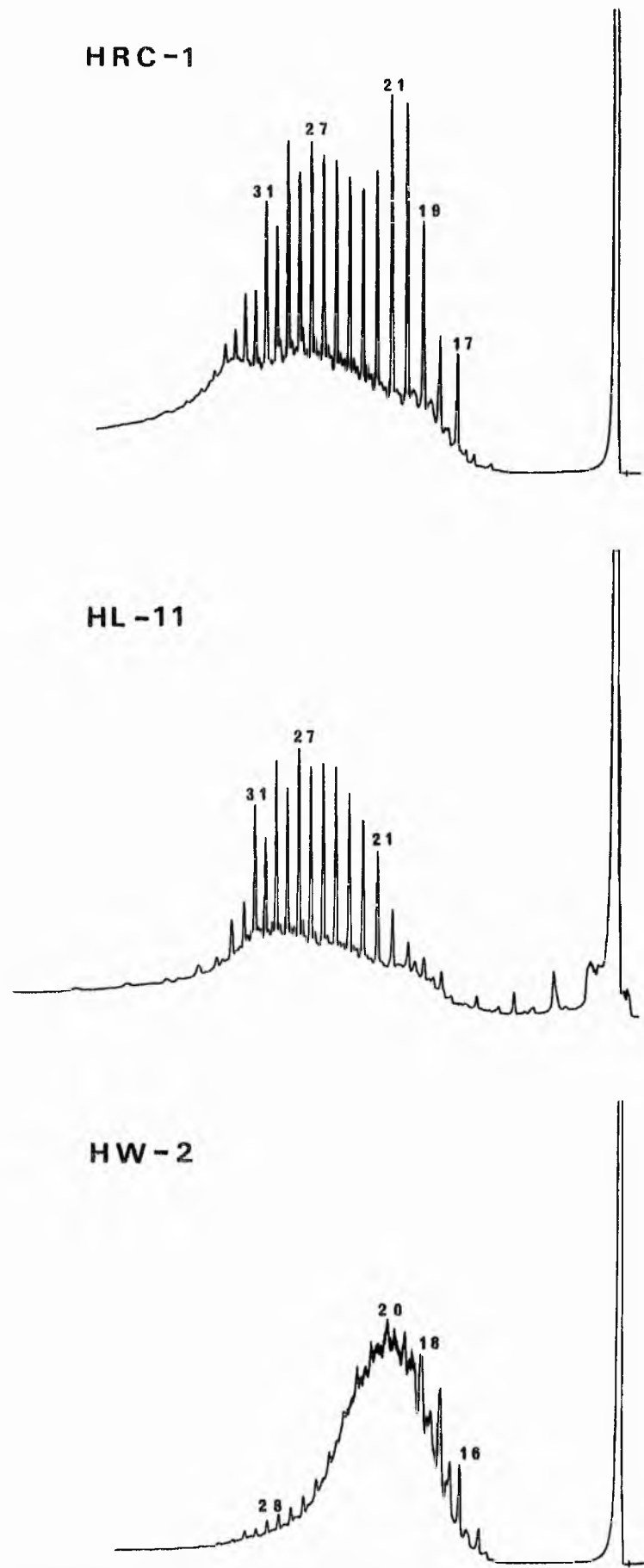


Figure 101. Gas-liquid chromatograms of the total alkanes extracted from samples HRC-1, HL-11, HW-2. Numbers above peaks are carbon chain lengths of coinjected n-alkanes.

Sample HW-1

| | | |
|------------------------|-------------------------------------|----------------------|
| Model of chromatograph | Varian 1200 | |
| Column | 5' x 1/8" | |
| Packing | 3% OV-1 on 100-120 mesh Varaport 30 | |
| Column temp. | 80-300°C | 6°/min. |
| Detector temp. | 300°C | Injector temp. 300°C |
| Attenuation | 32 x 1 | |
| Recorder | 1 mV | 12 in/hr. |
| Nitrogen | 40 psi | |

Sample HCL-4

| | | |
|------------------------|-------------------------------------|----------------------|
| Model of chromatograph | Varian 1400 | |
| Column | 5' x 1/8" | |
| Packing | 3% OV-1 on 100-120 mesh Varaport 30 | |
| Column temp. | 80-300°C | 6°/min. |
| Detector temp. | 300°C | Injector temp. 300°C |
| Attenuation | 16 x 10 ⁻¹¹ | |
| Recorder | 1 mV | 12 in/hr. |
| Nitrogen | 40 psi | |

Sample HG-1

| | | |
|------------------------|-------------------------------------|----------------------|
| Model of chromatograph | Varian 1400 | |
| Column | 5' x 1/8" | |
| Packing | 3% OV-1 on 100-120 mesh Varaport 30 | |
| Column temp. | 70-300°C | 6°/min. |
| Detector temp. | 300°C | Injector temp. 300°C |
| Attenuation | 8 x 10 ⁻¹⁰ | |
| Recorder | 1 mV | 12 in/hr. |
| Nitrogen | 40 psi | |

Figure 102. Gas-liquid chromatograms of the total alkanes extracted from samples HW-4, HCL-4, HG-1. Numbers above peaks are carbon chain lengths of coinjected n-alkanes.

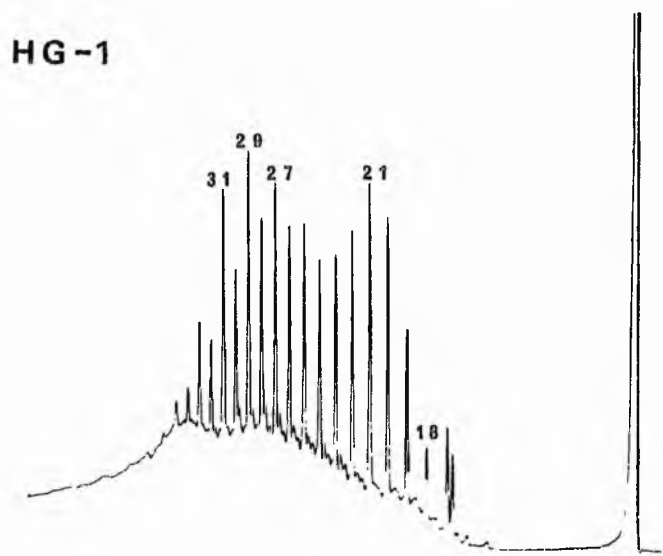
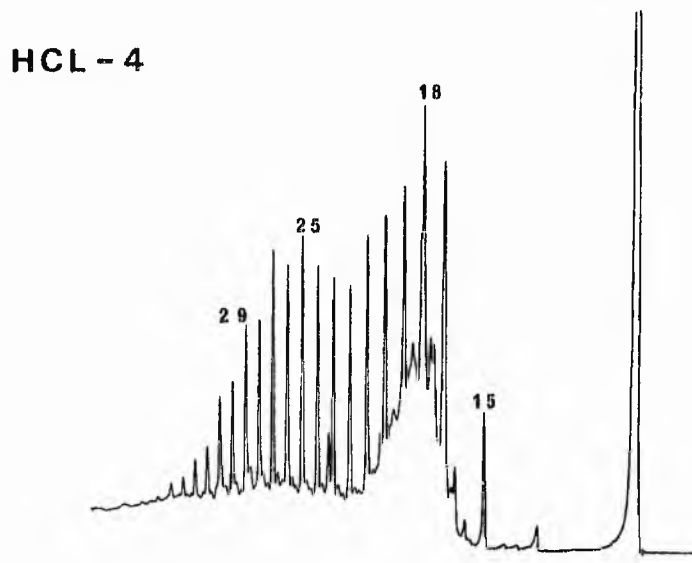
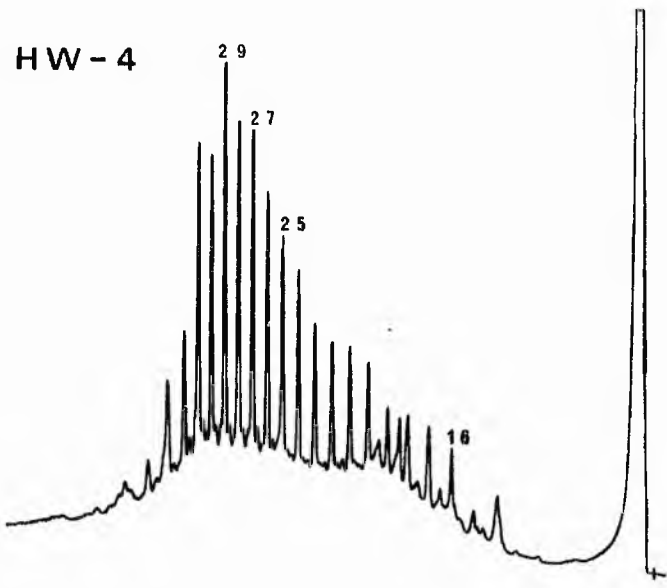


Figure 102.

Sample HW-3

| | | |
|------------------------|-------------------------------------|----------------------|
| Model of chromatograph | Varian 1200 | |
| Column | 5' x 1/8" | |
| Packing | 3% OV-1 on 100-120 mesh Varaport 30 | |
| Column temp. | 80-300°C | 6°/min. |
| Detector temp. | 300°C | Injector temp. 300°C |
| Attenuation | 64 x 1 | |
| Recorder | 1 mV | 12 in/hr. |
| Nitrogen | 40 psi | |

Sample HCL-1

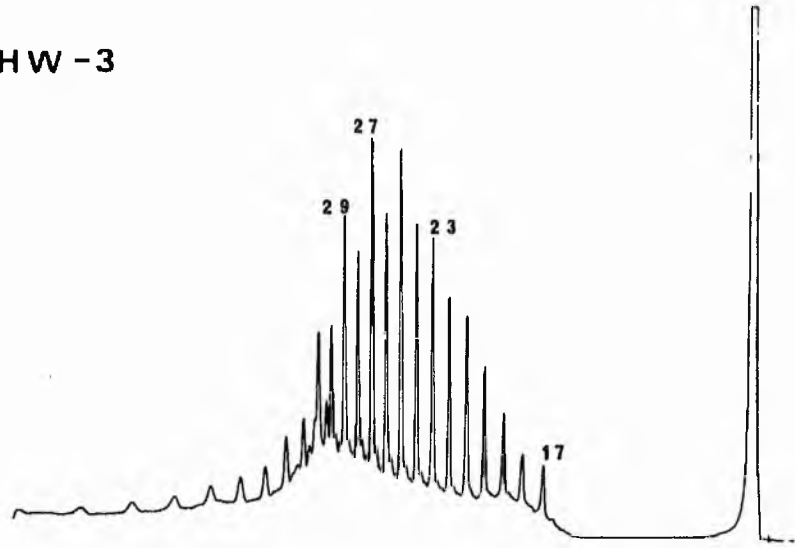
| | | |
|------------------------|---------------------------------------|----------------------|
| Model of chromatograph | Varian 1200 | |
| Column | 5' x 1/8" | |
| Packing | 3% OV-101 on 100-120 mesh Varaport 30 | |
| Column temp. | 80-300°C | 6°/min. |
| Detector temp. | 300°C | Injector temp. 300°C |
| Attenuation | 64 x 1 | |
| Recorder | 1 mV | 12 in/hr. |
| Nitrogen | 40 psi | |

Sample HCL-2

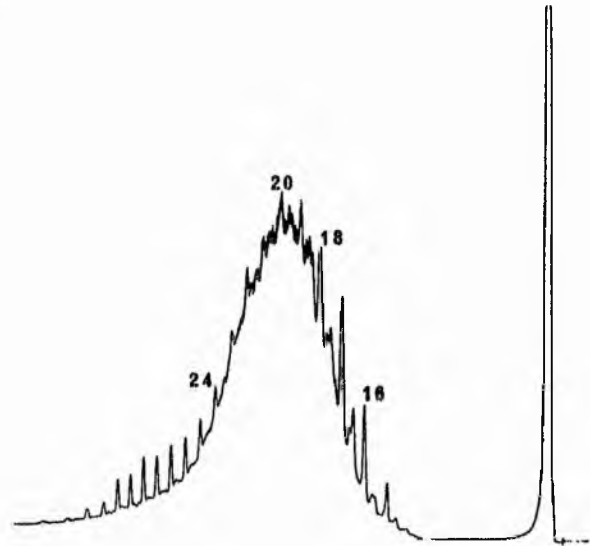
| | | |
|------------------------|---------------------------------------|----------------------|
| Model of chromatograph | Varian 1400 | |
| Column | 10' x 1/8" | |
| Packing | 3% OV-101 on 100-120 mesh Varaport 30 | |
| Column temp. | 70-300°C | 4°/min. |
| Detector temp. | 300°C | Injector temp. 300°C |
| Attenuation | 8 x 10 ⁻¹¹ | |
| Recorder | 1 mV | 12 in/hr. |
| Nitrogen | 40 psi | |

Figure 103. Gas-liquid chromatograms of the total alkanes extracted from samples HW-3, HCL-1, HCL-2. Numbers above peaks are carbon chain lengths of coinjected n-alkanes.

HW - 3



HCL-1



HCL-2

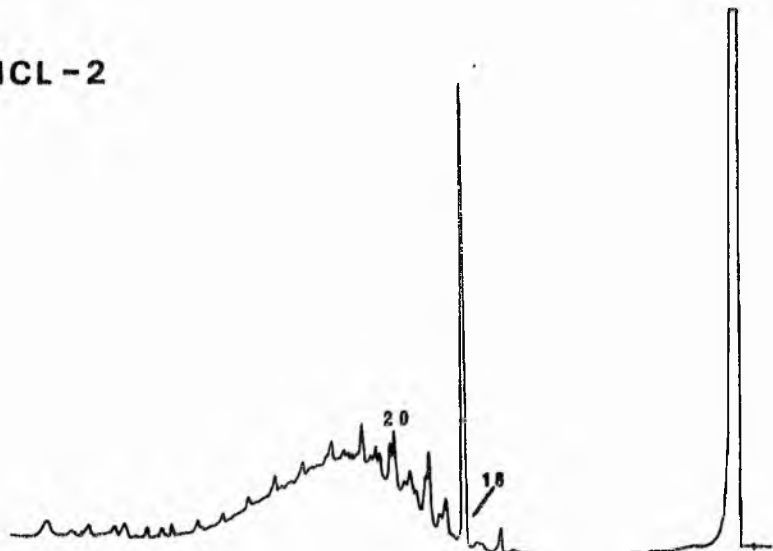


Figure 103.

Sample HCL-5

| | |
|------------------------|---------------------------------------|
| Model of chromatograph | Varian 1200 |
| Column | 5' x 1/8" |
| Packing | 3% OV-101 on 100-120 mesh Varaport 30 |
| Column temp. | 80-300°C 6°/min. |
| Detector temp. | 300°C Injector temp. 300°C |
| Attenuation | 32 x 1 |
| Recorder | 1 mV 12 in/hr. |
| Nitrogen | 40 psi |

Sample HCL-6

| | |
|------------------------|-------------------------------------|
| Model of chromatograph | Varian 1400 |
| Column | 5' x 1/8" |
| Packing | 3% OV-1 on 100-120 mesh Varaport 30 |
| Column temp. | 80-300°C 6°/min. |
| Detector temp. | 300°C Injector temp. 300°C |
| Attenuation | 8 x 10 ⁻¹⁰ |
| Recorder | 1 mV 12 in/hr. |
| Nitrogen | 40 psi |

Sample HCL-3

| | |
|------------------------|---------------------------------------|
| Model of chromatograph | Varian 1400 |
| Column | 5' x 1/8" |
| Packing | 3% OV-101 on 100-120 mesh Varaport 30 |
| Column temp. | 80-300°C 6°/min. |
| Detector temp. | 300°C Injector temp. 300°C |
| Attenuation | 128 x 10 ⁻¹¹ |
| Recorder | 1 mV 12 in/hr. |
| Nitrogen | 40 psi |

Figure 104. Gas-liquid chromatograms of the total alkanes extracted from samples HCL-5, HCL-6, HCL-3. Numbers above peaks are carbon chain lengths of coinjected n-alkanes.

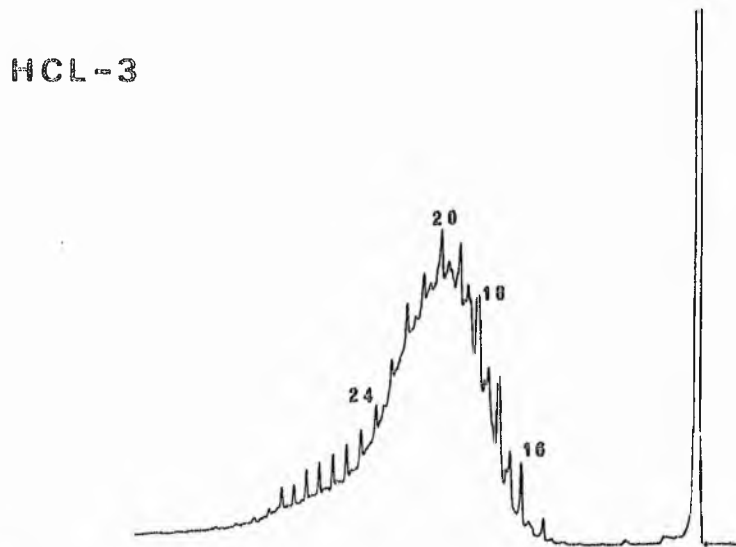
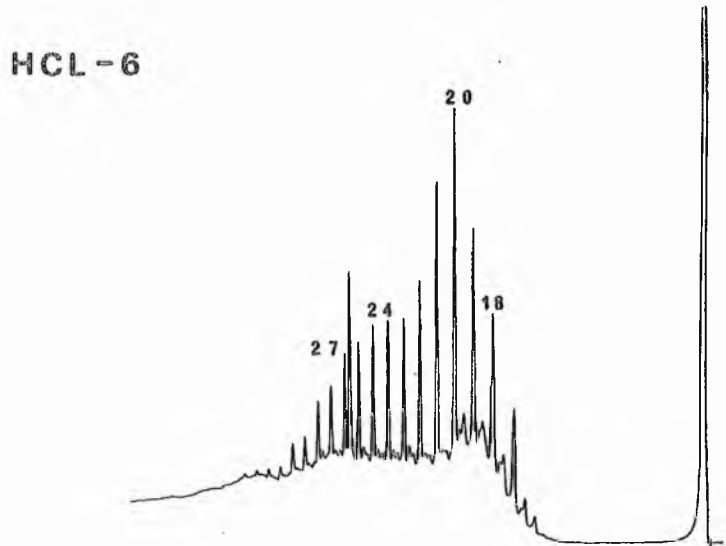
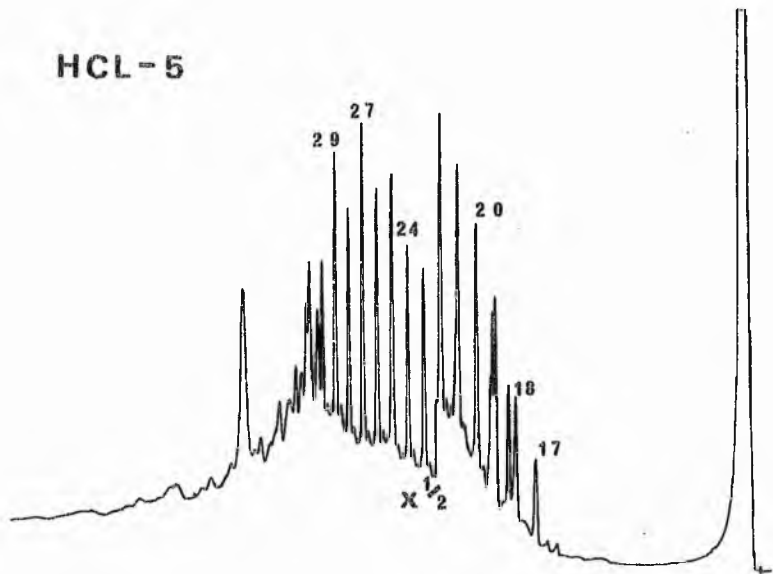


Figure 104.

Sample III-3

| | | |
|------------------------|-------------------------------------|----------------------|
| Model of chromatograph | Varian 1400 | |
| Column | 10' x 1/16" | |
| Packing | 5% OV-1 on 100-120 mesh Varaport 30 | |
| Column temp. | 80-300°C | 4°/min. |
| Detector temp. | 300°C | Injector temp. 300°C |
| Attenuation | 16 x 10 ⁻¹² | |
| Recorder | 1 mV | 12 in/hr. |
| Nitrogen | 40 psi | |

Sample III-14

| | | |
|------------------------|---------------------------------------|----------------------|
| Model of chromatograph | Varian 1400 | |
| Column | 5' x 1/8" | |
| Packing | 3% OV-101 on 100-120 mesh Varaport 30 | |
| Column temp. | 80-300°C | 6°/min. |
| Detector temp. | 300°C | Injector temp. 300°C |
| Attenuation | 32 x 10 ⁻¹¹ | |
| Recorder | 1 mV | 12 in/hr. |
| Nitrogen | 40 psi | |

Sample III-15

| | | |
|------------------------|---------------------------------------|----------------------|
| Model of chromatograph | Varian 1400 | |
| Column | 5' x 1/8" | |
| Packing | 3% OV-101 on 100-120 mesh Varaport 30 | |
| Column temp. | 80-300°C | 6°/min. |
| Detector temp. | 300°C | Injector temp. 300°C |
| Attenuation | 16 x 10 ⁻¹¹ | |
| Recorder | 1 mV | 12 in/hr. |
| Nitrogen | 40 psi | |

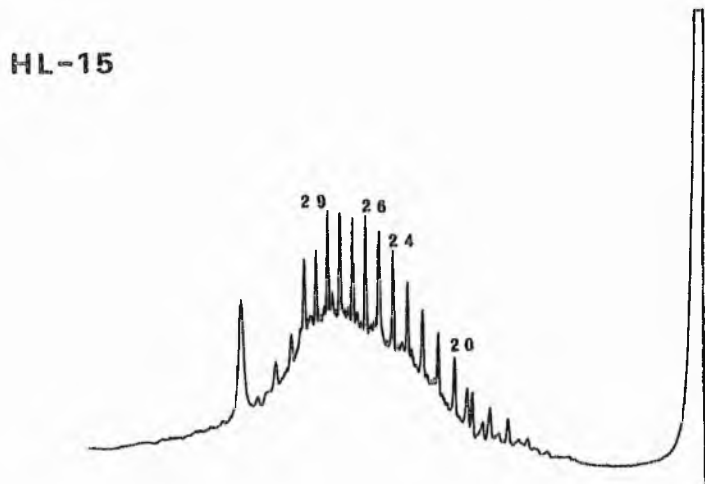
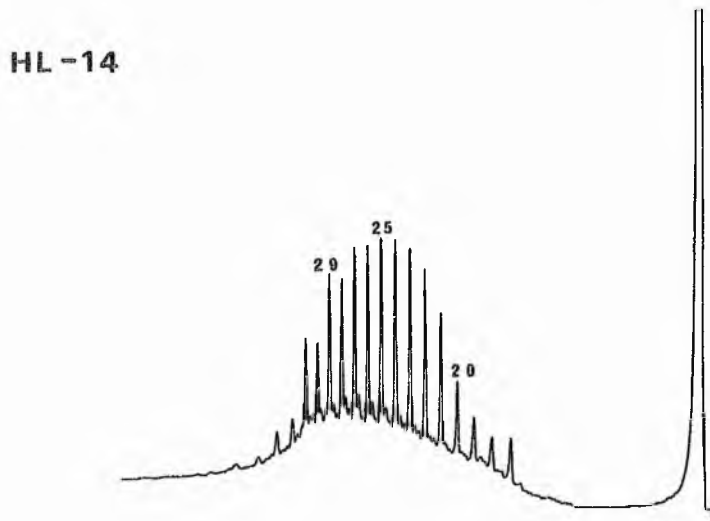
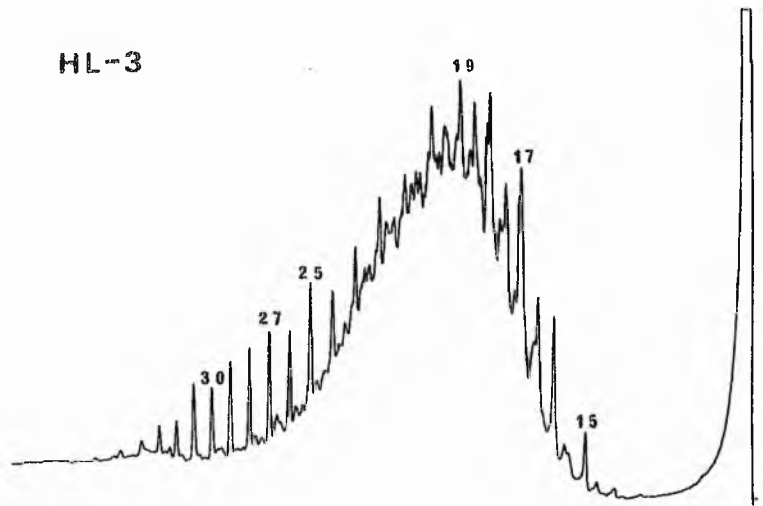


Figure 105. Gas-liquid chromatograms of the total alkanes extracted from samples HL-3, HL-14, HL-15. Numbers above peaks are carbon chain lengths of coinjected n-alkanes.

Sample HG-2

| | | |
|------------------------|---------------------------------------|----------------------|
| Model of chromatograph | Varian 1400 | |
| Column | 5' x 1/8" | |
| Packing | 3% OV-101 on 100-120 mesh Varaport 30 | |
| Column temp. | 80-300°C | 6°/min. |
| Detector temp. | 300°C | Injector temp. 300°C |
| Attenuation | 32 x 10 ⁻¹¹ | |
| Recorder | 1 mV | 12 in/hr. |
| Nitrogen | 40 psi | |

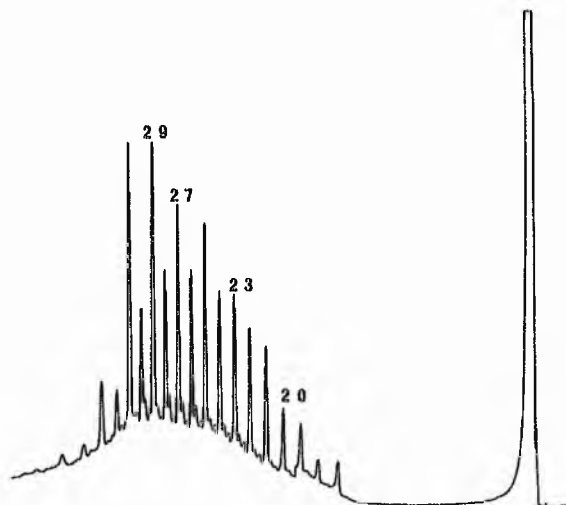
Sample HW-1

| | | |
|------------------------|-------------------------------------|----------------------|
| Model of chromatograph | Varian 1400 | |
| Column | 10' x 1/16" | |
| Packing | 5% OV-1 on 100-120 mesh Varaport 30 | |
| Column temp. | 80-300°C | 4°/min. |
| Detector temp. | 300°C | Injector temp. 300°C |
| Attenuation | 32 x 10 ⁻¹¹ | |
| Recorder | 1 mV | 12 in/hr. |
| Nitrogen | 40 psi | |

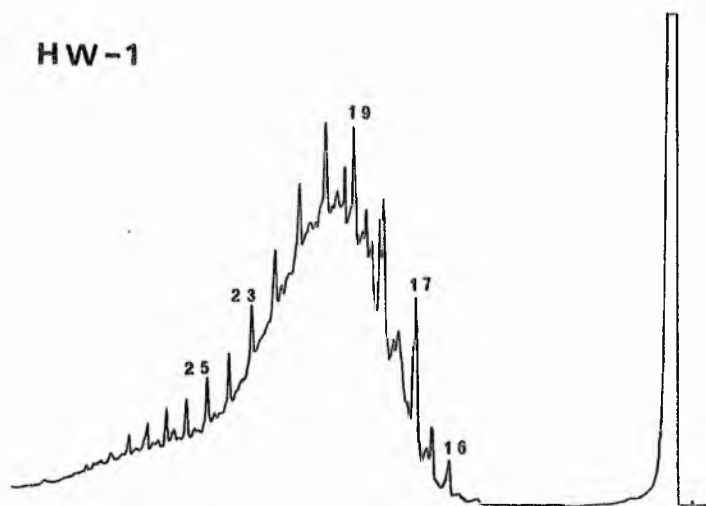
Sample HW-5

| | | |
|------------------------|-------------------------------------|----------------------|
| Model of chromatograph | Varian 1400 | |
| Column | 5' x 1/8" | |
| Packing | 3% OV-1 on 100-120 mesh Varaport 30 | |
| Column temp. | 70-300°C | 6°/min. |
| Detector temp. | 300°C | Injector temp. 300°C |
| Attenuation | 8 x 10 ⁻¹⁰ | |
| Recorder | 1 mV | 12 in/hr. |
| Nitrogen | 40 psi | |

HG-2



HW-1



HW-5

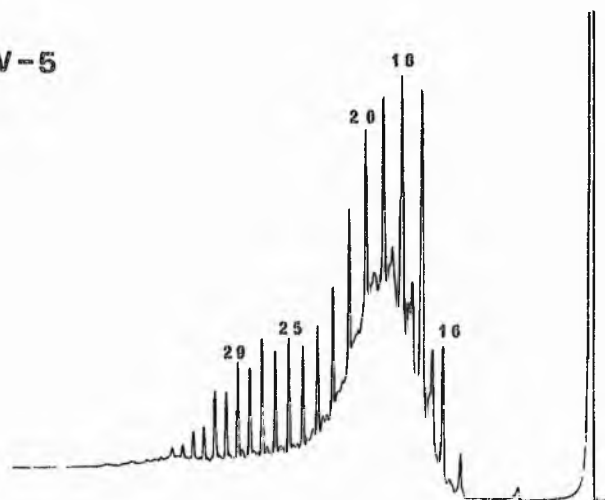


Figure 106. Gas-liquid chromatograms of the total alkanes extracted from samples HG-2, HW-1, HW-5. Numbers above peaks are carbon chain lengths of coinjected n-alkanes.

Sample CLAN-1

| | | |
|------------------------|-------------------------------------|----------------------|
| Model of chromatograph | Varian 1400 | |
| Column | 5' x 1/8" | |
| Packing | 3% OV-1 on 100-120 mesh Varaport 30 | |
| Column temp. | 80-300°C | 6°/min. |
| Detector temp. | 300°C | Injector temp. 300°C |
| Attenuation | 32 x 10 ⁻¹¹ | |
| Recorder | 1 mV | 12 in/hr. |
| Nitrogen | 40 psi | |

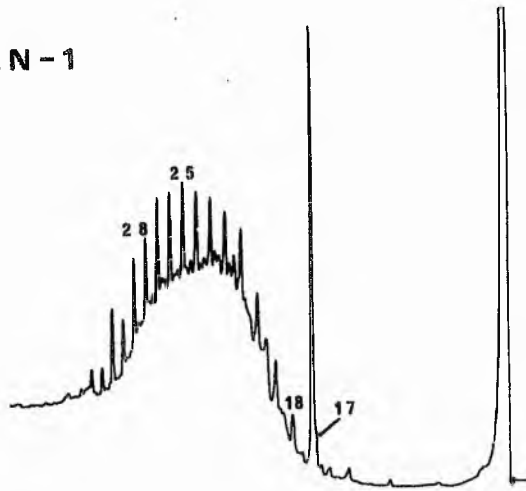
Sample CLAN-2

| | | |
|------------------------|-------------------------------------|----------------------|
| Model of chromatograph | Varian 1400 | |
| Column | 5' x 1/8" | |
| Packing | 3% OV-1 on 100-120 mesh Varaport 30 | |
| Column temp. | 70-300°C | 6°/min. |
| Detector temp. | 300°C | Injector temp. 300°C |
| Attenuation | 32 x 10 ⁻¹¹ | |
| Recorder | 1 mV | 12 in/hr. |
| Nitrogen | 40 psi | |

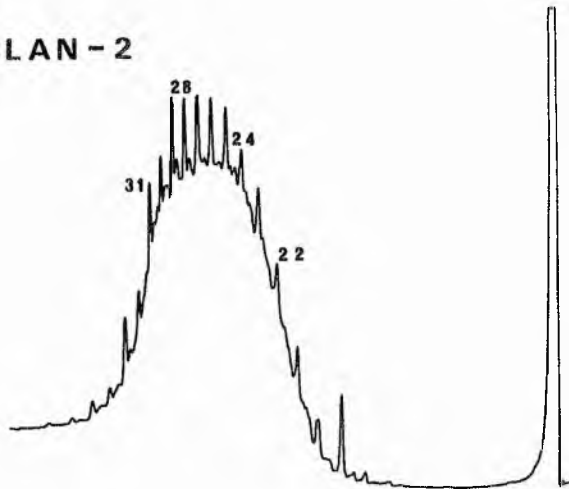
Sample CLAN-3

| | | |
|------------------------|-------------------------------------|----------------------|
| Model of chromatograph | Varian 1400 | |
| Column | 5' x 1/8" | |
| Packing | 3% OV-1 on 100-120 mesh Varaport 30 | |
| Column temp. | 70-300°C | 6°/min. |
| Detector temp. | 300°C | Injector temp. 300°C |
| Attenuation | 32 x 10 ⁻¹¹ | |
| Recorder | 1 mV | 12 in/hr. |
| Nitrogen | 40 psi | |

CLAN-1



CLAN-2



CLAN-3

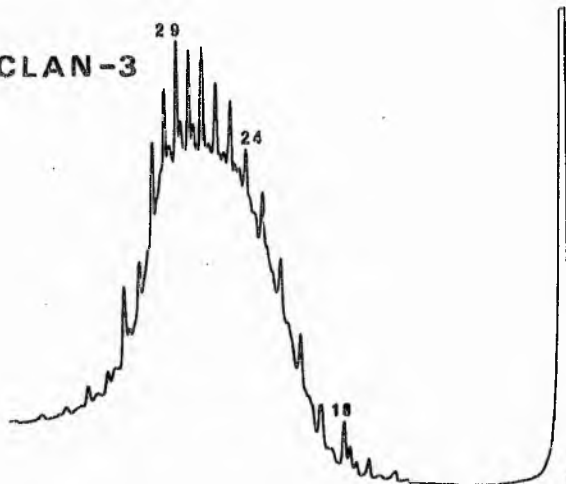


Figure 107. Gas-liquid chromatograms of the total alkanes extracted from samples CLAN-1, CLAN-2, CLAN-3. Numbers above peaks are carbon chain lengths of coinjected n-alkanes.

Sample CLAN-4

Model of chromatograph Varian 1400
Column 5' x 1/8"
Packing 3% OV-1 on 100-120 mesh Varaport 30
Column temp. 70-300°C 6°/min.
Detector temp. 300°C Injector temp. 300°C
Attenuation 32 x 10⁻¹¹
Recorder 1 mV 12 in/hr.
Nitrogen 40 psi

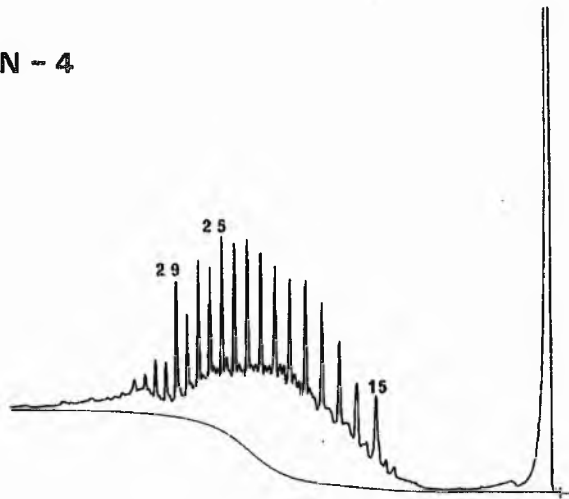
Sample CLAN-5

Model of chromatograph Varian 1400
Column 5' x 1/8"
Packing 3% OV-1 on 100-120 mesh Varaport 30
Column temp. 70-300°C 6°/min.
Detector temp. 300°C Injector temp. 300°C
Attenuation 16 x 10⁻¹¹
Recorder 1 mV 12 in/hr.
Nitrogen 40 psi

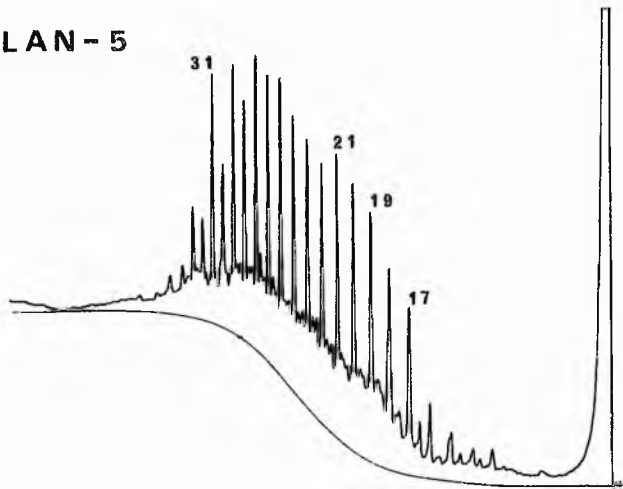
Sample CLAN-6

Model of chromatograph Varian 1400
Column 5' x 1/8"
Packing 3% OV-1 on 100-120 mesh Varaport 30
Column temp. 80-300°C 6°/min.
Detector temp. 300°C Injector temp. 300°C
Attenuation 16 x 10⁻¹¹
Recorder 1 mV 12 in/hr.
Nitrogen 40 psi

CLAN - 4



CLAN - 5



CLAN - 6

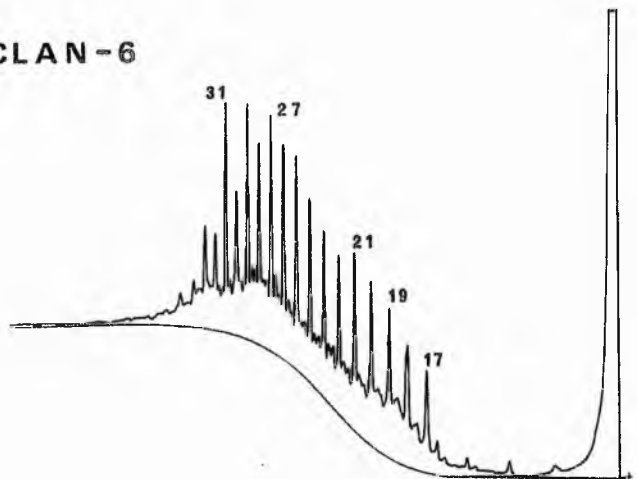


Figure 108. Gas-liquid chromatograms of the total alkanes extracted from samples CLAN-4, CLAN-5, CLAN-6. Numbers above peaks are carbon chain lengths of coinjected n-alkanes.

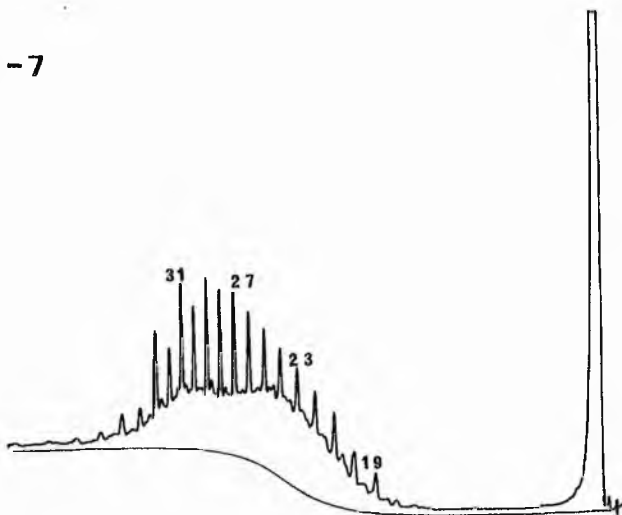
Sample CLAN-7

| | | |
|------------------------|-------------------------------------|----------------------|
| Model of chromatograph | Varian 1400 | |
| Column | 5' x 1/8" | |
| Packing | 3% OV-1 on 100-120 mesh Varaport 30 | |
| Column temp. | 80-300°C | 6°/min. |
| Detector temp. | 300°C | Injector temp. 300°C |
| Attenuation | 32 x 10 ⁻¹¹ | |
| Recorder | 1 mV | 12 in/hr. |
| Nitrogen | 40 psi | |

Sample CLAN 'TAR'

| | | |
|------------------------|-------------------------------------|----------------------|
| Model of chromatograph | Varian 1400 | |
| Column | 5' x 1/8" | |
| Packing | 3% OV-1 on 100-120 mesh Varaport 30 | |
| Column temp. | 70-300°C | 6°/min. |
| Detector temp. | 300°C | Injector temp. 300°C |
| Attenuation | 16 x 10 ⁻¹⁰ | |
| Recorder | 1 mV | 12 in/hr. |
| Nitrogen | 40 psi | |

CLAN-7



CLAN 'TAR'

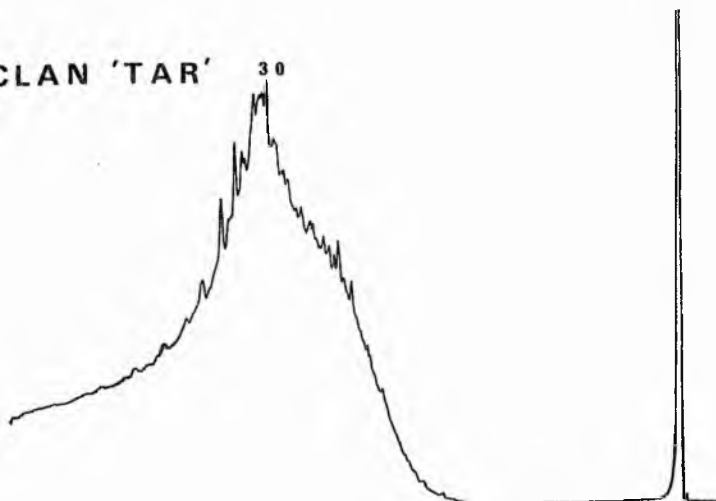


Figure 109. Gas-liquid chromatograms of the total alkanes extracted from sample CLAN-7 and from a contaminatory 'tar' found in a fracture at Clanyard Bay. Numbers above peaks are carbon chain lengths of coinjected n-alkanes.

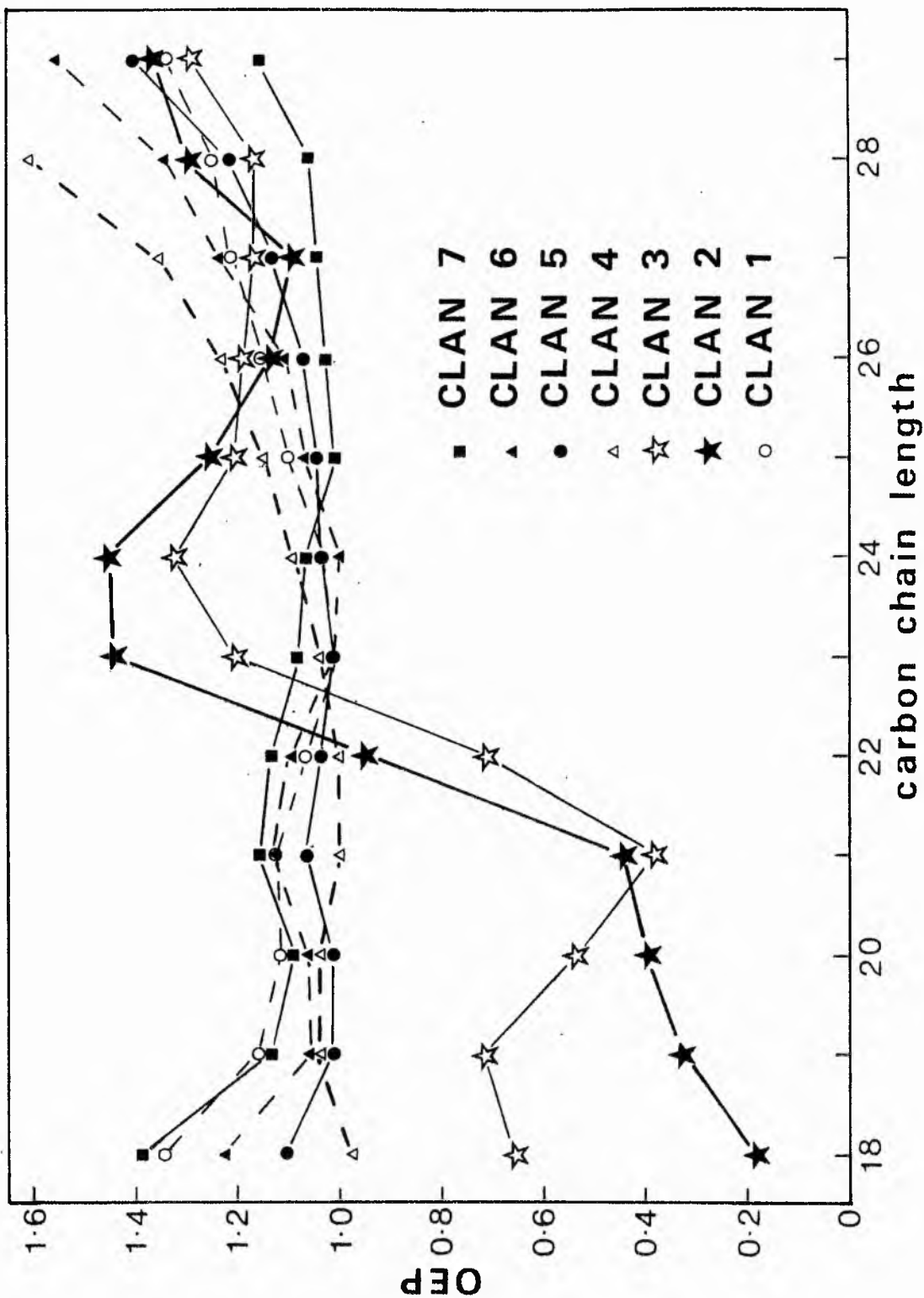


Figure 110. Plot of the variation in odd-even predominance values with respect to carbon chain length for samples collected adjacent the dyke at Clanyard Bay.

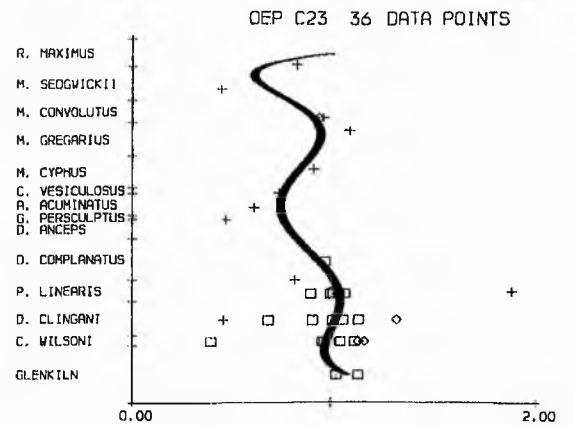
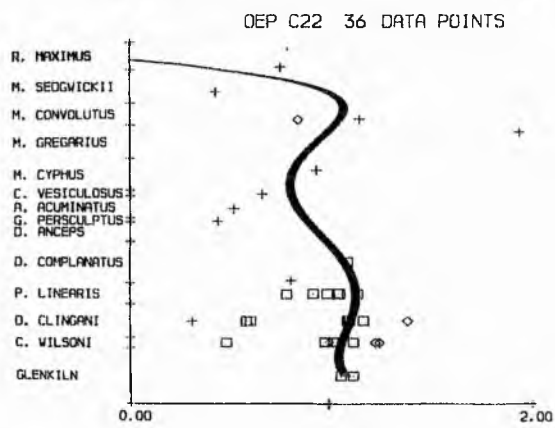
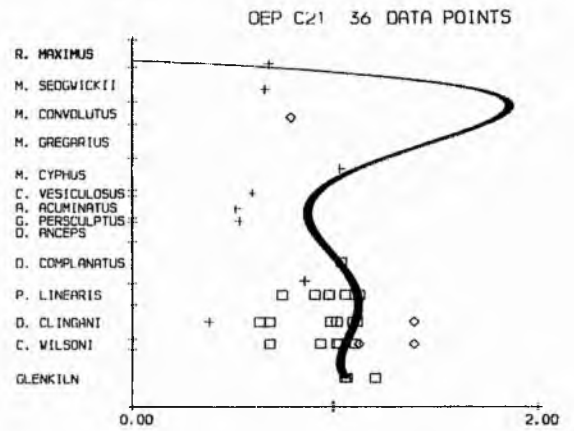
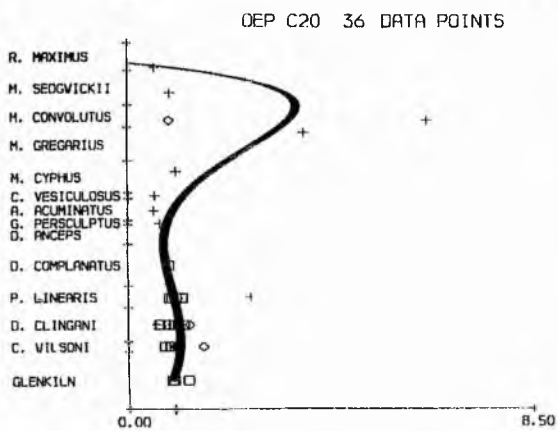
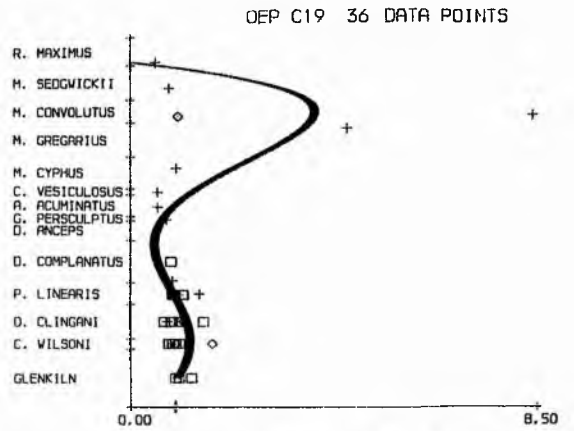
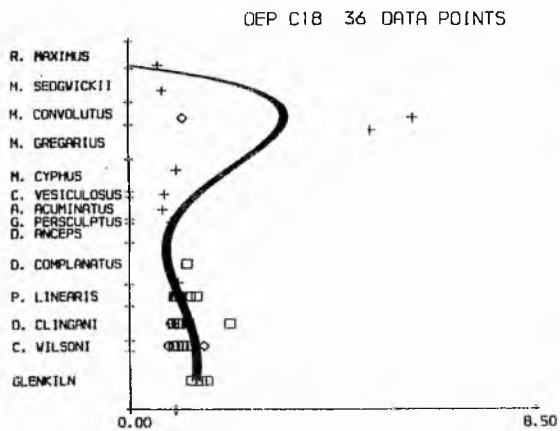


Figure 111. Plots illustrating the stratigraphic variation in the Moffat Shales of odd-even predominance values at various carbon chain lengths. Key to localities is given in Figure 94.

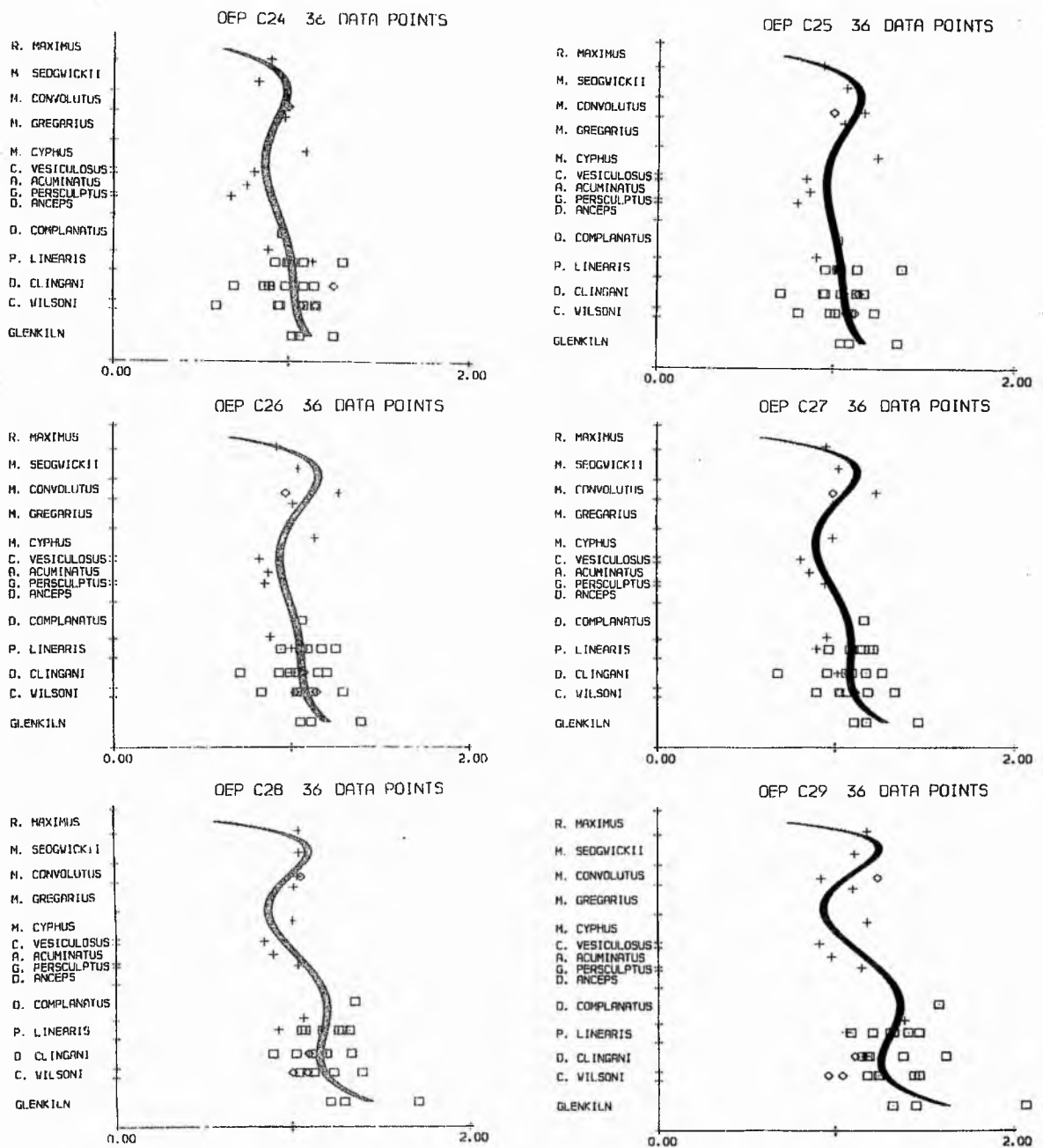


Figure 112. Plots illustrating the stratigraphic variation in the Moffat Shales of odd-even predominance values at various carbon chain lengths. Key to localities is given in Figure 94.

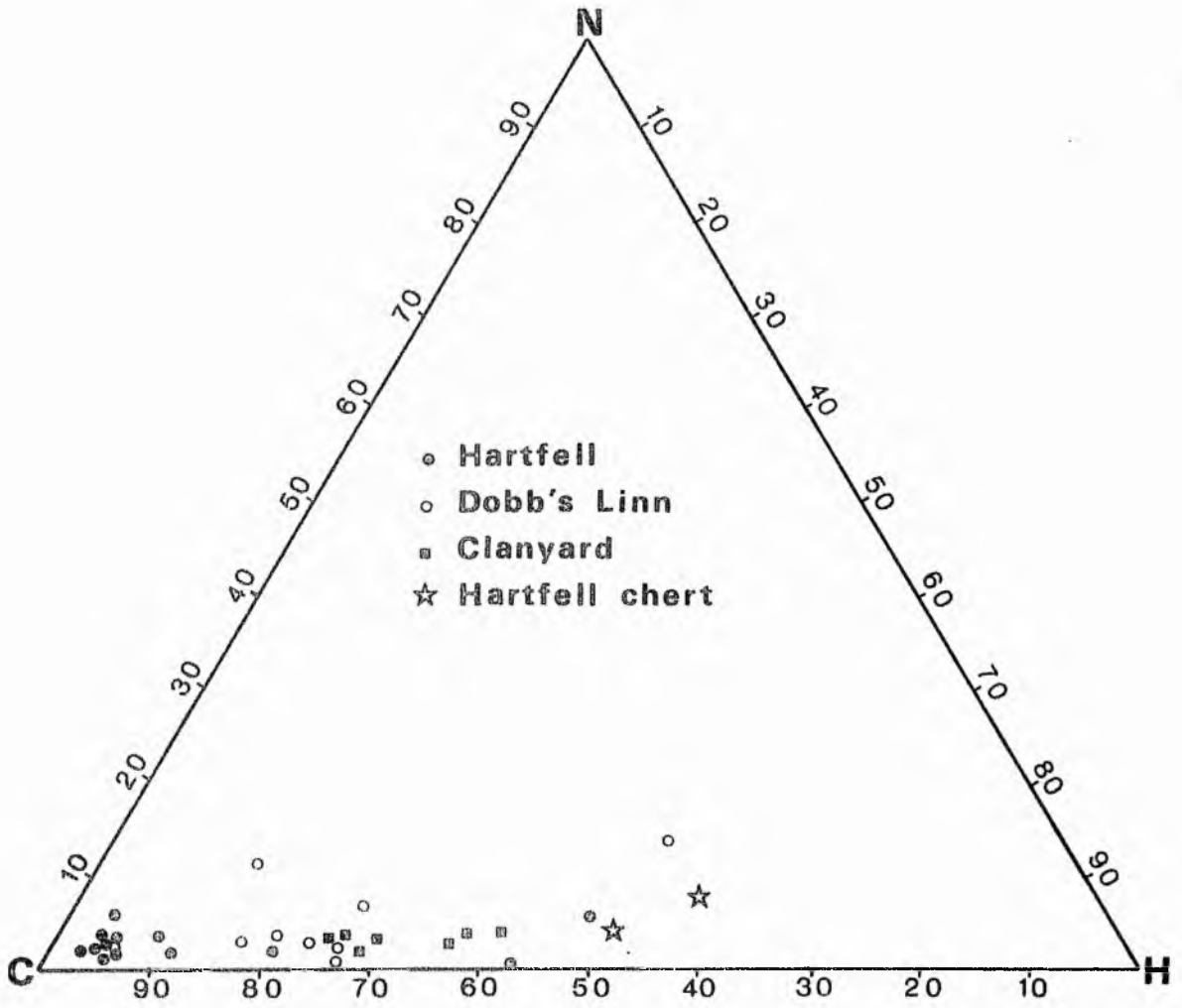


Figure 113. Triangular variation diagram illustrating the chemical variation (d.a.f.) of Moffat Shale kerogenous isolates.

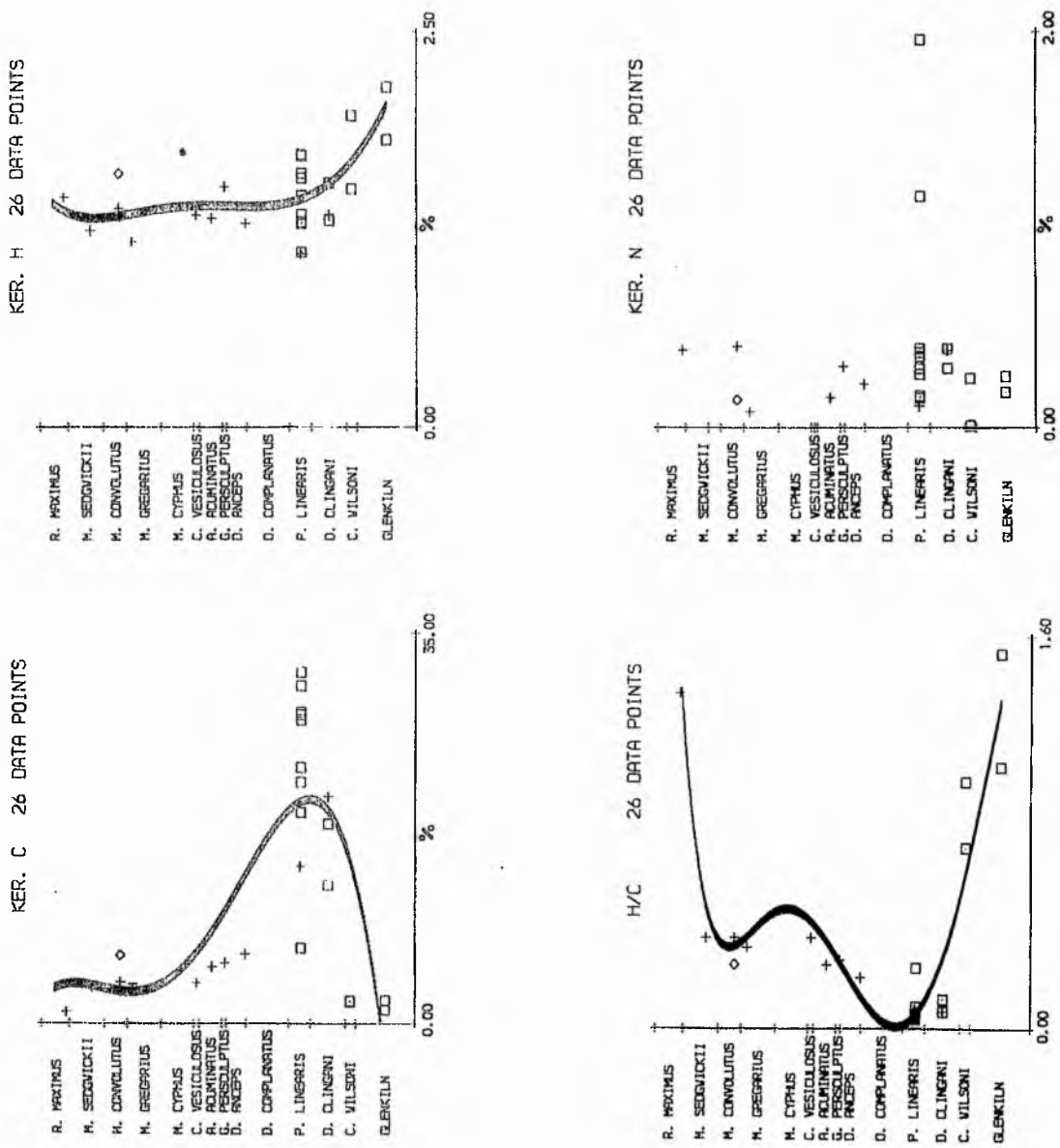


Figure 114. Plots illustrating the stratigraphic variation in the Moffat Shales of the elemental composition of Moffat Shale kerogen isolates. Key to localities is given in Figure 94.

Figure 115. X-ray diffraction traces between 25.5 and 27.5° two-theta for Moffat Shale kerogen isolates. Hartfell samples are arranged with respect to height up the cliff, f indicates position of major thrust. Dobb's Linn samples are arranged in stratigraphic order.

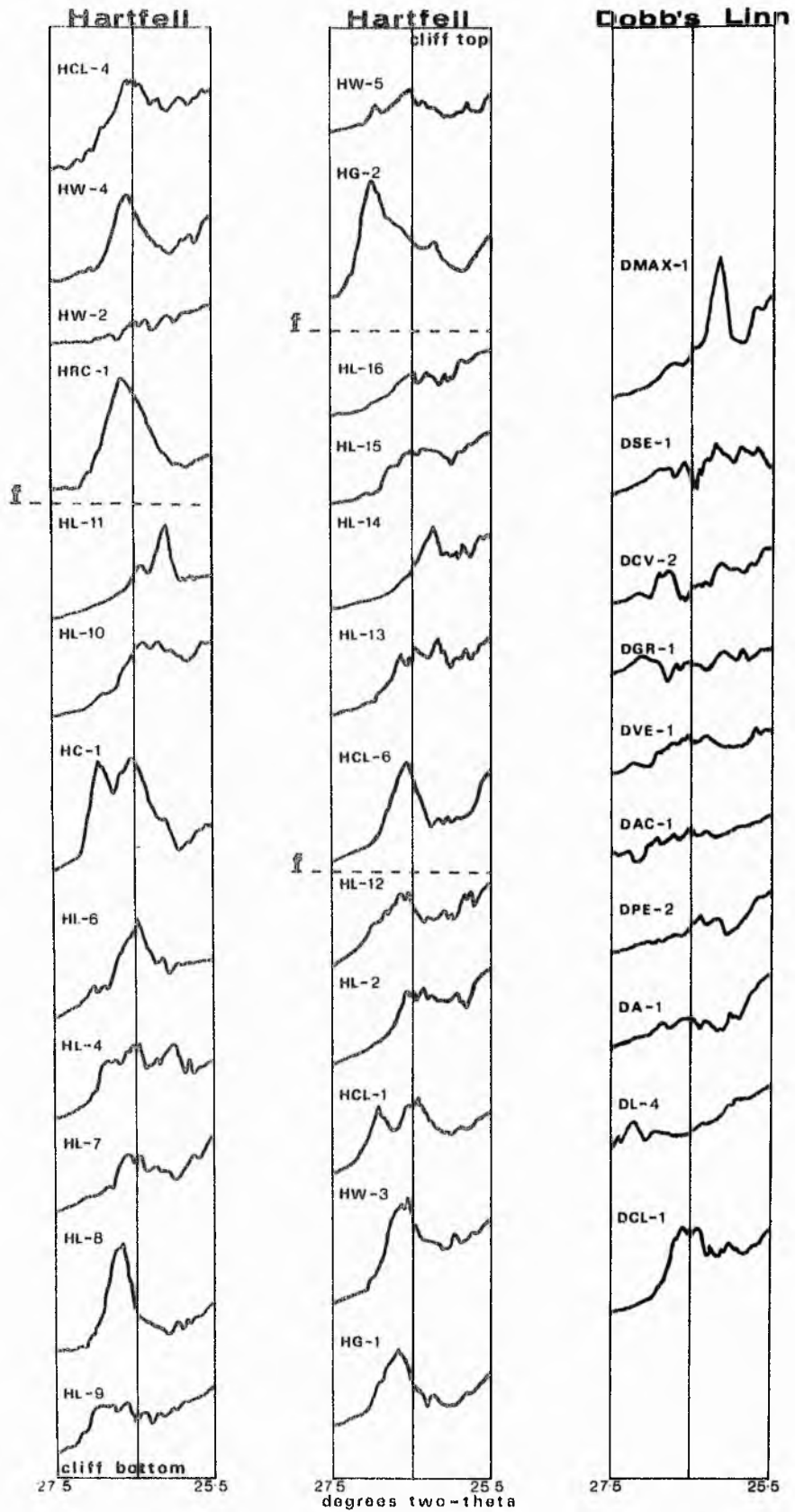


Figure 115.

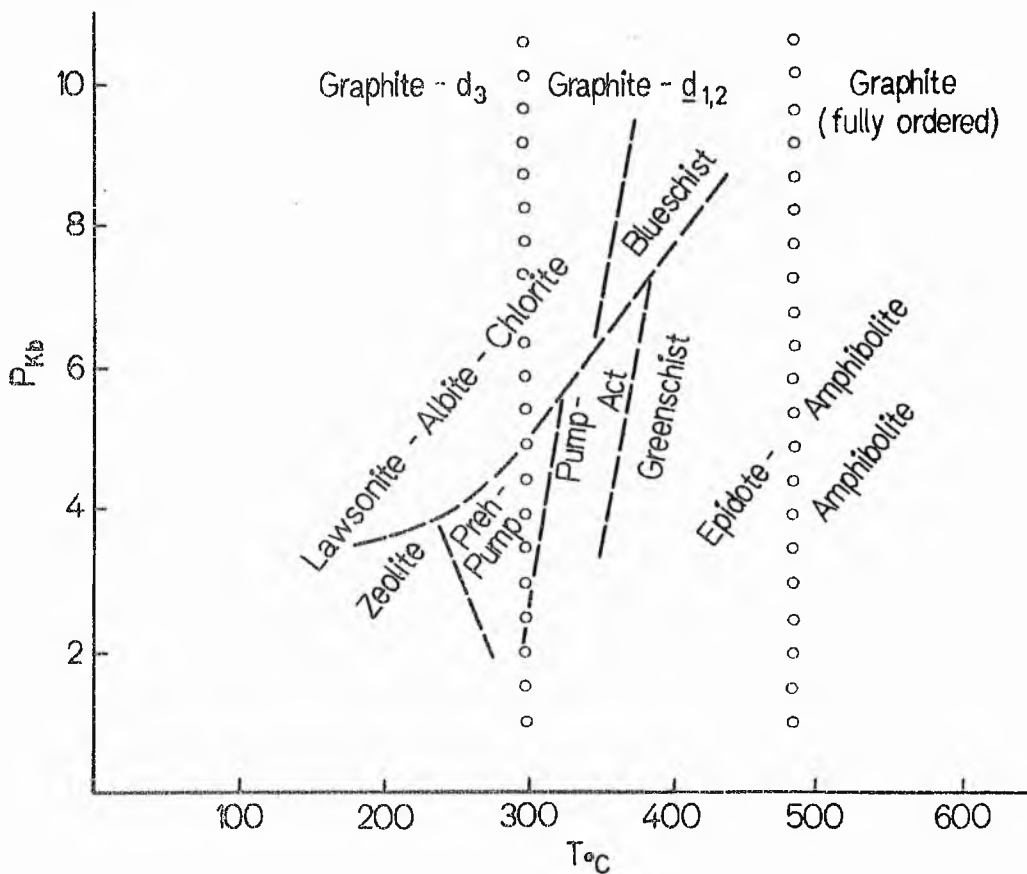


Figure 116. p - t - facies metamorphic grid, showing estimated conditions at which graphite and disordered graphite occur in nature. Estimated field, boundaries of graphite and graphite-d indicated by open circles, (after Landis 1971).

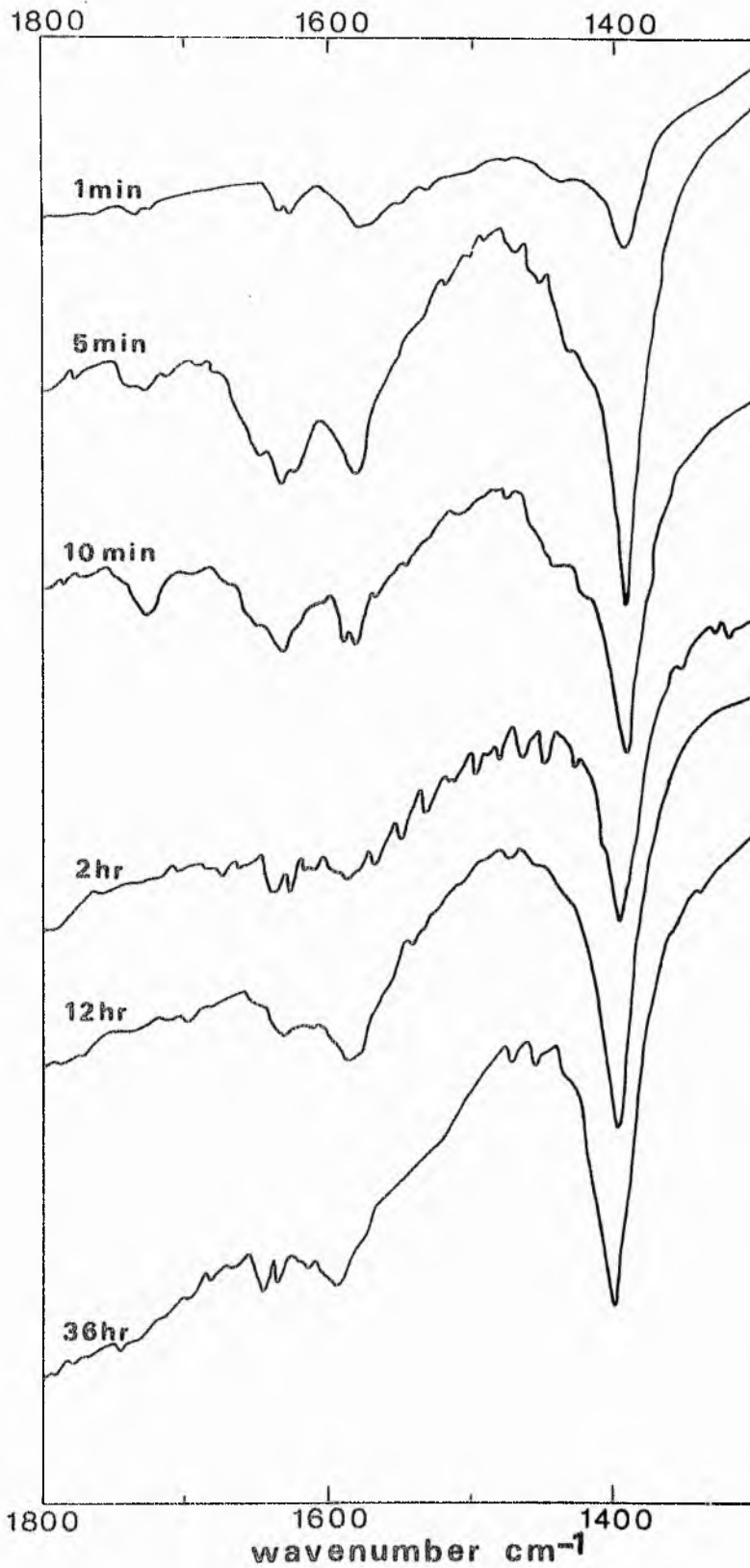


Figure 117. Infra-red spectra of sample NW-4 kerogen isolate recorded after crushing for different lengths of time.

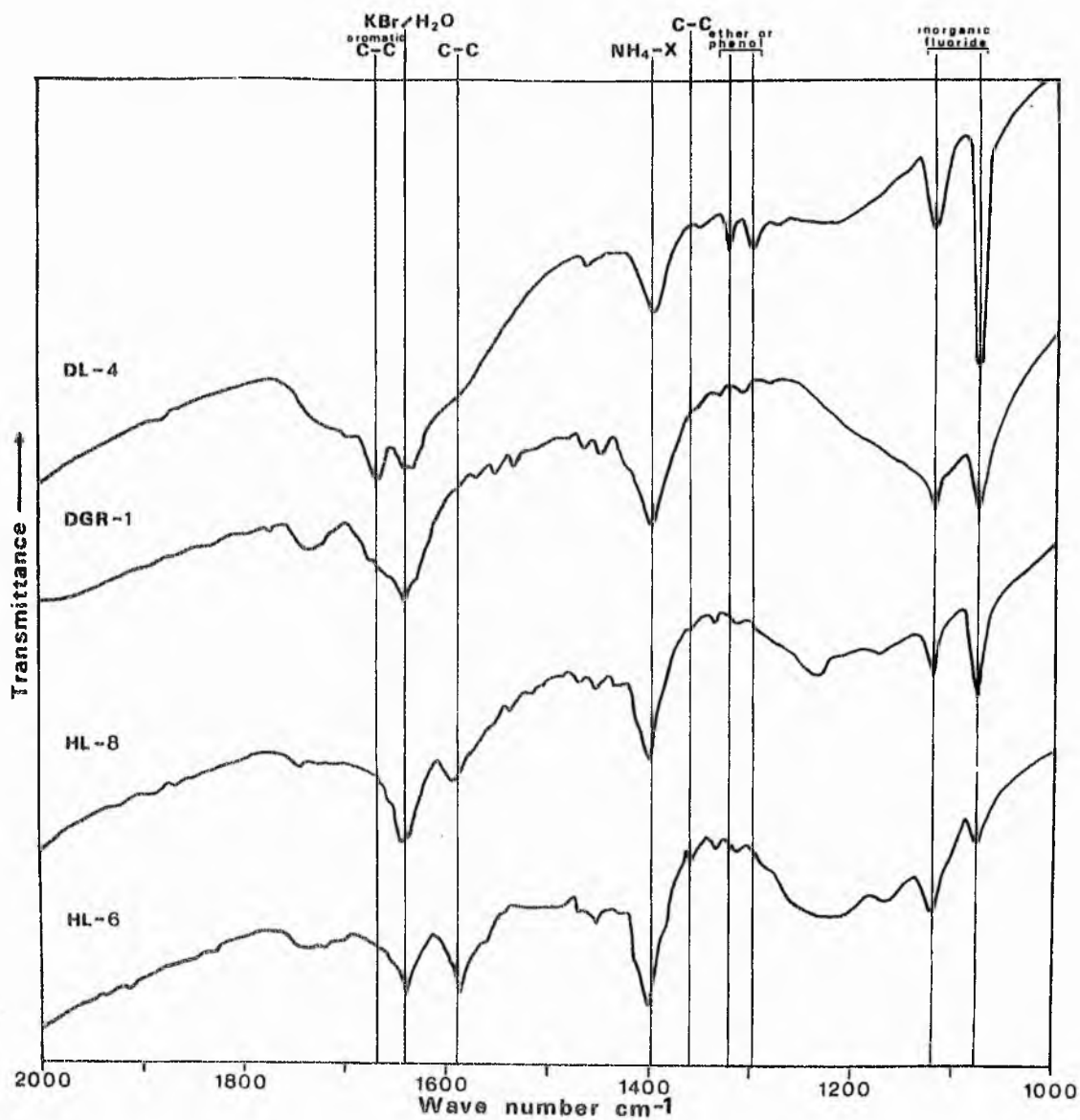


Figure 118. Infra-red spectra of the kerogen material isolated from samples DL-4, DGR-1, HL-8 and HL-6.

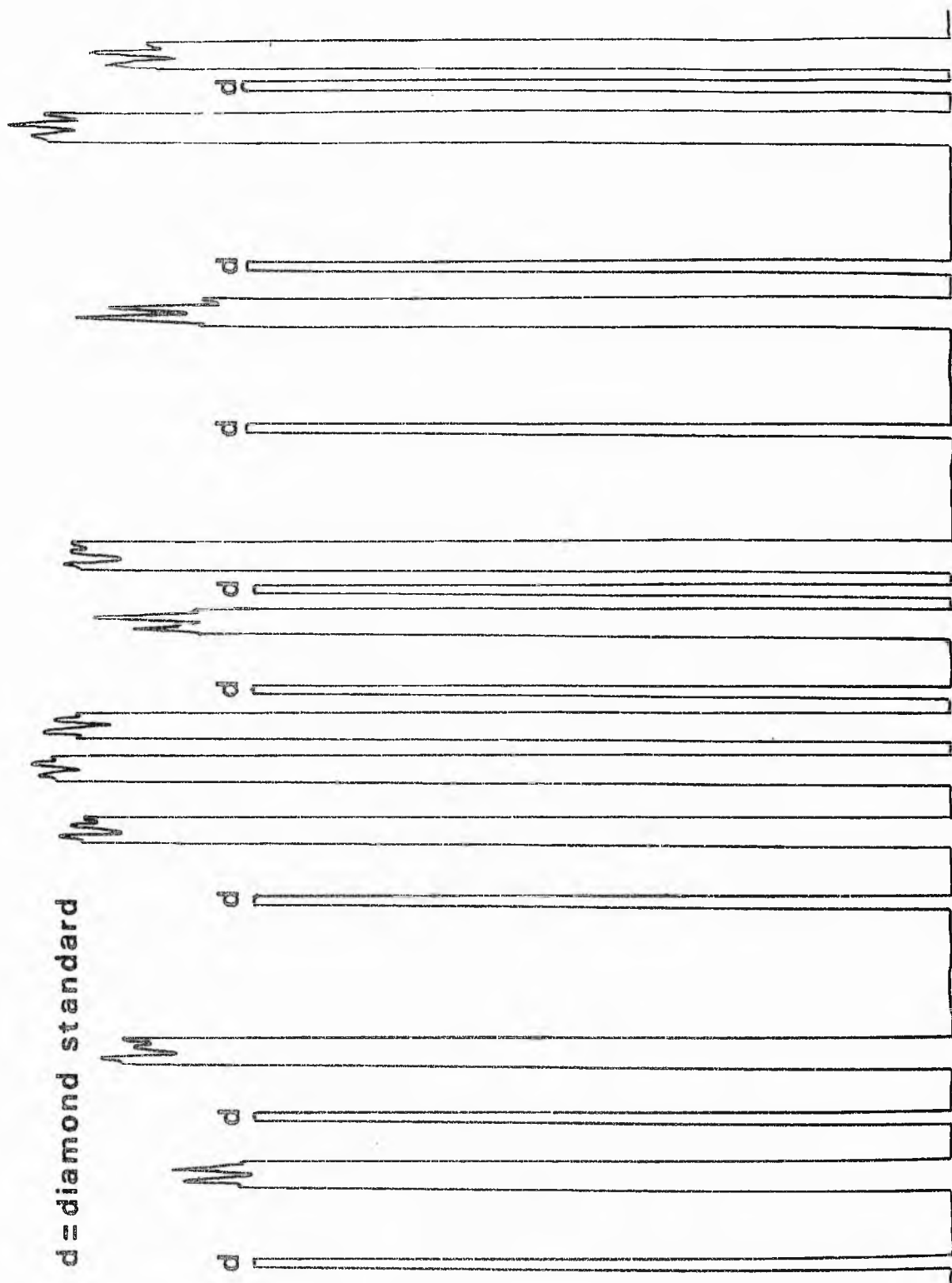


Figure 119. Chart recording of reflectivity-rotation measurements on graptolite particles in a block of mudstone cut parallel to the plane of the bedding.

Figure 120. Plot of the variation in graptolite fragments of maximum and minimum air reflectivity with respect to the angle the measurement surface makes with the plane of the bedding.

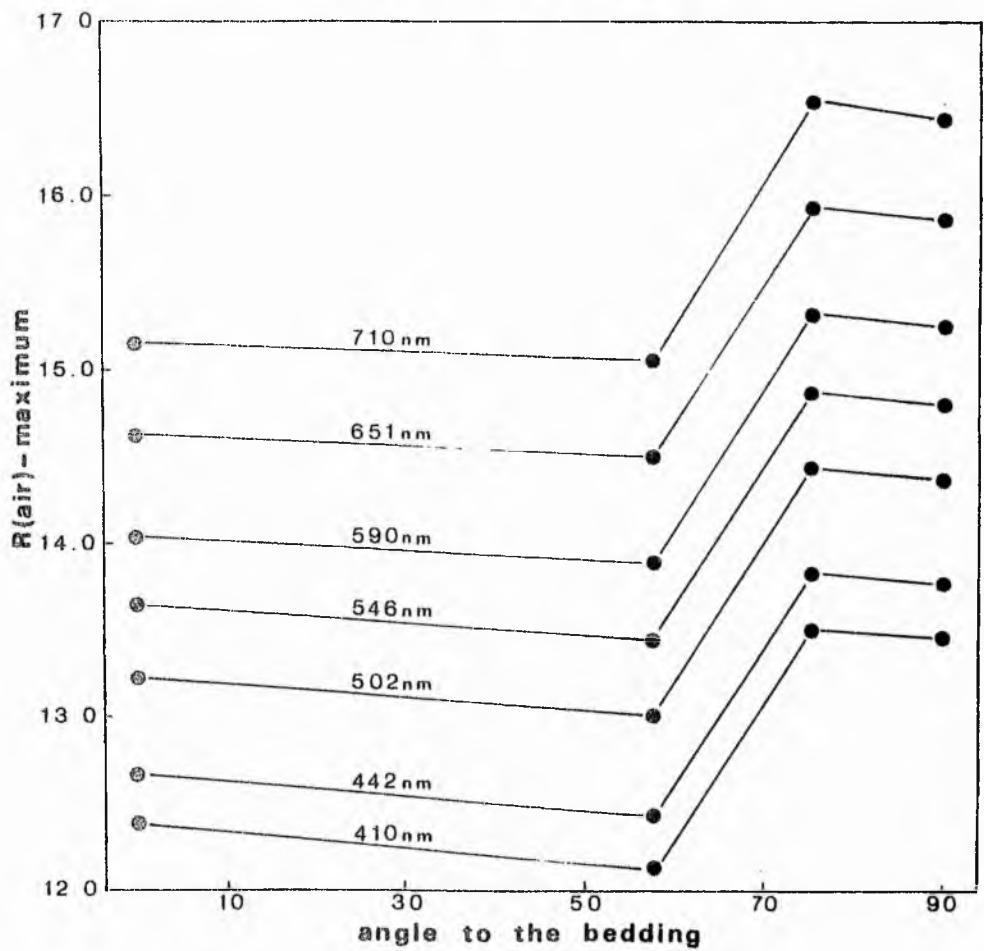
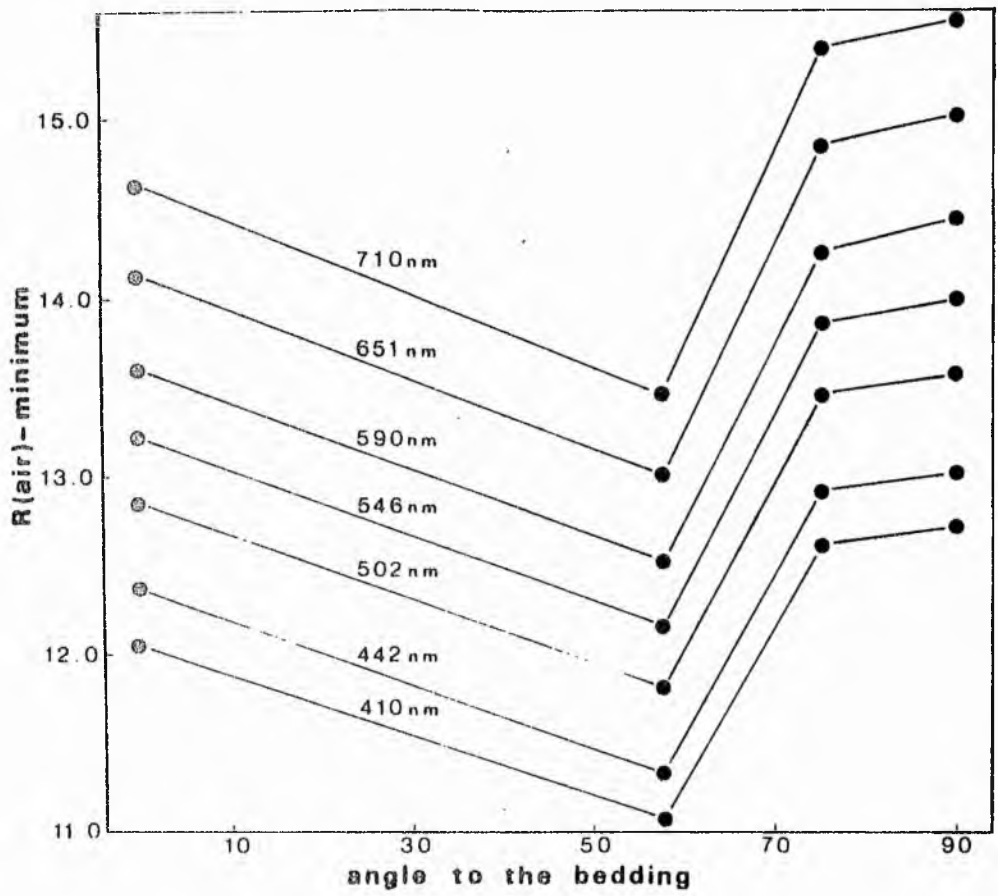


Figure 120.

Figure 121. Plot of the variation in graptolite fragments of oil and air reflectivity with wavelength for particles cut at various angles to the plane of the bedding.

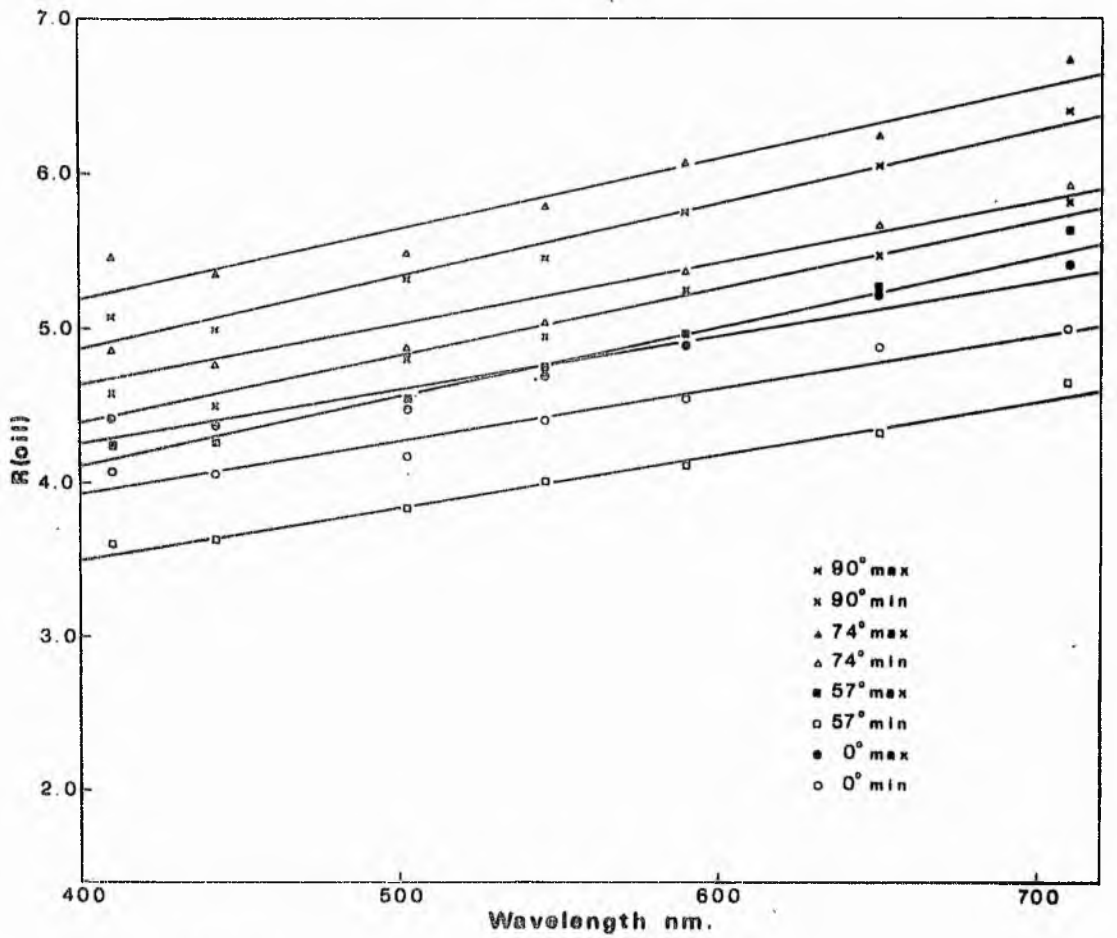
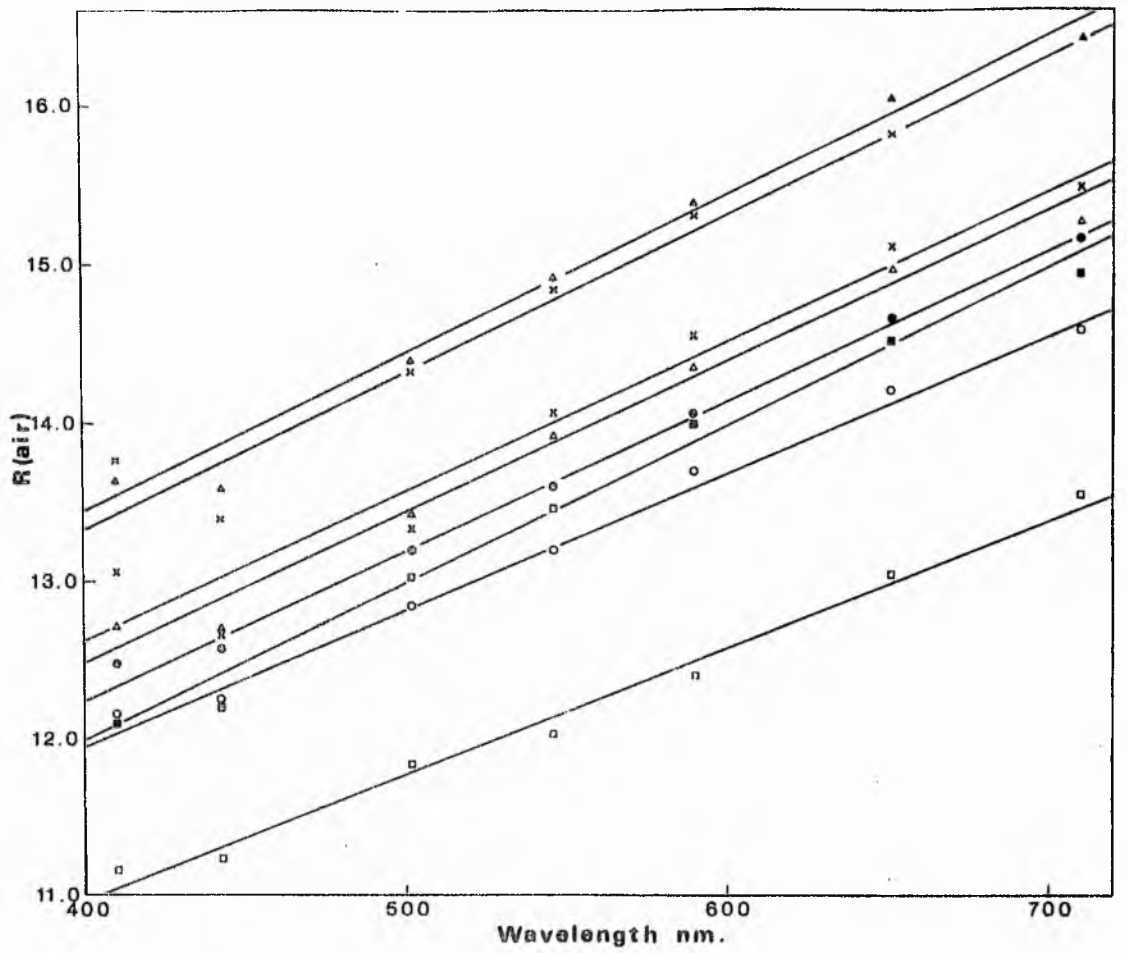


Figure 121.

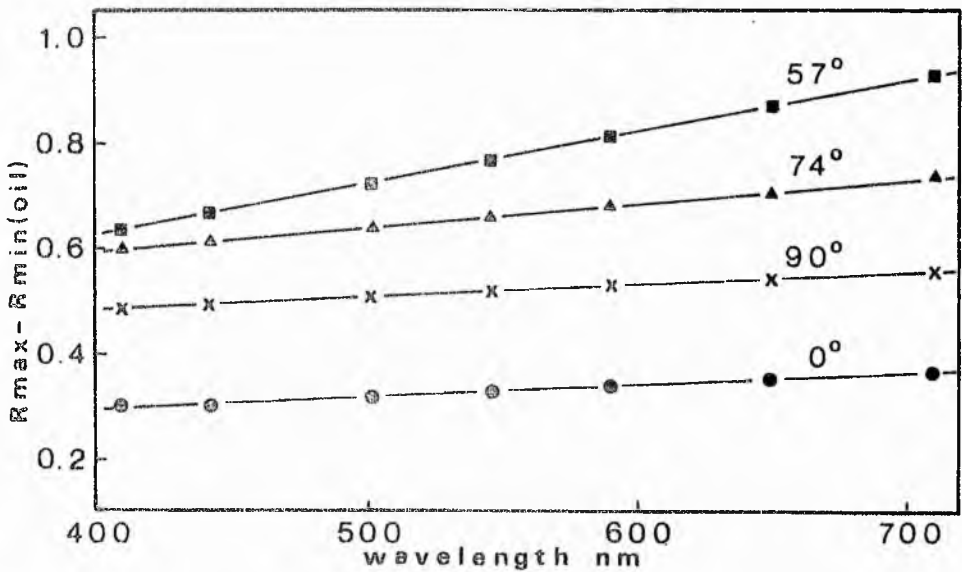
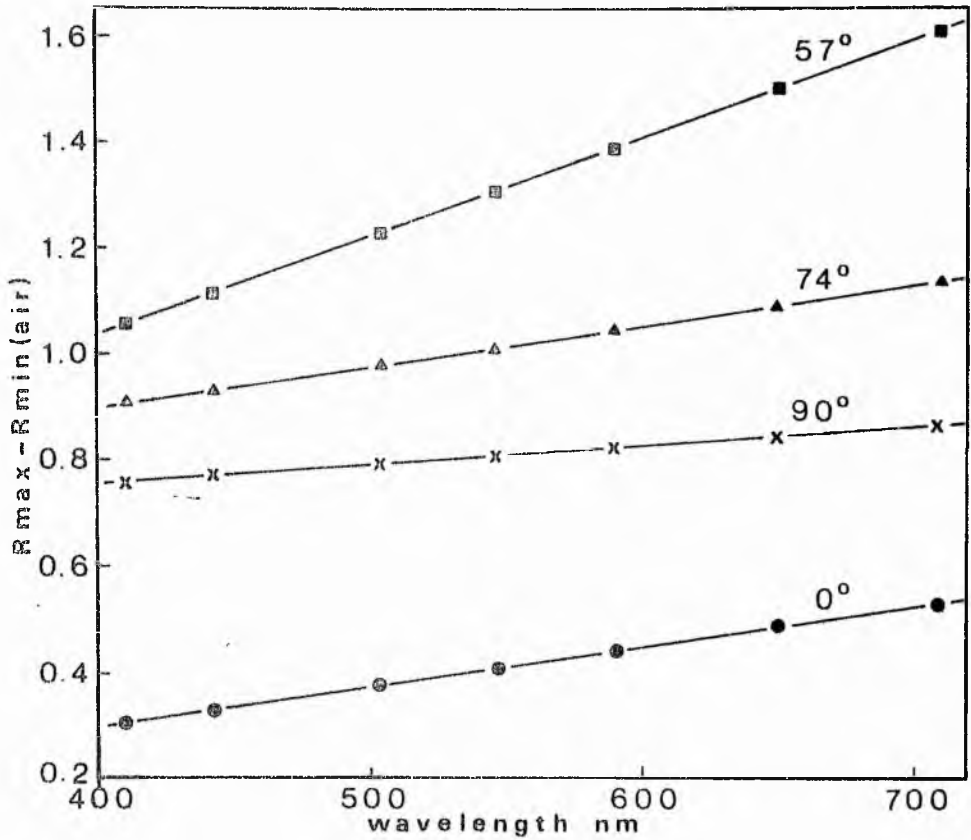
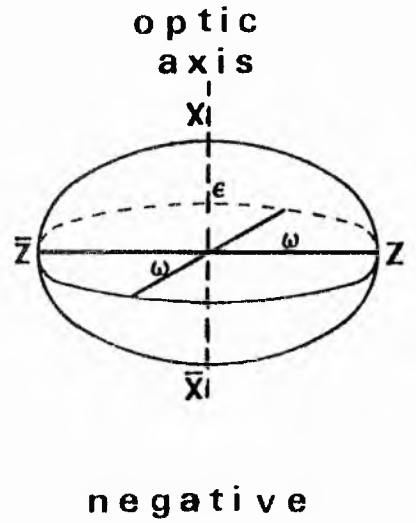
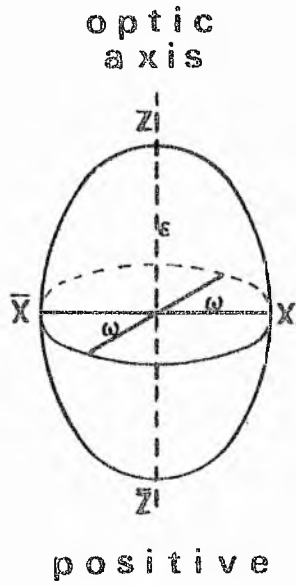


Figure 122. Plot of the variation in graptolite fragments of the difference between maximum and minimum reflectivity with wavelength for particles cut at various angles to the plane of the bedding.

uniaxial



biaxial

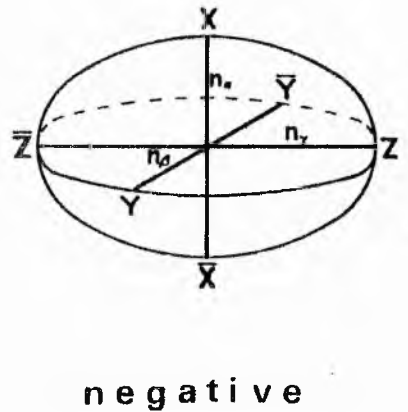
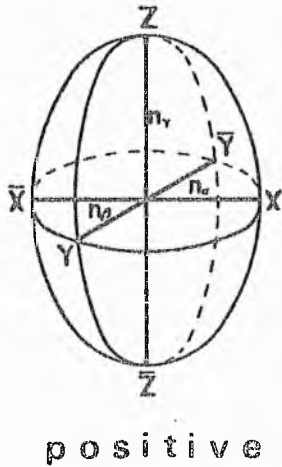


Figure 123. Indicatrices of uniaxial and biaxial crystals.

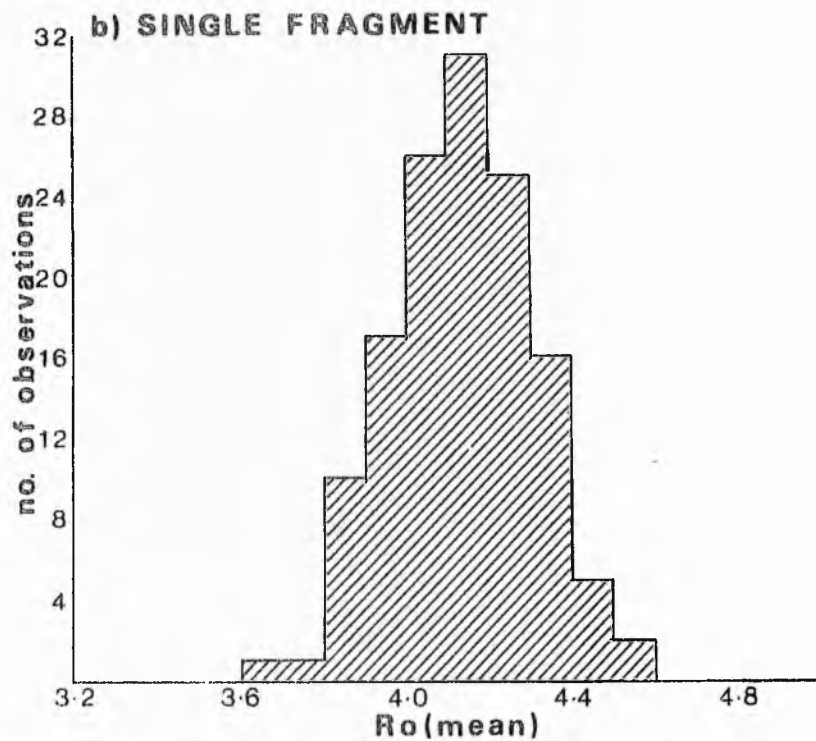
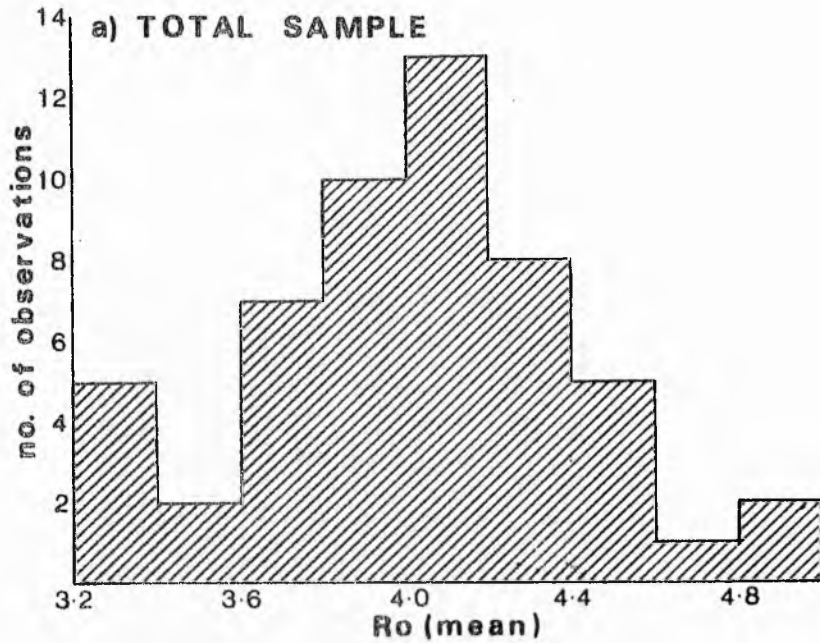


Figure 124. Histograms for the variation in reflectivity in sample LBR-29. a) variation within the sample b) variation across a single fragment.

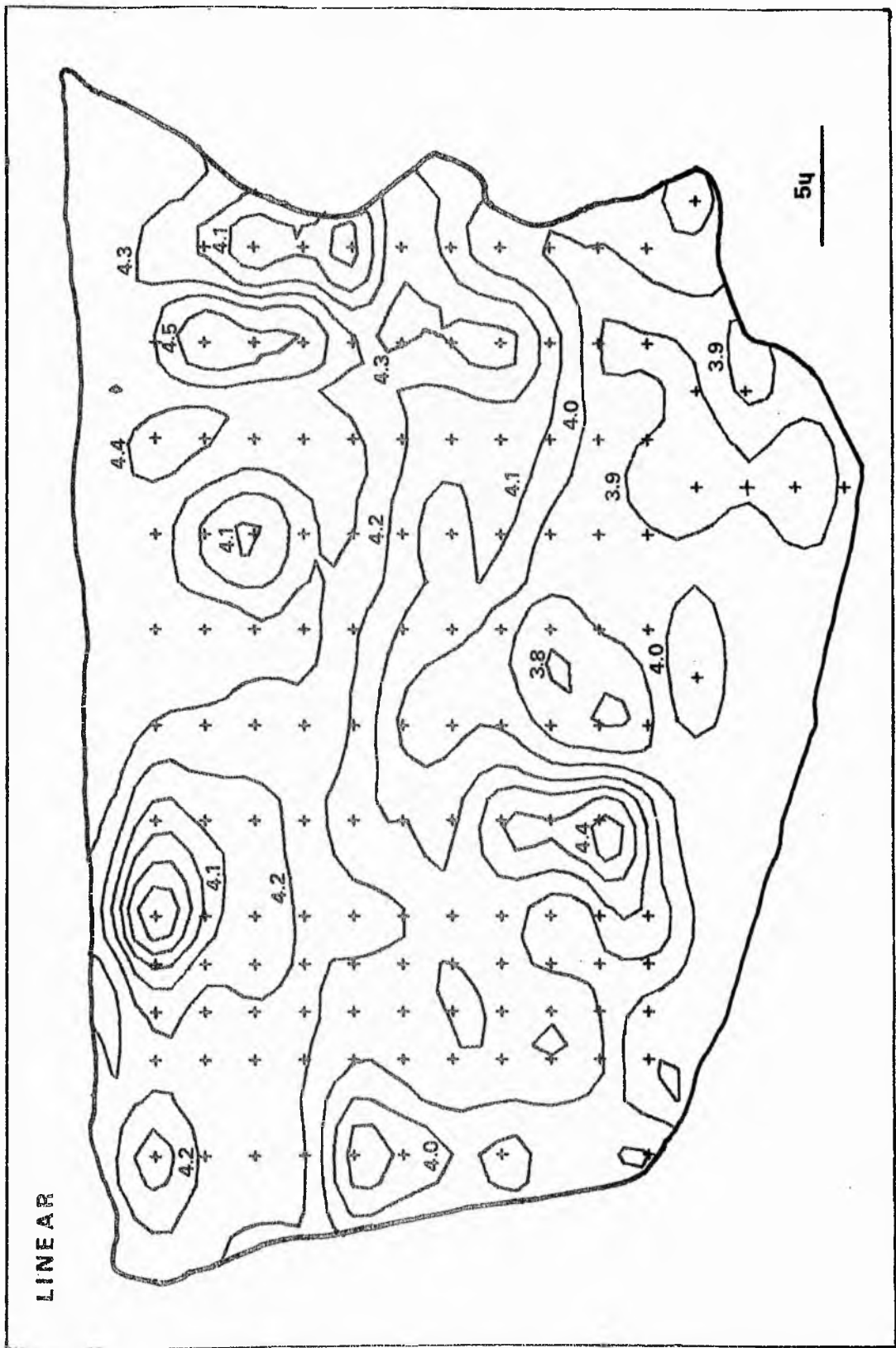


Figure 125. Linear iterative surface map for the variation in reflectivity over the surface of a graptolite fragment.

TSA OVER LBR/29 GRAPTOLITE FRAGMENT

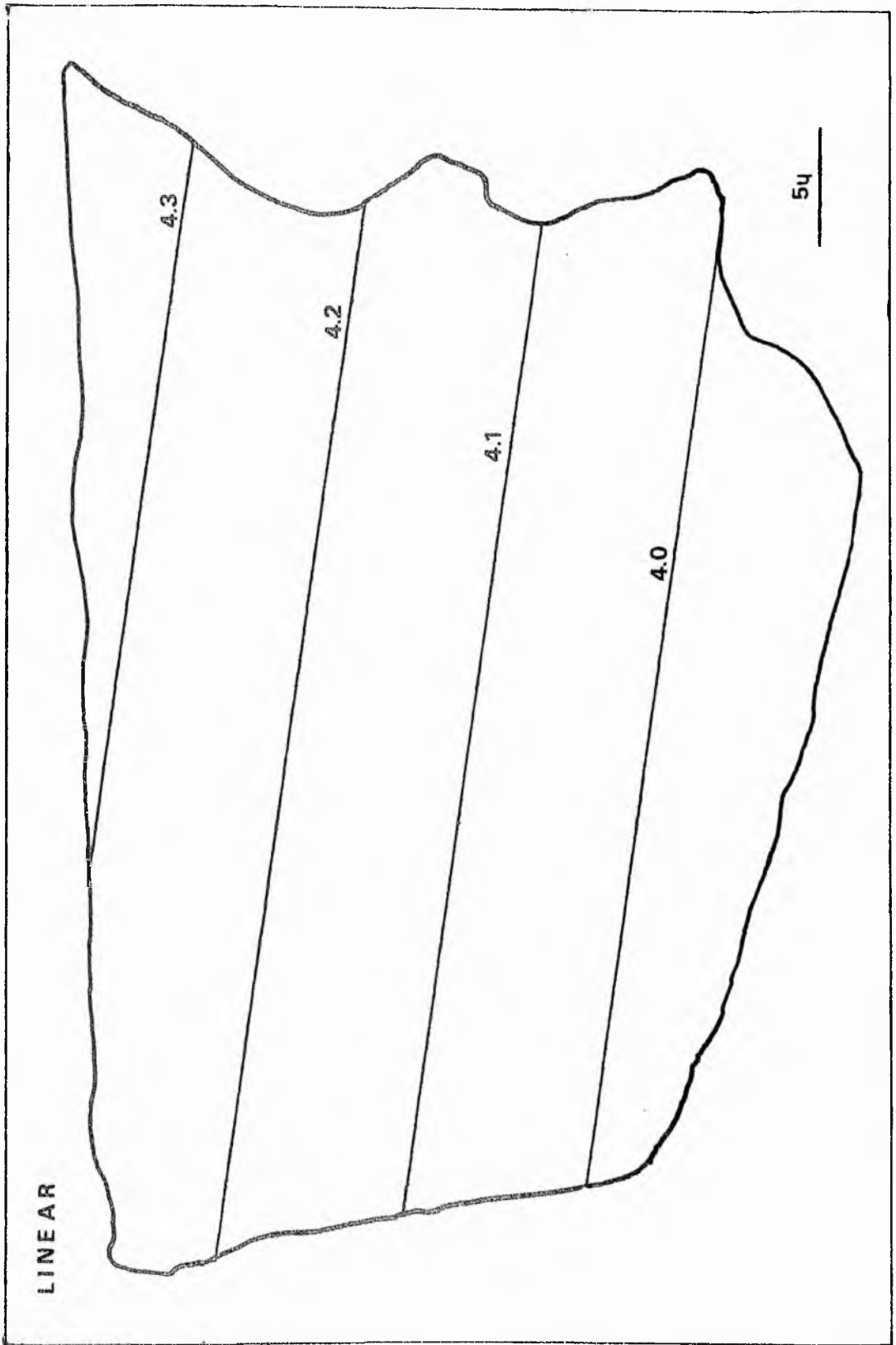


Figure 126. Linear surface global fit map for the variation in reflectivity over the surface of a graptolite fragment.

GLOBAL FIT SURFACE PLOT



Figure 127. Linear surface difference map for the variation in reflectivity over the surface of a graptolite fragment. Hatched areas are of positive difference, dotted areas of negative difference.

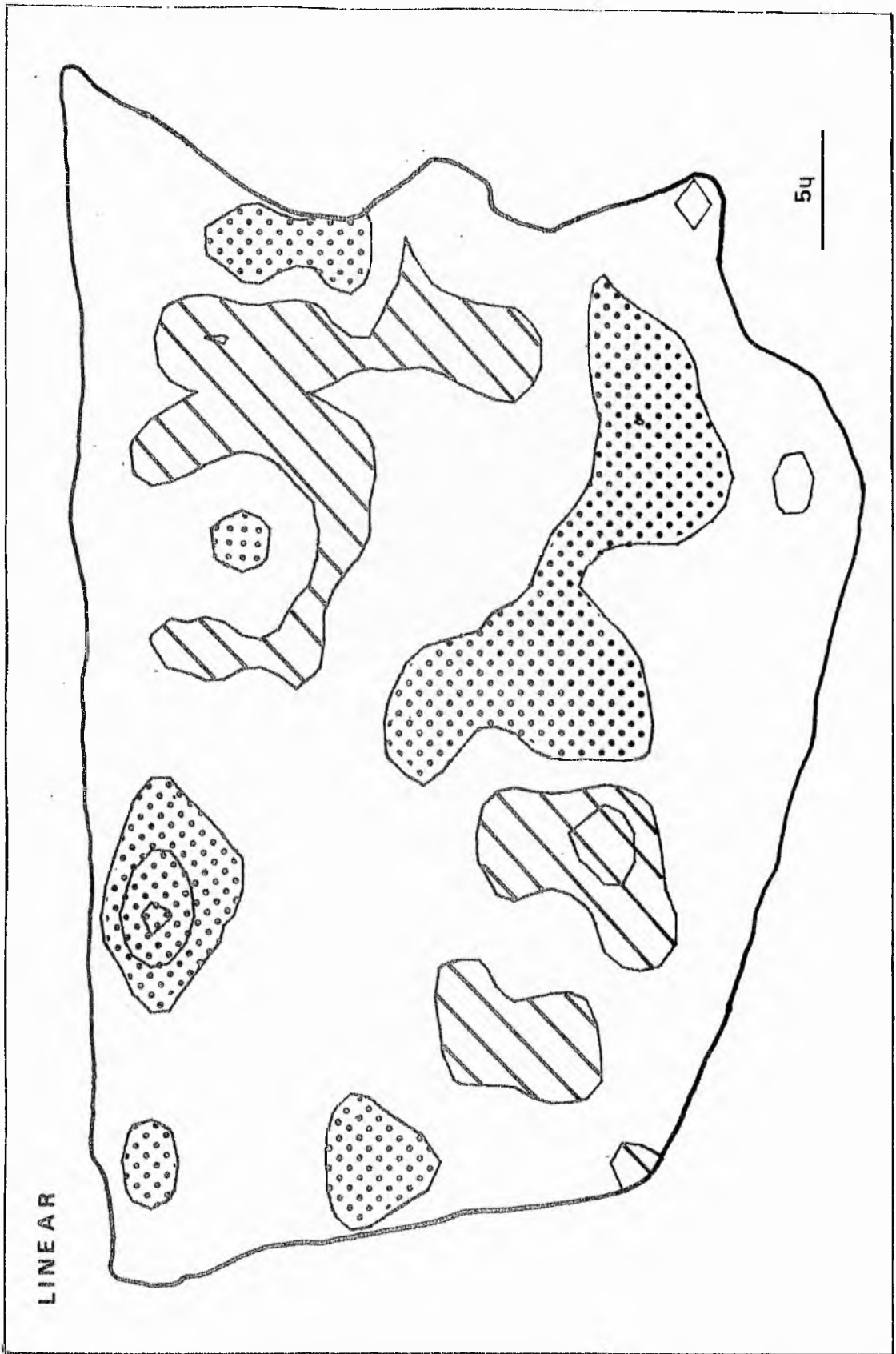


Figure 127.

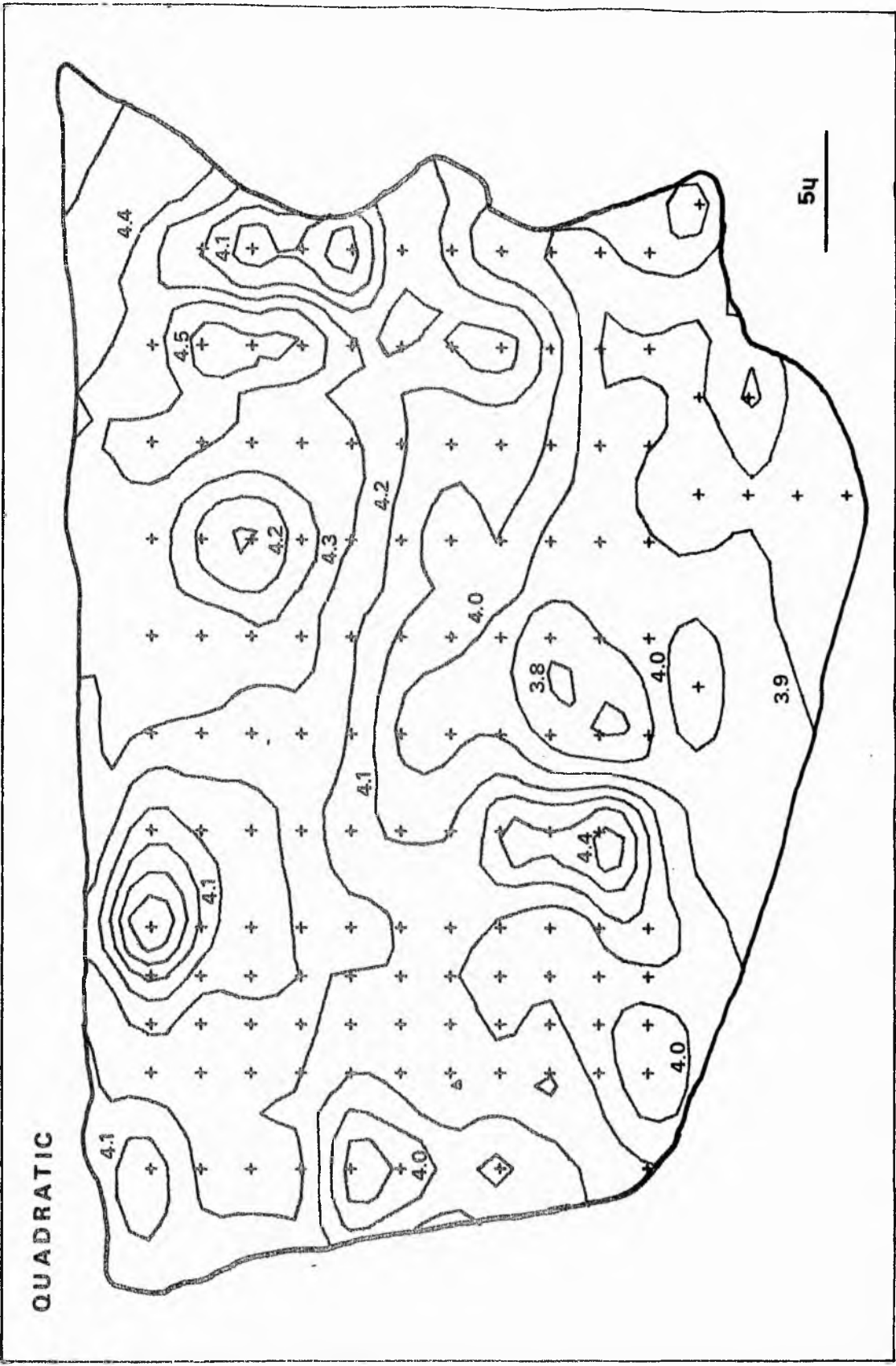


Figure 128. Quadratic iterative surface map for the variation in reflectivity over the surface of a graptolite fragment.

TSA OVER LBR/29 GRAPTOLITE FRAGMENT

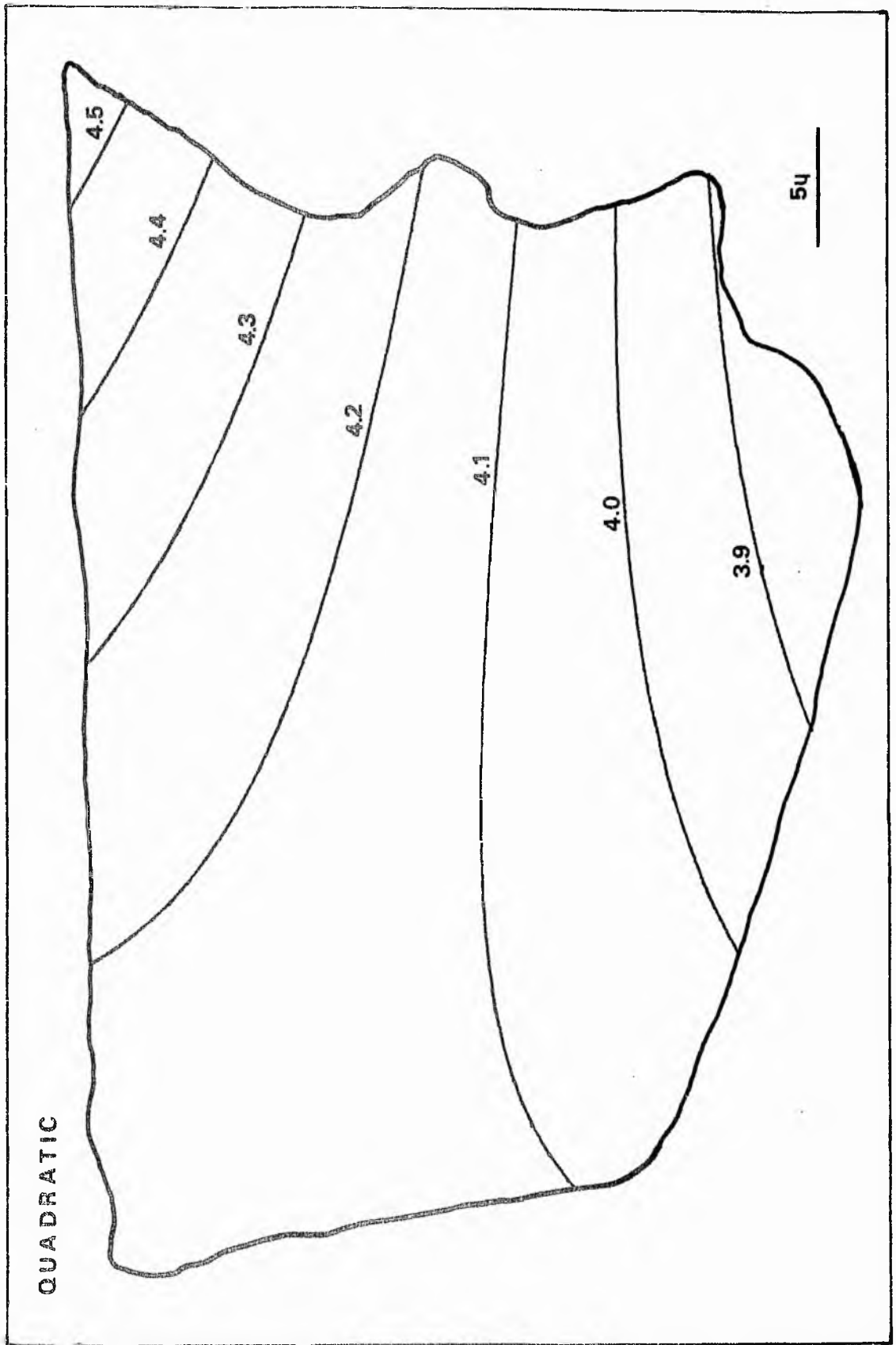


Figure 129. Quadratic surface global fit map for the variation in reflectivity over the surface of a graptolite fragment.

Figure 130. Quadratic surface difference map for the variation in reflectivity over the surface of a graptolite fragment. Hatched areas are of positive difference, dotted areas of negative difference.

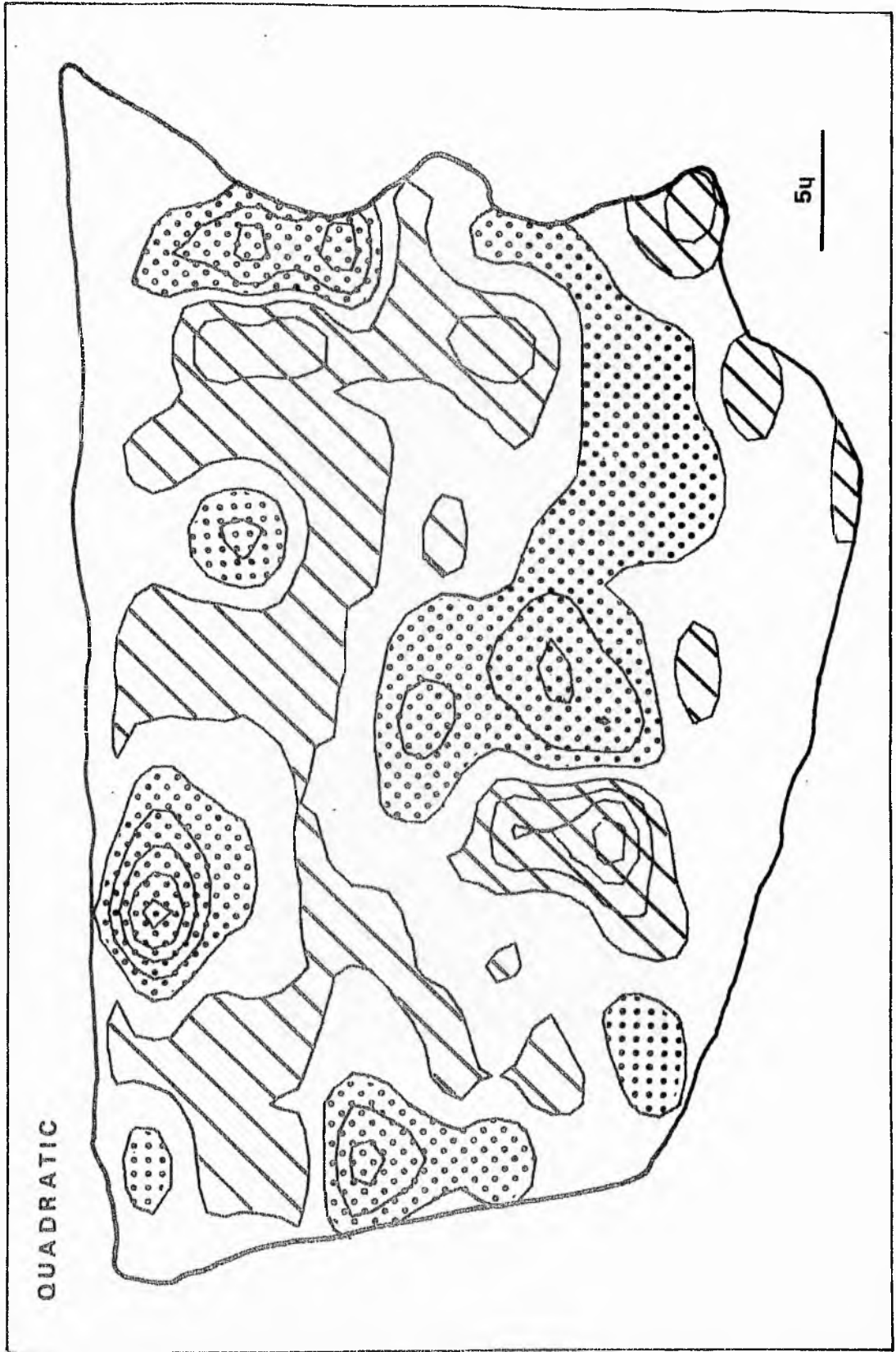


Figure 130.

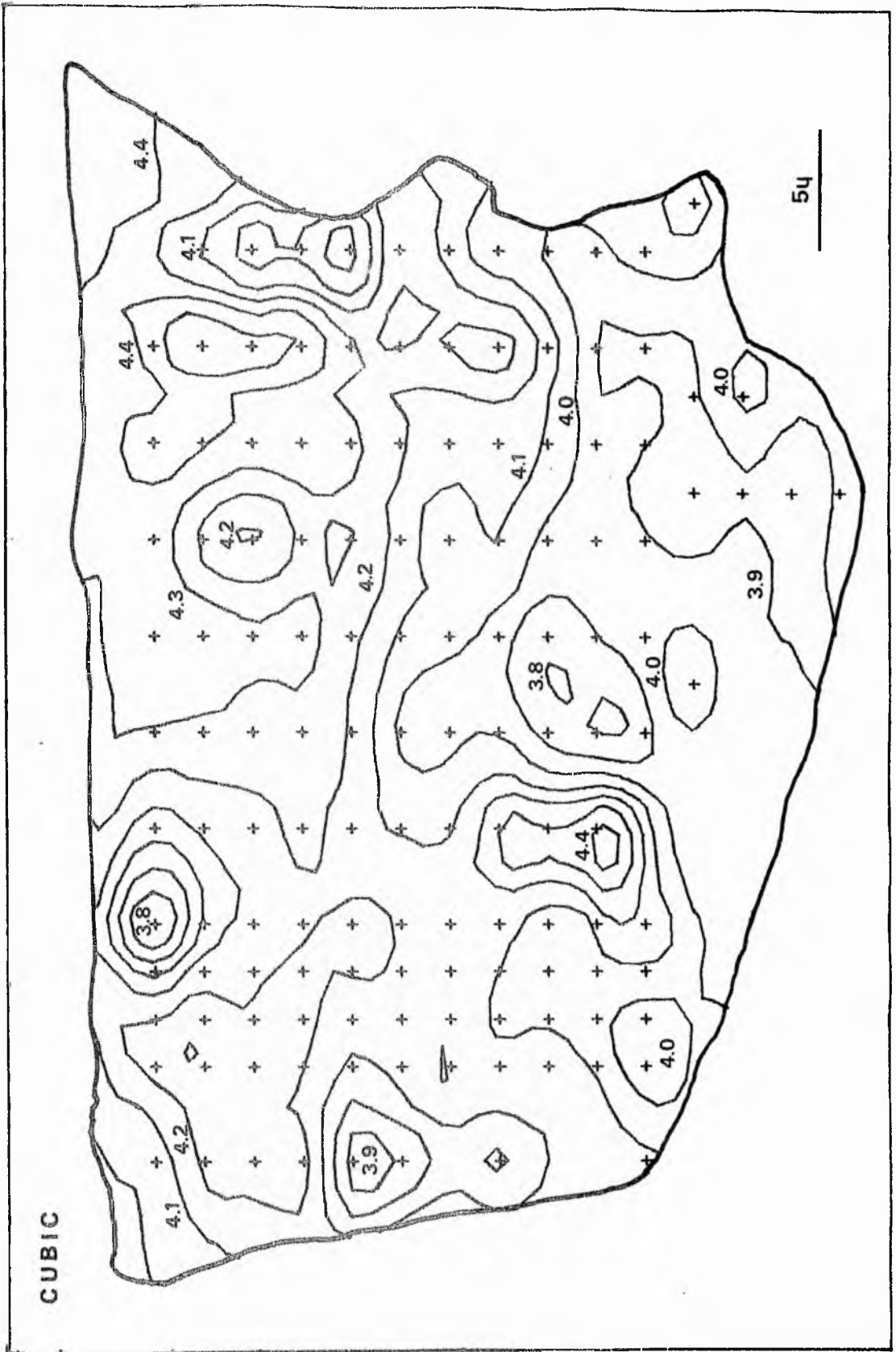
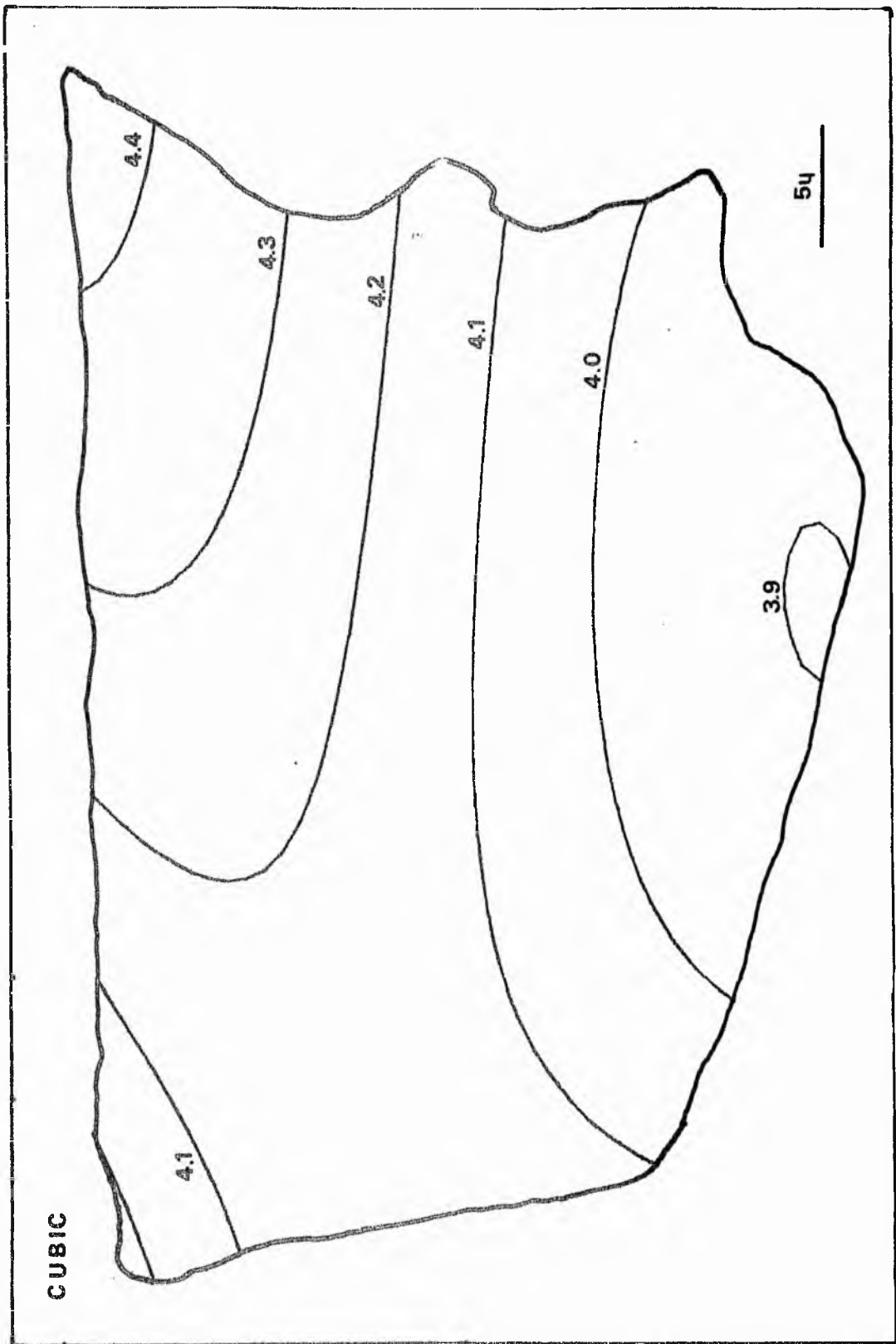


Figure 131. Cubic iterative surface map for the variation in reflectivity over the surface of a graptolite fragment.



GLOBAL FIT SURFACE PLOT

Figure 132. Cubic surface global fit map for the variation in reflectivity over the surface of a graptolite fragment.

Figure 133. Cubic surface difference map for the variation in reflectivity over the surface of a graptolite fragment. Hatched areas are of positive difference, dotted areas of negative difference.

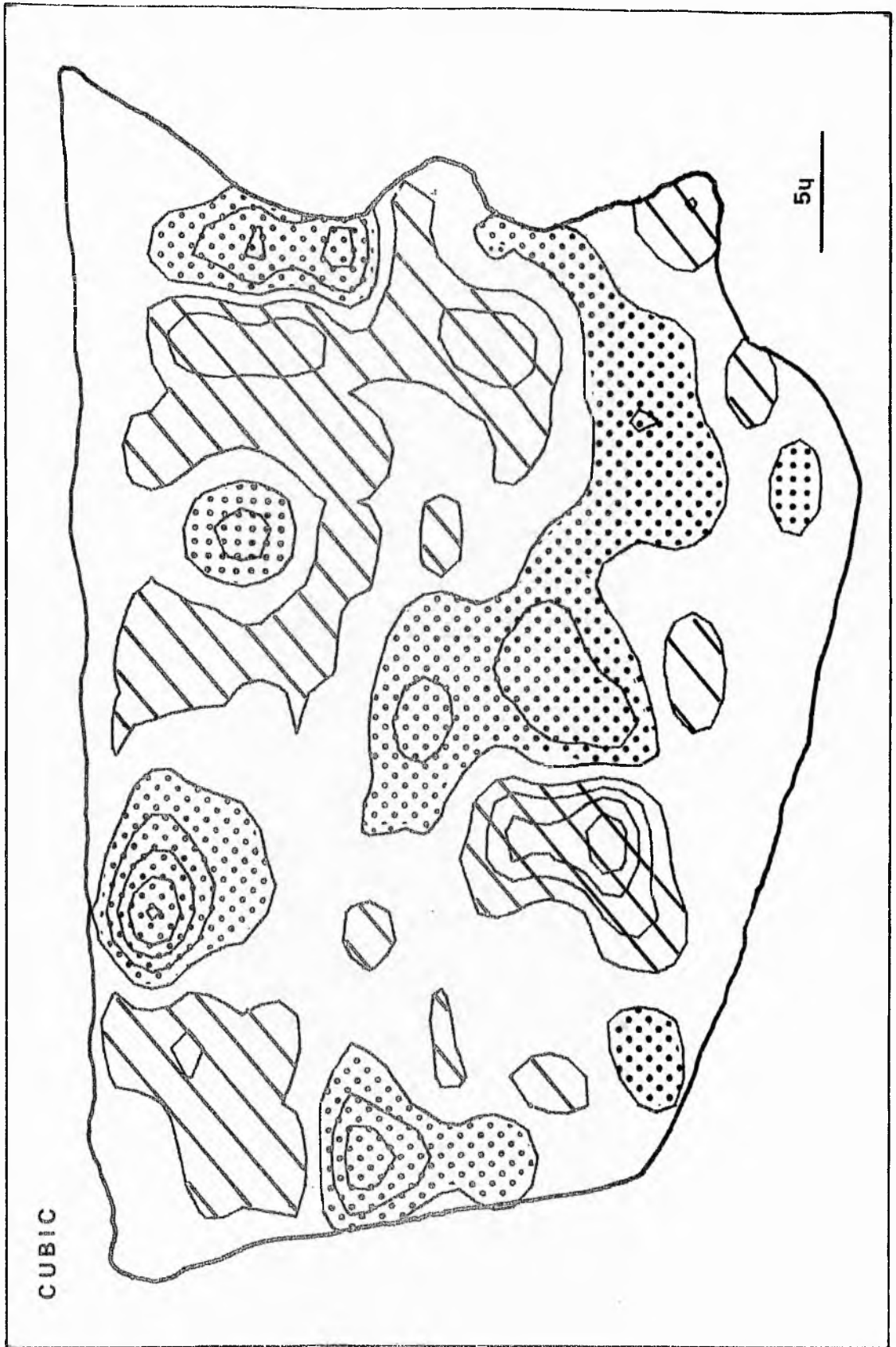


Figure 133.

DIFFERENCE MAP

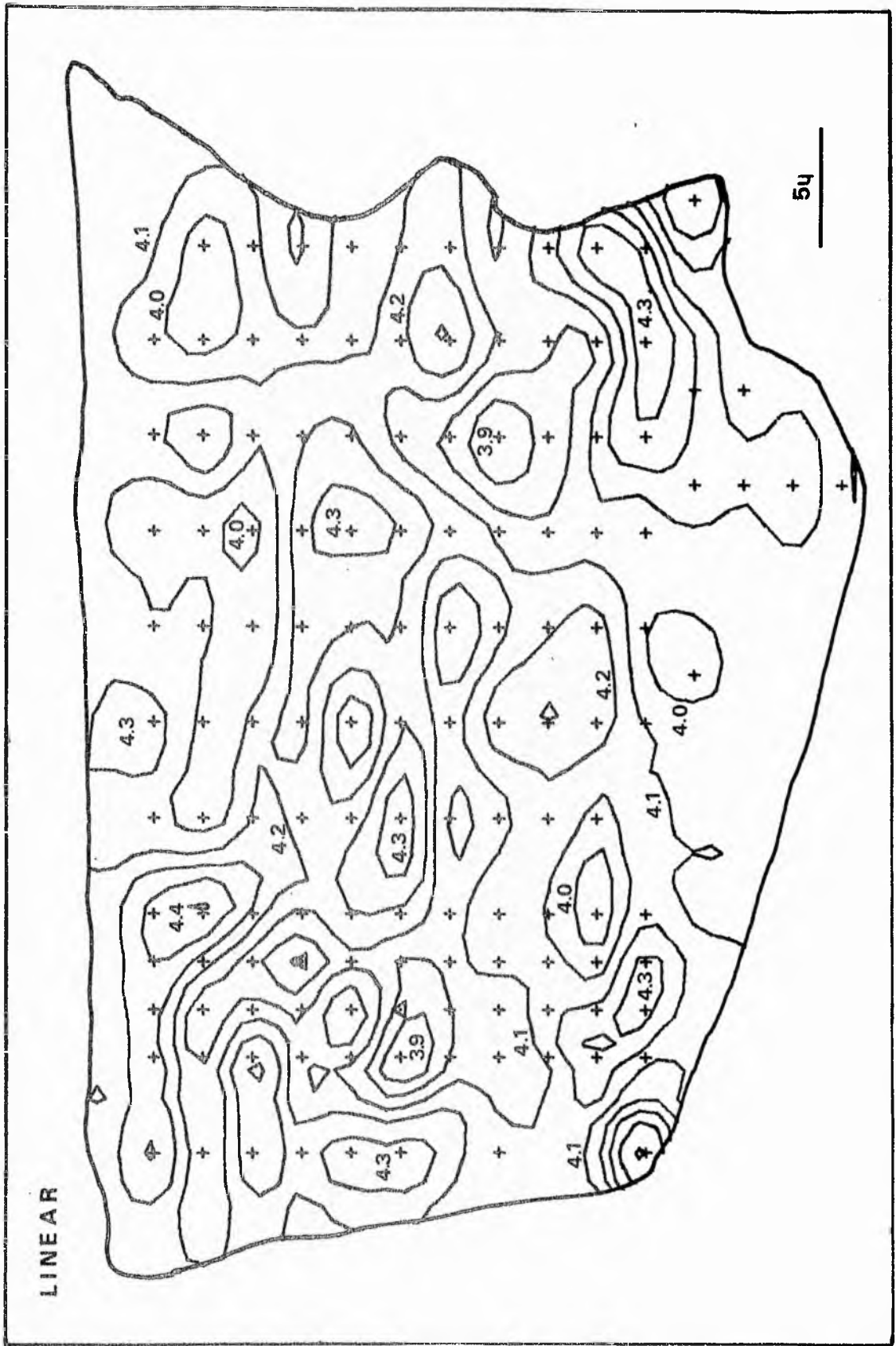
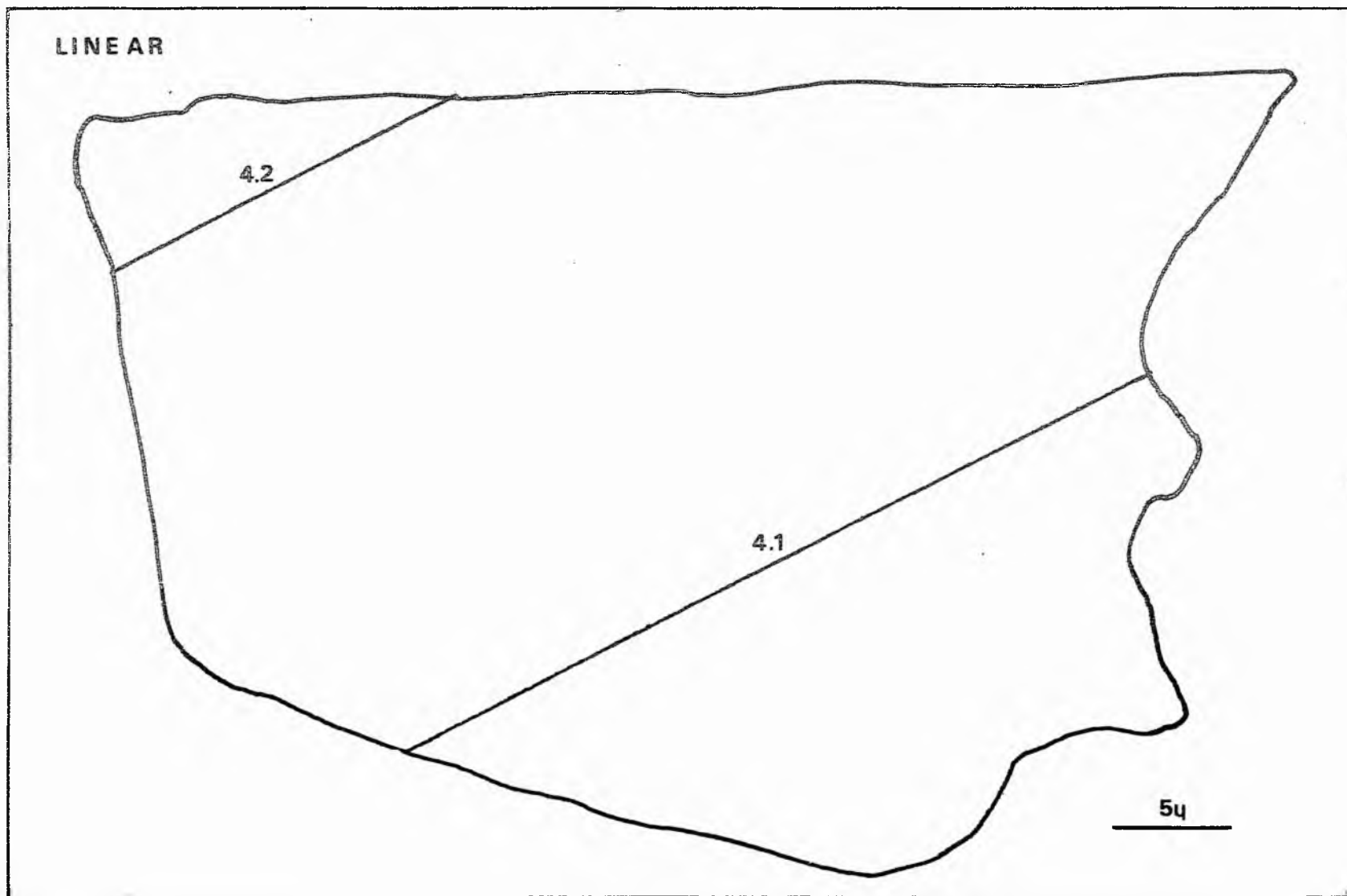


Figure 134. Linear iterative surface map for the variation in reflectance values produced at random over the surface of a graptolite fragment.

Figure 135. Linear surface global fit map for the variation in reflectance values produced at random over the surface of a graptolite fragment.

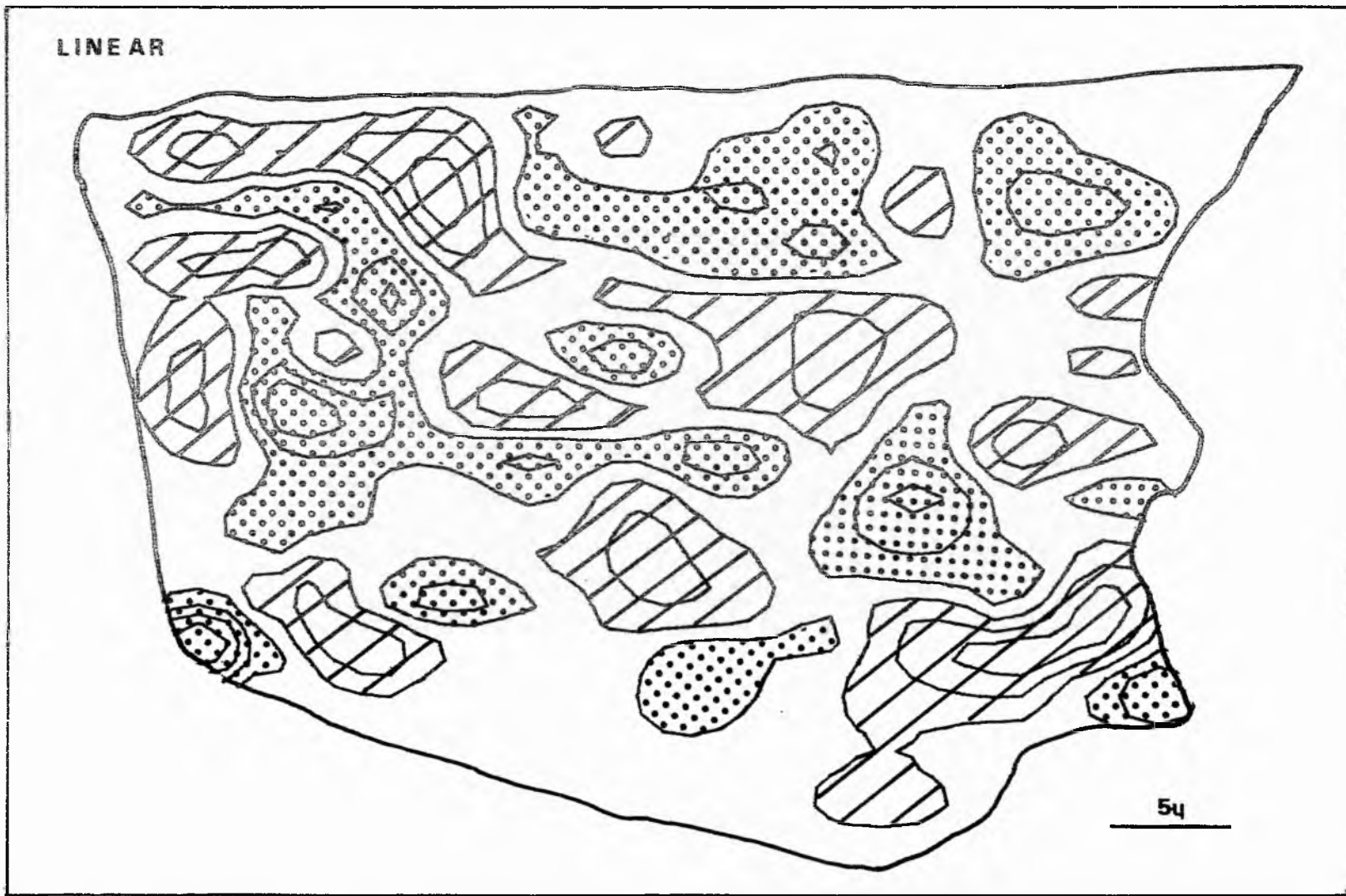
Figure 135.



GLOBAL FIT SURFACE PLOT

Figure 136. Linear surface difference map for the variation in reflectance values produced at random over the surface of a graptolite fragment. Hatched areas are of positive difference, dotted areas of negative difference.

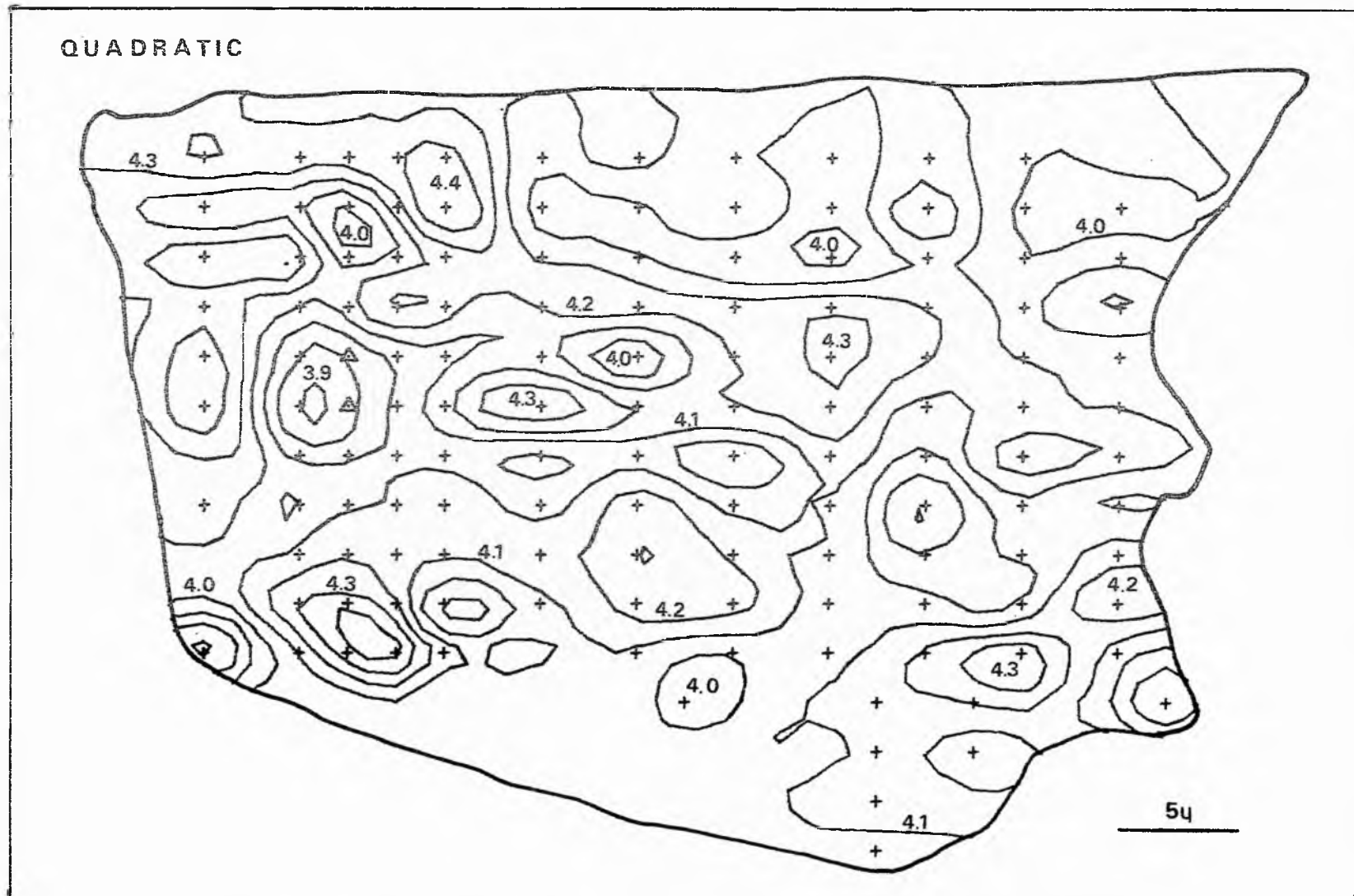
Figure 136.



DIFFERENCE MAP

Figure 137. Quadratic iterative surface map for the variation in reflectance values produced at random over the surface of a graptolite fragment.

Figure 137.



RANDOM VALUES FOR R0 OVER LBR/29 FRAGMENT

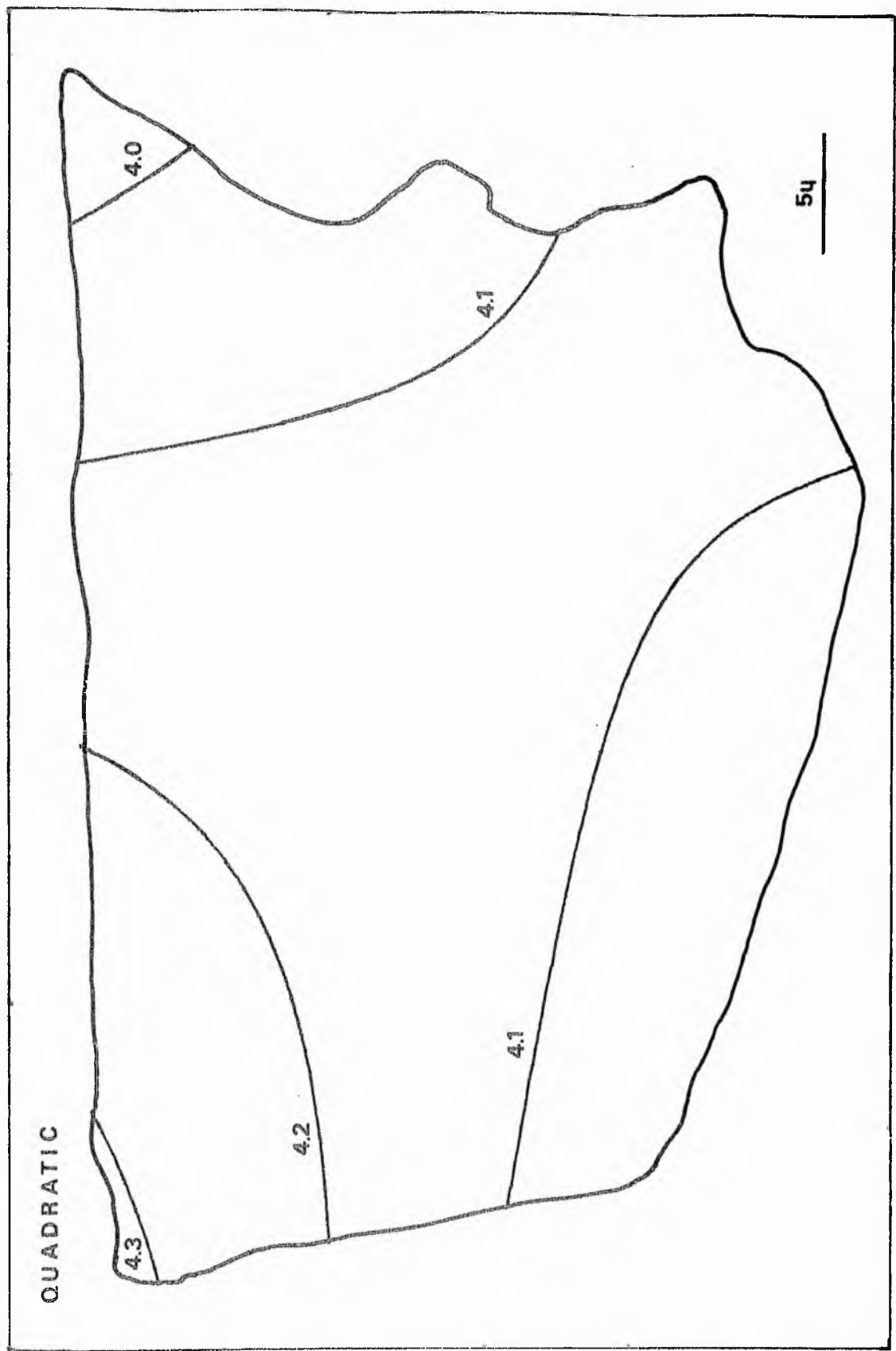
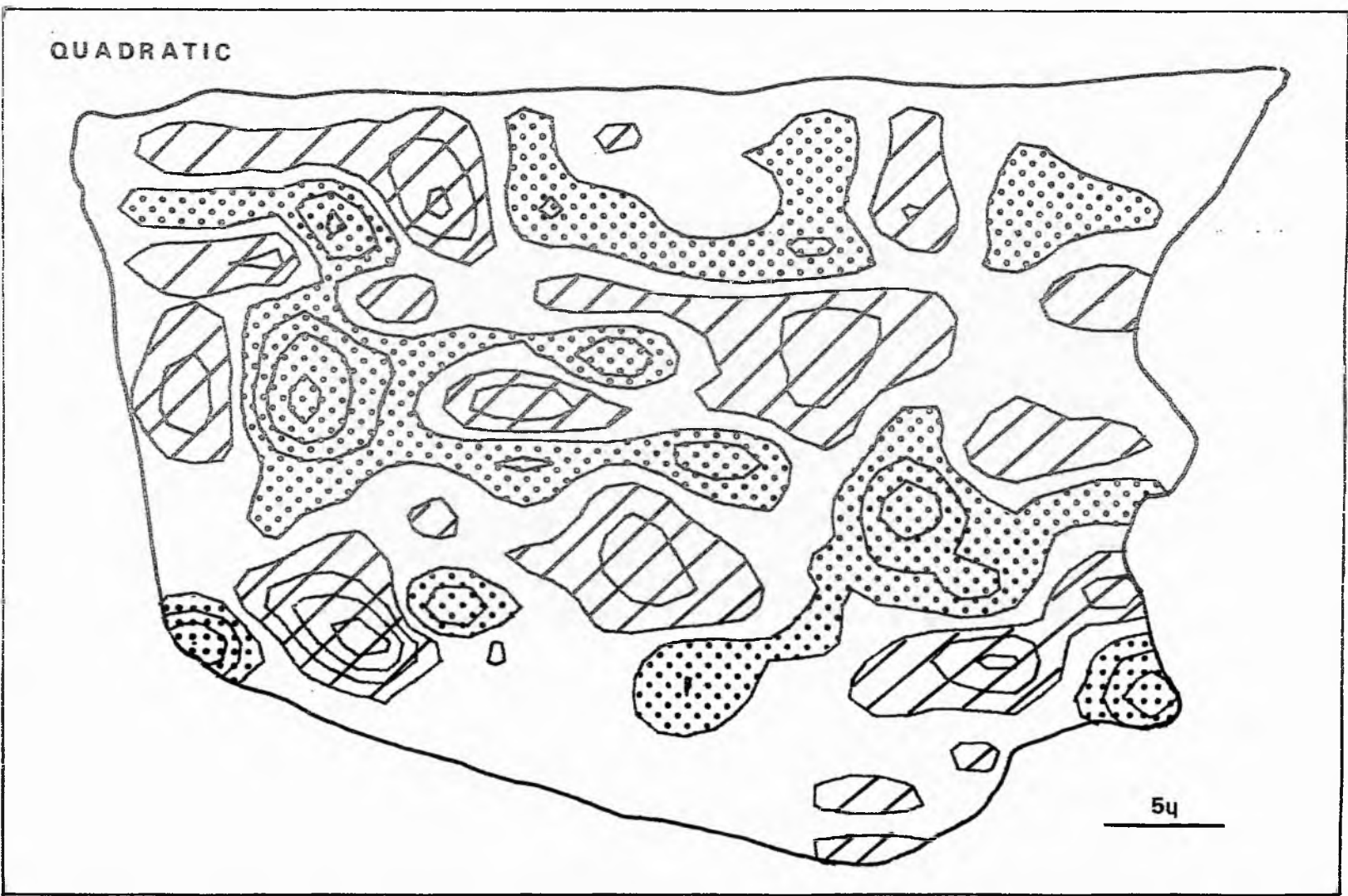


Figure 138. Quadratic surface global fit map for the variation in reflectance values produced at random over the surface of a graptolite fragment.

Figure 139. Quadratic surface difference map for the variation in reflectance values produced at random over the surface of a graptolite fragment. Hatched areas are of positive difference, dotted areas of negative difference.

Figure 139.



DIFFERENCE MAP

Figure 140. Cubic iterative surface map for the variation in reflectance values produced at random over the surface of a graptolite fragment.

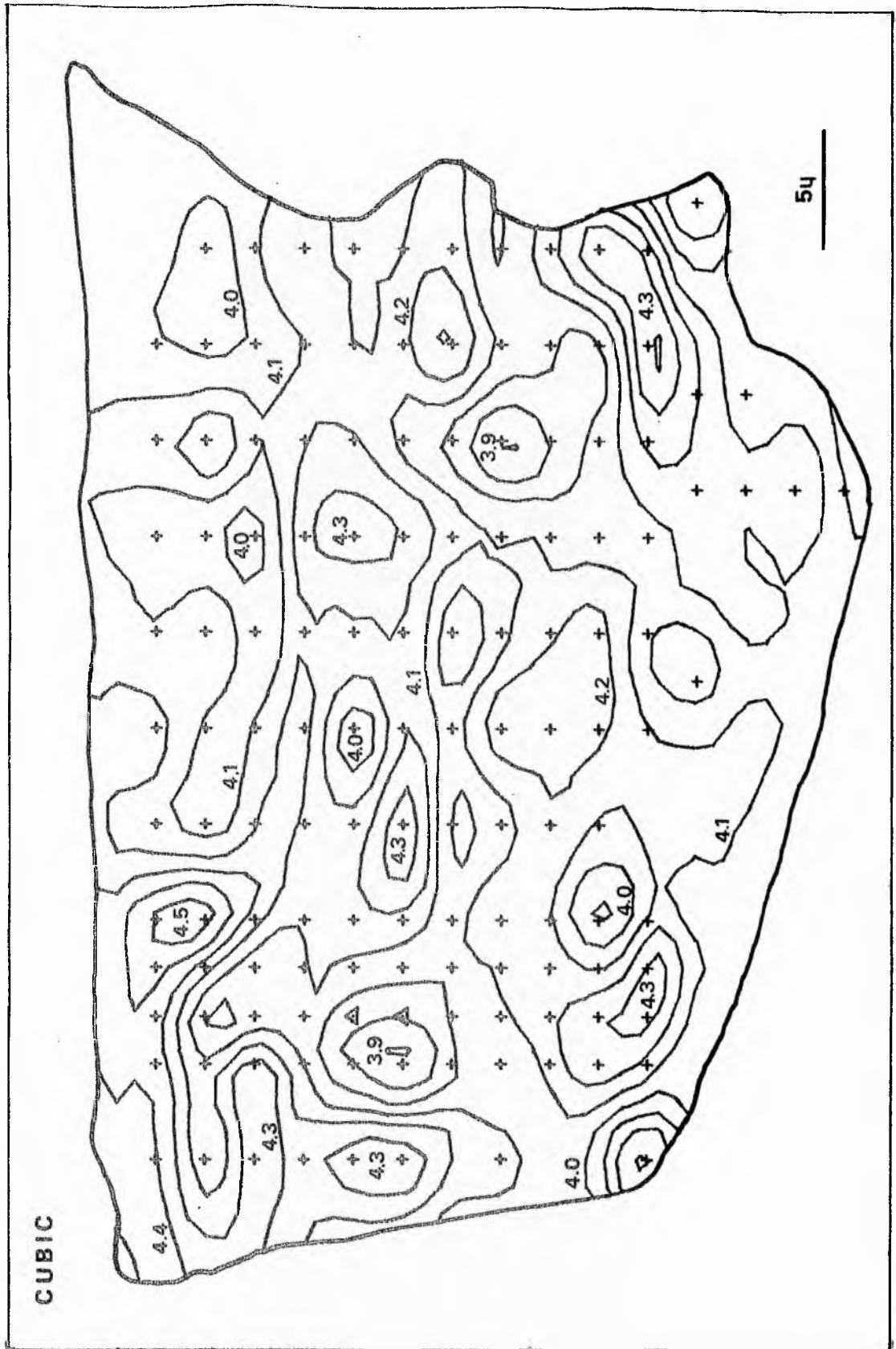
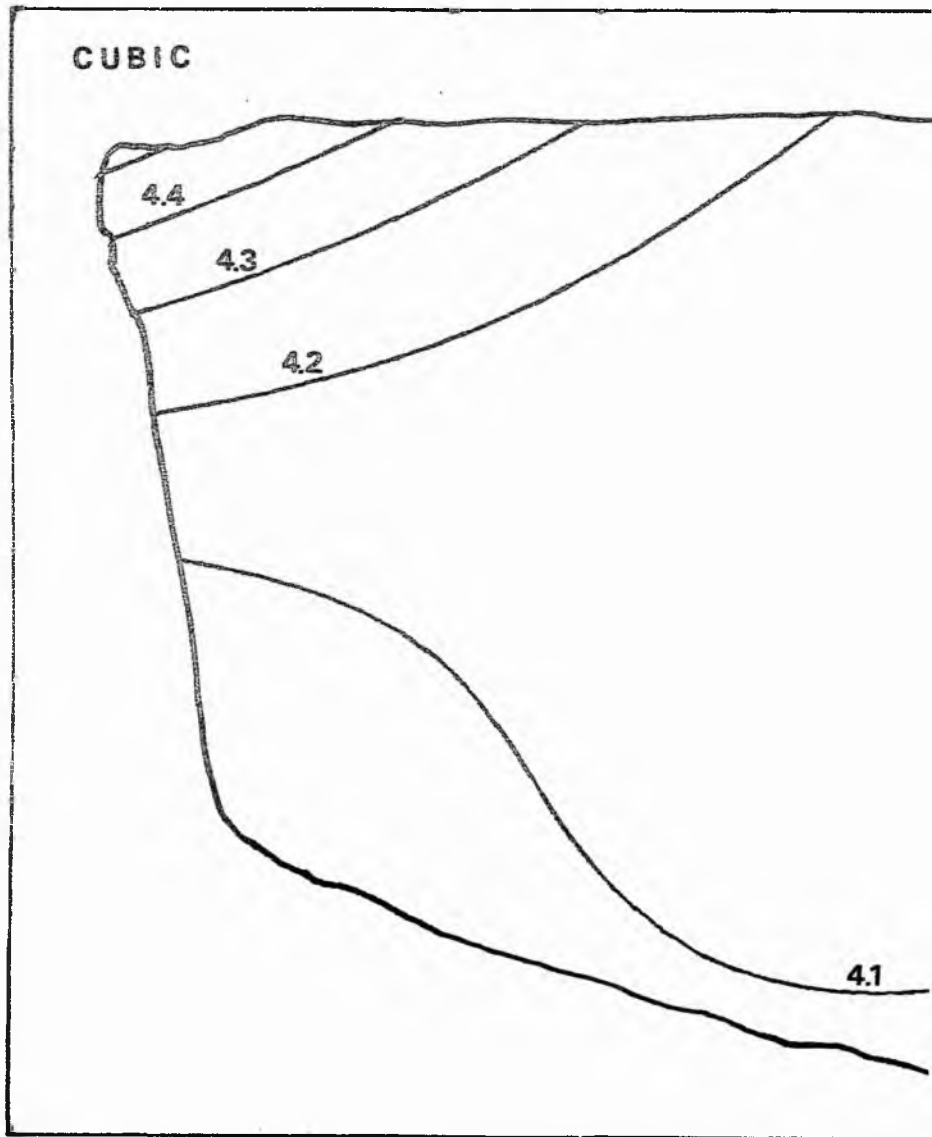


Figure 140.

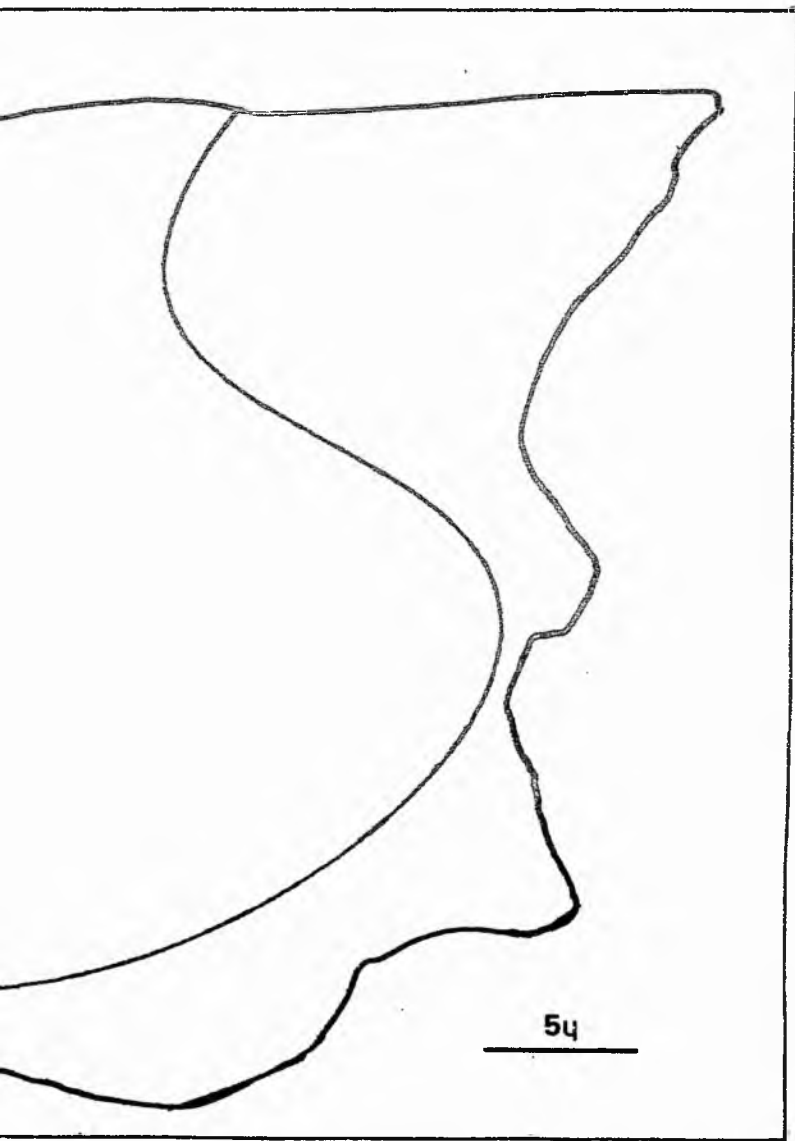
RANDOM VALUES FOR R0 OVER LBR/29 FRAGMENT

Figure 141. Cubic surface global fit map for the variation in reflectance values produced at random over the surface of a graptolite fragment.

Figure 141.



GLOBAL FIT SURFACE PLOT



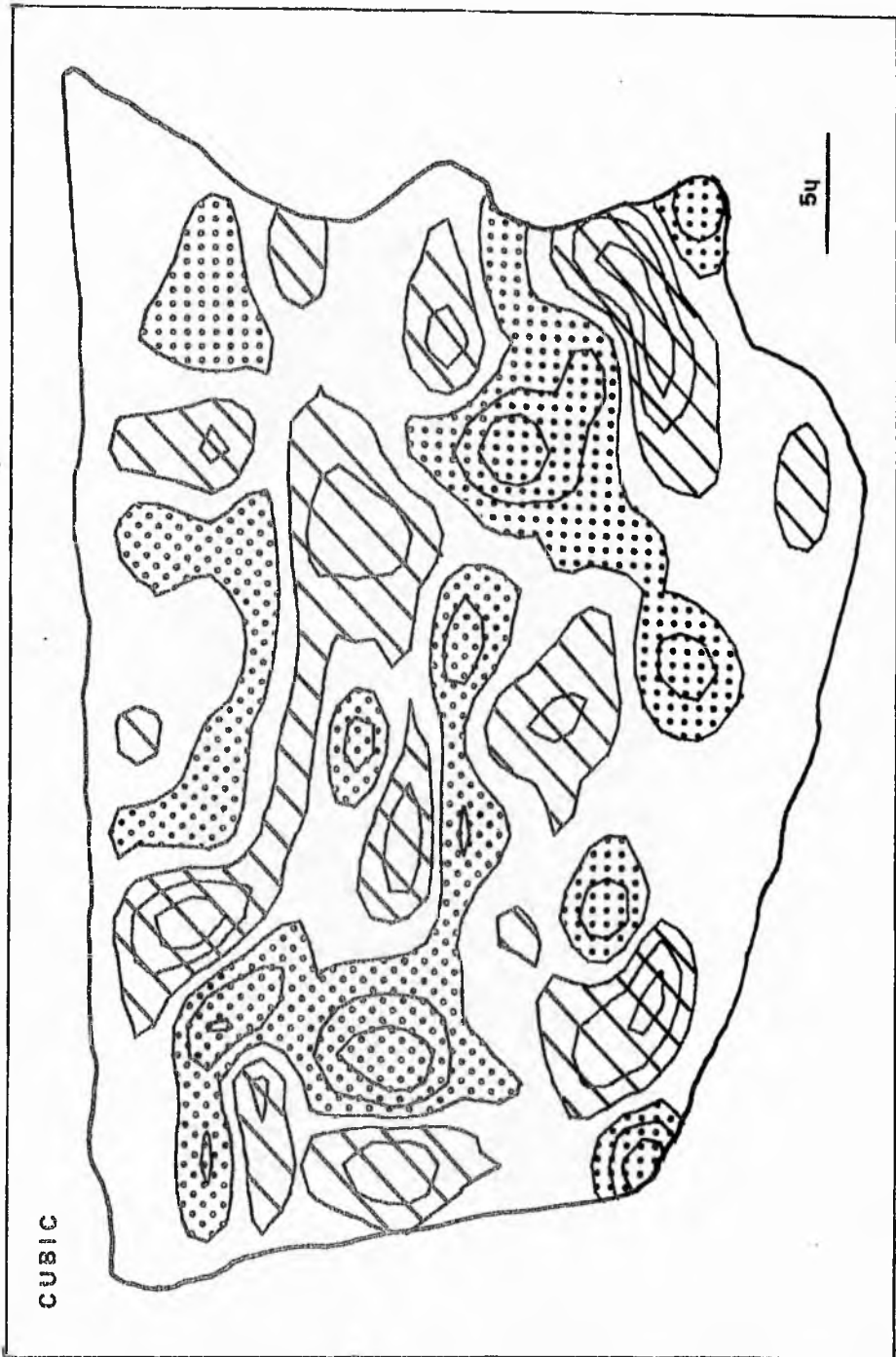


Figure 142. Cubic surface difference map for the variation in reflectance values produced at random over the surface of a graptolite fragment. Hatched areas are of positive difference, dotted areas of negative difference.

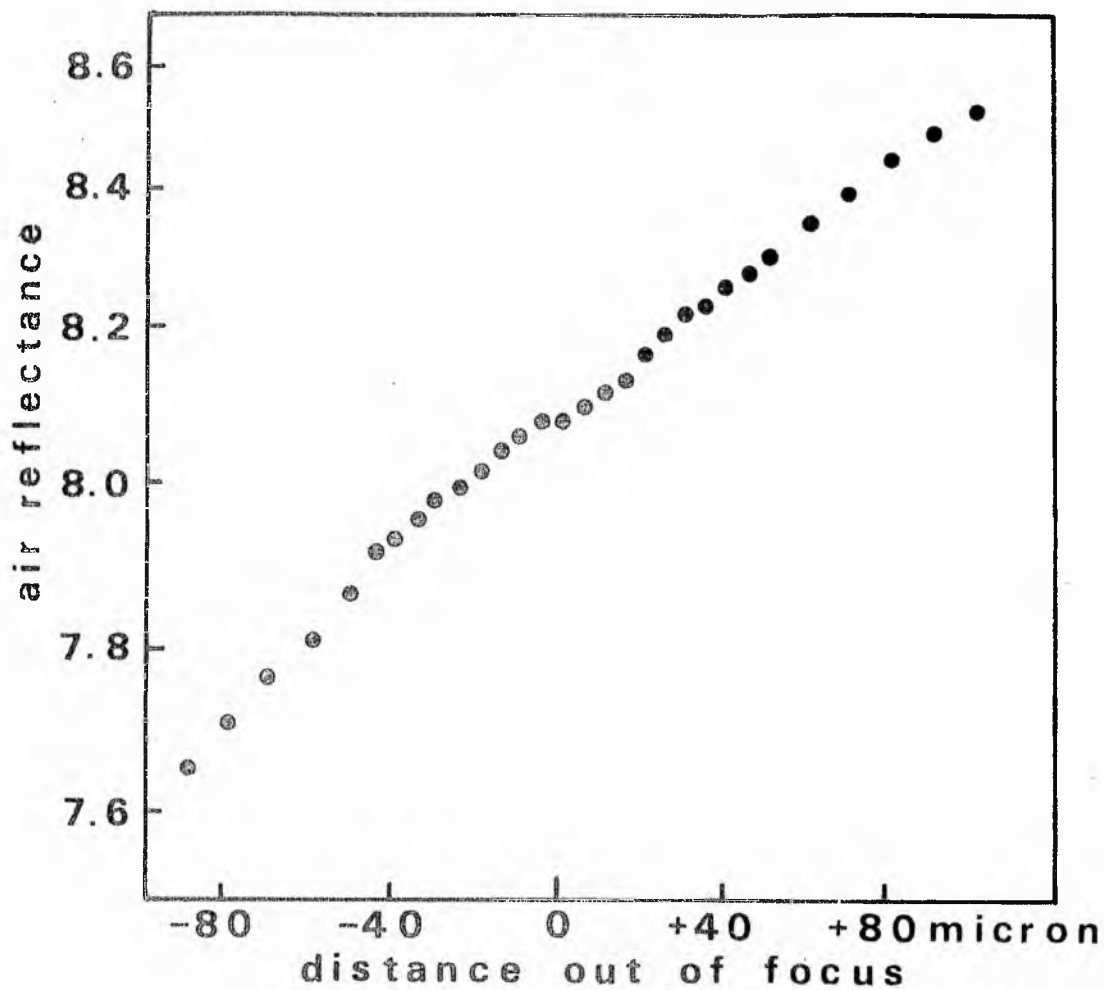


Figure 143. Plot of the variation in reflectivity with focal length (after Jones 1961).

Figure 145. Plots of the variation in reflectivity, refractive and absorptive indices of graptolite fragments from the LB-series of samples from the south side of the dyke at Clanyard Bay.

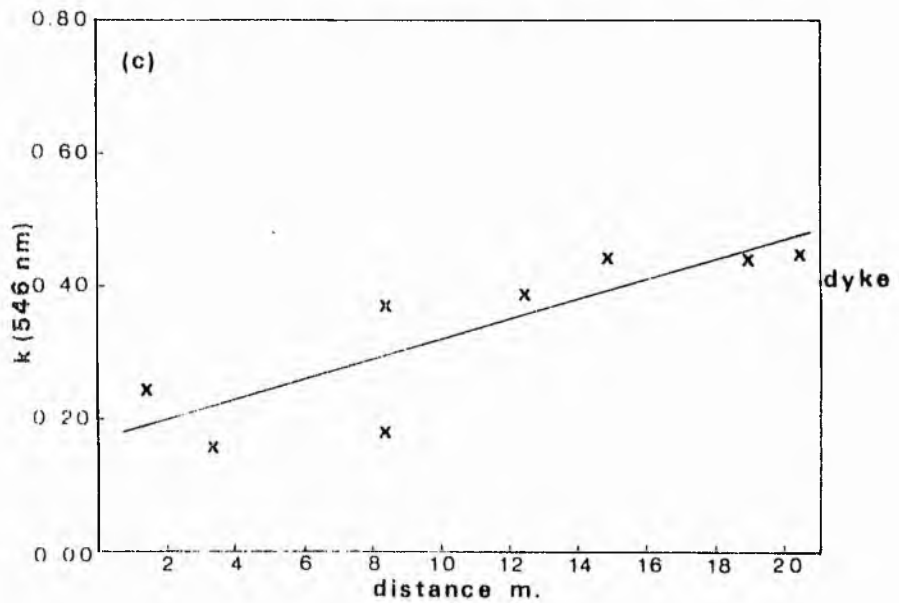
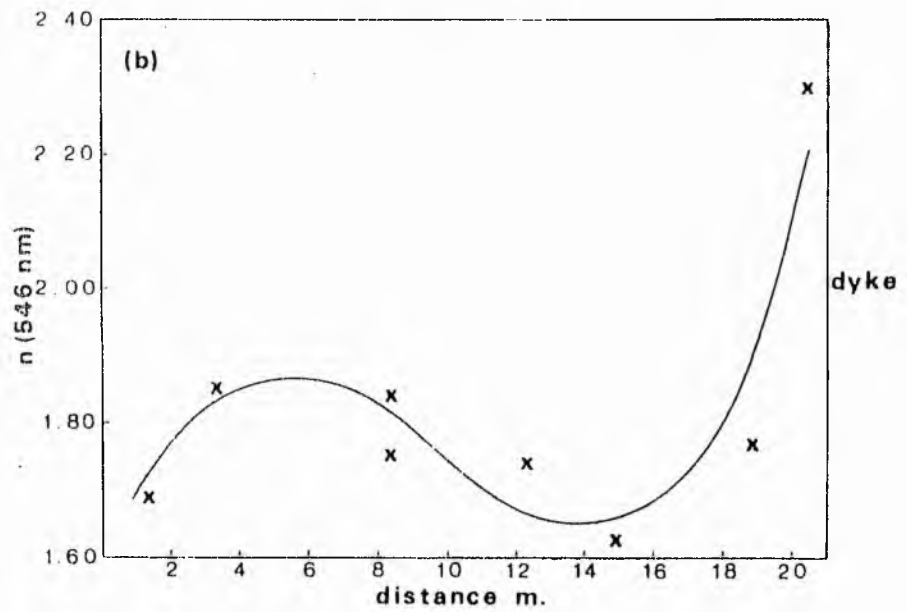
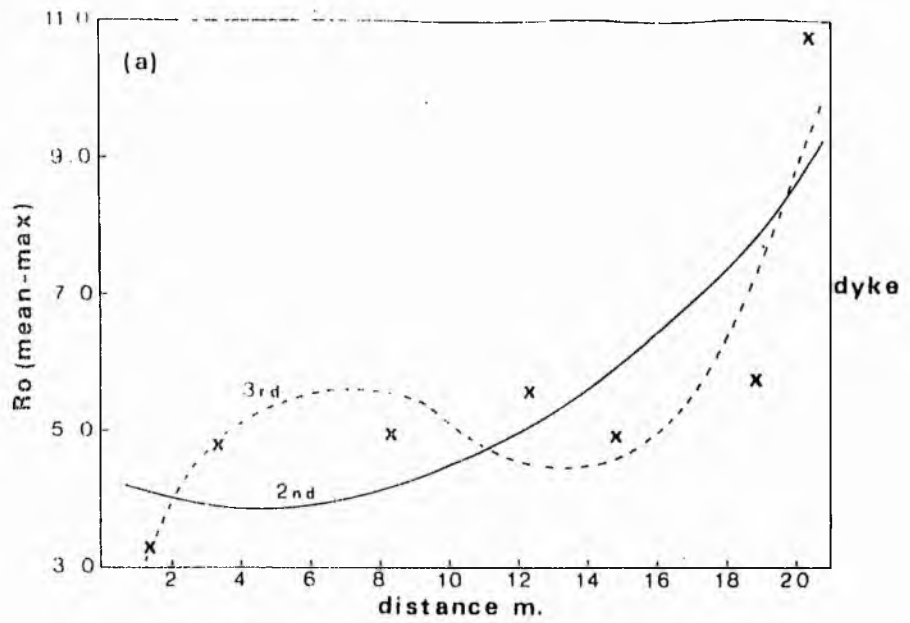


Figure 145. Distance refers to an arbitrary distance measured along the line of section.

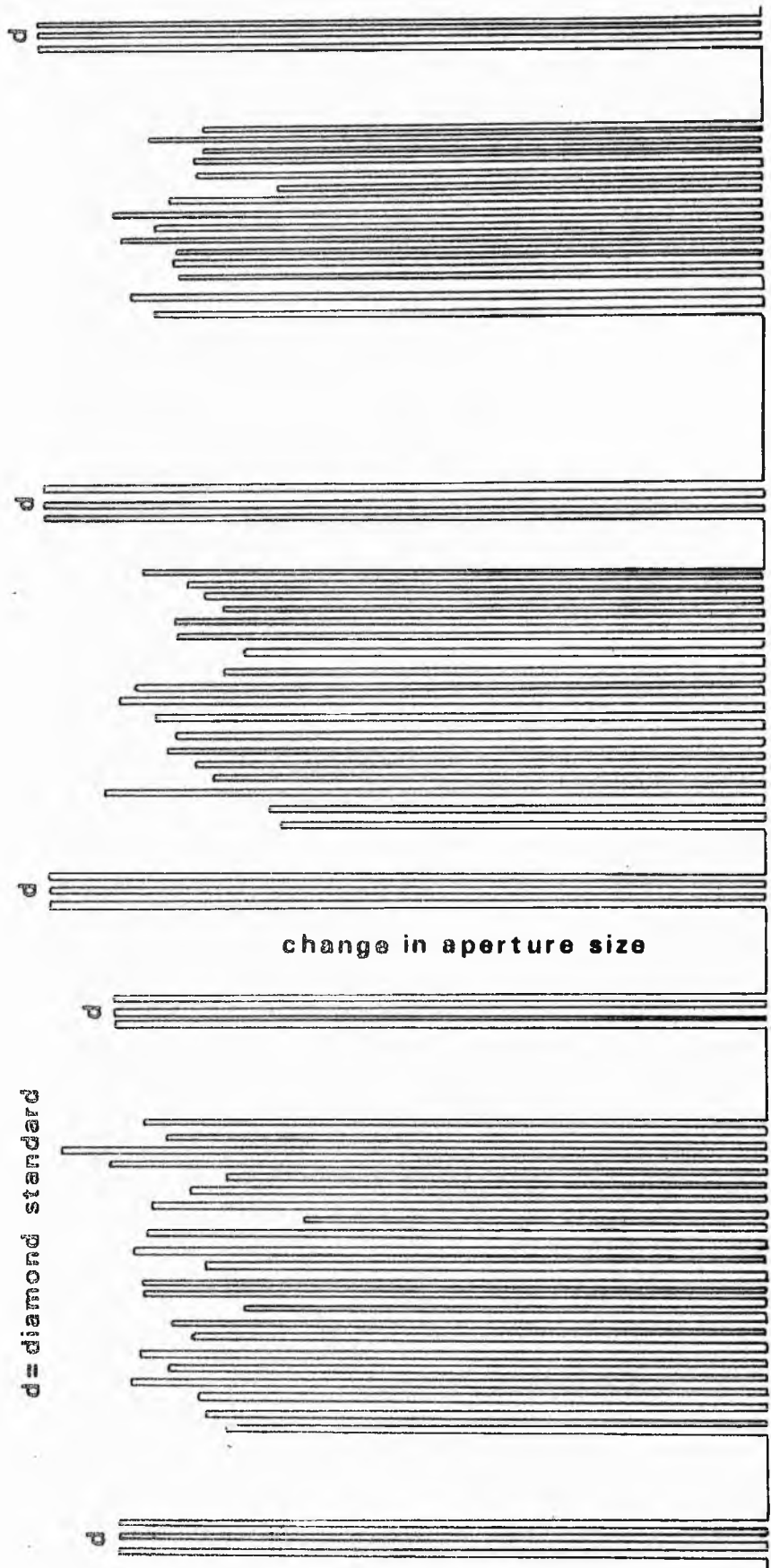


Figure 146. Representative chart recording obtained during the measurement of reflectivity of graptolite fragments.

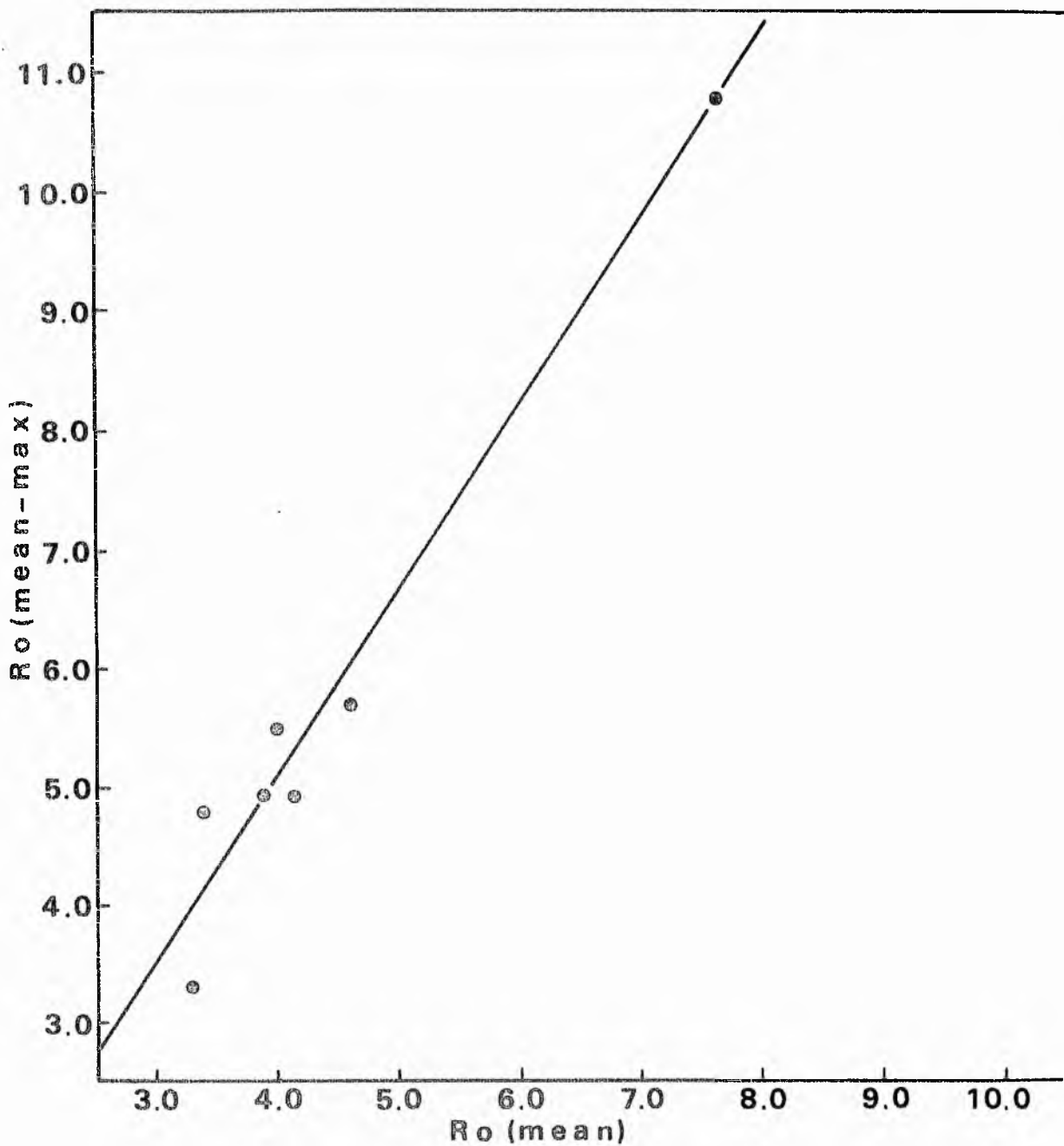


Figure 147. Plot illustrating the relationship for graptolite fragments from the south side of the dyke at Clanyard Bay between mean and mean-maximum reflectivities.

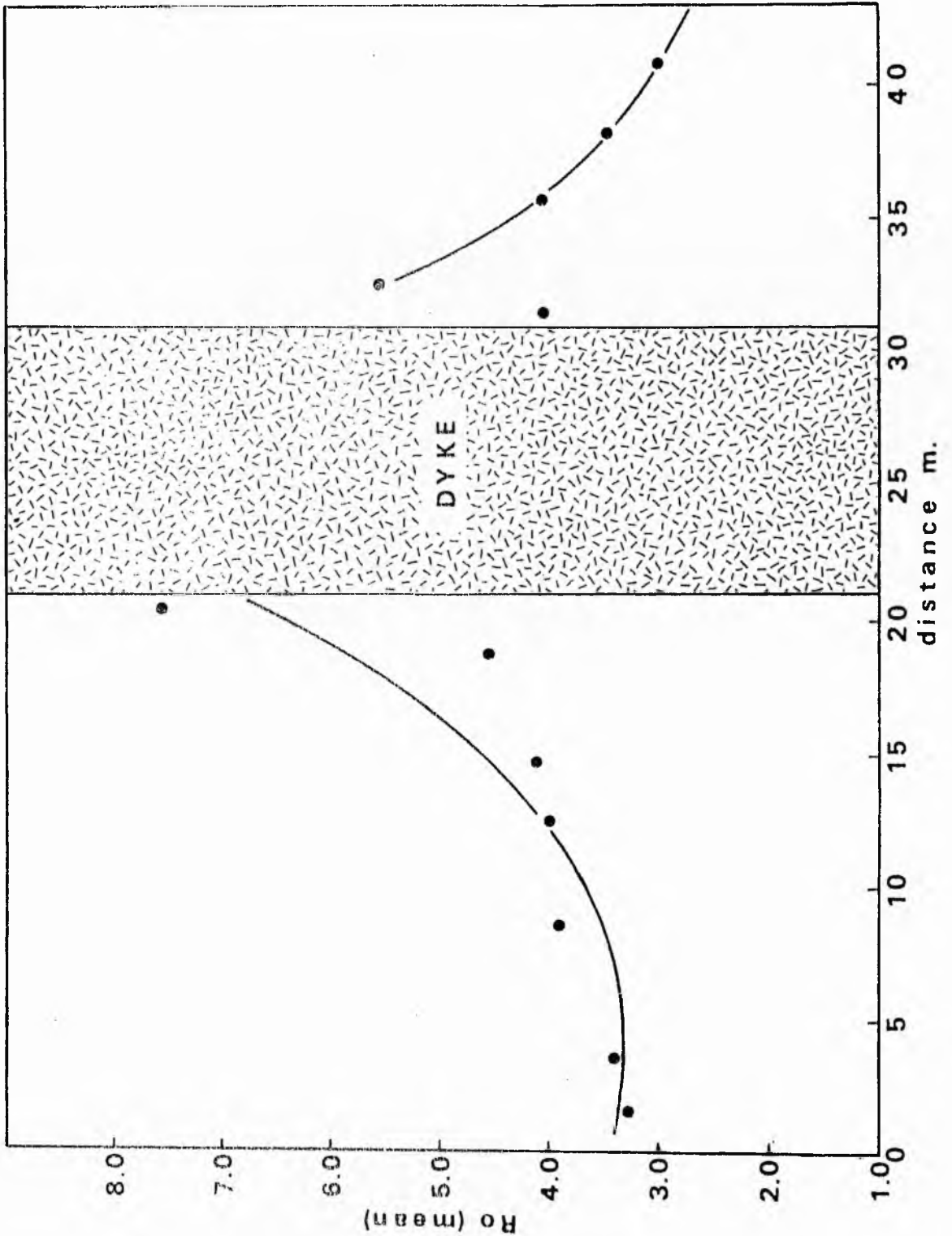


Figure 148. Plot of the variation in reflectivity of graptolite fragments along a measured section at Clanyard Bay (see Figure 144; LB-series). Distance refers to an arbitrary distance measured along the line of section.

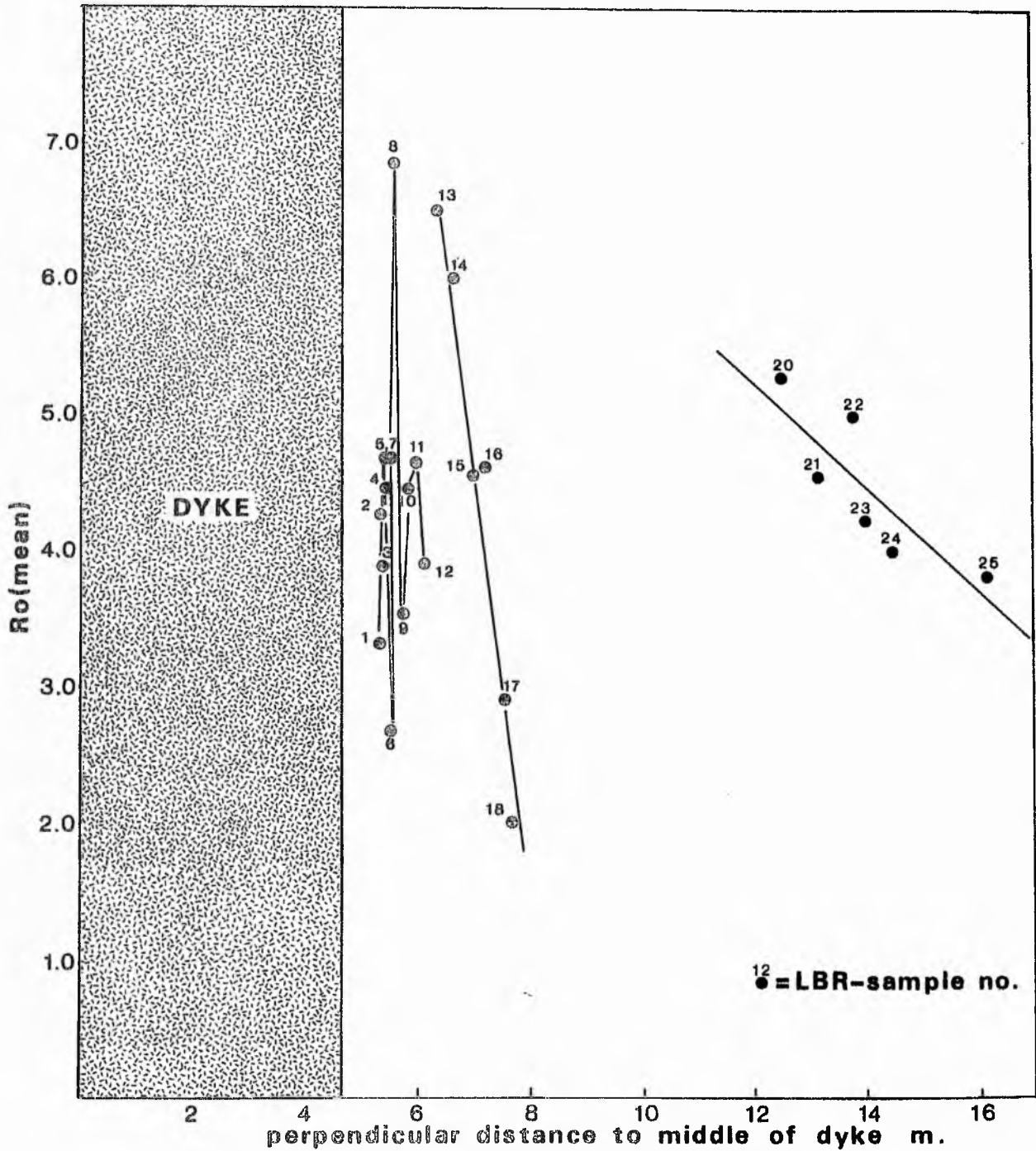


Figure 149. Plot of the variation in reflectivity of graptolite fragments with distance for samples collected from the north of the dyke at Clanyard Bay.

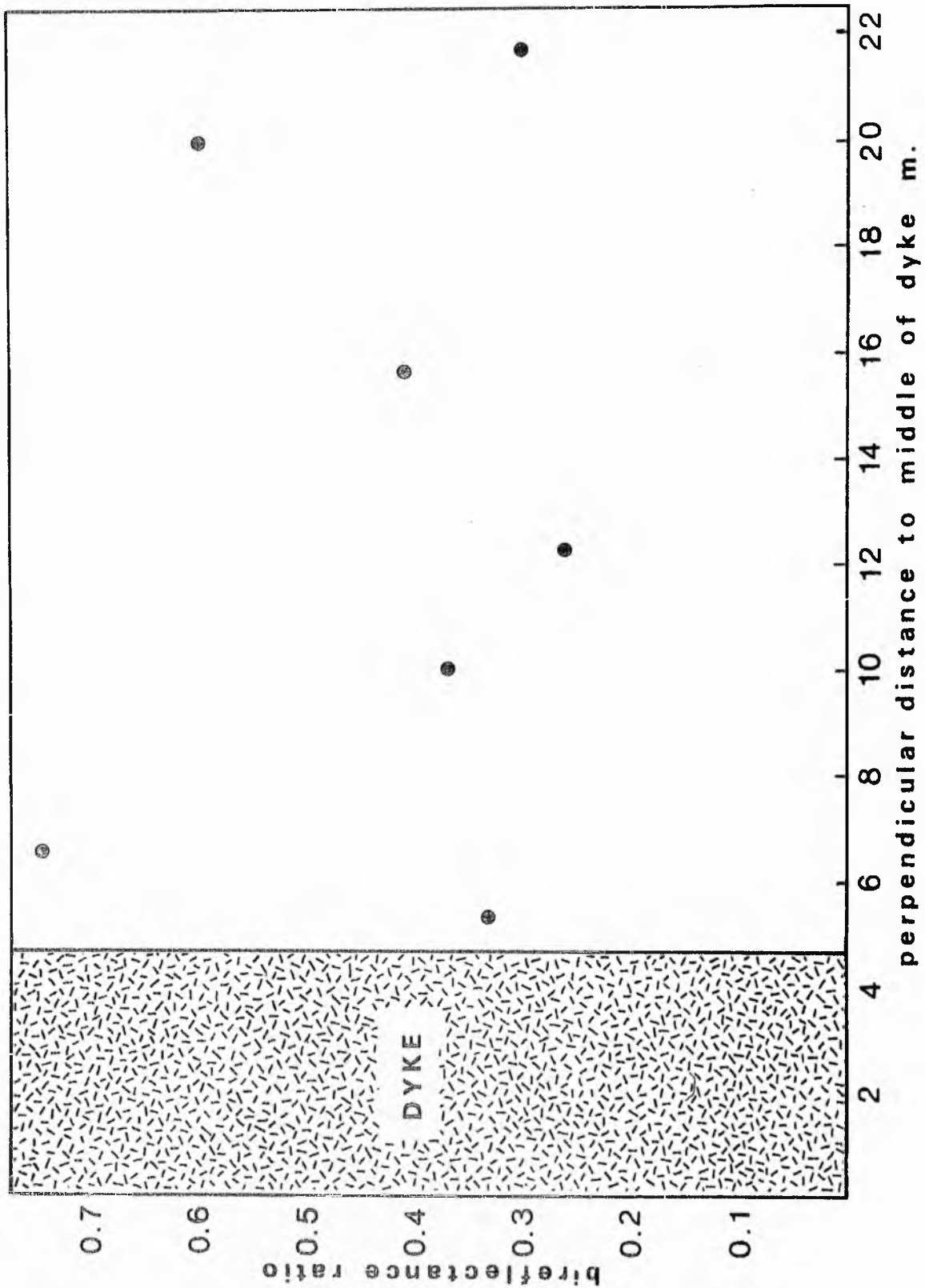


Figure 150. Plot of the variation in the bireflectance ratio of graptolite fragments with distance from an igneous dyke.

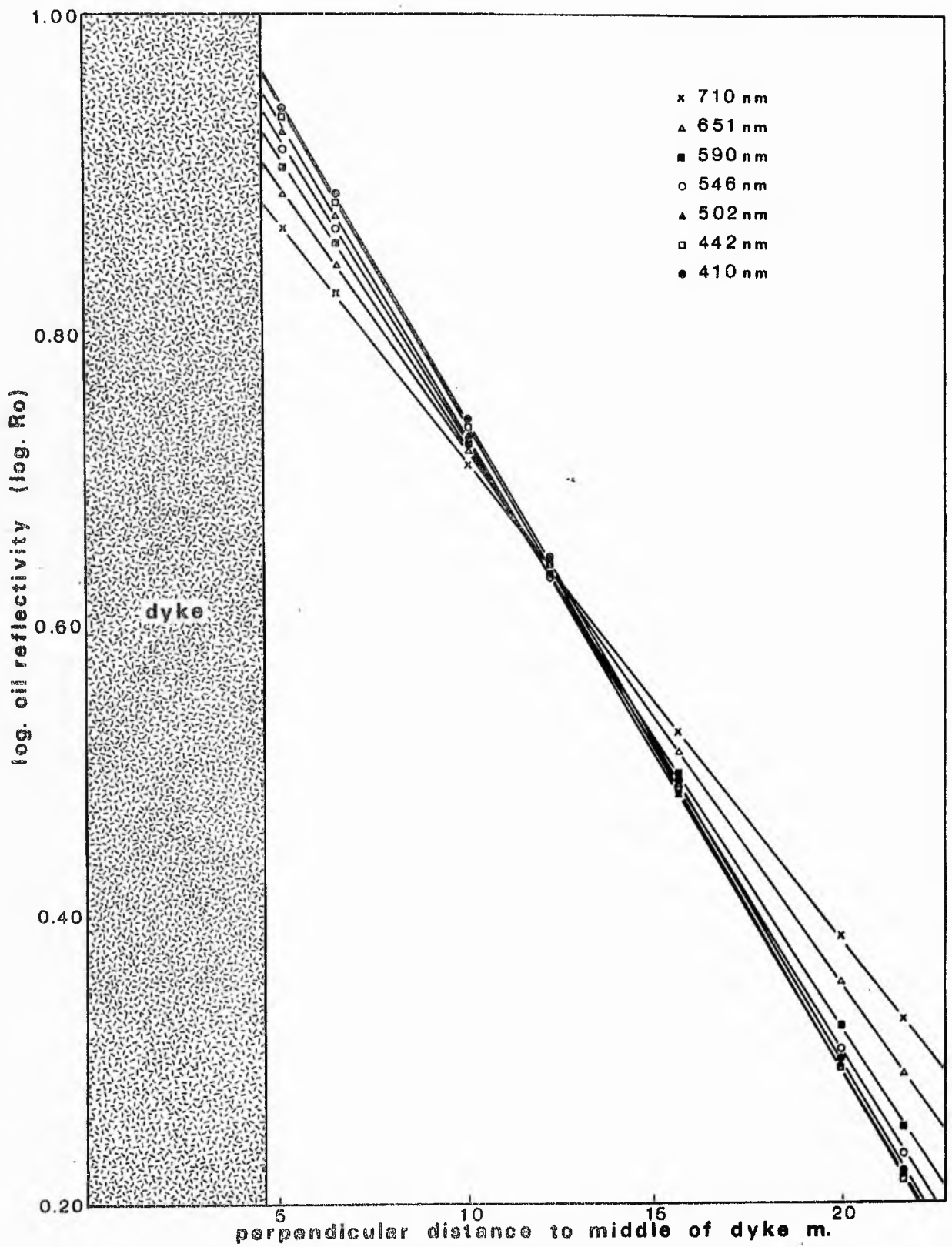


Figure 151. Plot illustrating the variation in reflectivity at selected wavelengths of graptolite fragments adjacent to an igneous dyke.

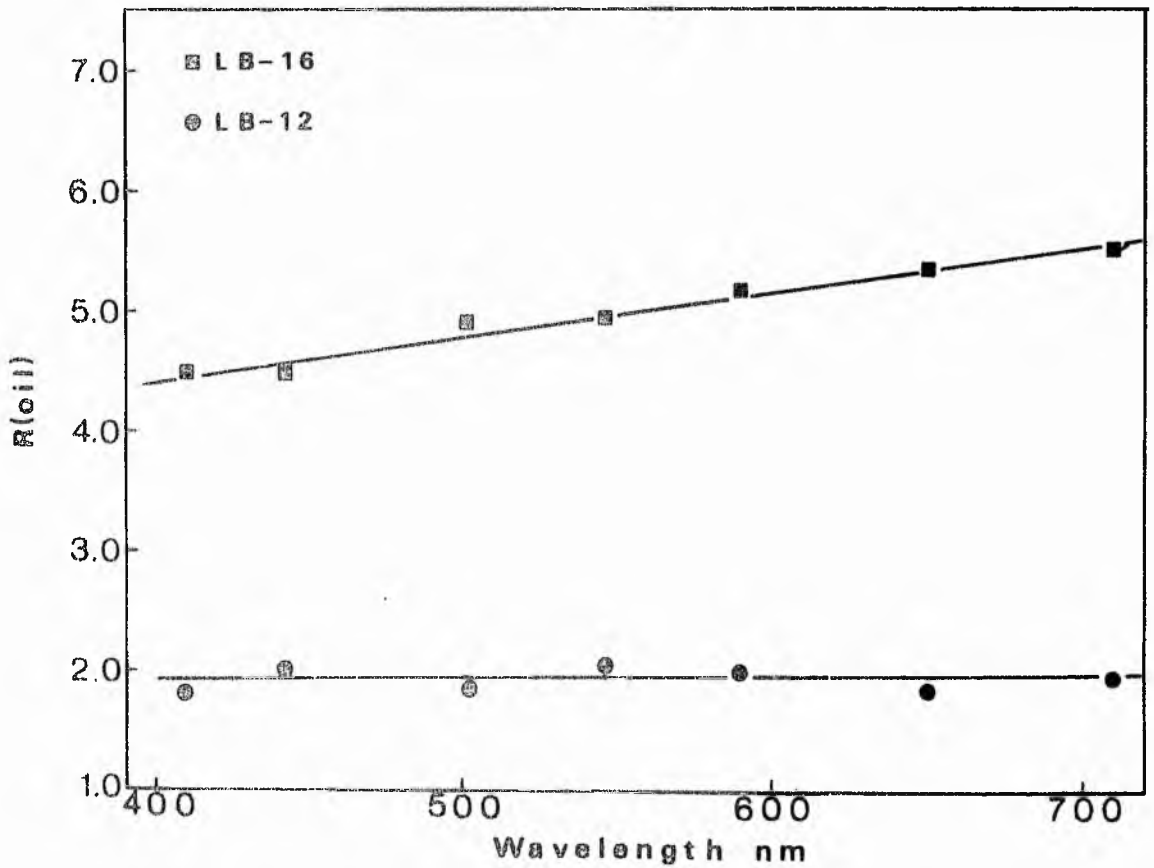
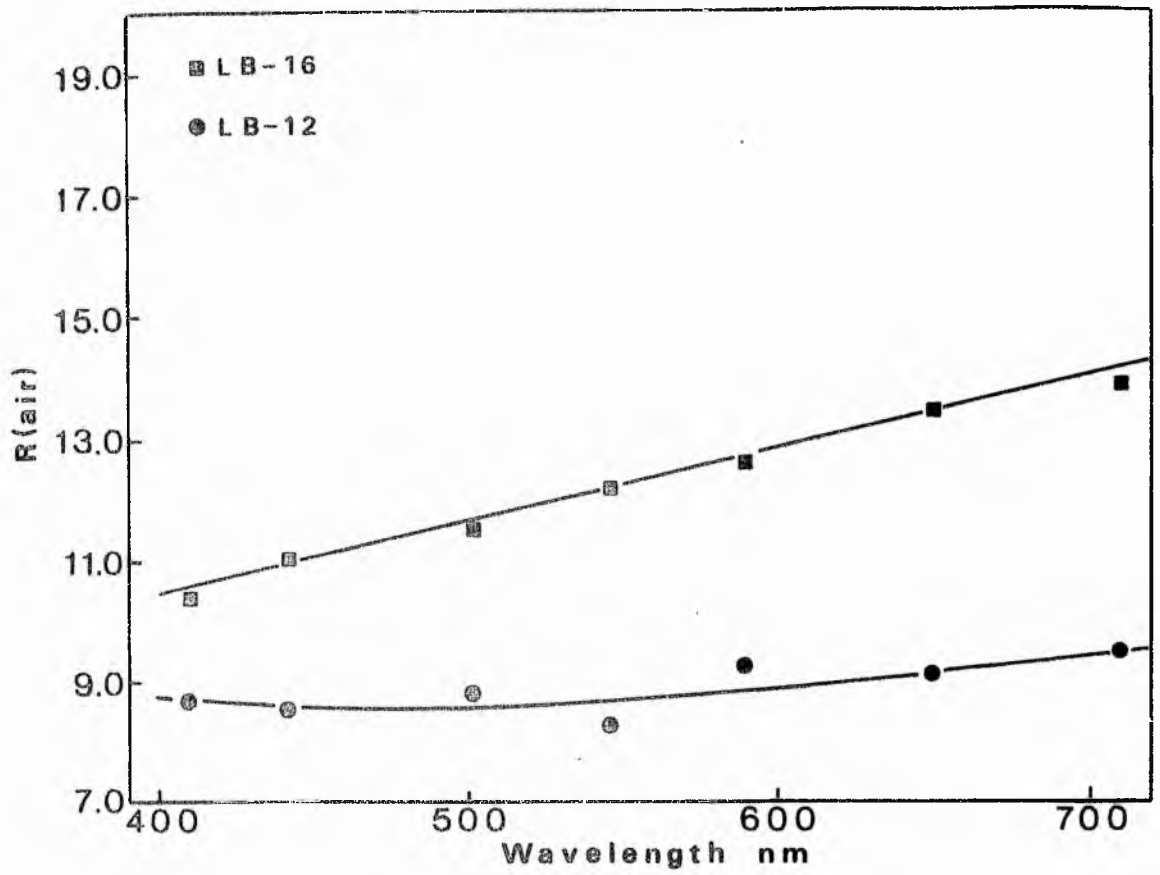


Figure 152. Plots illustrating the dispersion with wavelength of oil and air reflectivities in samples LB-12 and LB-16.

Figure 153. Plots illustrating the dispersion with wavelength of oil and air reflectivities in samples LB-17A, LB-15 and LB-13.

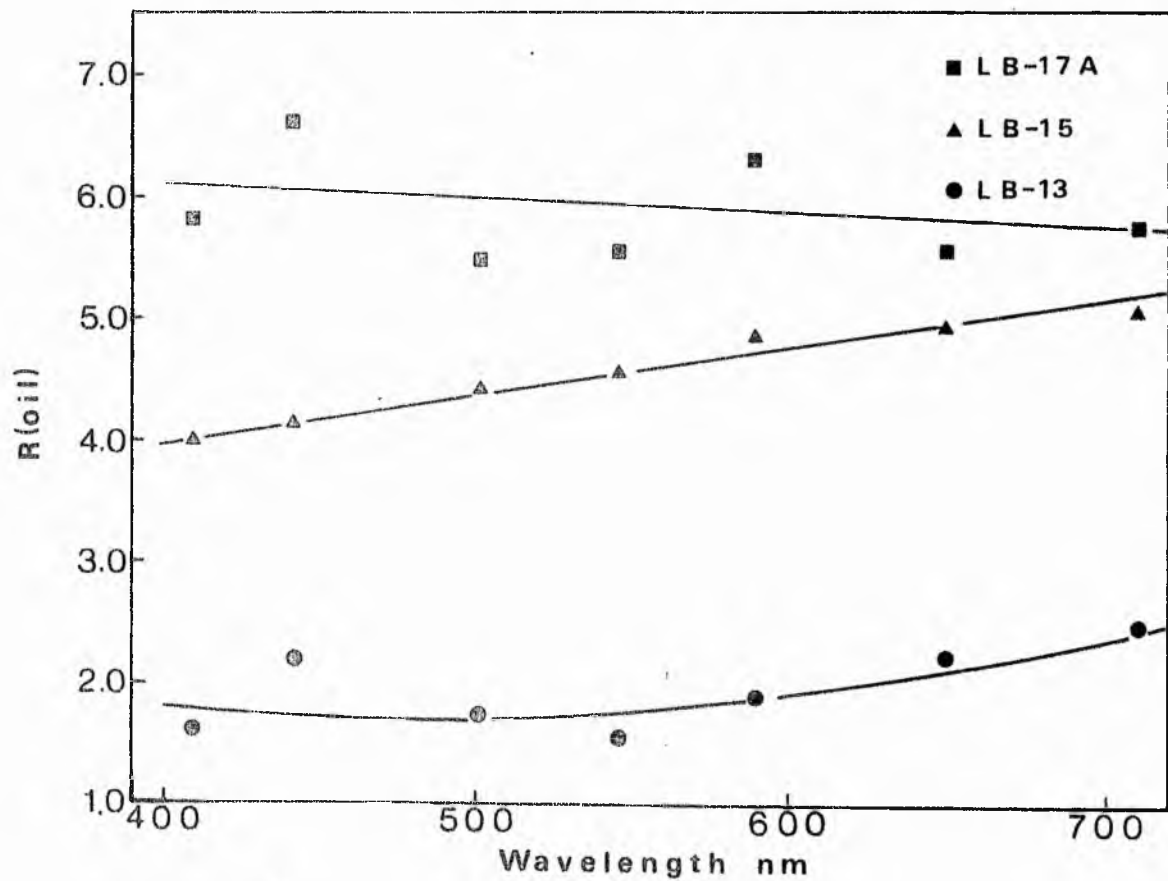
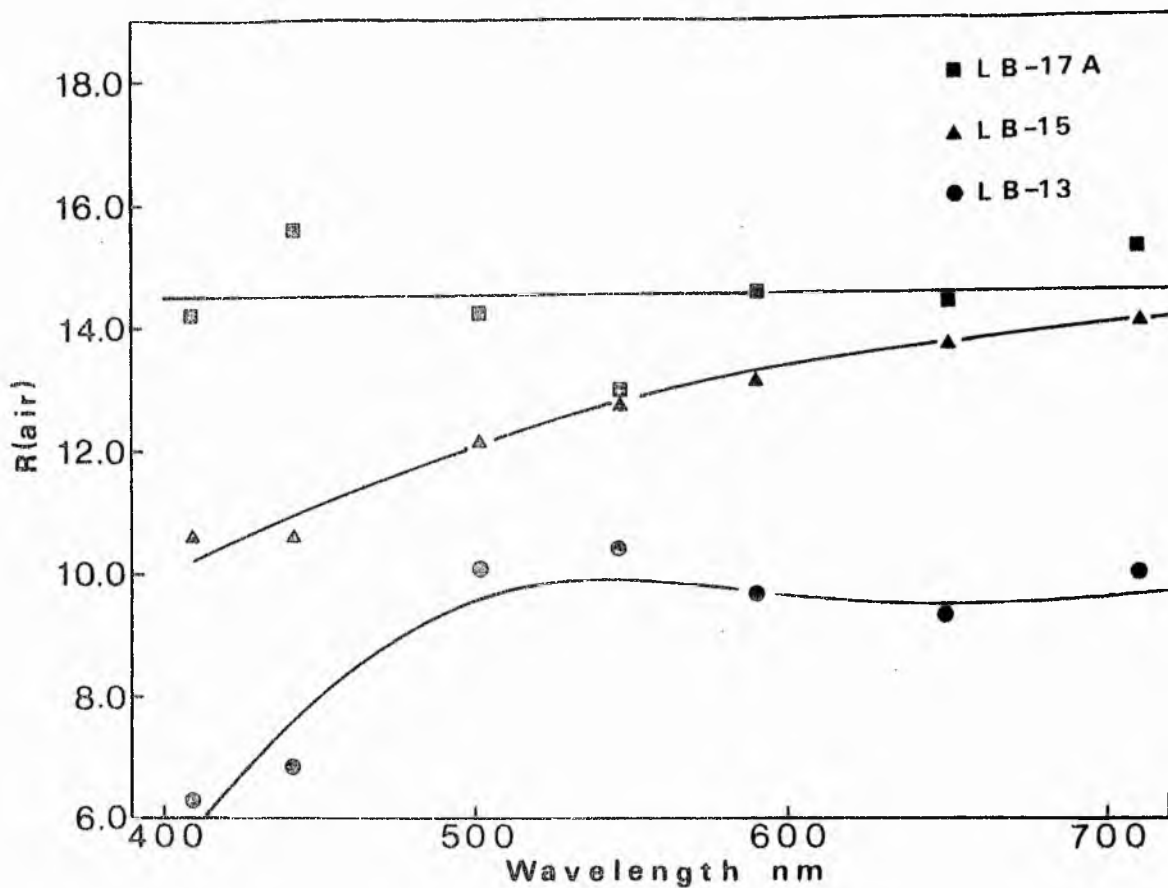


Figure 153.

Figure 154. Plots illustrating the dispersion with wavelength of oil and air reflectivities in samples LB-14 (1) and LB-14 (2).

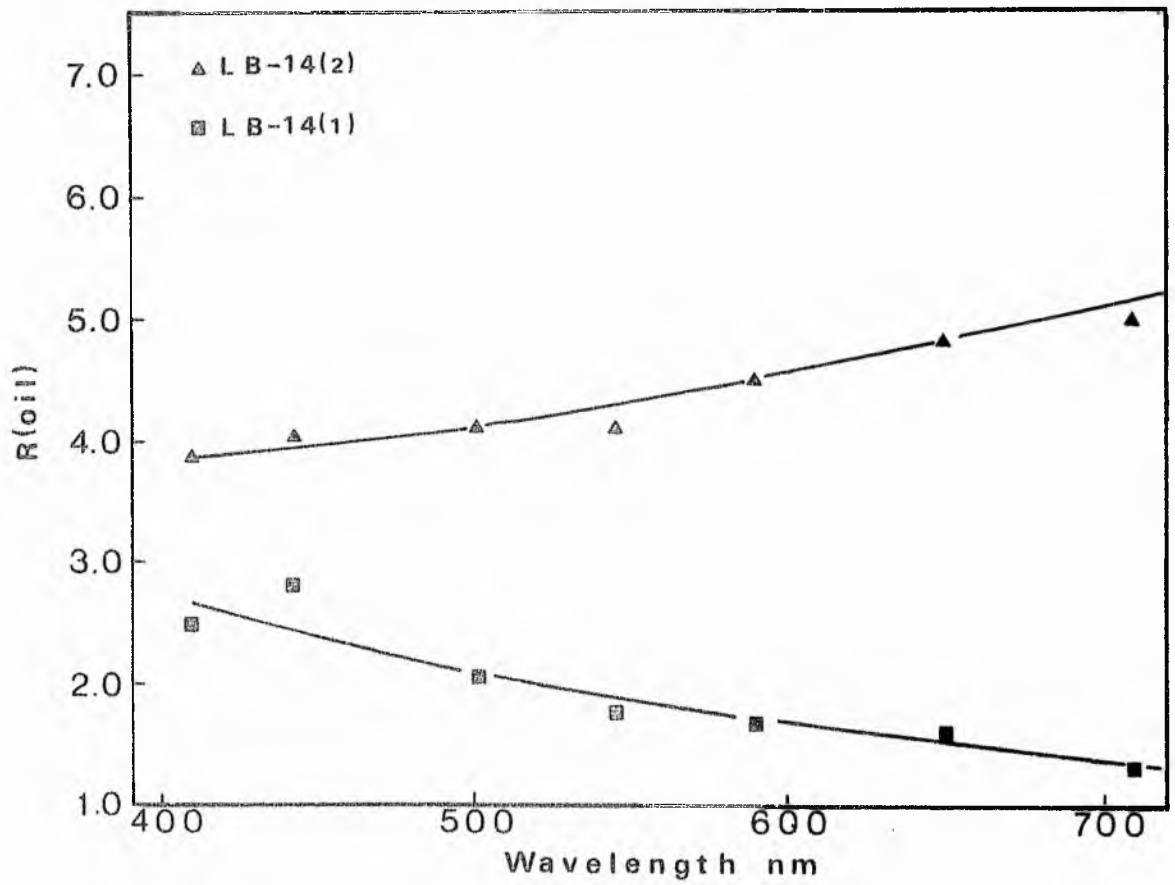
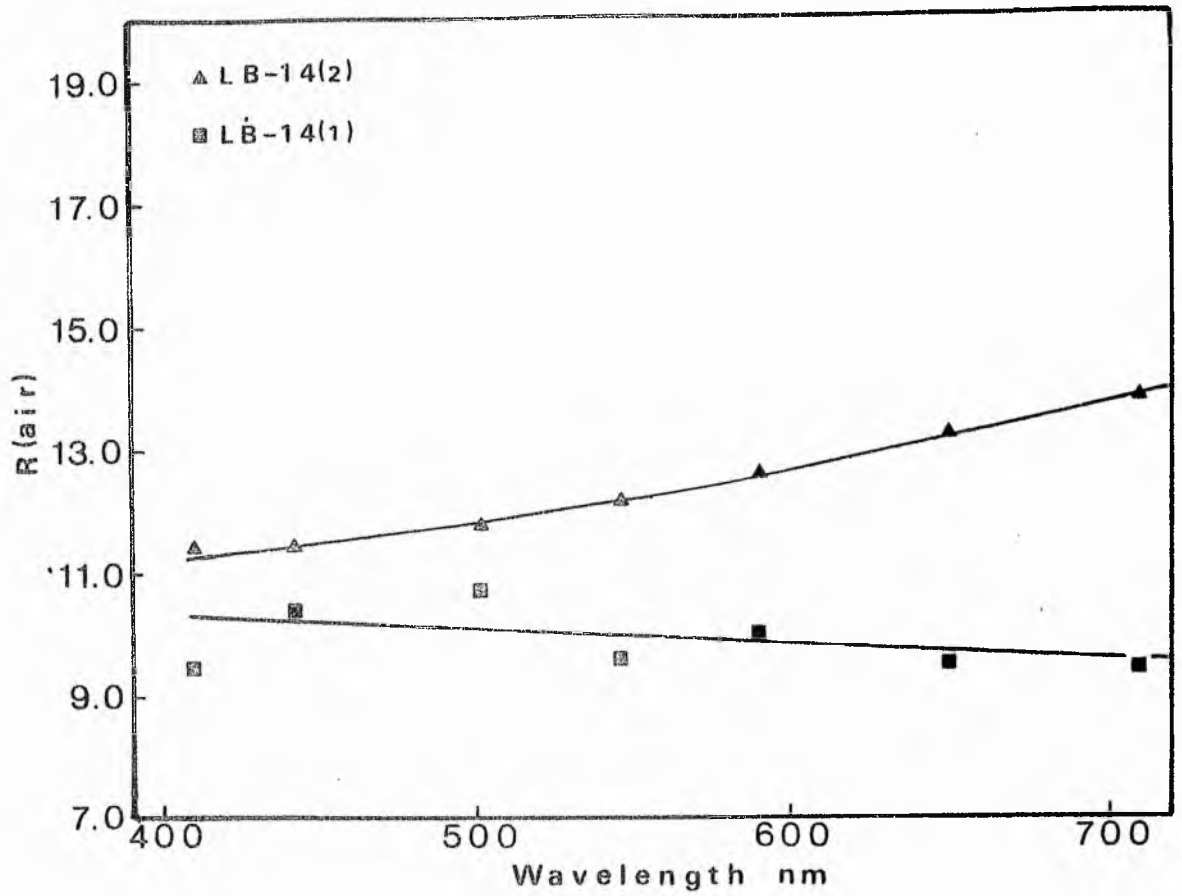


Figure 154.

Figure 155. Plots illustrating the dispersion with wavelength of oil and air reflectivities in sample LB-18.

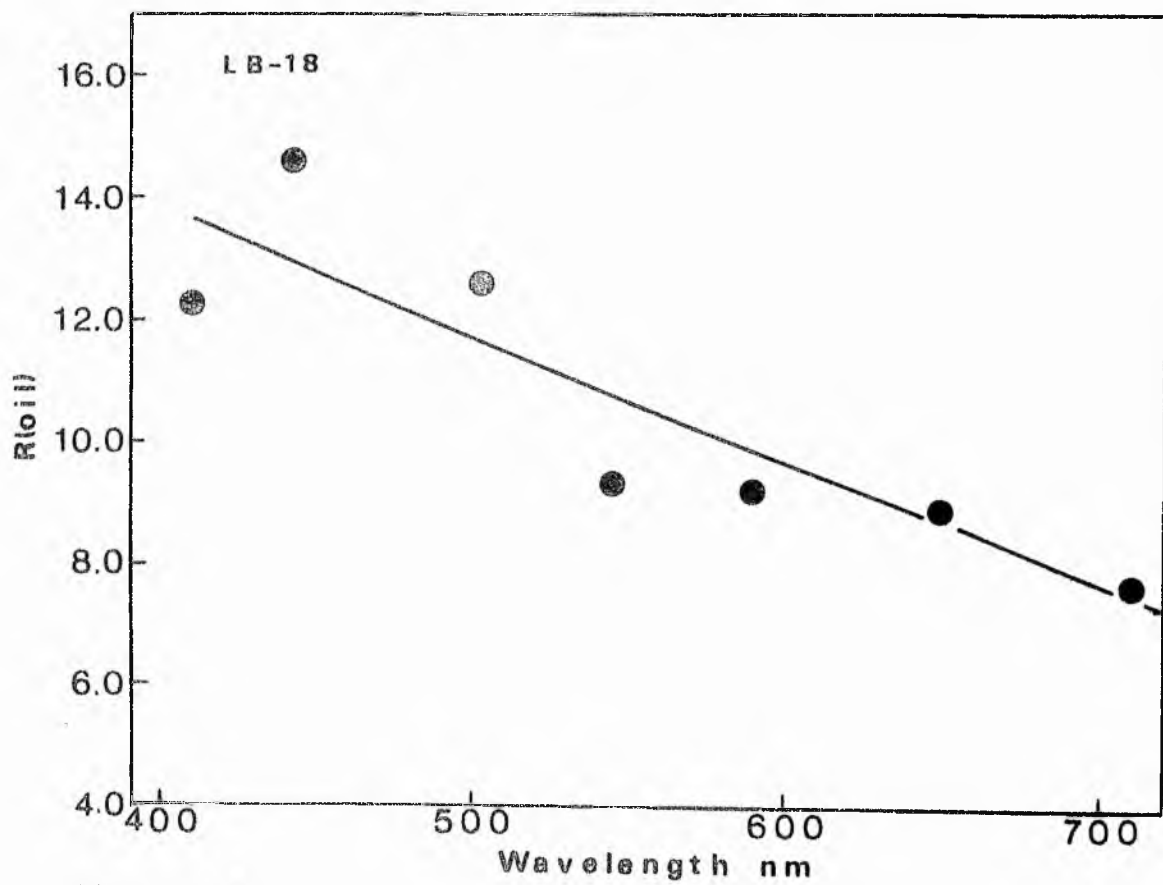
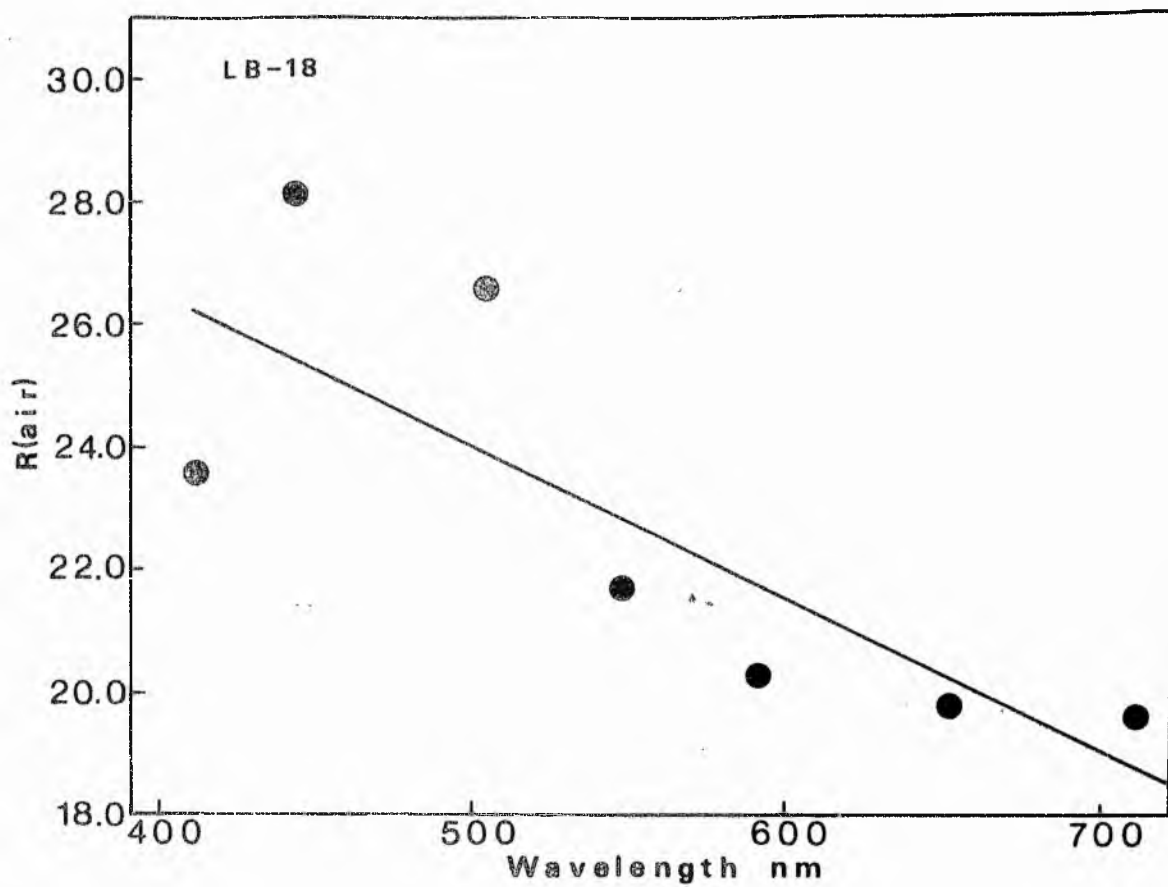


Figure 155.

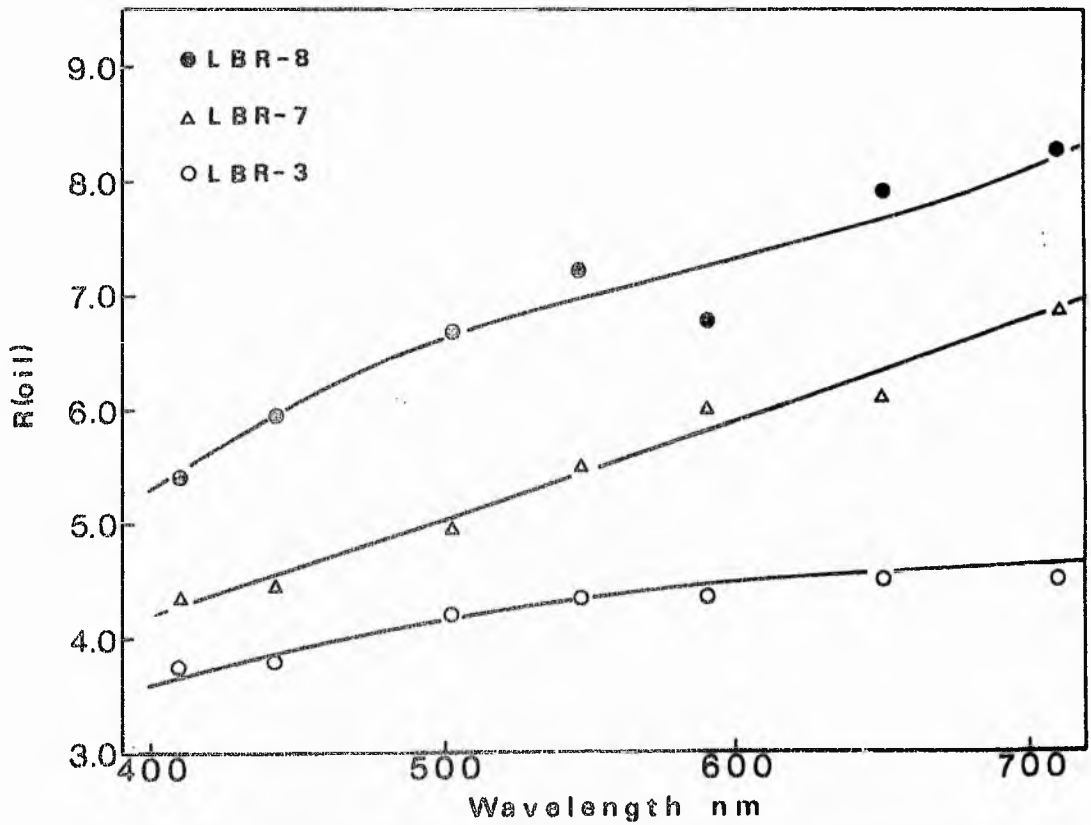
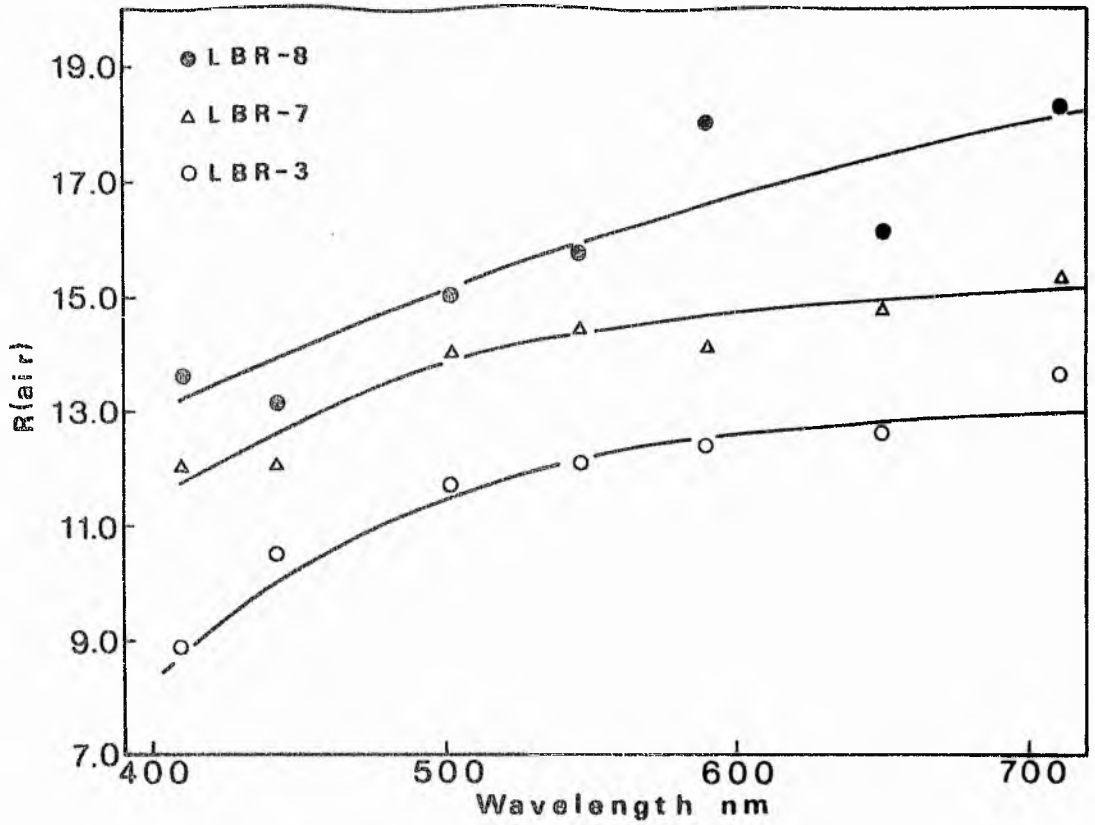


Figure 156. Plots illustrating the dispersion with wavelength of oil and air reflectivities in samples LBR-8, LBR-7 and LBR-3.

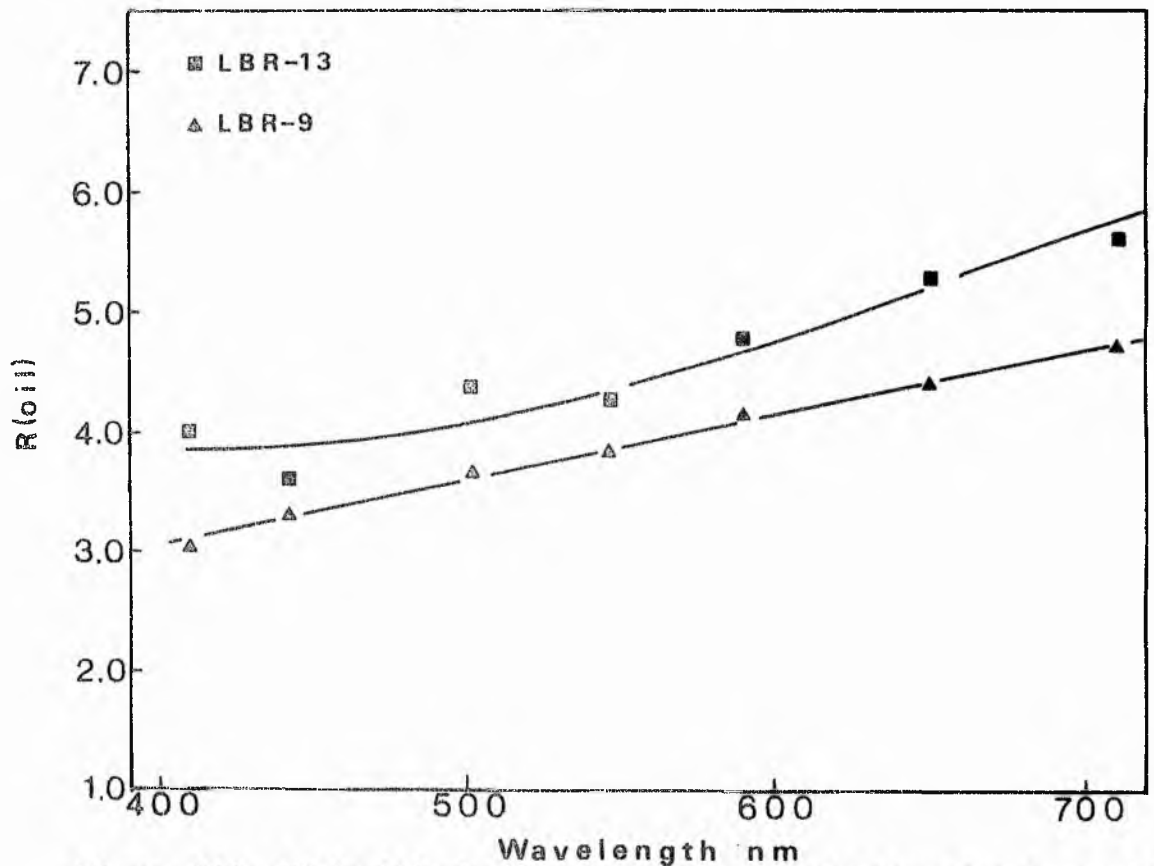
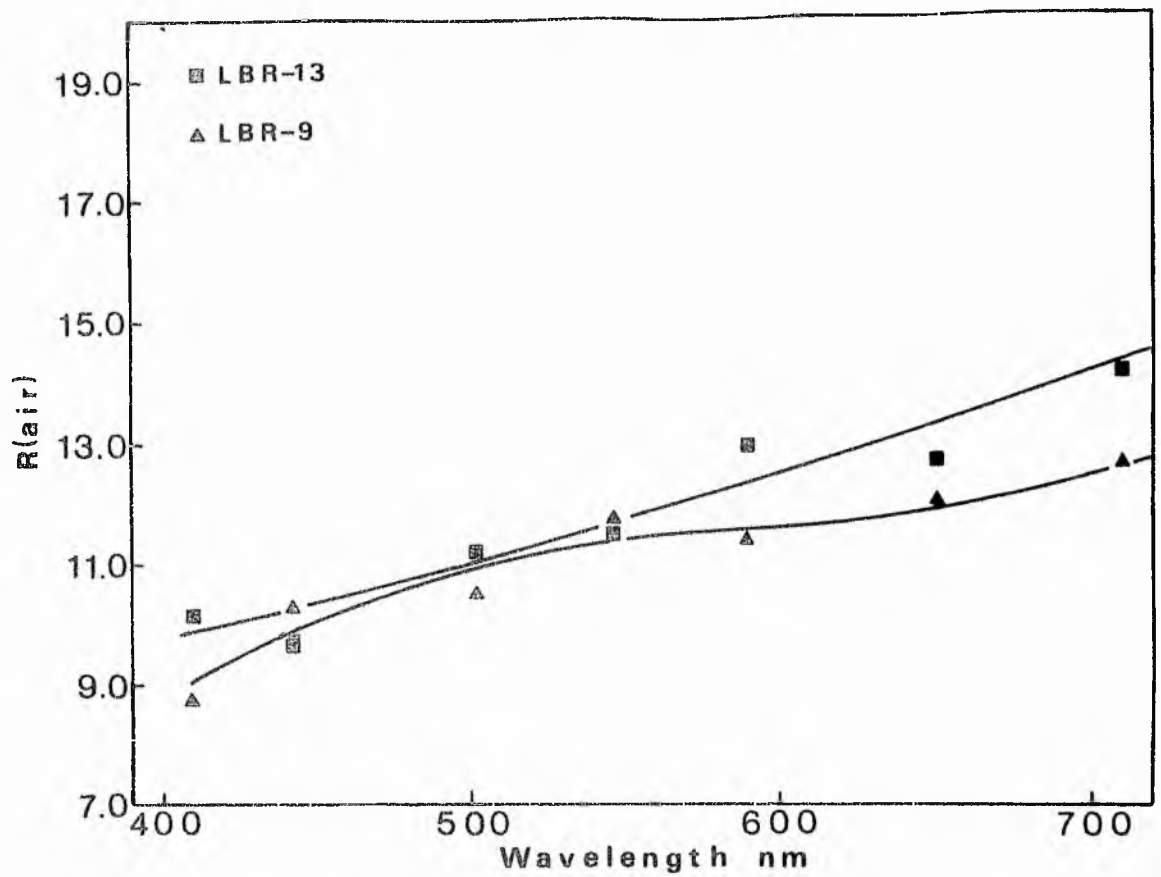


Figure 157. Plots illustrating the dispersion with wavelength of oil and air reflectivities in samples LBR-13 and LBR-9.

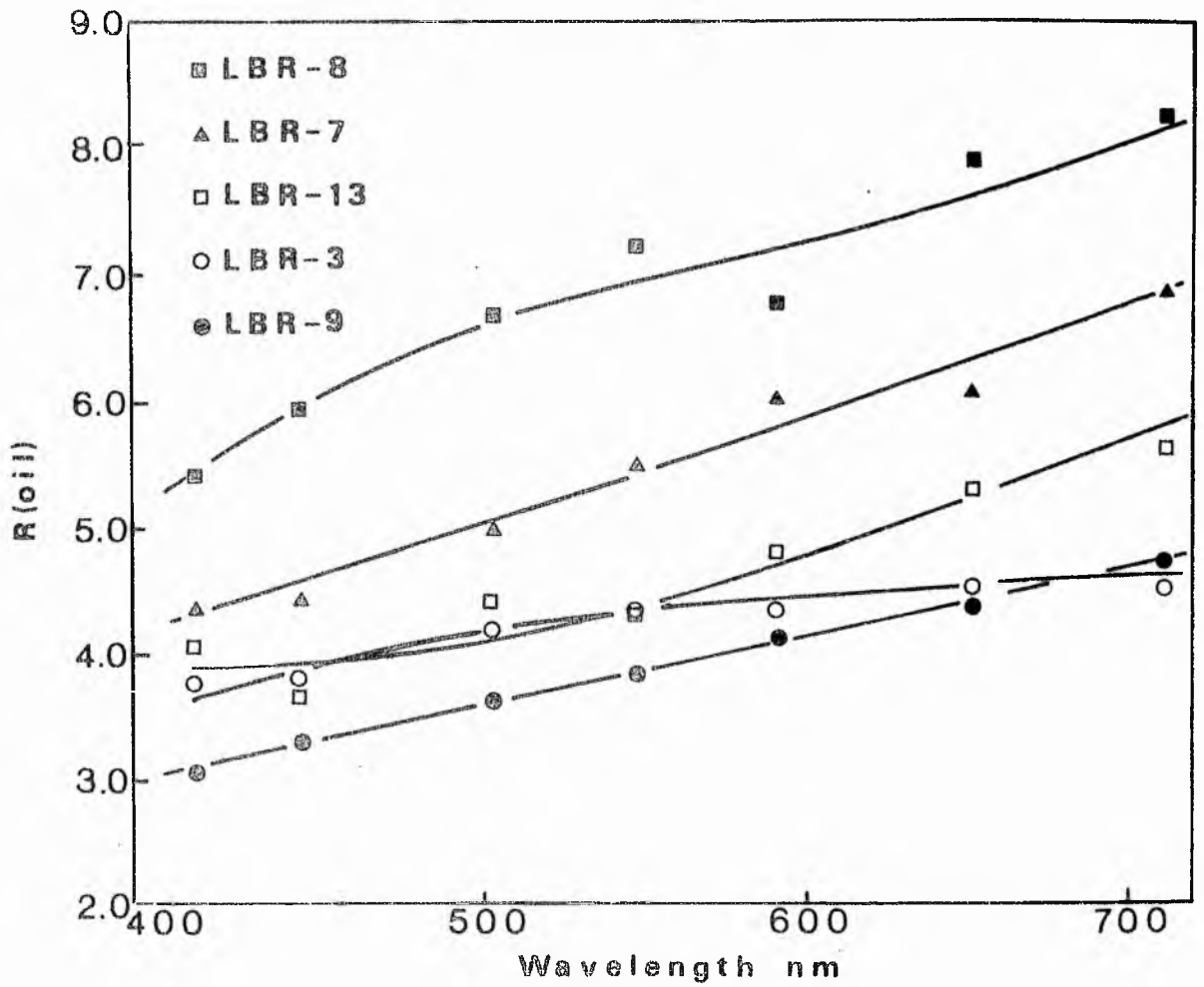


Figure 158. Composite plot illustrating the dispersion with wavelength of the reflectivity in samples from the LBR-series.

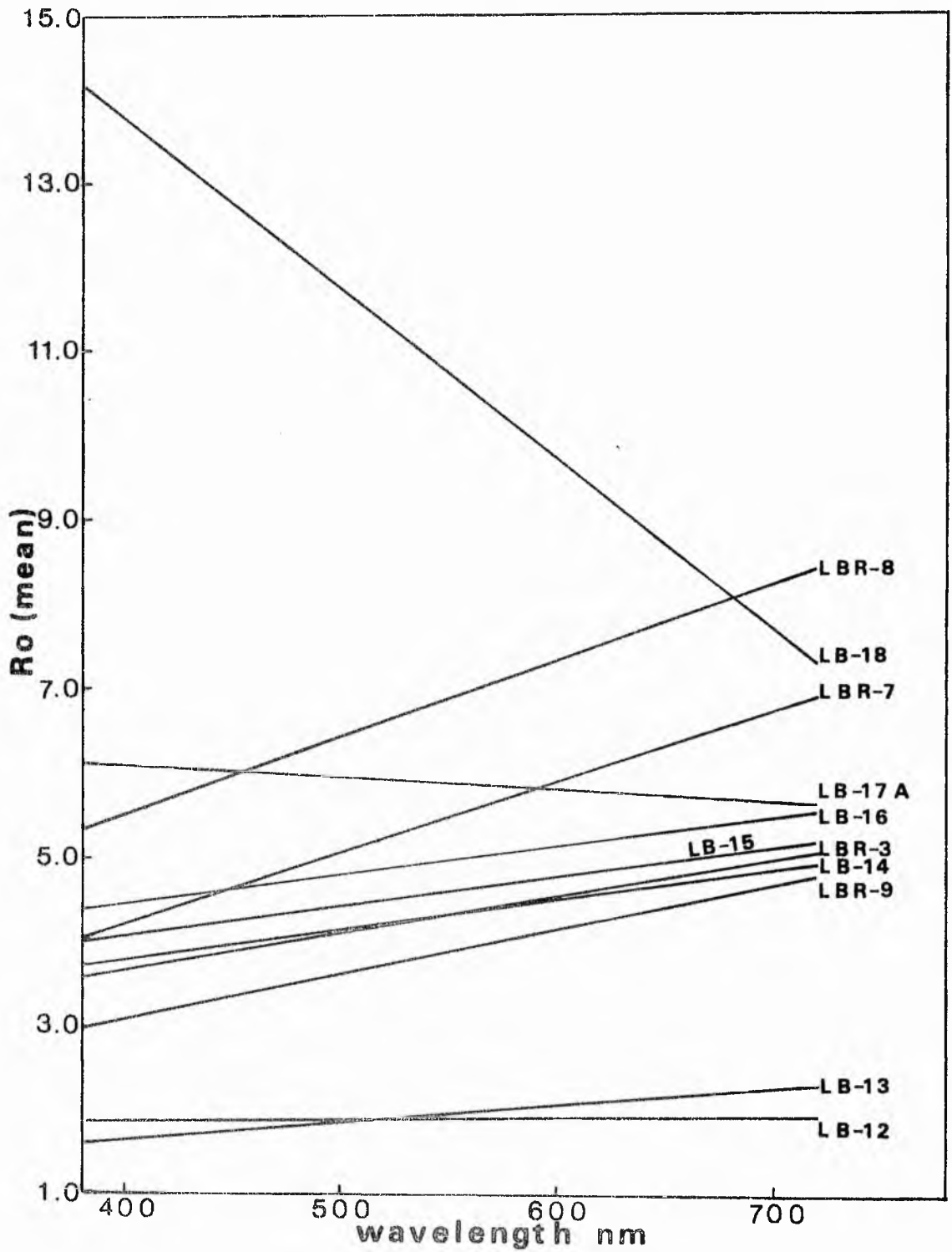


Figure 159. Plot of linear regression lines for the spectral variation of graptolite reflectivity.

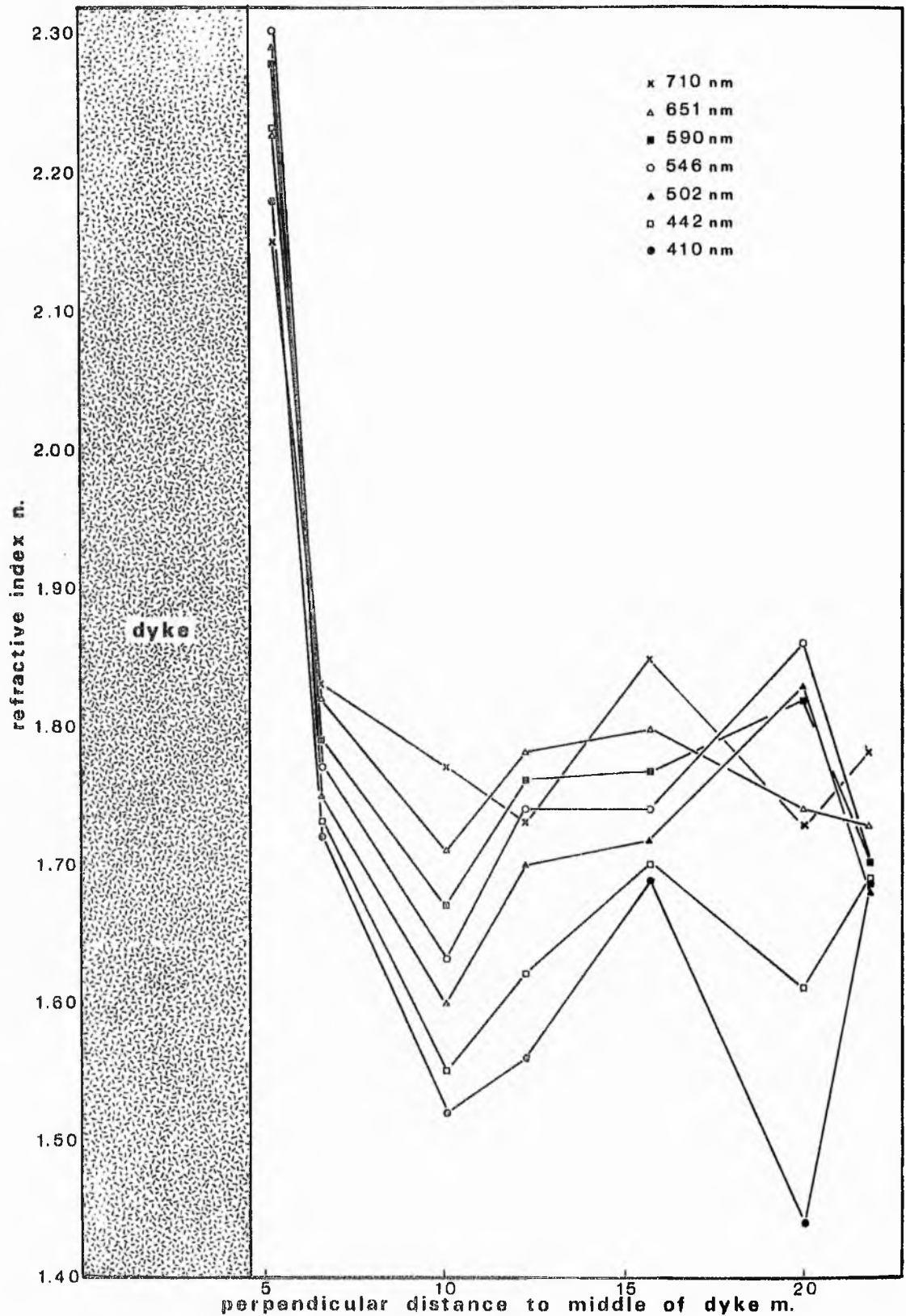


Figure 160. Plot illustrating the variation with distance from an igneous dyke of the refractive index of graptolite fragments.

Figure 161. Plots illustrating the dispersion with wavelength of the absorptive and refractive indices in samples LB-12 and LB-16.

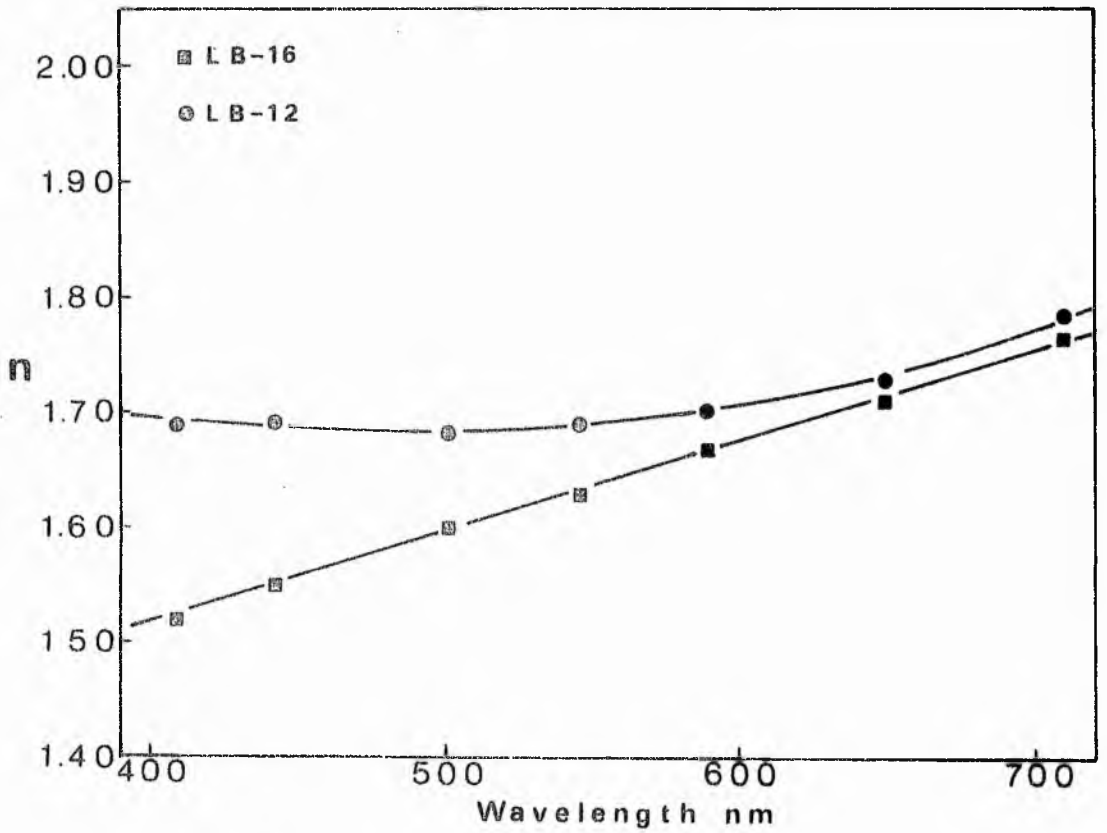
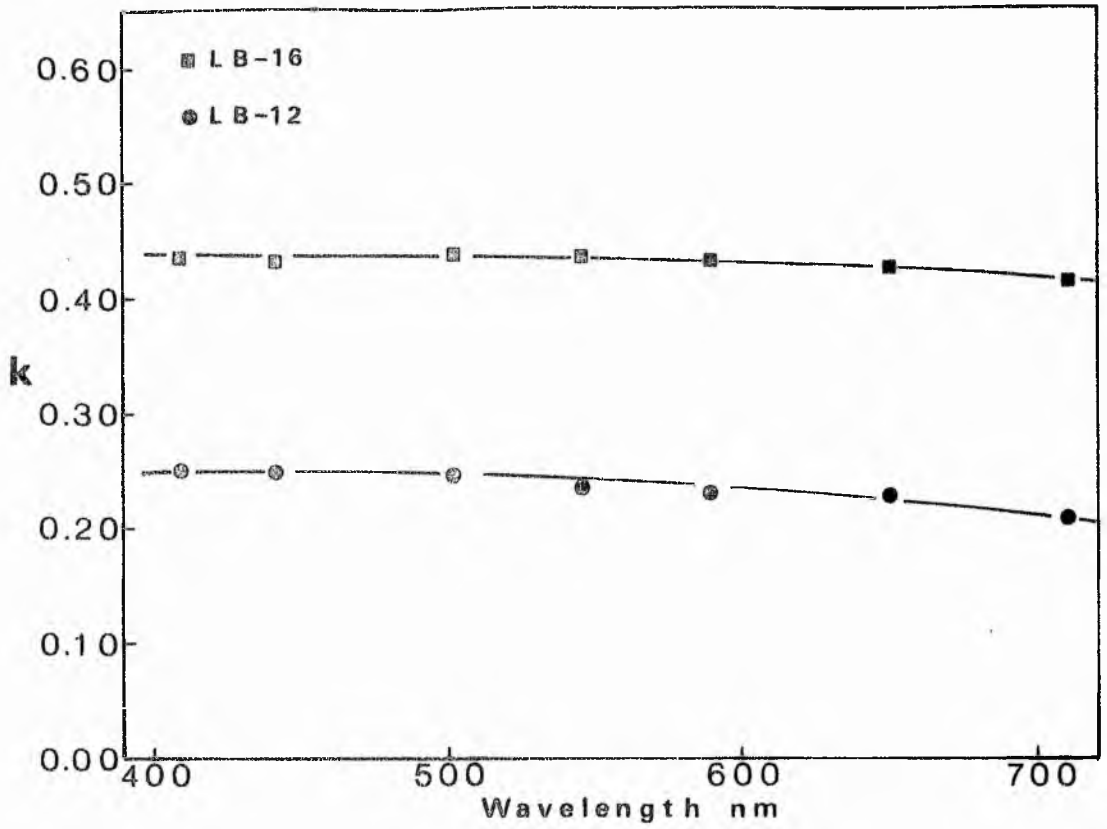


Figure 161.

Figure 162. Plots illustrating the dispersion with wavelength of the absorptive and refractive indices in samples LB-17A, LB-15 and LB-13.

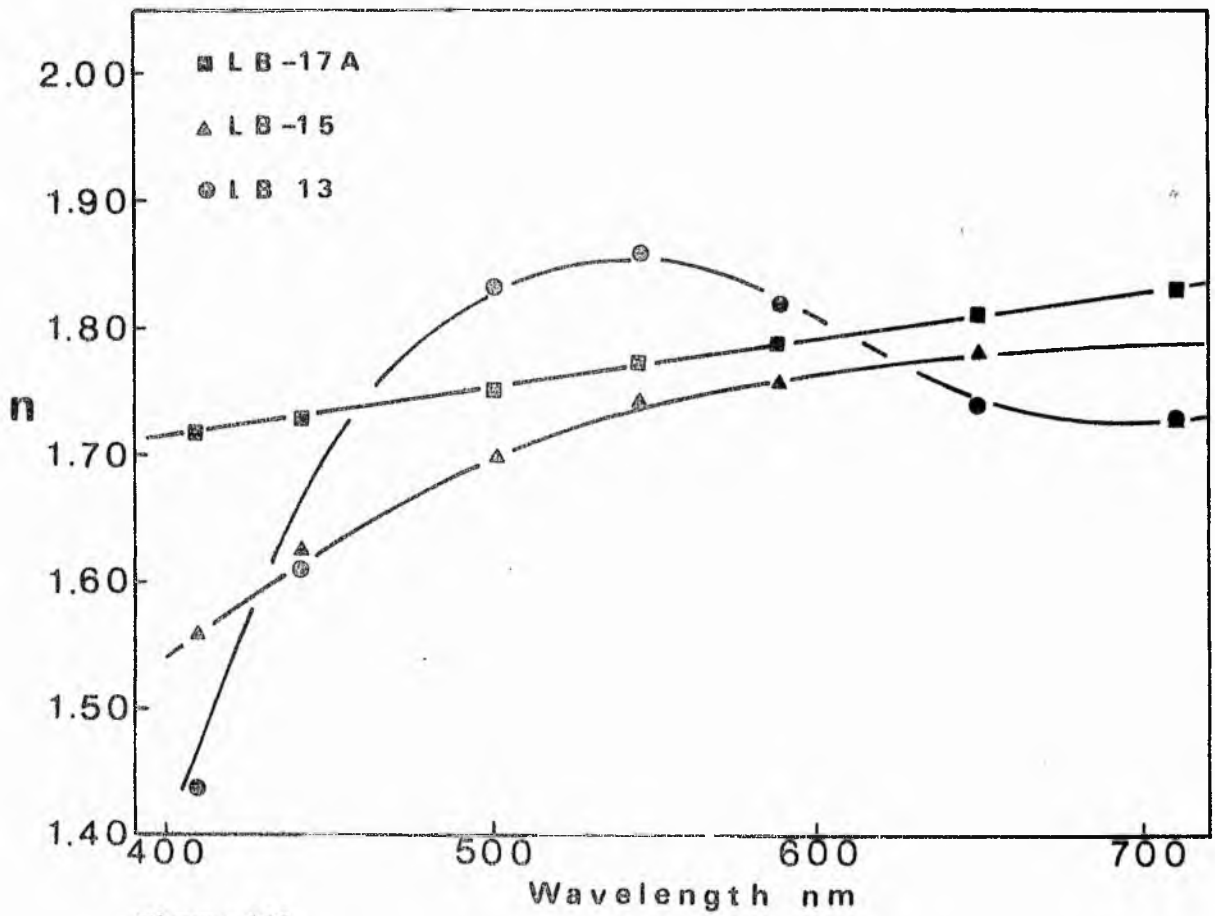
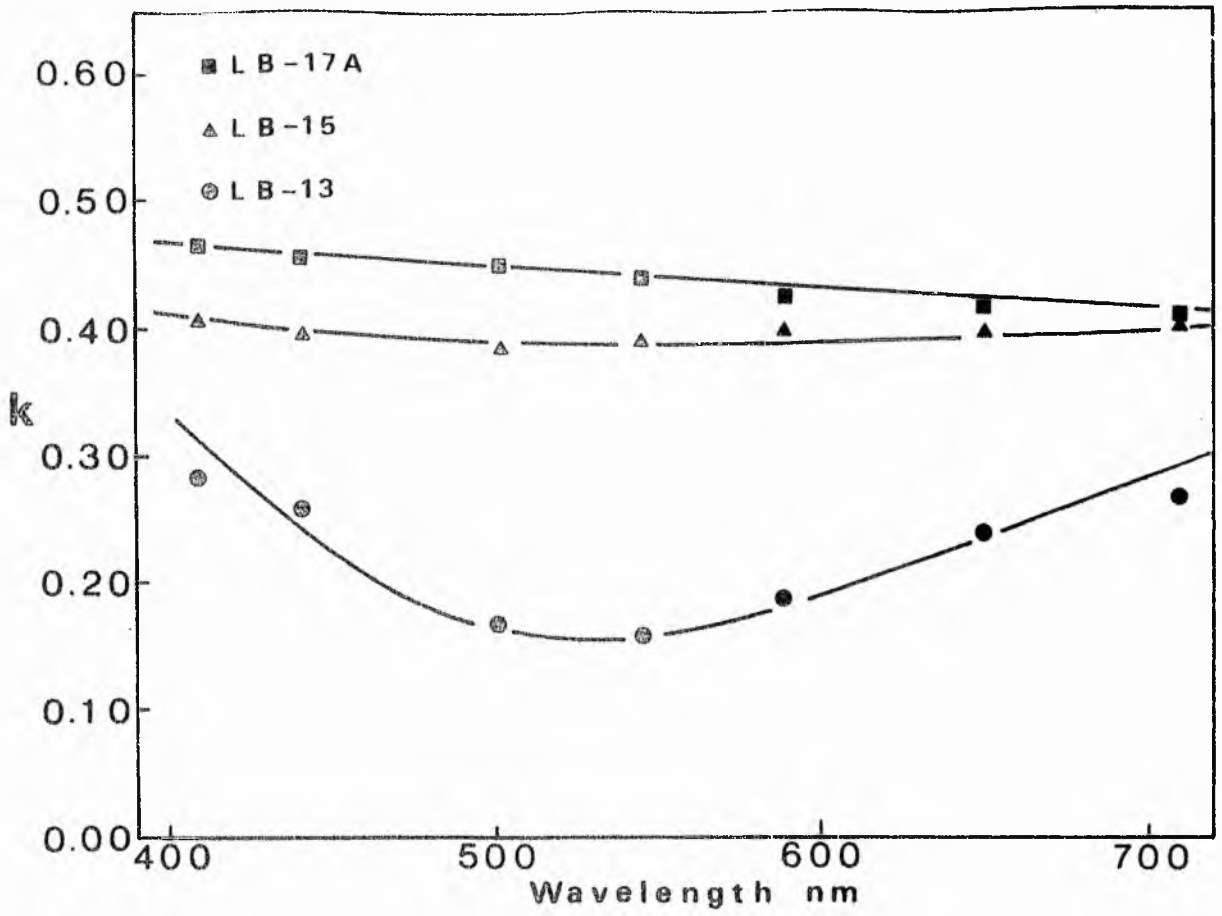


Figure 162.

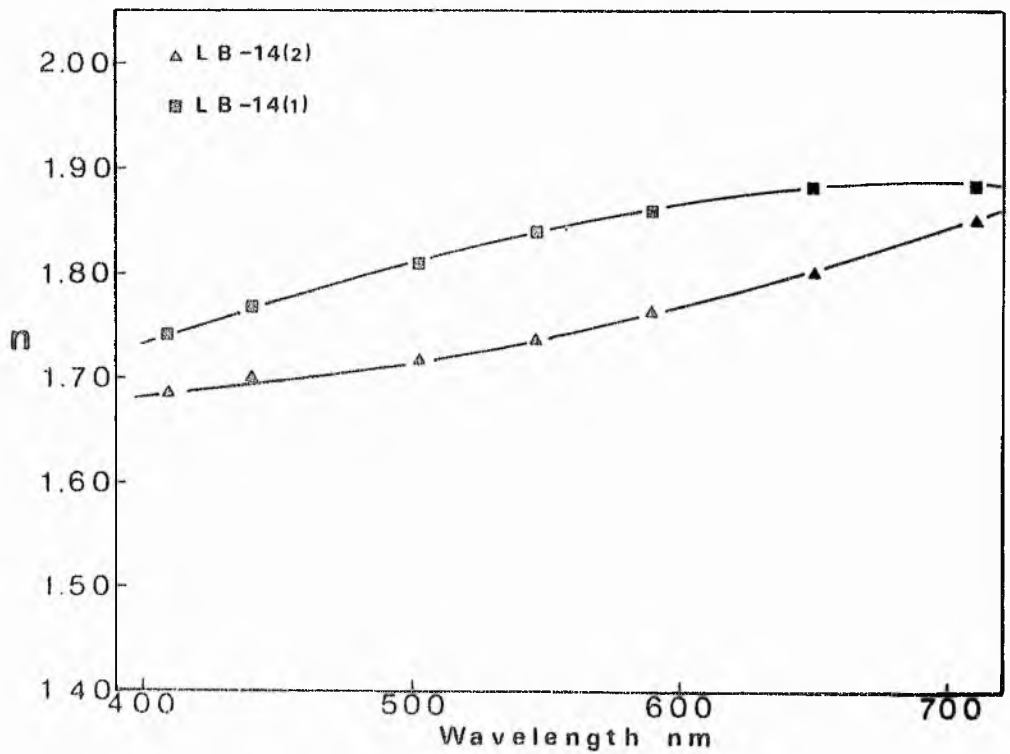
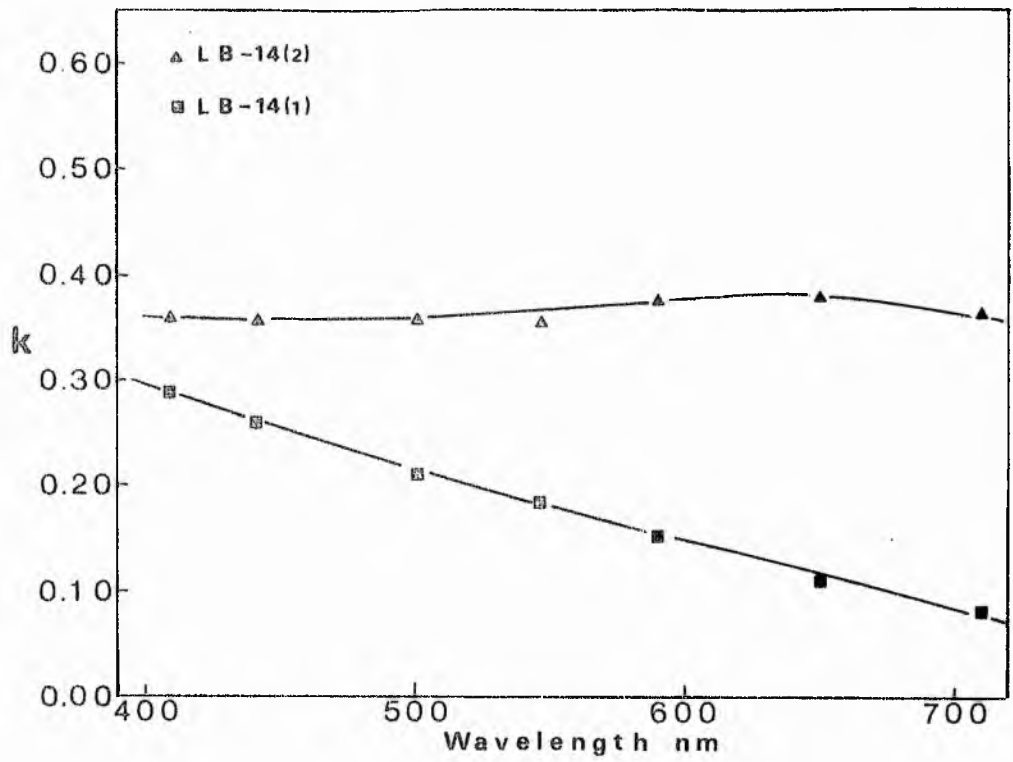


Figure 163. Plots illustrating the dispersion with wavelength of the absorptive and refractive indices in samples LB-14 (1) and LB-14 (2).

Figure 164. Plots illustrating the dispersion with wavelength of the absorptive and refractive indices in samples LBR-13 and LBR-9.

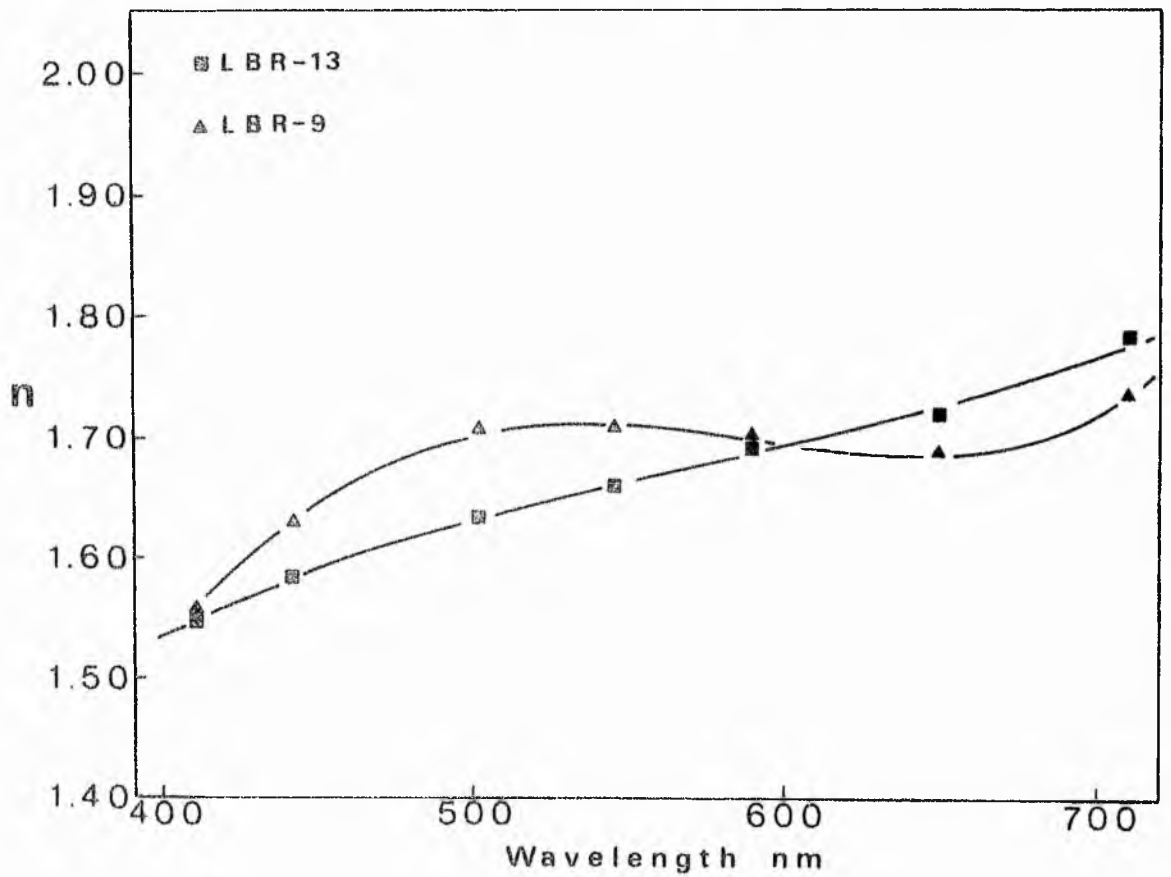
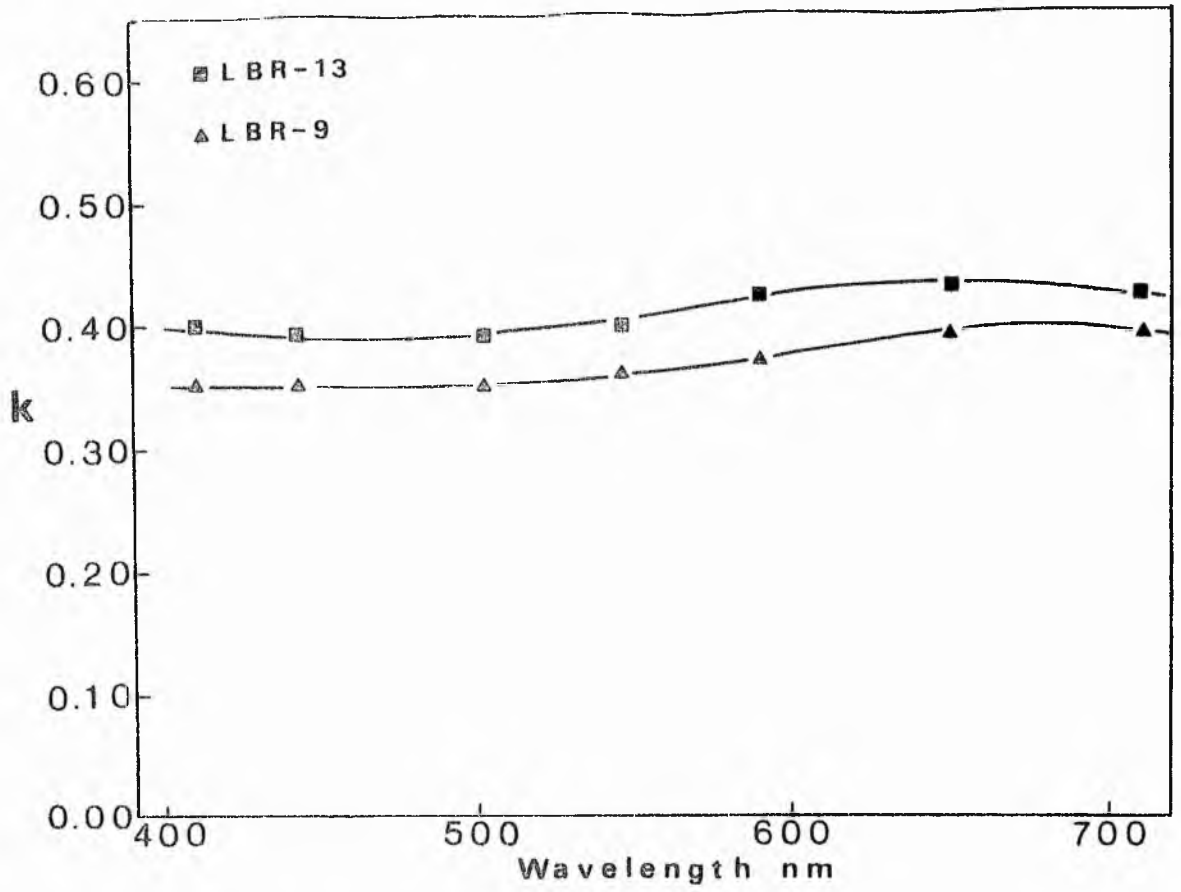


Figure 164.

Figure 165. Plots illustrating the dispersion with wavelength of the absorptive and refractive index in samples LBR-8, LBR-7 and LBR-3.

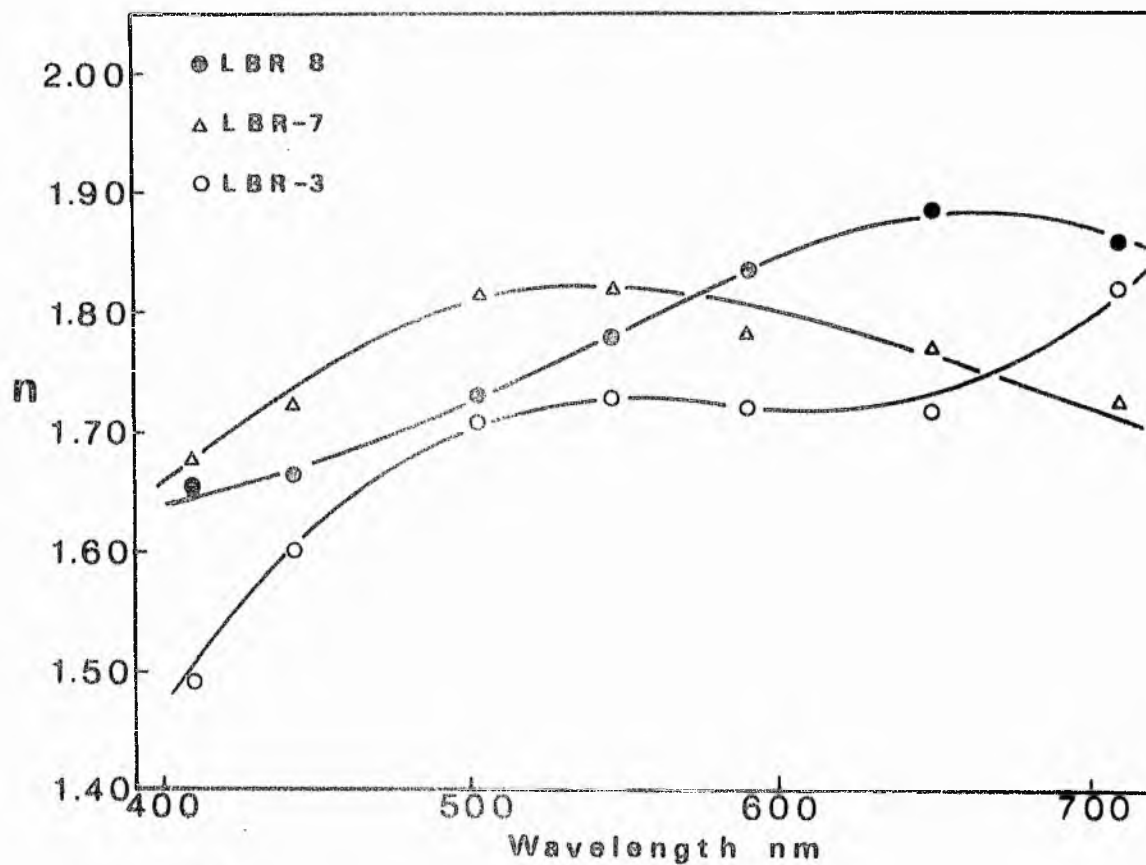
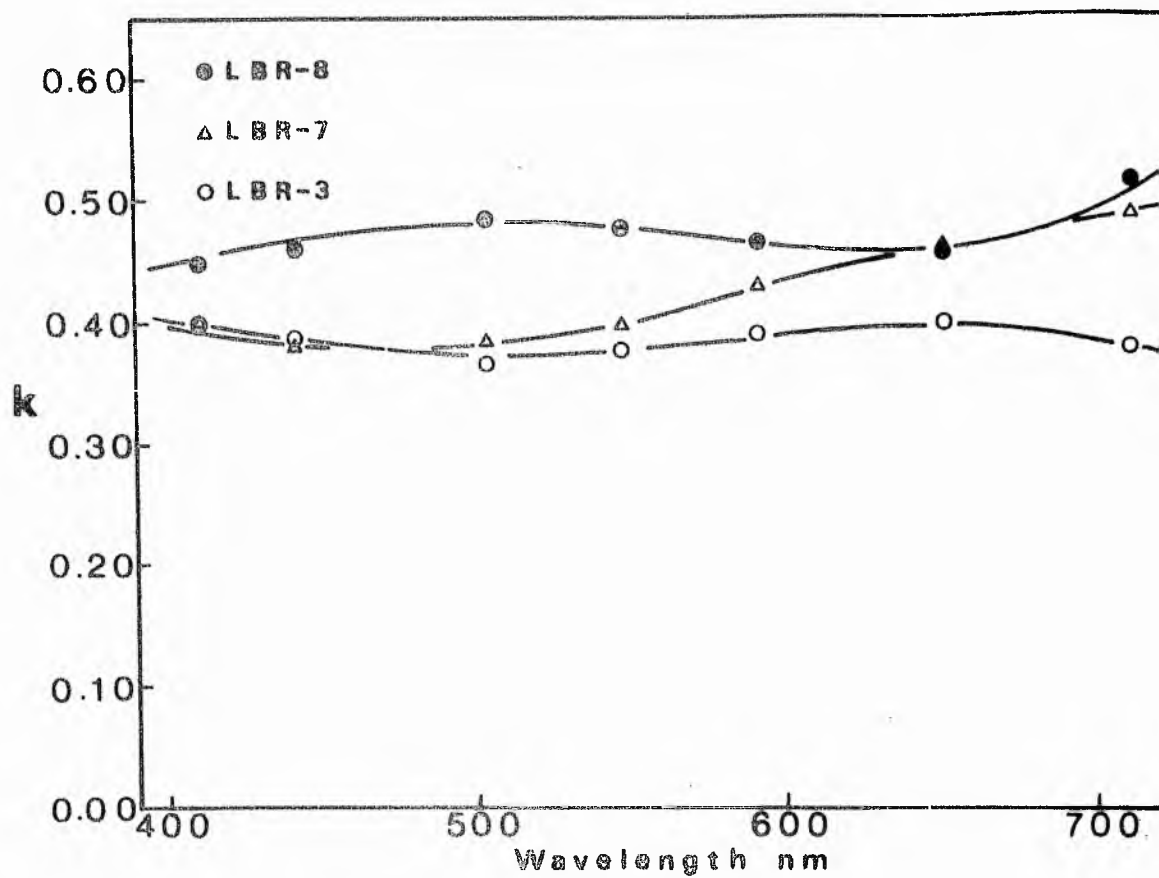


Figure 165.

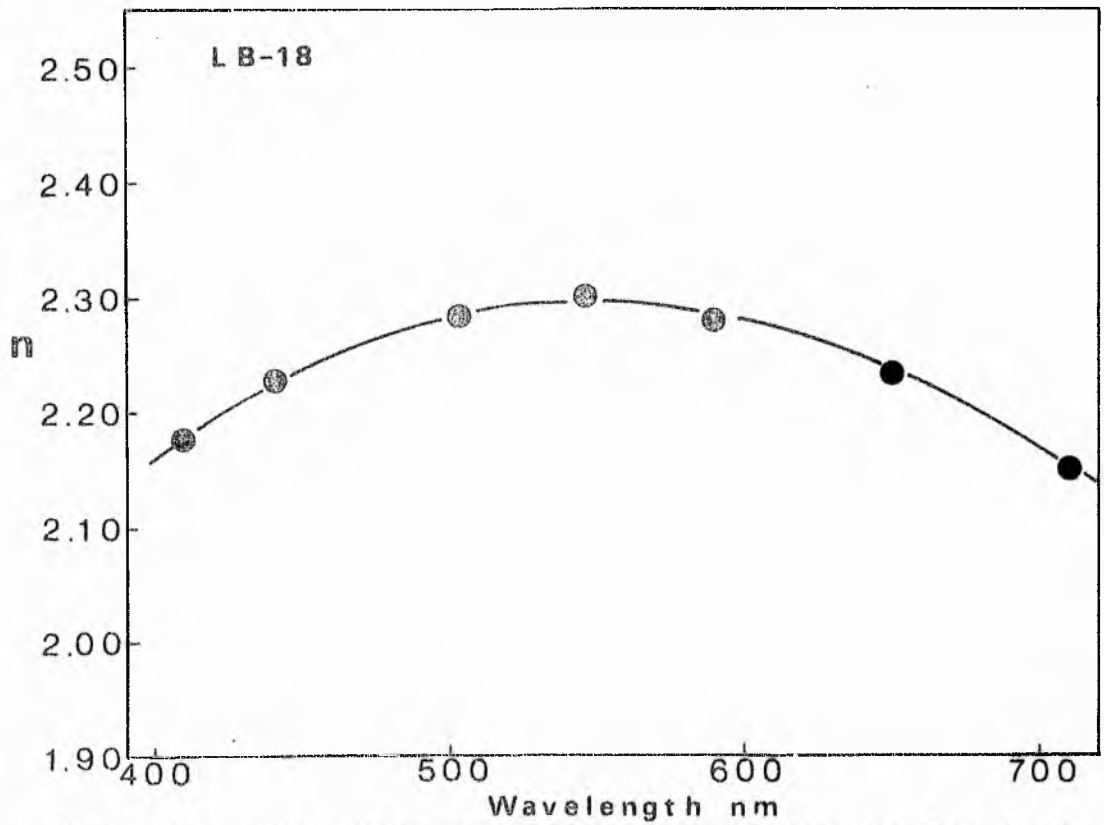
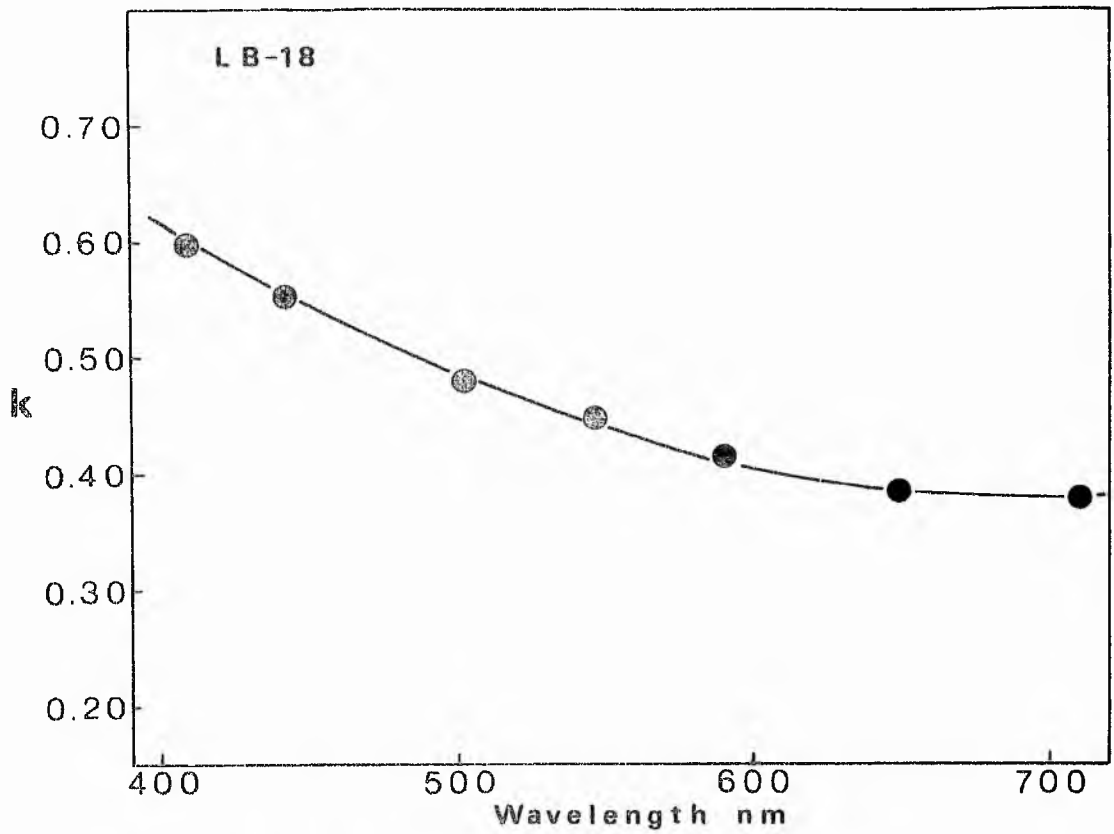


Figure 166. Plots illustrating the dispersion with wavelength of the absorptive and refractive index of sample LB-18.

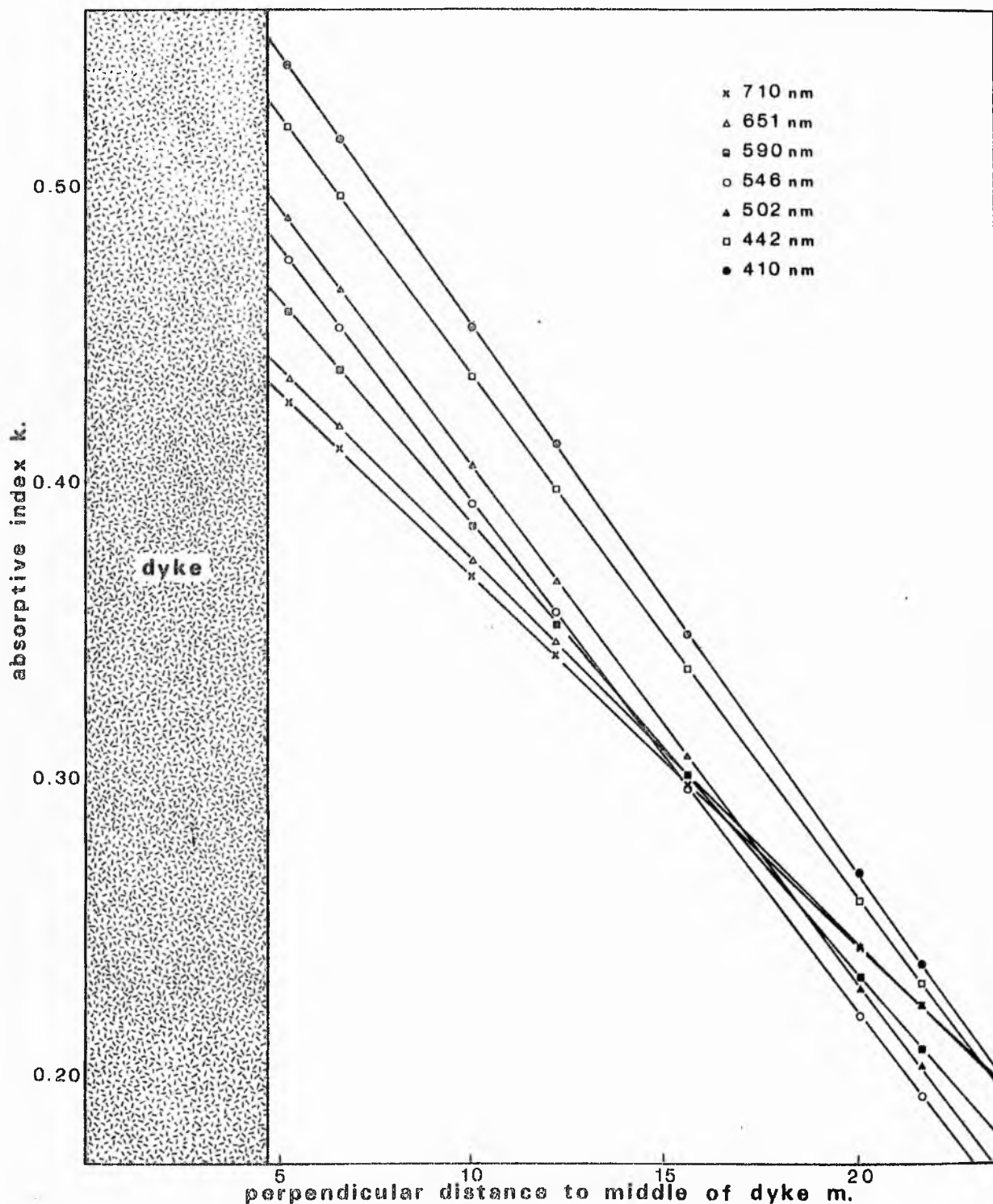


Figure 167. Linear regression lines for the variation of absorptive index of graptolite fragments with distance from the dyke at Clanyard Bay.

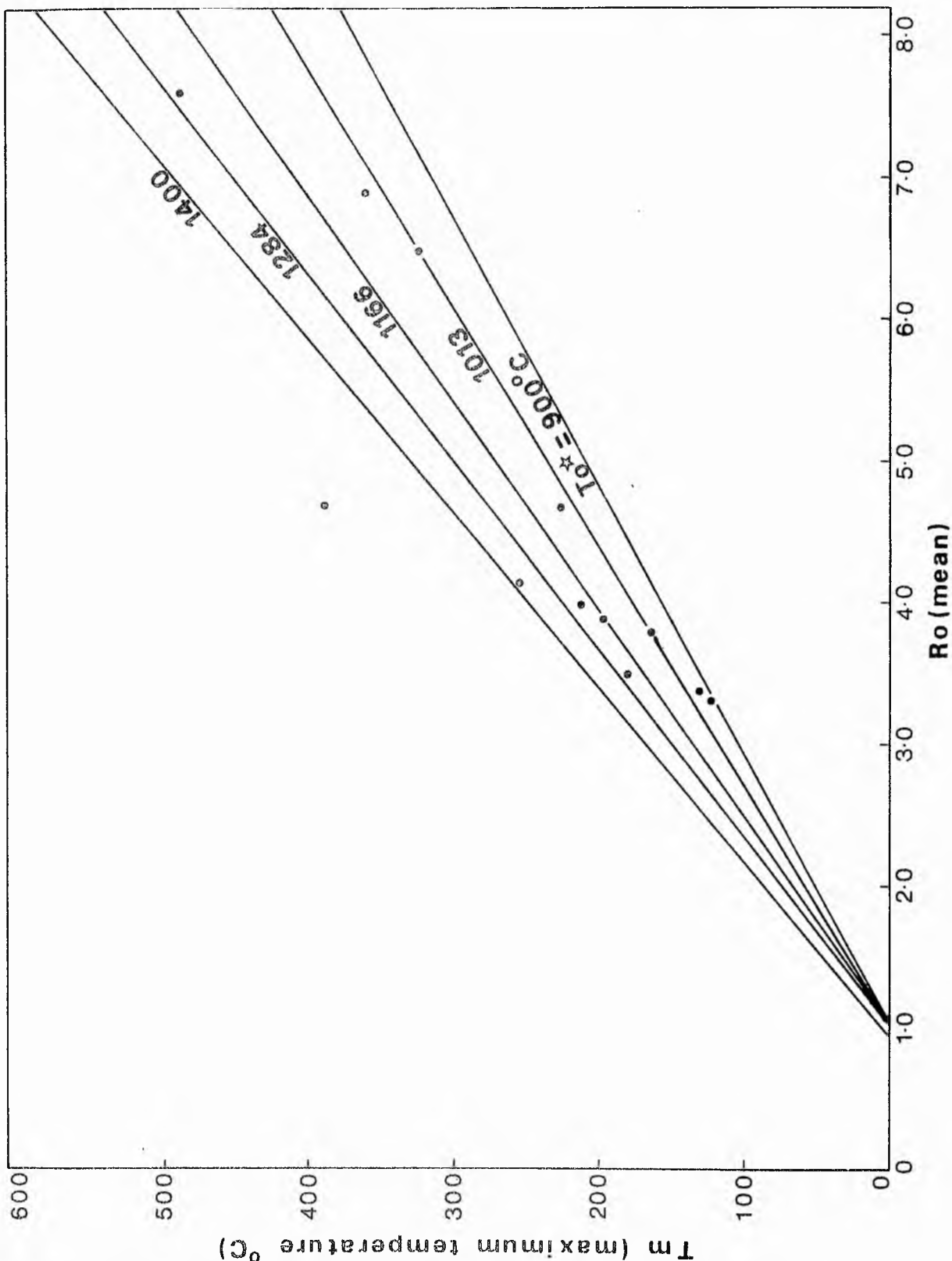


Figure 168. Plot of linear regression lines for various values of equivalent temperature (To^*) for the variation of reflectivity with temperature of graptolite fragments. Dots indicate variation for $To^* = 1166^\circ$.

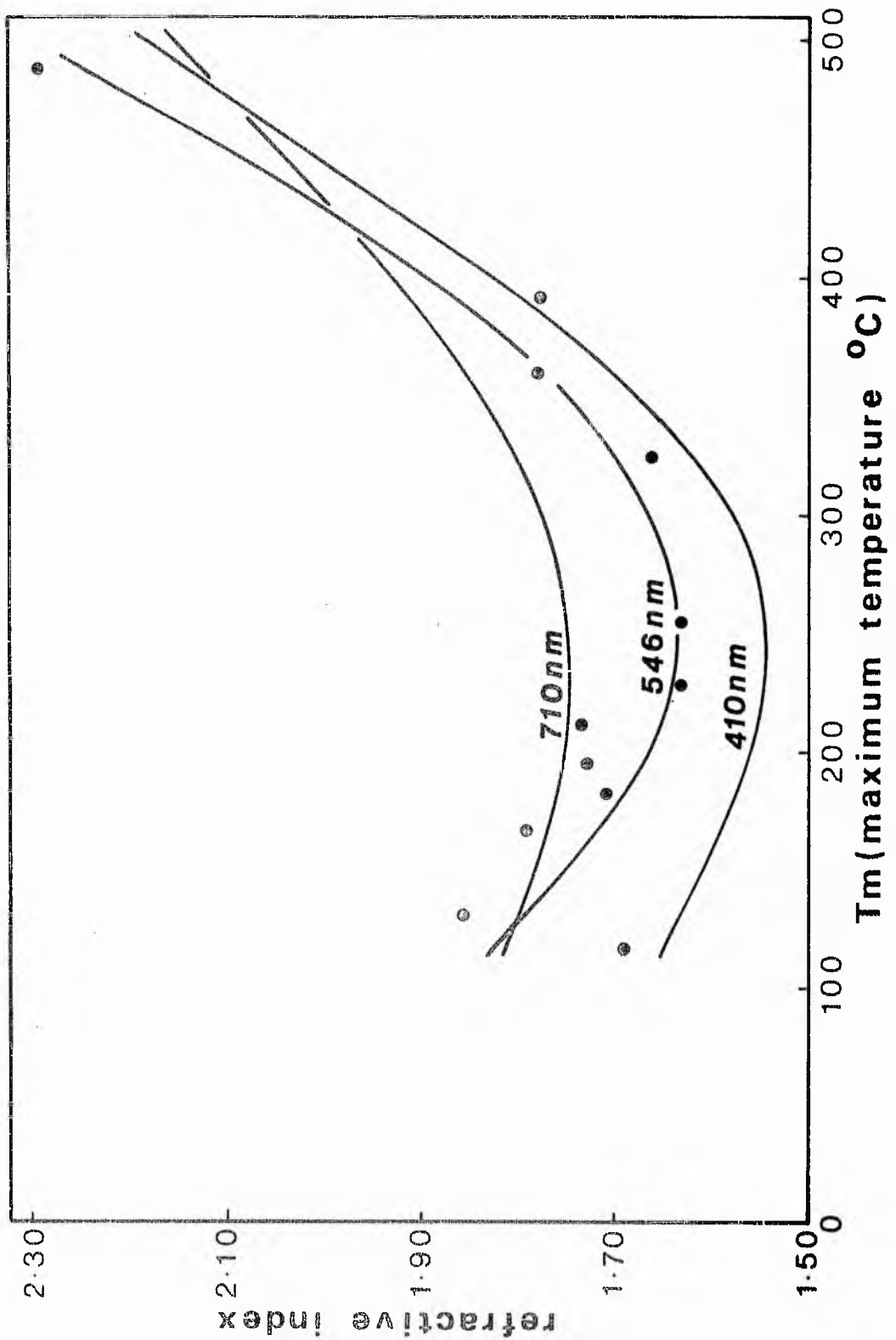


Figure 169. Plot of 'best-fit' regression lines at various wavelengths for the variation of refractive index with temperature of graptolite fragments.
 Dots indicate variation for wavelength = 546 nm.

Figure 170. Plot of the variation in refractive index with temperature of graptolite fragments. T_s , T_r and T_m are hypothetical positions for the onset of plasticity, onset of resolidification and onset of molecular reorganisation in the solid.

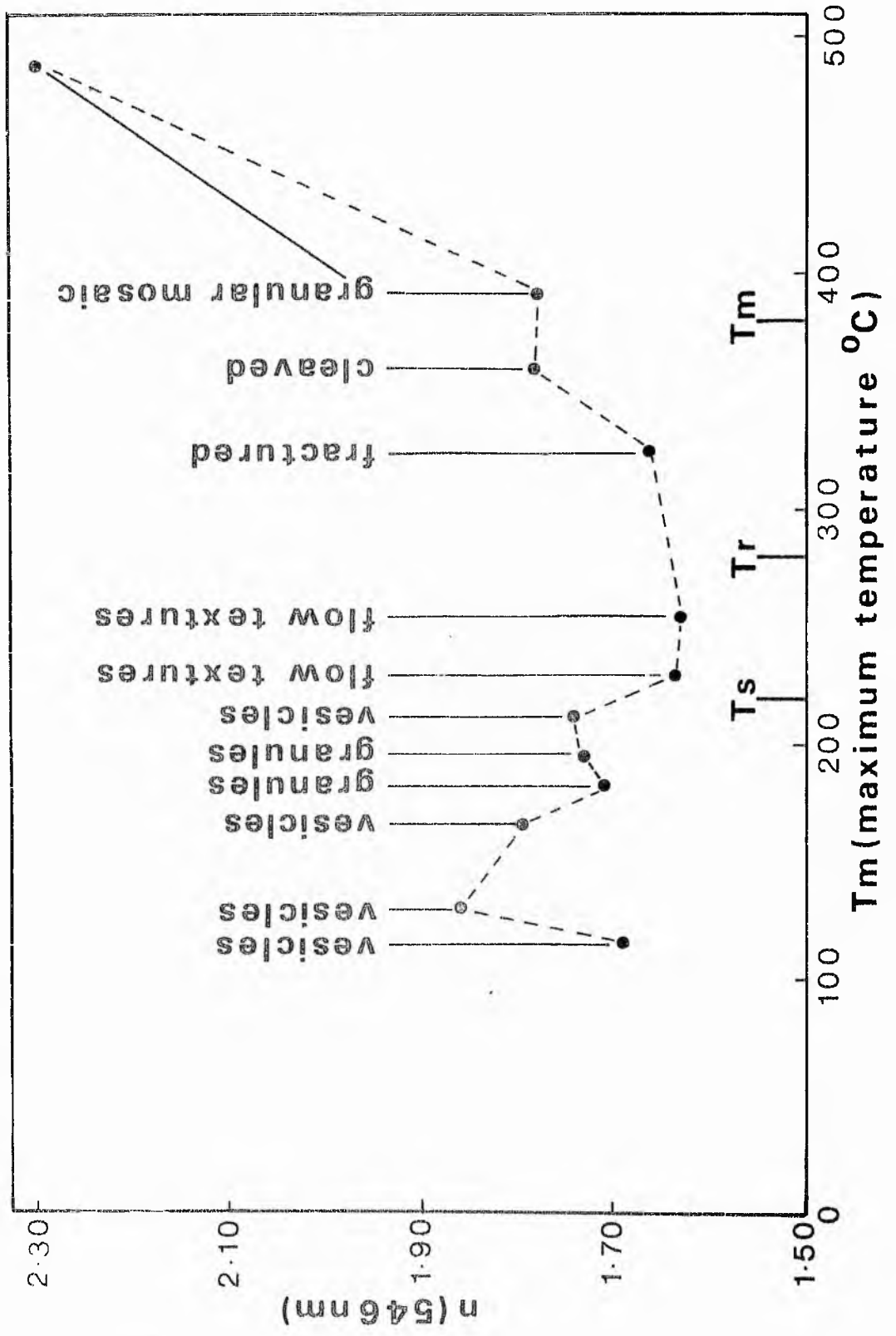


Figure 170.

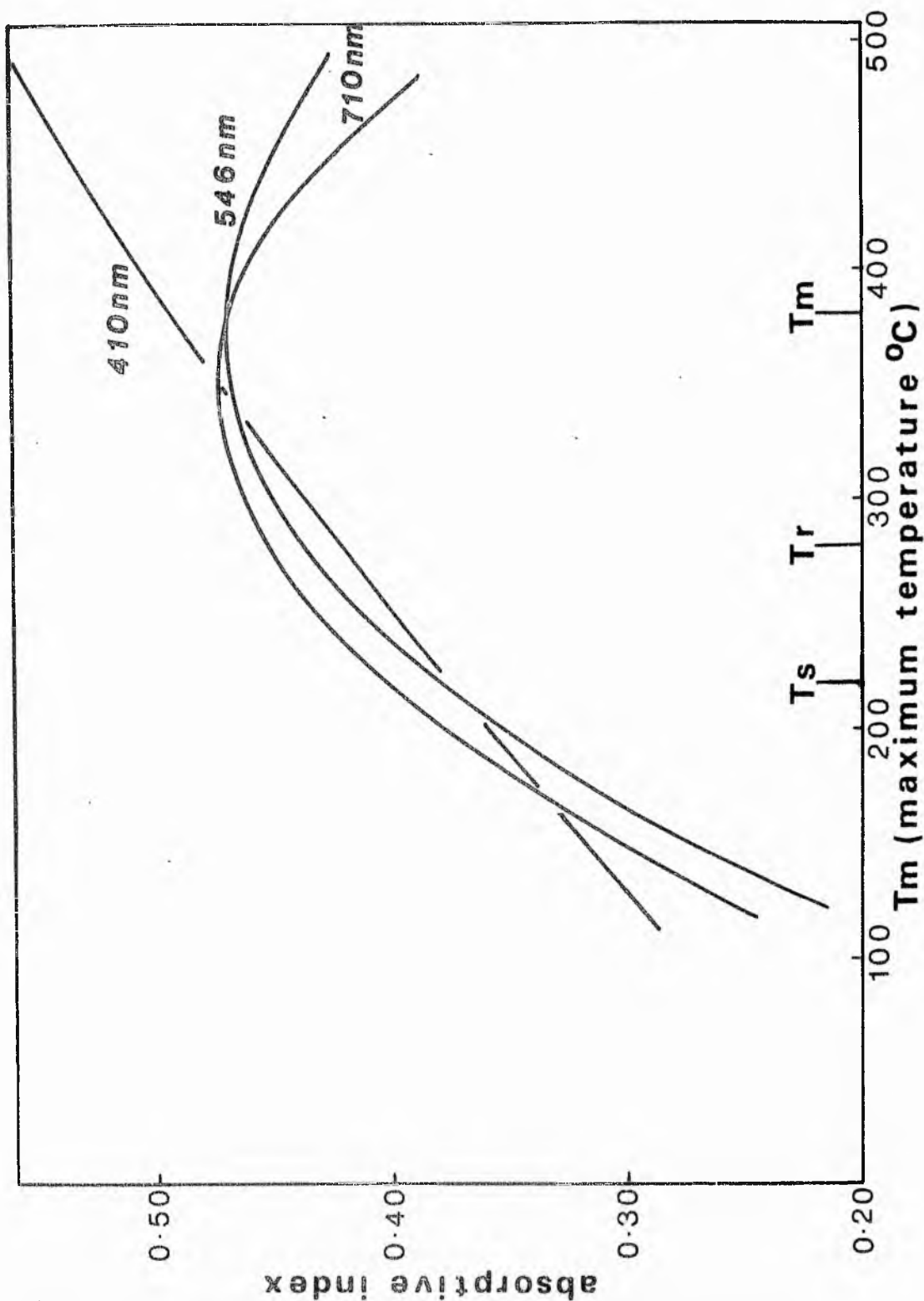
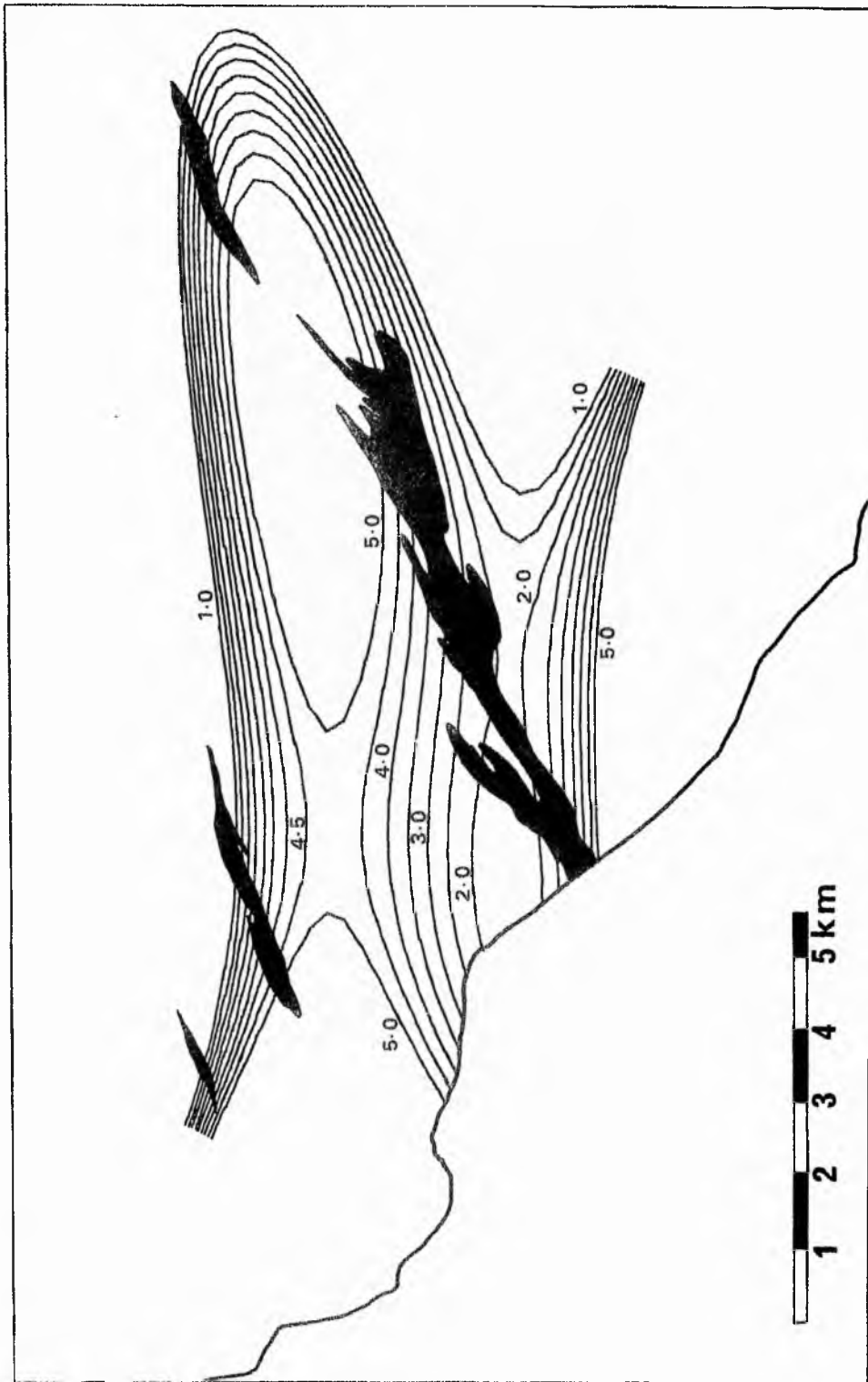
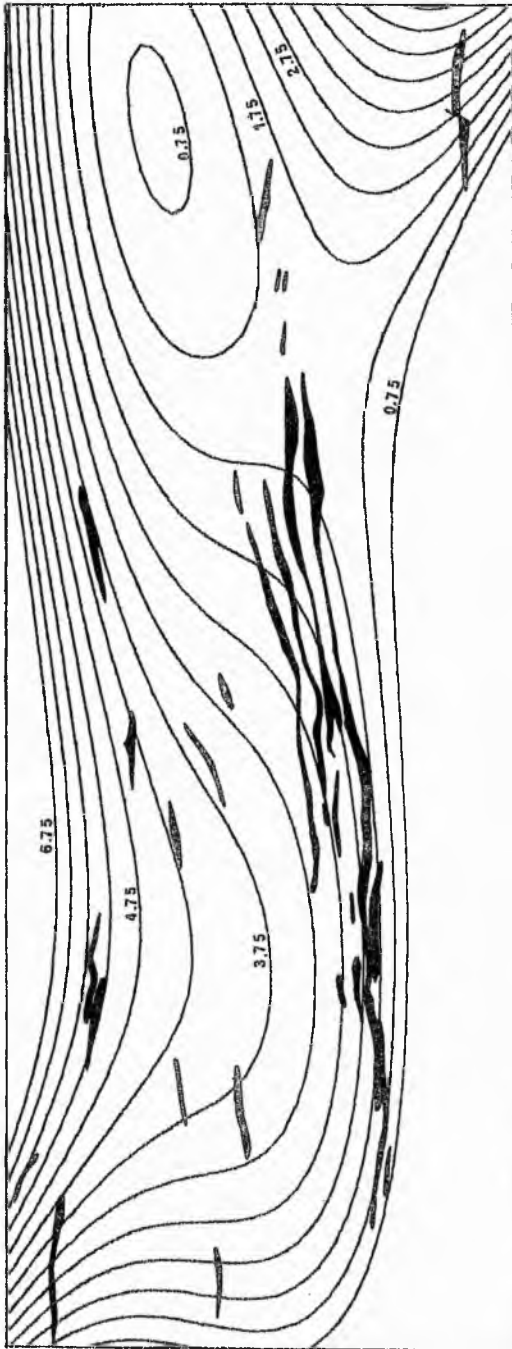


Figure 171. Plot of the variation of absorptive index with temperature for graptolite fragments. T_s , T_r and T_m are hypothetical positions for the onset of plasticity, onset of resolidification and onset of molecular reorganisation in the solid.

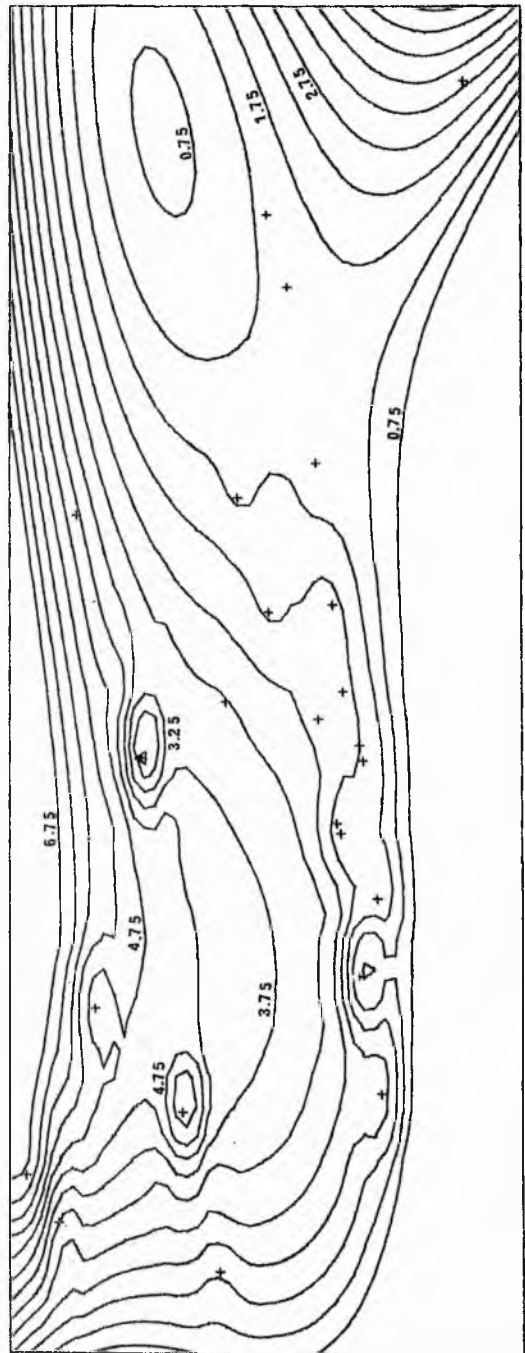


GLOBAL FIT SURFACE PLOT

Figure 172. Global-fit surface map for the variation of reflectivity in an area along the eastern margin of Luce Bay.



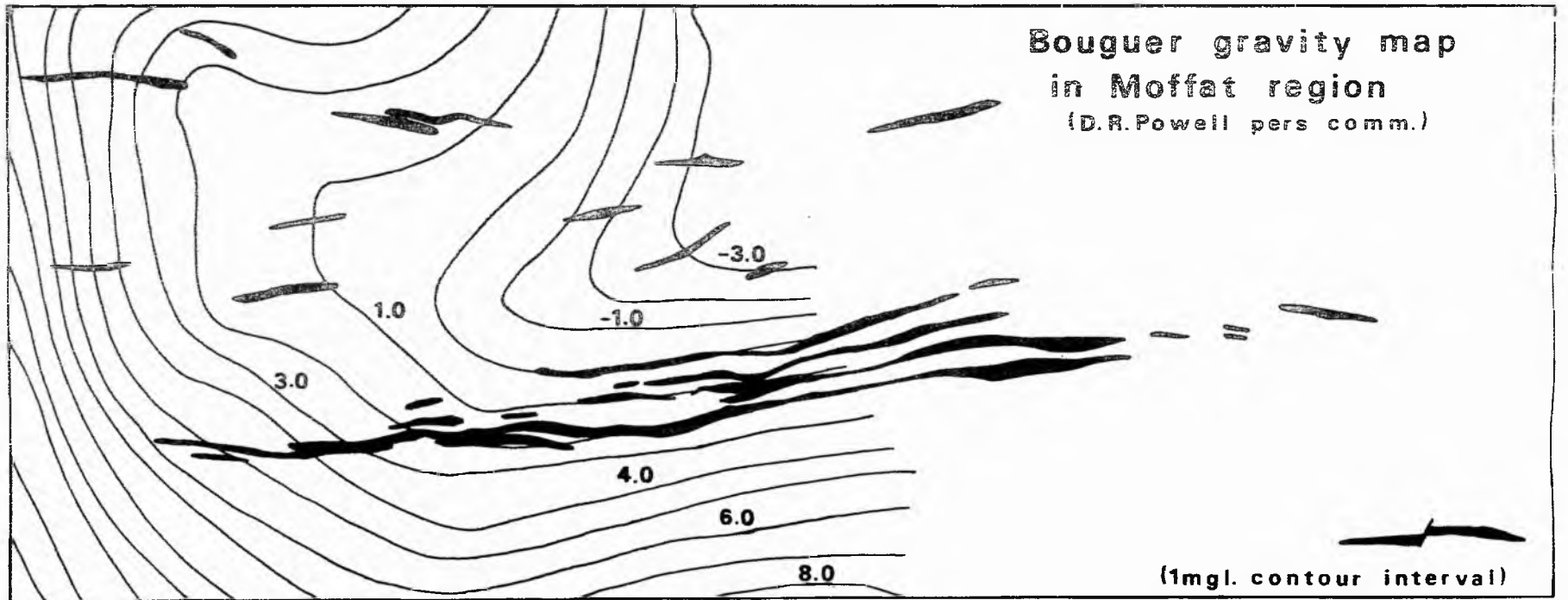
GLOBAL FIT SURFACE PLOT



REFLECTIVITY IN MOFFAT REGION

Figure 173. Global-fit and iterative surface maps for the variation of reflectivity in the Moffat Shales. For scale and orientation see Figure 4.

Figure 174. Bouguer gravity map for part of the Moffat region.



R (OIL) . 35 DATA POINTS

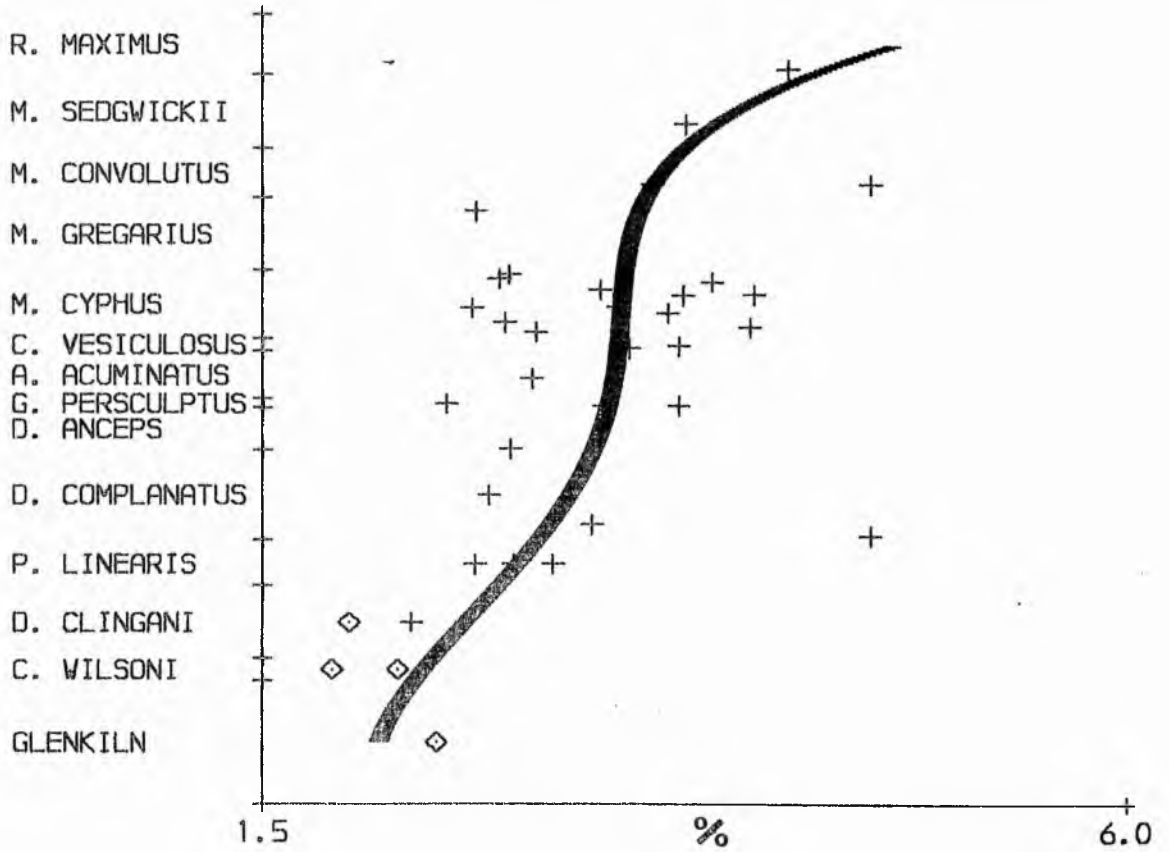


Figure 175. Plot illustrating the stratigraphic variation of reflectivity in the Moffat Shales. (Crosses indicate samples from Dobb's Linn, diamonds Glenkiln and Mounbenger).

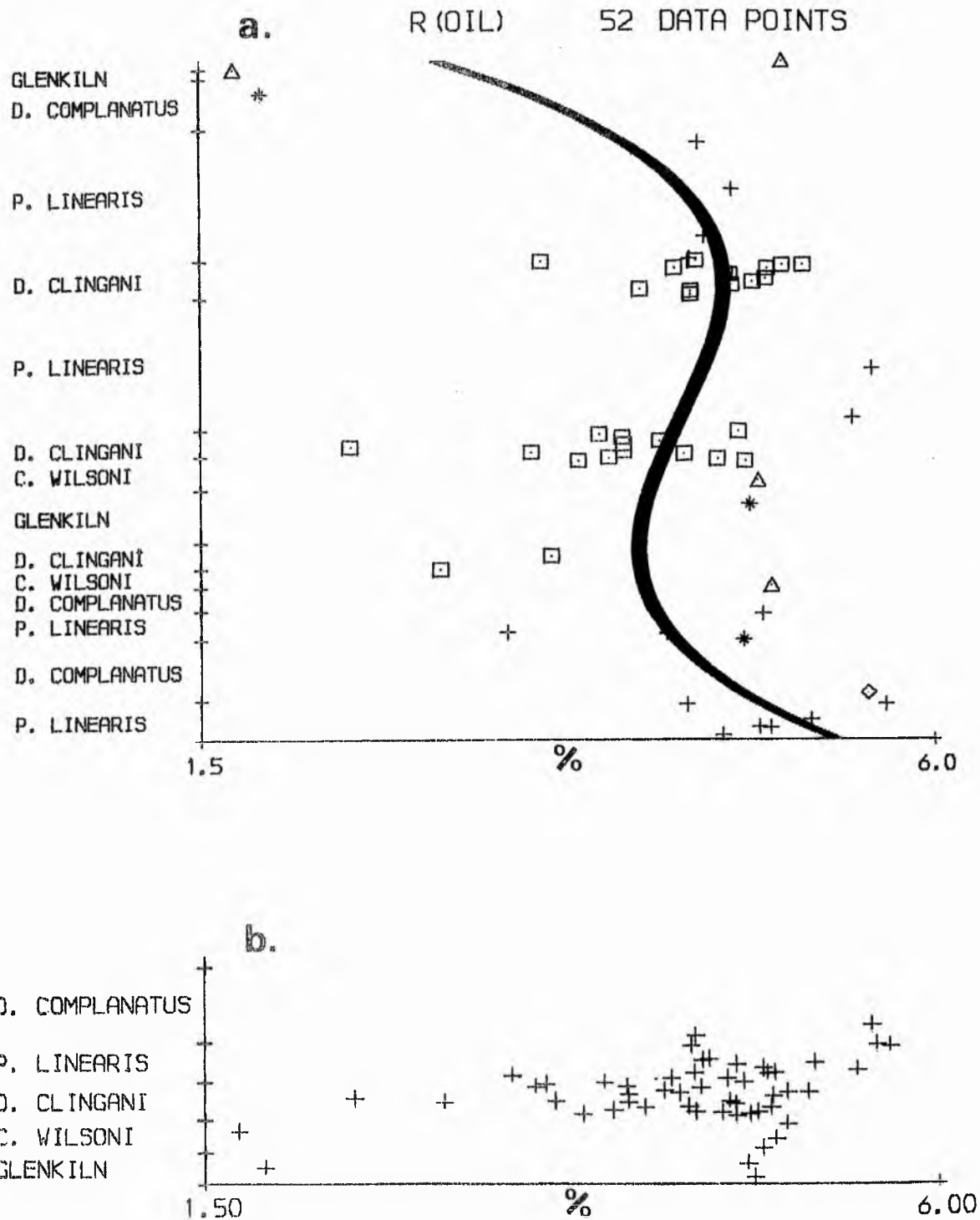


Figure 176. Plots illustrating the stratigraphic variation in reflectivity in the sediments of the north cliff at Hartfell.
 a) observed sequence, b) structurally restored sequence.

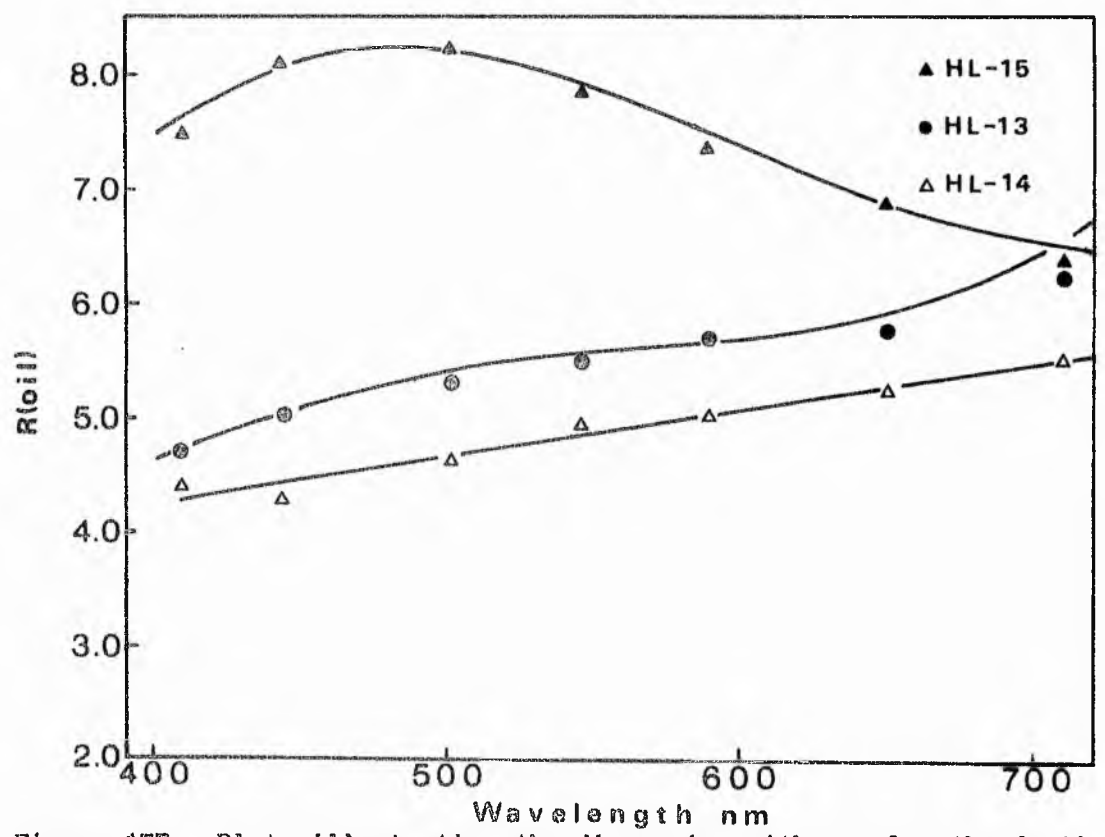
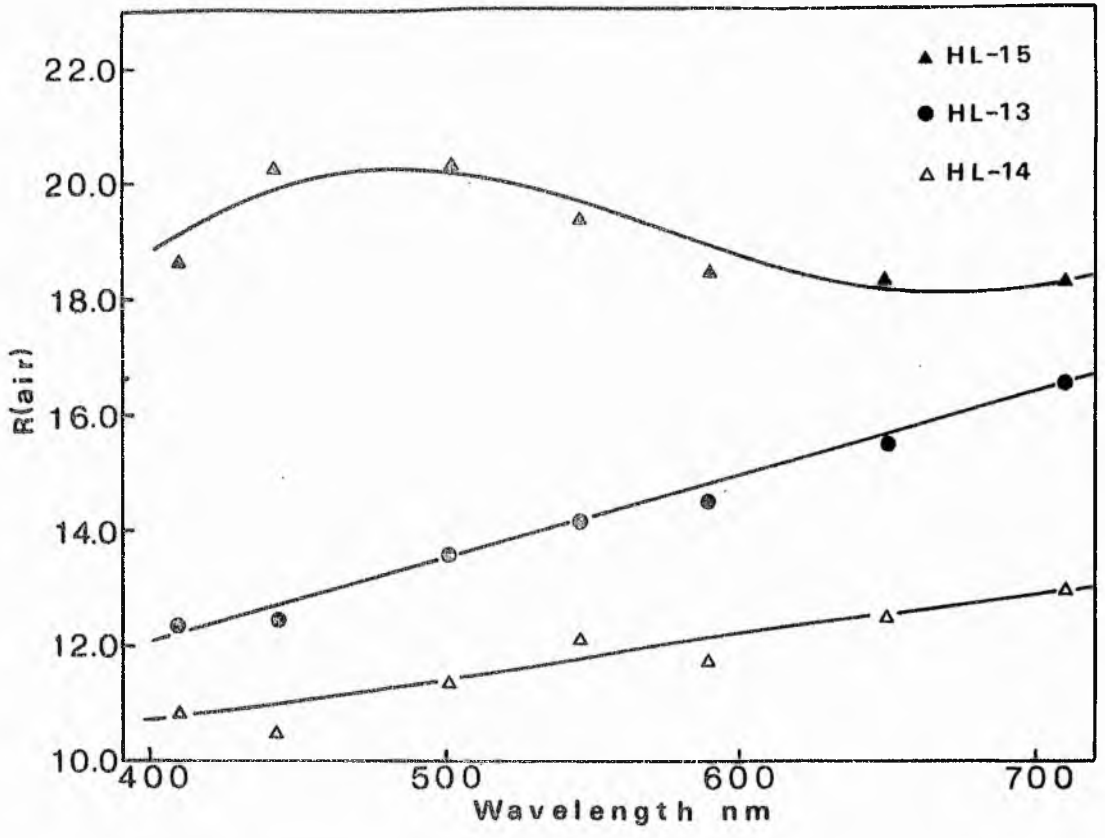


Figure 177. Plots illustrating the dispersion with wavelength of oil and air reflectivities in samples HL-15, HL-13 and HL-14.

Figure 178. Plots illustrating the dispersion with wavelength of oil and air reflectivities in samples HCL-26A, HCL-26 and HCL-31.

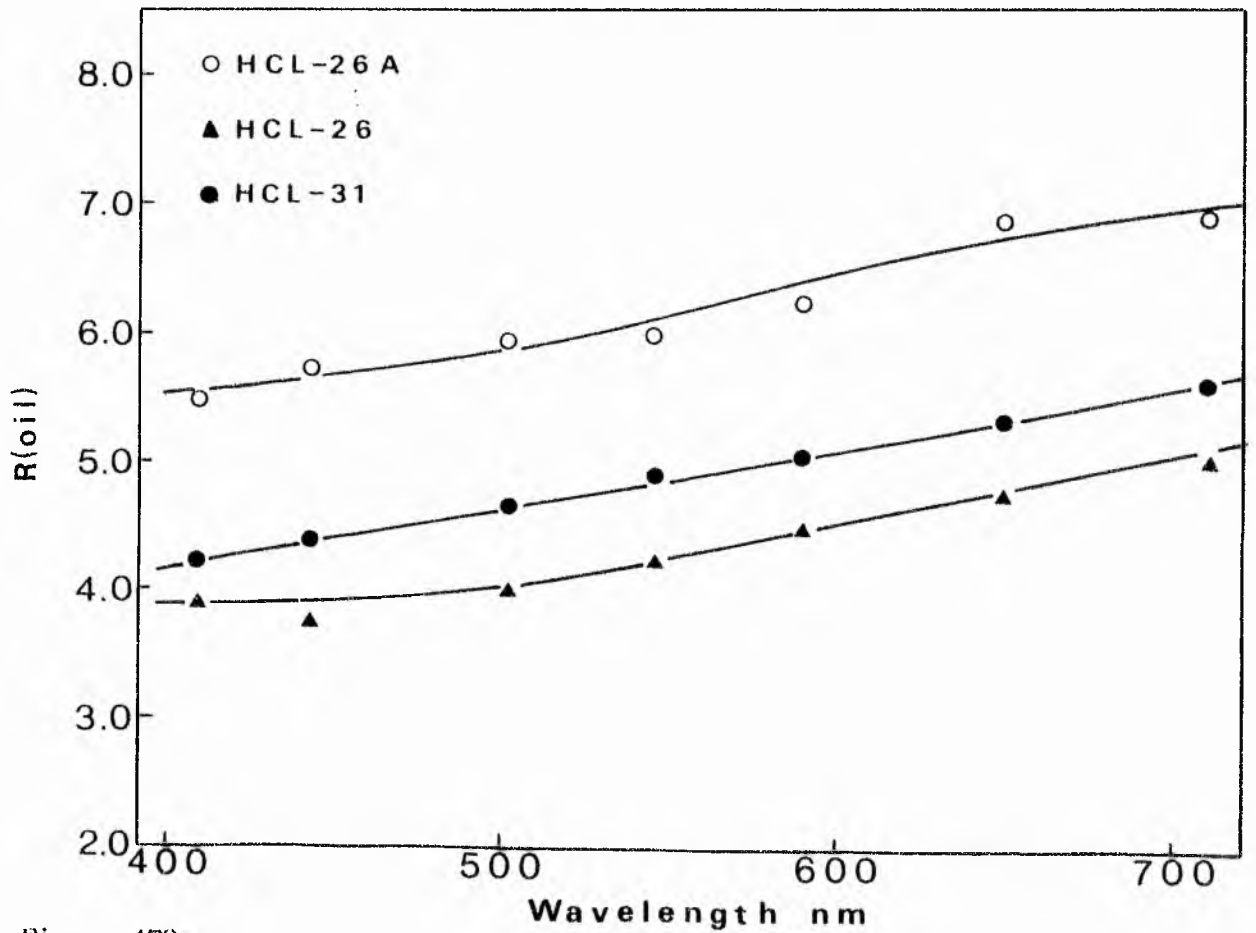
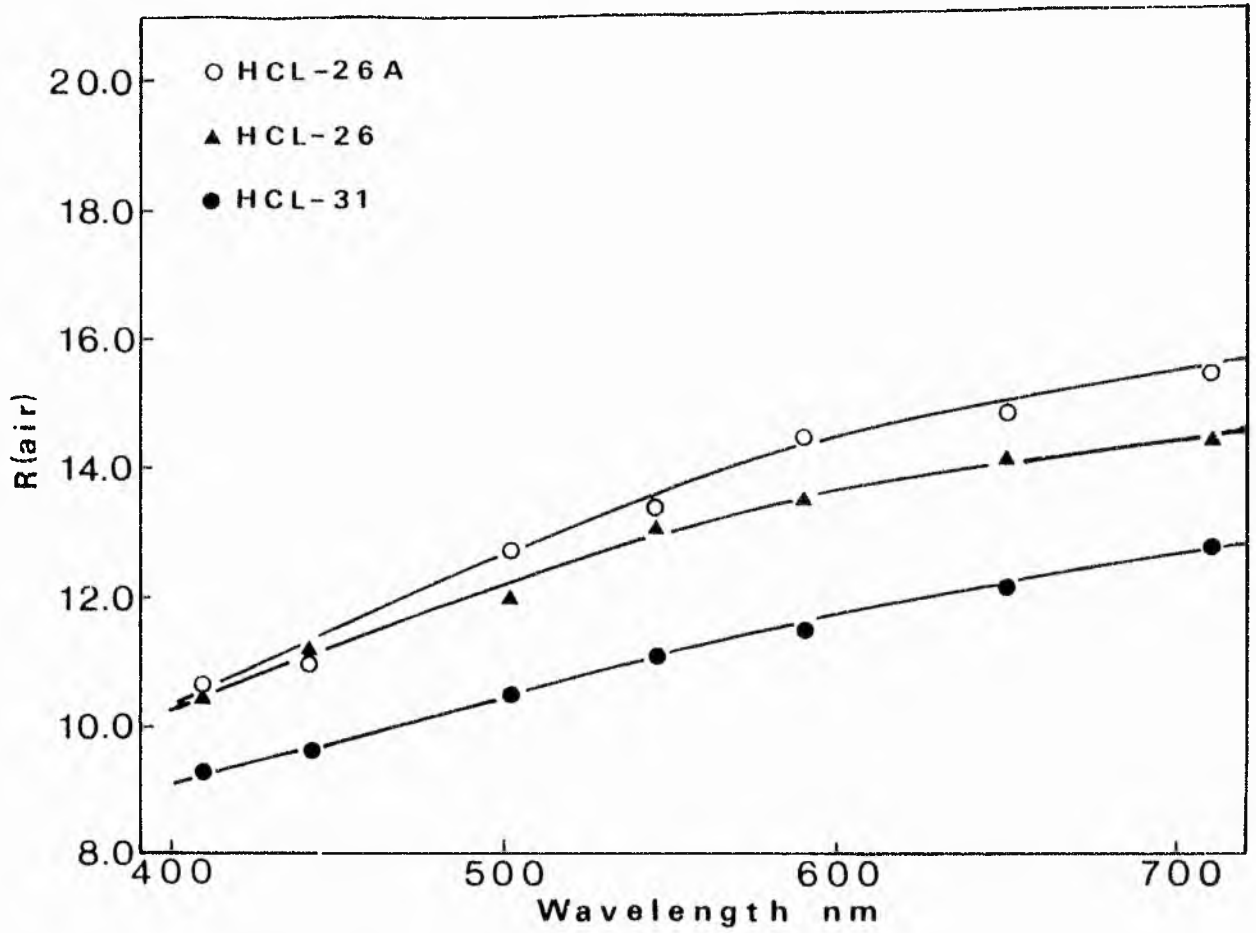


Figure 178.

Figure 179. Plots illustrating the dispersion with wavelength of oil and air reflectivities in samples HL-4 and HCL-16.

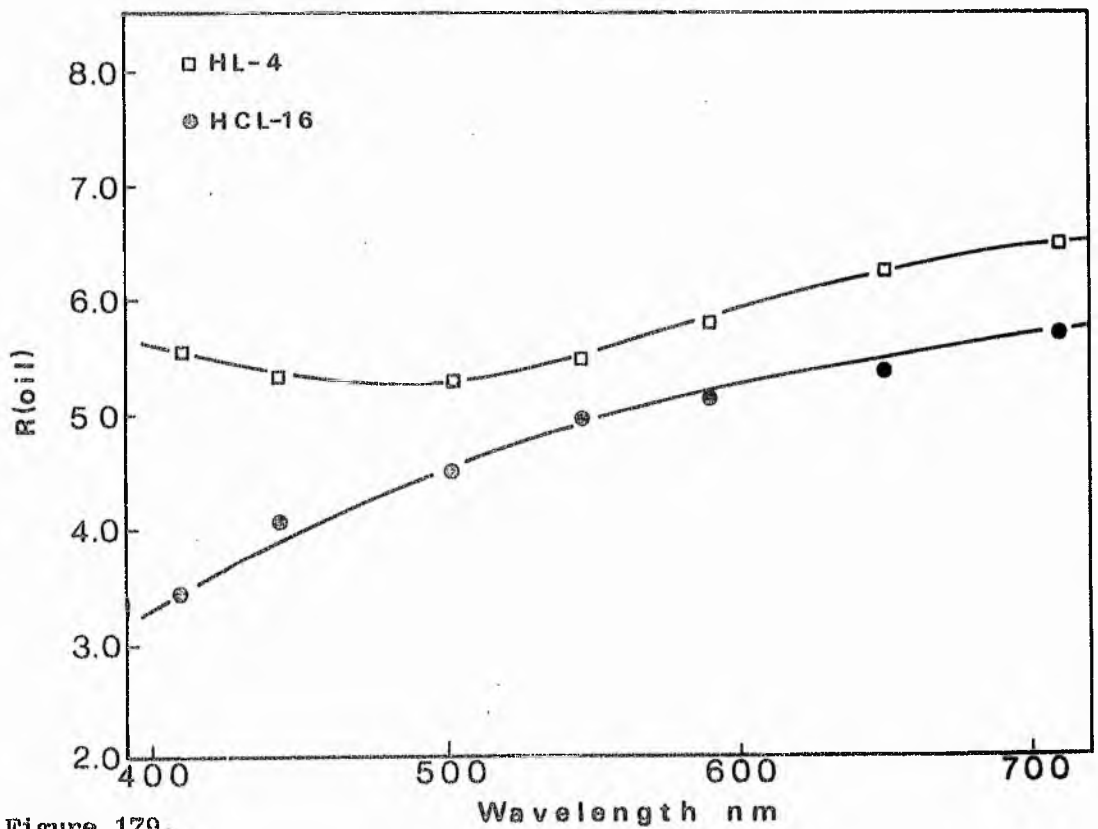
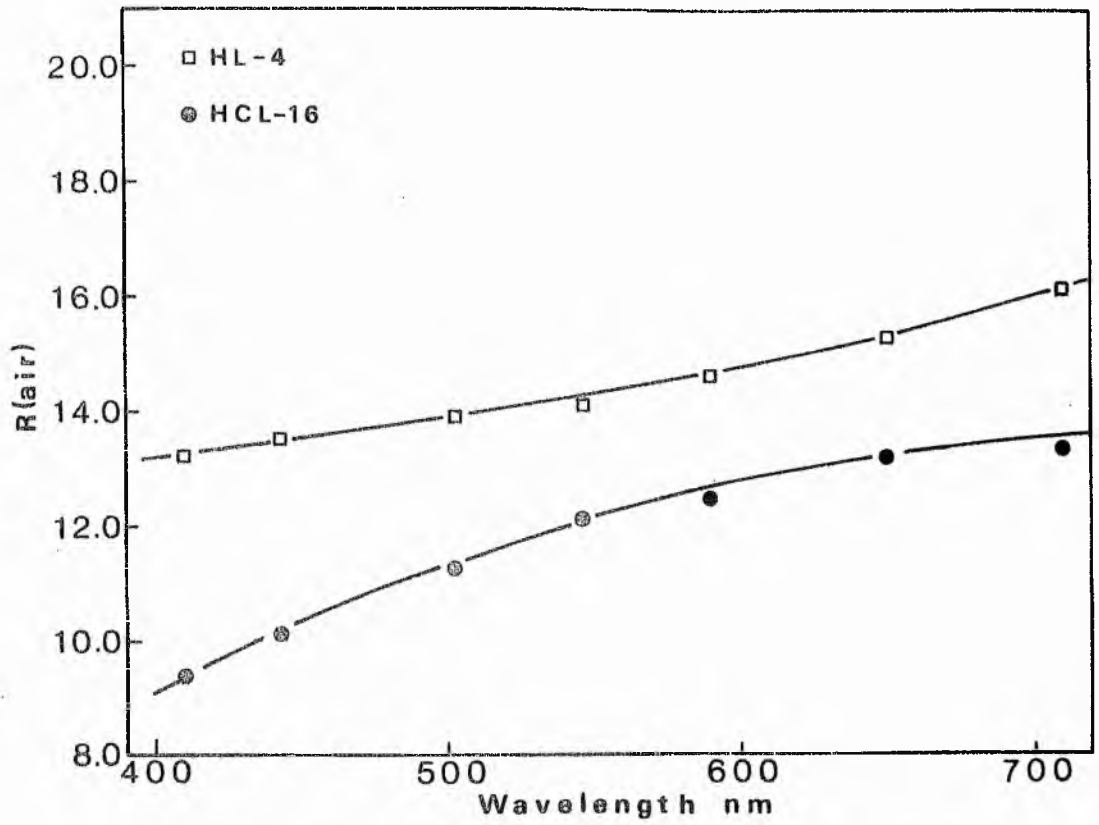


Figure 179.

Figure 180. Plots illustrating the dispersion with wavelength of the absorptive and refractive indices in samples HL-15, HL-13, HL-14.

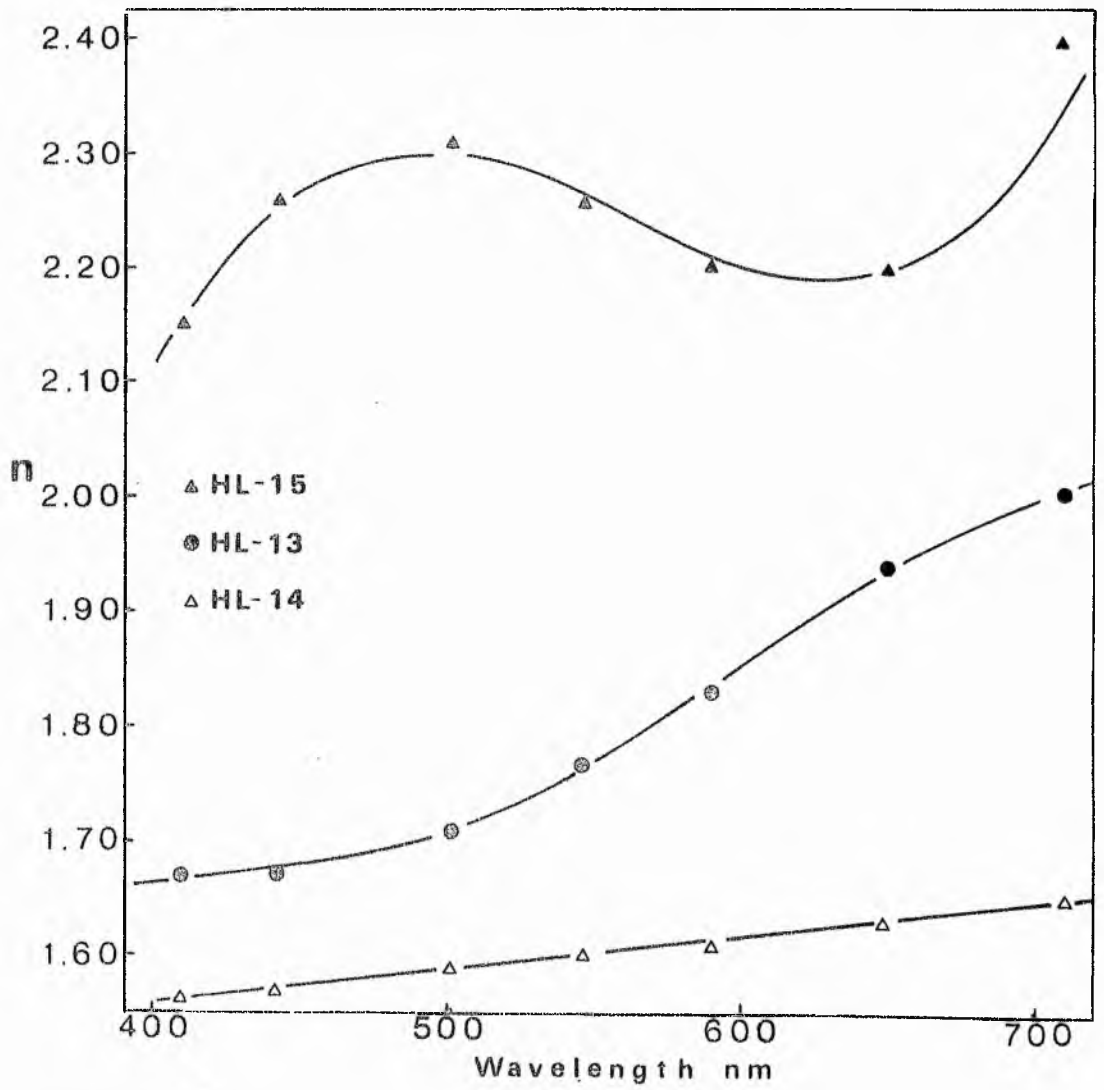
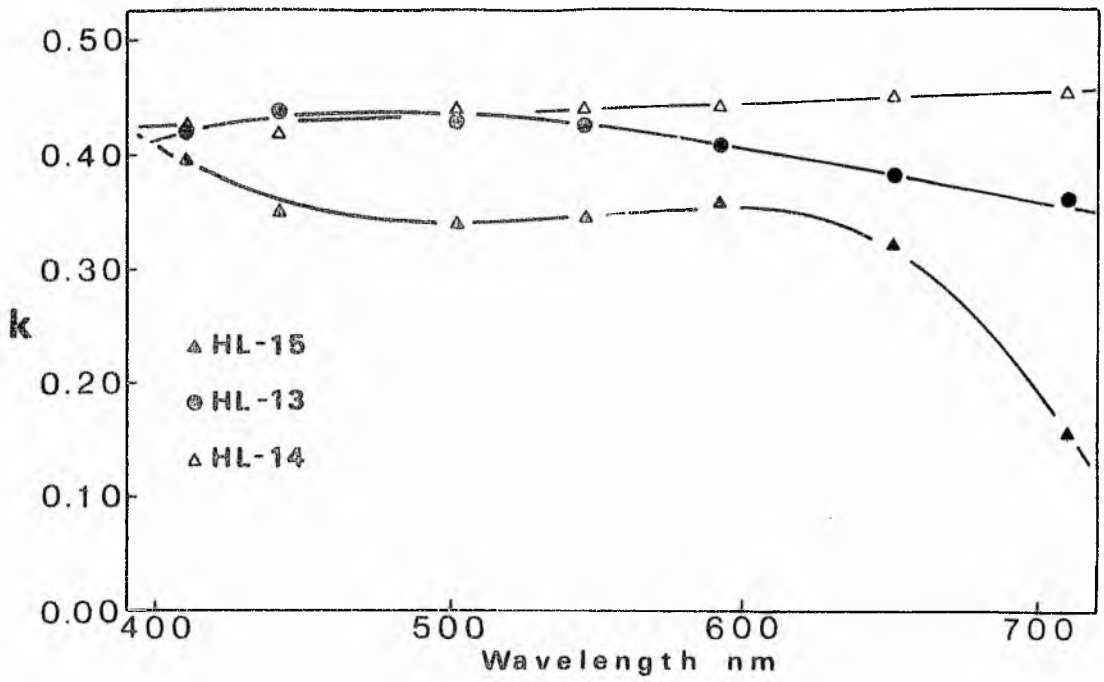


Figure 180.

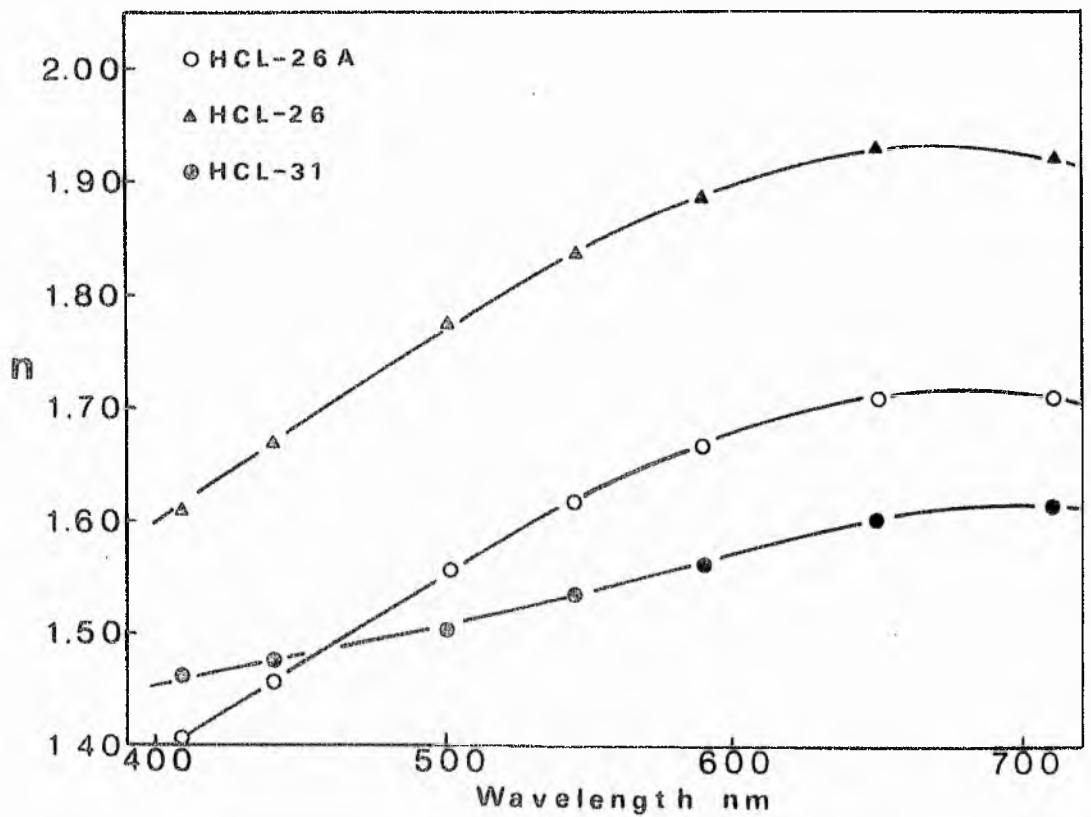
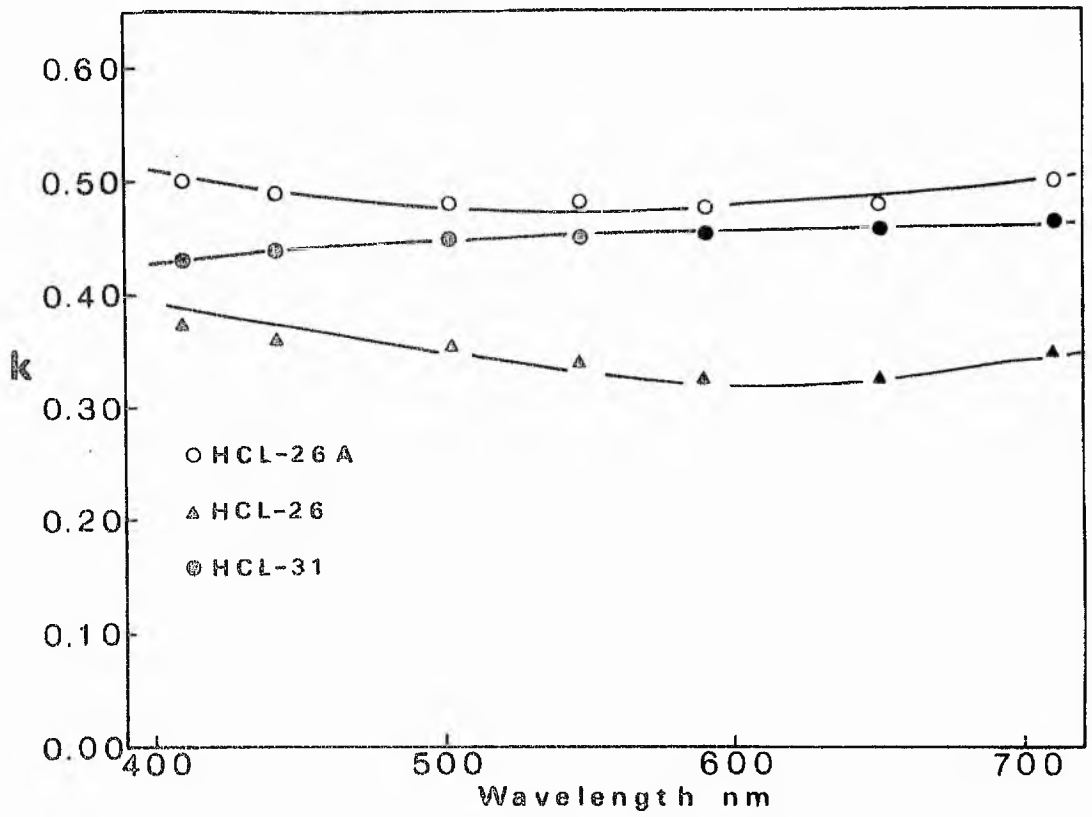


Figure 181. Plots illustrating the dispersion with wavelength of the absorptive and refractive indices in samples HCL-26A, HCL-26, HCL-31.



Figure 182. Plots illustrating the dispersion with wavelength of the absorptive and refractive indices in samples HL-4 and HCL-16.

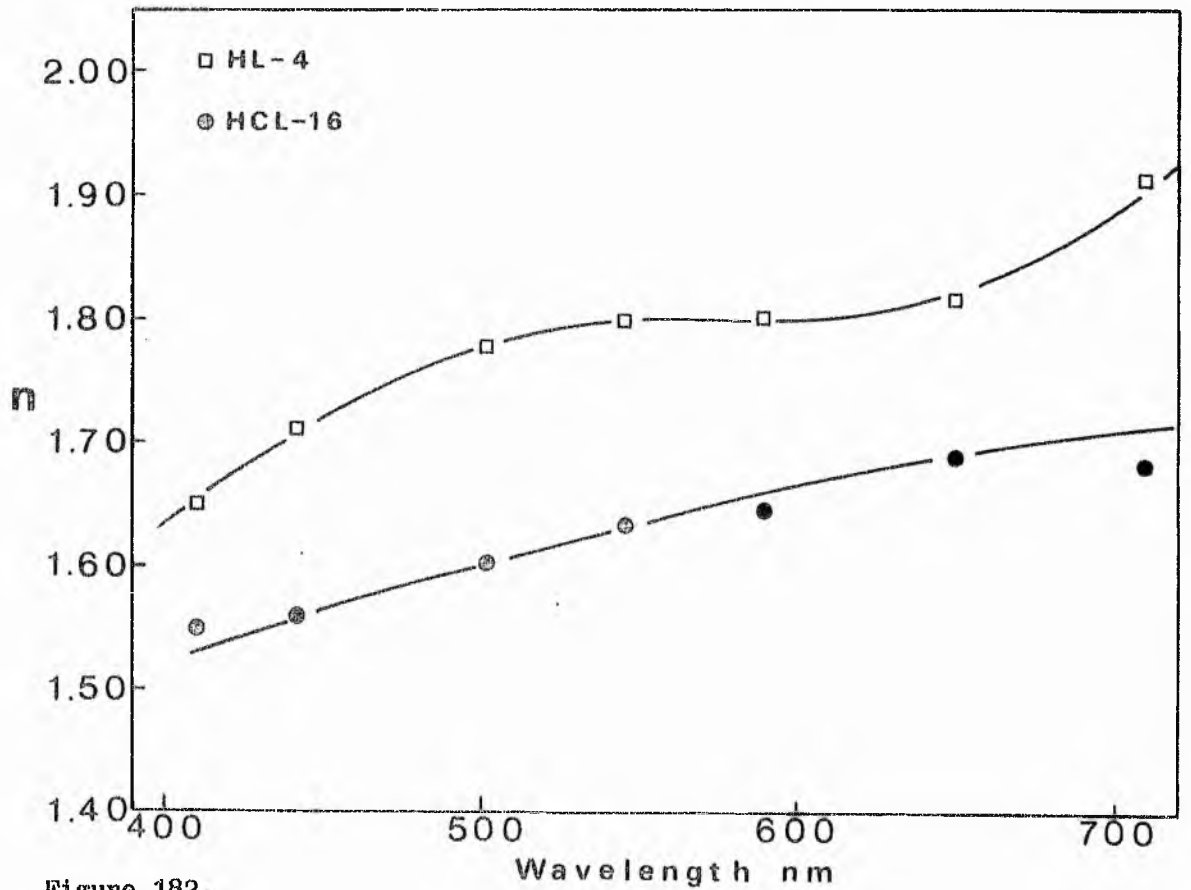
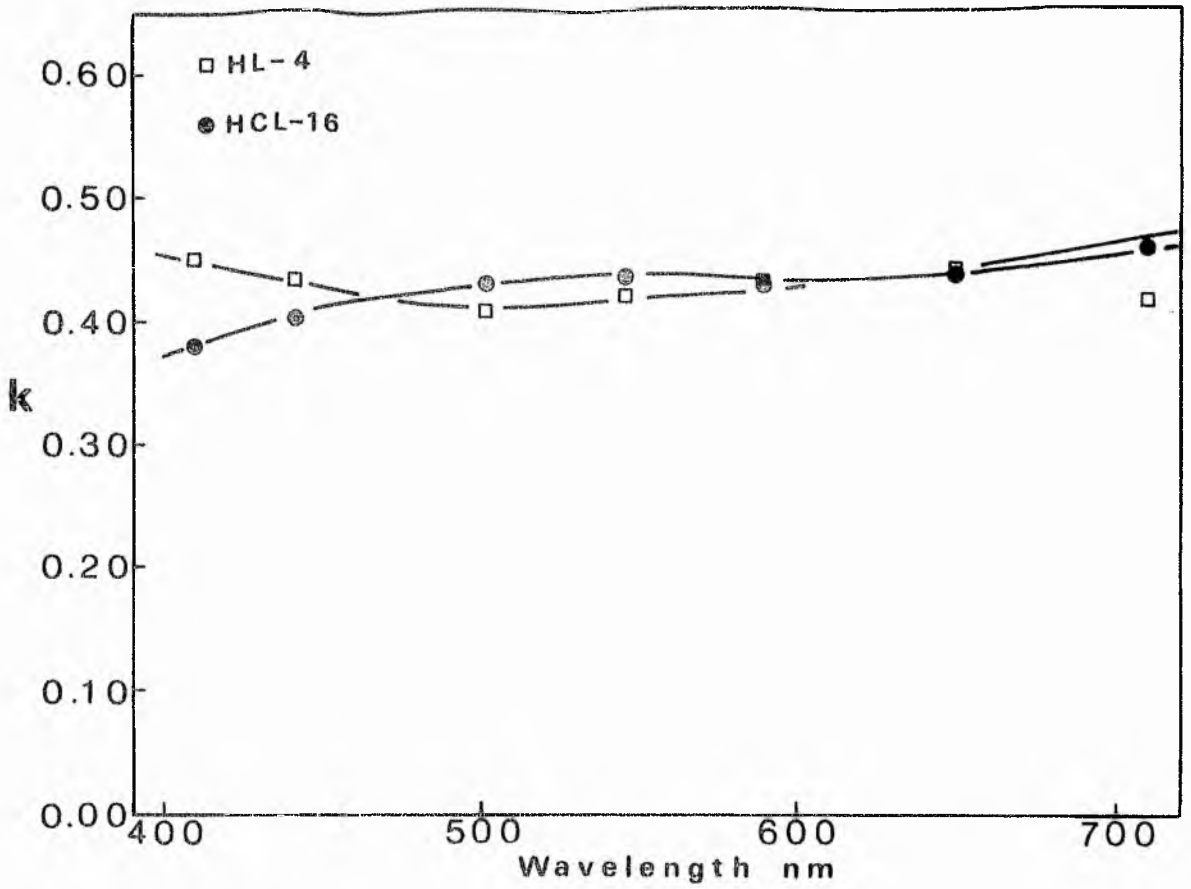


Figure 182.

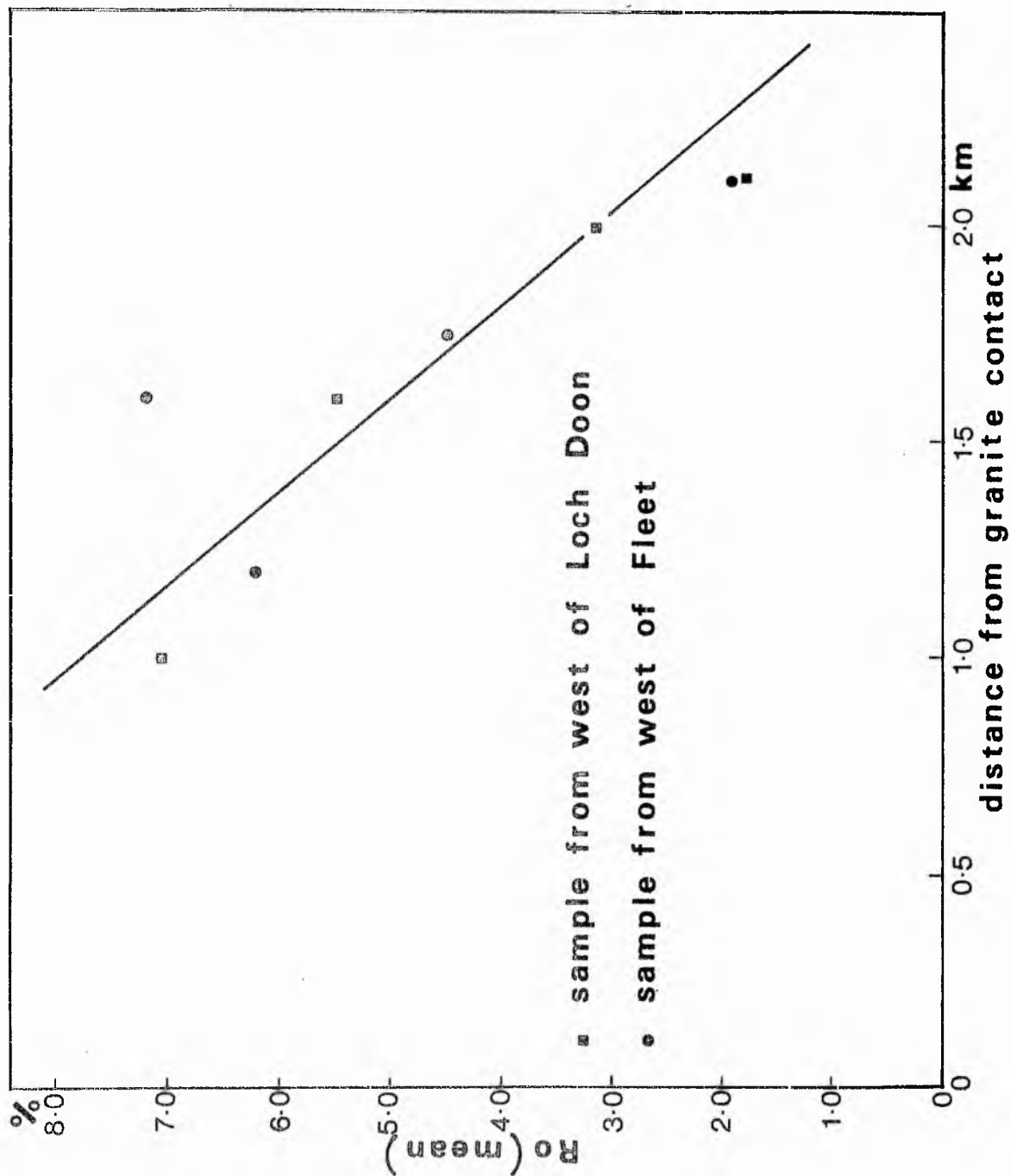


Figure 183. Plot of the variation in reflectivity of graptolite fragments with distance from igneous plutons.

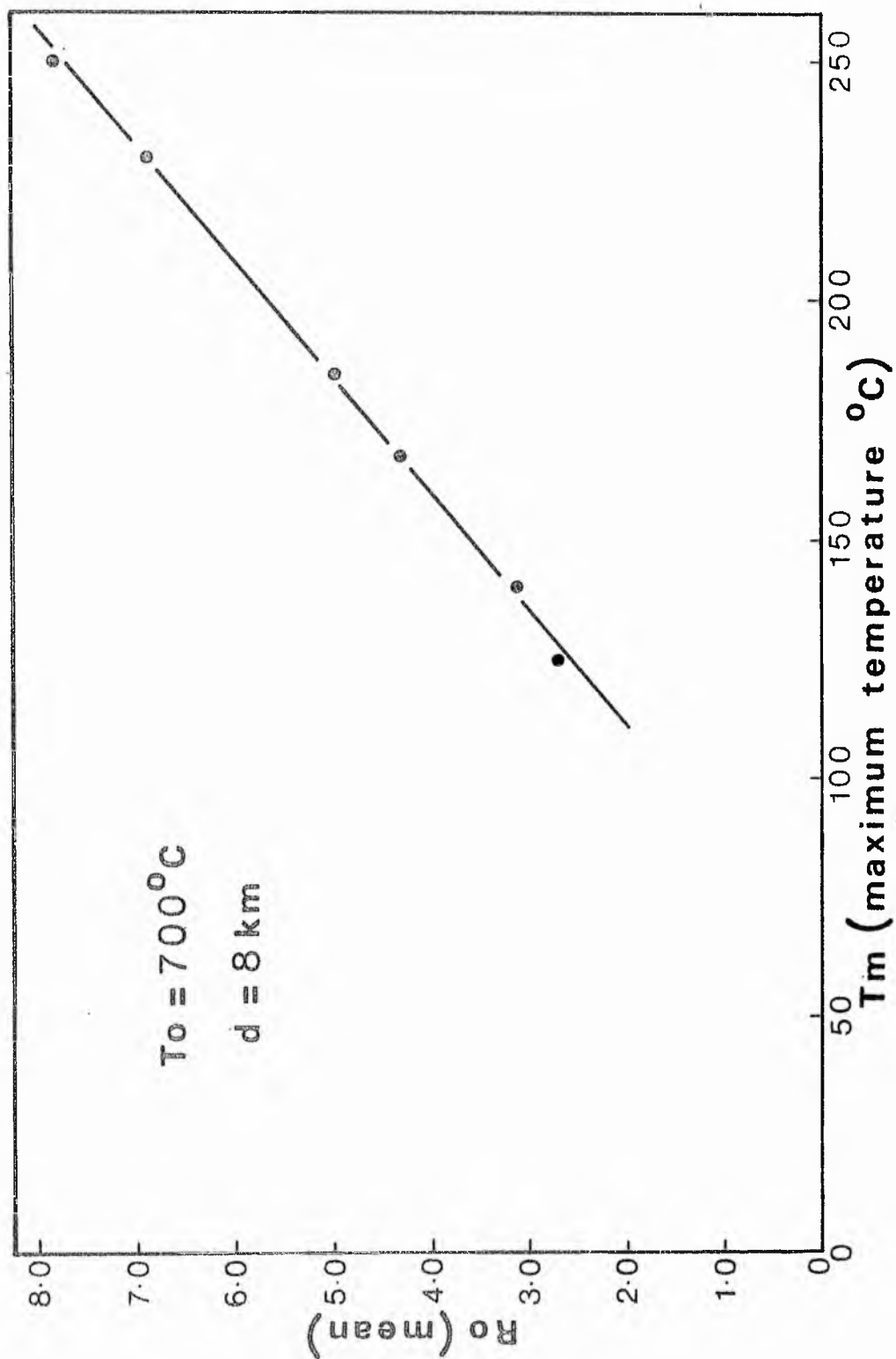


Figure 184. Plot of the variation in reflectivity with temperature for graptolites in the vicinity of igneous plutons.

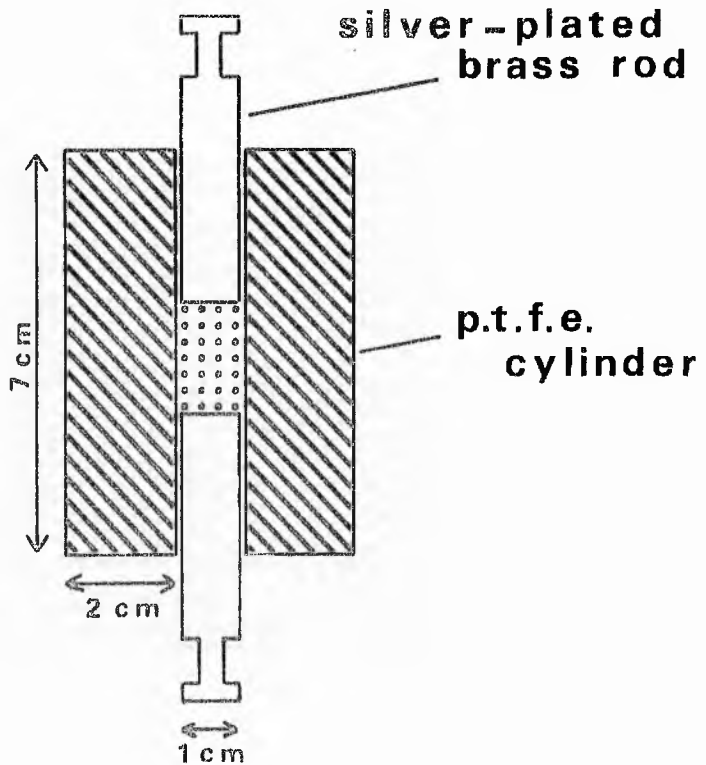
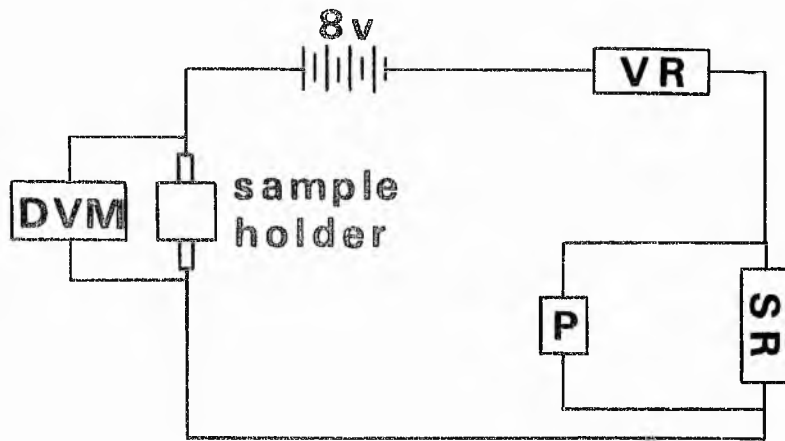


Figure 185. Electrical circuit and apparatus used to measure the resistivity of powdered rock samples; DVM, digital voltmeter; P, potentiometer; VR, variable resistance; SR, standard resistance.

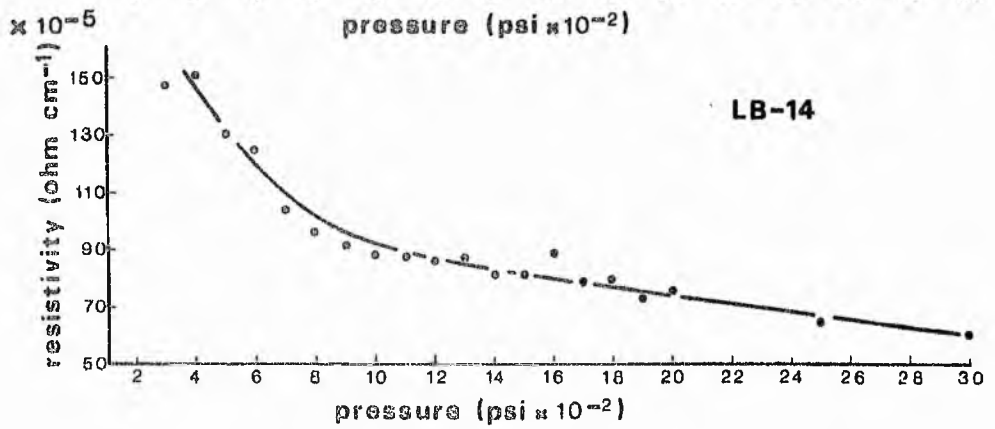
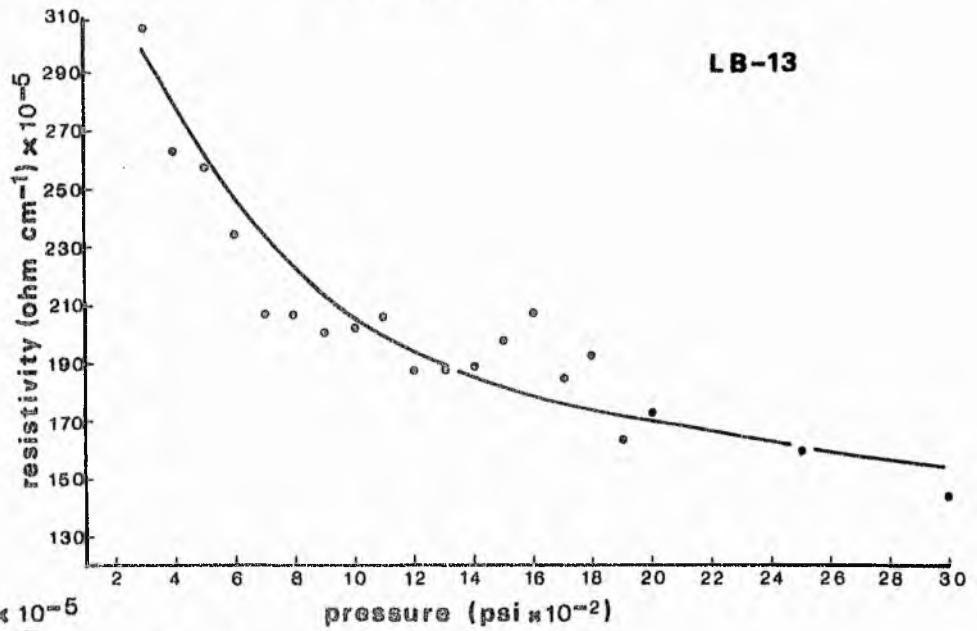
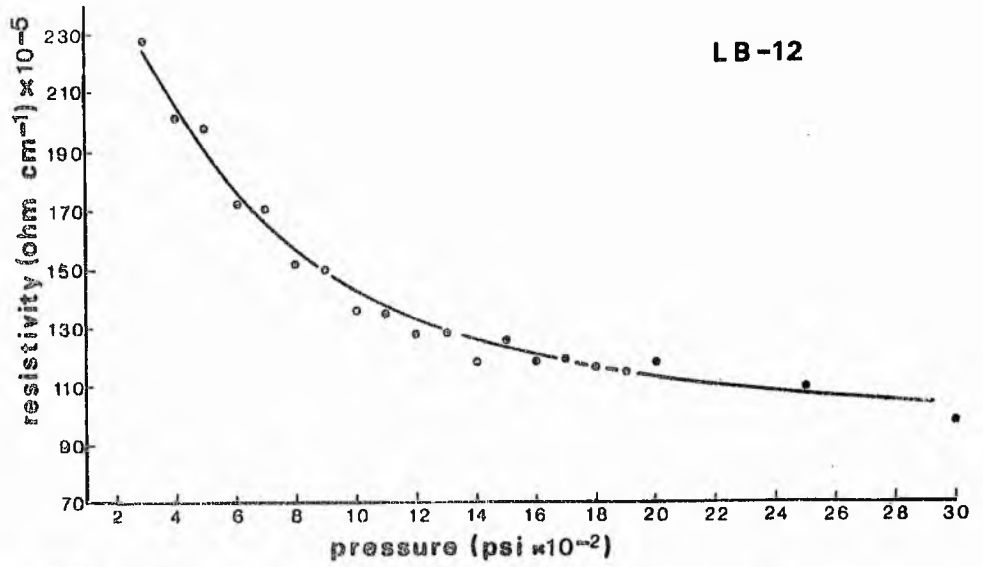


Figure 186. Plots of the variation in resistivity with pressure for samples from Clanyard Bay.

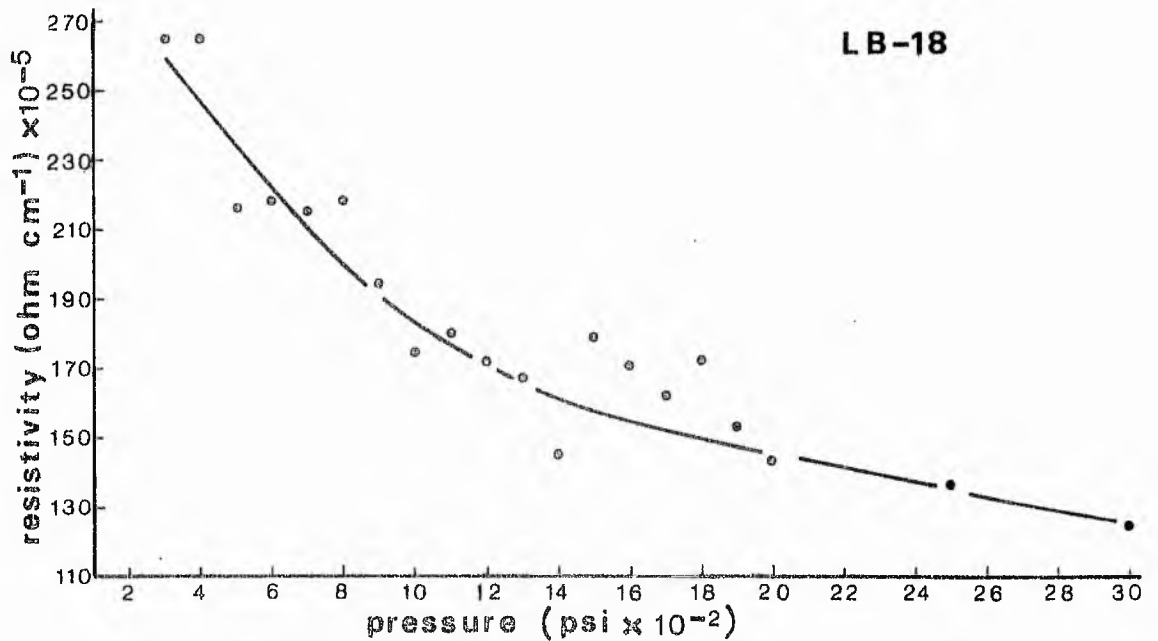
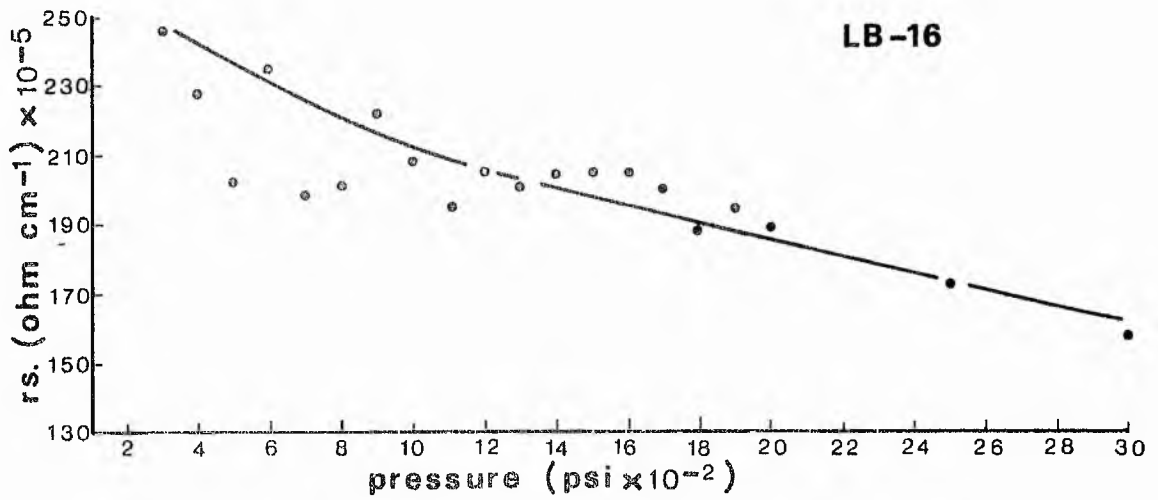
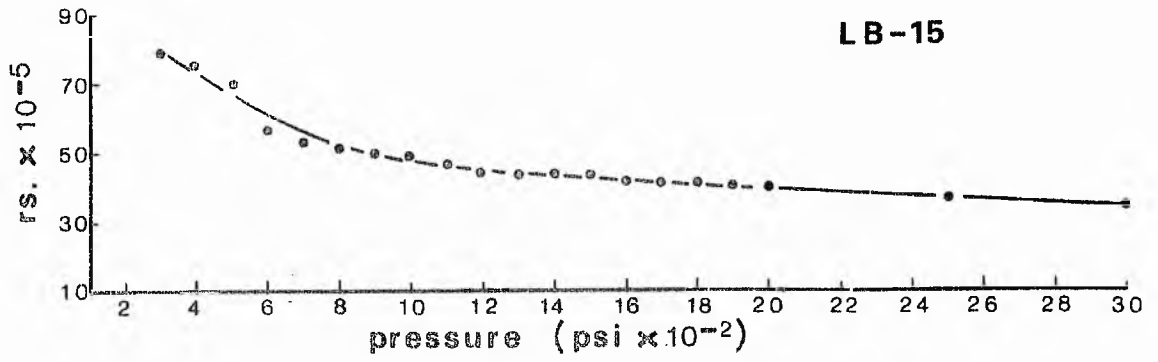


Figure 187. Plots of the variation in resistivity with pressure for samples from Clanyard Bay.

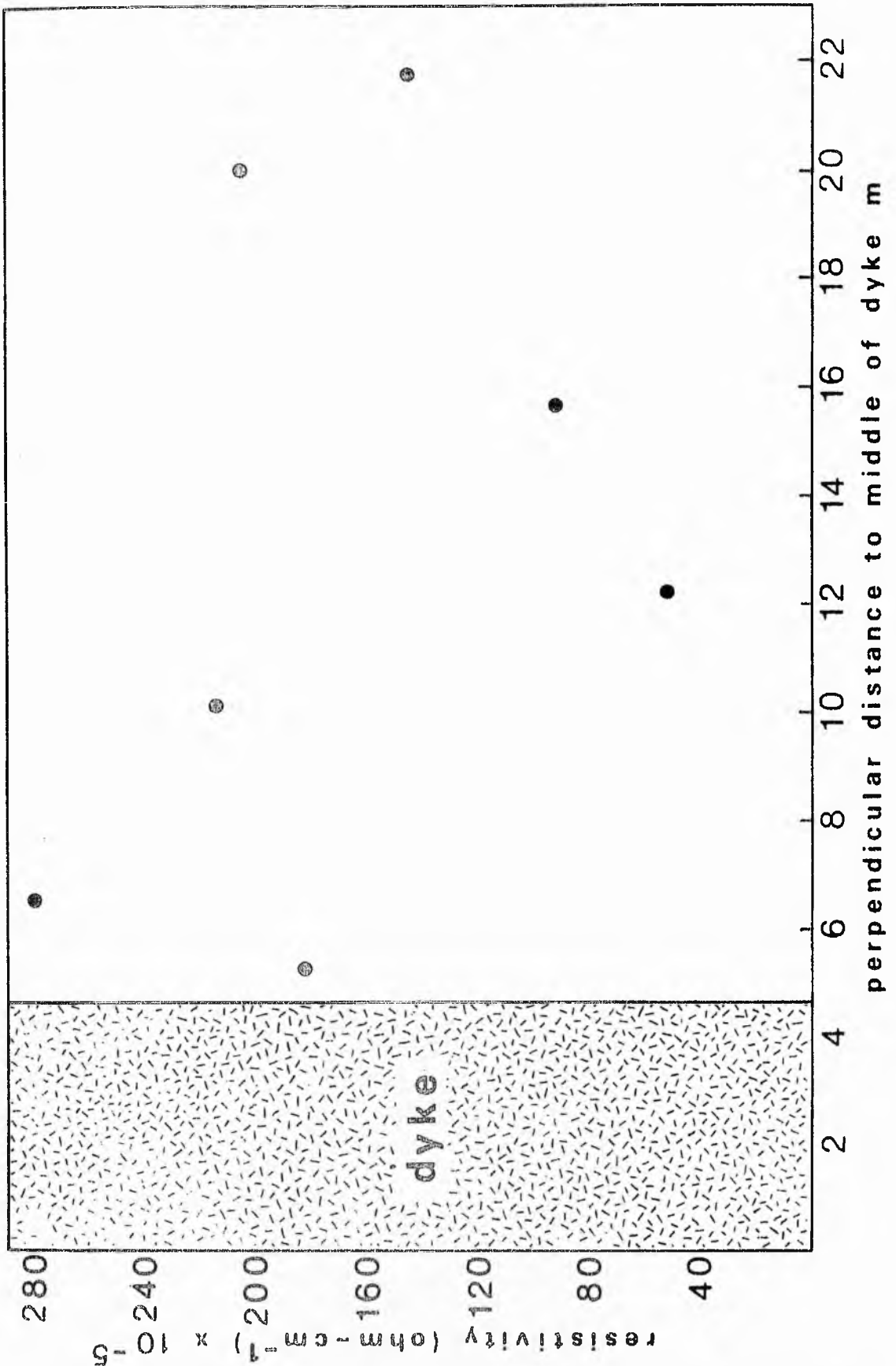


Figure 188. Plot of the variation in resistivity with distance from the dyke at Clanyard Bay.

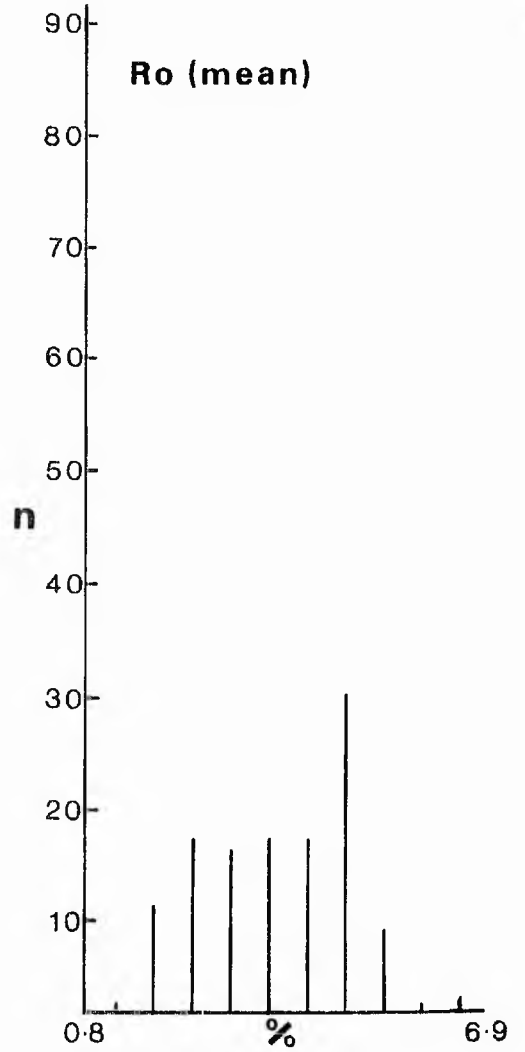
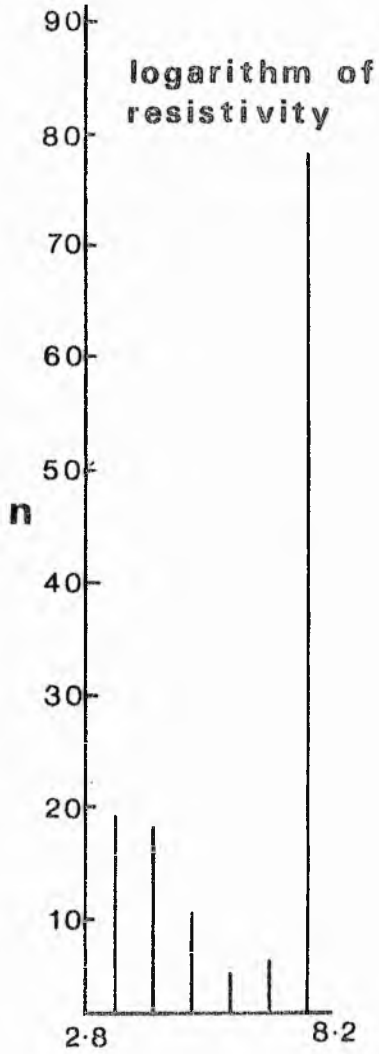
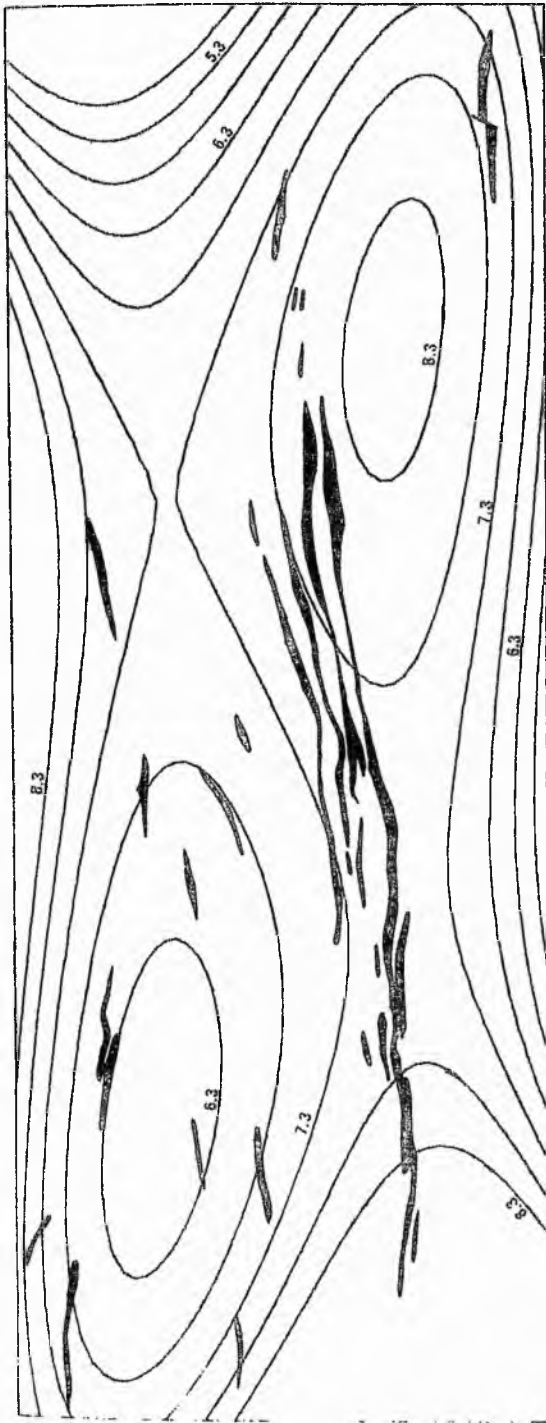
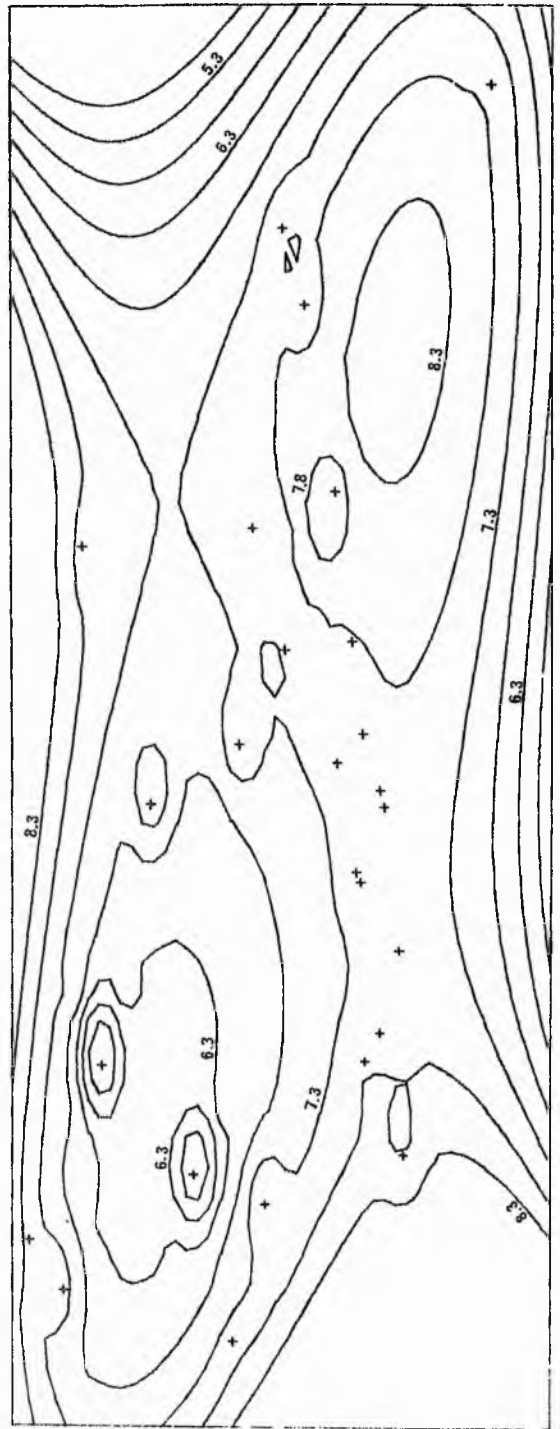


Figure 189. Histograms illustrating the variation in resistivity and reflectivity in the Moffat Shales in the vicinity of Moffat.



GLOBAL FIT SURFACE PLOT

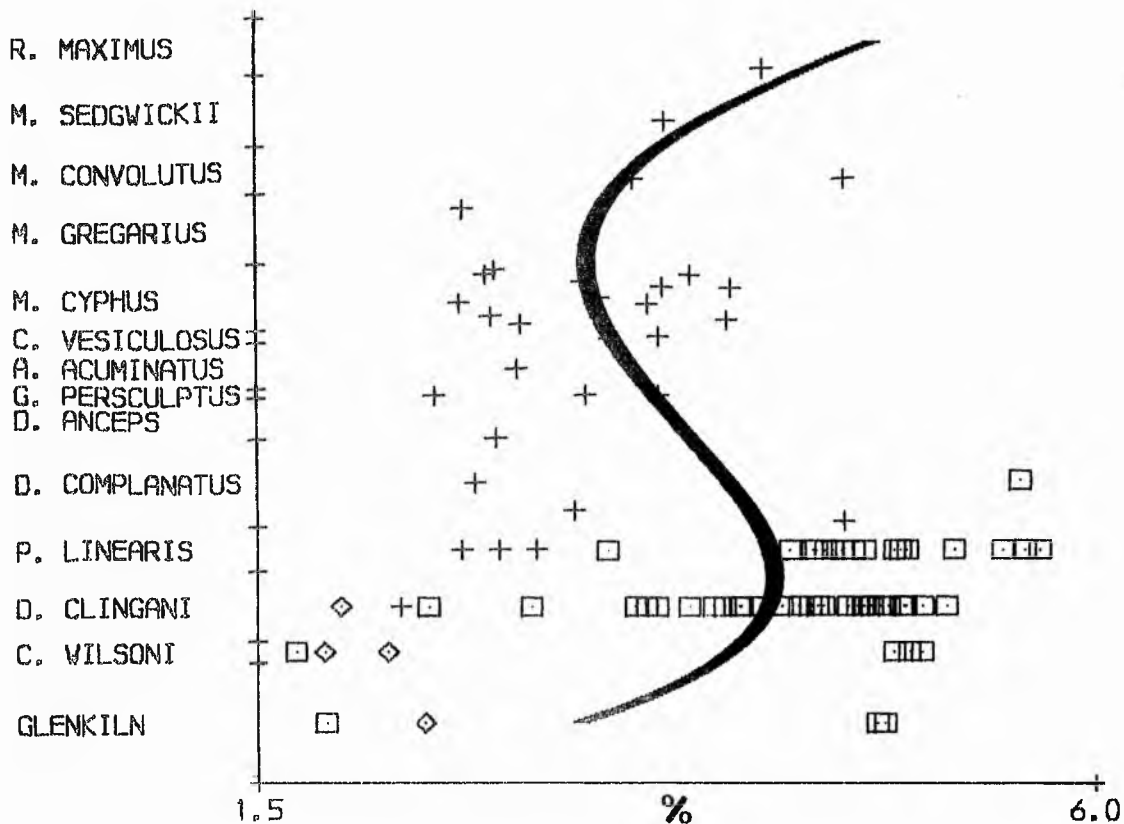


LOG RESISTIVITY IN MOFFAT REGION

Figure 190. Global-fit and iterative surface maps for the variation in resistivity in the Moffat Shales. For scale and orientation, compare Figure 4.

Figure 191. Plots illustrating the stratigraphic variation in reflectivity and resistivity in the Moffat Shales. For key see Figure 20.

R (OIL) 88 DATA POINTS



LOG RES 101 DATA POINTS

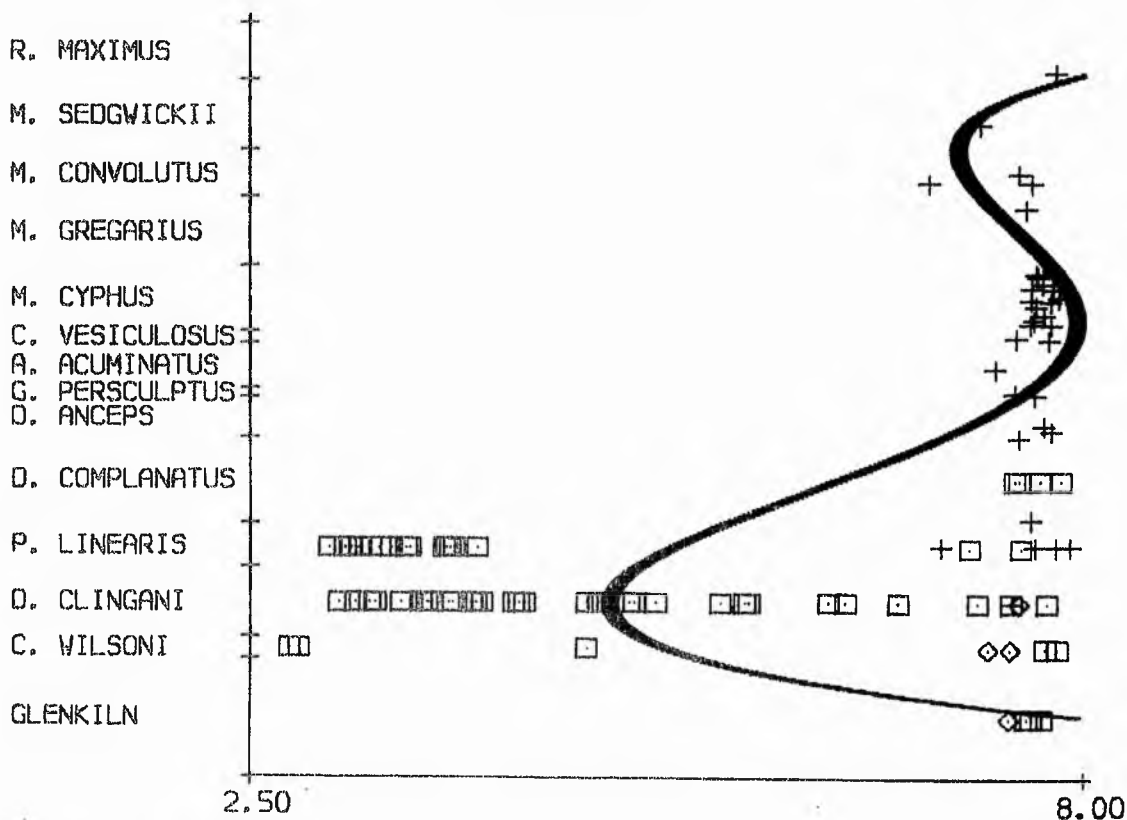


Figure 191.

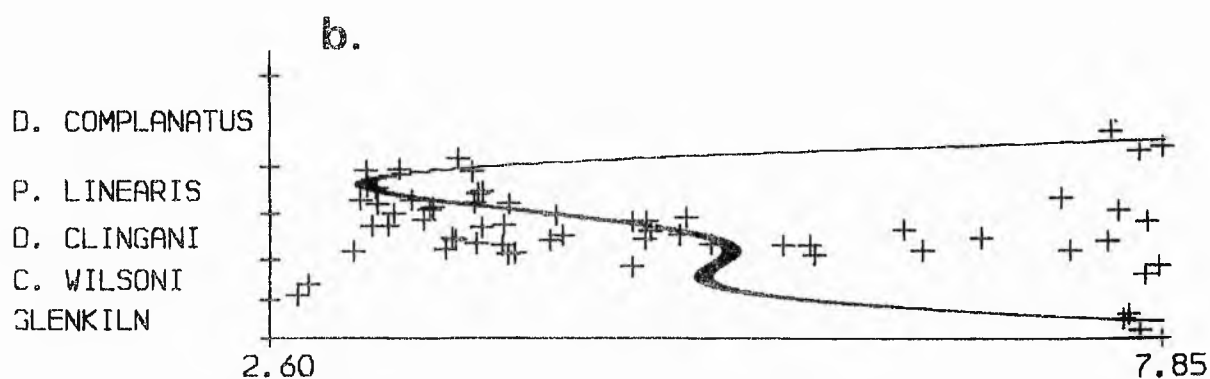
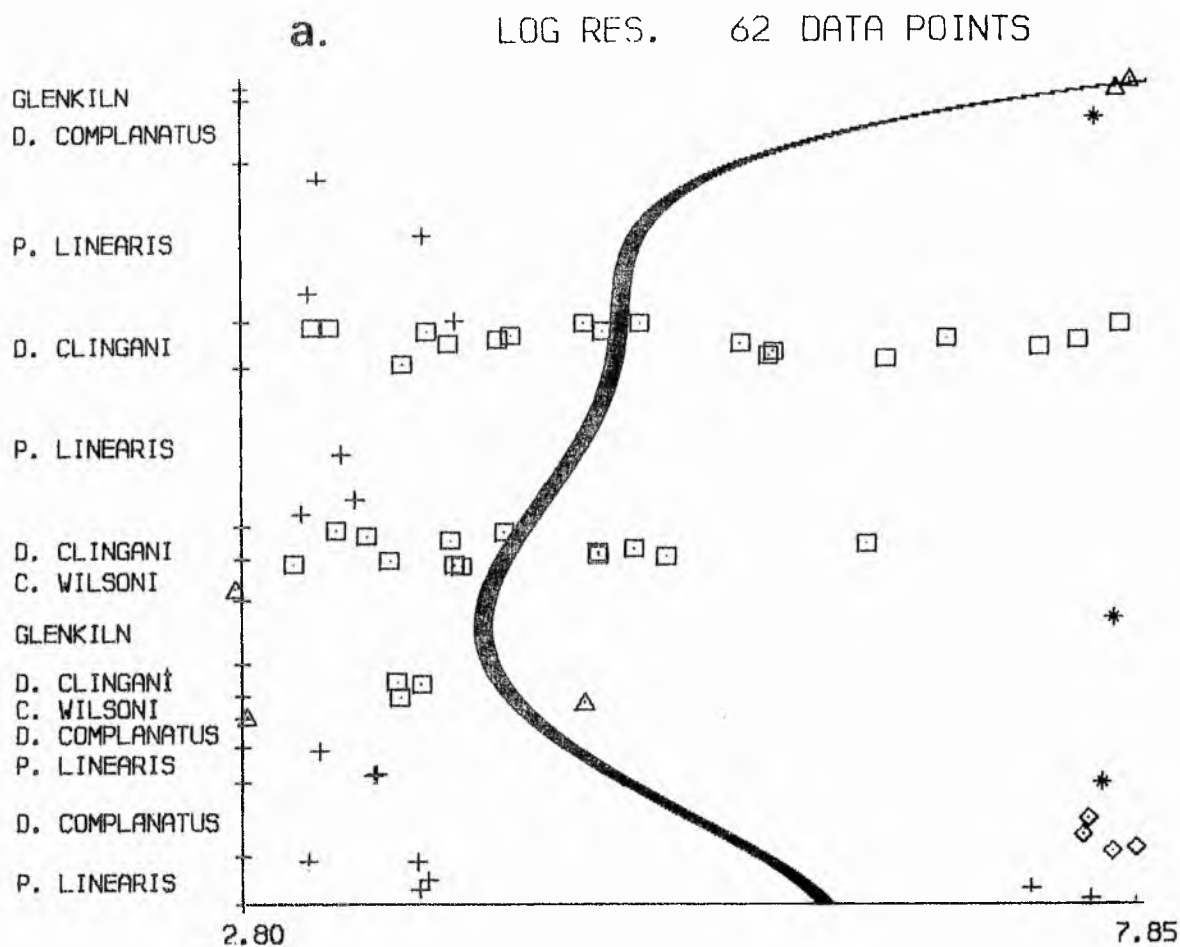


Figure 192. Plots illustrating the stratigraphic variation in resistivity of the sediments of the north cliff at Hartfell Scaur.
a) Sequence as observed, b) structurally restored sequence.

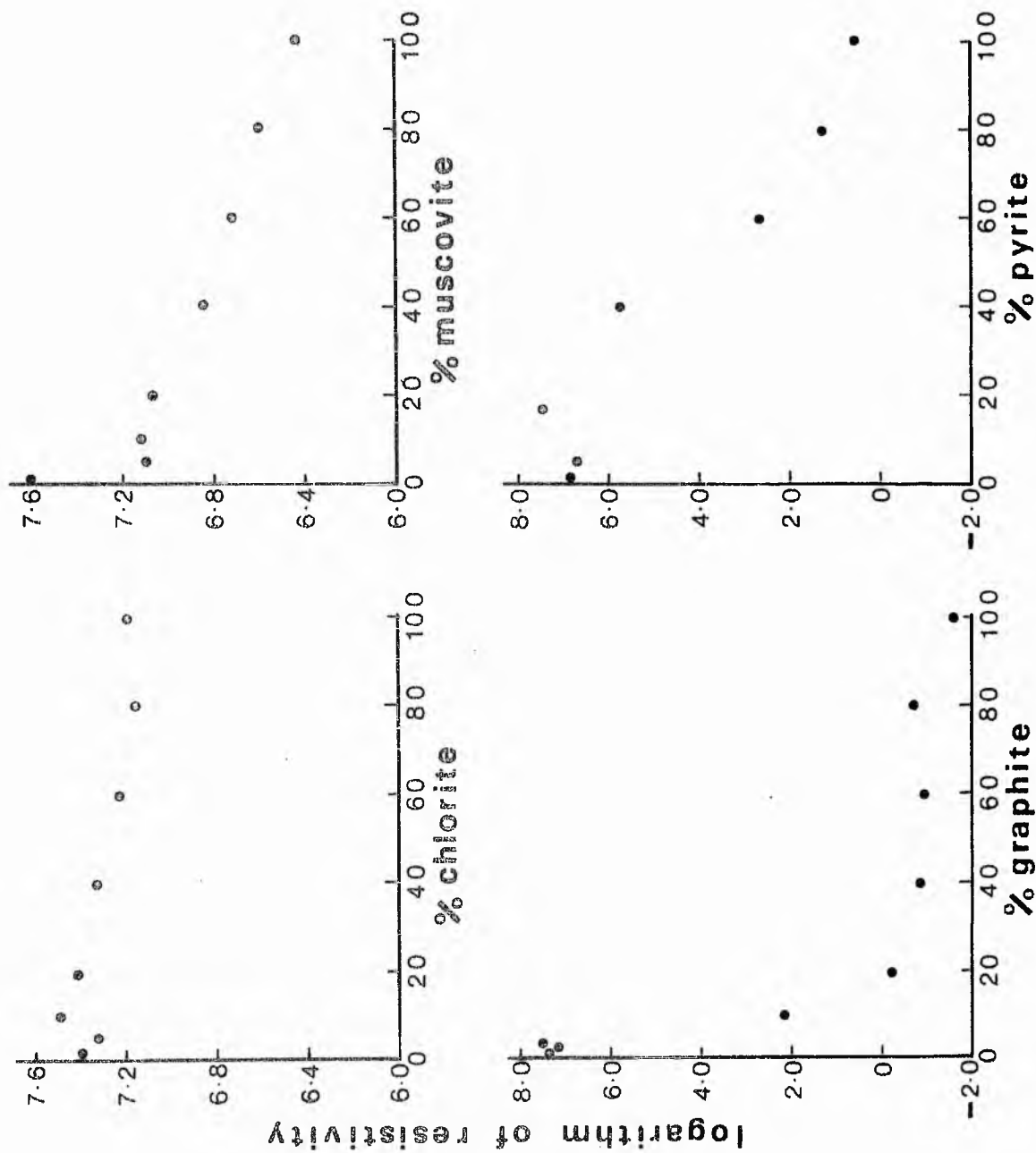


Figure 193. Plots of the variation in resistivity of two component mixtures of quartz with chlorite, muscovite, graphite and pyrite.

Sample n-trifluoro-acetyl (-) menthol derivatives of amino acids

| | |
|------------------------|-------------------------------------|
| Model of chromatograph | Varian 1400 |
| Column | 10' x 1/8" Glass |
| Packing | 3% OV-1 on 100-120 mesh Varaport 30 |
| Column temp. | 140-260°C 4°/min. |
| Detector temp. | 240°C Injector temp. 210°C |
| Attenuation | 16 x 10 ⁻¹¹ |
| Recorder | 1 mV 12 in/hr. |
| Nitrogen | 40 ml/min. |
| Isothermal | At 140°C for 5 mins. |

Sample n-propyl n-hepta fluoro butyric acetyl derivatives of amino acids

| | | |
|------------------------|---|-------|
| Model of chromatograph | Varian 1400 | acids |
| Column | 10' x 1/16" Glass | |
| Packing | 3% OV-1 on 100-120 mesh Varaport 30 | |
| Column temp. | 70-260°C 4°/min. | |
| Detector temp. | 290°C Injector temp. 230°C | |
| Attenuation | 128 x 10 ⁻¹¹ | |
| Recorder | 1 mV 12 in/hr. | |
| Nitrogen | 40 ml/min. | |
| Isothermal | At 70°C for 15 mins. | |
| Inject | 2 μ l Std. + 2 μ l acetic anhydride | |

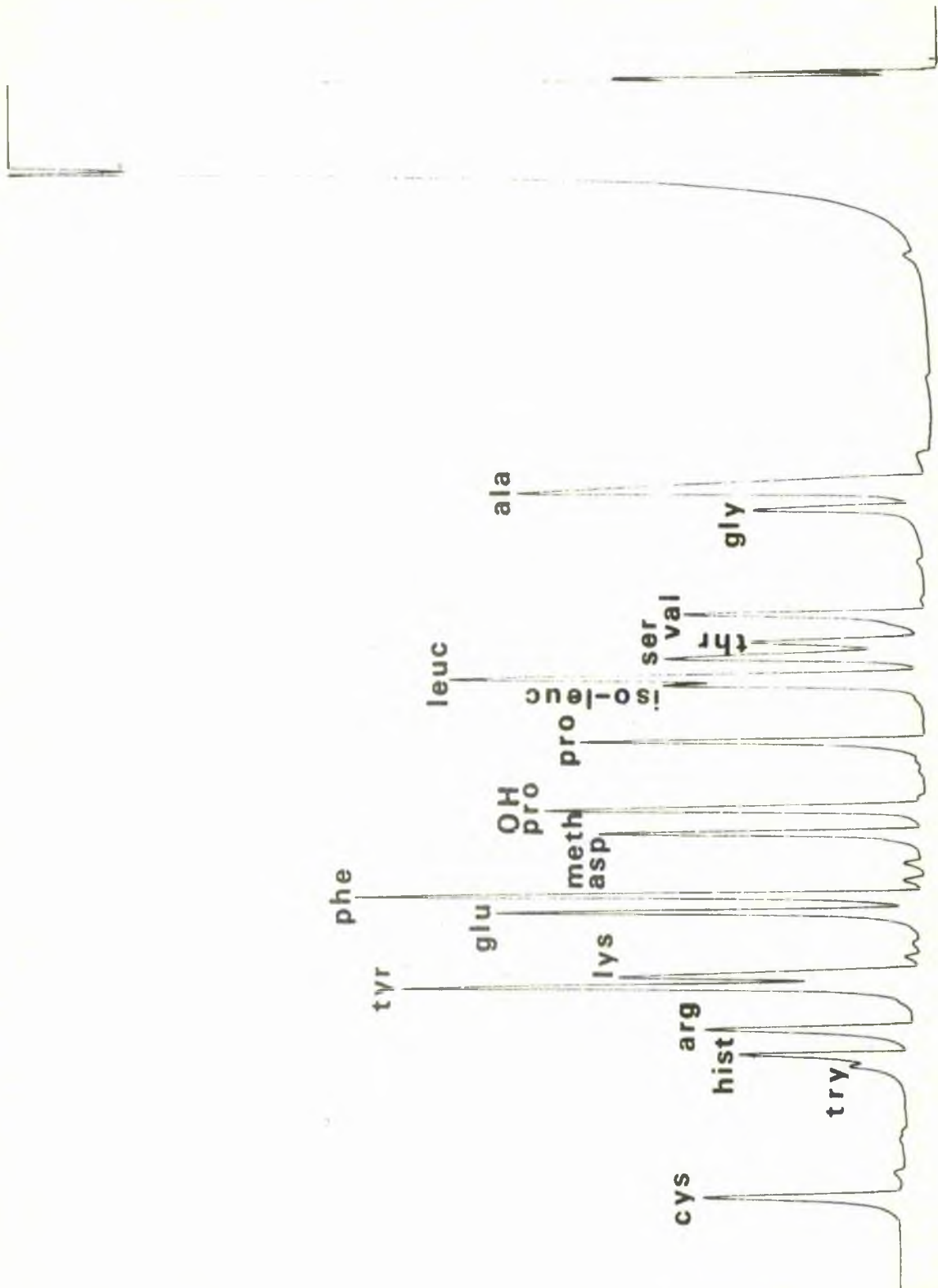


Figure 194. Gas-liquid chromatogram of the N-heptafluoro-butyl n-propyl derivatives of a standard series of amino acids. Chromatographic conditions in text.

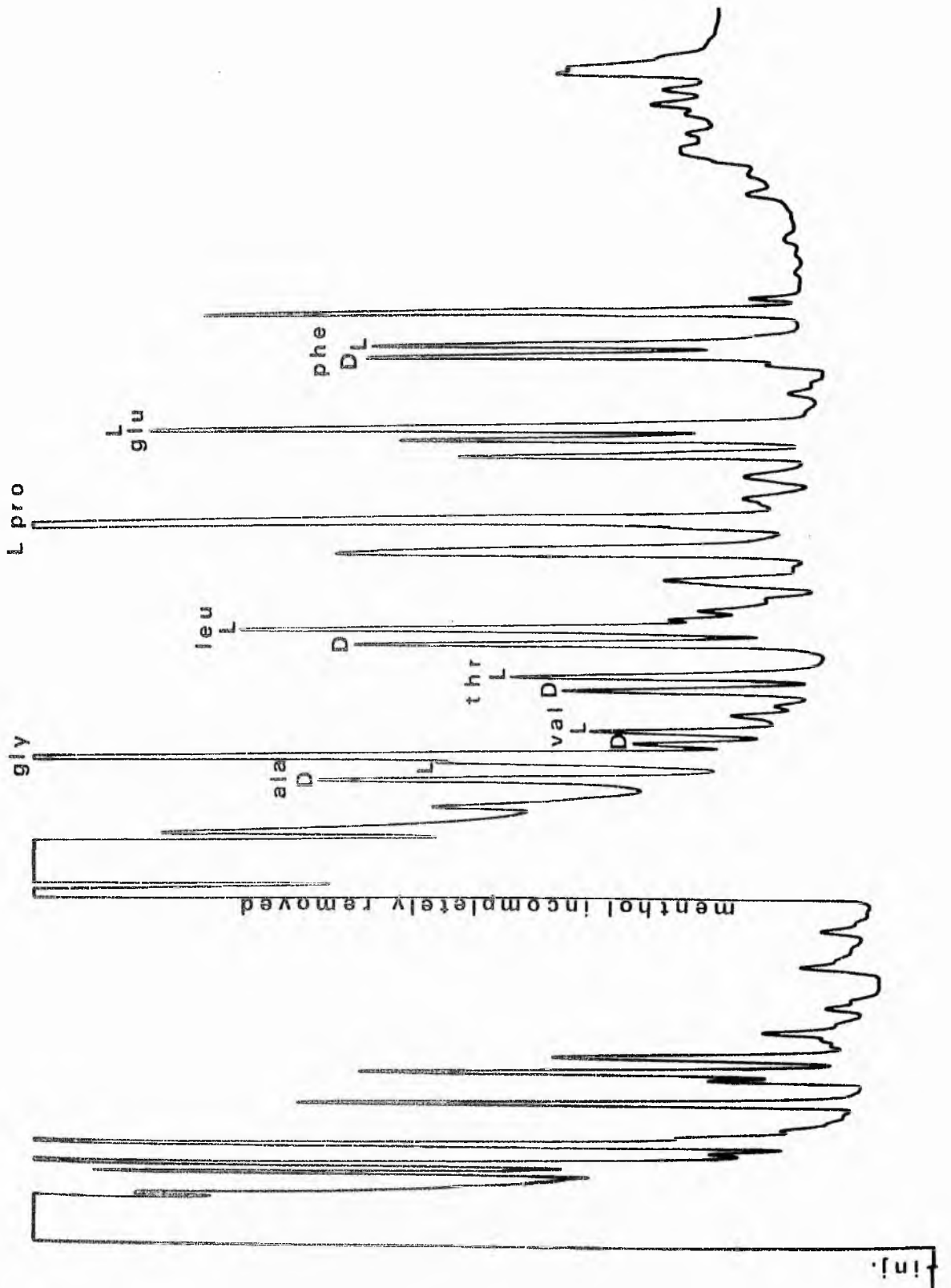


Figure 195. Gas-liquid chromatogram of the N-trifluoro-acetyl L-valyl-L-valine cyclohexyl esters of a standard series of amino acids. L indicates position of laevo enantiomer, D position of dextra enantiomer. Chromatographic conditions in text.

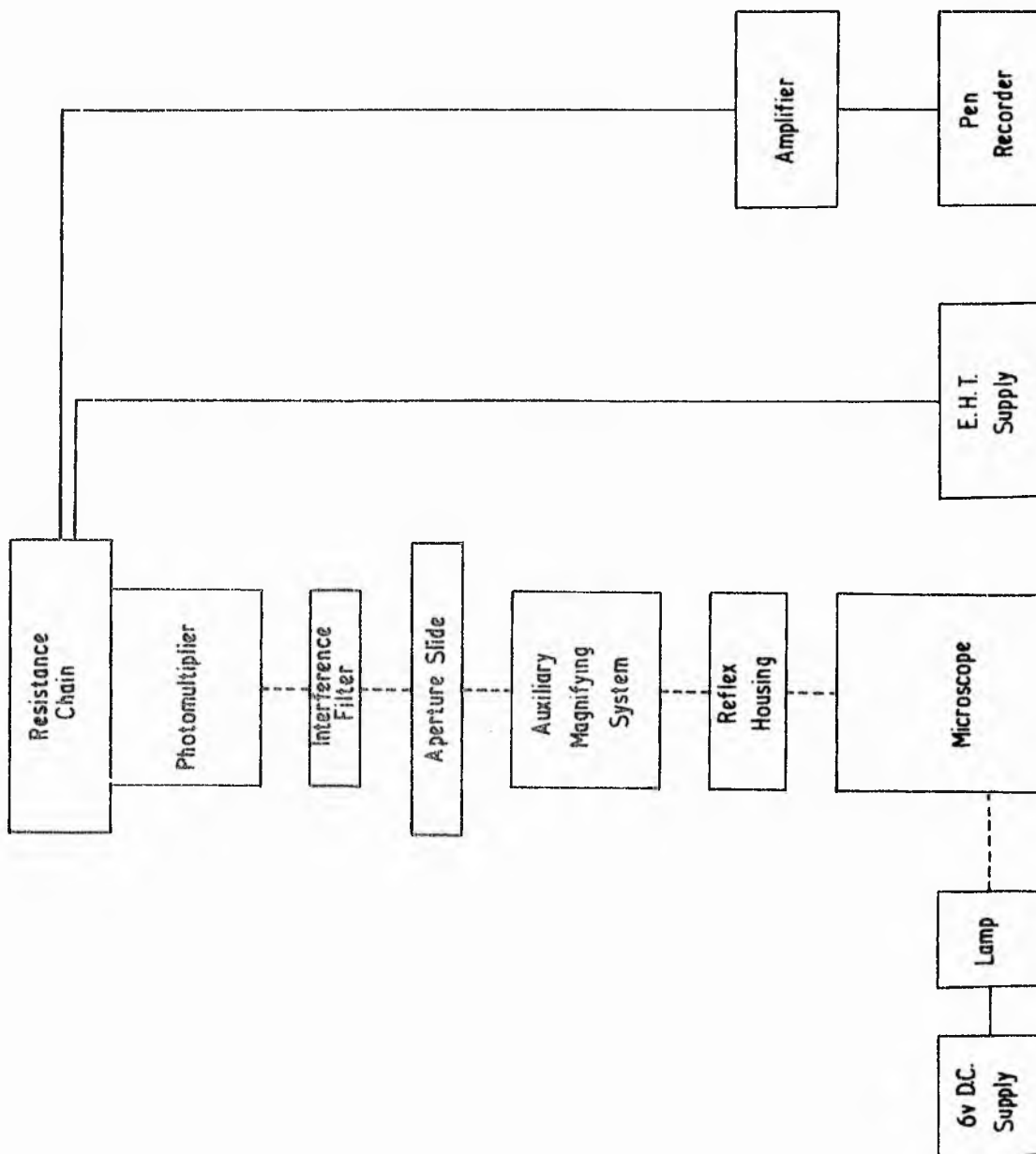


Figure 196. Schematic flow diagram of important elements in the microphotometer system, after Jones et al., (1968).

Key to Figure 197.

1. Photometer field diaphragm
2. Filter holder
3. Lamp carrier for incident light illumination
4. Light source
5. Current stabilizing mains unit
6. Photomultiplier
7. Four-leaf measuring diaphragm
8. Viewing shutter
9. Monocular viewer
10. Clamp for lamp carrier
11. Bertrand lens
12. Changing lever for photometer illumination / low power illumination
13. Microscope lamp carrier for incident light
14. Illumination changing slide
15. Objective lens
16. Microscope lamp attachment for transmitted light.

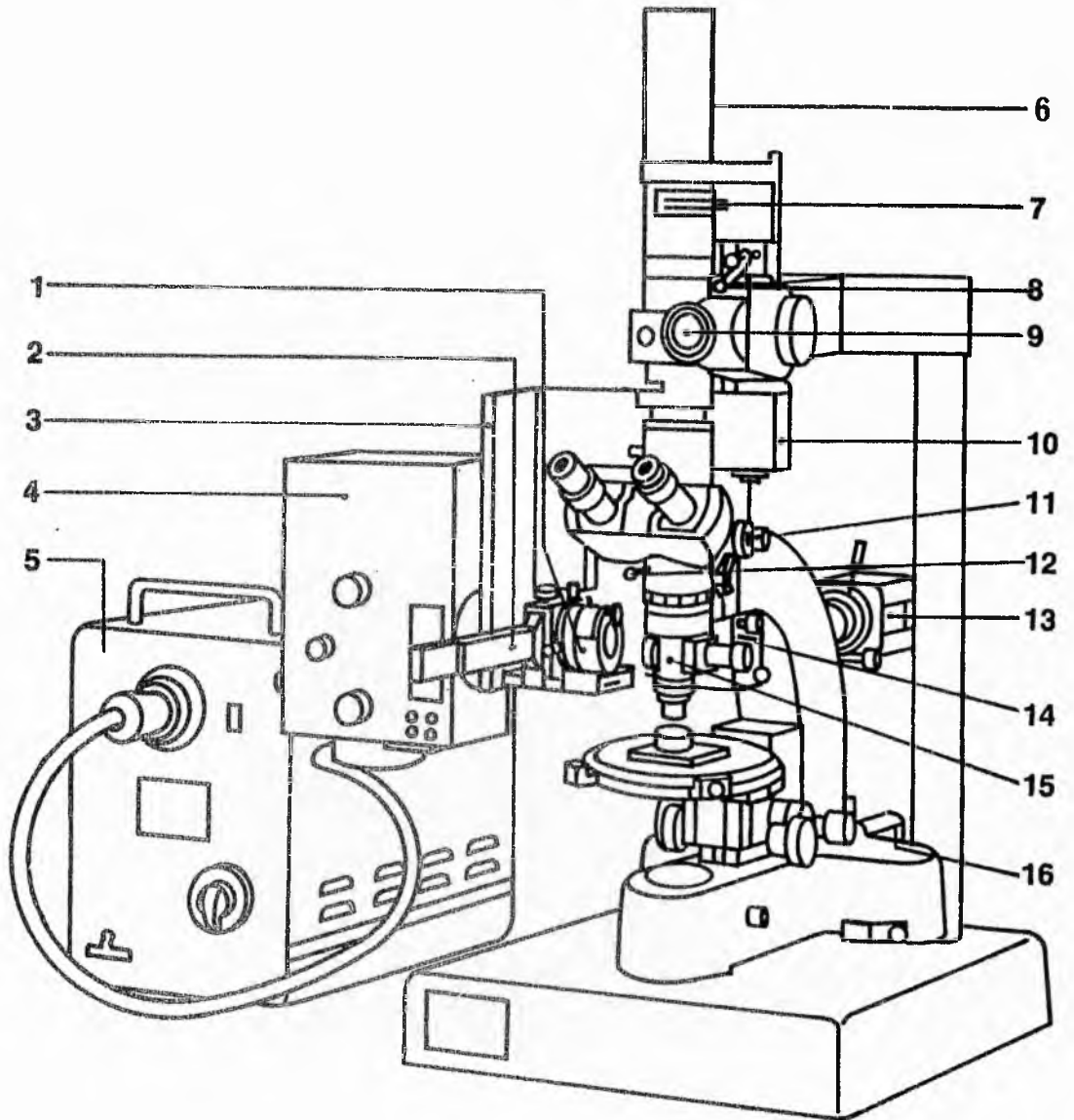
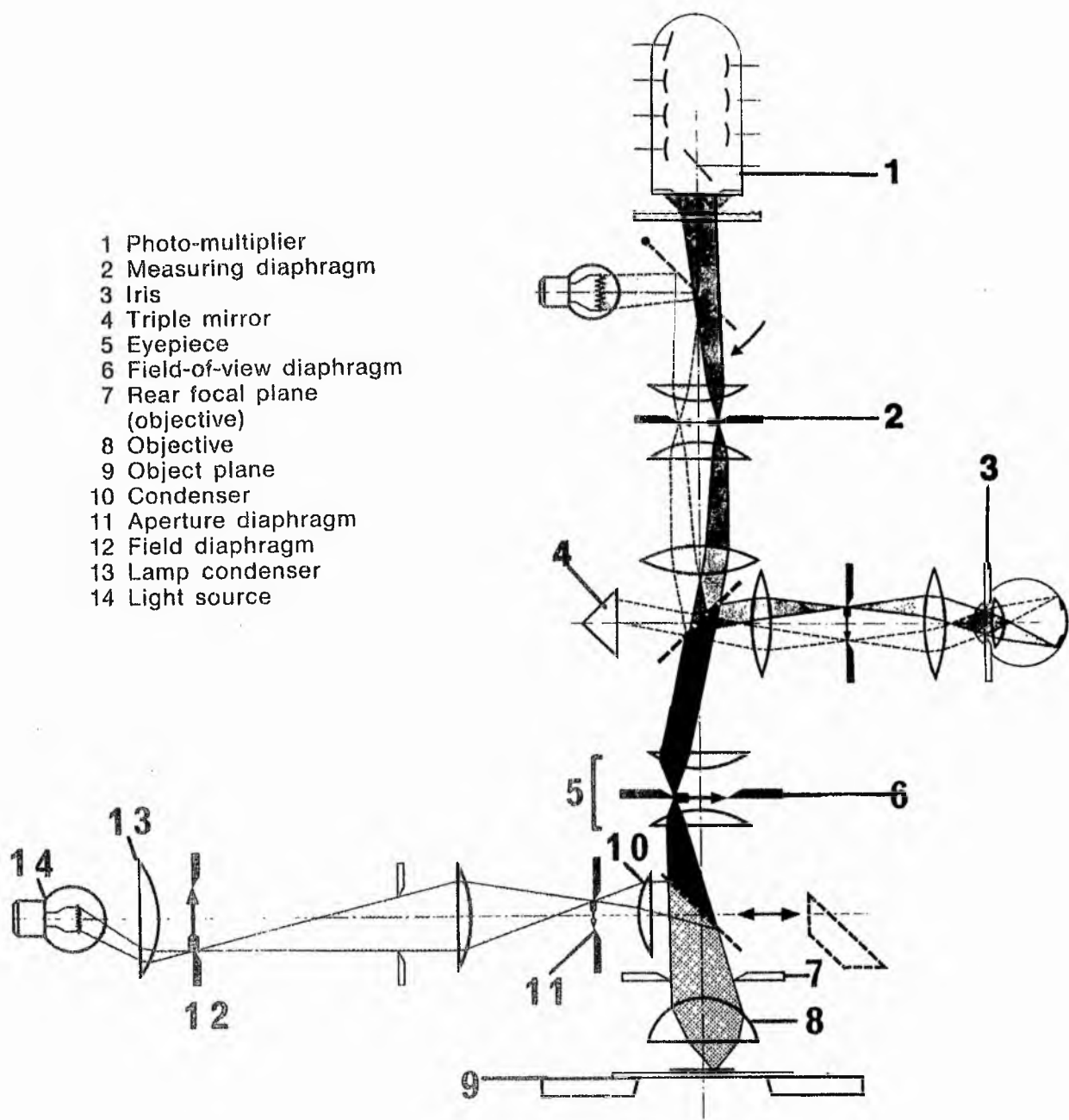


Figure 197. Drawing illustrating the position of the important elements in the Leitz Orthoplan microphotometer system. (For key see facing page).



- 1 Photo-multiplier
- 2 Measuring diaphragm
- 3 Iris
- 4 Triple mirror
- 5 Eyepiece
- 6 Field-of-view diaphragm
- 7 Rear focal plane (objective)
- 8 Objective
- 9 Object plane
- 10 Condenser
- 11 Aperture diaphragm
- 12 Field diaphragm
- 13 Lamp condenser
- 14 Light source

Figure 198. Light beam path for incident light in the Leitz Orthoplan system.

BEREK - PRISM REFLECTOR

PLANE-GLASS REFLECTOR

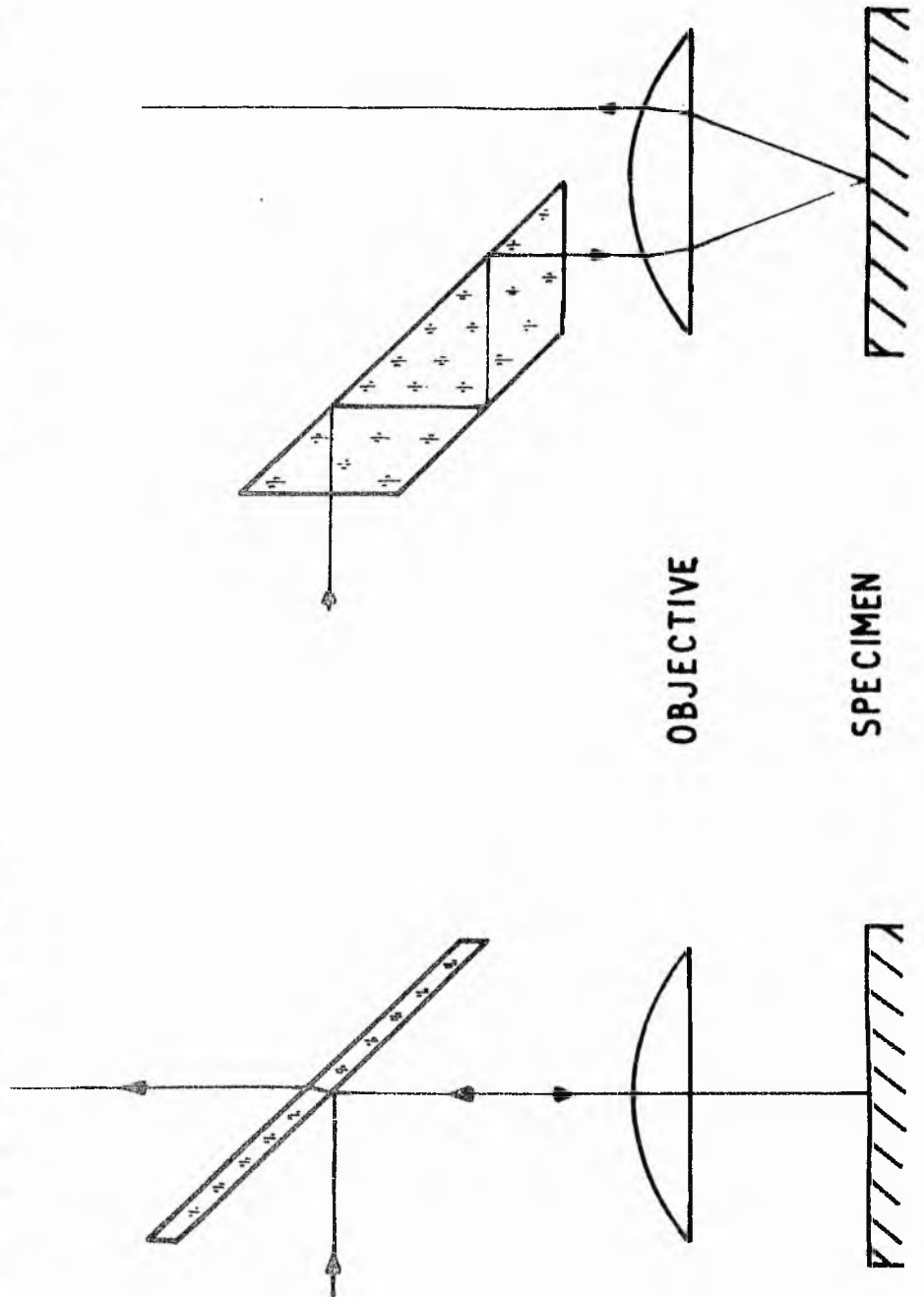


Figure 199. Diagrams of the light path in each of the two types of vertical illuminator which are incorporated in the Leitz Orthoplan system.

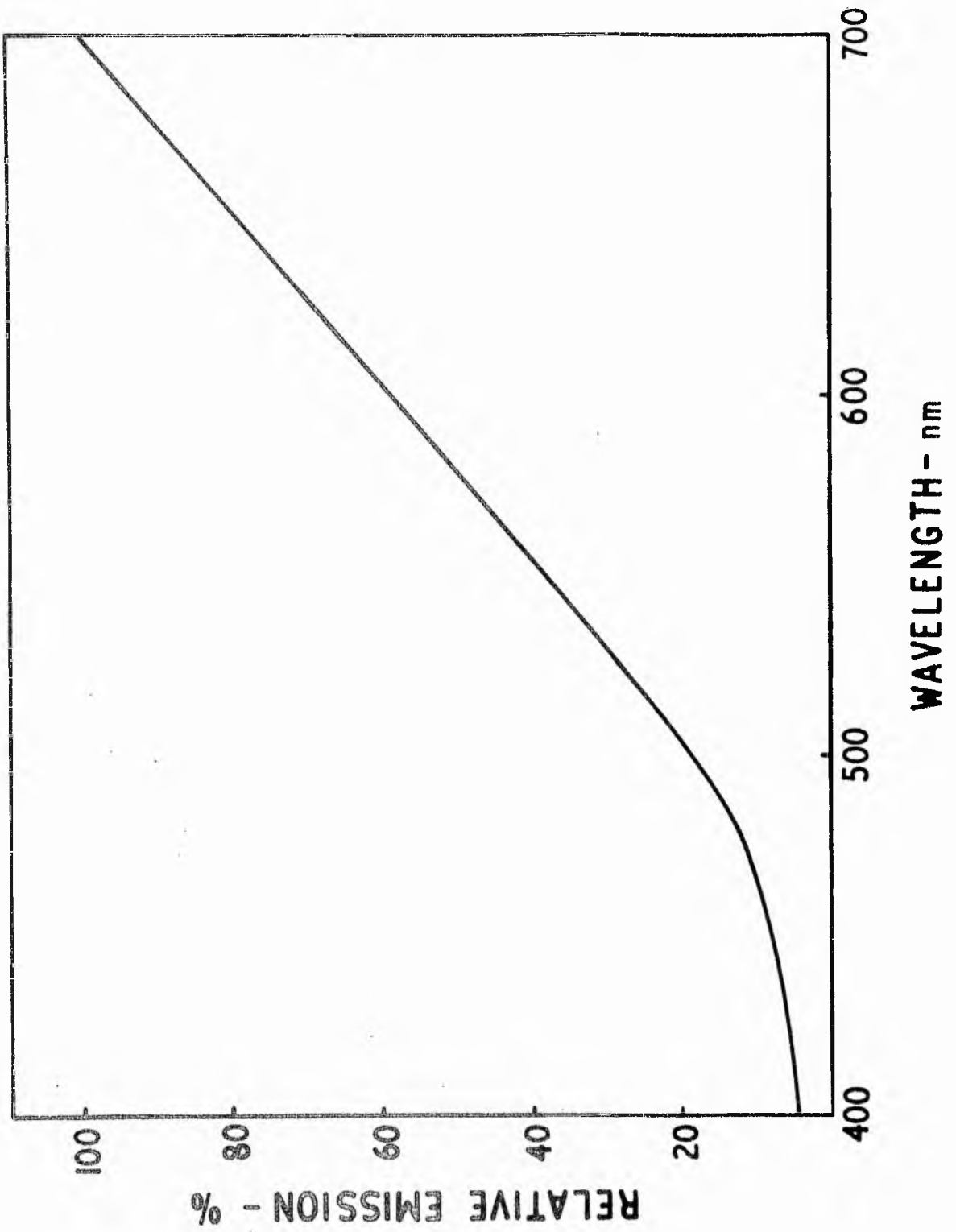


Figure 200. Graph of the spectral response of a tungsten lamp (after Shillaber 1949).

EMI.
TYPE 9592B

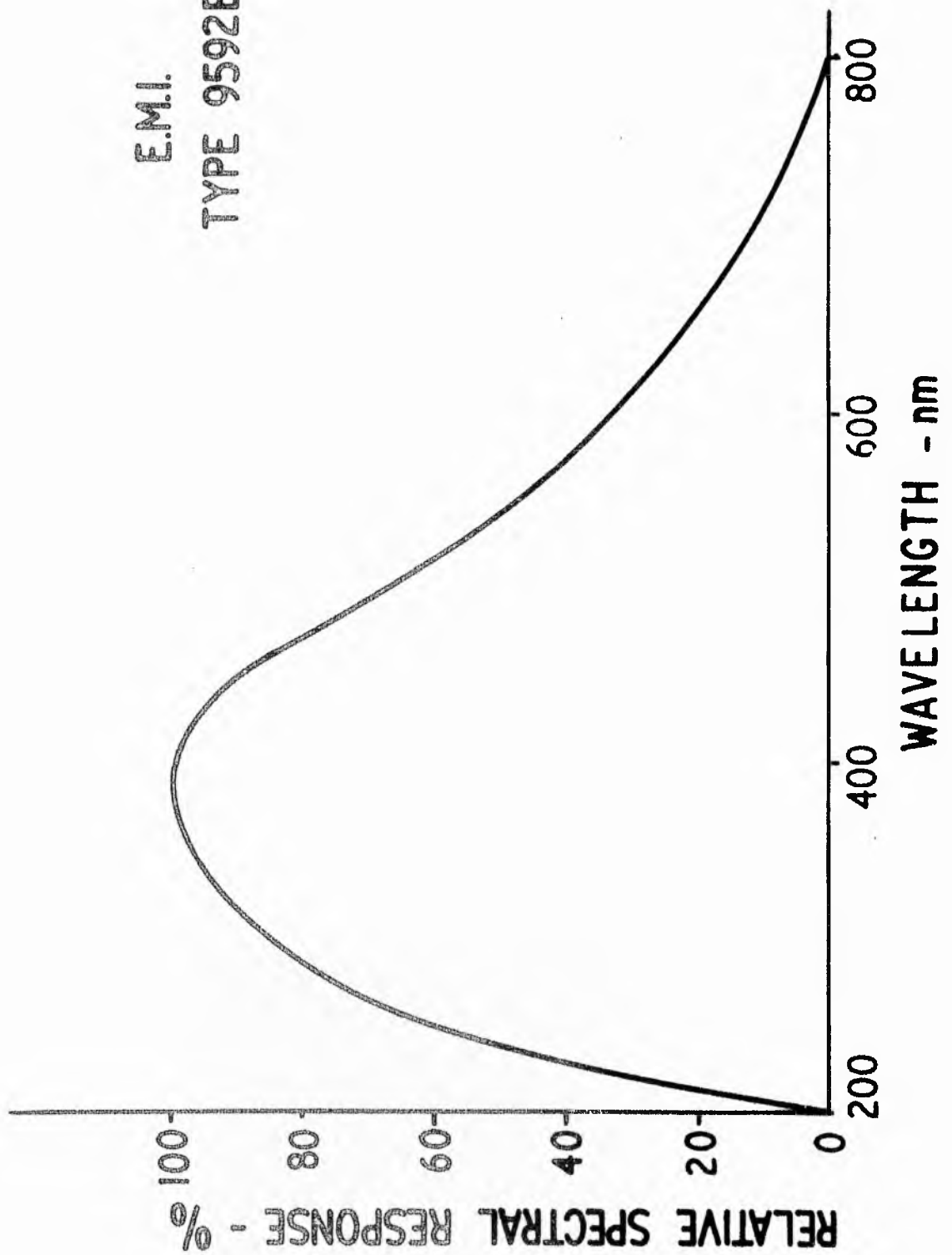


Figure 201. Graph of the spectral response of the EMI type 9592 photomultiplier.

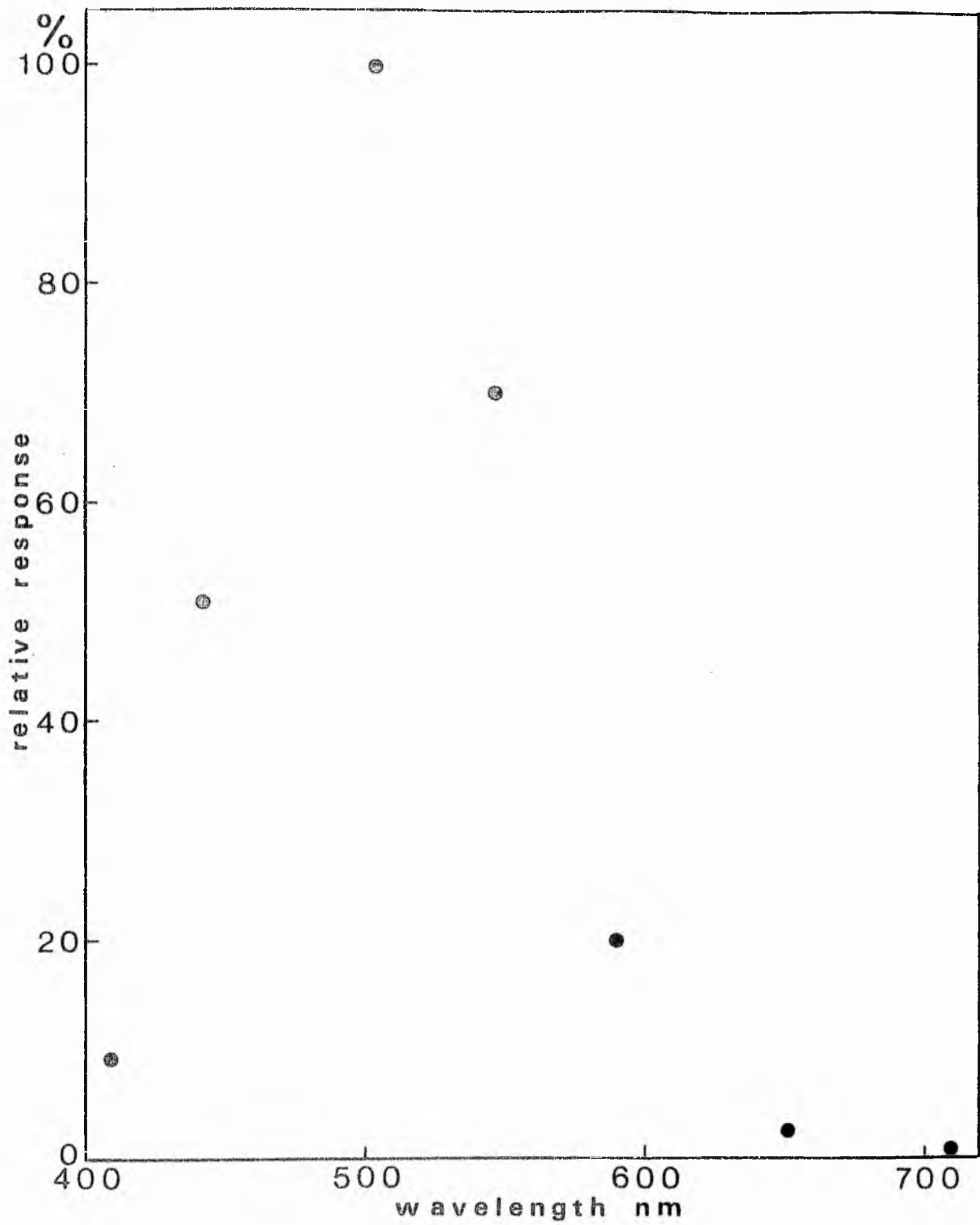


Figure 202. Plot of the spectral response of the Leitz Orthoplan microphotometer system.

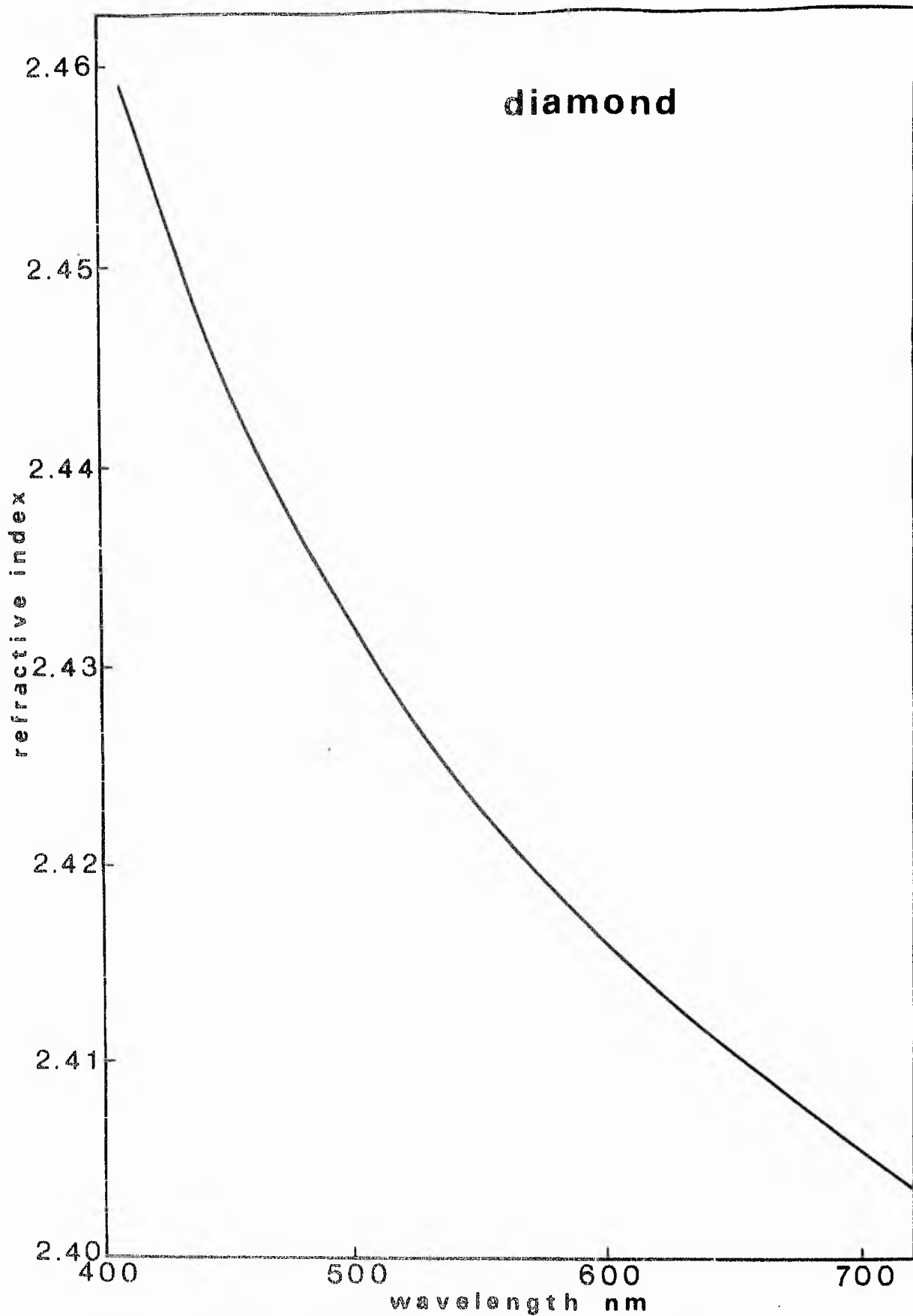


Figure 203. Plot of the dispersion with wavelength of the refractive index of diamond.

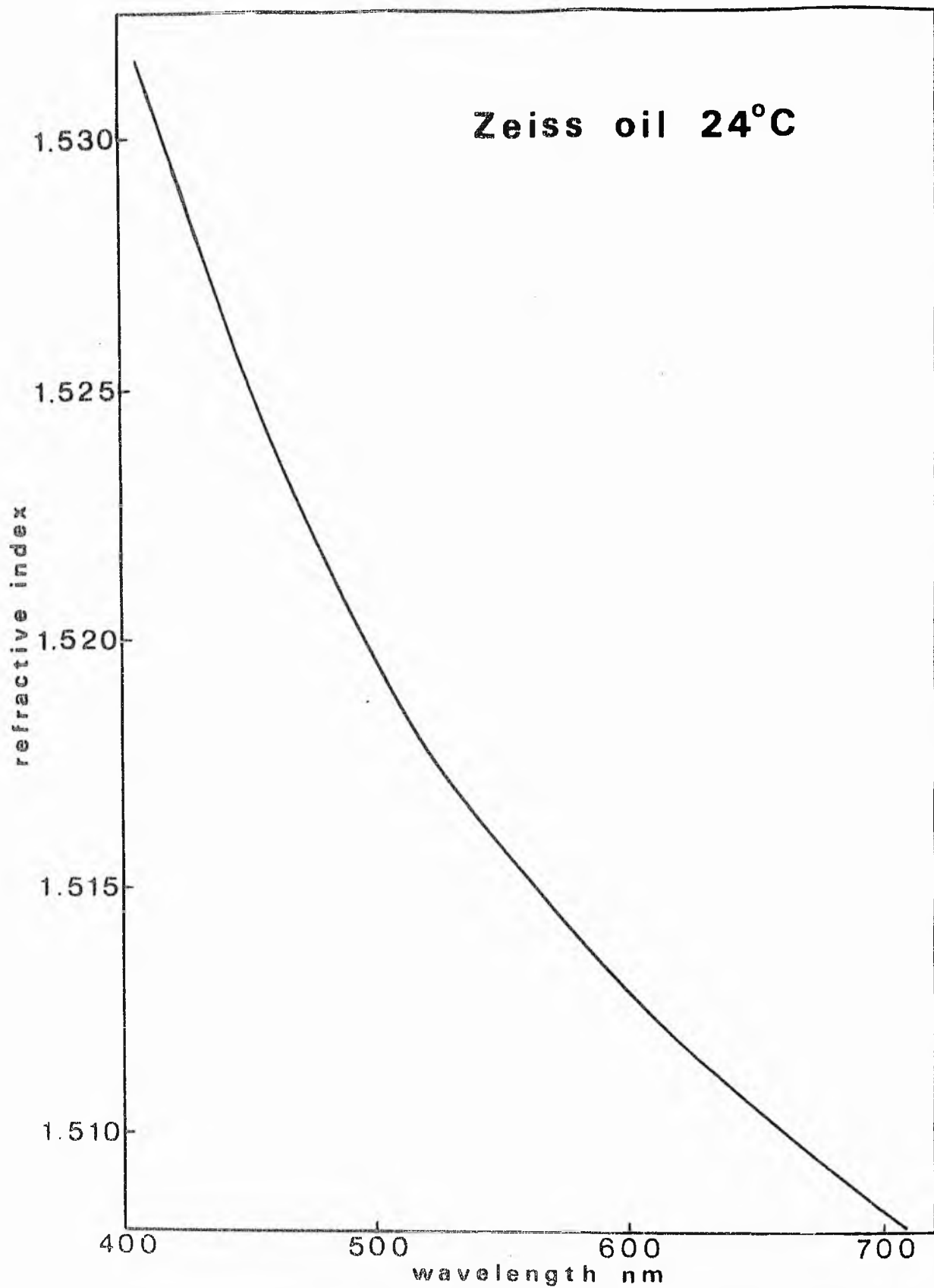


Figure 204. Plot of the variation with wavelength of the refractive index of Zeiss immersion oil at 24°C.

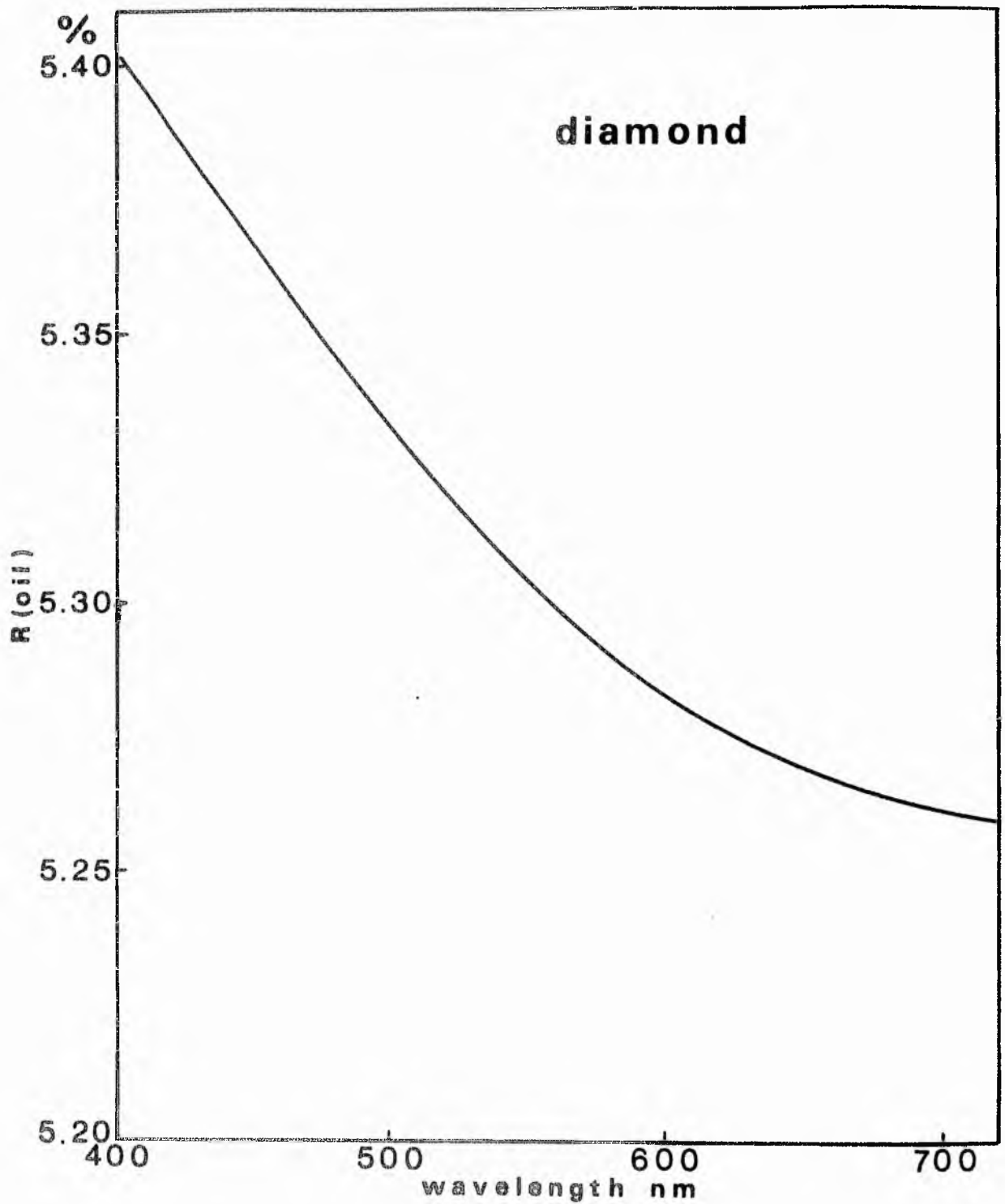


Figure 205. Plot of the dispersion with wavelength of the reflectivity of diamond in Zeiss immersion oil.

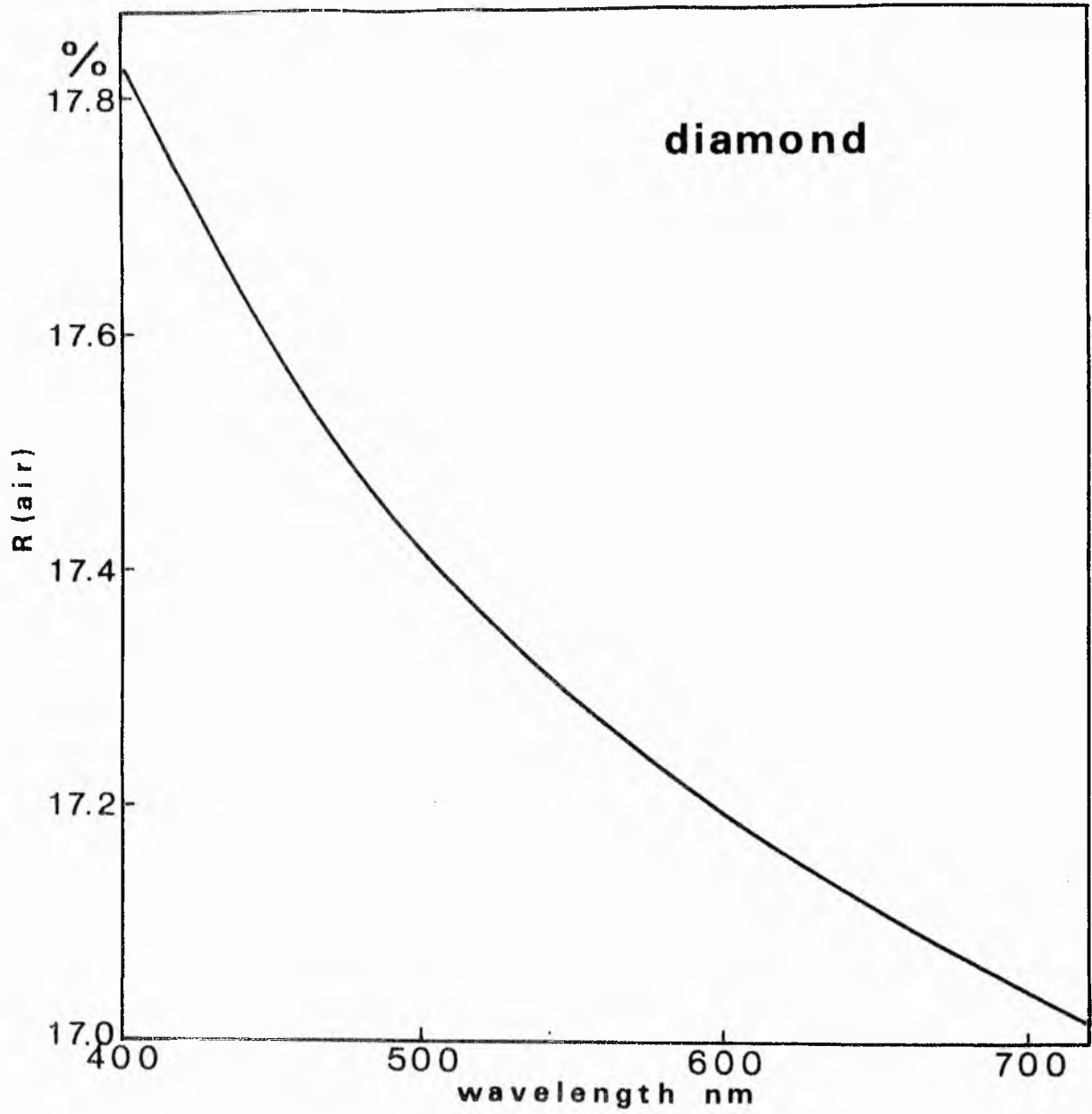


Figure 206. Plot of the dispersion with wavelength of the reflectivity of diamond in air.